A Study of the Reactivity and Coordination Chemistry of N-Heterocyclic Carbenes with Main Group Compounds

Jordan Waters

Christ Church College

University of Oxford

A thesis submitted for the degree of

Doctor of Philosophy in Inorganic Chemistry

Hilary 2017

Abstract

A Study of the Reactivity and Coordination Chemistry of N-Heterocyclic Carbenes with Main Group Compounds

Jordan Waters — Christ Church College

DPhil in Inorganic Chemistry — Hilary 2017

This thesis describes selected reactivity studies of the N-heterocyclic carbene, IPr, towards a range of main group compounds. The synthesis and characterisation of sixty-three compounds, all of which incorporate IPr as a ligand in one of three coordination modes, are detailed herein.

The deprotonation of IPr allowed for the isolation of an anionic source of the aIPr: ligand which was synthesised as a novel potassium salt and along with the previously reported lithium salt, was employed in reactions with group 12 and 14 bis(trimethylsilyl)amides and tetrahalides. The further chemistry of such novel products was investigated towards both electrophilic and nucleophilic reagents making use of both the pendant nucleophilic carbene functionality and the electrophilic main group centre.

An alternative route to such species was investigated by the spontaneous isomerisation of IPr in the coordination sphere of group 14 tetrabromides and group 15 tribromides. The scope of this reactivity was subsequently investigated and was found to provide a simpler route to access the abnormal coordination mode of IPr. The aIPr ligand which is generated may be deprotonated by additional IPr thereby affording aIPr: ligands. The addition of halide abstracting agents allowed for the synthesis of cationic species stabilised by the coordination of either IPr or aIPr ligands.

A unique, spontaneous reductive coupling of two phosphorus centres was discovered to take place upon heating a THF solution of (IPr)PBr_3. This allowed for the isolation of a bromide bridged P–P bond with reduced phosphorus centres. This facile reduction chemistry was further explored by reaction with mild reducing agents which provide access to low oxidation state phosphorus compounds in high yields. This chemistry was found to be possible (and more effective) due to the presence of the weaker phosphorus bond to bromine relative to the commonly employed chlorine ligands.

Acknowledgements

First and foremost, I want to thank my supervisor, Professor Jose Goicoechea for allowing me to be a member of the group and for the opportunity to work in an exciting field of chemistry. Likewise, for giving me the freedom to test random reactions, often with little outcome, and for his regular advice and support and non-stop encouragement for there were times when results may have been few and far between. He also proofread this entire thesis which was no mean feat.

Naturally, I would not have been able to undertake this project without the financial support which was provided by Christ Church College, the EPSRC and the University of Oxford.

I also want to specifically mention those who have directly contributed to this research. My three Part II students, Lajoy Tucker, Oliver Crossley and Thomas Everitt, along with a second year undergraduate summer student, Qien Chen, who were all delightful students to supervise and in return helped me in the various aspects of this research with numerous results and most importantly, growing single crystals. Additionally, I would like to thank Dr. Nick Rees for his invaluable assistance with an assortment of NMR experiments and his expert insight, Dr. William Myers for conducting the EPR experiments and Colin Sparrow for carrying out the EI-MS and GC-MS experiments.

I must also thank all of those I have shared the lab with over the years. Dr. Rob Turbervill for supervising me as a Part II and teaching me how to do synthetic chemistry and for his crude humour which is unlike anyone else I know. Dr. Gaby Espinoza Quintero for making the lab such a fun place to be and obviously for the unplanned evening excursions to the pub and to her gigs. Dr. Andy Jupp for being by my side almost constantly while he was in the group and for trying to teach me some basic English, I really should of listened. Dr. Tom Robinson for

providing a good dose of comedy as the old man of the group. David Lo for always having a smile on his face and a smoothie to hand. Érica Faria for a constant supply of delicious treats and Dr. Alex Hinz who has provided the lab with a long needed bit of German as well as actually helping me to learn how to do some computational chemistry.

Of course I would like to thank everyone else I have shared the lab with over the years: Gemma, Izzy, Dave, Mikey, Dan, Mike, James, Jamie, Claire, Jess, Chris, Marcel, Jonas, Michael, Dan, Harry, Geve, Stefans and Corey, along with everyone from the other organometallic groups on the top floor of the CRL.

Needless to say, I would also like to thank my family and most of all, the mother and Andy for their constant love and support despite me having remained a student for longer than they might have expected.

Finally, I would like to thank all my friends for providing me with a distraction from chemistry when it was most necessary, even though this likely ended up with me chatting about chemistry and them still not having a clue about what I actually did in the lab. Likewise, I need to thank Emma for being the best distraction from writing this thesis and encouraging me to keep going with it.

List of abbreviations

$\{^1H\}$	^1H decoupled
12-crown-4	1,4,7,10-tetraoxacyclododecane, $C_8H_{16}O_4$
18-crown-6	1,4,7,10,13,16-hexaoxacycloocatadecane, $C_{12}H_{24}O_6$
2,2,2-crypt	4,7,13,16,21,24-hexaoxa-1,10-diazabicyclo[8.8.8]hexacosane, $C_{18}H_{36}N_2O_6$
Å	Ångström
AIM	atoms in molecules
aIPr	abnormally bonded IPr
aIPr:	abnormally bonded and deprotonated IPr
Anal.	elemental analysis
Ar	aryl
atm	standard atmosphere
benzene	C_6H_6
br	broad
butyl	C_4H_9
°C	degrees Celsius
CAAC	cyclic(alkyl)(amino)carbene

CCD	charge-coupled device
Calcd	calculated
CSD	Cambridge Structural Database
Cp	cyclopentadienyl, C_5H_5
δ	chemical shift
Δ	difference or heating
d	doublet
d_n	deuterated with n deuterium atoms
D	dipolar coupling constant or diffusion constant
DBU	1,8-diazabicyclo[5.4.0]undec-7-ene, $C_9H_{16}N_2$
DCM	dichloromethane, CH_2Cl_2
diethyl ether	Et_2O
DFB	difluorobenzene, 1,2-$F_2C_6H_4$
DFT	density functional theory
dioxane	1,4-dioxane, $C_4H_8O_2$
Dipp	2,6-diisopropylphenyl
DOSY	diffusion-ordered spectroscopy
DTBMS	di-*tert*-butylmethylsilyl

EI-MS	electron impact mass spectrometry
EPR	electron paramagnetic resonance
ESI-MS	electrospray ionisation mass spectrometry
Et	ethyl, CH_2CH_3
fwhm	full width at half maximum
γ	gyromagnetic or magnetogyric ratio
g	gram
hexane	C_6H_{14}
HMPT	hexamethylphosphorus triamide, $P(NMe_2)_3$
HOMO	highest occupied molecular orbital
HSQC	heteronuclear single quantum coherence
Hz	Hertz
I	nuclear angular momentum quantum number
I^{i}Pr	1,3-bis(isopropyl)imidazol-2-ylidene, $:C(N(^iPr))_2(CH)_2$
IMes	1,3-bis(2,4,6-trimethylphenyl)imidazol-2-ylidene, $:C(N(Mes))_2(CH)_2$
^{i}Pr	isopropyl
IPh	1,3-bis(phenyl)imidazol-2-ylidene, $:C(N(Ph))_2(CH)_2$
IPr	1,3-bis(2,6-diisopropylphenyl)imidazol-2-ylidene, $:C(N(Dipp))_2(CH)_2$

I^{t}Bu	1,3-bis(*tert*-butyl)imidazol-2-ylidene, :C(N(^{t}Bu))$_2$(CH)$_2$
J	Joule
J	coupling constant
k	kilo
K	Kelvin
Kα	radiation emitted on transition of an electron from an L shell to K shell
HMDS	hexamethyldisilylamide, N(SiMe$_3$)$_2$
λ_{max}	wavelength of maximum absorption
L	litre
LUMO	lowest unoccupied molecular orbital
μ	micro or bridging ligand
m	milli or metre or multiplet
M	mega or molar, mol·dm^{-3}
m/*z*	mass to charge ratio
Me	methyl, CH_3
Mes	2,4,6-trimethylphenyl
min	minute
mol	mole

n	principle quantum number
n	nano
^{n}Bu	normal butyl, $CH_2CH_2CH_2CH_3$
naphthalene	bicyclo[4.4.0]deca-1,3,5,7,9-pentaene, $C_{10}H_8$
NHC	N-heterocyclic carbene
NMR	nuclear magnetic resonance
OAc	acetate, $[CH_3CO_2]^-$
OTf	triflate, $[CF_3SO_3]^-$
PEEK	polyether ether ketone
Ph	phenyl, C_6H_5
pK_a	$-\log_{10}(K_a)$ where K_a is the acid dissociation constant
ppm	parts per million
propyl	C_3H_7
pyridine	C_5H_5N
q	quartet
r	radius
R	carbon coordinated ligand
Σ	sum

s	singlet
sept	septet
t	triplet
Tbt	2,4,6-tris(bis(trimethylsilyl)methyl)phenyl
^{t}Bu	tertiary butyl, $C(CH_3)_3$
TDAE	tetrakis(dimethylamino)ethylene, $(Me_2N)_2C=C(NMe_2)_2$
terphenyl	2,6-$(Ar)_2C_6H_3$
tert	tertiary
THF	tetrahydrofuran, C_4H_8O
TMEDA	*N*,*N*,*N'*,*N'*-tetramethylethylenendiamine, $(CH_3)_2NCH_2CH_2N(CH_3)_2$
TMP	2,2,6,6-tetramethylpiperidine, $C_9H_{19}N$
toluene	methylbenzene, C_7H_8
Trip	2,4,6-triisopropylphenyl
TTMSS	tris(trimethylsilyl)silyl
UV/Vis	ultraviolet/visible
V	Volt
v	very
ν_{CO}	carbonyl stretching frequency

Contents

Chapter 1

Introduction

1.1 Main group elements

The main group elements are those which occur in groups 1 and 2 (s-block) and groups 13–18 (p-block) of the periodic table and their elemental forms comprise metals, metalloids, non-metals and noble gases. Interest in the chemistry of these elements has steadily increased over the years with the isolation of compounds that exhibit unforeseen bonding motifs and challenge our understanding of fundamental concepts in structure and bonding.

1.1.1 Inorganic chemistry of the main group elements

The majority of our understanding of chemistry is limited to the first row elements of the p-block due to their high natural abundance. Indeed, the whole field of organic chemistry is largely built around a handful of elements: carbon, hydrogen, oxygen and nitrogen. The remainder of the periodic table gives rise to the field of inorganic chemistry which has the concept of chemical periodicity at its heart. It was in the mid to late 1800s that Dimitri Mendeleev worked on developing what we now know as the periodic table of the elements whereby he was able to order and classify elements according to their chemical properties and was able to predict the existence of elements such as germanium 20 years prior to its discovery in 1886.[1] Since then, many of the elements that were unknown at the time, and including those that were, have been isolated as binary compounds such as carbides, nitrides and oxides.[2]

Naturally, similar materials comprising the heavier main group elements such as phosphides and selenides are also accessible, in fact, binary compounds such as gallium arsenide (GaAs) and zinc selenide (ZnS) are highly useful materials and used widely in the electronic industry in devices such as high speed transistors, lasers and optical communication systems.[3,4] These compounds are isovalent with the group 14 elements such as silicon and form part of a group of extensively used semiconductors and small band gap insulators.

Finally, binary compounds of the main group elements with hydrogen and the halogens form a very useful set of compounds which are typically used as precursors for further chemistry.[5] These species are typically molecular compounds, therefore it is possible to dissolve these compounds in organic solvents. There are a small number of exceptions, such as SnF_4, which form an insoluble polymeric material by the formation fluoride bridges. Similarly, $GaCl_3$ is only monomeric in the gas phase and will dimerise to give $Ga_2Cl_4(\mu\text{-}Cl)_2$ in the solid state, however the dimer remains highly soluble in many solvents.

1.1.2 Trends in bonding in main group compounds

Due to the small differences in the electronegativities of the p-block elements, bonding in compounds of the main group elements is predominantly covalent in nature. There is a general decrease in the strength of bonds as you descend a group due to the poorer overlap of the atomic orbitals involved in bonding. The strength of a covalent bond to an electronegative element (such as a halogen) generally decreases across a period due to the reduction in the ionic contribution.

The stoichiometry of the compounds formed by the main group elements, and their oxidation states, can be reliably predicted by consideration of the electronic configuration of the element. This is an extension of the commonly used octet rule which is based on the observation that the elements tend to combine in such as way so as to obtain eight electrons in their valence shell. The valence electron configuration of the group 14 elements is ns^2np^2, consequently, they are predicted to form four covalent bonds utilising all valence electrons and are thus termed tetravalent. However, as the group is descended, we find that there is an increasing stabilisation of the divalent state of the elements, an observation that suggests that the ns^2 electrons are less likely to be involved in bonding. This so called *inert pair effect* is

the result of the weaker E–X bonds due the heavier main group elements being unable to compensate for the promotional energy of the s electrons.[6]

This trend in stability of the *N*–2 oxidation state is noted in group 13, 14 and 15. This gives rise to the increasing stability of the +1, +2, and +3 oxidation state of the heavier elements in these groups respectively. Consequently, whereas BCl_3, CCl_4 and PCl_5 are all synthetically accessible and stable species, $TlCl_3$ is unstable above 40 °C with respect to loss of Cl_2 to give TlCl, $PbCl_4$ tends to decompose to $PbCl_2$ with loss of Cl_2 above 0 °C and $BiCl_5$ is unknown.

1.1.3 Unusual oxidation states in binary main group compounds

The tendency for the main group elements to form compounds in which they exist in the *N* or *N*–2 oxidation states results in these species having electron paired configurations and diamagnetic properties. Compounds with an empirical formula that suggests the presence of a main group element with an intermediate oxidation state and an unpaired electron would imply that such a species is paramagnetic. However, paramagnetic binary compounds of the main group elements are very rare; the compounds either disproportionate or dimerise with the formation of an element–element bond. Notable exceptions are the nitrogen oxides NO and NO_2. These are well known free radical species with nitrogen in the +2 and +4 oxidation states, respectively; these species are still susceptible to dimerisation at low temperatures.

There are numerous examples of group 13 dihalide species, $E^{II}X_2$ (E = Ga, In, Tl; X = Cl, Br, I) in which the main group element has a formal oxidation state of +2 and therefore an unpaired electron. This oxidation state is unstable with respect to disproportionation and the true formula for such compounds is $[E^{I}]^{+}[E^{III}X_4]^{-}$ which contains the elements in the more stable +1 and +3 (*N*–2 and *N*, respectively) oxidation states in the form of an $[E^{I}]^{+}$ cation and an $[E^{III}X_4]^{-}$ tetrahedral anion (Figure 1.1).

The number of compounds which form element–element bonds, and can therefore be considered as existing in an intermediate oxidation state, are also plentiful. For example, $SiCl_3$ contains silicon in the +3 oxidation, hence it has one unpaired electron and is a radical species. Such a molecule is unstable with respect to dimerisation and results in the formation of a two electron Si–Si covalent bond affording $Cl_3Si–SiCl_3$. This is also true of Si_2H_6 and Ge_2H_6 which are heavier group 14 analogues of ethane. $Cl_2B^{II}–B^{II}Cl_2$ can be synthesised by the reduction of the boron(III) precursor BCl_3 (Figure 1.1).[7]

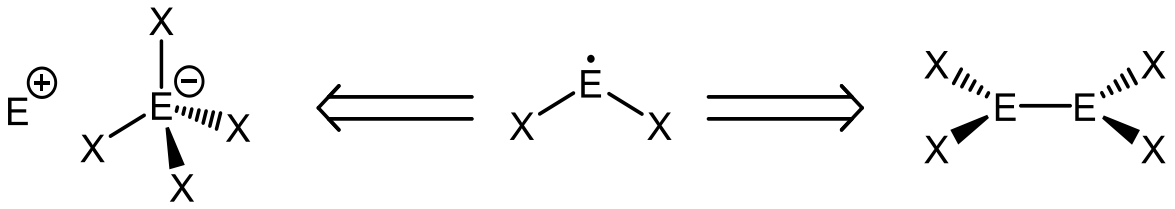

Figure 1.1: Representations of the true structures of group 13 dihalides.

Similarly, the group 15 elements in the +2 oxidation state are accessible through the formation of E–E bonds and the use of weakly oxidising reagents such as iodine (I_2). Stoichiometric addition of either phosphorus or arsenic to iodine does not afford the monomeric and paramagnetic $E^{II}I_2$ which would have an unpaired electron, but instead results in the formation of $E^{II}{}_2I_4$ with the formation of a single covalent E–E bond.[8] Similarly, the monohalides (and monohydrides) of the group 15 elements have also been studied both theoretically and experimentally. Nitrogen monofluoride (NF) which contains nitrogen in the +1 oxidation state, a so called nitrene with only six valence electrons, is a highly reactive intermediate and has been observed spectroscopically in the gas phase upon decomposition of fluorine azide (N_3F).[9,10] The triplet state of NF has two unpaired electrons in the two orthogonal nitrogen p orbitals, this diradical species is again highly unstable with respect to dimerisation and the formation of an N=N double bond generating FN=NF. The synthesis of bismuth monoiodide (BiI) results in a disproportionation of Bi^{I} to Bi^{0} and Bi^{II}, however, these unusually low

oxidation states of bismuth also results in the formation of Bi–Bi bonds in a structure that can be described as infinite chains of $I_2Bi^{II}–Bi^0–Bi^0–Bi^{II}I_2$ (Figure 1.2).[11]

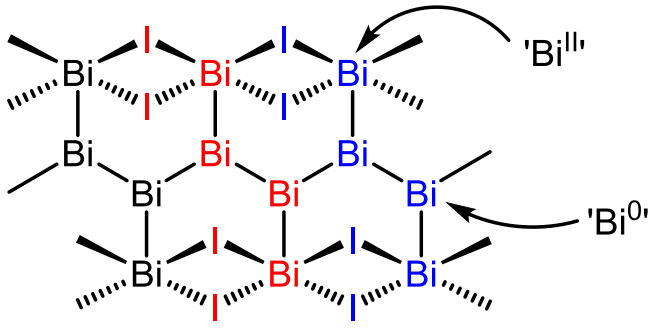

Figure 1.2: Solid state structure of $[Bi^0_2Bi^{II}_2I_4]_\infty$.

Whilst the monohalides of the heavy group 13 elements such as indium and thallium are isolable and stable species, the equivalent monomeric boron and aluminium halides are thermodynamically unstable.[12] Where boron only has four valence electrons in BCl for example, this species readily forms clusters of the form $(BCl)_n$. Both B_4Cl_4 and B_8Cl_8 have been isolated and crystallographically characterised in the form of a tetrahedron or square antiprism of boron atoms, respectively, further stabilised by additional bonding involving Cl p_π orbitals.[13–15] AlX (X = Cl, Br) can be generated and found to be thermodynamically stable at a temperature of 1000 °C and a pressure of 10^{-3} mbar. Schnöckel and Köhnlein developed a reactor that passes HX over liquid aluminium contained in a graphite oven. This generates gaseous AlX which can be immediately condensed onto a solid solvent matrix before disproportionation can occur.[16] AlX formed by this method can then be utilised in the synthesis of low valent aluminium clusters.[17,18] Gallium iodide ($Ga^{I}I$) is easily prepared by the sonication of gallium metal with half an equivalent of I_2 in toluene. The green powder that forms, whilst a versatile reagent as a source of gallium(I), has recently been shown to have a composition consistent with $[Ga^0]_2[Ga^I]^+[Ga^{III}I_4]^-$.[19,20]

1.1.4 Main group elements in negative oxidation states

In contrast to oxidation reactions that take place with electrophilic reagents such as oxygen, hydrogen and the halogens, high temperature solid state reactions between a group 1 or 2 electropositive metal with a main group element gives rise to a Zintl phase (A_xE_y where A = alkali or alkaline earth metal and E = p-block element) which contains electron rich clusters of the p-block elements in negative oxidation states. This reactivity can be dated back to 1891 when Joannis discovered that the reduction of elemental lead with sodium in liquid ammonia afforded a green solution containing lead anions.[21] However, it was Eduard Zintl who was able to identify the anion present in liquid ammonia, $[Pb_9]^{4-}$. Such highly anionic species, commonly referred to as Zintl ions, have since been studied in solution by use of multi-dentate, chelating cryptands and crown ethers in order to sequester the naked metal cation, thereby increasing their solubility and facilitating their crystallisation from solution.[22,23] Numerous Zintl clusters have been synthesised since Joannis' pioneering studies and have been employed as useful precursors to novel compounds. Despite this, the vast majority of these species have a maximum alkali metal content of one per p-block element; the general oxidation state of the p-block element in Zintl ions lies between 0 and –1. Some of the most common Zintl ions studied are those of the group 14 and 15 elements and have previously been the focus of research by the Goicoechea group and others.[24–28] Zintl ions such as $[E_9]^{4-}$ where E = Ge, Sn and Pb and $[E_7]^{3-}$ where E = P, As and Sb all contain main group elements with an average oxidation state of approximately –0.4 (Figure 1.3).[29] Ions such as $[Bi_2]^{2-}$ and $[P_4]^{4-}$, with the elements in the –1 oxidation state, are known and a few examples, such as $[Bi_4]^{6-}$, with an average oxidation state of –1.5 are also synthetically accessible.[30–32] Zintl phases such as sodium phosphide (Na_3P, with a formal phosphorus oxidation state of –3) can be synthesised from the elements and used as a source of P^{3-}, however the high lattice enthalpy precludes the dissolution of such a reactive species.

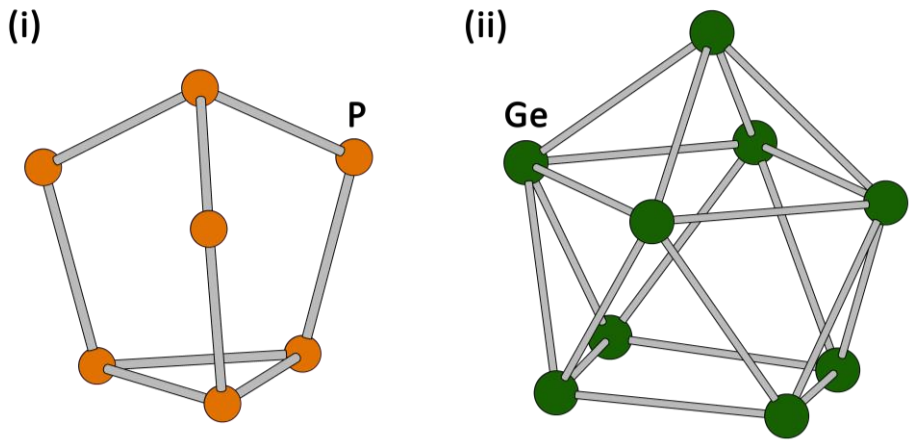

Figure 1.3: Ball and stick models of: (i) $[P_7]^{3-}$ and (ii) $[Ge_9]^{4-}$.

1.2 Ligands in main group chemistry

Needless to say, chemistry is not limited to binary compounds. The majority of chemistry involves the use of functionalised ligands. Carbon, nitrogen and oxygen can all be incorporated into ligands with varying steric and electronic properties. Some of the common varieties of carbon, nitrogen and oxygen based ligands are illustrated in Figure 1.4.

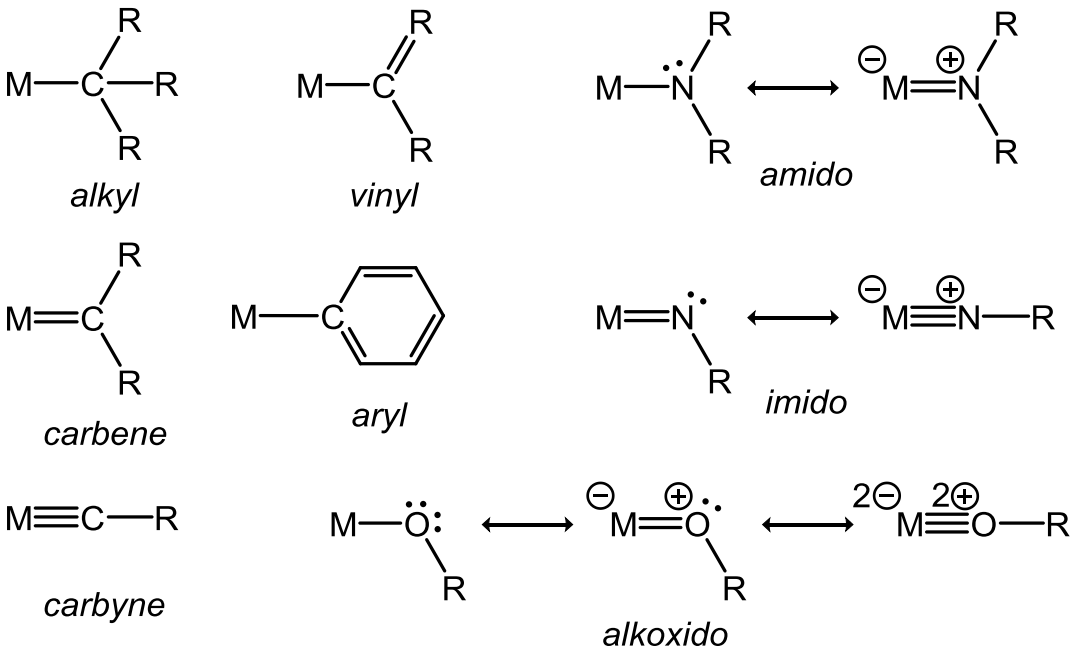

Figure 1.4: Possible coordination modes of various carbon, nitrogen and oxygen based ligands.

Molecular hydrides of carbon such as ethane, ethene (ethylene) and ethyne (acetylene) are well known and contain single, double and triple bonds, respectively. The ability of carbon to form compounds with a variety of bonding motifs results in the diverse chemistry that can be observed to occur naturally.

However, the heavier group 14 elements are not observed to naturally form multiply bonded species such as $H_2E{=}EH_2$ and HE≡EH. The now fairly outdated double bond rule states that elements whose principal quantum number is greater than two should not form multiple bonds with themselves or other elements. The basis for the rule is attributed to the decrease in orbital overlap on descending a p-block group in the periodic table.[33,34] This effect can be observed in the elemental form of the main group elements.[2] A very common comparison is that of the first row elements such as nitrogen and oxygen which readily form strong multiple bonds, hence exist as gaseous diatomic molecules, with the second row elements such as phosphorus and sulphur which in their elemental forms do not contain multiple bonds but instead oligomerise or polymerise in order to maximise the number of stronger single bonds. Where the single bond strengths for N–N and P–P are 161 $kJ{\cdot}mol^{-1}$ and 209 $kJ{\cdot}mol^{-1}$, respectively, the bond strength in N_2 is 946 $kJ{\cdot}mol^{-1}$ however, that of an equivalent P_2 triply bonded molecule has a bond strength of only 490 $kJ{\cdot}mol^{-1}$. It is clear to see that the sum of three single P–P bonds is greater than that of P≡P and so phosphorus has multiple elemental forms, all of which consist of networks of P–P single bonds.[35–37] Of great interest is the monomeric P_4 molecule which forms a strained tetrahedron and is a useful precursor for phosphorus chemistry. Identical arguments rationalise the diatomic structure of O_2 and the formation of single bonds in various sized rings of sulphur, predominantly S_8.

This rule was ultimately disproven with the synthesis of species such as disilenes ($R_2Si{=}SiR_2$),[38] diphosphenes (RP=PR),[39] and the phosphaalkyne P≡C^{t}Bu.[40] Since these first

examples, the chemistry of main group compounds containing multiple bonds has developed rapidly and can be considered a leading theme in main group chemistry. One modification to the rule is that where multiple bonds do form between the heavier main group elements, they are often weak or may be prone to oligomerisation. Multiple bonds between the elements are generally stabilised kinetically with sterically large groups and electronically with strongly electron donating groups. The possibility of multiple bonding between the main group elements has since been comprehensively reviewed by Fischer and Power.[41,42]

1.2.1 Classification of ligands

The concepts of oxidation state, coordination number and valency have been central to describing the structure and bonding in inorganic compounds.[43] Malcolm Green established a simple classification of each type of ligand as a method of conveniently describing the bonding interactions involved.[44] Ligands are typically described with either L, X (and R) or Z. The L notation is used to describe a neutral ligand which has a filled orbital with two electrons which are used to donate to an empty orbital on a Lewis acid. The X notation is used to describe a ligand with a formally singly occupied orbital which requires one electron from the metal or main group centre for bonding. Naturally, they can be described as an anionic two electron donor ligand. An R label is typically used to represent a carbon group or hydrogen atom whilst an X label is typically used to represent all other anionic groups such as halides or amido functionalities ($–NR_2$), however, these are often used interchangeably. Finally, the Z notation is used to describe a ligand which has an empty orbital which can accept an electron pair from a Lewis basic metal or main group centre. Ligands of this class are rare and are generally a Lewis acid such as BH_3, $AlMe_3$ or SiF_4.

Such classifications are important in modern main group chemistry as a method to accurately describe oxidation state, valency and therefore the electronic structure of novel compounds.

1.2.2 Sterically bulky ligands in the synthesis of persistent main group radicals

By employing sterically demanding bulky groups as ligands in place of very small groups such as halides or hydrides, it is possible to kinetically stabilise a diverse range of main group elements in unusual oxidation states and/or low coordination numbers resulting in persistent and stable radicals.[45] R type carbon or silicon based ligands have been frequently used; very common bulky ligands include Mes (2,4,6-trimethylphenyl), Dipp (2,6-diisopropylphenyl) and Trip (2,4,6-triisopropylphenyl) as carbon bonded ligands and DTBMS (di-*tert*-butylmethylsilyl) and TTMSS (tris(trimethylsilyl)silyl) as silicon based ligands. Some of the earliest work in this area was carried out by Olmstead and Power who were able to crystallographically characterise a previously postulated persistent boron based radical $[B(Mes)_3]^{\bullet-}$ as the $[Li(12\text{-crown-}4)_2]^+$ salt which was monomeric in solid state and solution and not susceptible to loss of a ligand and B–B bond formation (cf. B_2Cl_4).[46] The boron centre remains planar as the additional electron resides in boron orbital of predominantly p character. Despite similarity with these studies, it was not until 2013 that the triarylphosphine $P(Trip)_3$ (synthesised via the organocopper reagent TripCu with PCl_3) was shown to be easily oxidised by AgX (X = SbF_6 or $Al(OR^F)_4$ and $OR^F = OC(CF_3)_3$) to generate the corresponding radical cation (Scheme 1.1).[47]

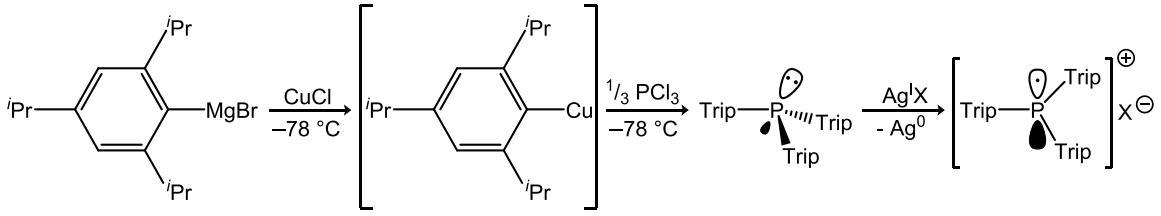

Scheme 1.1: Synthesis of a stable cationic radical triarylphosphine.

The normally pyramidal phosphine becomes trigonal planar on oxidation as a result of the bulky aryl groups resisting the effect of P 3s and P 3p hybridisation, an effect corroborated by computational analysis (as smaller aryl groups such as phenyl groups in $[PPh_3]^{\bullet+}$ would allow for some pyramidalisation). Equally, the same research groups were able to access the stable radical anion and cation of the tetraryldiborane $(Mes)_2B^{II}–B^{II}(Mes)(Ph)$ and the tetraryldiphosphine $(Trip)_2P^{II}–P^{II}(Trip)_2$, respectively.[48,49] Both reactions allow for multiple bonding character between the main group elements. In both examples, the unpaired electron resides in a π orbital equally distributed over both main group atoms as determined by equivalent coupling to the nuclei in the EPR spectra. A second reduction of the boron complex is possible to afford the diamagnetic dianion however in both anions the B–B bond length does not reflect the double bond character due to the increased electrostatic repulsion. Upon oxidation of the tetraryldiphosphine, the structure becomes less pyramidalised, in fact, removal of the second electron to afford the diamagnetic diphosphine dication results in complete flattening in the $[(Trip)_2P^{III}=P^{III}(Trip)_2]^{2+}$ core and what can now be described as a formal double bond between the two phosphorus atoms as evidenced by a shortening of the P–P bond distance.

Likewise, monomeric radical anions of the heavier group 13 elements are also accessible. Reduction of $E^{III}(Si^tBu_2Me)_3$ (E = Al, Ga) by an alkali metal (Li, Na or K) in THF generated the corresponding homoleptic radical anions $[E^{II}(Si^tBu_2Me)_3]^{\bullet-}$. As is to be expected of many persistent radical species, there is an immediate colour change, in these examples, to dark-red. The small hyperfine coupling constant for the radical anions again indicate a relatively planar structure is retained in solution and the unpaired electron resides predominantly in the Al 3p or Ga 4p orbital, respectively. Finally, neutral radicals of the group 14 elements (in the +3 oxidation state) were accessed via a different method (Figure 1.5). The radical complexes were obtained upon addition of multiple equivalents of an alkali metal silyl reagent ($MSiR_3$)

with a source of E^{II} (E = Ge, Sn, Pb) or Si^{IV} in $Si(Br)_2(Si(^tBu_2Me))_2$.[50–53] In these reactions, a salt metathesis reaction takes place followed by addition of a third silyl group to give $[E^{II}(SiR_3)]^-$ in all cases which is followed by a one electron oxidation by the original group 14 reagent, or by addition of $GeCl_2$·dioxane in the synthesis of $[Si^{III}(Si(^tBu_2Me)_2)_3]^{\bullet}$.

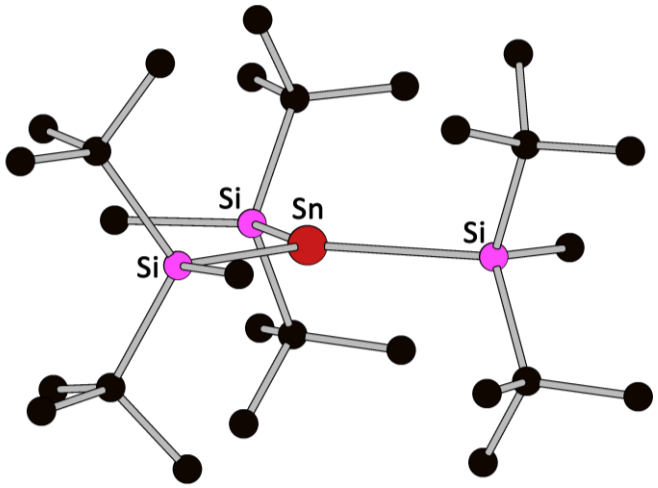

Figure 1.5: Ball and stick model of $[Sn(Si^tBu_2Me)_3]^{\bullet}$. Hydrogen atoms have been omitted for clarity.

In 2006, Nozaki and co-workers succeeded in synthesising a nucleophilic, anionic boron(I) species supported by a reduced diazabutadiene ligand.[54] Reduction of Dipp-diazabutadiene with magnesium metal followed by reaction with BBr_3 affords the precursor *N*,*N*'-bis(2,6-diisopropylphenyl)-2-bromo-2,3-dihydro-1*H*-1,3,2-diazaborole. A further two electron reduction with lithium powder and naphthalene allows for the isolation of the boryllithium, a species isoelectronic with an N-heterocyclic carbene (Scheme 1.2).

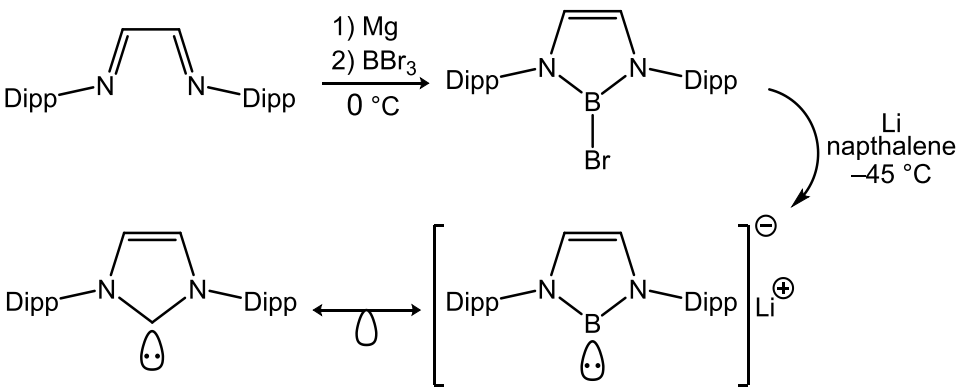

Scheme 1.2: Synthesis of a nucleophilic boryllithium.

This represents the first example of a nucleophilic boron based X type ligand and has therefore been found as a supporting ligand in many main group complexes.[55] The formally empty boron p orbital provides the ligand with a greater π acidity relative to NHCs (see Section 1.2.7) which results in a greater degree of π backbonding. Subsequently, many of the heavier analogues of boryllithium and NHCs have been synthesised such as an N-heterocyclic gallyl anion as the potassium salt,[56] and the N-heterocyclic silylene, germylene and stannylenes, albeit via appropriate modified synthetic methodologies.[57–59] Correspondingly, the heavier analogues can increasingly be described as a neutral diazabutadiene ligand supporting the main group element in the zero oxidation state with reduced π delocalisation. This was neatly demonstrated by facile exchange of the ligand in an N-heterocyclic stannylene (Scheme 1.3).[59]

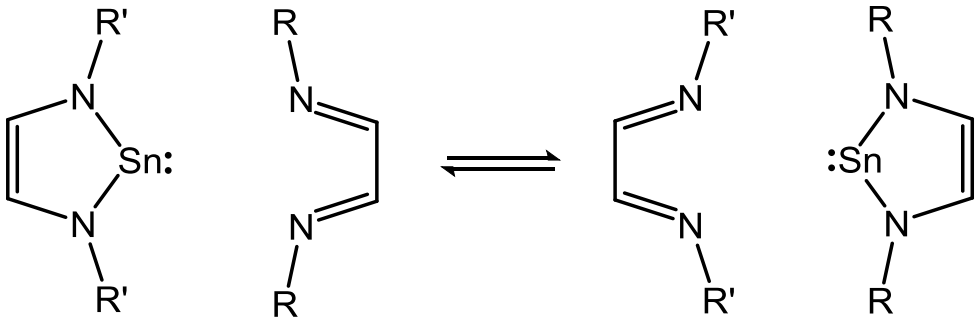

Scheme 1.3: Transfer of tin atoms between two diazabutadiene ligands.

The usefulness of the boryl substituent as a ligand in main group chemistry has been elegantly demonstrated in collaborations between the Aldridge, Jones and Mountford groups.[66–68] One of the most ground breaking results to come from these collaborations was published in 2014, involving the synthesis of stable $Ga^{II}X_2$, $In^{II}X_2$ and $Tl^{II}X_2$ radicals by making use of the sterically demanding boryl substituent. $E^{II}(boryl)_2$ were the first conclusive examples of monomeric $E^{II}X_2$ species and were shown to be thermally robust paramagnetic species.[63] As discussed previously, compounds of this composition are typically mixed valence species

($[E^{I}]^{+}[E^{III}X_4]^{-}$) or feature E–E bonds ($X_2E^{II}–E^{II}X_2$). Whilst the ligand may provide some ability for π backbonding for the partially filled metal based orbital, >70% of the spin density was determined to be metal-based by EPR spectroscopy.

Finally, Schulz and co-workers have used terphenyl groups as supporting ligands in the synthesis of a mixed phosphorus and arsenic biradicaloid present in the neutral complex ($P(\mu\text{-NTer})_2As$; Figure 1.6) which features a core P–N–As–N ring with significant biradical character and a HOMO with a larger coefficient on the As atom.[64]

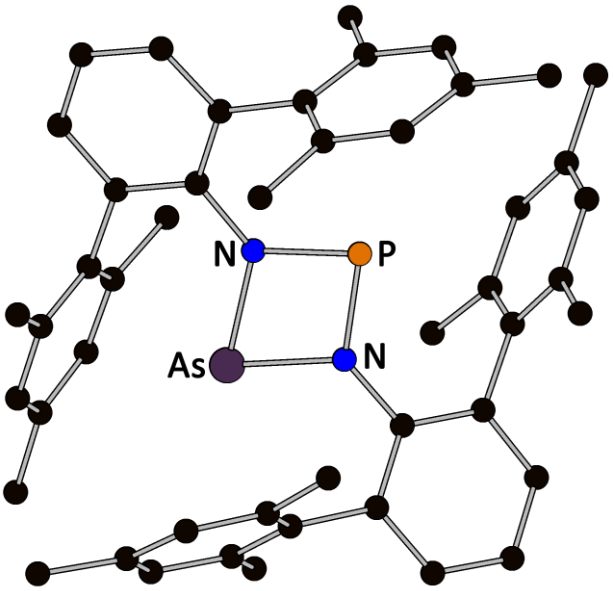

Figure 1.6: Ball and stick model of $P(\mu\text{-NTer})_2As$. Hydrogen atoms have been omitted for clarity.

1.2.3 Sterically bulky ligands in the synthesis of multiple bonds between the main group elements

Boryl ligands, whilst being strong electron donors capable of providing electron density for the stabilisation of low valent complexes, do also significantly benefit from the α nitrogen substituents which provide steric bulk and aid in kinetic stabilisation of reactive species. In this respect, aryl ligands (X type carbon bonded ligands) substituted in the 2,6 positions of the phenyl ring with secondary bulky aryl groups such as Mes or Dipp affords a ligand structure

very similar to that of imidazole based NHCs. So called *meta*-terphenyl ligands (or typically reffered to as just terphenyl ligands in this context) have been used widely as ligands in complexes of elements across the periodic table.[65] It was in the late 1990s that Power and co-workers were able to isolate mono-coordinate indium(I) and thallium(I) complexes as monomeric species bearing a terphenyl ligand (2,6-$Trip_2C_6H_3E$; E = In, Tl).[66,67] Both compounds could be synthesised by the addition of the ether solvate of the terphenyl lithium, 2,6-$Trip_2C_6H_3Li{\cdot}Et_2O$, to a suspension of InCl or TlCl in Et_2O at –78 °C or 0 °C, respectively. However, it was ten years later before a similar gallium(I) species could be synthesised by employing a bulkier terphenyl ligand (2,6-$Trip_2$-3,5-$^{i}Pr_2C_6H$) in order to disfavour dimerisation (Figure 1.7). The energy gain of this process could be systematically varied by changing the steric bulk on the ligand. Smaller terphenyl substituents were observed to afford monomeric species in solution which dimerise in the solid state.[68]

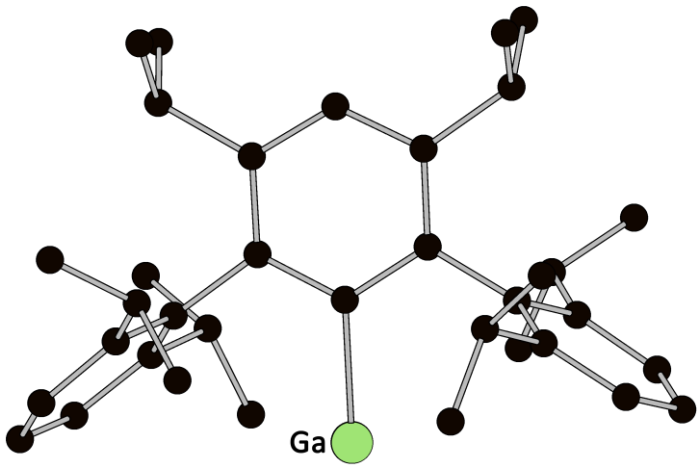

Figure 1.7: Ball and stick model of monomeric Ga(2,6-$Trip_2$-3,5-$^{i}Pr_2C_6H$).

1.2.4 Multiple bonds between the group 14 elements

The pioneering work of Lappert in the 1970s in the field of carbene analogues of the heavy group 14 elements paved the way for the discovery of the heavy group 14 analogues of alkenes with E=E double bonds (E = Ge, Sn, Pb).[69–71] Studies of $R_2E^{II}=E^{II}R_2$ species established key

periodic trends in structure and bonding for the group 14 elements. His work provided the first description of the now well established *trans* bent structure of E_2R_4 compounds of group 14, which contrasts with the planar arrangement of substituents in alkenes (Figure 1.8).[72–74] With the aid of molecular orbital calculations, it was shown that the electron density becomes increasingly localised on the main group element in a lone pair type orbital affording an increasingly bent structure on descending the group 14 elements. Such double bonded species were synthesised with moderately bulky ligands such as $CH(SiMe_3)_2$. A simple metathesis reaction using two equivalents of the organomagnesium or organolithium salt of the ligand with EX_2 or the stable heavy carbene analogues $E(NR_2)_2$ affords the products in high yields. The first disilene was not synthesised until 1981; tetramesityldisilene ($Mes_2Si=SiMes_2$) was obtained from the photolysis 2,2-bis(mesityl)hexamethyltrisilane ($Mes_2Si(SiMe_3)_2$) which is suggested to form via the formation of the divalent silicon intermediate, bis(mesityl)silylene (Mes_2Si:) which subsequently dimerises.[38] Evidence for this pathway was obtained by conducting the photolysis at low temperature and trapping the reactive intermediate with a suitable reagent.

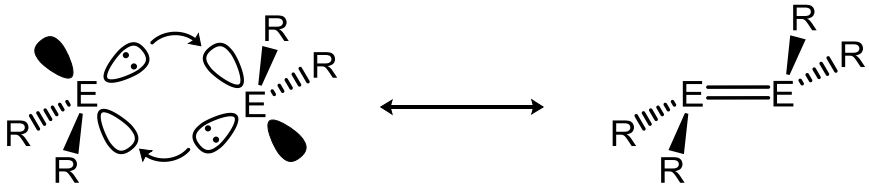

Figure 1.8: Illustration of how two singlet metallylene moieties dimerise in a *trans* bent geometry.

By extension, heavy group 14 analogues of alkynes have also been synthesised.[75] $RE^{I}{\equiv}E^{I}R$ (E = Ge, Sn, Pb; R = terphenyl) were synthesised by Power and co-workers by the reduction of the metallylene precursor $RE^{II}X$ (X = Cl, Br) with potassium to obtain the digermyne and distannyne.[76,77] $LiAlH_4$ was used to obtain the diplumbyne, presumably via RPbH as an intermediate, which generates RPb≡PbR with loss of H_2.[78] The first silylyne was synthesised

by Sekiguchi and co-workers by employing bulky silicon based ligands and reduction of the tetrabrominated precursor ([Si]–$SiBr_2$–$SiBr_2$–[Si] where [Si] = Si(^{i}Pr)($CH(SiMe_3)_2$)$_2$) with KC_8.[79] An identical *trans* bent structure is observed in all compounds, again with an increase in angle on descending the group 14 elements. A simultaneous lengthening of the multiple bond relative to known single bond lengths indicates a reduction in multiple bond character (Table 1.1). This results in a bonding description increasingly unlike that of carbon and more towards that of a dimetallylene with bonding more accurately described as a single bond comprised of significant p orbital character, hence the long bond length observed in the lead species.

	E–E Bond length (Å)	**Typical E–E single bond lengths (Å)**	**R–E–E angle (°)**
RCCR	1.20	1.54	180
RSiSiR	2.062(1)	2.34	137.4(1)
RGeGeR	2.285(1)	2.44	128.7(1)
RSnSnR	2.668(1)	2.81	125.2(1)
RPbPbR	3.188(1)	2.84	94.3(1)

Table 1.1: Bond lengths and angles in group 14 alkyne analogues.[76–79]

Replacement of the X type terphenyl ligand with a bulky amido XL type ligand was shown to be possible and allows for the synthesis of a novel RGeGeR type compound. The ligand of choice is one commonly employed in the Jones group and can be seen to be a terphenyl substituted amide ligand, $N(SiMe_3)(Ar^*)$ where Ar^* = 2,6-$(CHPh_2)_2$-4-MeC_6H_2.[80] The electronic properties of the ligand has an important effect on the molecular orbital energies.

The weaker bonding present in multiply bonded heavy main group elements results in a smaller energy gap between bonding and antibonding molecular orbitals. Therefore, many of the aforementioned complexes possess a small energy difference between HOMO and LUMO and these highly reactive p-block compounds, with frontier orbitals closely resembling those

of transition metals, display reactivity towards small molecules such as H_2, NH_3 or C_2H_4 which had only been known for transition metals previously.[81,82]

Transition metals have been used as catalysts for the delivery of dihydrogen to organic substrates, the key mechanistic step being the oxidative addition of H_2 to the metal centre. It has been shown that highly reactive p-block compounds could have potential to undergo similar chemistry; in 2005, the germanium alkyne analogue was shown to react directly with dihydrogen under ambient conditions to give the hydrogenated products RGe(H)=Ge(H)R, $RGe(H)_2$–$Ge(H)_2R$ and $RGe(H)_3$. Calculations for the mechanism of the tin analogue, which reacts to give $RSn(\mu\text{-}H)_2SnR$ exclusively, confirms the synergic interaction of the filled π orbital interacting with σ^* of H_2 and the filled σ orbital of H_2 donating into the n_+ non-bonding ligand orbital. In 2009, ethylene was shown to reversibly react with the distannyne complex to afford a 1,4-distannabicyclo[2.2.0]butane structure, a vital step forward in the use of main group elements as transition metals (Scheme 1.4).[83]

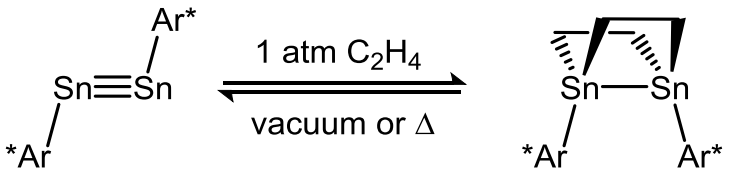

Scheme 1.4: Reversible activation of C_2H_4 by a terphenyl substituted distannyne.

The addition of a nitrogen lone pair on the amido ligand allow for additional donation of electron density into the empty π^* type orbitals of the digermylene/digermyne complex. The increased bond order between the ligand and germanium centre favours the digermylene description of bonding with a substantial increase in Ge–Ge bond length to 2.709(3) Å (cf. 2.285(1) Å for the terphenyl substituted complex). The effect of the nitrogen substituent is to decrease the HOMO–LUMO energy gap resulting in increased reactivity and the

complex was shown to oxidatively add dihydrogen across one of the germanium centres, much like a transition metal.

A recent landmark discovery to come from the Aldridge group involved the isolation of a heavier group 14 analogue of vinylidene.[84] An NHC stabilised boryl germanium chloride (NHC)–GeCl(B(NDippCH)$_2$) was treated with excess potassium metal to afford a dianionic, formally Ge^0 compound, [RGe^0=Ge^{0}R]$^{2-}$ (R = B(NDippCH)$_2$). Describing the bonding as a Ge=Ge double bond with a bond length of 2.392(1) Å is consistent with the bond lengths observed in the two electron reduced analogue of the terphenyl substituted digermyne which has a bond length of 2.391(1) Å.[85] A subsequent two electron oxidation by reaction with Cp_2Fe^+ or Ph_3C^+ affords R_2Ge^{II}=Ge^0 (Figure 1.9). The relative energies of various isomers of heavier analogues of ethyne have previously been calculated,[86] and for HGeGeH, the linear alkyne-like structure was calculated to be high in energy, as already demonstrated by the significant bending present in terphenyl substituted species.

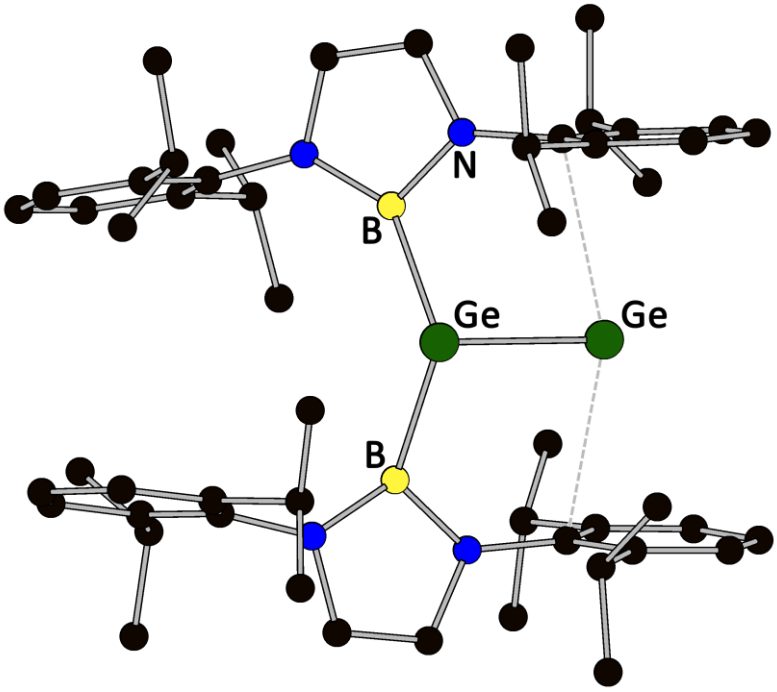

Figure 1.9: Ball and stick model of ((NDippCH)$_2$B)$_2$Ge=Ge. Hydrogen atoms have been omitted for clarity.

The lowest energy isomer was calculated to be the double bridged butterfly isomer $Ge(\mu\text{-}H)_2Ge$ at –192 kJ·mol^{-1} relative to the linear isomer, however due to the size of the large terphenyl and boryl groups, this geometry is sterically unflavoured. The vinylidene isomer $H_2Ge{=}Ge$ was calculated to lie –132 kJ·mol^{-1} lower in energy than the linear isomer. Hence, the remarkable discovery of the vinylidene isomer of R_2E_2 is clearly driven by the unique properties of the boryl ligand and the relatively low energy profile with which the ligand can move across the Ge_2 moiety, presumably via a monobridged intermediate. The Ge=Ge bond length was measured to be 2.312(1) Å, shorter than that of the reduced precursor and consistent with multiple bonding character. Finally, weak π interactions of the flanking aryl groups stabilising the Ge^0 centre were found to structurally distort the boryl ligand.

1.2.5 Multiple bonds between the group 15 elements

A similar protocol of reducing high oxidation state precursors can be used in order to synthesise doubly bonded species of the group 15 elements bearing bulky terphenyl type ligands. The formal addition of two electrons to the valence orbitals of the main group elements results in an isolobal analogy between RE=ER where E = P, As, Sb, Bi and the two electron reduced group 14 alkyne analogues $[RE{=}ER]^{2-}$. The diphosphene was achieved by an equivalent methodology of reduction of $RPCl_2$ which proceeds via a postulated phosphinidene intermediate and dimerises to afford the diphosphene.[39] Synthesis of the diarsene was precluded by the spontaneous elimination of HCl and decomposition of the precursor, $RAsCl_2$ (R = 2,4,6-^{t}Bu$_3$C$_6$H$_2$). Reduction of the analogous difluoride to afford the dihydride could subsequently be coupled with $(Me_3Si)_2CHAsCl_2$ to generate an asymmetric diarsene in the presence of a base such as DBU.[87] This new pathway then allowed the coupling of two different group 15 elements and the reaction with $(Me_3Si)_2CHPCl_2$ affords a double bonded phosphaarsene R'P=AsR (Scheme 1.5). The first distibene and dibismuthene were

realised around ten years later when an even bulkier terphenyl ligand, Tbt (2,4,6-tris(bis(trimethylsilyl)methyl)phenyl), was employed. However, synthesis of these compounds utilised HMPT (hexamethylphosphorus triamide, $P(NMe_2)_3$) as a reducing agent when combined with either the 1,3,5,2,4,6-triselenatristibane or 1,3,5,2,4,6-triselenatribismane ($(TbtESe)_3$; E = Sb, Bi).[88,89]

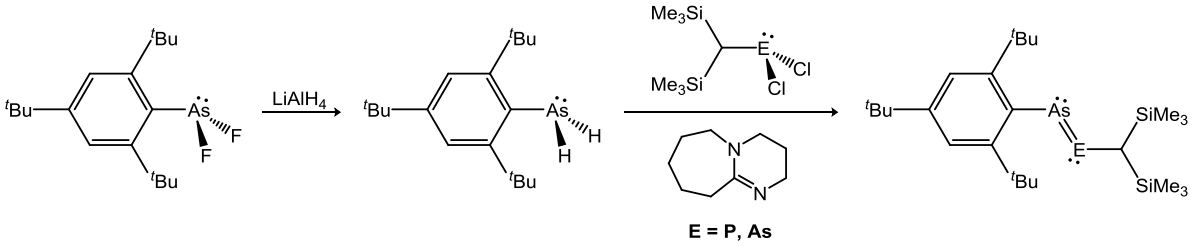

Scheme 1.5: Synthesis of an asymmetric diarsene and phosphaarsene from a bulky aryl arsine.

Finally, boryllithium can be used as a reducing agent in the synthesis of an alternatively substituted distibene and dibismuthene.[62] Addition of the boryllithium to a bulky amido substituted antimony or bismuth dihalide results in reduction of the metal centre and, via a postulated amido stibinidene or bismuthinidene, dimerisation affords the amido distibene. However, further addition of the boryl reagent to the bismuthinidene displaces the amide ligand and the boryl substituted dibismuthene is isolated in this case upon dimerisation. Both complexes display the expected *trans* bent geometry, and the dibismuthene was fortuitously crystallised as two rotamers whereby the central Bi–Bi moiety lies either in or out of plane with the boryl ligands. This indicates the energy difference between the two geometries is low and NMR data suggests that the ligands are conformationally free in solution.

1.2.6 Multidentate ligands

The almost limitless possibilities of ligand design allows for the fine tuning of steric and electronic properties. One fundamental change to an organic ligand is the incorporation of

more than one binding site, typically through heteroatoms such as nitrogen or oxygen. Multidentate ligands benefit from a chelate effect in the synthesis of the coordination complex; the pre-organised ligand results in a large entropy gain on coordination. Multidentate ligands can be classified as mixed ligands, for example, the NacNac (β-diketiminate) ligand derived from the condensation of an amine with acetylacetonate (Hacac). Deprotonation of the backbone affords a monoanionic, bidentate ligand which can be classified as LX. Naturally, the electron density is delocalised over the ligand and generally each nitrogen bonds equally to the metal centre. These ligands reach many fields of chemistry, however, most notably in recent years, bulky guanidinate $[ArNC(NR'_2)NAr]^-$ and NacNac ligands have been used extensively in the Jones group in the stabilisation of low oxidation state compounds. In 2007, these ligands allowed for the synthesis and isolation of stable magnesium(I) compounds which exhibit Mg–Mg bonds (Scheme 1.6).[90–92] As magnesium is a group 2 element, the Mg–Mg bond present in the magnesium(I) species, $[Mg(ArNC(NR'_2)NAr)]_2$, was calculated to possess 93.2% 3s character. These highly soluble organometallic reagents have since been proven to be useful reducing agents with a high reduction potential, capable of controlled reduction of numerous main group complexes; many of these reductions were also reported to have been unsuccessful with commonly employed reducing agents such as alkali metals. NacNac ligands have also been used for the stabilisation of highly reactive group 2 hydride complexes.[92,93]

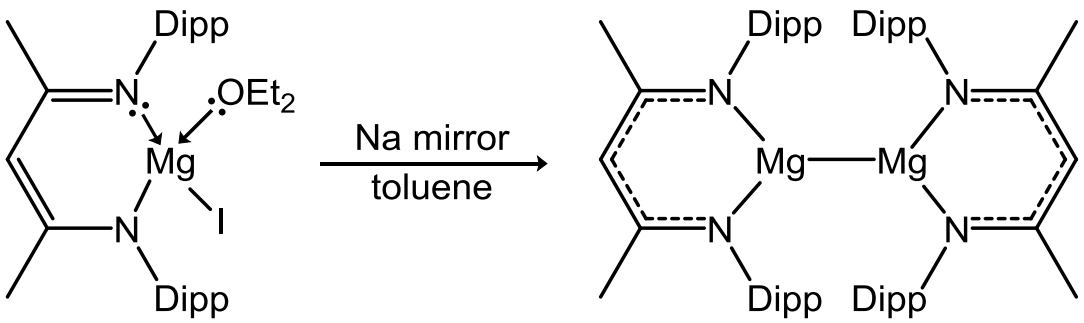

Scheme 1.6: Synthesis of a NacNac supported Mg^I–Mg^I single bond.

The use of β-diketiminate ligands naturally also extends to the p-block elements. The low valent, monomeric $Ga^{I}[(NDippCMe)_2CH]$ was synthesised by addition of the solvent free lithium-NacNac salt to a suspension of gallium(I) iodide in toluene followed by an excess of potassium (Figure 1.10).[94] The analogous aluminium(I) compound was isolated upon a two-electron reduction of $Al^{III}(I)_2[(NDippCMe)_2CH]$ with potassium.[95] The core EN_2C_3 ring is essentially planar in both compounds which may suggest delocalisation of the 6π electrons affording aromaticity, however, the higher ionic contribution to bonding to the metal centre means that they are best described by a bidentate monoanionic ligand complexed to the E^{I} cation.

By extension, diazabutadienes (RN=C(H)–C(H)=NR) have also been used in coordination chemistry for the isolation of low valent, low oxidation state main group compounds. Whilst formally a diimine, and therefore an L_2-type ligand, they are typically redox active and can be easily reduced to the monoanionic and dianionic species with either alkali metals or on coordination to an electron rich p-block element; the reduced diazabutadienes can then be viewed as either LX or X_2 ligands, respectively. Research carried out by Gudat and co-workers in extension from earlier results obtained by Reeske and Cowley demonstrated that redox chemistry takes place on reaction of bulky substituted diazabutadienes with various boron and phosphorus trihalides.[96,97] For example, an N-heterocyclic phosphenium cation could be synthesised by addition of DippN=C(H)–C(H)=NDipp to PI_3 with formal elimination of I_2 (Figure 1.10). The P^{III} cation was subsequently crystallised as the triiodide salt. Similarly Jones and co-workers discovered that InCl would undergo a one electron oxidation on reaction with Dipp-diazabutadiene (affording a one electron reduction of the ligand) to yield a paramagnetic indium(II) complex bearing an In–In bond.[98] EPR measurements confirmed the electron density to be largely delocalised on the NCCN fragment of each ligand.

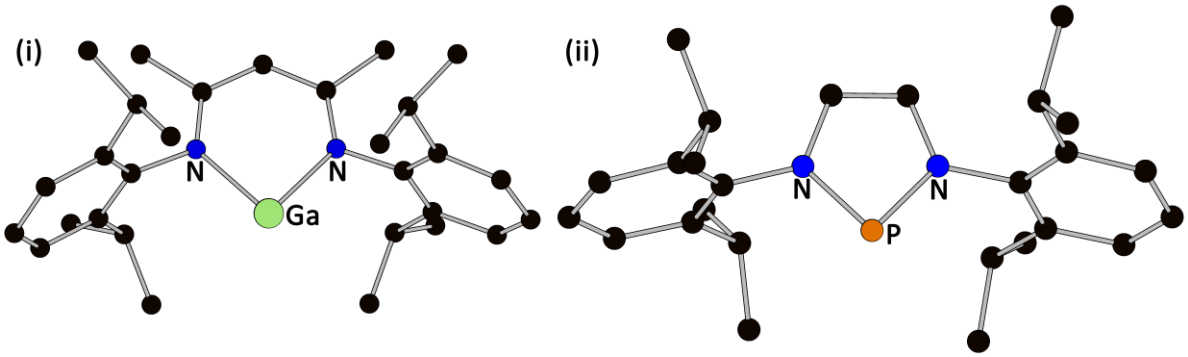

Figure 1.10: Ball and stick model of: (i) Ga[(NDippCMe)$_2$CH] and (ii) [P(NDippCH)$_2$]$^+$. Hydrogen atoms have been omitted for clarity.

1.2.7 N-Heterocyclic carbenes

A similar description of a reduced dianionic diazabutadiene coordinated to a carbon(II) dication can be employed to describe the bonding in N-heterocyclic carbenes (NHCs), the discovery of which has undeniably transformed modern main group chemistry.[99] There now exist numerous methodologies for the synthesis of a wide range of functionalised NHCs. One of the most common methods for synthesis of moderately bulky NHCs involves the deprotonation of the cationic imidazolium salt precursor with a suitably strong base such as KO^{t}Bu or ^{n}BuLi. A carbene is defined as a divalent carbon atom with a six electron valence shell. Traditionally considered a highly reactive intermediate, such carbon(II) species can be prone to dimerisation to afford C=C alkenic double bonds (as described by the Wanzlick equilibrium).[100] Some of the first isolated NHCs were suggested to be possible due to the large flanking substituents which kinetically stabilise the carbene centre in order to disfavour dimerisation. It is now known that the electronic stabilisation afforded by the adjacent nitrogen atoms is a much more important factor (Figure 1.11). NHCs can be described as a dianionic diazabutadiene ligand coordinated to a dicationic carbon(II) atom. Naturally, the strong σ bonding between the nitrogen and carbon atoms is supplemented by the favourable multiple bonding character afforded by donation of π electron density from the adjacent

nitrogen lone pair which lies in the nitrogen p orbital. Donation of electron density into the LUMO, an unoccupied carbon p orbital increases the HOMO–LUMO gap, increasing the stability of such species. This is reflected in the C–N bond lengths which lie somewhere in between a single and double bond.[101–103] The large energy gap, and the cyclic nature of the carbene forcing a bent geometry at the carbene carbon, favours the singlet state with the two remaining carbon valence electrons occupied in an sp^2 type orbital in the plane of the imidazole ring. Until 1996, the extent of π delocalisation had been considered of negligible importance, especially with respect to the imidazolium salt precursors. Both Apeloig and Frenking independently concluded that delocalisation does occur in unsaturated NHCs and so increases the formally vacant p_π occupancy to 56% of a perfectly delocalised π bond; only 40% delocalisation occurs in the saturated analogues.[104,105] Such delocalisation results in a 6π electron ring fulfilling the conditions required for aromatic character, further stabilising the low valent carbon centre.

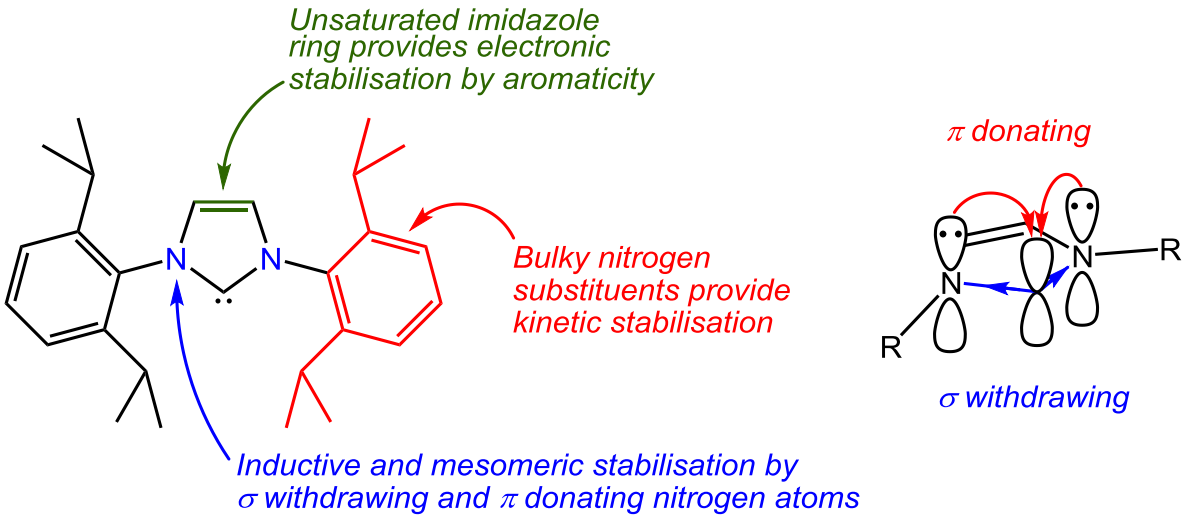

Figure 1.11: Structural and electronic features of an NHC.

NHCs are significantly nucleophilic due to their singlet ground state and partial p_π occupation. They behave as monodentate, two electron donor L type ligands, bonding to metals in a fashion analogous to tri-substituted phosphines allowing comparisons to be made about their

ligand properties.[106] Nolan and co-workers measured the ν_{CO} stretching frequencies (A_1 mode) of NHC complexes of Ni(0) carbonyls and compared the values with analogous phosphine complexes, demonstrating that NHCs were better σ donors.[107] It is also possible to determine the relative π acceptor properties of NHCs by measuring the ^{31}P NMR chemical shift of NHC–phenylphosphinidene adducts (NHC=P(Ph)). The chemical shifts of such adducts are considerably spread out and are very sensitive to more subtle changes in the electronic structure of NHCs.[108] The π accepting ability of NHCs is considerably poor due to π donation from the adjacent α substituents.[109] This effect is most pronounced in unsaturated aromatic imidazolylidenes.

As a result, NHCs are neutral two electron carbon based donor ligands which have highly tuneable steric and electronic properties that can be tailored for subsequent chemical applications. These neutral carbon based ligands compliment the range of previously employed neutral ligands (such as ethers, amines and phosphines) and anionic ligands (such as amides, alkoxides and aryl groups). It comes a no surprise that the popularity of NHCs has exploded over the last twenty years due to their ability to stabilise a range of low coordinate, low oxidation state main group (and transition metal) compounds.

1.3 The isolobal analogy

The principle of an isolobal relationship between two chemical moieties has been used by chemists as a method of understanding bonding in organometallic species by relating said moieties with known organic compounds with well understood frontier orbital arrangements. As described by Hoffmann in his Nobel lecture in 1981, two fragments can be considered to be isolobal if the number, symmetry properties, approximate energy and shape of frontier orbitals and the number of electrons in them are similar – not identical, but similar.[110] The

latter point is key in that this allows us to describe the frontier orbital arrangement of a simple organic moiety with that of a more complex metal fragment and predict the existence of a new complex bearing said metal fragment in place of the organic moiety. This is a simple model that can only be used for predicting isolobal complexes as the model makes no predictions about the thermodynamic or kinetic stability of a resulting complex. Originally a method used to describe bonding in transition metal complexes and clusters, the analogy has been extended to describe the relationship between various compounds of the main group elements. Isolobal complexes can be described as isoelectronic if the compounds share the same number of valence electrons and structure. In this respect, the boryl anion and an NHC are isoelectronic and they are both isolobal with the N-heterocyclic phosphenium ion $[P(NDipp)_2(CH)_2]^+$ (Figure 1.12).

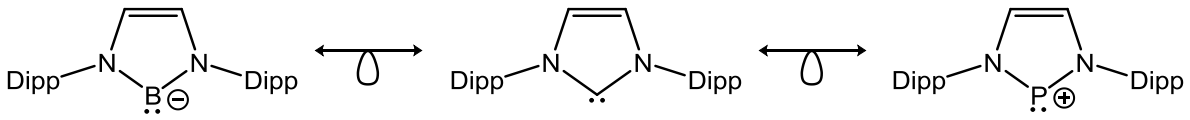

Figure 1.12: Illustration of the isolobal relationship between a boryl anion, NHC and a phosphenium cation.

Similarly, the monomeric indium(I) terphenyl complex can be considered isoelectronic with a carbonyl group (Figure 1.13). The indium species was shown to function as a ligand in coordination to the 16 electron $Mn(\eta^5\text{-}C_5H_5)(CO)_2$ fragment.[66] Also, the anionic terphenyl ligand itself is isoelectronic with a neutral 2,6-diaryl pyridine ligand and a thallium(I) complex of the ligand has been synthesised.[111] However, the experimentally observed Tl–N distance is significantly greater, and as a result of significant electrophilic character of the Tl^I cation, the complex is stabilised by numerous π interactions with the ligand aryl groups and two fluorobenzene solvent molecules.

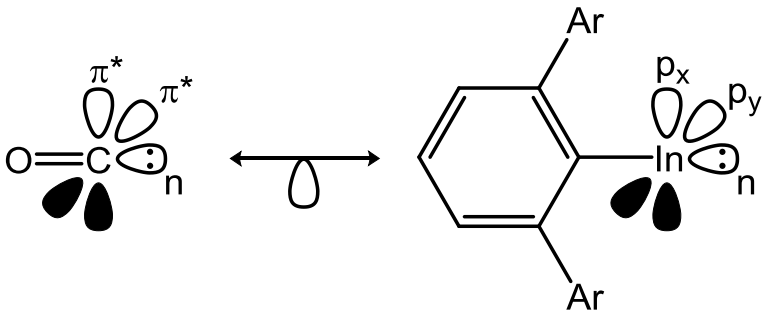

Figure 1.13: Example of an isolobal analogy, pictured here that between CO and R–In.

1.4 NHCs as stabilising ligands of main group multiple bonds

As already mentioned, NHCs are strong, two electron carbon based σ donors. Arguably the most common family of NHCs used in synthesis are those consisting of a five membered imidazole based core ring with an unsaturated backbone, i.e. imidazol-2-ylidenes. These neutral ligands (L type donor ligands) allow for the stabilisation of very low oxidation state complexes. Where X type ligands such as aryl groups formally contribute one electron to bonding, there is a requirement for the element involved in bonding to also contribute one electron in order to form a covalent bond thereby increasing the formal oxidation state of the element. NHCs provide two electrons for bonding, hence any theoretical replacement of an X type ligand with an NHC would afford a one electron reduction of the bonding element, assuming the overall charge remains the same. It is easy to see how NHCs are perfectly designed to access neutral complexes of the main group elements in low oxidation states.

Beginning only nine years ago in 2008, the Robinson group sought to access the diatomic allotropes of main group elements using NHCs as stabilising ligands.[112] The first diatomic allotrope to come to fruition was that of the NHC stabilised disilicon $LSi^0{=}Si^0L$ (Figure 1.14).[113] The formal oxidation state of zero, means this species can be viewed as essentially a source of elemental silicon. The NHC used, $:C(N(2,6\text{-}^{i}Pr_2C_6H_3))_2(CH)_2$, was a

Dipp substituted, unsaturated imidazol-2-ylidene commonly reffered to as IPr. The nomenclature used for NHCs that are based on an imidazole ring involves an 'I' (for imidazol-2-ylidene) followed by the abbreviation of the nitrogen bound substituent, in this case 'Dipp'. The NHC should be reffered to as IDipp however, for this very common NHC, IPr has been extensively used in the literature. Addition of IPr to $SiCl_4$ results in quantitative formation of the Lewis acid-base adduct $(IPr)SiCl_4$. This species contains a hypervalent silicon atom, however, in this complex the two axial chlorine ligands form a long three-centre, four-electron interaction which is a common description for hypervalent molecules ($Si–Cl_{ax}$ = 2.189(1) Å).[114] The two equatorial chlorine ligands form conventional two-centre, two-electron bonds to the silicon with a shorter bond length ($Si–Cl_{eq}$ = 2.070(1) Å). Reduction of this complex with four equivalents of potassium intercalated graphite (KC_8) in THF resulted in the formation IPr→Si=Si←IPr in 23% yield as dark red crystals.

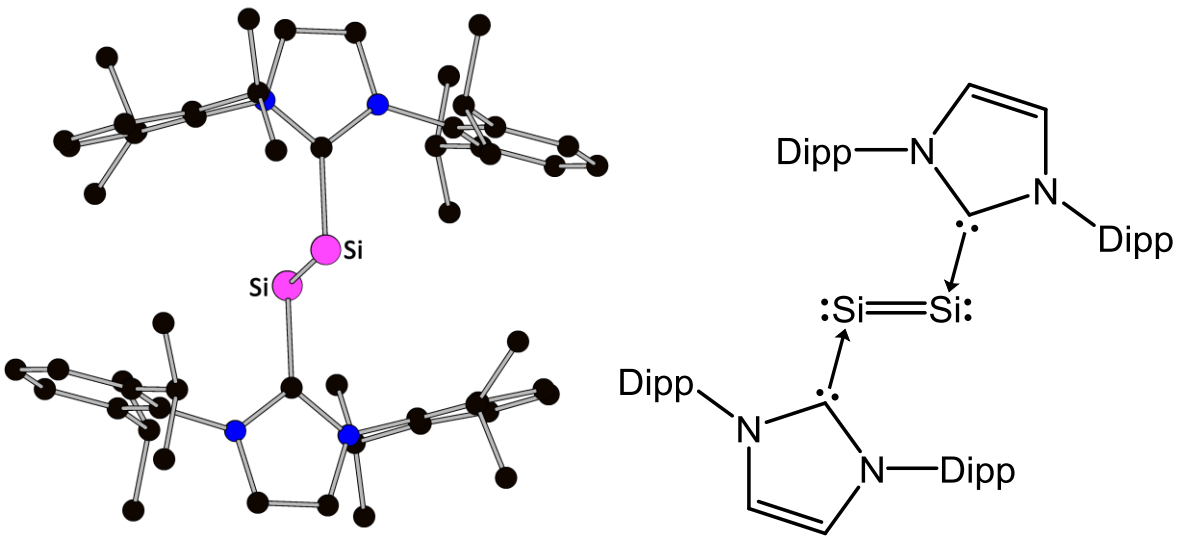

Figure 1.14: Ball and stick model (left) and Lewis structure (right) of $(IPr)_2Si_2$. Hydrogen atoms have been omitted for clarity.

The nature of bonding in NHC complexes has been the subject of fierce debate in recent years.[115,116] The neutral donor nature of bonding in NHCs has led to a common representation of the ligand as a Lewis base donor, utilising arrows to suggest electron donation in Lewis

structures, i.e. IPr→Si=Si←IPr.[117] This representation however can lead to misleading conclusions about the nature of the bonding in a compound. A theoretical study of various hypothetical NHC stabilised acetylenes (NHC→(C_2H_2)←NHC) were used as a case study to test how far the analogy of an NHC stabilised species can be pushed.[118] In this case, the highly electron donating groups in the hypothetical tetraaminobutadiene were calculated to be best described by two dative bonds from the NHC and a C_2H_2 fragment in a highly excited electronic state. An alternative is to represent such molecules with a resonance structure involving a formal covalent bond and the generation of zwitterionic species. Ultimately, a calculation of the contribution of each resonance structure will provide the most suitable representation of the bonding involved, and qualitatively, can be assumed on the basis of the strength of the NHC–E interaction. Whilst π backbonding is poor in NHC complexes, there may be significant contribution for certain elements. It is important to remember that there is no one correct Lewis representation and that bonding may be a hybrid of many contributing resonance structures (Figure 1.15).

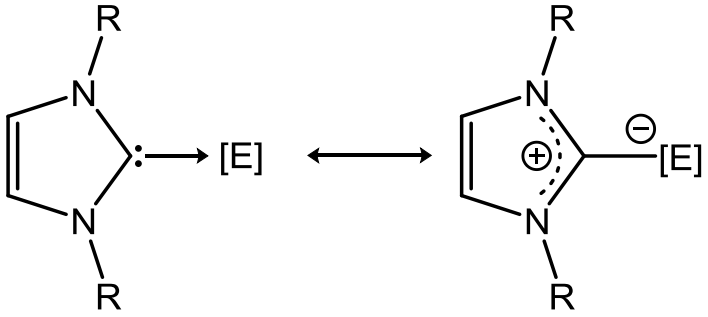

Figure 1.15: Two major contributing resonances structures describing the bonding of NHCs to a main group complex [E].

The isolation of a formally disilicon(0) species sparked interest in using IPr as a ligand for the synthesis of low oxidation state compounds of the main group elements. The Robinson group subsequently succeeded in accessing IPr stabilised diphosphorus and diarsenic using related synthetic methods in 57% and 19% yields starting from the IPr adducts of PCl_3 and $AsCl_3$,

respectively.[119,120] These moderate to low yields indicate the problems associated with the harsh conditions used for reduction and the uncontrolled mechanism by which multiple intermediate oxidation state species must come together to form the E–E bond. The IPr stabilised diphosphorus molecule was calculated so have moderate π backdonation and therefore, moderate P=C double bond character. The use of IPr as a ligand results in a formal P–P single bond despite the formal zero oxidation state of the phosphorus atoms.

Multiple other diatomic main group elements in the zero oxidation state stabilised by IPr have since been reported. IPr adducts of digermanium and ditin were synthesised by the Jones group by reduction of the IPr adduct of the element dihalide precursors with their novel Mg^{I} reducing agent (as discussed previously in Section 1.2.6).[121,122] Finally, and most notably, IPr stabilised tetrabromodiborane could be reduced with sodium napthalenide to afford the NHC stabilised B_2 which features a B≡B triple bond.[123] Donation of the IPr lone pair into the vacant sp hybridised boron orbital, resulting in the expected linear structure, affords the IPr–diboryne which is isolobal with an alkyne.

The Bertrand group have also extensively developed the chemistry of an alternative carbene with a single nitrogen substituent. Replacement of one of the nitrogen substituents of an NHC by a quaternary carbon centre reduces the amount of π electron donation into the empty p orbital of the carbene centre. This has the effect of both increasing the electrophilicity and nucleophilicity of such cyclic(alkyl)(amino)carbenes (CAACs).[124,125] The use of these species as ligands in main group chemistry has been extensively studied and provides a useful comparison for coordination when compared to similar imidazol-2-ylidene stabilised complexes. Numerous compounds of main group diatomics coordinated by CAAC ligands have been synthesised and show significantly greater backbonding to the ligand and cumulene character when compared to NHCs.[126–129]

1.5 Chemistry of NHC stabilised main group diatomics

Following the isolation of a family of IPr stabilised diatomic molecules of the main group elements, the possibility for further reactivity was subsequently explored. Remarkable work in the Bertrand group involved the chemical oxidation of the diphosphorus species. One and two electron oxidation reactions afforded the IPr stabilised radical cation and diamagnetic dication of P_2, specifically $[IPr–P–P–IPr]^{\bullet+}$ and $[IPr–P=P–IPr]^{2+}$ as the $[B(C_6F_5)_4]^-$ and $[CF_3SO_3]^-$ salts, respectively.[130] These species have formal bond order of one and a half and two, respectively, as electron density is removed from the phosphorus atoms and π bonding becomes possible between the two elements. The equivalent radical cation and dication of diarsenic were also subsequently synthesised and characterised by Robinson and co-workers.[131] Unexpectedly, the oxidation of IPr stabilised diarsenic was achieved by addition of gallium trichloride ($GaCl_3$) in appropriate stoichiometries. One equivalent affords the one electron oxidation whilst a second equivalent binds to the liberated chloride ion, hence both cations were isolated as $[GaCl_4]^-$ salts. This reaction demonstrates how electron rich these species are as gallium halides are not well known oxidising agents. Alternatively, the reduction of $(IPr)_2P_2$ was investigated by addition to lithium metal. Rather than the simple two electron reduced $[(IPr)_2P_2]^{2-}$, instead what was isolated was an IPr stabilised phosphinidene that had undergone a lithiation of the NHC backbone with the proton migrating to the phosphorus atom to afford a PH moiety (Scheme 1.7).[132]

In light of these results, the Robinson group have spearheaded investigations into the wide variety of chemistry that such species can undergo (in particular the IPr stabilised diphosphorus and disilicon compounds). Such reactions include those with BH_3 in a series of hydroboration reactions which result in the formation of a variety of silicon containing species

or the coordination of a bridging $[BH_2]^+$ cation (with a $[B_2H_7]^-$ counter anion) upon reaction with diphosphorus.[133,134]

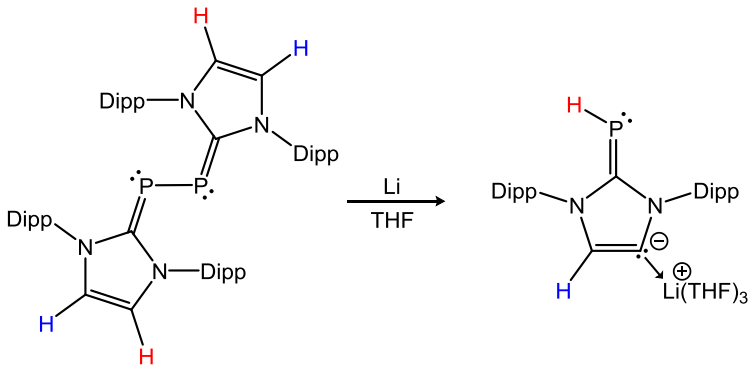

Scheme 1.7: Reduction of $(IPr)_2P_2$ with lithium metal to afford a carbene stabilised phosphinidene.

The addition of a proton source to such compounds has resulted in the isolation of protonated species that can be described as IPr stabilised $[HSi_2]^+$ or $[HP_2]^+$ (Scheme 1.8).[135,136] Simple complexation with alkali metals or copper chloride has also been investigated.[137] More interesting is the oxidation chemistry of such species with oxidants such as iodine or oxygen. Oxidation of $(IPr)_2Si_2$ with I_2 results in the formation of $(IPr)_2Si_2I_2$. Halide abstraction from this species affords the disilicon(I) cation $[(IPr)_2Si_2I]^+$ which is analogous to the product resulting from protonation of the parent compound.[138] The controlled addition of dry dioxygen allowed for the isolation of elusive silicon oxides stabilised by IPr.[139] SiO_2 is an abundant material that is known to form a strong network of single Si–O in contrast to CO_2.

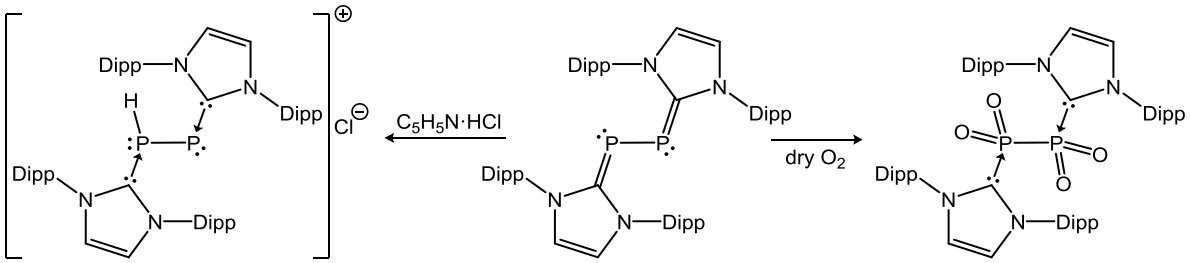

Scheme 1.8: Reactivity of the NHC stabilised diphosphorus $(IPr)_2P_2$ towards a proton source and dry O_2 gas.

The landmark discovery that IPr is capable of stabilising multiple silicon oxides, namely Si_2O_3 and Si_2O_4 illustrates the enormous potential of these ligands in synthesis. By the same method, diphosphorus tetroxide was synthesised and represents a pathway into studying the reactivity of these highly reactive phosphorus oxides (Scheme 1.8).[140]

1.6 Coordination chemistry of NHCs

NHCs now represent an indispensable ligand in many areas of chemistry.[141–150] They are widely used in the formation of transition metals complexes and a simple search of the Cambridge Structural Database reveals almost eight thousand crystallographically characterised NHC–transition metal complexes compared to approximately six hundred crystallographically characterised NHC complexes of the heavy group 13, 14 and 15 elements i.e. the 2nd to 5th row main group elements. Bonding in NHCs is dominated by the so-called "classical" coordination via the carbene (C2) position as expected. NHCs bonding in such a manner were documented for over thirty years prior to other coordination modes being discovered.

1.6.1 Abnormal or mesoionic NHCs (aNHCs or MICs)

1.6.1.1 Transition metal complexes bearing abnormal NHCs

The first documented example of a so-called "abnormal" (or mesoionic) NHC complex was reported by Crabtree and co-workers and was isolated from the reaction of 2-pyridylmethylimidazolium salts with the iridium polyhydride $IrH_5(PPh_3)_2$.[151,152] The term mesoionic describes that fact that a charge neutral Lewis structure cannot be drawn for this coordination mode. An abnormal NHC (aNHC) can be understood as a formal intramolecular migration of the imidazole backbone proton to the carbene carbon (Figure 1.16). Crabtree

observed that direct metallation of an imidazolium at either the C2 or C4 position was found to be a result of either steric factors, due to the nature of the R group associated with the imidazol-2-ylidene ring, or electronic factors associated with the counter-anion and the nature of the solvent.[153,154] The abnormal bonding mode was unambiguously confirmed by X-ray crystallography and the presence of a low field resonance in the ^{1}H NMR spectrum at 8.72 ppm corresponding to the acidic imidazolium proton. Considering the difference in the calculated acidities of the C2 and C4 bound protons in the imidazolium salt (pK_a = 24 and 33, respectively),[155] it is surprising that the in situ metallation can occur exclusively at the C4 position. The regioselectivity is being controlled by the steric bulk of the R group, hence when R = Mes, the sole isomer in the C4 metallated product, whereas when R = ^{n}Bu or ^{i}Pr, a mixture of the normal and abnormally bonded species are observed.

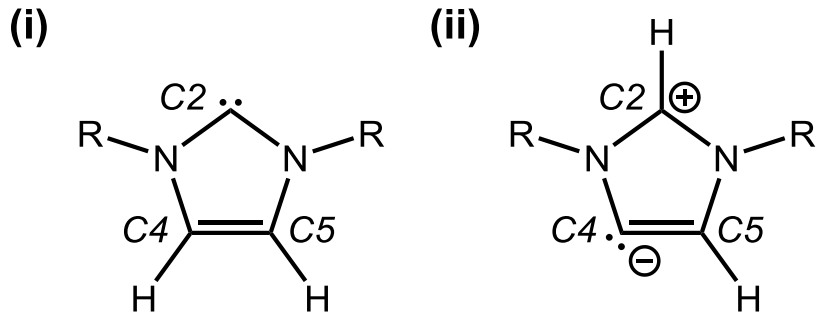

Figure 1.16: Bonding modes of (i) classical NHCs and (ii) abnormal NHCs.

Following this discovery, there has been a noticeable increase in the number of new complexes bearing C4-bonded NHCs. Several reviews highlighting the importance and prevalence of this bonding mode have since been published.[156–159] There are several reports of C4-bonded NHC complexes of palladium, which in all likelihood is due to the extensive studies carried out with catalytically active C2-bonded NHC palladium complexes.[160–162] However, there are many other novel complexes of aNHCs bonded to ruthenium, rhodium and iridium.

Along with metal mediated C–H activation, abnormal NHC complexes have also been accessed fortuitously by a free base induced isomerisation (such as in the addition of multiple equivalents of NHC). In an attempt to isolate the two-coordinate nickel complex. $[(IPr)Ni(NO)]^+$, the three coordinate $[(IPr)(aIPr)Ni(NO)]^+$ was actually isolated. In the presence of uncoordinated NHC (or two equivalents for an improved yield), the NHC acts as a base to deprotonate the coordinated ligand. Isomerisation of the NHC to generate the abnormal complex is often favoured due to steric relief from the two very bulky α Dipp substituents.[163] The isomerised ligand proceeds to deprotonate the in situ generated imidazolium salt thereby regenerating IPr which then proceeds to coordinate the electrophilic nickel centre. Alternatively, a normal to abnormal rearrangement was found to occur upon refluxing a toluene solution of the three-coordinate iron(II) or cobalt(II) complexes $(IPr)M(N(SiMe_3)_2)_2$ (M = Fe, Co).[164,165] This reaction is assumed to go via cleavage of the M–C bond which generates some free IPr in solution. The free IPr is then capable of acting as a base thereby facilitating isomerisation of the IPr under the forcing reflux conditions. This reaction demonstrates that abnormal bonding in NHC complexes may be thermodynamically controlled. The formation of a stronger σ M–C bond is indicated by the reduction in bond length (cf. 2.182(2) and 2.117(2) Å for the Fe–NHC and aNHC complex, respectively).

1.6.1.2 Main group complexes bearing abnormal NHCs

The isomerisation of NHCs coordinated to main group complexes has also been studied experimentally. Parallel arguments for the formation of such compounds apply. They are accessed from either the specific addition of excess NHC (either catalytic or stoichiometric excess), or in refluxing solvents in order to break the Lewis acid–base bond between the NHC ligand and the main group moiety. Examples which demonstrate the normal to abnormal

isomerisation of NHCs include trimethyl group 13 complexes, i.e. I^{t}Bu→EMe$_3$ where E = Al, Ga and In, (IPr)Sn(OTf)$_2$ (Scheme 1.9) and [(IPr)PCl$_2$][OTf].[166–169]

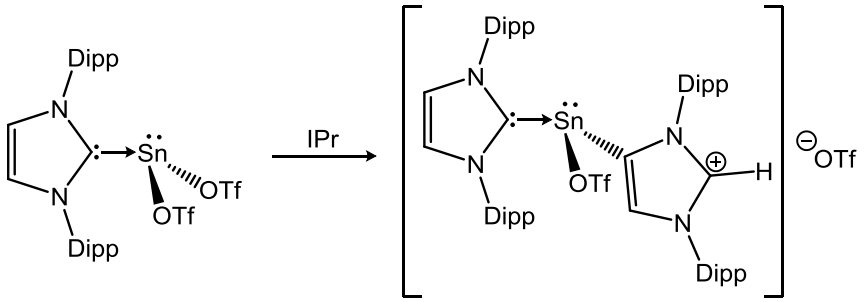

Scheme 1.9: Isomerisation of IPr in (IPr)Sn(OTf)$_2$ induced by the stoichiometric addition of IPr.

The asymmetric [(IPr)(aIPr)PCl$_2$]$^+$ cation could be isolated as the triflate salt in 96% yield upon addition of IPr to [(IPr)PCl$_2$][OTf] (which was obtained by the addition of PCl$_3$ to IPr and Me$_3$SiOTf in fluorobenzene). Impressively, a two electron reduction afforded the phosphanide [(IPr)(aIPr)P]$^+$ which contains a two-coordinate phosphorus(I) centre with two lone pairs which were shown to be available for coordination by the addition of two equivalents of AuCl (Scheme 1.10).[168]

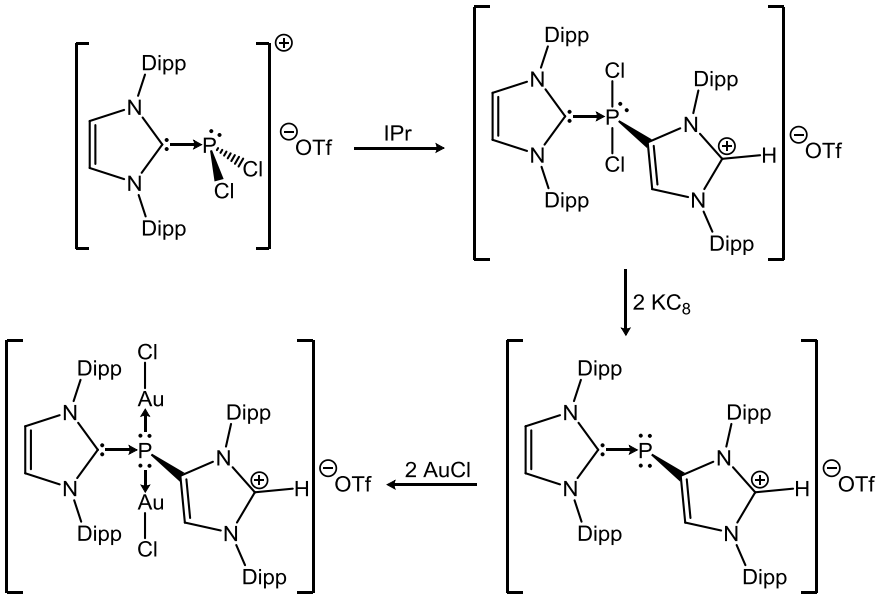

Scheme 1.10: Synthesis of a phosphanide by the isomerisation of an IPr ligand followed by chemical reduction with KC$_8$.

These results highlight the conditions whereby such isomerisation reactions take place. They all occur upon coordination of an NHC ligand to highly Lewis acidic species ($AlMe_3$, $Sn(OTf)_2$ and PCl_2^+). The effect of these main group moieties when bonded to the C2 position of an NHC is to inductively withdraw electron density from the imidazole ring, thus increasing the acidity of the backbone imidazole proton. Evidence for this kind of reactivity was demonstrated by Arduengo and co-workers in 1997 prior to the discovery of transition metal aNHC complexes. Addition of CCl_4 to a THF solution of IMes (1,3-bis(2,4,6-trimethylphenyl)-imidazol-2-ylidene) yields 1,3-bis(2,4,6-trimethylphenyl)-4,5-dichloroimidazol-2-ylidene.[170] The reaction proceeds by in situ generation of a trichloromethyl anion which is basic enough to deprotonate the chlorinated imidazolium cation (Scheme 1.11). The resulting mesoionic 1,3-bis(mesityl)-2-chloro-imidazol-4-ylidene reacts with additional CCl_4 to chlorinate the C4 position. This process is then repeated to give the dichlorinated product. The greater stability afforded over IMes is apparent since IMes is too strong a base to tolerate acidic solvents such as chloroform.

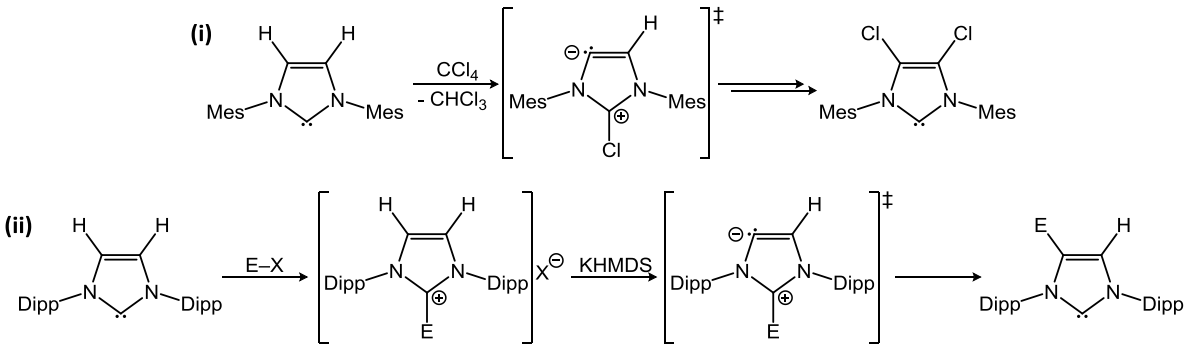

Scheme 1.11: (i) Chlorination of IMes by CCl_4 and (ii) the subsequent generalised C4 functionalisation of IPr using E–X followed by KHMDS as a base.

Subsequently, the scope of this reactivity was exploited by Bertrand and co-workers who demonstrated that addition of IPr to various electrophilic reagents (E–X where E = PhC(O), PPh_2; X = Cl; and E = CF_3SO_2, Me_3Si; X = CF_3SO_3) generated the imidazolium adducts.[171]

Addition of potassium bis(trimethylsilyl)amide (KHMDS) led to the deprotonation of the imidazolium cation to generate an "abnormal" carbene as an intermediate, however intramolecular rearrangement yielded the C4-functionalised NHC (Scheme 1.11).

The first isolable "abnormal" carbene was synthesised by Bertrand and co-workers in 2009 by utilizing an imidazolium salt with a non-labile phenyl group blocking the C2 position.[172] Deprotonation using two equivalents of KHMDS led to the formation of the free aNHC, which could be isolated as a green powder and was stable in solution and as a solid for several days under an inert atmosphere. The quantitative exchange of IPr for the stable abnormal NHC during the reaction with IPr→$SiCl_2$ is indicative of the greater σ donor strength of the abnormal NHC. Furthermore, stable adducts with $GeCl_2$ and $SnCl_2$ were also synthesised (Scheme 1.12).[173,174]

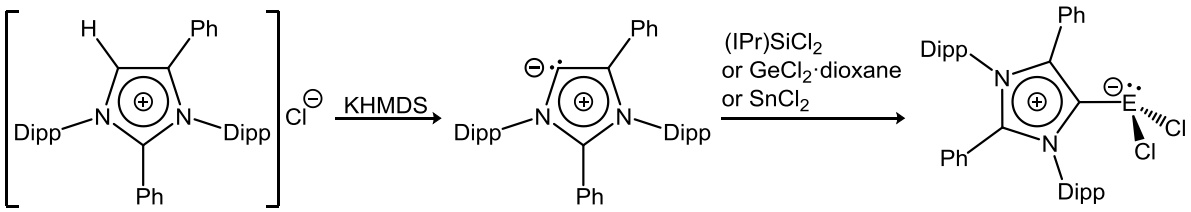

Scheme 1.12: Synthesis of the first free abnormal NHC and the subsequent coordination to group 14 dichlorides.

1.6.2 Ditopic carbanionic NHCs

Ditopic carbanionic NHCs are the result of a formal deprotonation of a neutral NHC to give an anionic ligand capable of bonding through the "classical" C2 and "abnormal" C4 carbene centres simultaneously, hence this has also led to the description of these species as anionic "dicarbenes" (NHDCs) however the use of aNHC: (Scheme 1.13) better represents the bonding of such ligands. To date, such species are limited to NHCs with unsaturated alkenic backbones. The synthesis of such ligands can be separated into three methods, namely via

metal-mediated C–H activation, chemical reduction and direct deprotonation. The capability of ditopic carbanionic NHCs to bridge two metal centres through different carbon atoms of the imidazole ring closely resembles the bonding mode of neutral 1,2,4-triazole-3,5-diylidenes.[175,176] This type of NHC allows for bonding to the C4 carbene centre (which has significant vinylic character), a bonding mode closely related to that observed for transition metal complexes of abnormally bonded carbenes.

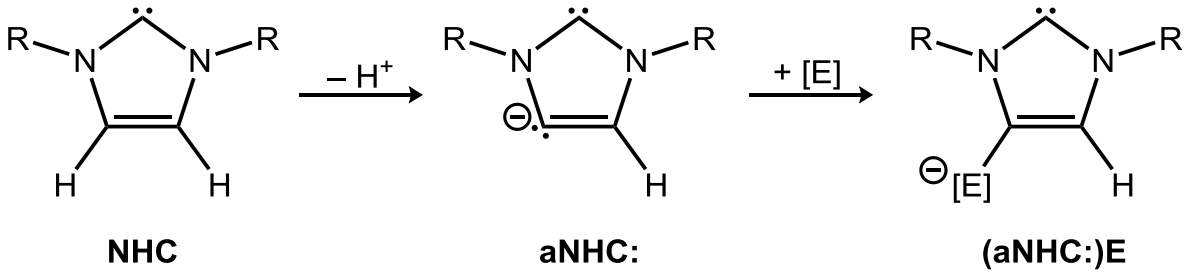

Scheme 1.13: Nomenclature used for ditopic carbanionic N-heterocyclic carbenes.

A comprehensive review of the chemistry of known ditopic carbanionic NHCs was published in 2015.[177] There are limited examples of metal-mediated activation routes to ditopic carbanionic NHC complexes, however the first example of an NHC bonded to two transition metals through the C2 and C4 positions simultaneously was obtained by such a method by Meyer and co-workers.[178] Reaction of an N-pyridazine functionalised imidazolium salt with dimeric allyl palladium chloride produces the mononuclear palladium complex which on standing, dimerises and is accompanied by an imidazole C–H bond activation with loss of propene to afford the dinuclear, ditopic carbanionic NHC complex. Similar palladium complexes were synthesised by Albrecht and co-workers by the C4–I bond activation by palladium(0) species.[179]

1.6.2.1 Chemical reduction

Addition of electropositive alkali metals to NHC complexes of the elements has been shown to afford a reduced NHC complex in the form of ditopic carbanionic NHCs. In an attempt to chemically reduce NHC complexes of the f-elements, Arnold and Liddle discovered that with formal loss of dihydrogen, the reduction of an amido tethered NHC complex of yttrium or samarium with potassium napthalenide afforded a ditopic carbanionic NHC with yttrium or samarium bonded to the C4 carbon and the C2 carbene coordinated to a potassium ion.[180] Investigations into the reduction of the uncoordinated NHC ligand allowed for the characterisation of the radical anion demonstrating the electron resides in the π-system of the NHC upon reduction.

Chemical reduction of transition metal complexes has been actively studied by the Goicoechea group. Reduction of a variety of bis(mesityl) transition metal and group 12 complexes with IPr allows for the isolation of complexes bearing two aIPr: ligands, both bonded to the metal centre through the anionic C4 position.[181–183] Reduction of (IPr)M(Mes)$_2$ (M = Mn, Fe, Zn, Cd) with KC_8 afforded a mixture of [(aIPr:)$_2$M(Mes)]$^-$ and [M(Mes)$_3$]$^-$ (and formally H_2) as potassium salts which could be purified by fractional crystallisation (Scheme 1.14). The nomenclature for ditopic carbanionic NHC ligands that I have used here will continue to be used throughout this thesis where aIPr: represents a C4 bonded IPr ligand with a deprotonated C2 position available for bonding and represented with a lone pair (note that aIPr referrers to the abnormal isomer of the C2 coordinated IPr). The presence of an available carbenic position in the ligand was demonstrated by the reaction of the complexes with various Lewis acids such as BH_3, $AlMe_3$ and CO_2; the bonding interaction remains very similar to that of the adduct formed by the free NHC with the aforementioned Lewis acids.[184–186]

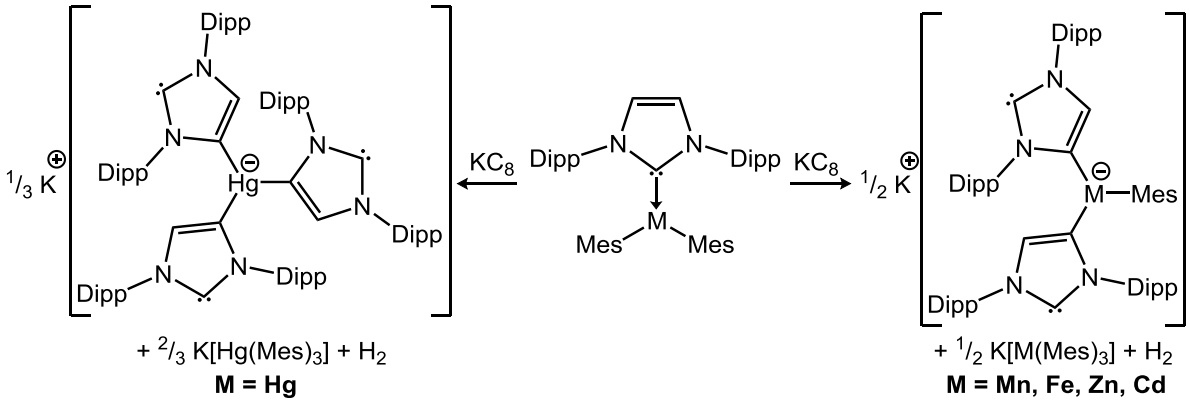

Scheme 1.14: Reduction of IPr–transition metal and group 12 bis(mesityl) complexes that afford complexes bearing aIPr: ligands.

Interestingly, IPr does not form a complex with $Hg(Mes)_2$ as evidenced by DOSY NMR spectroscopy and that upon reduction of a stoichiometric mixture of the two with KC_8, a mercury complex bearing three aIPr: ligands in a trigonal planar arrangement about the Hg^{II} metal centre could be isolated (Scheme 1.14).

1.6.2.2 Deprotonation

The most common method for the synthesis of aNHC: ligands, and arguably the simplest synthetic route, is the direct deprotonation of the free NHC. It was not until 2010 that Robinson and co-workers demonstrated that ^{n}BuLi could be used to deprotonate IPr in hexane to yield the anionic deprotonated NHC $[:C(N(2,6\text{-}^{i}Pr_2C_6H_3))_2(CH)CLi]_\infty$ ($[Li(aIPr:)]_\infty$) in near quantitative yield as an amorphous solid.[187] $[Li(aIPr:)]_\infty$ provides a useful starting material for the potential synthesis of novel complexes bearing (aIPr:) as a ligand. The polymeric solid readily dissolves in THF or TMEDA and could be used for the synthesis of a variety of triorganozincates upon addition of $ZnEt_2$.[188]

Understanding the chemistry of NHCs in highly reductive media is important for the rational synthesis of polar organometallic reagents. Very recently, Hevia and co-workers have developed a range of methods for the synthesis of aNHC: ligands coordinated to a variety of

metals such as magnesium, iron, zinc and gallium. This work has provided insights into the chemical reactivity of NHCs under reductive reaction conditions with some surprising results. Addition of IPr to a hexane solution of GaR_3 (R = CH_2SiMe_3) affords colourless crystals of the adduct (IPr)GaR_3 in 75% yield.[189] Remarkably, addition of the polar organometallic reagent $LiCH_2SiMe_3$ does not result in the lithiation of the NHC backbone to afford an aNHC:, as is the case when (IPr)BH_3 is treated with ^{n}BuLi.[190] Instead, co-complexation of the lithium reagent and the formation of the NHC stabilised lithium gallate (IPr)Li(μ-CH_2SiMe_3)$_2$Ga(CH_2SiMe_3)$_2$ is observed. A similar reactivity was reported for (IPr)Zn^{t}Bu$_2$ with ^{t}BuLi in hexane.[191] C4 gallation was achieved by direct deprotonation with MR (M = Li, Na, K; R = CH_2SiMe_3) followed by the addition of GaR_3; the ditopic carbanionic NHC complex [(aIPr:)GaR_3]$^-$ could be crystallised coordinated to a THF solvated alkali metal cation through the C2 position (Scheme 1.15).[189,192]

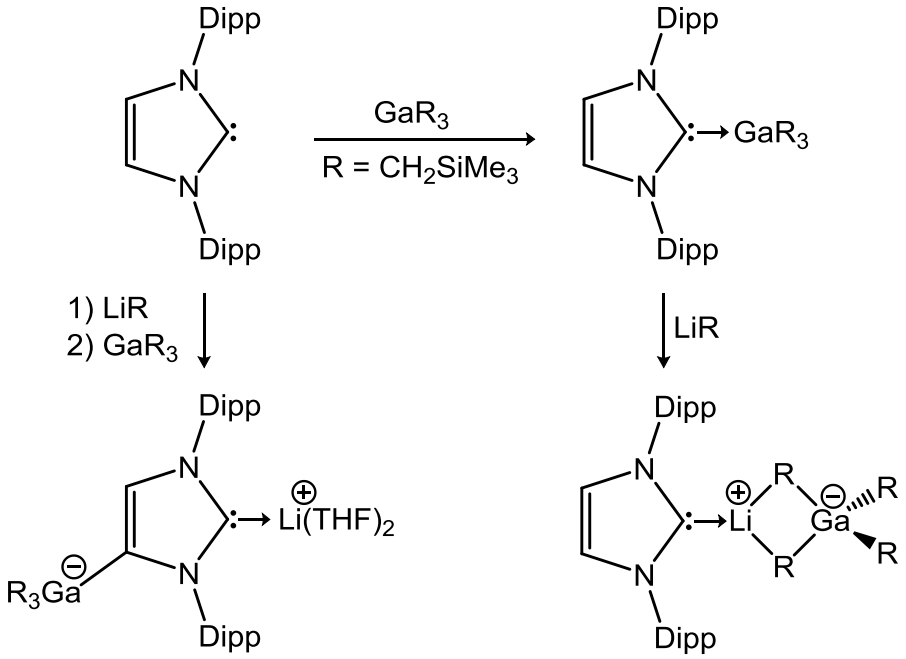

Scheme 1.15: Synthesis of a heteroleptic gallate and a homoleptic tetraalkyl gallate.

A similar reaction profile was observed for the IPr complex with Fe(HMDS)$_2$ when combined with organosodium bases.[193] Finally, Mulvey and co-workers investigated the direct

magnesiation of IPr by the inverse-crown complex $[KMg(TMP)_2(^nBu)]_6$ in a mixture of THF and methylcyclohexane. This affords the magnesiate $[(aIPr:)_2Mg(^nBu)(THF)]^-$ as the potassium salt.[194] Likewise, $[(aIPr:)_3Mg(THF)]^-$ could be isolated as the sodium salt upon reaction of IPr with a stoichiometric amount of $[(TMEDA)NaMg(TMP)_2(^nBu)]$ in hexane. The complex crystallises with the magnesium centre in a highly distorted tetrahedral geometry due to the three bulky aIPr: ligands adopting a pseudo-trigonal planar geometry. Perhaps even more unexpected, was the result of reacting IPr with the pre-inverse-crown $[Na_4Mg_2(TMP)_6(^nBu)_2]$ in a hydrocarbon solvent. The bimetallic complex is capable of deprotonation of the C4 imidazole proton accompanied by a directed magnesiation of the *para* position of the Dipp substituent resulting in an inverse-crown complex.

The further reactivity of these C4 functionalised NHCs was demonstrated by the addition of various electrophiles. Group 13 functionalised aNHC: species proceeded to react with Me_3SiCl, MeOTf or $(Ph_3P)AuCl$ with retention of the group 13 species bonded to the C4 carbon of the imidazole.[192,195,196] In contrast, reaction of the zincate species $[(aIPr:)Zn^tBu_2]^-$ with two equivalents of $(Ph_3P)AuCl$ afforded the dinuclear gold complex $(Ph_3P)Au(aIPr{\cdot}AuCl)$ as a result of the increased polarity of the Zn–C bond relative to the of B–C or Ga–C bond.[191]

1.7 Project aims

At the time of starting this DPhil research, the chemistry of ditopic carbanionic NHCs was a new and growing field. Building on the work carried out during my Part II project which involved the reduction of IPr complexes of group 12 metals, Chapter 2 will discuss the investigation of lithium and potassium salts of deprotonated IPr as reagents for the synthesis of novel complexes of the group 12 and 14 metals. Chapter 3 will discuss the development of

this chemistry with a focus on the reactivity of the alkali metal salt of aIPr: with a variety of group 12 and 14 halide precursors for the development of novel Lewis acidic group 14 complexes bearing a ligand with an unquenched NHC functional group. This chapter will also include an examination of the chemistry of IPr complexes of the group 14 element halides under reflux conditions to afford aIPr and aIPr: complexes via an alternative synthetic route. The reactivity of IPr with the group 15 bromides and the stability of these complexes on heating was subsequently studied and these results will be discussed in Chapter 4. This chapter will also describe the synthesis of the cationic species formed upon bromide abstraction from the various IPr and aIPr complexes. The unique redox chemistry that was observed to take place on heating a solution of (IPr)PBr_3 and the subsequent reduction chemistry as a novel route into low oxidation state IPr stabilised diphosphorus compounds will be discussed in Chapter 5. Finally, Chapter 6 will detail some of the preliminary investigations into the use of IPr as a supporting ligand for the synthesis of highly Lewis acidic species that may provide useful precursors to novel low oxidation state compounds of various p-block elements by systematic reduction with the use of mild reducing agents. Chapter 7 provides all experimental data for the compounds reported in this thesis along with details of the synthetic methods and characterisation techniques.

1.8 References

(1) Strathern, P. *Mendeleyev's Dream: The Quest for the Elements*; Berkley Publishing Group: New York, 2000.

(2) Earnshaw, N. N.; Greenwood, A. *Chemistry of the Elements (Second Edition)*; Butterworth-Heinemann: Oxford, 1997.

(3) Mokkapati, S.; Jagadish, C. *Materials Today* **2009**, *12* (4), 22–32.

(4) del Alamo, J. A. *Nature* **2011**, *479* (7373), 317–323.

(5) *Inorganic Syntheses, http://www.inorgsynth.com/*, DOI: 10.1002/SERIES2146.

(6) Drago, R. S. *J. Phys. Chem.* **1958**, *62* (3), 353–357.

(7) Urry, G.; Wartik, T.; Moore, R. E.; Schlesinger, H. I. *J. Am. Chem. Soc.* **1954**, *76* (21), 5293–5298.

(8) Hewitt, J. T.; Winmill, T. F. *J. Chem. Soc., Trans.* **1907**, *91*, 962–964.

(9) Benard, D. J.; Winker, B. K.; Seder, T. A.; Cohn, R. H. *J. Phys. Chem.* **1989**, *93* (12), 4790–4796.

(10) Heidner, R. F.; Helvajian, H.; Holloway, J. S.; Koffend, J. B. *J. Phys. Chem.* **1989**, *93* (23), 7813–7818.

(11) Schnering, H. G. v.; Benda, H. v.; Kalveram, C. *Z. Anorg. Allg. Chem.* **1978**, *438* (1), 37–52.

(12) Dohmeier, C.; Loos, D.; Schnöckel, H. *Angew. Chem. Int. Ed. Engl.* **1996**, *35* (2), 129–149.

(13) Urry, G.; Wartik, T.; Schlesinger, H. I. *J. Am. Chem. Soc.* **1952**, *74* (22), 5809–5809.

(14) Atoji, M.; Lipscomb, W. N. *Acta Cryst.* **1953**, *6* (6), 547–550.

(15) Jacobson, R. A.; Lipscomb, W. N. *J. Am. Chem. Soc.* **1958**, *80* (20), 5571–5572.

(16) Schnöckel, H.; Köhnlein, H. *Polyhedron* **2002**, *21* (5–6), 489–501.

(17) Tacke, M.; Schnöckel, H. *Inorg. Chem.* **1989**, *28* (14), 2895–2896.

(18) Mocker, M.; Robl, C.; Schnöckel, H. *Angew. Chem. Int. Ed. Engl.* **1994**, *33* (17), 1754–1755.

(19) Green, M. L. H.; Mountford, P.; Smout, G. J.; Speel, S. R. *Polyhedron* **1990**, *9* (22), 2763–2765.

(20) Widdifield, C. M.; Jurca, T.; Richeson, D. S.; Bryce, D. L. *Polyhedron* **2012**, *35* (1), 96–100.

(21) Joannis, A. C. *C. R. Hebd. Seances Acad. Sci.* **1891**, *113*, 795.

(22) Fässler, T. F. *Structure and Bonding*; Springer: Berlin - Heidelberg, 2011, pp. 91–131.

(23) Scharfe, S.; Kraus, F.; Stegmaier, S.; Schier, A.; Fässler, T. F. *Angew. Chem. Int. Ed.* **2011**, *50* (16), 3630–3670.

(24) Zhou, B.; Denning, M. S.; Kays, D. L.; Goicoechea, J. M. *J. Am. Chem. Soc.* **2009**, *131* (8), 2802–2803.

(25) Knapp, C. M.; Large, J. S.; Rees, N. H.; Goicoechea, J. M. *Chem. Commun.* **2011**, *47* (14), 4111–4113.

(26) Espinoza-Quintero, G.; Duckworth, J. C. A.; Myers, W. K.; McGrady, J. E.; Goicoechea, J. M. *J. Am. Chem. Soc.* **2014**, *136* (4), 1210–1213.

(27) Lips, F.; Clérac, R.; Dehnen, S. *J. Am. Chem. Soc.* **2011**, *133* (36), 14168–14171.

(28) Li, F.; Sevov, S. C. *J. Am. Chem. Soc.* **2014**, *136* (34), 12056–12063.

(29) Turbervill, R. S. P.; Goicoechea, J. M. *Chem. Rev.* **2014**, *114* (21), 10807–10828.

(30) Xu, L.; Bobev, S.; El-Bahraoui, J.; Sevov, S. C. *J. Am. Chem. Soc.* **2000**, *122* (8), 1838–1839.

(31) Kraus, F.; Hanauer, T.; Korber, N. *Inorg. Chem.* **2006**, *45* (3), 1117–1123.

(32) Benda, C. B.; Fässler, T. F. *Z. Anorg. Allg. Chem.* **2014**, *640* (1), 40–45.

(33) Pitzer, K. S. *J. Am. Chem. Soc.* **1948**, *70* (6), 2140–2145.

(34) Jutzi, P. *Angew. Chem. Int. Ed. Engl.* **1975**, *14* (4), 232–245.

(35) Simon, A.; Borrmann, H.; Craubner, H. *Phosphorus and Sulfur* **1987**, *30* (1–2), 507–510.

(36) Thurn, H.; Krebs, H. *Acta Cryst. B* **1969**, *25* (1), 125–135.

(37) Hultgren, R.; Gingrich, N. S.; Warren, B. E. *J. Chem. Phys.* **1935**, *3* (6), 351–355.

(38) West, R.; Fink, M. J.; Michl, J. *Science* **1981**, *214* (4527), 1343–1344.

(39) Yoshifuji, M.; Shima, I.; Inamoto, N.; Hirotsu, K.; Higuchi, T. *J. Am. Chem. Soc.* **1981**, *103* (15), 4587–4589.

(40) Becker, G.; Gresser, G.; Uhl, W. *Z. Naturforsch. B* **1981**, *36 b*, 16–19.

(41) Power, P. P. *Chem. Rev.* **1999**, *99* (12), 3463–3504.

(42) Fischer, R. C.; Power, P. P. *Chem. Rev.* **2010**, *110* (7), 3877–3923.

(43) Parkin, G. *J. Chem. Educ.* **2006**, *83* (5), 791.

(44) Green, M. L. H. *J. Organomet. Chem.* **1995**, *500* (1–2), 127–148.

(45) Power, P. P. *Chem. Rev.* **2003**, *103* (3), 789–810.

(46) Olmstead, M. M.; Power, P. P. *J. Am. Chem. Soc.* **1986**, *108* (14), 4235–4236.

(47) Pan, X.; Chen, X.; Li, T.; Li, Y.; Wang, X. *J. Am. Chem. Soc.* **2013**, *135* (9), 3414–3417.

(48) Grigsby, W. J.; Power, P. *Chem. Eur. J.* **1997**, *3* (3), 368–375.

(49) Pan, X.; Su, Y.; Chen, X.; Zhao, Y.; Li, Y.; Zuo, J.; Wang, X. *J. Am. Chem. Soc.* **2013**, *135* (15), 5561–5564.

(50) Sekiguchi, A.; Fukawa, T.; Nakamoto, M.; Lee, V. Y.; Ichinohe, M. *J. Am. Chem. Soc.* **2002**, *124* (33), 9865–9869.

(51) Sekiguchi, A.; Fukawa, T.; Lee, V. Y.; Nakamoto, M. *J. Am. Chem. Soc.* **2003**, *125* (31), 9250–9251.

(52) Becker, M.; Förster, C.; Franzen, C.; Hartrath, J.; Kirsten, E.; Knuth, J.; Klinkhammer, K. W.; Sharma, A.; Hinderberger, D. *Inorg. Chem.* **2008**, *47* (21), 9965–9978.

(53) Drost, C.; Griebel, J.; Kirmse, R.; Lönnecke, P.; Reinhold, J. *Angew. Chem. Int. Ed.* **2009**, *48* (11), 1962–1965.

(54) Segawa, Y.; Yamashita, M.; Nozaki, K. *Science* **2006**, *314* (5796), 113–115.

(55) Segawa, Y.; Suzuki, Y.; Yamashita, M.; Nozaki, K. *J. Am. Chem. Soc.* **2008**, *130* (47), 16069–16079.

(56) Schmidt, E. S.; Jockisch, A.; Schmidbaur, H. *J. Am. Chem. Soc.* **1999**, *121* (41), 9758–9759.

(57) Denk, M.; Lennon, R.; Hayashi, R.; West, R.; Belyakov, A. V.; Verne, H. P.; Haaland, A.; Wagner, M.; Metzler, N. *J. Am. Chem. Soc.* **1994**, *116* (6), 2691–2692.

(58) Herrmann, W. A.; Denk, M.; Behm, J.; Scherer, W.; Klingan, F.-R.; Bock, H.; Solouki, B.; Wagner, M. *Angew. Chem. Int. Ed. Engl.* **1992**, *31* (11), 1485–1488.

(59) Gans-Eichler, T.; Gudat, D.; Nieger, M. *Angew. Chem. Int. Ed.* **2002**, *41* (11), 1888–1891.

(60) Protchenko, A. V.; Birjkumar, K. H.; Dange, D.; Schwarz, A. D.; Vidovic, D.; Jones, C.; Kaltsoyannis, N.; Mountford, P.; Aldridge, S. *J. Am. Chem. Soc.* **2012**, *134* (15), 6500–6503.

(61) Protchenko, A. V.; Blake, M. P.; Schwarz, A. D.; Jones, C.; Mountford, P.; Aldridge, S. *Organometallics* **2015**, *34* (11), 2126–2129.

(62) Dange, D.; Davey, A.; Abdalla, J. A. B.; Aldridge, S.; Jones, C. *Chem. Commun.* **2015**, *51* (33), 7128–7131.

(63) Protchenko, A. V.; Dange, D.; Harmer, J. R.; Tang, C. Y.; Schwarz, A. D.; Kelly, M. J.; Phillips, N.; Tirfoin, R.; Birjkumar, K. H.; Jones, C.; Kaltsoyannis, N.; Mountford, P.; Aldridge, S. *Nat. Chem.* **2014**, *6* (4), 315–319.

(64) Hinz, A.; Schulz, A.; Villinger, A. *Angew. Chem. Int. Ed.* **2015**, *54* (2), 668–672.

(65) Kays, D. L. *Organomet. Chem.* **2010**, *36*, 56–76.

(66) Haubrich, S. T.; Power, P. P. *J. Am. Chem. Soc.* **1998**, *120* (9), 2202–2203.

(67) Niemeyer, M.; Power, P. P. *Angew. Chem. Int. Ed.* **1998**, *37* (9), 1277–1279.

(68) Zhu, Z.; Fischer, R. C.; Ellis, B. D.; Rivard, E.; Merrill, W. A.; Olmstead, M. M.; Power, P. P.; Guo, J. D.; Nagase, S.; Pu, L. *Chem. Eur. J.* **2009**, *15* (21), 5263–5272.

(69) Davidson, P. J.; Harris, D. H.; Lappert, M. F. *J. Chem. Soc., Dalton Trans.* **1976**, 2268–2274.

(70) Cotton, J. D.; Davidson, P. J.; Lappert, M. F. *J. Chem. Soc., Dalton Trans.* **1976**, 2275–2286.

(71) Gynane, M. J. S.; Harris, D. H.; Lappert, M. F.; Power, P. P.; Rivière, P.; Rivière-Baudet, M. *J. Chem. Soc., Dalton Trans.* **1977**, 2004–2009.

(72) Hitchcock, P. B.; Lappert, M. F.; Miles, S. J.; Thorne, A. J. *J. Chem. Soc., Chem. Commun.* **1984**, 480–482.

(73) Goldberg, D. E.; Hitchcock, P. B.; Lappert, M. F.; Thomas, K. M.; Thorne, A. J.; Fjeldberg, T.; Haaland, A.; Schilling, B. E. R. *J. Chem. Soc., Dalton Trans.* **1986**, 2387–2394.

(74) Kira, M. *Organometallics* **2011**, *30* (16), 4459–4465.

(75) Power, P. P. *Organometallics* **2007**, *26* (18), 4362–4372.

(76) Stender, M.; Phillips, A. D.; Wright, R. J.; Power, P. P. *Angew. Chem. Int. Ed.* **2002**, *41* (10), 1785–1787.

(77) Phillips, A. D.; Wright, R. J.; Olmstead, M. M.; Power, P. P. *J. Am. Chem. Soc.* **2002**, *124* (21), 5930–5931.

(78) Pu, L.; Twamley, B.; Power, P. P. *J. Am. Chem. Soc.* **2000**, *122* (14), 3524–3525.

(79) Sekiguchi, A.; Kinjo, R.; Ichinohe, M. *Science* **2004**, *305* (5691), 1755–1757.

(80) Li, J.; Schenk, C.; Goedecke, C.; Frenking, G.; Jones, C. *J. Am. Chem. Soc.* **2011**, *133* (46), 18622–18625.

(81) Pearson, R. G. *J. Am. Chem. Soc.* **1988**, *110* (7), 2092–2097.

(82) Power, P. P. *Nature* **2010**, *463* (7278), 171–177.

(83) Peng, Y.; Ellis, B. D.; Wang, X.; Fettinger, J. C.; Power, P. P. *Science* **2009**, *325* (5948), 1668–1670.

(84) Rit, A.; Campos, J.; Niu, H.; Aldridge, S. *Nat. Chem.* **2016**, *8* (11), 1022–1026.

(85) Pu, L.; Phillips, A. D.; Richards, A. F.; Stender, M.; Simons, R. S.; Olmstead, M. M.; Power, P. P. *J. Am. Chem. Soc.* **2003**, *125* (38), 11626–11636.

(86) Nagase, S.; Kobayashi, K.; Takagi, N. *J. Organomet. Chem.* **2000**, *611* (1–2), 264–271.

(87) Cowley, A. H.; Lasch, J. G.; Norman, N. C.; Pakulski, M. *J. Am. Chem. Soc.* **1983**, *105* (16), 5506–5507.

(88) Tokitoh, N.; Arai, Y.; Sasamori, T.; Okazaki, R.; Nagase, S.; Uekusa, H.; Ohashi, Y. *J. Am. Chem. Soc.* **1998**, *120* (2), 433–434.

(89) Tokitoh, N.; Arai, Y.; Okazaki, R.; Nagase, S. *Science* **1997**, *277* (5322), 78–80.

(90) Green, S. P.; Jones, C.; Stasch, A. *Science* **2007**, *318* (5857), 1754–1757.

(91) Westerhausen, M. *Angew. Chem. Int. Ed.* **2008**, *47* (12), 2185–2187.

(92) Bonyhady, S. J.; Jones, C.; Nembenna, S.; Stasch, A.; Edwards, A. J.; McIntyre, G. J. *Chem. Eur. J.* **2010**, *16* (3), 938–955.

(93) Harder, S.; Brettar, J. *Angew. Chem. Int. Ed.* **2006**, *45* (21), 3474–3478.

(94) Hardman, N. J.; Eichler, B. E.; Power, P. P. *Chem. Commun.* **2000**, 1991–1992.

(95) Cui, C.; Roesky, H. W.; Schmidt, H.-G.; Noltemeyer, M.; Hao, H.; Cimpoesu, F. *Angew. Chem. Int. Ed.* **2000**, *39* (23), 4274–4276.

(96) Reeske, G.; Cowley, A. H. *Inorg. Chem.* **2007**, *46* (4), 1426–1430.

(97) Herrmannsdörfer, D.; Kaaz, M.; Puntigam, O.; Bender, J.; Nieger, M.; Gudat, D. *Eur. J. Inorg. Chem.* **2015**, *2015* (29), 4819–4828.

(98) Baker, R. J.; Farley, R. D.; Jones, C.; Kloth, M.; Murphy, D. M. *Chem. Commun.* **2002**, 1196–1197.

(99) Hopkinson, M. N.; Richter, C.; Schedler, M.; Glorius, F. *Nature* **2014**, *510* (7506), 485–496.

(100) Denk, M. K.; Hatano, K.; Ma, M. *Tetrahedron Lett.* **1999**, *40* (11), 2057–2060.

(101) Arduengo III, A. J.; Harlow, R. L.; Kline, M. *J. Am. Chem. Soc.* **1991**, *113* (1), 361–363.

(102) Arduengo III, A. J.; Rasika Dias, H. V.; Harlow, R. L.; Kline, M. *J. Am. Chem. Soc.* **1992**, *114* (14), 5530–5534.

(103) Arduengo III, A. J.; Krafczyk, R.; Schmutzler, R.; Craig, H. A.; Goerlich, J. R.; Marshall, W. J.; Unverzagt, M. *Tetrahedron* **1999**, *55* (51), 14523–14534.

(104) Heinemann, C.; Müller, T.; Apeloig, Y.; Schwarz, H. *J. Am. Chem. Soc.* **1996**, *118* (8), 2023–2038.

(105) Boehme, C.; Frenking, G. *J. Am. Chem. Soc.* **1996**, *118* (8), 2039–2046.

(106) Crabtree, R. H. *J. Organomet. Chem.* **2005**, *690* (24–25), 5451–5457.

(107) Dorta, R.; Stevens, E. D.; Scott, N. M.; Costabile, C.; Cavallo, L.; Hoff, C. D.; Nolan, S. P. *J. Am. Chem. Soc.* **2005**, *127* (8), 2485–2495.

(108) Back, O.; Henry-Ellinger, M.; Martin, C. D.; Martin, D.; Bertrand, G. *Angew. Chem. Int. Ed.* **2013**, *52* (10), 2939–2943.

(109) Lee, M.-T.; Hu, C.-H. *Organometallics* **2004**, *23* (5), 976–983.

(110) Hoffmann, R. *Angew. Chem. Int. Ed. Engl.* **1982**, *21* (10), 711–724.

(111) Mansaray, H. B.; Tang, C. Y.; Vidovic, D.; Thompson, A. L.; Aldridge, S. *Inorg. Chem.* **2012**, *51* (23), 13017–13022.

(112) Wang, Y.; Robinson, G. H. *Dalton Trans.* **2011**, *41* (2), 337–345.

(113) Wang, Y.; Xie, Y.; Wei, P.; King, R. B.; Schaefer III, H. F.; Schleyer, P. v. R.; Robinson, G. H. *Science* **2008**, *321* (5892), 1069–1071.

(114) Green, M. L. H.; Parkin, G. *Dalton Trans.* **2016**, *45* (47), 18784–18795.

(115) Himmel, D.; Krossing, I.; Schnepf, A. *Angew. Chem. Int. Ed.* **2014**, *53* (2), 370–374.

(116) Frenking, G. *Angew. Chem. Int. Ed.* **2014**, *53* (24), 6040–6046.

(117) Zhao, L.; Hermann, M.; Holzmann, N.; Frenking, G. *Coord. Chem. Rev.* **2017**, DOI: 10.1016/j.ccr.2017.03.026.

(118) Georgiou, D. C.; Zhao, L.; Wilson, D. J. D.; Frenking, G.; Dutton, J. L. *Chem. Eur. J.* **2017**, *23* (12), 2926–2934.

(119) Wang, Y.; Xie, Y.; Wei, P.; King, R. B.; Schaefer III, H. F.; Schleyer, P. v. R.; Robinson, G. H. *J. Am. Chem. Soc.* **2008**, *130* (45), 14970–14971.

(120) Abraham, M. Y.; Wang, Y.; Xie, Y.; Wei, P.; Schaefer III, H. F.; Schleyer, P. v. R.; Robinson, G. H. *Chem. Eur. J.* **2010**, *16* (2), 432–435.

(121) Sidiropoulos, A.; Jones, C.; Stasch, A.; Klein, S.; Frenking, G. *Angew. Chem. Int. Ed.* **2009**, *48* (51), 9701–9704.

(122) Jones, C.; Sidiropoulos, A.; Holzmann, N.; Frenking, G.; Stasch, A. *Chem. Commun.* **2012**, *48* (79), 9855–9857.

(123) Braunschweig, H.; Dewhurst, R. D.; Hammond, K.; Mies, J.; Radacki, K.; Vargas, A. *Science* **2012**, *336* (6087), 1420–1422.

(124) Lavallo, V.; Canac, Y.; Präsang, C.; Donnadieu, B.; Bertrand, G. *Angew. Chem. Int. Ed.* **2005**, *44* (35), 5705–5709.

(125) Soleilhavoup, M.; Bertrand, G. *Acc. Chem. Res.* **2015**, *48* (2), 256–266.

(126) Back, O.; Kuchenbeiser, G.; Donnadieu, B.; Bertrand, G. *Angew. Chem. Int. Ed.* **2009**, *48* (30), 5530–5533.

(127) Kretschmer, R.; Ruiz, D. A.; Moore, C. E.; Rheingold, A. L.; Bertrand, G. *Angew. Chem. Int. Ed.* **2014**, *53* (31), 8176–8179.

(128) Mondal, K. C.; Samuel, P. P.; Roesky, H. W.; Aysin, R. R.; Leites, L. A.; Neudeck, S.; Lübben, J.; Dittrich, B.; Holzmann, N.; Hermann, M.; Frenking, G. *J. Am. Chem. Soc.* **2014**, *136* (25), 8919–8922.

(129) Böhnke, J.; Braunschweig, H.; Ewing, W. C.; Hörl, C.; Kramer, T.; Krummenacher, I.; Mies, J.; Vargas, A. *Angew. Chem. Int. Ed.* **2014**, *53* (34), 9082–9085.

(130) Back, O.; Donnadieu, B.; Parameswaran, P.; Frenking, G.; Bertrand, G. *Nat. Chem.* **2010**, *2* (5), 369–373.

(131) Abraham, M. Y.; Wang, Y.; Xie, Y.; Gilliard, Jr., R. J.; Wei, P.; Vaccaro, B. J.; Johnson, M. K.; Schaefer III, H. F.; Schleyer, P. v. R.; Robinson, G. H. *J. Am. Chem. Soc.* **2013**, *135* (7), 2486–2488.

(132) Wang, Y.; Xie, Y.; Abraham, M. Y.; Gilliard, Jr., R. J.; Wei, P.; Schaefer III, H. F.; Schleyer, P. v. R.; Robinson, G. H. *Organometallics* **2010**, *29* (21), 4778–4780.

(133) Abraham, M. Y.; Wang, Y.; Xie, Y.; Wei, P.; Schaefer III, H. F.; Schleyer, P. v. R.; Robinson, G. H. *J. Am. Chem. Soc.* **2011**, *133* (23), 8874–8876.

(134) Wang, Y.; Xie, Y.; Abraham, M. Y.; Wei, P.; Schaefer III, H. F.; Schleyer, P. v R.; Robinson, G. H. *Chem. Commun.* **2011**, *47* (32), 9224–9226.

(135) Arz, M. I.; Straßmann, M.; Geiß, D.; Schnakenburg, G.; Filippou, A. C. *J. Am. Chem. Soc.* **2016**, *138* (13), 4589–4600.

(136) Wang, Y.; Hickox, H. P.; Xie, Y.; Wei, P.; Cui, D.; Walter, M. R.; Schaefer III, H. F.; Robinson, G. H. *Chem. Commun.* **2016**, *52* (33), 5746–5748.

(137) Chen, M.; Wang, Y.; Xie, Y.; Wei, P.; Gilliard, Jr., R. J.; Schwartz, N. A.; Schaefer III, H. F.; Schleyer, P. v. R.; Robinson, G. H. *Chem. Eur. J.* **2014**, *20* (30), 9208–9211.

(138) Arz, M. I.; Geiß, D.; Straßmann, M.; Schnakenburg, G.; Filippou, A. C. *Chem. Sci.* **2015**, *6* (11), 6515–6524.

(139) Wang, Y.; Chen, M.; Xie, Y.; Wei, P.; Schaefer III, H. F.; Schleyer, P. v. R.; Robinson, G. H. *Nat. Chem.* **2015**, *7* (6), 509–513.

(140) Wang, Y.; Xie, Y.; Wei, P.; Schaefer III, H. F.; Schleyer, P. v. R.; Robinson, G. H. *J. Am. Chem. Soc.* **2013**, *135* (51), 19139–19142.

(141) Bourissou, D.; Guerret, O.; Gabbaï, F. P.; Bertrand, G. *Chem. Rev.* **2000**, *100* (1), 39–92.

(142) Bertrand, G. *Carbene Chemistry: From Fleeting Intermediates to Powerful Reagents*; Marcel Dekker: New York, 2002.

(143) Herrmann, W. A. *Angew. Chem. Int. Ed.* **2002**, *41* (8), 1290–1309.

(144) Díez-González, S.; Nolan, S. P. *Coord. Chem. Rev.* **2007**, *251* (5–6), 874–883.

(145) Hahn, F. E.; Jahnke, M. C. *Angew. Chem. Int. Ed.* **2008**, *47* (17), 3122–3172.

(146) Jacobsen, H.; Correa, A.; Poater, A.; Costabile, C.; Cavallo, L. *Coord. Chem. Rev.* **2009**, *253* (5–6), 687–703.

(147) Díez-González, S.; Marion, N.; Nolan, S. P. *Chem. Rev.* **2009**, *109* (8), 3612–3676.

(148) Mercs, L.; Albrecht, M. *Chem. Soc. Rev.* **2010**, *39* (6), 1903–1912.

(149) Díez-González, S. *N-Heterocyclic Carbenes: From Laboratory Curiosities to Effective Synthetic Tools*; RSC Publishing: Cambridge, 2010.

(150) Cazin, C. S. J. *N-Heterocyclic Carbenes in Transition Metal Catalysis and Organocatalysis, Catalysis by Metal Complexes*; Springer: Dordrecht, The Netherlands, 2011.

(151) Gründemann, S.; Kovacevic, A.; Albrecht, M.; Robert, J. W. F.; Crabtree, H. *Chem. Commun.* **2001**, 2274–2275.

(152) Gründemann, S.; Kovacevic, A.; Albrecht, M.; Faller, J. W.; Crabtree, R. H. *J. Am. Chem. Soc.* **2002**, *124* (35), 10473–10481.

(153) Appelhans, L. N.; Zuccaccia, D.; Kovacevic, A.; Chianese, A. R.; Miecznikowski, J. R.; Macchioni, A.; Clot, E.; Eisenstein, O.; Crabtree, R. H. *J. Am. Chem. Soc.* **2005**, *127* (46), 16299–16311.

(154) Kovacevic, A.; Meadows, K. R.; Counts, M.; Arthur, D. J. *Inorg. Chim. Acta* **2011**, *373* (1), 259–261.

(155) Magill, A. M.; Yates, B. F. *Aust. J. Chem.* **2004**, *57* (12), 1205–1210.

(156) Arnold, P. L.; Pearson, S. *Coord. Chem. Rev.* **2007**, *251* (5–6), 596–609.

(157) Albrecht, M. *Chem. Commun.* **2008**, 3601–3610.

(158) Schuster, O.; Yang, L.; Raubenheimer, H. G.; Albrecht, M. *Chem. Rev.* **2009**, *109* (8), 3445–3478.

(159) Crabtree, R. H. *Coord. Chem. Rev.* **2013**, *257* (3–4), 755–766.

(160) Hadei, N.; Kantchev, E. A. B.; O'Brie, C. J.; Organ, M. G. *Org. Lett.* **2005**, *7* (17), 3805–3807.

(161) Heckenroth, M.; Kluser, E.; Neels, A.; Albrecht, M. *Angew. Chem. Int. Ed.* **2007**, *46* (33), 6293–6296.

(162) Lebel, H.; Janes, M. K.; Charette, A. B.; Nolan, S. P. *J. Am. Chem. Soc.* **2004**, *126* (16), 5046–5047.

(163) Varonka, M. S.; Warren, T. H. *Organometallics* **2010**, *29* (4), 717–720.

(164) Day, B. M.; Pugh, T.; Hendriks, D.; Guerra, C. F.; Evans, D. J.; Bickelhaupt, F. M.; Layfield, R. A. *J. Am. Chem. Soc.* **2013**, *135* (36), 13338–13341.

(165) Day, B. M.; Pal, K.; Pugh, T.; Tuck, J.; Layfield, R. A. *Inorg. Chem.* **2014**, *53* (19), 10578–10584.

(166) Schnee, G.; Nieto Faza, O.; Specklin, D.; Jacques, B.; Karmazin, L.; Welter, R.; Silva López, C.; Dagorne, S. *Chem. Eur. J.* **2015**, *21* (49), 17959–17972.

(167) Turbervill, R. S. P.; Goicoechea, J. M. *Aust. J. Chem.* **2013**, *66* (10), 1131–1137.

(168) Schwedtmann, K.; Holthausen, M. H.; Feldmann, K.-O.; Weigand, J. J. *Angew. Chem. Int. Ed.* **2013**, *52* (52), 14204–14208.

(169) Schwedtmann, K.; Schoemaker, R.; Hennersdorf, F.; Bauzá, A.; Frontera, A.; Weiss, R.; Weigand, J. J. *Dalton Trans.* **2016**, *45* (28), 11384–11396.

(170) Arduengo III, A. J.; Davidson, F.; Dias, H. V. R.; Goerlich, J. R.; Khasnis, D.; Marshall, W. J.; Prakasha, T. K. *J. Am. Chem. Soc.* **1997**, *119* (52), 12742–12749.

(171) Mendoza-Espinosa, D.; Donnadieu, B.; Bertrand, G. *J. Am. Chem. Soc.* **2010**, *132* (21), 7264–7265.

(172) Aldeco-Perez, E.; Rosenthal, A. J.; Donnadieu, B.; Parameswaran, P.; Frenking, G.; Bertrand, G. *Science* **2009**, *326* (5952), 556–559.

(173) Singh, A. P.; Ghadwal, R. S.; Roesky, H. W.; Holstein, J. J.; Dittrich, B.; Demers, J.-P.; Chevelkov, V.; Lange, A. *Chem. Commun.* **2012**, *48* (61), 7574–7576.

(174) Singh, A. P.; Samuel, P. P.; Mondal, K. C.; Roesky, H. W.; Sidhu, N. S.; Dittrich, B. *Organometallics* **2013**, *32* (1), 354–357.

(175) Guerret, O.; Solé, S.; Gornitzka, H.; Teichert, M.; Trinquier, G.; Bertrand, G. *J. Am. Chem. Soc.* **1997**, *119* (28), 6668–6669.

(176) Guerret, O.; Solé, S.; Gornitzka, H.; Trinquier, G.; Bertrand, G. *J. Organomet. Chem.* **2000**, *600* (1–2), 112–117.

(177) Waters, J. B.; Goicoechea, J. M. *Coord. Chem. Rev.* **2015**, *293–294*, 80–94.

(178) Scheele, U. J.; Dechert, S.; Meyer, F. *Chem. Eur. J.* **2008**, *14* (17), 5112–5115.

(179) Krüger, A.; Kluser, E.; Müller-Bunz, H.; Neels, A.; Albrecht, M. *Eur. J. Inorg. Chem.* **2012**, *2012* (9), 1394–1402.

(180) Arnold, P. L.; Liddle, S. T. *Organometallics* **2006**, *25* (6), 1485–1491.

(181) Musgrave, R. A.; Turbervill, R. S. P.; Irwin, M.; Goicoechea, J. M. *Angew. Chem. Int. Ed.* **2012**, *51* (43), 10832–10835.

(182) Waters, J. B.; Turbervill, R. S. P.; Goicoechea, J. M. *Organometallics* **2013**, *32* (18), 5190–5200.

(183) Musgrave, R. A.; Turbervill, R. S. P.; Irwin, M.; Herchel, R.; Goicoechea, J. M. *Dalton Trans.* **2014**, *43* (11), 4335–4344.

(184) Curran, D. P.; Solovyev, A.; Makhlouf Brahmi, M.; Fensterbank, L.; Malacria, M.; Lacôte, E. *Angew. Chem. Int. Ed.* **2011**, *50* (44), 10294–10317.

(185) Shih, W.-C.; Wang, C.-H.; Chang, Y.-T.; Yap, G. P. A.; Ong, T.-G. *Organometallics* **2009**, *28* (4), 1060–1067.

(186) Duong, H. A.; Tekavec, T. N.; Arif, A. M.; Louie, J. *Chem. Commun.* **2004**, 112–113.

(187) Wang, Y.; Xie, Y.; Abraham, M. Y.; Wei, P.; Schaefer III, H. F.; Schleyer, P. v. R.; Robinson, G. H. *J. Am. Chem. Soc.* **2010**, *132* (41), 14370–14372.

(188) Wang, Y.; Xie, Y.; Abraham, M. Y.; Gilliard, Jr., R. J.; Wei, P.; Campana, C. F.; Schaefer III, H. F.; Schleyer, P. v. R.; Robinson, G. H. *Angew. Chem. Int. Ed.* **2012**, *51* (40), 10173–10176.

(189) Uzelac, M.; Hernán-Gómez, A.; Armstrong, D. R.; Kennedy, A. R.; Hevia, E. *Chem. Sci.* **2015**, *6* (10), 5719–5728.

(190) Jana, A.; Azhakar, R.; Tavčar, G.; Roesky, H. W.; Objartel, I.; Stalke, D. *Eur. J. Inorg. Chem.* **2011**, *2011* (25), 3686–3689.

(191) Armstrong, D. R.; Baillie, S. E.; Blair, V. L.; Chabloz, N. G.; Diez, J.; Garcia-Alvarez, J.; Kennedy, A. R.; Robertson, S. D.; Hevia, E. *Chem. Sci.* **2013**, *4* (11), 4259–4266.

(192) Uzelac, M.; Kennedy, A. R.; Hernán-Gómez, A.; Fuentes, M. Á.; Hevia, E. *Z. Anorg. Allg. Chem.* **2016**, *642* (22), 1241–1244.

(193) Maddock, L. C. H.; Cadenbach, T.; Kennedy, A. R.; Borilovic, I.; Aromí, G.; Hevia, E. *Inorg. Chem.* **2015**, *54* (18), 9201–9210.

(194) Martínez-Martínez, A. J.; Fuentes, M. Á.; Hernán-Gómez, A.; Hevia, E.; Kennedy, A. R.; Mulvey, R. E.; O'Hara, C. T. *Angew. Chem. Int. Ed.* **2015**, *54* (47), 14075–14079.

(195) Wang, Y.; Xie, Y.; Abraham, M. Y.; Wei, P.; Schaefer III, H. F.; Schleyer, P. v. R.; Robinson, G. H. *Organometallics* **2011**, *30* (6), 1303–1306.

(196) Kronig, S.; Theuergarten, E.; Daniliuc, C. G.; Jones, P. G.; Tamm, M. *Angew. Chem. Int. Ed.* **2012**, *51* (13), 3240–3244.

Chapter 2

Synthesis of aIPr: complexes of group 12 and 14 bis(trimethylsilyl)amides

2.1 Introduction and objectives

2.1.1 The deprotonated N-heterocyclic carbene

NHCs and aNHCs are considered carbenes in the broadest possible sense. The true definition of a carbene requires the carbon centre to be two-coordinate and have six valence electrons. The only carbene for which this definition is accurate is the transient :CH_2.[1,2] Carbenes have only become isolable due to the conjugative effect of substituents which increases the HOMO–LUMO energy gap and prevents dimerisation. In the case of free aNHCs, there are no examples where the C2 substituent is a proton as isomerisation would always afford the free NHC due to basicity differences, hence, protic aNHCs are isolated upon coordination to another species and the 'carbene' centre is three-coordinate. The bonding mode of aNHCs through the C4 carbon is significantly vinylic in character with little to no backbonding and can be considered to be much closer to an R type ligand than an L type ligand. It was discovered in 2010 that treatment of the N-heterocyclic carbene, IPr, with ^{n}BuLi in hexane at ambient temperature quantitatively affords an anionic N-heterocyclic dicarbene which has also been termed a ditopic carbanionic N-heterocyclic carbene to better represent the nature of such a species (Scheme 2.1).

A deprotonated NHC with two nitrogen atoms in the imidazole ring is isoelectronic with triazole based bis(NHC)s. These latter species have been used in ionic silver polymers and can be reasonably termed dicarbenes due to the presence of two neutral Lewis basic carbon atoms.[3] The lithiated salt ($[Li(aIPr:)]_\infty$) is a convenient precursor for the synthesis of compounds bearing aIPr: ligands. $[Li(THF)(aIPr:)]_\infty$ could also be synthesised (albeit in lower yield) by the reduction of IPr with lithium metal in THF and crystallised as a coordination polymer with one THF coordinated to each lithium cation.[4]

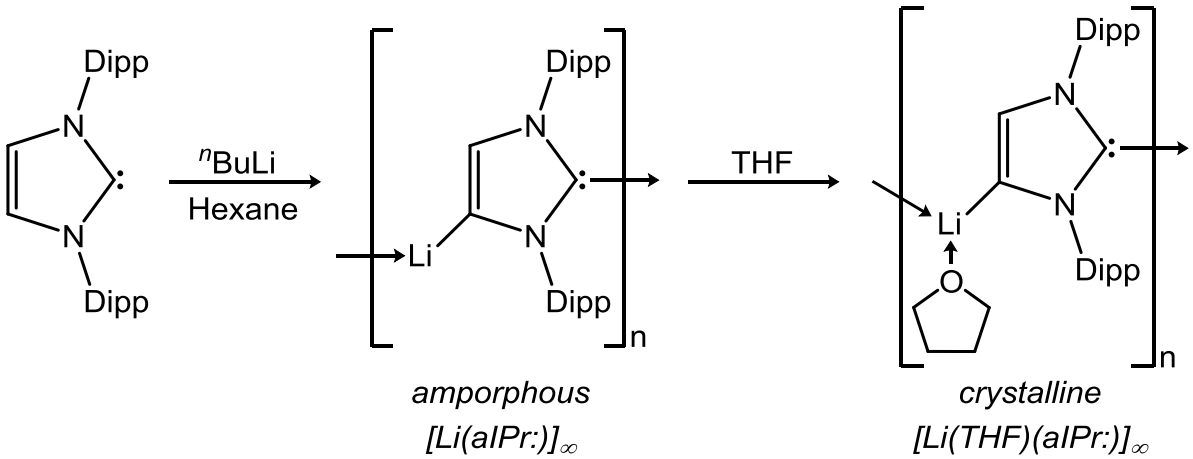

Scheme 2.1: Deprotonation of IPr with ^{n}BuLi to afford $[Li(aIPr:)]_{\infty}$ which can be crystallised from THF with one molecule of THF coordinated to lithium.

2.1.2 Group 14 bis(trimethylsilyl)amides

The low-valent group 14 amides $E[N(SiMe_3)_2]_2$ (E = Ge, Sn, Pb) were synthesised and their physical properties analysed in 1977 by Lappert and co-workers.[5]

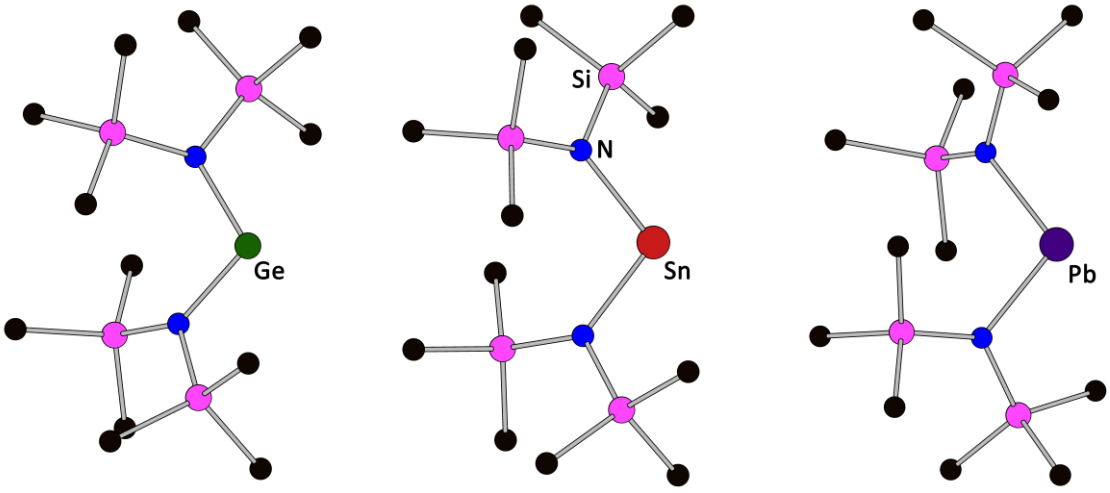

Figure 2.1: Ball and stick models of $E[N(SiMe_3)_2]_2$ which clearly show a monomeric structure.

$Sn[N(SiMe_3)_2]_2$ had been reported one year earlier in a preliminary publication by Lappert suggesting a monomeric structure. The same compound was reported in 1974 by Schaeffer and Zuckerman to be dimeric.[6,7] These divalent group 14 bis(trimethylsilyl)amide complexes were shown by Lappert to be monomeric by cryoscopy in benzene. They are thermochromic,

low melting point solids or liquids that are thermally stable and can be purified by distillation. The monomeric structure for all complexes was ultimately proven by X-ray crystallography (Figure 2.1).[8,9] The reduction in N–E–N bond angle from Ge to Sn and Pb (107.1(2)°, 104.7(2)° and 103.6(7)°, respectively) is consistent with the reduction in sp hybridisation characteristic of descending a group in the periodic table

2.1.3 Chapter outline

The recent report of an alkali metal salt of a ditopic carbanionic NHC provided a useful entry point to investigate the chemistry of such ligands. This salt can be used to access compounds which contain unquenched classical NHC functionality. With the aim of moving away from the method of chemical reduction, this chapter will discuss our investigations into the use of alkali metal salts as precursors for the synthesis of novel compounds bearing aIPr: as a ligand, including the preparation of the novel potassium salt of IPr and the differences in reactivity of the two reagents $[Li(aIPr:)]_\infty$ and $[K(aIPr:)]_\infty$.

This chapter will focus on the reactivity of these reagents with the group 14 bis(trimethylsilyl)amide reagents. These species serve as a convenient source of group 14 metallylenes, that is, stable low-valent group 14 precursors that have proven useful in accessing novel group 14 complexes with a range of substituents.[10]

2.2 Alkali metal salts of deprotonated IPr

2.2.1 Synthesis of $[:C(N(2,6\text{-}^{i}Pr_2C_6H_3))_2(CH)CK]_n$ ($[K(aIPr:)]_\infty$) (1)

The recent isolation of a lithium salt of a deprotonated NHC ($[Li(aIPr:)]_\infty$) prompted us to investigate whether the aIPr: species could be isolated as the free anion, $[:C(N(2,6\text{-}^{i}Pr_2C_6H_3))_2(CH)C:]^-$. With this objective in mind, we sought to synthesise the

organopotassium compound [:C(N(2,6-^{i}Pr$_2$C$_6$H$_3$))$_2$(CH)CK]$_n$ (**1**) which was achieved by a cation exchange reaction between [Li(aIPr:)]$_\infty$ and KO^{t}Bu in Et$_2$O much like the synthesis of so-called superbasic Schlosser's bases.[11,12] These have also been termed LICKOR superbases due to the precursor reagents, an organolithium ('LiC') in combination with a potassium alkoxide ('KOR'). Attempts to sequester the potassium cation in **1** with 2,2,2-crypt resulted in decomposition of the cryptand and the generation of free IPr on protonation of the carbanionic backbone. This is entirely consistent with the high Brønsted basicity of the proposed anion. Regardless, the synthesis of a new alkali metal salt of deprotonated IPr provides a new useful precursor for the synthesis of novel compounds bearing aIPr: ligands.

Addition of diethyl ether to a mixture of [Li(aIPr:)]$_\infty$ and KO^{t}Bu at –78 °C results in the formation of an orange solution. Upon warming to room temperature, the solution can be concentrated in vacuo and a mixture of THF and hexane added to induce crystallisation of [:C(N(2,6-^{i}Pr$_2$C$_6$H$_3$))$_2$(CH)CK(THF)$_2$]$_n$ ([K(THF)$_2$(aIPr:)]$_\infty$) as a colourless, crystalline coordination polymer (Scheme 2.2).[13] The high solubility of the LiO^{t}Bu by-product allows for the isolation of the lithium free salt as confirmed by the absence of a resonance in the ^{7}Li NMR spectrum of the precipitate. After filtration, the solid was washed with a combination of hexane and cold THF until the washings were clear at which point the solid is dried thoroughly under vacuum. It was found that the THF coordinated to the potassium ion is readily liberated under vacuum as determined by ^{1}H NMR spectroscopy (Figure 2.4), hence, after extended drying at room temperature, **1** can be isolated solvent free in at least 56% yield (a yield only limited by the hydrolysis of reagents during manipulation).

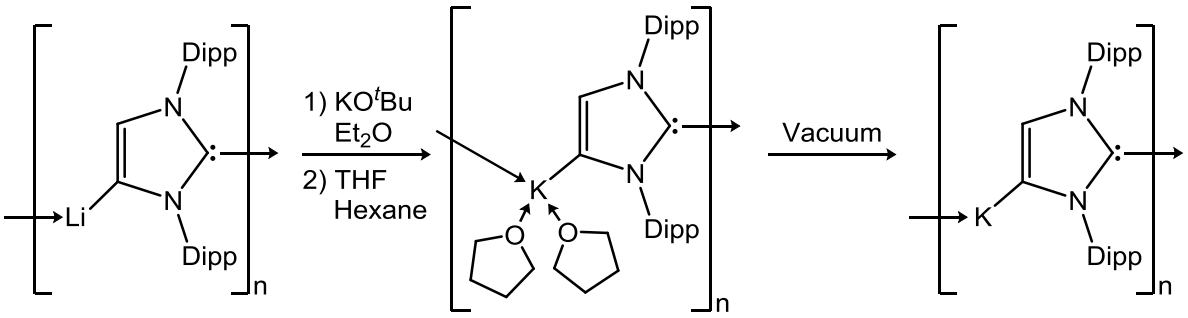

Scheme 2.2: Synthesis of **1**.

2.2.2 Characterisation of 1

Single crystals of **1**·2THF suitable for single crystal X-ray diffraction were obtained by either slow diffusion of hexane into a saturated THF solution, or by slow cooling of a warm THF solution saturated with **1**. There are bonding interactions between the potassium cations and both the classical C2 carbene carbon and that of the abnormal C4, carbanionic position of the aIPr: ligand (K1–C1 = 2.905(2) Å and K1–C3 = 2.812(2) Å) as pictured in Figure 2.2 and 2.3. The observed bond lengths show a shorter bond length between K^+ and the formally anionic carbon centre as a result of the greater electrostatic attraction (Σr_{cov} = 2.70 Å).[14]

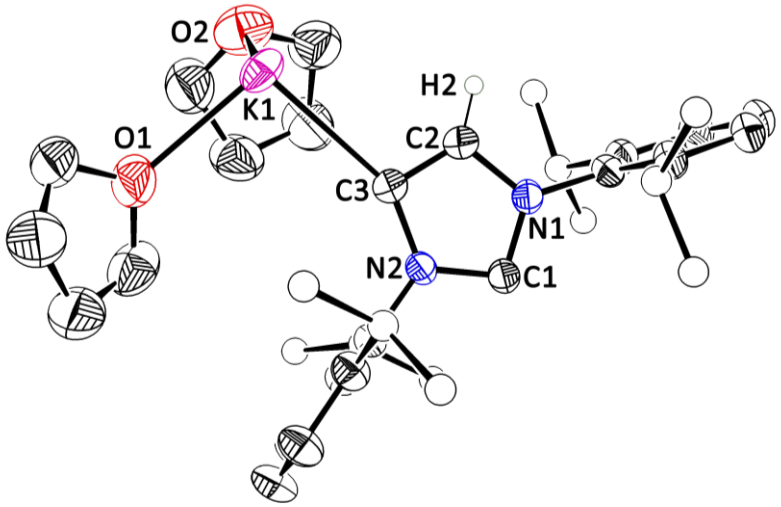

Figure 2.2: Molecular structure of the monomeric unit of **1**·2THF. Anisotropic displacement ellipsoids pictured are set at 50% probability. Hydrogen atoms (with the exception of the imidazole proton labelled H2) have been omitted for clarity. Atoms of the ^{i}Pr groups and H2 are pictured as spheres of arbitrary radii.

Unsurprisingly, there are no significant differences between the anionic moiety $[:C(N(2,6\text{-}^{i}Pr_2C_6H_3)_2)(CH)C]^-$ in **1** and the previously reported $[Li(THF)]^+$ salt, $[Li(THF)(aIPr:)]_\infty$.[4] $[K(THF)_2(aIPr:)]_\infty$ crystallises in the orthorhombic space group $P2_12_12_1$ and reveals one-dimensional zig-zag chains along the crystallographic *b* axis in which the aIPr: ligands are bridged by potassium cations coordinated by two molecules of THF (Figure 2.3).

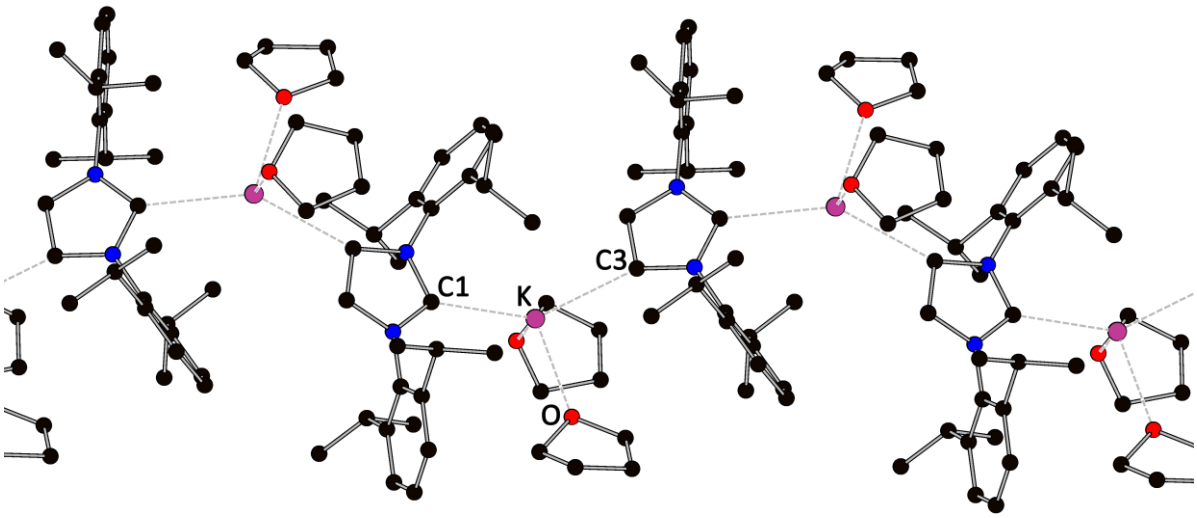

Figure 2.3: Ball and stick model showing one-dimensional coordination polymer chains of $[K(THF)_2(aIPr:)]_\infty$ within the crystal structure. Hydrogen atoms have been omitted for clarity.

$[K(aIPr:)]_\infty$ is sparingly soluble in THF at ambient temperature however this does not prohibit the possibility of obtaining both ^1H and $^{13}C\{^1H\}$ NMR spectra of **1** saturated in d_8-THF. Other solvents such as acetonitrile, DFB, dichloromethane, pyridine and toluene are incompatible with such a highly reducing and Brønsted basic species. Likewise, **1** shows no solubility in non-polar solvents such as benzene and Et_2O. The NMR spectra obtained in d_8-THF are consistent with an asymmetric, backbone deprotonated IPr moiety.

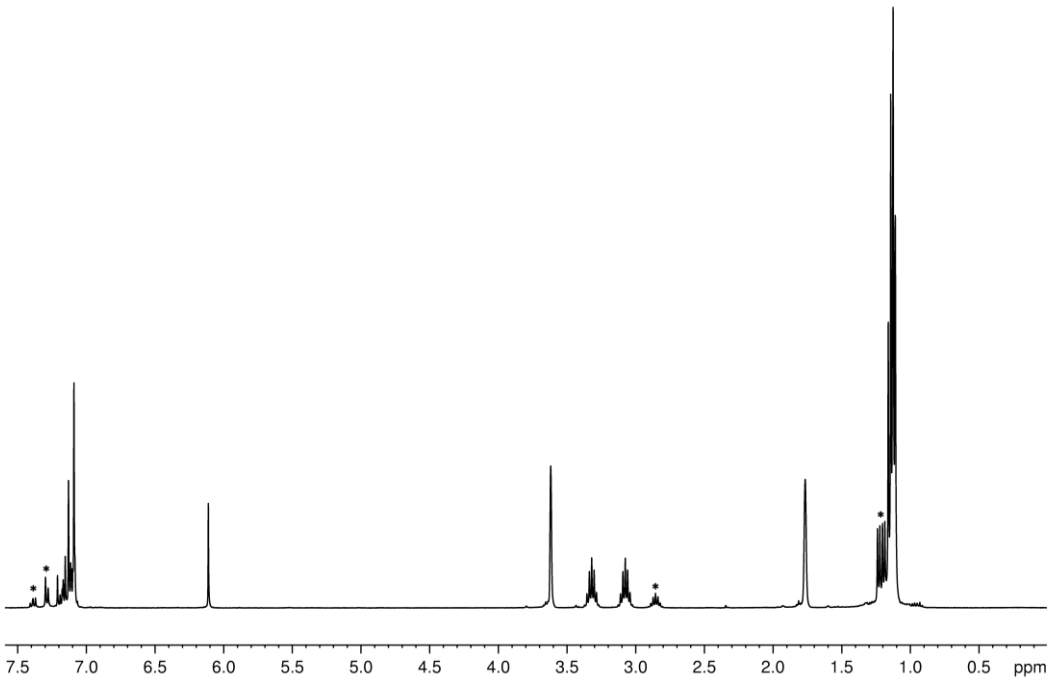

Figure 2.4: ^{1}H NMR spectrum of **1** in d_8-THF. Resonances marked with * are due to free IPr presumably formed by hydrolysis.

The NMR spectra of all other aIPr and aIPr: complexes reported in this thesis show very similar resonances and so the general NMR spectrum will be discussed in detail here. The most indicative set of resonances that signify an asymmetric species are the two methine resonances which result from the two different Dipp substituents (3.28 and 3.04 ppm) and the single alkenic proton resonance at 6.07 ppm which integrate in a 2 : 2 : 1 ratio. Four overlapping doublet resonances are also observed for the diastereotopic methyl substituents of the ^{i}Pr groups of the two Dipp substituents. Finally, the aromatic proton resonances appear as a *pseudo*-doublet and triplet for the *meta*- and *para*-Dipp protons, respectively. Similarly, the $^{13}C\{^{1}H\}$ spectrum displays resonances due to the carbenic carbon, carbanionic carbon and the protonated alkenic carbon at 215.1, 176.3 and 126.8 ppm, respectively.

2.3 Adducts between $[K(aIPr:)]_\infty$ and $E[N(SiMe_3)_2]_2$

2.3.1 Synthesis of 1 : 1 adducts between $[K(aIPr:)]_\infty$ and $E[N(SiMe_3)_2]_2$ (E = Zn, Sn)

Evidently, it seems unlikely that $[aIPr:]^-$ may be isolated without an accompanying metal interaction. Addition of **1** to $E[N(SiMe_3)_2]_2$ in a 1 : 1 stoichiometric ratio affords the three coordinate anionic complexes $[E\{C[N(2,6\text{-}^iPr_2C_6H_3)]_2(CH)C\}\{N(SiMe_3)_2\}_2]^-$ (E = Zn, **2**; Sn, **3**) and the potassium cation can then be sequestered with the use of 2,2,2-crypt or 18-crown-6 which allows the carbenic site to remain uncoordinated and available for further coordination (Scheme 2.3). The ^{1}H NMR spectra for the crude reaction mixtures in d_8-THF are consistent with complexes bearing an aIPr: ligand with no proton bonded to the C2 carbon. The most diagnostic resonances in the ^{1}H NMR spectra are those arising from the alkenic proton and the two methine resonances which are observed at 6.92, 3.23 and 3.03 ppm for **2** and 7.01, 3.26 and 3.06 ppm for **3**, respectively. Both **2** and **3** are indefinitely stable in solution at room temperature with no apparent change in the NMR spectra.

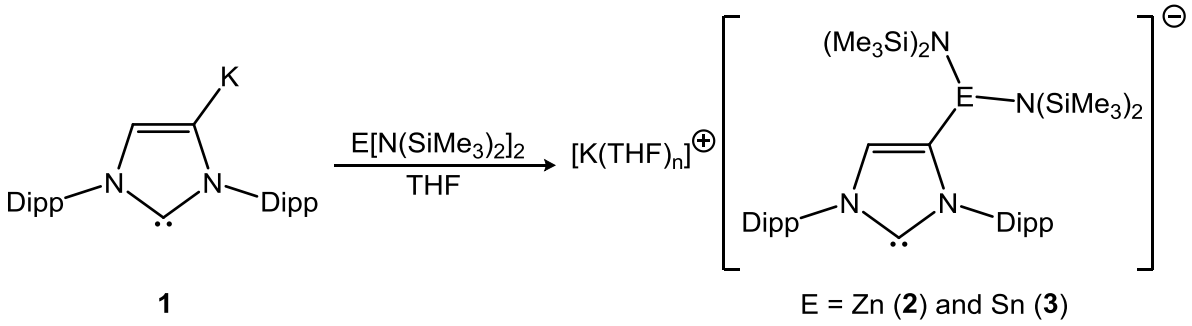

1

E = Zn (**2**) and Sn (**3**)

Scheme 2.3: Synthesis of $[K(THF)_n][\mathbf{2}]$ and $[K(THF)_n][\mathbf{3}]$.

Further evidence for the formation of the three coordinate complexes was obtained by the use of electrospray ionisation mass spectrometry (ESI-MS) which reveals molecular ions at *m*/*z* values of 773.9 and 826.2 for **2** and **3**, respectively.

2.3.2 Crystallisation of 2 and 3

Single crystals of **2** and **3** could be grown by the addition of a suitable sequestering agent followed by slow diffusion of hexane into a THF solution of the products. This method afforded the crystalline salts [K(2,2,2-crypt)][**2**]·THF and [K(18-crown-6)(THF)][**3**]·$^{1}/_{2}$THF (Figure 2.5). As expected, the zinc(II) complex was found to adopt a trigonal planar geometry ($\Sigma_{\text{bond angles}}$ = 360.0°) whereas the tin(II) complex was found to adopt a trigonal pyramidal geometry on account of the stereochemically active lone pair of electrons ($\Sigma_{\text{bond angles}}$ = 300.1°).

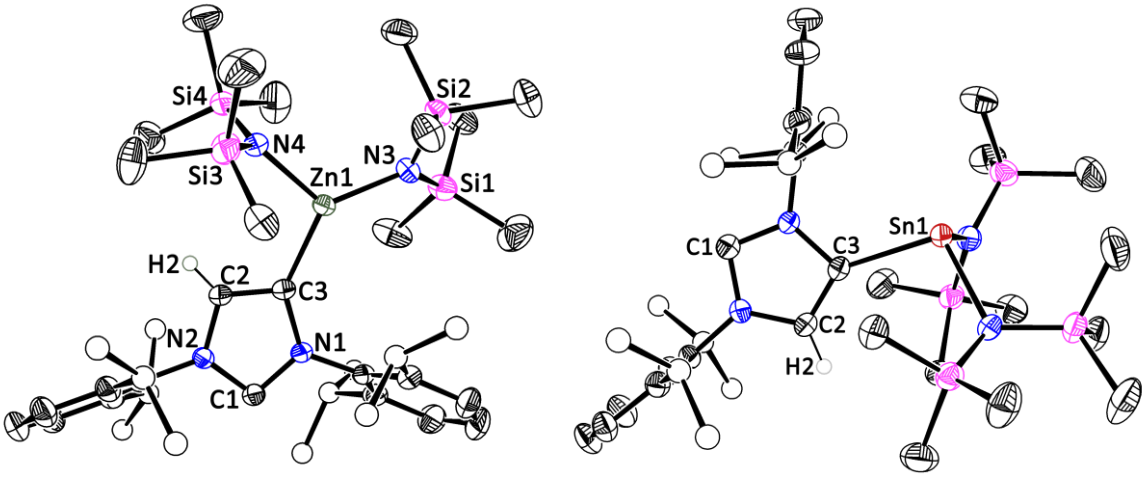

Figure 2.5: Structures of anions **2** (left) and **3** (right) in [K(2,2,2-crypt)][**2**] and [K(18-crown-6)(THF)$_2$][**3**]. Anisotropic displacement ellipsoids pictured are set at 50% probability. Hydrogen atoms (with the exception of the imidazole proton labelled H2) have been omitted for clarity. Atoms of the ^{i}Pr groups and H2 are pictured as spheres of arbitrary radii.

The E–C bond lengths of 2.008(1) and 2.277(3) Å for **2** and **3**, respectively, are consistent with the difference in covalent radius of tin relative to zinc (Δd = 0.27 Å and Δr_{cov} = 0.17–0.32 Å).[14,15] Similarly, the E–N bond lengths were observed to be on average, 0.25 Å longer for **3**. The closely related [(aIPr:)$_2$Zn(Mes)]$^-$ (Scheme 1.14) shows very similar bond lengths from the metal to the aIPr: ligands (2.023(2) and 2.009(2) Å).[16]

2.3.3 Synthesis of 1 : 1 adducts between $[K(aIPr:)]_\infty$ and $E[N(SiMe_3)_2]_2$ (E = Ge, Pb)

By the same methodology, addition of $[K(aIPr:)]_\infty$ to one equivalent of the germanium and lead bis(trimethylsilyl)amides in THF reveals the formation of $[(aIPr:)E\{N(SiMe_3)_2\}_2]^-$ (E = Ge, **4**; Pb, **5**) by ^{1}H NMR spectroscopy. The NMR spectra are very similar to those of **2** and **3** and display the asymmetry of a coordinated aIPr:. ^{1}H NMR spectroscopy studies reveal the presence of a single alkenic proton and two methine resonances (6.83, 3.48 and 3.08 ppm for **4** and 7.00, 3.19 and 3.06 ppm for **5**, respectively). However, unlike **2** and **3**, anions **4** and **5** were unstable in solution when left to stand for several hours at ambient temperature.

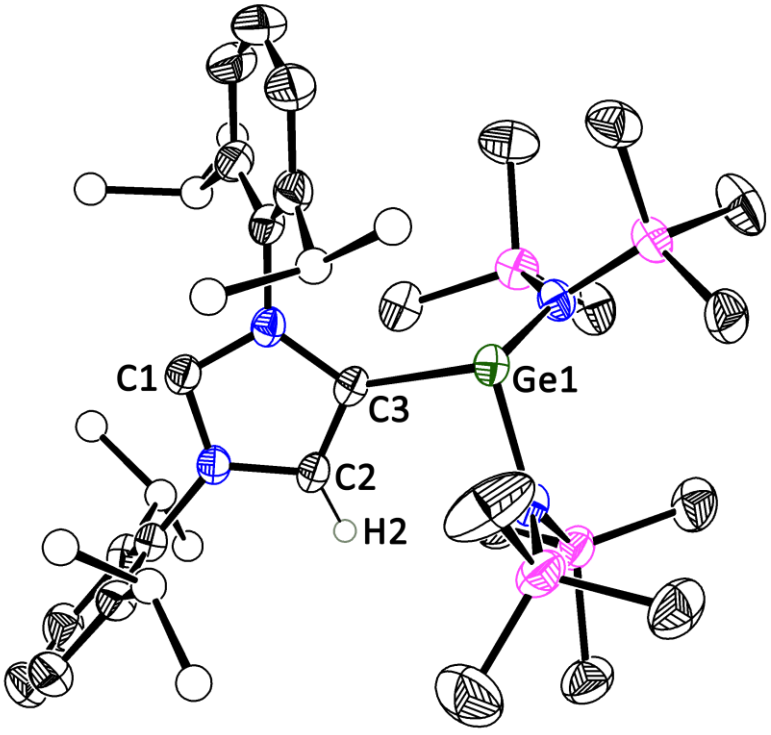

Figure 2.6: Structure of anion **4** in $[K(18\text{-crown-6})(THF)_2]_2$[**4**][**6**]·THF. Anisotropic displacement ellipsoids pictured are set at 50% probability. Hydrogen atoms (with the exception of the imidazole proton labelled H2) have been omitted for clarity. Atoms of the ^{i}Pr groups and H2 are pictured as spheres of arbitrary radii.

The ^{1}H NMR spectra for both species increased in complexity over time giving rise to new complexes. Due to the relative instability of **4** and **5** in solution, compositionally pure samples

could not be obtained. However, **4** was fortuitously co-crystallised along with an equivalent of the decomposition product **6** (*vide infra*) in $[K(18\text{-crown-6})(THF)_2]_2[\mathbf{4}][\mathbf{6}]\cdot THF$ by diffusion of hexane into a freshly prepared THF reaction mixture (Figure 2.6).

Compound **4** exhibits a trigonal pyramidal structure much like that observed for **3** ($\Sigma_{\text{bond angles}} = 304.6°$). The larger sum of angles is consistent with the increase in steric clash between the substituents when bonded to a smaller element centre ($\Delta r_{cov} = 0.19$ Å).[15] By extension, the E–C bond length (2.059(2) Å) is 0.22 Å smaller than the equivalent bond length in **3**.

2.3.4 Synthesis of 2 : 1 adducts between $[K(aIPr:)]_\infty$ and $E[N(SiMe_3)_2]_2$ (E = Ge, Pb)

Solutions of **4** and **5** were found to decompose on standing and electrospray mass spectrometry revealed a mass envelope at 1008.9 in a mass spectrum of the reaction mixture in the synthesis of **4**. This can be ascribed to the 2 : 1 adduct product $[(aIPr:)_2Ge\{N(SiMe_3)_2\}]^-$ (**6**) which was found to co-crystallise with the 1 : 1 adduct. **4** and **5** are presumed to decompose via a Schlenk-like equilibrium to afford the bis(aIPr:) complexes (Scheme 2.4). This decomposition pathway was not found to take place for the zinc and tin species, **2** and **3**. The products that form suggest that the mechanism may go via a germylene or plumbylene intermediate that may dimerise to allow migration of the aIPr: ligand. Such a species is unlikely to be liberated as a free species in solution at room temperature. Such low-coordinate complexes could form on the elimination of the potassium amide ($K[N(SiMe_3)_2]$) which is a stable species in solution. Correspondingly, both decomposition reactions result in the stoichiometric formation of $[E\{N(SiMe_3)_2\}_3]^-$.

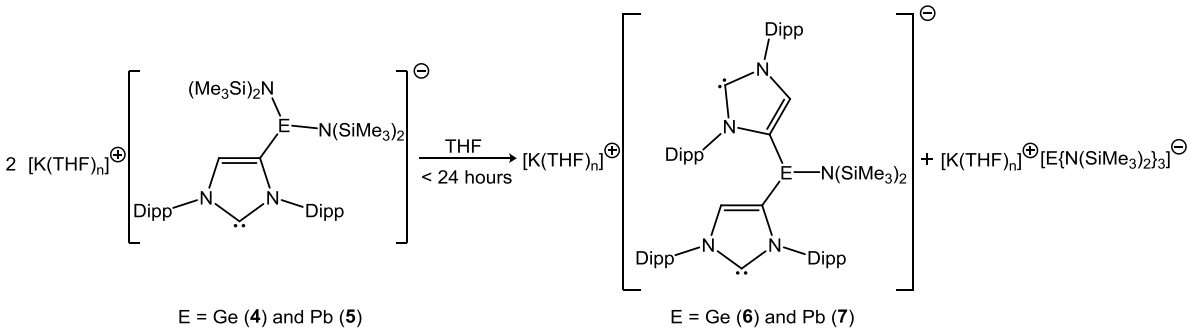

Scheme 2.4: Synthesis of **6** and **7** by decomposition of **4** and **5**.

Alternatively, addition of two equivalents of $[K(aIPr:)]_\infty$ to the group 14 reagents allows for the high yielding synthesis of $[(aIPr:)_2E\{N(SiMe_3)_2\}]^-$ (E = Ge, **6**; Pb, **7**) with $K[N(SiMe_3)_2]$ as a by-product. Analysis of ^1H NMR spectra of both **6** and **7** reveals restricted rotation about the N–Dipp bonds due to a doubling in the number of NMR resonances observed for these groups. The diagnostic, single alkenic proton resonance in both spectra at 6.93 and 6.96 ppm for **6** and **7**, respectively, indicates the symmetry equivalence of the two coordinated aIPr: ligands. In the case of **6**, additional restricted rotation is observed for the Ge–N bond which gives rise to two resonances for the $SiMe_3$ groups as a result of the shorter bond distances to the smaller main group element. The $^{13}C\{^1H\}$ NMR spectra are also consistent with this analysis and reveal inequivalent *ortho*- and *meta*-Dipp resonances with eight arising from these nuclei and an additional four resonances from the *ipso*- and *para*-Dipp carbon nuclei. Finally, $^{29}Si\{^1H\}$ NMR confirms the restricted Ge–N rotation in **6** which gives rise to two separate resonances at –2.6 and –3.5 ppm.

Addition of 18-crown-6 to both reaction mixtures followed by slow diffusion of hexane into the THF solution allows for the crystallisation of both as $[K(18\text{-crown-6})(THF)_2]^+$ salts (Figure 2.7). The by-product $[K(18\text{-crown-6})(THF)_2][N(SiMe_3)_2]$ was removed in the filtrate due to its high solubility in the solvent mixture of THF and hexane.

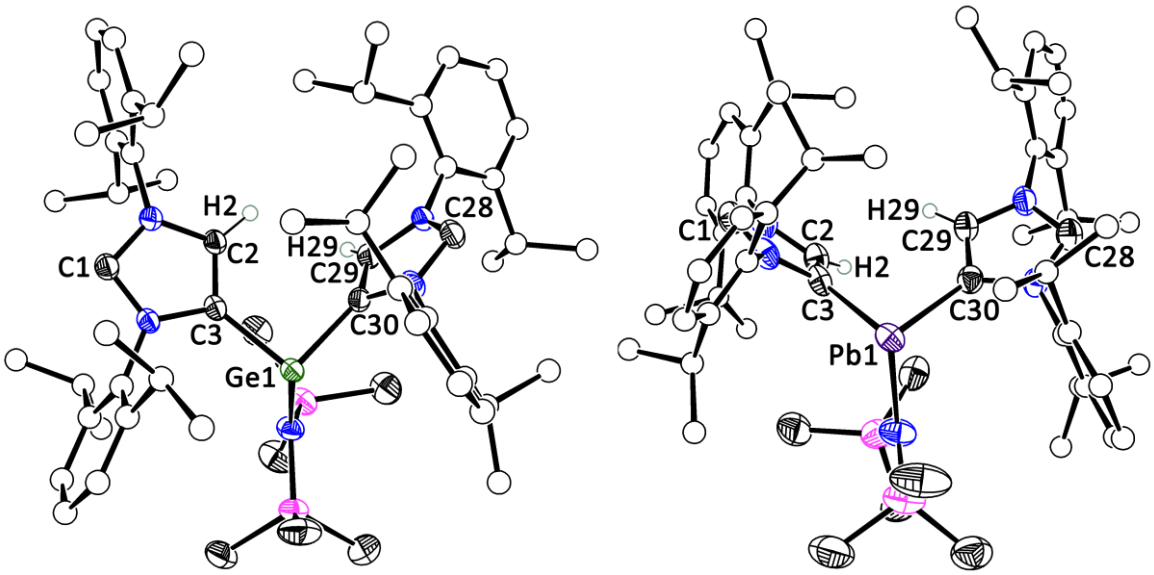

Figure 2.7: Structures of anions **6** (left) and **7** (right) in [K(18-crown-6)(THF)$_2$][**6**]·THF and [K(18-crown-6)(THF)$_2$][**7**]·THF. Anisotropic displacement ellipsoids pictured are set at 50% probability. Hydrogen atoms (with the exception of the imidazole protons labelled H2 and H29) have been omitted for clarity. Atoms of the Dipp groups, H2 and H29 are pictured as spheres of arbitrary radii.

The molecular structures determined by single crystal X-ray diffraction clearly show the presence of two aIPr: ligands with one remaining amide ligand arranged in a trigonal pyramidal geometry ($\Sigma_{\text{bond angles}}$ = 300.1° and 290.9° for **6** and **7**, respectively). The structures illustrate how sterically congested these species are and are consistent with the restricted rotation observed by NMR spectroscopy. The Ge–C bond lengths (2.067(2) and 2.038(2) Å) are very similar to that observed in **4** and the Pb–C bond lengths, were found to be 2.362(5) and 2.339(5) Å, which are in line with the greater covalent radius of lead relative to germanium (Δr_{cov} = 0.25 Å).[15]

2.4 Adducts between $[Li(aIPr:)]_\infty$ and $E[N(SiMe_3)_2]_2$

2.4.1 Synthesis of 2 : 1 adducts between $[Li(aIPr:)]_\infty$ and $E[N(SiMe_3)_2]_2$ (E = Ge, Sn, Pb)

As reported previously when using $[K(aIPr:)]_\infty$ as an aIPr: source, the lithium salts of **6**, and **7** could be synthesised in reasonable yield by the addition of two equivalents of $[Li(aIPr:)]_\infty$ to main group reagents in THF to afford the isostructural complexes $(aIPr:)(aIPr{\cdot}Li(THF)_2)E\{N(SiMe_3)_2\}$ (E = Ge, **8**; Sn, **9**; Pb, **10**). All complexes were crystallised by slow diffusion of hexane into a THF solution (Figure 2.8, 2.9 and 2.10). NMR spectroscopy reveals restricted rotation about the N–Dipp bonds in all species. As observed in anion **6**, **8** has restricted rotation about the Ge–N bond giving rise to two separate $SiMe_3$ resonances in the ^1H and ^{13}C NMR spectra.

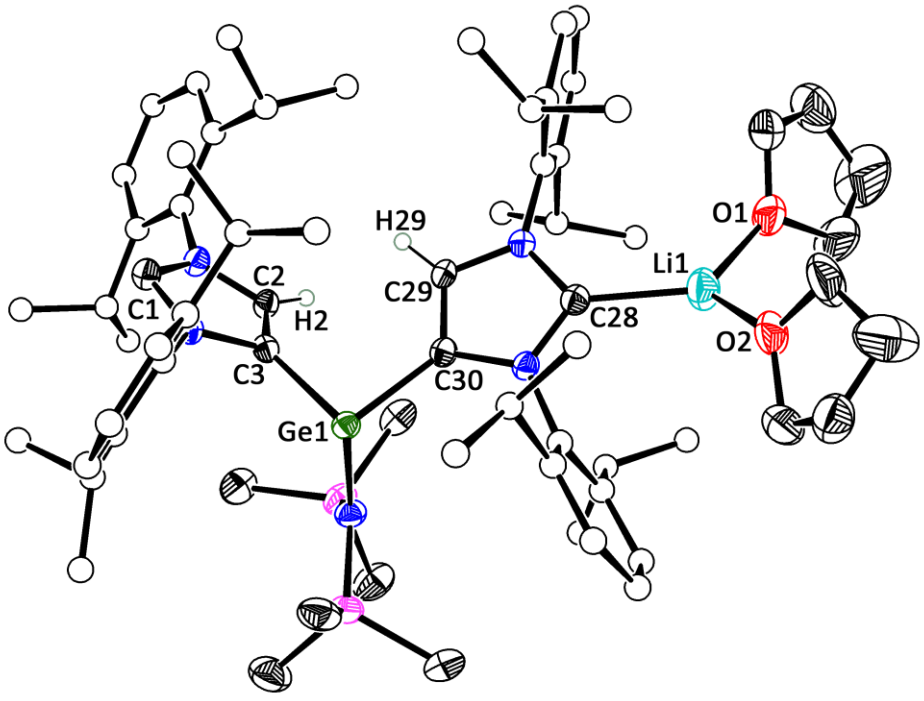

Figure 2.8: Molecular structure of **8**. Anisotropic displacement ellipsoids pictured are set at 50% probability. Hydrogen atoms (with the exception of the imidazole protons labelled H2 and H29) have been omitted for clarity. Atoms of the Dipp groups, H2 and H29 are pictured as spheres of arbitrary radii.

The ^{1}H resonance for the $SiMe_3$ group is broad in the case of **9** suggesting free, however, hindered rotation about the Sn–N bond. Finally, only one sharp resonance is observed for the $SiMe_3$ groups in **10** as expected due to the larger covalent radius of the lead atom and reduced steric hindrance.

These species crystallise well in the absence of any sequestering agent as the lithium cation remains coordinated by one of the free NHCs of the complex (along with two molecules of THF) in a trigonal planar arrangement. The lithium cation is likely completely solvated when dissolved in THF as evidenced by a single alkenic resonance in the ^{1}H NMR spectra indicating the equivalence of the two aIPr: ligands in solution.

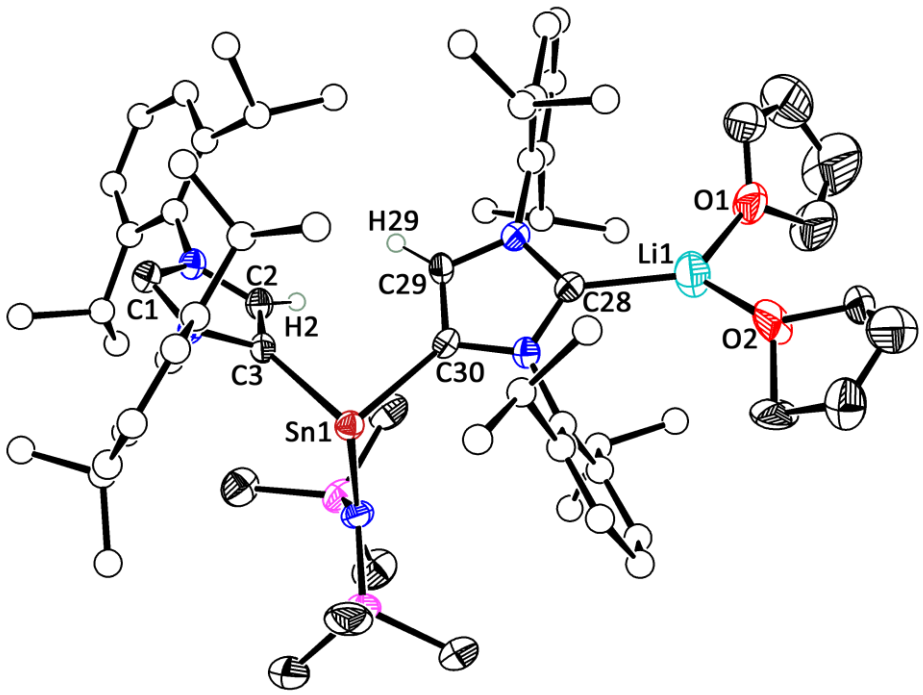

Figure 2.9: Molecular structure of **9**. Anisotropic displacement ellipsoids pictured are set at 50% probability. Hydrogen atoms (with the exception of the imidazole protons labelled H2 and H29) have been omitted for clarity. Atoms of the Dipp groups, H2 and H29 are pictured as spheres of arbitrary radii.

The coordination of the NHC moiety to a hard Lewis acid, the lithium cation, shows no effect on the bonding interaction between the ligand and the central main group element. In **8**–**10**,

the E–C3 and E–C30 bond lengths were found to be identical for each species within experimental error (2.065(2) and 2.061(2) Å in **8**; 2.261(2) and 2.255(2) Å in **9**; 2.358(3) and 2.352(3) Å in **10**). These values are also consistent with the bond lengths observed in the potassium salts **6** and **7**. It would appear as though the bonding interaction through the abnormal position of an NHC is independent of coordination of the classical NHC position to other species.

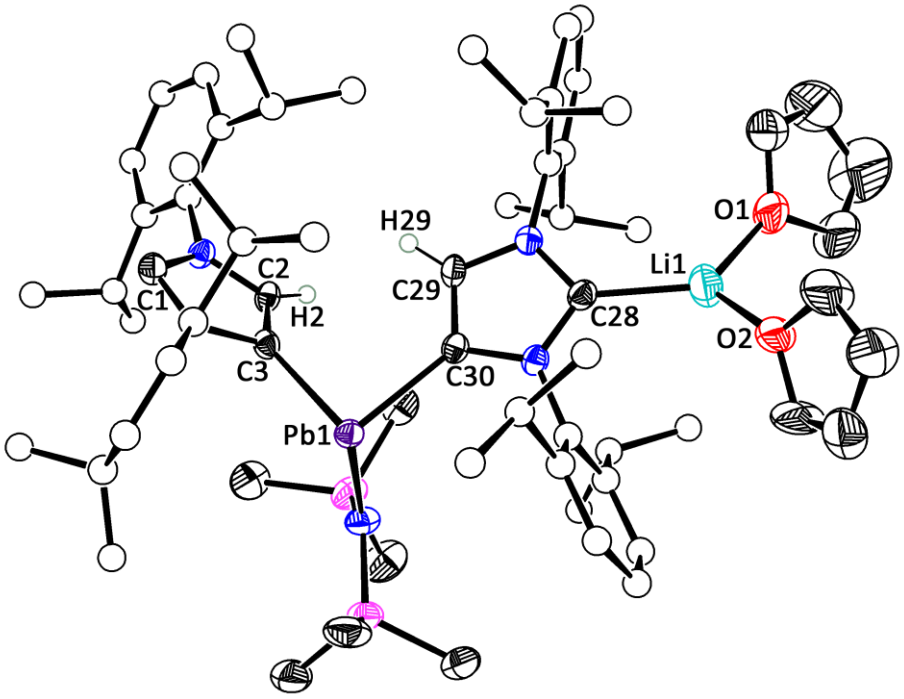

Figure 2.10: Molecular structure of **10**. Anisotropic displacement ellipsoids pictured are set at 50% probability. Hydrogen atoms (with the exception of the imidazole protons labelled H2 and H29) have been omitted for clarity. Atoms of the Dipp groups, H2 and H29 are pictured as spheres of arbitrary radii.

2.4.2 Reactions of a 1 : 1 stoichiometry of $[Li(aIPr:)]_\infty$ with $E[N(SiMe_3)_2]_2$

In contrast to reactions involving **1**, when the lithium salt was employed, it was noted that the reaction mixtures maintained a deeper colour, from green to yellow and orange in the synthesis of **8**, **9** and **10**, respectively. This prompted us to investigate the reactivity of just one equivalent of $[Li(aIPr:)]_\infty$ with $E[N(SiMe_3)_2]_2$.

2.4.2.1 Reaction of $[Li(aIPr:)]_\infty$ with $Ge[N(SiMe_3)_2]_2$

Addition of one equivalent of $[Li(aIPr:)]_\infty$ to $Ge[N(SiMe_3)_2]_2$ in THF gives rise to a deep green colour when the reaction mixture is not cooled below 0 °C. Unfortunately, despite extensive efforts to characterise the green product, this was not possible due to extensive decomposition which rapidly follows its synthesis as evidenced by the decolouration of the reaction mixture within about one hour to give an orange solution from which **8** and $Li[N(SiMe_3)_2]$ could be isolated. The highly coloured complex is likely to be a two coordinate germylene-like species which may be possible due to the higher affinity of the liberated $[N(SiMe_3)_2]^-$ to form stable aggregates with the lithium cation in solution.

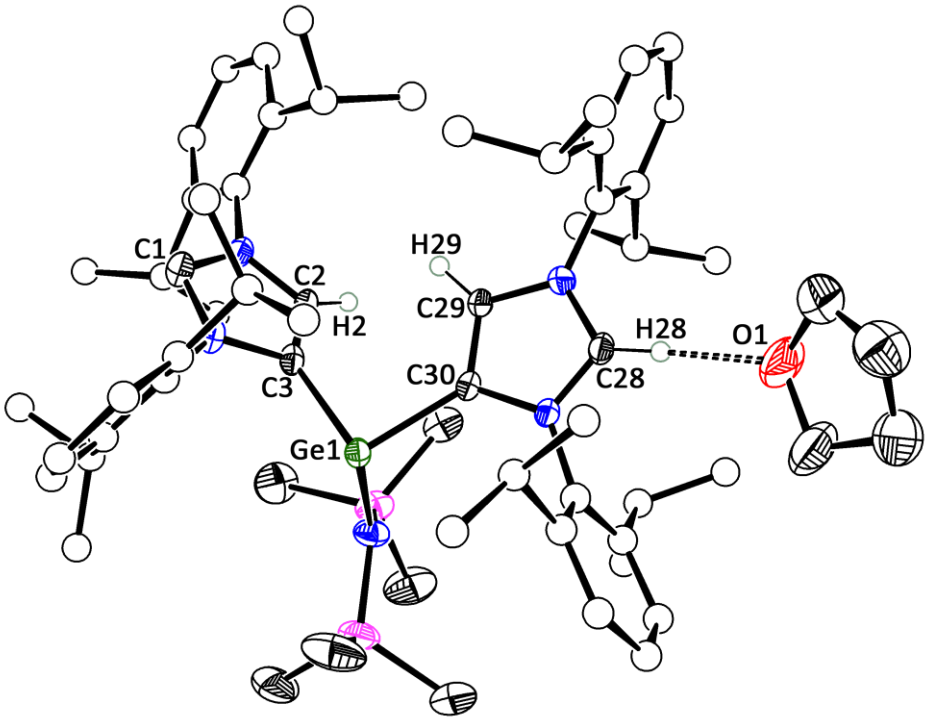

Figure 2.11: Molecular structure of **11**·THF. Anisotropic displacement ellipsoids pictured are set at 50% probability. Hydrogen atoms (with the exception of the imidazole protons labelled H2, H28 and H29) have been omitted for clarity. Atoms of the Dipp groups, H2, H28 and H29 are pictured as spheres of arbitrary radii.

The green colour was persistent when the mixture was maintained below –25 °C and upon immediate removal of the solvent from the reaction mixture at this temperature allowed for

the isolation of a green amorphous powder. However, upon dissolution in d_8-THF, the product that could be isolated was the protonated version of **8**. The neutral, zwitterionic complex [(aIPr)(aIPr:)Ge{N(SiMe$_3$)$_2$}]·THF, **11**·THF, could be characterised and crystallised from a concentrated THF solution. **11** could also be synthesised directly from **8** by the addition of an acid such as [H(OEt$_2$)$_2$][B(3,5-{CF$_3$}$_2$C$_6$H$_3$)$_4$].

Similar to **8**, **9** and **10**, coordination of one of the free NHC moieties does not significantly affect the abnormal bonding interaction, and in **11**, protonation has only a marginal effect of increasing the Ge1–C30 bond length when compared to Ge1–C3 (2.076(2) and 2.064(2) Å, respectively) (Figure 2.11).

2.4.2.2 Reaction of [Li(aIPr:)]$_\infty$ with Sn[N(SiMe$_3$)$_2$]$_2$

Addition of [Li(aIPr:)]$_\infty$ to one equivalent of Sn[N(SiMe$_3$)$_2$]$_2$ in d_8-THF suggests the formation of **3** as determined by ^{1}H NMR spectroscopy. However, upon slow diffusion of hexane into a THF solution of this reaction mixture, single crystals of a novel distannane species, **12**, crystallised (Scheme 2.5).[17] In solution, it is reasoned that the ligands present in these complexes may be fairly labile (especially under such highly basic reactions conditions) hence, upon addition of hexane, aggregates consisting of Li[N(SiMe$_3$)$_2$] are free to form in solution upon elimination of one of the ligands. The exact nature of the amide moiety is not known and is likely to be a mixture of different species whose concentration may vary significantly as hexane diffuses into the solution, substantially changing the properties of the solvent such as the polarity. Upon elimination of one equivalent of Li[N(SiMe$_3$)$_2$], the postulated stannylene intermediate that forms would be susceptible to dimerisation to form a distannene. At this point, the by-product is suitably basic enough to result in the deprotonation of one of the SiMe$_3$ groups which forms part of the distannene intermediate. The carbanion

which forms rapidly attacks the Sn=Sn double bond thereby forming a five-membered heterocycle containing a single Sn–Sn bond.

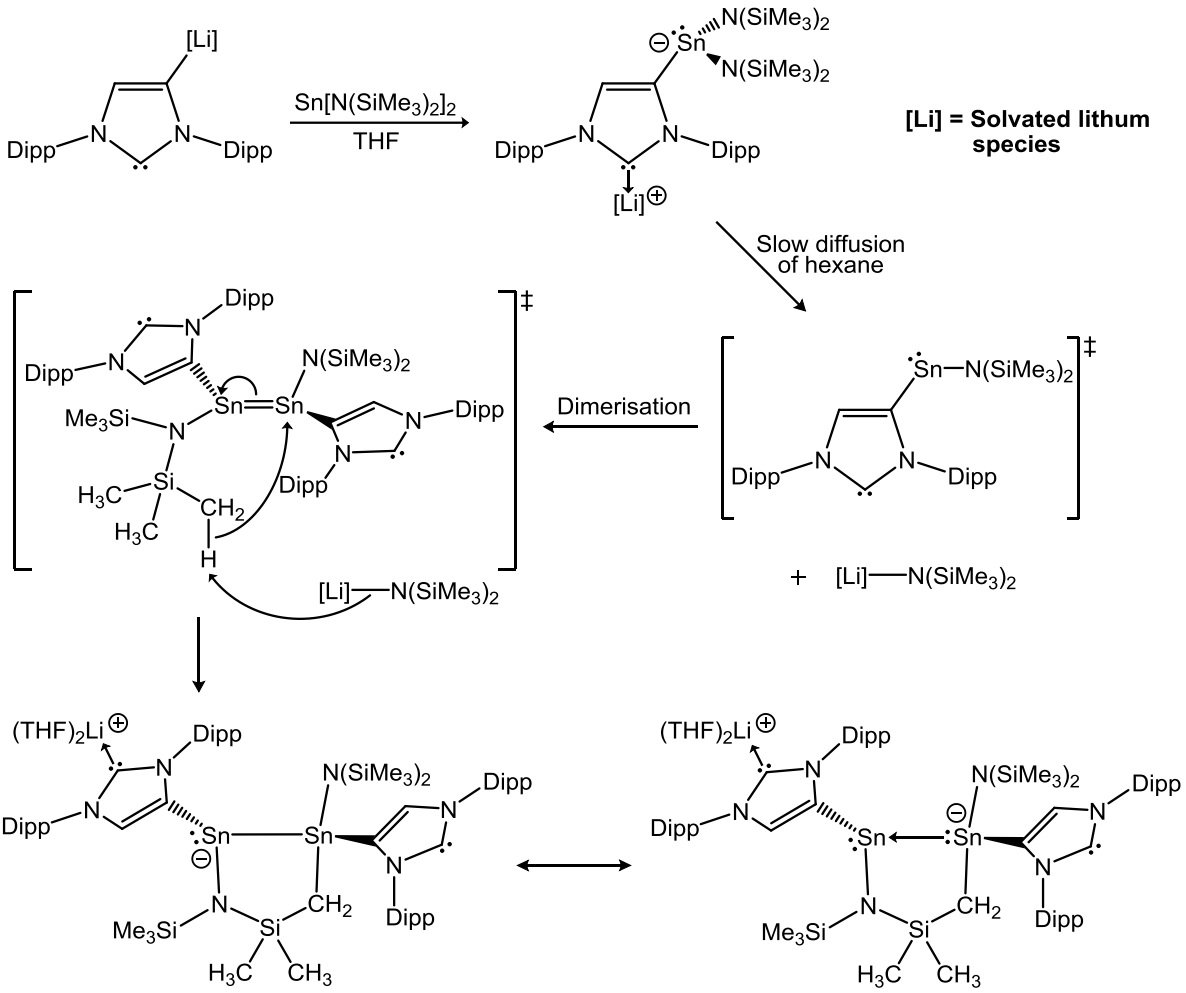

Scheme 2.5: Postulated mechanism for the formation of the distannane, **12**.

There are a handful of reported examples of the bis(trimethylsilyl)amide ligand being deprotonated in basic reaction media. Metallacycle formation such a this has been previously observed in main group complexes and those of the transition metals and the actinides.[18–22] The basicity of the amide by-product is likely also increased due to the presence of free NHC moieties in solution. The free NHC is capable, and has been shown to readily coordinate lithium cations, hence, any amide aggregate which may form in solution is likely to be more

basic, much like the enhancement of the reactivity of ^{n}BuLi by the addition of a chelating ligand such as TMEDA (tetramethylethylenediamine).[23]

The distannane, **12**, was isolated in 54% crystalline yield and characterised by ^{1}H, ^{13}C{^{1}H}, ^{29}Si{^{1}H} and ^{119}Sn{^{1}H} NMR spectroscopy. The two distinct aIPr: ligands can be easily identified by the diagnostic imidazole proton resonances which appear at 7.04 and 6.89 ppm in the ^{1}H NMR spectrum in d_8-THF. In line with a large degree of restricted rotation about the N–Dipp bonds, individual methine resonances which integrate to a single proton can be identified at 3.33, 3.19, 3.06, 2.95 and 2.89 ppm along with three more overlapping methine resonances with an integral of three between 2.78 and 2.87 ppm. Correspondingly, there are numerous overlapping doublet resonances attributable to the various methyl groups of the Dipp substituents between 0.93 and 1.46 ppm. The formation of the metallacycle can be clearly demonstrated by the inequivalence of the $SiMe_3$ groups.

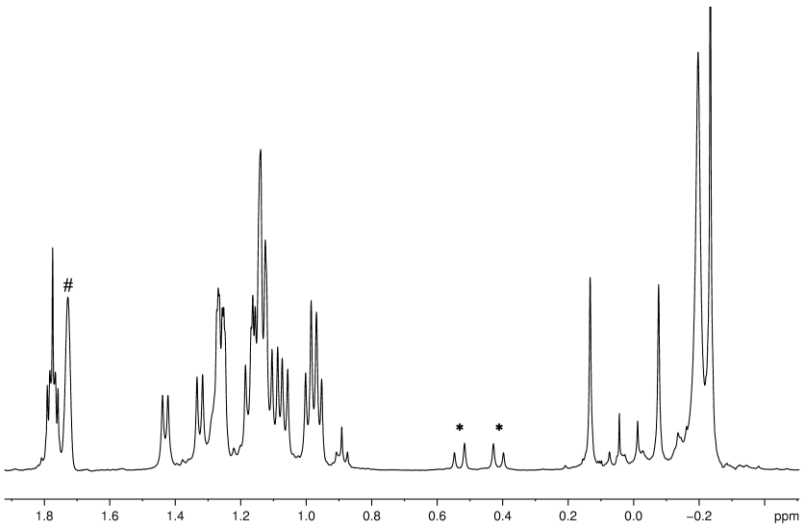

Figure 2.12: ^{1}H NMR spectrum of the aliphatic region of **12** in d_8-THF. Resonances marked with * are due to the CH_2 bridge of the metallacycle. The resonance marked with # is due to residual protons in the NMR solvent.

Most notably, the two inequivalent methyl groups bound to the silicon atom which forms part of the five-membered metallacycle appear as two separate resonances in the ^{1}H NMR

spectrum at 0.13 and –0.08 ppm. Likewise, the two inequivalent protons of the tin bound carbon atom which forms part of the five-membered metallacycle appear as two doublets which couple to one another with a coupling constant of 12 Hz (Figure 2.12). The asymmetric metallacycle can also be observed by the presence of three resonances in the $^{29}Si\{^{1}H\}$ NMR spectrum in an approximate 2 : 1 : 1 ratio as expected. The $^{13}C\{^{1}H\}$ NMR spectrum gives rise to two highly downfield resonances at 221.9 and 215.7 ppm which can be assigned to the two NHC carbons. The resonance at 215.7 ppm is broadened with a *full width at half maximum* (fwhm) of approximately 20 Hz which likely results from coupling to the 92.4% abundant, quadrupolar, ^{7}Li nucleus which has a nuclear spin of $^{3}/_{2}$. Lastly, the ^{119}Sn NMR spectrum clearly shows two resonances at –12.5 and –126.2 ppm due to the presence of two inequivalent tin environments.

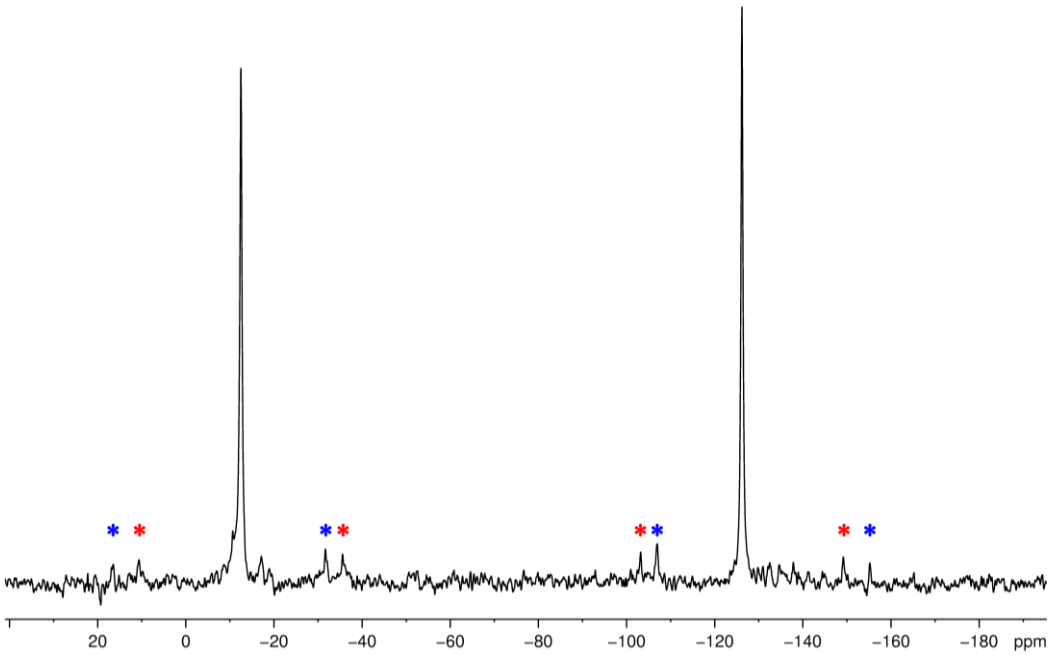

Figure 2.13: $^{119}Sn\{^{1}H\}$ NMR spectrum of **12** in d_8-THF. Resonances marked with * are satellites which result from ^{119}Sn coupling to ^{117}Sn. Resonances marked with * are satellites which result from ^{119}Sn coupling to ^{119}Sn.

The chemical shifts are indicative of shielded tin environments and neither are consistent with a stannylene which give rise to highly downfield shifted resonances, hence the resonance

structure (Scheme 2.5, left) which shows a formal Sn–Sn bond is likely a better description that that of a stannylene stabilised by lone pair donation from a trigonal pyramidal tin(II) anion. The bonding between the two tin centres is further corroborated by the large coupling constant observed as satellites in the $^{119}Sn\{^{1}H\}$ NMR spectrum. The $^{1}J_{^{119}Sn-^{117}Sn}$ is measured to be approximately 8600 Hz and is symmetrically disposed about the central resonance as expected (Figure 2.13, resonances marked with *). The $^{1}J_{^{119}Sn-^{119}Sn}$ coupling constant was measured to be just under 9000 Hz (Figure 2.13, resonances marked with *). These satellites are not symmetric about the main resonance and this is easily explained due to second order effects. The ratio the difference in chemical shift ($\Delta\delta$) and the coupling constant (J) is relatively small (i.e. $\Delta\delta/J \approx 2.4$).

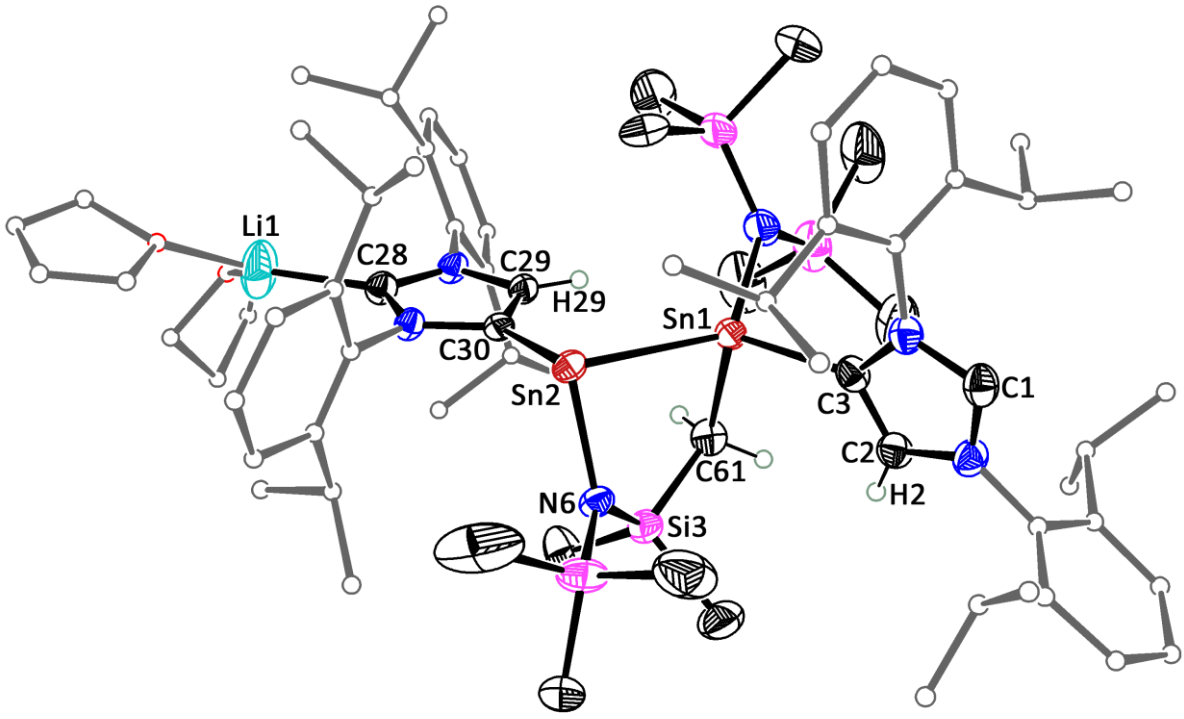

Figure 2.14: Molecular structure of **12**. Anisotropic displacement ellipsoids pictured are set at 50% probability. Hydrogen atoms (with the exception of the imidazole protons labelled H2 and H29 and the unlabelled protons bonded to C61) have been omitted for clarity. Atoms of the Dipp groups, THF molecules, H2 and H29 are pictured as spheres of arbitrary radii.

These second order effects result in the inner resonance of the respective doublet increasing in intensity and the outer resonance decreasing; the main resonance lying at the intensity

weighted mid-point of the satellite and not just equidistant from the two resonances. The coupling constants are particularly large for a $^{1}J_{Sn–Sn}$ coupling constant which may be indicative of a strong single bond between the two tin centres; coupling constants for hexaorganoditins lie approximately in the range of 2000–4000 Hz.[24] The structure of **12** was unambiguously confirmed by single crystal X-ray diffraction which shows the formation of a strained Sn–Sn–N–Si–C metallacycle (Figure 2.14).

The five-membered metallacycle in **12** shows a significant amount of distortion as indicated by the very small angles about the tin atoms. More specifically, the Sn1–Sn2–N6 and Sn2–Sn1–C61 bond angles were found to be 83.7(1)° and 93.3(1)°, respectively. The geometry about Sn2 is trigonal pyramidal, $\Sigma_{\text{bond angles}}$ = 272.4°, which is significantly more distorted than those observed in the previous tin complexes **3** and **9**. Sn2 however, adopts a distorted tetrahedral geometry due to the inherent strain brought about by the five-membered ring. A four-coordinate geometry index, τ_4, was developed in 2007 and is a simple metric to analyse how tetrahedral or square planar a complex may be, much like the τ_5 parameter which quantifies the five-coordinate geometry as either trigonal bipyramidal or square based pyramidal.[25] These parameters are calculated through the use of the two largest bond angles, however numerous structural distortions can result in deformation of a perfect tetrahedral geometry, hence a new τ_4' parameter was developed to differentiate between the largest (β) and second largest bond angles (α).[26]

$$\tau_4 = \frac{360° - (\alpha + \beta)}{360° - 2\theta} \; and \; \tau_4' = \frac{(\beta - \alpha)}{360° - \theta} + \frac{180° - \beta}{180° - \theta} \; where \; \theta = cos^{-1}(-\frac{1}{3})$$

A value of one would be expected for a perfect tetrahedron and zero for a square planar geometry. Hence the τ_4 and τ_4' value for Sn1 (where α = 116.4(1)° and β = 128.4(1)°) can be calculated to be 0.817 and 0.780, respectively, and these values indicate a fair degree of

distortion from a perfect tetrahedral geometry (whereas, for example, the τ_4 and τ_4' values for Si3 are 0.958 and 0.955, respectively, indicating a near perfect tetrahedral geometry).

The Sn1–C3 and Sn2–C30 bond lengths, 2.186(4) and 2.256(3) Å, respectively, are within the expected range of bond lengths observed for abnormal bonding of an NHC to a tin centre. Bonding of the aIPr: coordinated to the lithium cation does show a significantly longer bond length, however, this distance is very similar to that observed in the previous complexes. It is the Sn1–C3 bond length that is particularly short relative to previous Sn–C bond distances and likely is a result of the increased electrophilicity of Sn1 which arises from the donation of the lone pair into a vacant orbital on Sn2 forming a covalent bond and a four-coordinate tin centre (although still formally tin(II)). The Sn–Sn bond length is measured to be 2.869(1) Å which is slightly longer than that expected based on the covalent radius of tin (r_{cov} = 1.39 Å; Σr_{cov} = 2.78 Å),[15] and is slightly longer than the distances observed in hexaphenylditin and a similar heterocyclic compound which resulted from loss of hydrogen from the trimethylsilylamide ligand, $[Sn\{N(SiMe_3)_2\}\{N(SiMe_3)(SiMe_2CH_2)\}]_2$.[20,27] The Sn–Sn bond lengths are 2.770(4) and 2.737(2) Å, respectively, however, a search of the Cambridge Structural Database reveals a wide range in Sn–Sn bond lengths which easily extend beyond 3 Å indicating the elasticity of the bond whose length may be significantly influenced by the steric influence of the ligands as much as the electronic properties of the bonding interaction.

2.4.2.3 Reaction of $[Li(aIPr:)]_\infty$ with $Pb[N(SiMe_3)_2]_2$

When $[Li(aIPr:)]_\infty$ was added to a solution of $Pb[N(SiMe_3)_2]_2$ in a 1 : 1 ratio, the solution again turned a yellow colour, as was the case in the 2 : 1 addition. When carried out in d_8-THF, numerous products could be observed, but not accurately identified in the ^{1}H NMR spectrum of the crude reaction mixture. Slow diffusion of hexane into the THF reaction mixture allowed for the formation of yellow crystals of a product that could be identified by single crystal

X-ray diffraction. The product, **13**, could be identified as the plumbyl species, **10**, which was coordinated to a plumbylene metallacycle (formed by the deprotonation of the amide ligand much like that observed in the formation of **12**) through the pendant NHC moiety. During the crystallisation process, extensive decomposition was observed through the deposition of metallic lead. As the product, **13**, has the core structure observed in **10**, which was the product of the 2 : 1 stoichiometric reaction between $[Li(aIPr:)]_\infty$ and $Pb[N(SiMe_3)_2]_2$, a higher yielding synthetic route was devised. Addition of $Pb[N(SiMe_3)_2]_2$ to a solution of **10** resulted in the quantitative formation of **13** over 24 hours with the generation of $HN(SiMe_3)_2$ as a by-product (Scheme 2.6).[17]

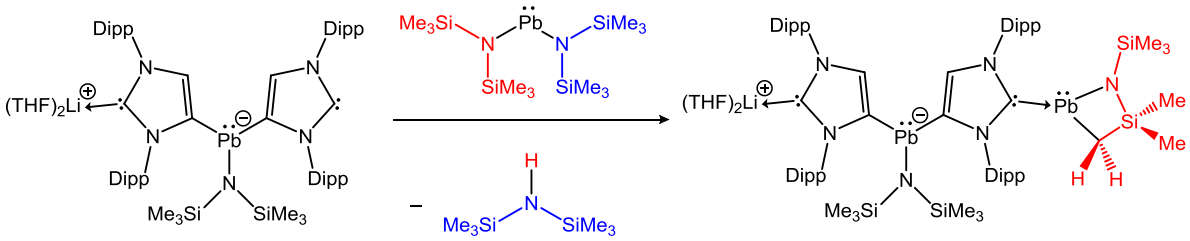

Scheme 2.6: Synthesis of **13** by the addition of $Pb[N(SiMe_3)_2]_2$ to **10**.

It may be possible that in a reaction of 1 : 1 stoichiometry that numerous species form, potentially of the same form as that observed for **12**, i.e. as species with a Pb–Pb bond incorporated into a metallacycle, however, if such a species were to form, it would be reasonable to assume that the strength of bonding between the two lead atoms is quite weak and may be susceptible to decomposition under the reaction conditions which generates $Li[N(SiMe_3)_2]$ and $HN(SiMe_3)_2$ as by-products.

The ^1H NMR spectrum of **13** in d_8-THF clearly shows dynamic behaviour in solution. Firstly, one may expect to observe separate resonances for the two alternatively substituted NHC ligands. However, what is observed is a single alkenic resonance at 7.04 ppm which integrates to two protons and can be ascribed to protons on the imidazole ring. It might also be expected

that the number of resonances observed for the methine and methyl groups to double with respect to those observed for **10**, however there is very little change in the chemical shift of the resonances and the number of resonances remains identical. This result would imply that both ligands are identical in solution, hence, the plumbylene metallacycle moiety must equally reside on both NHC ligands or be free and non-coordinating in solution. Diffusion-Ordered NMR Spectroscopy (DOSY) is a valuable NMR experiment that allows determination of the diffusion constant of species in solution. By applying a gradient, molecules can be spatially labelled based upon their position in the NMR tube, and after allowing diffusion to occur over a specified delay time, their new position can be decoded with a second gradient. The rate of diffusion (and the diffusion constant, *D*) is inversely proportional to the hydrodynamic radius of the species, i.e. larger molecules are slower to diffuse in solution and so have a lower diffusion constant and a smaller attenuation of the NMR resonance would be observed. ^{1}H DOSY NMR reveals that all resonances attributable to **13**, i.e. both the plumbyl core and the plumbylene moiety diffuse at the same rate in solution hence must always be associated in solution on the timescale of the NMR experiment. The calculated value *D* was between 4.5×10^{-10} and 5.5×10^{-10} $m^2\cdot s^{-1}$ for all resonances, cf. 1.5×10^{-9} $m^2\cdot s^{-1}$ calculated for the $HN(SiMe_3)_2$ by-product. What this means is that the plumbylene metallacycle is not a free species in solution as it would have a higher diffusion constant due to its smaller hydrodynamic radius relative to **10**. Therefore, it must be the case that the plumbylene metallacycle is free to change coordination from one of the NHC ligands to one of another species in solution, hence, both ligands appear identical by NMR spectroscopy.

Conclusive evidence for the formation of the four-membered Pb–N–Si–C metallacycle comes from the resonances which arise from the $SiMe_3$ groups. At room temperature, the ^{1}H NMR spectrum reveals four singlet (however broad) resonances at –0.20, –0.41, –0.51 and –1.67 ppm in a ratio of 18 : 6 : 9 : 2 and these can be easily assigned to the $N(SiMe_3)_2$ group

of the core, the two methyl groups of the metallacycle, the terminal N–$SiMe_3$ group, and the CH_2 group bonded to the lead atom forming the plumbylene. However, it would be expected that the methyl group and the CH_2 protons should give separate resonances as part of a rigid metallacycle. It can then be concluded that at room temperature, there is rapid inversion of configuration at the plumbylene lead atom resulting in the equivalence of these resonances (Figure 2.15).

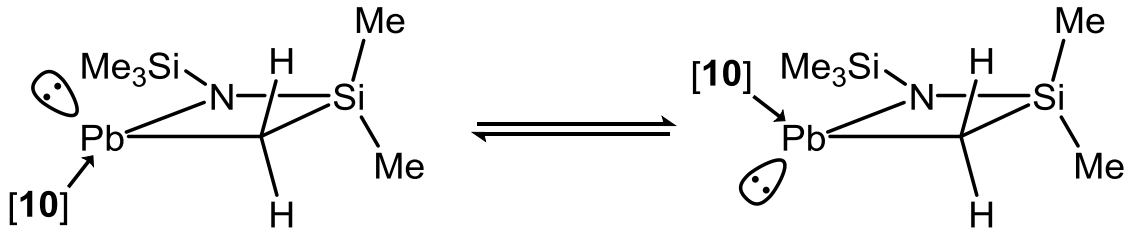

Figure 2.15: Illustration of the inversion of configuration that takes place in **13**.

This dynamic process could be observed by variable temperature ^1H NMR spectroscopy (Figure 2.16). On cooling the NMR sample from 298 K to 238 K, the single resonances observed for the CH_2 group and the two methyl groups broaden and separate into two resonances each due to the inequivalence of the two positions above and below the metallacycle. The two methyl groups give rise to resonances at –0.33 and –0.53 ppm which each integrate to three protons. Furthermore, the CH_2 protons give rise to doublet resonances due to coupling to one another at –1.17 and –2.26 ppm with a coupling constant of 11 Hz. The highly upfield resonances are consistent with the environment of the CH_2 group which is bonded to a lead atom. These sets of resonances were observed to coalesce between 258 K and 278 K. Additionally, upon heating the sample to 338 K, the broad resonances continued to reduce in line width as the rate of inversion increases.

Finally, **13** could also be characterised by $^{13}C\{^1H\}$, $^{29}Si\{^1H\}$ and $^{207}Pb\{^1H\}$ NMR spectroscopy. Two very broad resonances were observable in the $^{13}C\{^1H\}$ NMR spectrum at

200.0 and 193.9 ppm with a fwhm of approximately 500 and 100 Hz, respectively, due to the dynamic processes occurring at room temperature. These can be assigned to the C2 and C4 carbons of the imidazole ring. All carbon resonances for the silicon bound carbons can be observed and identified, except for the CH_2 carbon which is bonded to the lead atom of the plumbylene. It was however, possible to observe cross peaks for this resonance in a Heteronuclear Single Quantum Coherence (HSQC) NMR experiment at 218 K. A cross peak was observed at 22.0 ppm in the ^{13}C domain which correlates with both doublet resonances which were observed for the inequivalent protons of the CH_2 bridge.

As was the case in **12**, three resonances can be observed in the $^{29}Si\{^{1}H\}$ NMR spectrum of **13** as expected. Finally, the room temperature $^{207}Pb\{^{1}H\}$ NMR spectrum displays two extremely broad resonances at 2840.6 and 1674.6 ppm which can be assigned to the plumbylene lead atom and the central plumbyl lead atom.

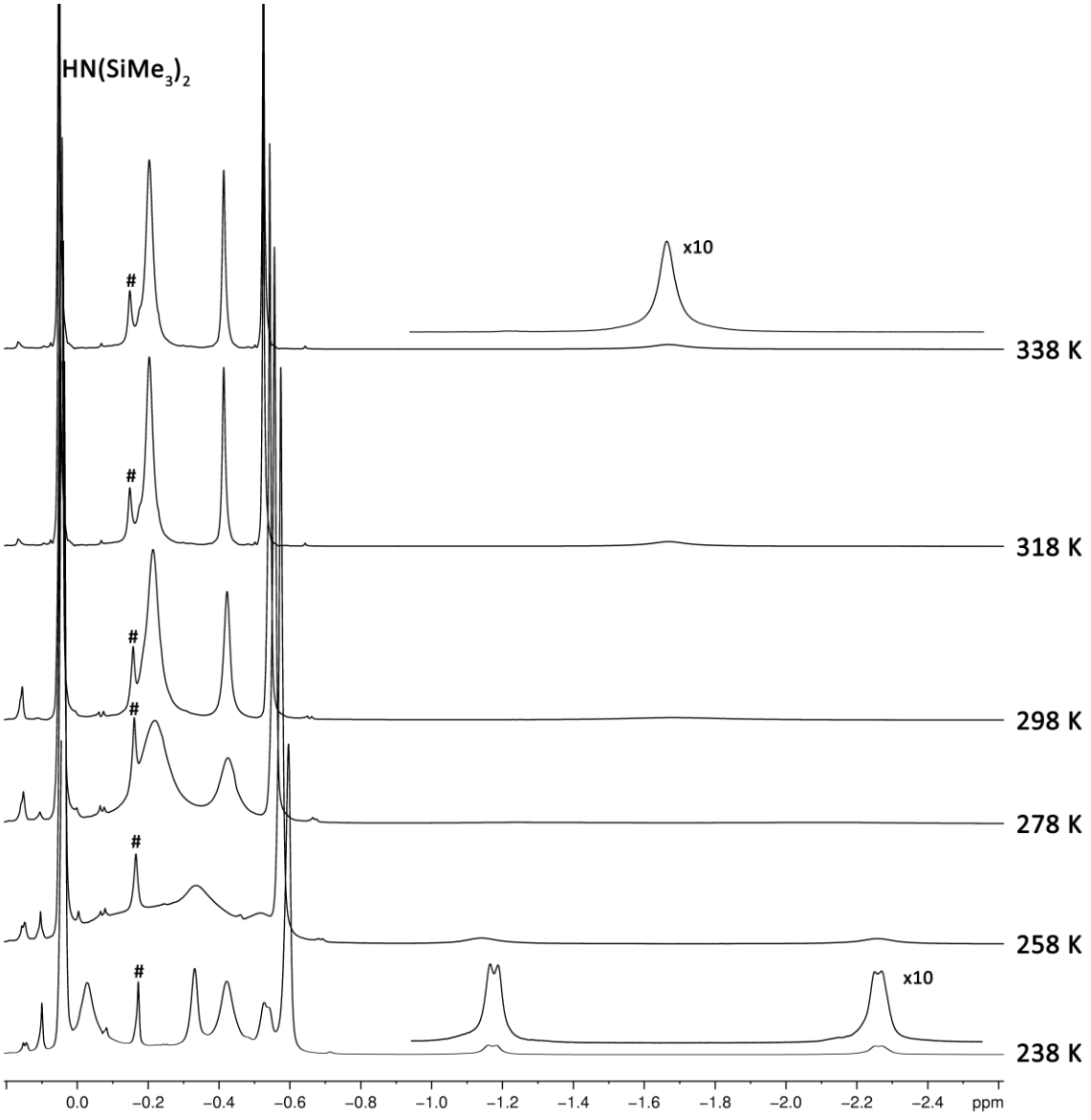

Figure 2.16: Variable temperature ^{1}H NMR of **13** in d_8-THF at 20 K intervals from 238 K to 338 K. Resonances marked with # arise from an unknown impurity.

The structure of **13** was unambiguously confirmed by single crystal X-ray diffraction. Single crystals were grown by slow diffusion of hexane into a THF solution. **13** was also fortuitously crystallised with the plumbylene moiety in both configurations providing crystallographic evidence for the inversion process which was suggested to take place (Figure 2.17 and 2.18). Both isomers were found to crystallise in the Sohncke space group, that is one without a mirror plane or inversion symmetry, $P2_1$. Both samples were determined to be enantiopure crystals with Flack parameters calculated at 0.069(5) and 0.046(3).[28]

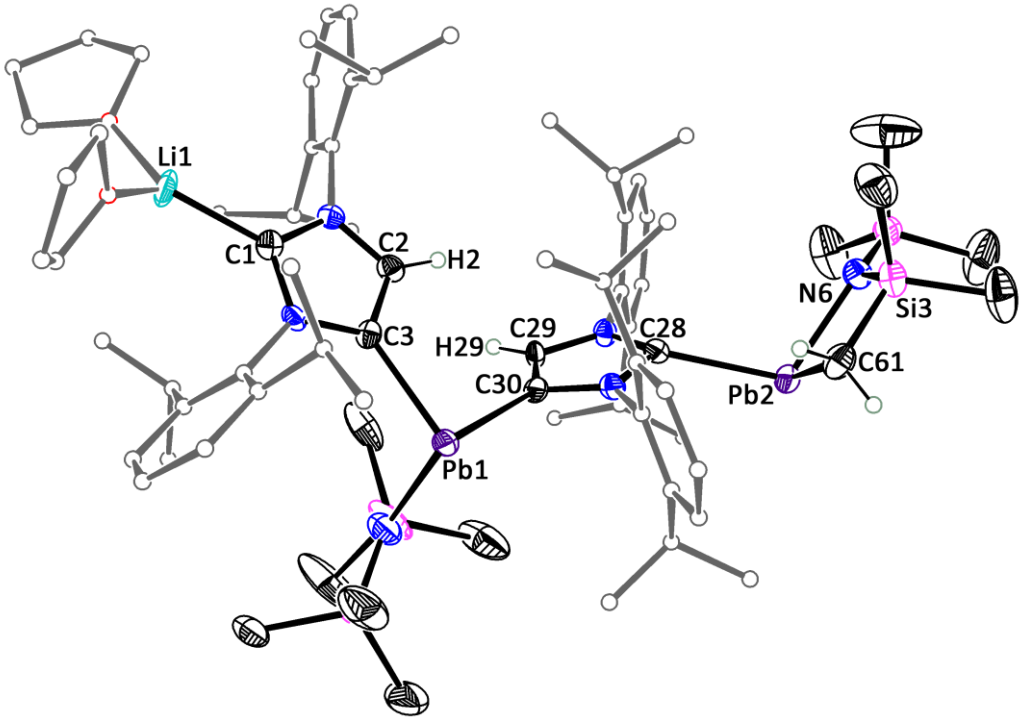

Figure 2.17: Molecular structure of one isomer of **13**. Anisotropic displacement ellipsoids pictured are set at 50% probability. Hydrogen atoms (with the exception of the imidazole protons labelled H2 and H29 and the unlabelled protons bonded to C61) have been omitted for clarity. Atoms of the Dipp groups, THF molecules and hydrogen atoms are pictured as spheres of arbitrary radii.

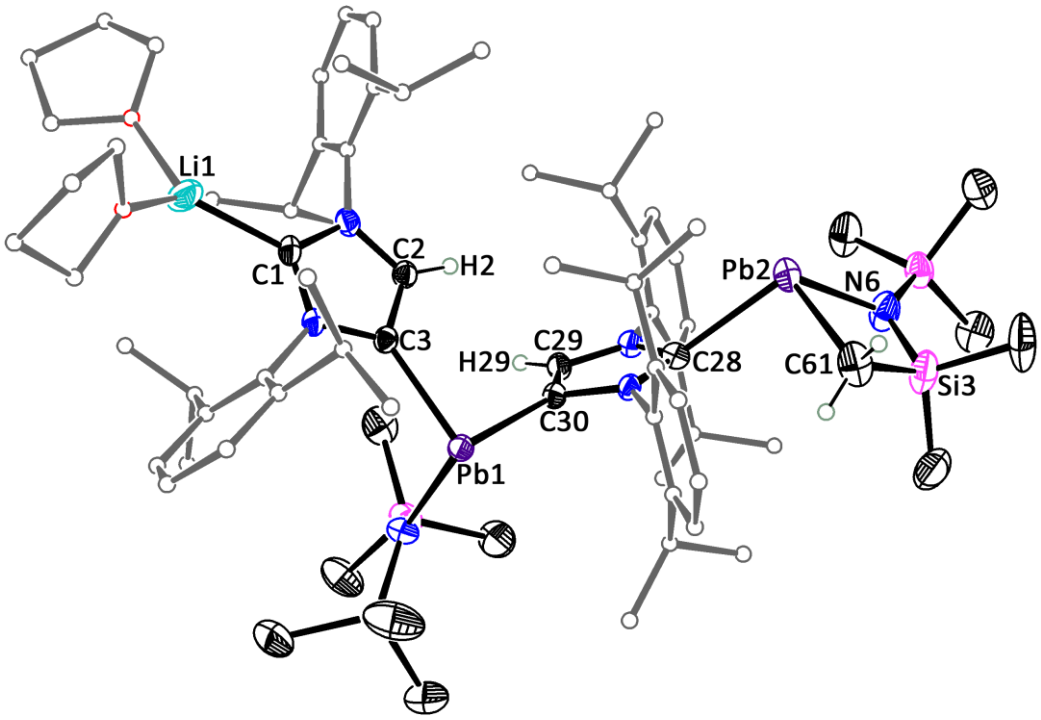

Figure 2.18: Molecular structure of one isomer of **13**. Anisotropic displacement ellipsoids pictured are set at 50% probability. Hydrogen atoms (with the exception of the imidazole protons labelled H2 and H29 and the unlabelled protons bonded to C61) have been omitted for clarity. Atoms of the Dipp groups, THF molecules and hydrogen atoms are pictured as spheres of arbitrary radii.

The structural parameters for both isomers of **13** were found to be very similar, if not identical within experimental error. The Pb1–C3 bond lengths were observed to be 2.356(9) and 2.366(8) Å and the Pb1–C30 bond lengths 2.394(9) and 2.403(9) Å. The Pb1–C30 bond lengths are notably longer than those of the previously recorded Pb–C bond lengths by up to 0.5 Å which may indicate a weaker bonding interaction as a result of the presence of the coordinating plumbylene metallacycle.

The Pb2–C28 bond distance was found to vary between the two isomers, however, both were still significantly longer than the other Pb–C distances observed in all previous complexes at 2.472(9) and 2.522(9) Å. The large difference between the two isomers may just be a result of crystal packing. The bond lengths of Pb2 to both N6 and C61 were found to be shorter than other Pb–N and Pb–C bond lengths observed elsewhere. The Pb2–C61 distances, for example, are 2.325(13) and 2.327(11) Å and likely result due to the inherent strain of the four-membered metallacycle which preferentially brings the substituents closer so as to increase the N6–Pb2–C61 bond angle which can be measured to be highly acute, 72.7(4)° and 73.2(4)°. In these two low energy conformations, the lead atom of the plumbylene unit retains a trigonal pyramidal geometry as observed in **7** and **10** ($\Sigma_{\text{bond angles}}$ = 280.0° and 280.2°). Finally, the plumbylene unit does not coordinate directly in the plane with the carbene carbon of the NHC. This can be seen by the slight distortion from trigonal planar as would be expected for the carbene carbon ($\Sigma_{\text{bond angles}}$ = 351.5° and 351.7°). This is likely due to the steric bulk of the Dipp groups which forces the plumbylene metallacycle to coordinate slightly out of the plane of the imidazole ring.

2.5 Conclusions

This chapter has described the synthesis of a new alkali metal salt of a ditopic carbanionic NHC, **1**, $[K(aIPr:)]_\infty$, from the alkali metal exchange of lithium in the known compound $[Li(aIPr:)]_\infty$ for potassium. The use of **1** as a synthon for the generation of novel polar organometallic species was demonstrated by the 1 : 1 and 2 : 1 addition products with group 12 and 14 bis(trimethylsilyl)amides. The equivalent reactivity with the lithium salt demonstrated a mixture of reactivity. Along with the formation of similar lithium salts of the novel polar organometallic species, the lithium by-products influence the further reactivity of such species resulting in the formation of novel stannylene and plumbylene complexes **12** and **13**.

2.6 References

(1) Demore, W. B.; Benson, S. W. *Advances in Photochemistry, Volume 2*; John Wiley & Sons, Inc.: Hoboken, 1964, pp 219–261.

(2) Gleiter, R.; Hoffmann, R. *J. Am. Chem. Soc.* **1968**, *90* (20), 5457–5460.

(3) Guerret, O.; Solé, S.; Gornitzka, H.; Teichert, M.; Trinquier, G.; Bertrand, G. *J. Am. Chem. Soc.* **1997**, *119* (28), 6668–6669.

(4) Wang, Y.; Xie, Y.; Abraham, M. Y.; Wei, P.; Schaefer III, H. F.; Schleyer, P. v. R.; Robinson, G. H. *J. Am. Chem. Soc.* **2010**, *132* (41), 14370–14372.

(5) Gynane, M. J. S.; Harris, D. H.; Lappert, M. F.; Power, P. P.; Rivière, P.; Rivière-Baudet, M. *J. Chem. Soc., Dalton Trans.* **1977**, 2004–2009.

(6) Cotton, J. D.; Davidson, P. J.; Lappert, M. F. *J. Chem. Soc., Dalton Trans.* **1976**, 2275–2286.

(7) Schaeffer, C. D.; Zuckerman, J. J. *J. Am. Chem. Soc.* **1974**, *96* (22), 7160–7162.

(8) Chorley, R. W.; Hitchcock, P. B.; Lappert, M. F.; Leung, W.-P.; Power, P. P.; Olmstead, M. M. *Inorg. Chim. Acta* **1992**, *198–200*, 203–209.

(9) Fjeldberg, T.; Hope, H.; Lappert, M. F.; Power, P. P.; Thorne, A. J. *J. Chem. Soc., Chem. Commun.* **1983**, 639–641.

(10) Lappert, M.; Protchenko, A.; Power, P.; Seeber, A. *Subvalent Amides of Silicon and the Group 14 Metals*; John Wiley & Sons, Ltd.: Chichester, 2008, pp 263–326.

(11) Schlosser, M.; Strunk, S. *Tetrahedron Lett.* **1984**, *25* (7), 741–744.

(12) Schlosser, M. *Pure Appl. Chem.* **1988**, *60* (11), 1627–1634.

(13) Waters, J. B.; Goicoechea, J. M. *Dalton Trans.* **2014**, *43* (38), 14239–14248.

(14) Pyykkö, P.; Atsumi, M. *Chem. Eur. J.* **2009**, *15* (1), 186–197.

(15) Cordero, B.; Gómez, V.; Platero-Prats, A. E.; Revés, M.; Echeverría, J.; Cremades, E.; Barragán, F.; Alvarez, S. *Dalton Trans.* **2008**, 2832–2838.

(16) Waters, J. B.; Turbervill, R. S. P.; Goicoechea, J. M. *Organometallics* **2013**, *32* (18), 5190–5200.

(17) Waters, J. B.; Tucker, L. S.; Goicoechea, J. M. *Organometallics* **2017**, DOI: 10.1021/acs.organomet.7b00352.

(18) Bradley, D. C.; Dawes, H. M.; Hursthouse, M. B.; Powell, H. R. *Polyhedron* **1988**, *7* (19–20), 2049–2051.

(19) Yu, X.; Bi, S.; Guzei, I. A.; Lin, Z.; Xue, Z.-L. *Inorg. Chem.* **2004**, *43* (22), 7111–7119.

(20) Veith, M.; Gasthauer, M.; Zimmer, M.; Huch, V. *Z. Anorg. Allg. Chem.* **2007**, *633* (13–14), 2274–2277.

(21) Bell, N. L.; Maron, L.; Arnold, P. L. *J. Am. Chem. Soc.* **2015**, *137* (33), 10492–10495.

(22) Johnson, K. R. D.; Hayes, P. G. *Polyhedron* **2016**, *108*, 43–49.

(23) Chalk, A. J.; Hoogeboom, T. J. *J. Organomet. Chem.* **1968**, *11*, 615–618.

(24) Mitchell, T. N. *J. Organomet. Chem.* **1974**, *70* (1), C1–C2.

(25) Yang, L.; Powell, D. R.; Houser, R. P. *Dalton Trans.* **2007**, 955–964.

(26) Okuniewski, A.; Rosiak, D.; Chojnacki, J.; Becker, B. *Polyhedron* **2015**, *90*, 47–57.

(27) Preut, H.; Haupt, H.-J.; Huber, F. *Z. Anorg. Allg. Chem.* **1973**, *396* (1), 81–89.

(28) Flack, H. D.; Bernardinelli, G. *Chirality* **2008**, *20* (5), 681–690.

Chapter 3

Synthesis of aIPr and aIPr: complexes of group 12 and 14 halides

3.1 Introduction and objectives

3.1.1 Reactivity of [Li(aIPr:)]$_\infty$ with main group halides

Various alkali metal salts have been shown to be useful in the synthesis of a range of (aIPr:)GaR_3 complexes (see Section 1.6.2.2). The subsequent chemistry of the remaining carbene functionality was also demonstrated by the addition of a variety of electrophiles such as MeOTf, MeOH, Me_3SiCl and allyl bromide (H_2C=CH–CH_2Br).[1,2] The Robinson group have investigated the reactivity of [Li(aIPr:)]$_\infty$ with main group halides such as $GaCl_3$ and $SiCl_4$. The use of halide reagents allows for the subsequent functionalisation of the resulting complexes, while the presence of a Lewis acidic main group element may afford interesting reactivity.

The deprotonation of the NHC adduct (IPr)BEt_3 has been shown to proceed via the backbone deprotonated complex (aIPr·BEt_3)Li$(THF)_3$. Upon addition of ^{n}BuLi to the adduct at –78 °C, the C4 lithiated species can be isolated and used for further coordination chemistry using the backbone of the imidazole ring.[3] In refluxing THF, this complex isomerises to afford the C4–borylated complex (aIPr·Li$(THF)_2$)BEt_3, a complex previously reported to form by the addition of [Li(aIPr:)]$_\infty$ directly to BEt_3 in toluene. These two compounds serve as a source of an anionic deprotonated IPr ligand that can coordinate with the C2 or C4 position (whereby the other position is occupied by the BEt_3 group). This was subsequently demonstrated by the reactivity of both isomers with $GaCl_3$. Both isomers are assumed to react with $GaCl_3$ by coordination of the lithiated carbon with the gallium centre. However, subsequent work up of both reaction mixtures resulted in decomposition, likely through solvent mediated protonation. The C2 coordinated BEt_3 group in the postulated [(aIPr·BEt_3)$GaCl_3$]$^-$ is liberated and the resulting anionic species is protonated to afford the zwitterionic (aIPr)$GaCl_3$, the

abnormal isomer of (IPr)$GaCl_3$.[4] In the alternative isomer, the C4 coordinated BEt_3 group loses ethyllithium, likely through protonolysis of the postulated $[(aIPr{\cdot}GaCl_3)BEt_3]^-$ resulting in the isolation of the zwitterionic $(aIPr{\cdot}GaCl_3)BEt_2$. It would appear, although not a conclusive result, as though elimination of LiCl does not occur in these complexes to afford a three-coordinate gallium centre and that only adduct formation occurs.

A salt metathesis reaction, with elimination of LiCl, was possible by the addition of $[Li(aIPr:)]_\infty$ to $SiCl_4$ in hexane or to R_2SiCl_2 (R = Me or Ph) in toluene.[5,6] The addition of either one or two equivalents of the lithium reagent in an non-polar solvent such as hexane or toluene allowed for the synthesis of silicon functionalised IPr ligands upon elimination of the alkali metal salt, LiCl.

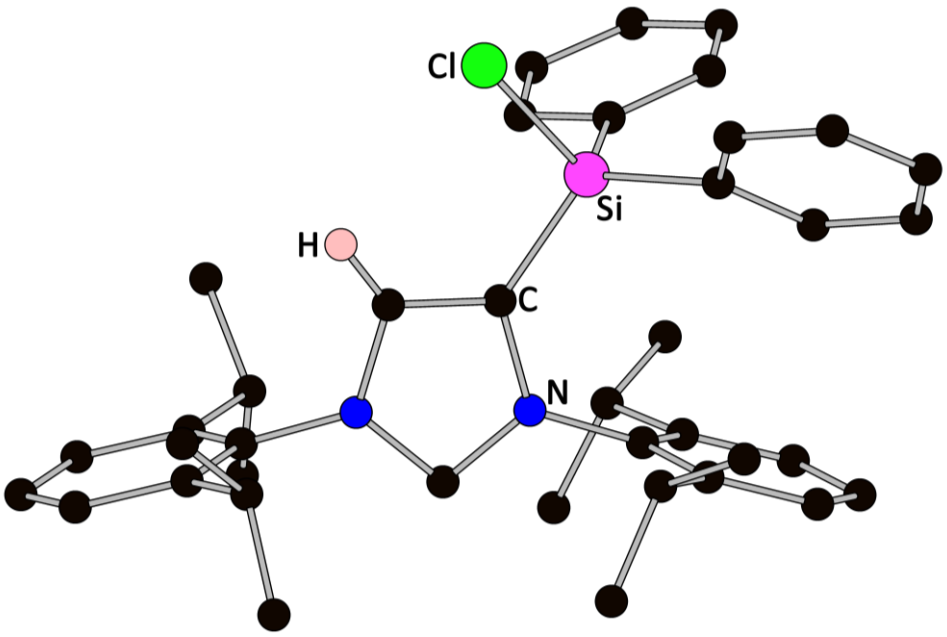

Figure 3.1: Ball and stick model of (aIPr:)$SiClPh_2$. Hydrogen atoms (with the exception of the imidazole proton) have been omitted for clarity.

Neutral products such as (aIPr:)$SiCl_3$, (aIPr:)$SiClPh_2$ (Figure 3.1) and (aIPr:)$_2SiPh_2$ could be isolated in reasonable to high yield from such reaction mixtures. Finally, the availability of the carbene functionality was demonstrated by coordination to copper(I) chloride, or by

protonation by an acidic reagent such as $HNEt_3Cl$ or CH_2Cl_2 (Scheme 3.1). On reaction of (aIPr:)$SiCl_3$ with CH_2Cl_2, a redistribution of the abnormal IPr ligands results in the isolation of the cationic complex, $[(aIPr)_2SiCl_3]^+$ presumably with the elimination of half an equivalent of $SiCl_4$. It is interesting to note that ligand transfer can take place despite the acidity of the solvent, which could result in the generation of the imidazolium salt on protonation of the silylated C4 carbon.

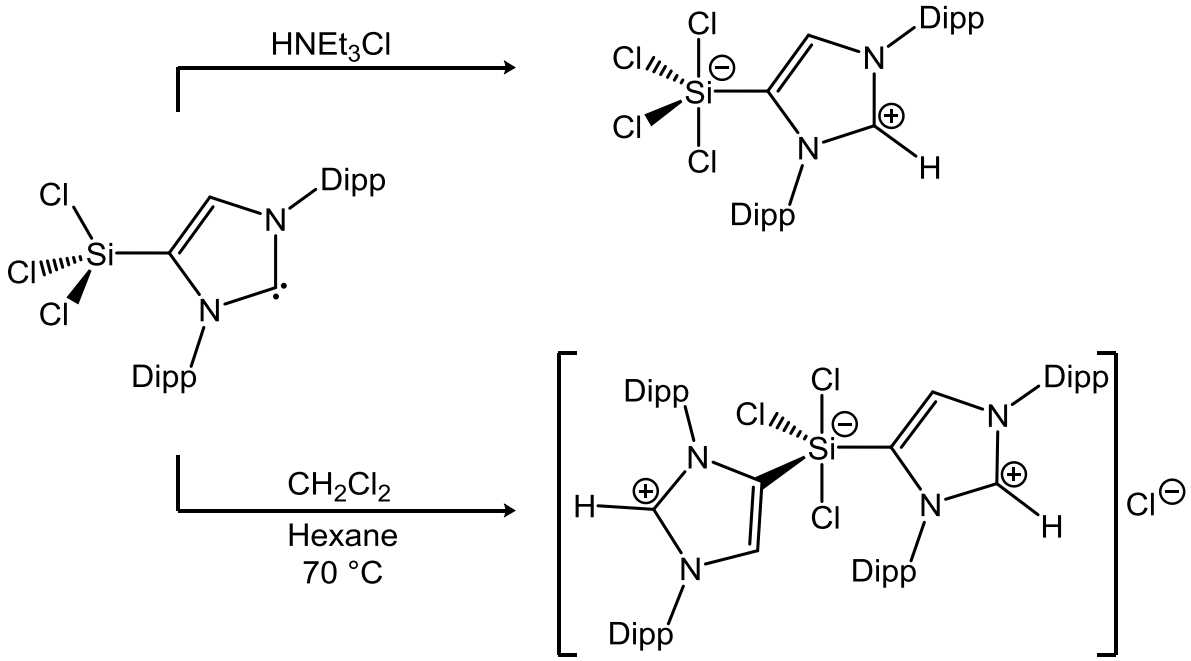

Scheme 3.1: aIPr products which result from protonation of (aIPr:)$SiCl_3$ by $HNEt_3Cl$ or CH_2Cl_2.

This year, Robinson and co-workers were able to synthesise a multi-metallic compound bearing aIPr: ligands. Reaction of (aIPr:)$SiCl_3$ with $[(\eta^5\text{-}C_5H_4Li)_2Fe]_3(TMEDA)_2$ results in the formation of the silyl bridged ferrocene bearing an aIPr: ligand coordinated to the silicon atom.[7] Subsequent reaction with $GeCl_2$·dioxane affords the corresponding $GeCl_2$ adduct through use of the remaining carbene functionality (Figure 3.2). Reaction of two equivalents of (aIPr:)$SiClMe_2$ with $[(\eta^5\text{-}C_5H_4Li)_2Fe]_3(TMEDA)_2$ allows for the formation of a bis(aIPr:) species whereby the ferrocene moiety is functionalised with two $SiMe_2$(aIPr:) groups. Similarly, coordination of $GeCl_2$ by the free carbene moieties was shown to be possible and

the postulated reduction of such compounds could result in the formation of organometallic polymers linked through main group diatomics, i.e. Ge_2. These results indicate the usefulness of such ligands in synthesis and the possibility for bis(aIPr:) species to employed for the synthesis of organometallic polymers.

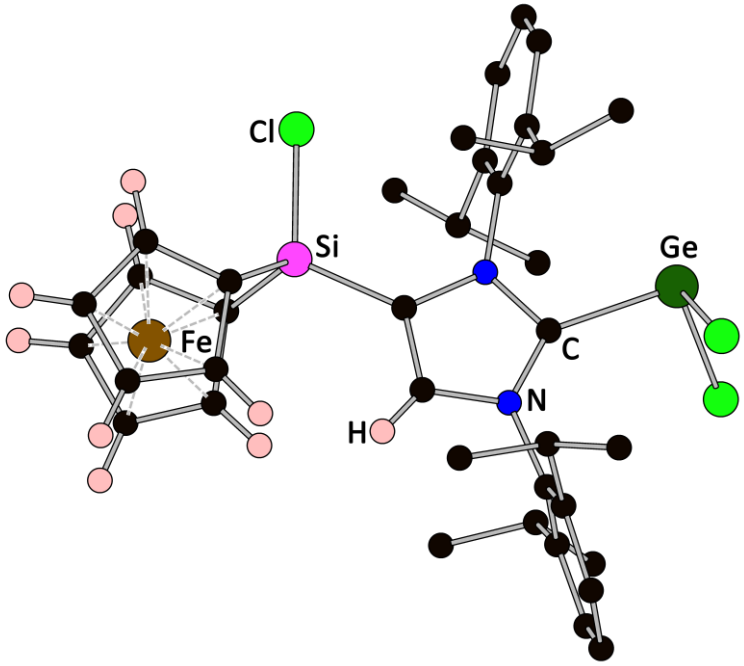

Figure 3.2: Ball and stick model of (aIPr·$GeCl_2$)SiCl{(C_5H_4)$_2$Fe}. Hydrogen atoms (with the exception of the imidazole proton and Cp protons) have been omitted for clarity.

3.1.2 Chapter outline

These results illustrate the synthetic utility of [Li(aIPr:)]$_\infty$ as a reagent in the synthesis of main group complexes bearing aIPr: ligands. We sought to compare and contrast the use of both [Li(aIPr:)]$_\infty$ and [K(aIPr:)]$_\infty$ as reagents for the synthesis of main group complexes bearing aIPr: ligands. This chapter will discuss the synthesis of mercury, silicon, germanium and tin halide complexes bearing aIPr: ligands and the subsequent chemistry of such species.

3.2 Synthesis of novel mercury compounds

3.2.1 Synthesis of (aIPr:)$_2$Hg (14)

As a method of synthesising neutral main group complexes bearing aIPr: ligands, we sought to access the organomercury compound (aIPr:)$_2$Hg (**14**) by a salt metathesis reaction of two equivalents of [M(aIPr:)]$_\infty$ (M = Li or K) with $HgCl_2$ (Scheme 3.2). This proof-of-concept reaction allowed for the determination of the conditions under which **14**, and any further novel species, could be synthesised. It was determined that (aIPr:)$_2$Hg can be synthesised by the addition of [Li(aIPr:)]$_\infty$ in THF or toluene, however in the former, the LiCl by-product is soluble in the reaction solvent hence the product must be extracted into a non-coordinating solvent such as toluene or hexane in order to separate it from the metal halide. A 57% yield of **14** was obtained by reaction of [K(aIPr:)]$_\infty$ with $HgCl_2$ in THF, thereby generating KCl which is insoluble and forms a viscous precipitate during the reaction and can be removed by filtration.

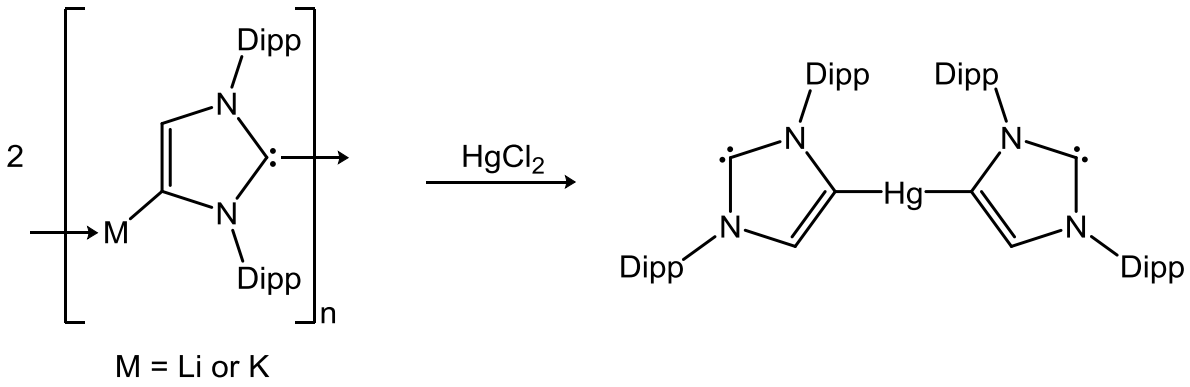

Scheme 3.2: Synthesis of **14** from either [Li(aIPr:)]$_\infty$ or [K(aIPr:)]$_\infty$ with $HgCl_2$.

14 was characterised by ^{1}H, ^{13}C{^{1}H} and ^{199}Hg{^{1}H} NMR spectroscopy. The ^{1}H NMR spectrum of **14** in d_8-THF was very similar to that observed for **1**; a single alkenic resonance observed at 6.94 ppm which integrates to two protons can be ascribed to the imidazole protons

and the two expected methine resonances appear at 2.76 and 2.70 ppm. Likewise, the carbenic carbon, carbanionic carbon and the protonated alkenic carbon resonances were observed in the $^{13}C\{^{1}H\}$ NMR spectrum at 222.4, 162.0 and 129.1 ppm. The carbanionic carbon centre shows the greatest change in chemical shift relative to that observed for **1** in d_8-THF ($\Delta\delta$ = 14.3 ppm cf. 176.3 ppm for **1**). Finally, a single resonance was observed at –635.0 ppm in the $^{199}Hg\{^{1}H\}$ NMR spectrum in d_8-THF, however, this shifts to –551.4 ppm upon dissolution in C_6D_6 indicating a possible interaction between the two-coordinate mercury centre and the coordinating THF molecules in solution which results in a significant upfield shift.

14 was crystallised from a saturated hexane solution at –35 °C (Figure 3.3). The colourless crystals that form have a visually octahedral shape, potentially indicative of the underlying crystal symmetry. Crystals of **14** could not be grown from any other solvent combinations. Multiple attempts to analyse the crystals formed from the cooled hexane solution produced a cubic unit cell where a = 66.9373(3) Å. A full data set was obtained using both Mo Kα and Cu Kα at 150 K. A solution was obtained by solving the structure in $Fd\bar{3}c$, a face centred cubic space group with 192 molecules in the unit cell and there was no apparent twinning giving rise to the high order space group. The crystal structure solution provides evidence for the formation of the expected (aIPr:)$_2$Hg, however, there is significant electron density that remains unaccounted for and is likely highly disordered hexane which is free to diffuse through the large pores that lie in the crystal structure. This is further substantiated by the observation that the colourless crystals rapidly desolvated once removed from the mother liquor. In order to select crystals of **14** suitable for a single crystal X-ray diffraction experiment, the crystals must be mounted from a pre-chilled microscope slide containing a mixture of Paratone-N® oil and the mother liquor rapidly upon removal from the crystallisation flask. Attempts to account for the disordered solvent using the SQUEEZE[8] tool

in the program *PLATON* were unsuccessful due to the large volume of the unit cell which significantly increased the computational efforts for the calculation. As a result, the final structure solution is currently not of publishable standard, however, the molecular structure of **14** can be determined hence discussed with appropriate caution.

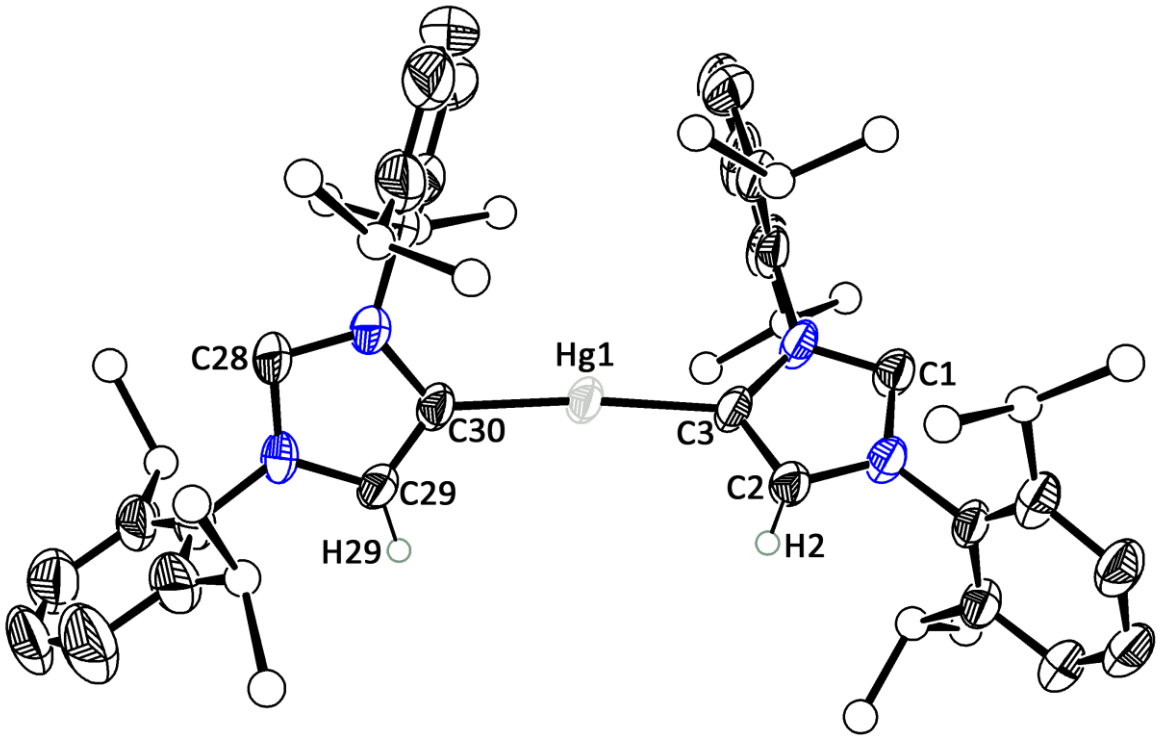

Figure 3.3: Molecular structure of **14**. Anisotropic displacement ellipsoids pictured are set at 50% probability. Hydrogen atoms (with the exception of the imidazole protons labelled H2 and H29) have been omitted for clarity. Atoms of the ^{i}Pr groups, H2 and H29 are pictured as spheres of arbitrary radii.

The geometry about the mercury atom was found to be approximately linear which is to be expected for a diorganomercury compound (C30–Hg1–C3 = 173.4(2)°). This is likely distorted due to the orientation that the aIPr: ligands adopt which brings two of the Dipp substituents towards one another as opposed to the maximum distance apart. This may be a π-stacking effect by interaction of the aromatic rings with that of the mercury centre. The Hg1–C3 and Hg1–C30 bond lengths were observed to be 2.045(6) and 2.048(6) Å. These distances are shorter than average Hg–C bond lengths and within the sum of covalent radii

(Σr_{cov} = 2.05 Å).[9] Although there is no obvious preferred orientation of the ligands, a torsion angle between C29–C30–C3–C2 of 38.8° arises from the stacking of the two eclipsing Dipp groups. Finally, further evidence for the formation of **14** was obtained by electron impact mass spectrometry (EI-MS) which displayed a mass envelope at 976.2751 which can be ascribed to the molecular ion, $[(aIPr)_2Hg]^+$ (Calcd 976.5318) .

3.2.2 Further chemistry of (aIPr:)$_2$Hg

Confirmation of the synthesis of **14** was also obtained by the investigation into its further reactivity. Addition of an equivalent of $[K(aIPr:)]_\infty$ to **14** in THF results in the formation of the previously reported trigonal planar species $[(aIPr:)_3Hg]^-$ (**15**) as the potassium salt which was crystallised as the $[K(2,2,2\text{-crypt})]^+$ salt upon addition of 2,2,2-crypt (Scheme 3.3). **15** was characterised by ^{1}H, ^{13}C{^{1}H} and ^{199}Hg{^{1}H} NMR spectroscopy. The trigonal planar geometry of **15** results in the imidazole proton being directed to lie above the aromatic ring of an adjacent Dipp group resulting in a significant upfield shift (δ = 4.37 ppm). It was possible to identify ^{199}Hg satellites in the ^{13}C{^{1}H} NMR spectrum of **15** in d_8-THF; coupling constants of 1526 Hz and 153 Hz were observed for the carbanionic carbon directly bonded to the mercury atom and the alkenic imidazole carbon, two bonds from the mercury centre. Finally, at single resonance was observed in the ^{199}Hg{^{1}H} spectrum at 14.0 ppm.

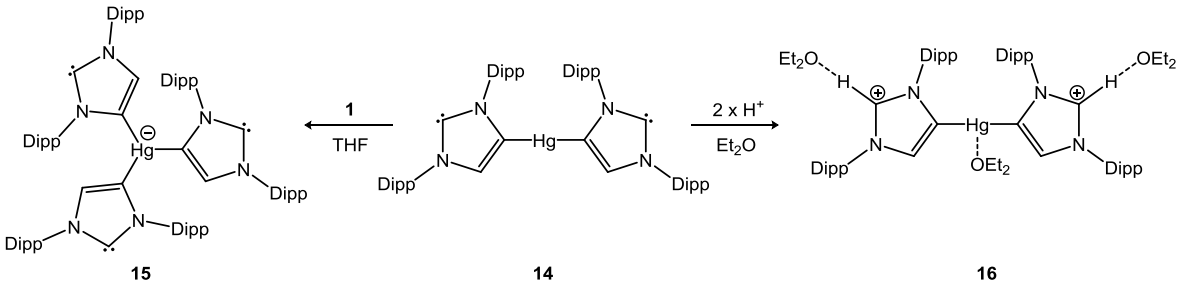

Scheme 3.3: Synthesis of **15** by addition of $[K(aIPr:)]_\infty$ or **16** by addition of Brookhart's acid to **14**.

Final evidence came from the protonation of **14** using an acid with a non-coordinating anion. Two equivalents of Brookhart's acid, $[H(OEt_2)_2][B(3,5\text{-}\{CF_3\}_2C_6H_3)_4]$,[10] was added to a diethyl ether solution of **14** resulting in the protonation of both vacant carbene moieties and the generation of a dicationic diorganomercury salt, **16** (Scheme 3.3), which is the first example of an abnormal NHC–Hg compound. $[(aIPr{\cdot}Et_2O)_2Hg(Et_2O)]^{2+}$ crystallises as a tris(diethyl ether) solvate whereby two solvent molecules form a strong hydrogen bonding interaction with the imidazole proton which remains fairly acidic. A third molecule coordinates the mercury centre and all three diethyl ether molecules are retained under vacuum as evidenced by ^{1}H NMR spectroscopy and by elemental analysis of a crystalline sample. Protonation of the carbene moiety was clearly demonstrated by the presence of a deshielded doublet resonance in the ^{1}H NMR spectrum at 9.82 ppm with a 1 Hz coupling constant. The coupling arises due to the four bond coupling to the other imidazole proton which can be observed at 7.86 ppm. Again this resonance is shifted upfield relative to that of **14** due to the positive charge that now exists on the imidazole ring. The three imidazole carbon resonances for the carbanionic carbon centre, the protonated C2 imidazole carbon and the protonated alkenic carbon appear at 162.8, 142.8 and 133.9 ppm, respectively. Finally, a single resonance was observed in the ^{199}Hg{^{1}H} NMR spectrum at –997.5 ppm in d_8-THF. This is significantly shifted from that observed at –635.0 ppm for **14** in d_8-THF and it is likely that the solvent would displace the coordinated diethyl ether molecule which crystallises in **16**, hence, protonation must have a pronounced effect on the bonding of the ligand to the mercury centre. The dicationic nature of **16** was observed in the electrospray mass spectrum which reveals a mass envelope at 489.2803 (Calcd 489.2732) which can be ascribed to $[(aIPr)_2Hg]^{2+}$ and displays peaks at half mass intervals as expected for a dicationic species.

Colourless single crystals of [**16**]$[B(3,5\text{-}\{CF_3\}_2C_6H_3)_4]_2$ were grown by slow diffusion of hexane into a diethyl ether solution of the reaction mixture (Figure 3.4).

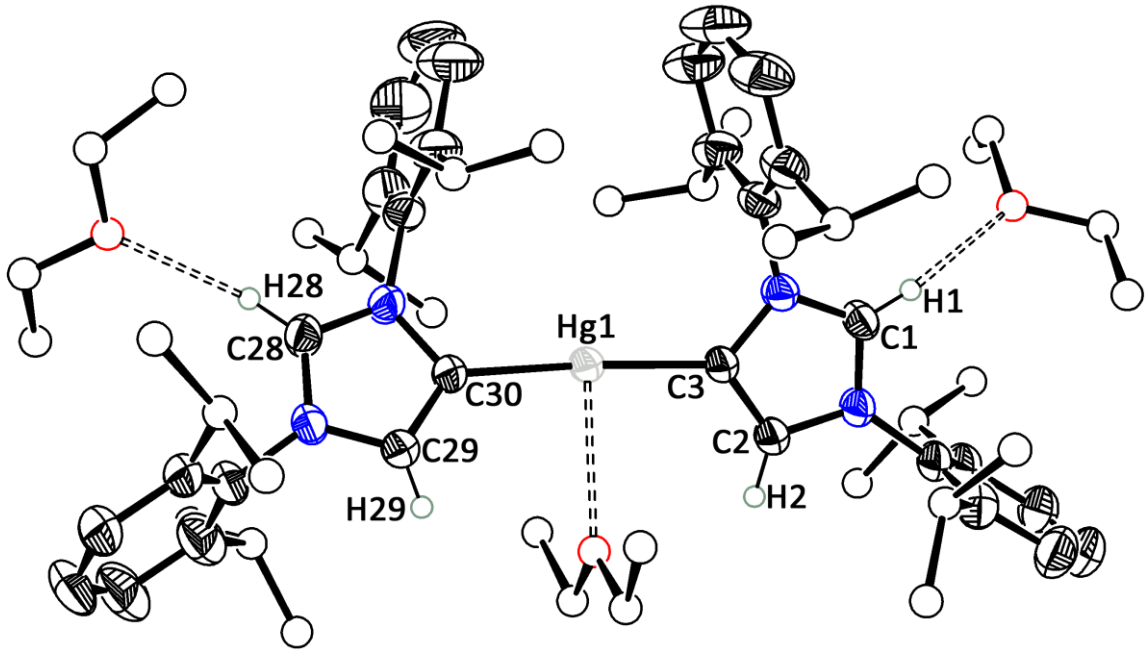

Figure 3.4: Structure of dication **16** in [**16**][B(3,5-{CF_3}$_2$$C_6H_3$)$_4$]$_2$. Anisotropic displacement ellipsoids pictured are set at 50% probability. Hydrogen atoms (with the exception of the imidazole protons labelled H1, H2, H28 and H29) have been omitted for clarity. Atoms of the ^{i}Pr groups, diethyl ether molecules and hydrogen atoms are pictured as spheres of arbitrary radii.

There is an apparent increase in both Hg–C bond lengths upon protonation (Hg1–C3 and Hg1–C30 = 2.062(2) and 2.066(2) Å) however, due to the large uncertainty of the measured values for **14**, this may not be statistically significant. Regardless, **16** shows a similar linear geometry about the mercury centre where C30–Hg1–C3 = 176.4(1)° and the overall geometry is very similar whereby two Dipp substituents are oriented towards one another despite the obvious steric clash that may result. This is more justifiable in the crystal structure of **16** due to the presence of a diethyl ether molecule coordinating the mercury centre on the opposite side. A similar torsion of 19.9° can be measured for the equivalent C29–C30–C3–C2.

3.2.3 Normal IPr complexes of mercury

16 can be considered as the abnormal isomer of the dicationic mercury complexes first synthesised by Wanzlick and Schönherr in 1968 during their original studies of nucleophilic carbenes.[11,12] The phenyl substituted imidazolium was used to synthesise the dicationic NHC

complex $[(IPh)_2Hg]^{2+}$ by the addition of the imidazolium chlorate salt [IPhH][ClO_4] to mercury(II) acetate ($Hg(OAc)_2$) resulting in the liberation of acetic acid. The molecular structure was subsequently confirmed using X-ray crystallography by Luger and Ruban.[13]

In order to provide a simple comparison in bonding between normal and abnormal NHC complexes, we sought to synthesise the dicationic normal IPr complex $[(IPr)_2Hg]^{2+}$. Addition of two equivalents of IPr to a solution of $HgCl_2$ in THF, along with one or two equivalents of $Na[B(3,5\text{-}\{CF_3\}_2C_6H_3)_4]$,[14,15] resulted in the monocationic, three-coordinate mercury complex $[(IPr)_2HgCl]^+$, **17** (Figure 3.5). Despite the excess of $Na[B(3,5\text{-}\{CF_3\}_2C_6H_3)_4]$, one chloride anion remained coordinate to the mercury centre resulting in only the monocationic, T-shaped complex.

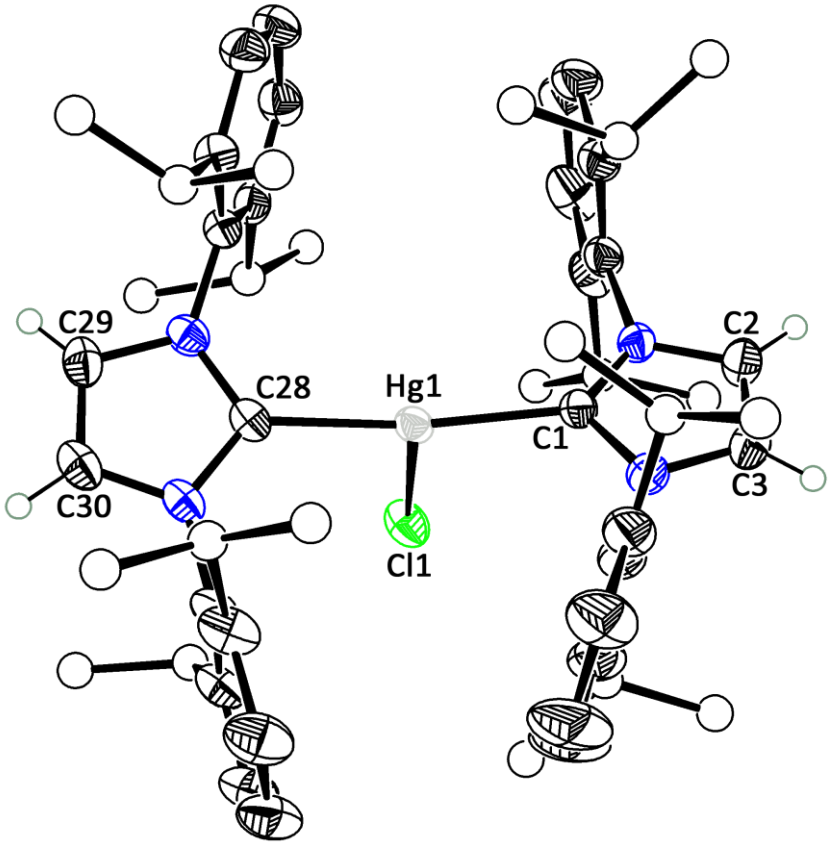

Figure 3.5: Structure of cation **17** in [**17**][$B(3,5\text{-}\{CF_3\}_2C_6H_3)_4$]. Anisotropic displacement ellipsoids pictured are set at 50% probability. Hydrogen atoms (with the exception of the imidazole protons) have been omitted for clarity. Atoms of the ^{i}Pr groups and hydrogen atoms are pictured as spheres of arbitrary radii.

17 was characterised by multielement NMR spectroscopy and reveals symmetrically coordinated IPr ligands with a single alkenic resonance at 7.84 ppm in d_8-THF. Similarly, one bond and three bond coupling between the imidazole carbons and the mercury atom can be observed as satellites in the $^{13}C\{^1H\}$ NMR spectrum and were found to be 2644 Hz and 75 Hz, respectively. Similarly, a single resonance was observed at –700.2 ppm in the $^{199}Hg\{^1H\}$ NMR spectrum.

The Hg1–C1 and Hg1–C28 bond lengths were observed to be 2.112(3) and 2.111(3) Å, respectively, by X-ray crystallography. The significantly longer bond lengths relative to those observed in **14** and **16** is likely due to a combination of reasons. The increased steric clash between the flanking Dipp groups would push the two ligands further apart and the additional coordination from the chloride ligand would reduce the electrophilicity of the central metal ion. Finally, the bonding to the backbone of the imidazole of IPr is significantly vinylic in character and more strongly electron donating the classical C2 carbene carbon. The bond length is also greater than that observed for the adduct $(IPr)HgCl_2$ which has a Hg–C bond length of 2.090(4) Å.[16] The geometry about the mercury atom is a T-shaped planar geometry where $\Sigma_{\text{bond angles}} = 360.0°$. However, the two IPr ligands coordinate in an approximately linear fashion, (likely due to the steric bulk of the ligand), where the C1–Hg1–C28 bond angle is 165.8(1)° with a N1–C1–C28–N3 torsion of 26.4°. Additionally, **17** was characterised by a mass envelope at 1013.5015 (Calcd 1013.5152) in the ESI-MS in DCM and no dissociation to afford the dicationic $[(IPr)_2Hg]^{2+}$ was observed.

An alternative method to synthesise $[(IPr)_2Hg]^{2+}$ was investigated. Addition of imidazolium salts to HgO has been observed to afford the aforementioned adduct $(IPr)HgCl_2$ with elimination of H_2O. This oxide route is a common method employed in the synthesis of silver–NHC complexes for subsequent transmetallation reactions.[17,18] Refluxing a THF

solution of [IPrH][B(3,5-{CF_3}$_2$$C_6H_3$)$_4$] with HgO allowed for the isolation of a trace amount of the target species [(IPr)$_2$Hg]$^{2+}$. Unfortunately, this method did got allow for the synthesis of enough material for characterisation due to the high insolubility of HgO in THF. An image of the molecular structure of [(IPr)$_2$Hg]$^{2+}$ as determined by single crystal X-ray diffraction suggesting such a complex is synthetically accessible is included in Appendix A, Figure A.1.

3.3 Synthesis of novel silicon and germanium compounds

3.3.1 Synthesis of (aIPr:)$_2$EX$_2$ (E = Si, Ge; X = Cl, Br)

With an interest in synthesising compounds that contain both a Lewis acidic centre and Lewis basic centre in the same molecule, we sought to introduce aIPr: as a ligand with group 14 tetrahalides. Following a similar protocol for the synthesis of (aIPr:)$_2$Hg by a salt metathesis reaction, addition of two equivalents of either the lithium or potassium salt of IPr to EX_4 resulted in the formation of the neutral, four-coordinate species (aIPr:)$_2$EX$_2$ (E = Si, Ge; X = Cl, Br) (Scheme 3.4). Such species contain a Lewis acidic EX_2 core and the aIPr: ligands retain the unquenched Lewis basicity of the carbene moiety within the same molecule. The reaction of the tetrahalides with [Li(aIPr:)]$_\infty$ could be carried out in either toluene or THF (the product requiring extraction from the lithium halide if THF was used as a reaction solvent) or by reaction with [K(aIPr:)]$_\infty$ in THF (whereby the potassium halide forms an insoluble viscous precipitate which can be removed by filtration). These reactions can be carried out at room temperature and proceeded very rapidly; when [Li(aIPr:)]$_\infty$ was used as a reagent, dark reaction solutions were obtained from which the product must be carefully purified by crystallisation, hence, [K(aIPr:)]$_\infty$ was found to have advantages as a reagent which gave rise to cleaner reaction mixtures.

The $(aIPr:)_2EX_2$ products were found to be highly soluble in hexane allowing for crystallisation from this solvent. This high solubility also allows for the reaction to be carried out in hexane as the reaction solvent; both $[Li(aIPr:)]_\infty$ and $[K(aIPr:)]_\infty$ are insoluble in hexane, however, all the tetrahalides are soluble (or miscible) with hexane, and the reaction proceeds presumably at the solid surface and this controls the rate of reaction. Hence, under these conditions, all reactions were complete after stirring for one day and the product was obtained in greatest yield with this method after filtration from the metal halide and removal of the solvent in vacuo.

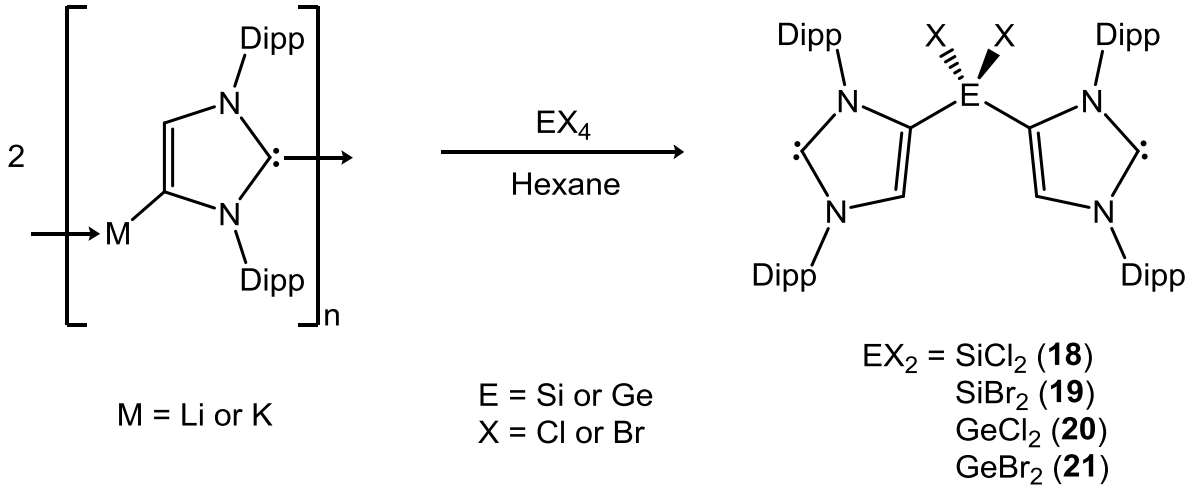

Scheme 3.4: Synthesis of $(aIPr:)_2EX_2$ by the addition of $[M(aIPr:)]_\infty$ to EX_4.

18–**21** can all be isolated in greater than 50% crystalline yields from hexane. All compounds give rise to very similar ^1H NMR spectra which show the presence of an aIPr: ligand. The most diagnostic resonance being the imidazole proton can be observed at 7.52 and 7.47 ppm for the silicon compounds **18** and **19** in d_8-THF, respectively. These resonances are observed to shift upon dissolution in C_6D_6 to 7.34 and 7.37 ppm, respectively. Likewise, the single imidazole resonance can be found shifted upfield at 6.88 and 6.93 ppm for **20** and **21** respectively, in C_6D_6. Accordingly, two septet methine resonances and four doublet methyl

resonances can be observed for all compounds and found between 2.83 and 2.90 ppm and between 1.05 and 1.32 ppm, respectively, in C_6D_6.

Additionally, $^{13}C\{^1H\}$ NMR spectroscopy indicates the presence of the uncoordinated carbene moiety as all compounds display a highly downfield resonance which can be assigned to the carbene carbon (δ = 226.6, 226.8, 225.9 and 225.8 ppm for **18**–**21**, respectively). Surprisingly, the carbanionic imidazole carbon is not found to change in chemical shift depending on the nature of the main group moiety and are observed at very similar chemical shifts in all samples. The resonances for **18**–**21** can be observed at 126.4, 126.2, 127.0 and 126.8 ppm, respectively. Likewise, the protonated imidazole carbon is observed at similar chemical shifts for the same main group element and the effect of the halogen is negligible (δ = 135.3 and 135.1 ppm for **18** and **19**, respectively and δ = 132.3 and 132.0 ppm for **20** and **21**, respectively).

Finally, **18** and **19** were characterised by a single resonance in the $^{29}Si\{^1H\}$ NMR spectra with chemical shifts of –18.0 and –36.9 ppm, where as expected, there is a significant shift in the resonance on changing the halogen from a chloride to bromide. The chemical shift of **18** compares well to that of (aIPr:)$SiCl_3$ (δ = –13.5 ppm) and both are shifted downfield when compared with (aIPr:)$SiClMe_2$ (δ = 9.9 ppm).[7] It was possible to observe silicon satellites in the $^{13}C\{^1H\}$ NMR spectrum of **18** only, in d_8-THF owing to the relatively low natural abundance of ^{29}Si (4.68%).[19] The I = $^1/_2$ nucleus results in a splitting to give rise to a doublet centred about the main resonance and can be observed for both the carbanionic carbon directly bonded to the silicon atom and for the protonated imidazole carbon. The coupling constants were measured to be 113 Hz and 16 Hz, respectively, and as expected, the one bond coupling constant is of an order of magnitude greater than that of the two bond coupling constant and within the range expected for ^{13}C–^{29}Si coupling.[20]

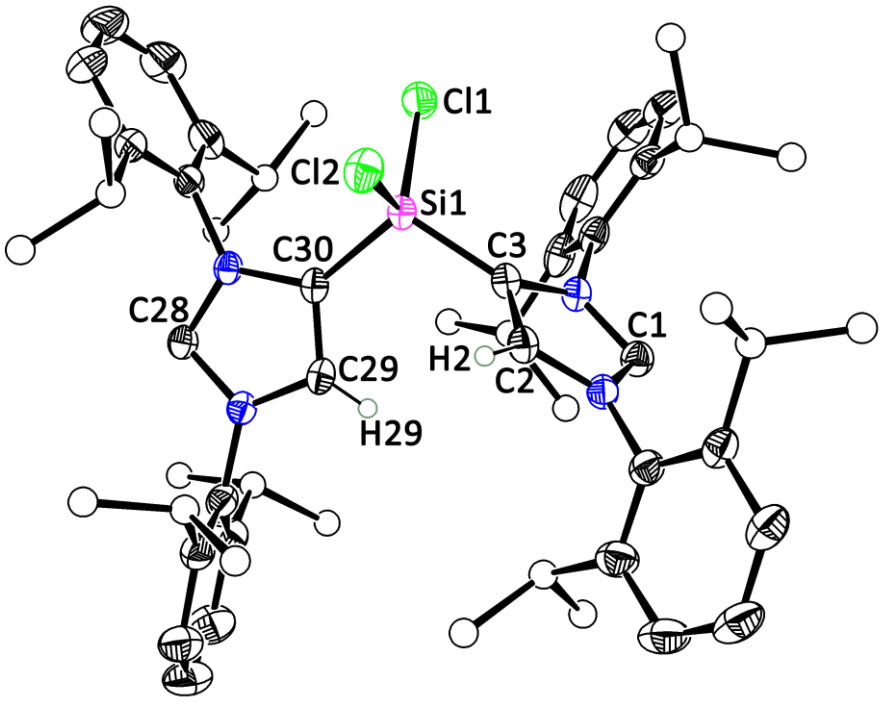

Figure 3.6: Molecular structure of **18**. Anisotropic displacement ellipsoids pictured are set at 50% probability. Hydrogen atoms (with the exception of the imidazole protons labelled H2 and H29) have been omitted for clarity. Atoms of the ^{i}Pr groups, H2 and H29 are pictured as spheres of arbitrary radii.

Analysis of the molecular structure of **18** and **19** by single crystal X-ray diffraction reveals that both compounds adopt a tetrahedral geometry about the silicon atom (Figure 3.6 and 3.7). **18** crystallises in the space group, $P\bar{1}$, with two molecules in the asymmetric unit (along with a single molecule of hexane). The structural parameters do not vary significantly between the two molecules and in most cases are identical. The distorted nature of the solid state structure of both **18** and **19** results in the inequivalence of the two aIPr: ligands and both structures can be described as being C_1 symmetric, whereby the only symmetry element the structures contain is that of the identity, *E*. Obviously, in solution, the free rotation about the C–Si bonds renders both ligands equivalent as evidenced by ^{1}H and ^{13}C{^{1}H} NMR spectroscopy.

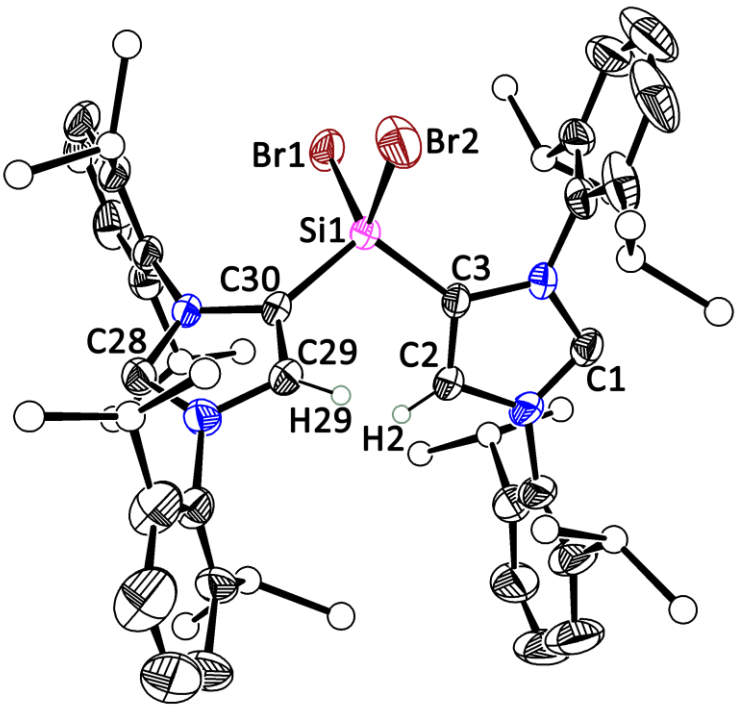

Figure 3.7: Molecular structure of **19**. Anisotropic displacement ellipsoids pictured are set at 50% probability. Hydrogen atoms (with the exception of the imidazole protons labelled H2 and H29) have been omitted for clarity. Atoms of the ^{i}Pr groups, H2 and H29 are pictured as spheres of arbitrary radii.

The distortion from tetrahedral in both compounds can be calculated using the τ_4' parameter which was introduced in Section 2.4.2.2. The τ_4' parameter can be calculated to be 0.938 and 0.947 for **18** and **19**, respectively. These values indicate very little distortion from a perfect tetrahedral geometry about the silicon centre. This slight distortion can be seen in the slight reduction in bond angle between the two aIPr: ligands and correspondingly, between the two halide ligands; the C–Si–C bond angles are 108.0(1)° and 106.7(1)° in **18** and **19**, respectively, whilst the Cl–Si–Cl angle is measured to be 106.3(6)° and the Br–Si–Br angle is 105.8(1)°.

In both structures, the plane of the imidazole ring of one aIPr: ligand approximately bisects the X–Si–X bond angle. The large steric bulk of the Dipp substituents results in the twisting of the other aIPr: ligand whereby the plane of the imidazole ring lies approximately in the plane of one of the Si–X bonds. This results in a slight discrepancy in the bond lengths

observed for each Si–X bond in **18** and **19**, which is likely a steric effect due to the packing of the ligands. The Si–Cl bond lengths observed in **18** are 2.025(2) and 2.039(2) Å for one molecule and 2.024(1) and 2.051(1) Å for the second molecule. This is the biggest difference observed between the two molecules due to the slightly different orientations of the distorted aIPr: ligand, however, all other bond lengths are similar and so only one molecule will be discussed hereafter. The Si–Br bond lengths were found to be 2.193(1) and 2.200(1) Å; the shorter Si–X bonds were found to be that of the halogen which lies approximately in the plane of one of the imidazole rings. Both Si–Cl bond lengths are within the range of the sum of covalent radii (Σr_{cov} = 2.13 Å),[9] and within the range of experimentally determined distances which range predominantly from 2.006 to 2.074 Å (Mean = 2.050 Å, Standard deviation = 0.022) based on a CSD search for R_2SiCl_2 (R = carbon coordinated ligand) compounds. Similarly, both Si–Br bond lengths are within the sum of covalent radii (Σr_{cov} = 2.31 Å),[9] and surprisingly, a similar search for structurally authenticated R_2SiBr_2 compounds in the CSD provides only eight results. These distances range from 2.216(1) to 2.270(1) Å and reveals that the Si–Br bond lengths observed in **19** are shorter than all other R_2SiBr_2 species.[21,22]

The Si–C bond lengths are all very similar to that calculated for the sum of covalent radii (Σr_{cov} = 1.84 Å).[9] In **18**, the C–Si bond lengths were observed to be 1.839(3) and 1.835(3) Å and very little change is observed in the bromide species where the Si–C bond lengths are 1.838(2) and 1.849(2) Å. These distances are all shorter than those observed for the normal IPr adducts of the silicon halides such as (IPr)$SiCl_4$, (IPr)$SiBr_4$ and the ionic species [(IPr)$SiBr_3$]Br (1.928(2), 1.935(2) and 1.880(9) Å, respectively).[23–25] This is to be expected due to the greater nucleophilic character of the C4 position of the imidazole relative to the C2 position. It is interesting to note that these bond lengths are similar to those observed in (*N*-methylpyrrol-2-yl)silanes which bear an electronically similar ligand.[26,27]

Analysis of the molecular structure of **20** and **21** by crystallography also reveals a tetrahedral geometry about the germanium centre. **20** crystallises in the *P*1 space group with a molecular geometry that can be described as being C_2 symmetric whereby the C_2 rotation axis bisects the Cl–Ge–Cl and C–Ge–C bond angles (Figure 3.8). The asymmetry of the aIPr: ligand and the relation of one ligand to another by a C_2 rotation axis (rather than a mirror plane) results in a chiral geometry and can crystallise in a space group with no inversion symmetry, i.e. *P*1.

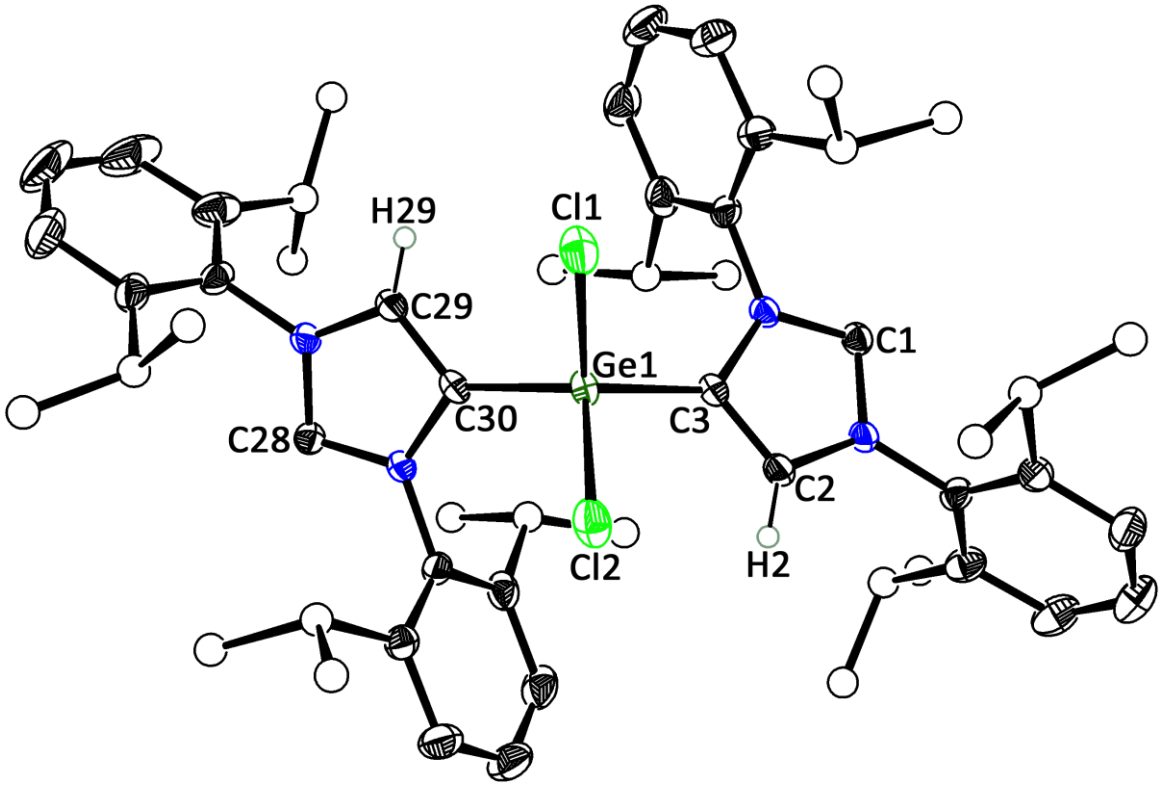

Figure 3.8: Molecular structure of **20**. Anisotropic displacement ellipsoids pictured are set at 50% probability. Hydrogen atoms (with the exception of the imidazole protons labelled H2 and H29) have been omitted for clarity. Atoms of the ^{i}Pr groups, H2 and H29 are pictured as spheres of arbitrary radii.

The large steric bulk of the ligands results in an expansion of the C3–Ge1–C30 bond angle (125.4(2)°) from a perfect tetrahedral angle. The distortion can be measured by calculation of the τ_4' parameter which is 0.838 and shows a reasonable distortion from a perfect tetrahedral geometry. The increased conformational flexibility in **20** and **21** allows for such species to adopt different conformations upon crystallisation. **21** crystallises in the orthorhombic space

group *Pbca* with eight molecules in the unit cell and **21** adopts a geometry whereby the imidazole proton, H2, is directed towards the open face of an adjacent Dipp group; this conformation is likely stabilised by π-interactions with the slightly acidic imidazole proton (Figure 3.9). This stabilising effect results in a slight decrease in the C3–Ge1–C30 bond angle relative to **20** (119.2(2)°) and the geometry about the germanium centre is slightly less distorted from tetrahedral when compared with **20** (τ_4' = 0.885).

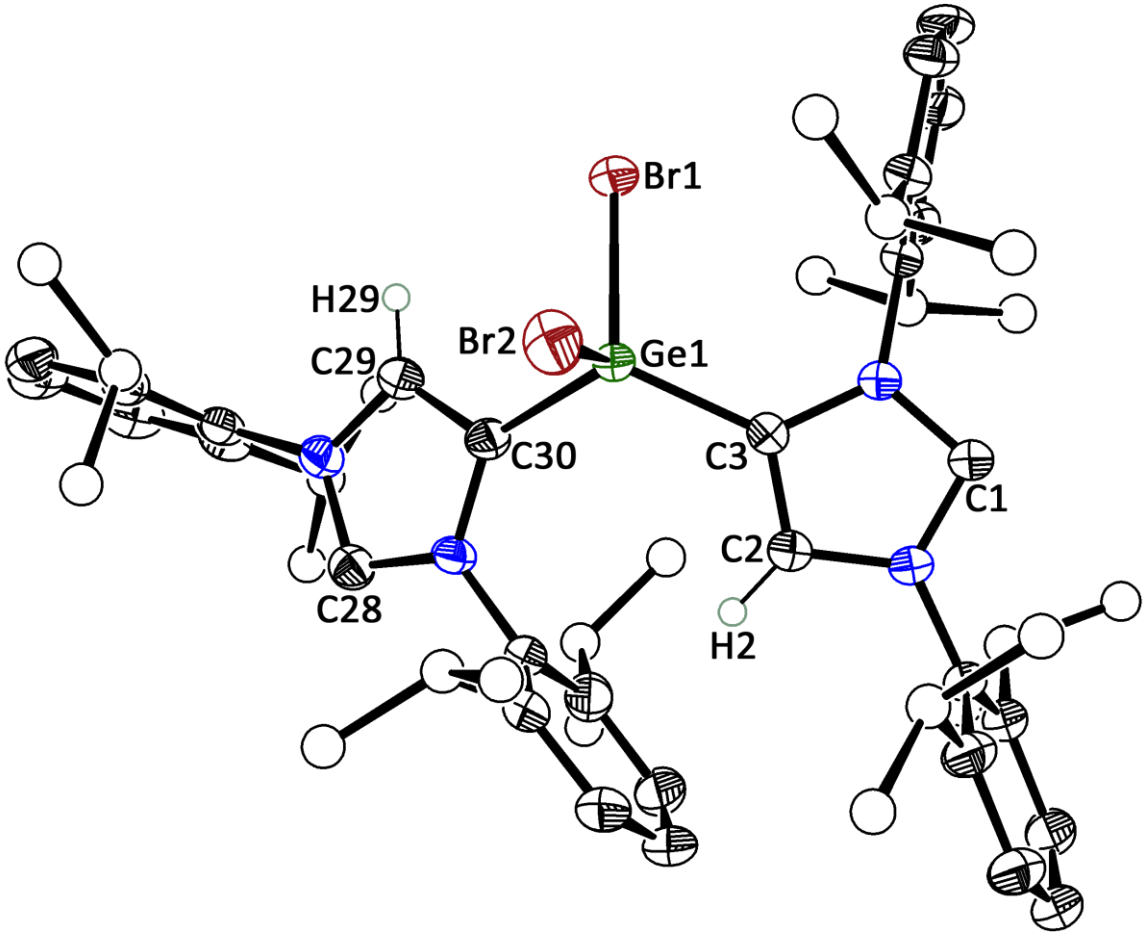

Figure 3.9: Molecular structure of **21**. Anisotropic displacement ellipsoids pictured are set at 50% probability. Hydrogen atoms (with the exception of the imidazole protons labelled H2 and H29) have been omitted for clarity. Atoms of the ^{i}Pr groups, H2 and H29 are pictured as spheres of arbitrary radii.

As expected, there is an increase in the Ge–C bond lengths in **20** and **21** relative to the Si–C bond lengths in **18** and **19** in line with the increase in covalent radius of germanium relative to silicon (Δr_{cov} = 0.09 Å). The Ge1–C3 and Ge1–C30 bond lengths observed in **20** are

1.916(3) and 1.919(3) Å, respectively, and in **21** were found to be similar at 1.922(4) and 1.927(4) Å, respectively. Again, these bond lengths are shorter than that observed for the normal IPr adducts, (IPr)$GeCl_4$ (1.992(2) Å). Similarly, an increase in the Ge–X bond lengths relative to the Si–X bond lengths in **18** and **19** was observed. The Ge–Cl bond lengths in **20** were found to be identical due to the symmetric nature of the geometry adopted upon crystallisation (2.145(1) and 2.146(1) Å), whereas the asymmetric geometry of **21** results in two significantly different Ge–Br bond lengths. The Ge1–Br1 bond length, which lies approximately in the plane of the two imidazole rings, was measured to be shorter than that of the Ge1–Br2 bond length (2.285(1) and 2.316(1) Å, respectively).

(IPr)$GeBr_4$ has not be synthesised and for structural comparison, we sought to synthesise the adduct by combination of the ligand, IPr, with $GeBr_4$ in THF. Upon addition of $GeBr_4$ to a THF solution of IPr, a colourless crystalline precipitate slowly begins to form. The precipitate was identified as the imidazolium salt, [IPrH]Br, by ^{1}H NMR spectroscopy and single crystal X-ray diffraction. The generation of the protic species was postulated to form due to deprotonation of (IPr)$GeBr_4$ by IPr in solution which may be the result of the adduct existing in equilibrium with the free IPr and $GeBr_4$.

As the C4 deprotonated species are unstable and unobserved in solution, isomerisation of the ligand occurs rapidly and the stronger sigma donation of the C4 carbon results in the elimination of a bromide ligand and subsequent crystallisation of the imidazolium salt due to its insolubility in THF. This would formally give rise to (aIPr:)$GeBr_3$. It was possible to access **21** cleanly by addition of multiple equivalents of IPr, presumably forming (aIPr:)$GeBr_3$ as an intermediate. Addition of $GeBr_4$ to four equivalents of IPr in THF, followed by heating at 65 °C for four days, results in the crystallisation of two equivalents of [IPrH]Br·THF and **21** in a 60% yield after extraction into toluene (Scheme 3.5). It was also possible to synthesise

the silicon–bromide compound, **19**, by an equivalent methodology in a 47% yield. It is important to note that this reaction only proceeds for the silicon and germanium tetrabromides and when the reaction is carried out using either $SiCl_4$ of $GeCl_4$, formation of **18** or **20** is not observed.

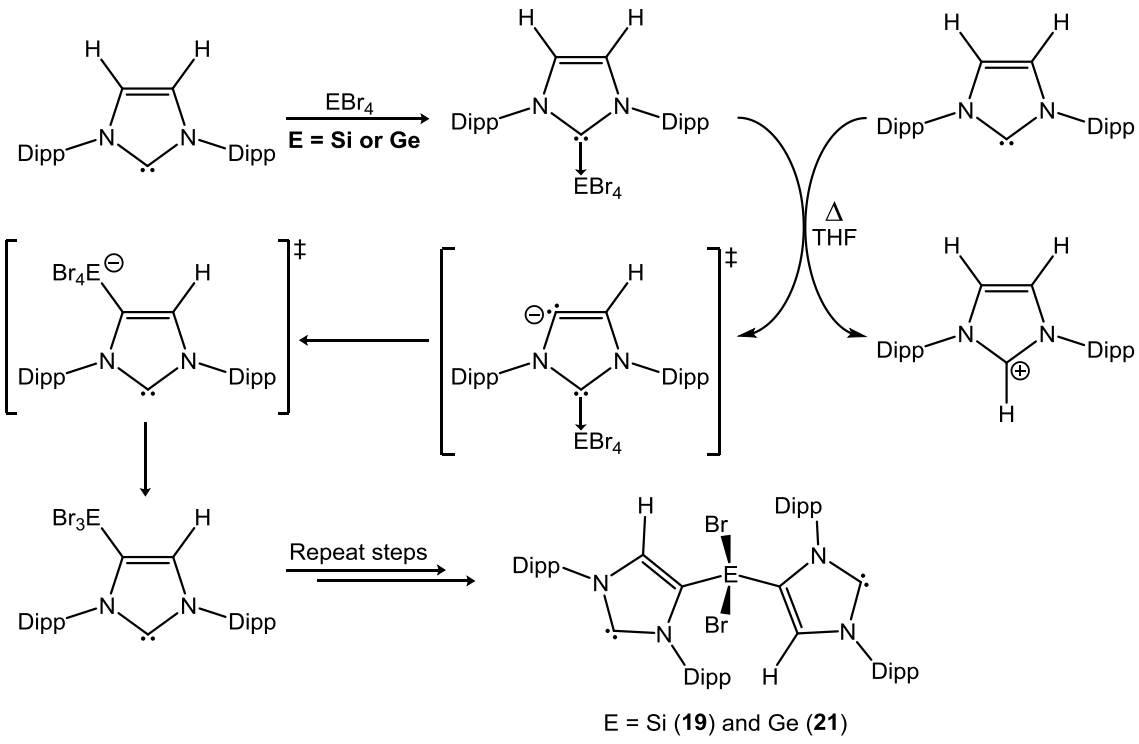

Scheme 3.5: Synthesis of (aIPr:)$_2$EBr$_2$ by the addition of four equivalents of IPr to EBr$_4$ in THF.

Upon addition of four equivalents of IPr to $SiCl_4$ in THF, it was possible to identify $[(aIPr)_2SiCl_3]Cl{\cdot}THF$ by single crystal X-ray diffraction as it readily crystallises from the reaction solution by the formation of a coordination polymer connected by a series of H1–Cl4–H28 hydrogen bonds (See Appendix A, Figure A.2). $[(aIPr)_2SiCl_3]Cl$ consists of two equivalents of abnormally bonded IPr ligands and forms by formal proton migration from the backbone to the C2 position of two IPr ligands. Such a species has already been synthesised by protonation of (aIPr:)$SiCl_3$ by CH_2Cl_2 (Scheme 3.1).[5] $[(aIPr)_2SiCl_3]Cl$ was crystallised as a THF solvate whereby a single THF molecule hydrogen bonds to the two backbone imidazole protons of $[(aIPr)_2SiCl_3]^+$. However, due to the co-crystallisation of the intermediate [IPrH]Cl,

[(aIPr)$_2$SiCl$_3$]Cl could not be obtained as a compositionally pure material via this route. Therefore, it can be concluded that the presence of E–Br bonds, which are notably weaker than equivalent E–Cl bonds, allows for the favourable crystallisation of [IPrH]Br and the generation of the neutral bis(aIPr:) species, **19** and **21** upon heating in THF which drives the reaction to completion.

Addition of GeBr$_4$ to a diethyl ether solution of IPr with the aim of the product precipitating from the reaction solution was also ineffective. As opposed to the precipitation of (IPr)GeBr$_4$, a reduction of the germanium centre from Ge^{IV} to Ge^{II} was observed in the isolation of (IPr)GeBr$_2$ (**22**) from the reaction solution (Figure 3.10).

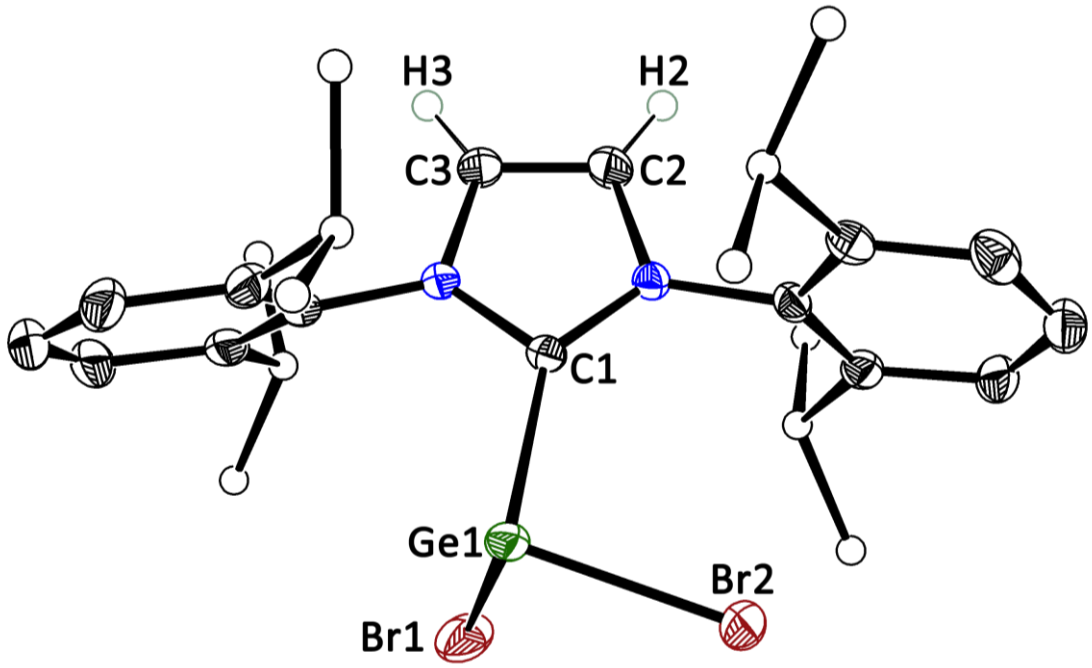

Figure 3.10: Molecular structure of **22**. Anisotropic displacement ellipsoids pictured are set at 50% probability. Hydrogen atoms (with the exception of the imidazole protons labelled H2 and H3) have been omitted for clarity. Atoms of the ^{i}Pr groups, H2 and H3 are pictured as spheres of arbitrary radii.

The equivalent of Br$_2$ which is liberated from the germanium centre is assumed to be lost by reaction of the adduct with free IPr in solution to generate [IPrBr]Br which crystallises immediately from the reaction solution, and half an equivalent of GeBr$_4$ remains unreacted.

Analysis of the colourless crystals by single crystal X-ray diffraction provides evidence for the formation of such a compound (See Appendix A, Figure A.3); similar species such as [IMesBr]Br·3MeCN have been crystallographically characterised and illustrate the formation of a bromoimidazolium salt which also halogen bonds with the free bromide ion and is synthesised by the addition of $C_2H_4Br_2$ to IMes in MeCN.[28] (IPr)$GeBr_2$ was crystallised from diethyl ether at –35 °C and characterised by ^1H and $^{13}C\{^1H\}$ NMR spectroscopy.

The ^1H NMR spectrum of **22** in d_8-THF reveals a single symmetric IPr ligand with a characteristic upfield shift of the imidazole resonance relative to free IPr due to the electron withdrawing effect of the $GeBr_2$ (δ = 7.67 ppm, cf. δ = 7.16 ppm for IPr). Additionally, two resonances can be observed for the imidazole carbons in the $^{13}C\{^1H\}$ NMR spectrum at 169.1 and 126.9 ppm for the carbene carbon and protonated alkenic carbons, respectively. The measured Ge1–C1 bond lengths are notably longer (2.114(2) Å) than the Ge–C bond lengths observed in **20**, **21** and (IPr)$GeCl_4$ due to the weaker coordination of the C2 position relative to the C4 position and the reduced electrophilicity of $GeBr_2$ relative to $GeCl_4$. The analogous silicon species, (IPr)$SiBr_2$, can be synthesised by reduction of (IPr)$SiBr_4$ with two equivalents of KC_8 and shows a similarly long Si–C bond length of 1.989(3) Å.[25] The geometry about the germanium centre is trigonal pyramidal, as would be expected for a base stabilised Ge^{II} complex, where $\Sigma_{\text{bond angles}}$ = 286.7°.

3.3.2 Protonation of (aIPr:)$_2EX_2$

Much like the synthesis of the dicationic mercury salt, [**16**][B(3,5-{CF_3}$_2C_6H_3$)$_4$]$_2$, we sought to investigate the protonation chemistry of (aIPr:)$_2EX_2$, **18**–**21**. The use of acids with a non-coordinating (or weakly coordinating) anion such as Brookhart's acid, [H(OEt_2)$_2$][B(3,5-{CF_3}$_2C_6H_3$)$_4$],[10] or trifluoromethanesulfonic acid, CF_3SO_3H, allows for the protonation of the carbene moiety thereby generating cationic complexes (Scheme 3.6).

Similar cationic species (i.e. compounds bearing aIPr ligands) can be formed by halide abstraction from protonated complexes bearing a halide ligand (See Section 3.4.3 and Chapter 4).

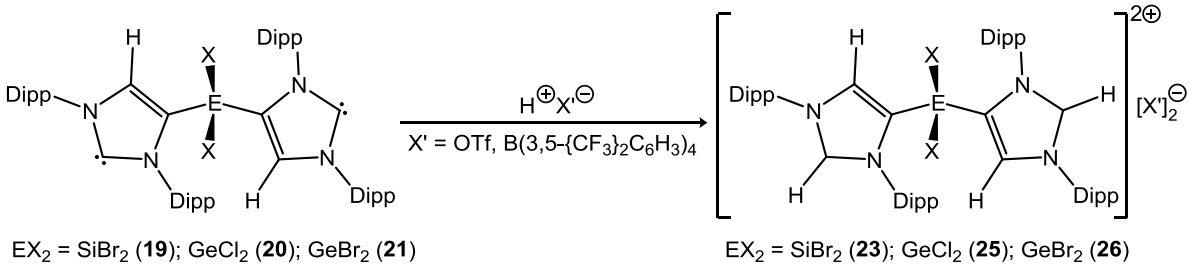

Scheme 3.6: Protonation of $(aIPr:)_2EX_2$ by the addition of triflic acid or Brookhart's acid.

Addition of two equivalents of triflic acid (HOTf) to a DFB solution of $(aIPr:)_2SiBr_2$ (**19**) results in the protonation of the two free carbene positions and the formation of the dicationic species, $[(aIPr)_2SiBr_2][OTf]_2$ (**23**). Evidence for the protonation of **19** comes from the ^{1}H NMR spectrum of **23** in CD_2Cl_2 which displays a highly deshielded singlet resonance at 9.84 ppm which can be assigned to the acidic imidazolium proton bonded to the C2 carbon. The cationic charge introduced by protonation also results in a downfield shift of the backbone imidazole proton resonance in the ^{1}H NMR spectrum and can be observed at 8.40 ppm (cf. 7.47 ppm for **19** in d_8-THF). Similarly, an upfield shift of the carbene resonance can be observed in the $^{13}C\{^1H\}$ NMR spectrum and the protonated imidazole C2 carbon is observed at 144.9 ppm which is a clear indication of the loss of carbenic character of this carbon. The chemical shift is much more similar to that of the protonated alkenic carbon of the imidazole (δ = 137.2 ppm). Finally, the silicon bound carbon can be observed at a very similar chemical shift of 127.0 ppm when compared to **19** (126.4 ppm in d_8-THF and 126.2 ppm in C_6D_6) indicating that the environment of this carbon is not significantly affected by the protonation of the ligand. Finally, a single resonance is observed in the $^{29}Si\{^1H\}$ NMR spectrum at

–42.6 ppm and is only slightly shifted downfield relative to that observed for **19** (–38.9 ppm in d_8-THF and –36.9 ppm in C_6D_6).

23 is highly moisture sensitive and susceptible to hydrolysis. This can be explained by the high electrostatic interaction between the electron deficient cationic species and the electron rich nature of the oxygen atom in water coupled with the high oxophilicity of silicon, i.e. silicon–oxygen bonds are very strong and provide a driving force for hydrolysis. Analysis of **23** by electrospray mass spectrometry results in the hydrolysis of **23** (due to the high dilution required for analysis) and species of the form $[(aIPr)_2Si(OH)_2]^{2+}$ can be observed. This presumably forms with appropriate loss of HBr. The predominant mass envelope observed at 987.5142 can be assigned to $[(aIPr)_2Si(OH)_2(OTf)]^+$ (Calcd 987.5096) which can be viewed to be the hydrolysis product of the dication present in the gas phase with a triflate anion. This technique provides no evidence for the structure of the complex and the non-coordinating nature of the triflate anion means it is unlikely that that triflate anion is bound to silicon and may fly with the dication due to electrostatic attraction. Likewise, a mass envelope observed at 461.3559 can be assigned to $[(aIPr)_2Si(OH)_2(CH_2Cl_2)]^{2+}$ (Calcd 461.2552). The dicationic nature of the hydrolysis product is evident by the spacing between the peaks of the mass envelope which are separated by half a mass unit.

Similarly, attempts to obtain single crystals of [**23**][OTf]$_2$ suitable for single crystal X-ray diffraction were also thwarted by hydrolysis due to the presence of adventitious moisture. It was possible to crystallographically characterise the hydrolysis product (See Appendix A, Figure A.4) as the triflate salt providing crystallographic evidence for this species that can be observed via ESI-MS. It was possible to grow single crystals containing **23** suitable for single crystal X-ray diffraction, however, these were observed to contain approximately 50% of an intermediate hydrolysis product which can be modelled as $[(aIPr)_2SiBr(OH)]^{2+}$.

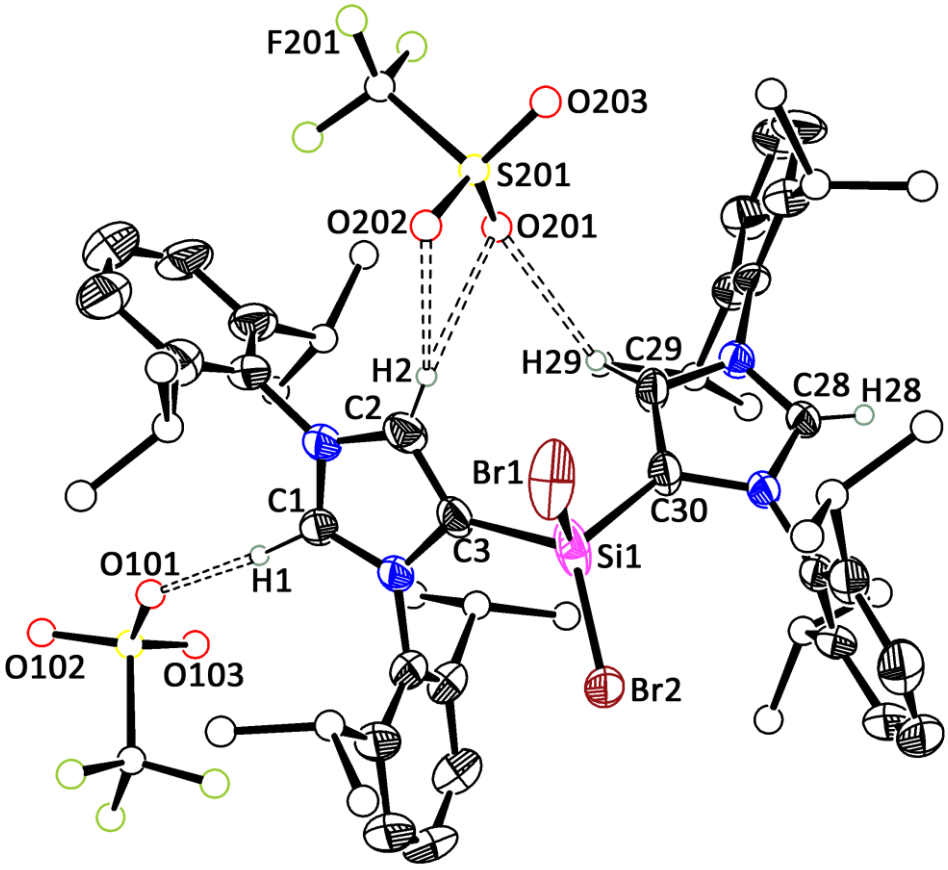

Figure 3.11: Molecular structure of [**23**][OTf]$_2$. Anisotropic displacement ellipsoids pictured are set at 50% probability. Hydrogen atoms (with the exception of the imidazole protons labelled H1, H2, H28 and H29) have been omitted for clarity. Atoms of the ^{i}Pr groups, the triflate anions and hydrogen atoms are pictured as spheres of arbitrary radii.

The molecular structure of **23** reveals the presence of triflate anions which form hydrogen bonds to electron deficient imidazole protons. Indeed, one triflate anion forms two hydrogen bonds bridging two different molecules of **23** forming a coordination polymer. As pictured in Figure 3.11, there is a hydrogen bonding interaction between O101 and H1 and there is a second hydrogen bond between O102 and H28 of another molecule of **23**. The second triflate anion forms hydrogen bonds to the backbone imidazole protons H2 and H29. Presumably due to packing effects, there is a close contact between H2 and two of the triflate oxygen atoms (O201 and O202). O201 bridges the two imidazole protons H2 and H29. These interactions are likely to be absent in solution due to the equivalence of the two ligands as determined by ^{1}H NMR spectroscopy.

A distortion from tetrahedral geometry about the silicon atom is evident by calculating the τ_4' parameter which is 0.902. This likely results due to the presence of the triflate anions which structurally distort **23** due to favourable hydrogen bonding interactions. A slight increase in Si–C bond lengths relative to **18** and **19** can be observed (1.858(5) and 1.862(5) Å) and may indicate a slightly weaker bonding interaction of the protonated aIPr ligand with respect to the anionic aIPr: ligand.

The high Lewis acidity of **23** is also evidenced through its reactivity towards THF. Addition of two equivalents of triflic acid to **19** in THF results in the formation of $[(aIPr)_2Si(OCH_2CH_2CH_2CH_2Br)_2]^{2+}$ (**24**). Similarly, the high oxophilicity of silicon accompanied by the significant increase in electrostatic interactions which result from protonation of the ligand allows for the formation of a Si–O bond by THF coordination. It is assumed that subsequent elimination of a bromide ligand allows for the nucleophilic ring opening of the coordinated THF molecule by reaction with the free bromide anion. [**24**][OTf]$_2$ can be isolated in 85% yield indicating almost instantaneous ring opening of THF under the reaction conditions. Again, protonation of the aIPr: ligand was evidenced by the appearance of a downfield resonance at 9.57 ppm in CD_2Cl_2 along with a resonance attributable to the backbone imidazole proton which is again downfield shifted with respect to **19** (δ = 8.10 ppm). The ring opened THF molecule results in the formation of an asymmetric $(CH_2)_4$ chain for which multiple highly coupled resonances can be observed in the ^{1}H NMR spectrum. Due to the inductive electron withdrawing effect of the electronegative oxygen and bromine substituents, the directly bonded methylene groups resonate at a similar chemical shift and result in an overlapping multiplet between 3.24 and 3.29 ppm which integrates to a total of eight protons. The two carbon resonances can be observed separately at 65.1 and 33.5 ppm in the $^{13}C\{^1H\}$ NMR spectrum for the oxygen and bromine bound carbons, respectively. Two further multiplets (*pseudo*-quintets) can be observed between 1.45 and 1.53 ppm and between

1.18 and 1.27 ppm which integrate to four protons each for the two central methylene groups. Likewise, two further carbon resonances are observed at 30.3 and 28.6 ppm confirming the presence of the ring opened THF molecule.

Single crystals of [**24**][OTf]$_2$ were grown by slow diffusion of hexane into a THF solution. Analysis by single crystal X-ray diffraction reveals two equivalents of [**24**][OTf]$_2$ in the asymmetric unit in $P\bar{1}$.

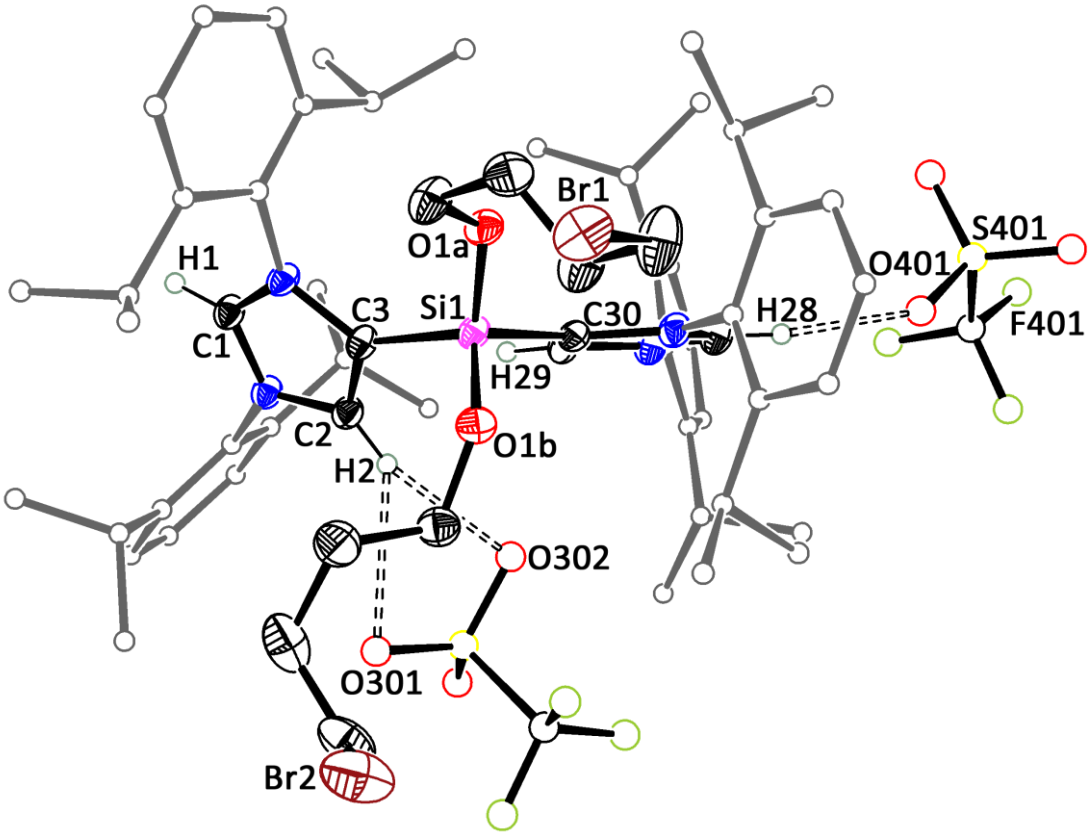

Figure 3.12: Molecular structure of [**24**][OTf]$_2$. Anisotropic displacement ellipsoids pictured are set at 50% probability. Hydrogen atoms (with the exception of the imidazole protons labelled H1, H2, H28 and H29) have been omitted for clarity. Atoms of the ^{i}Pr groups, the triflate anions and hydrogen atoms are pictured as spheres of arbitrary radii.

The slight distortion of silicon from tetrahedral in **24** can again be quantified by the τ_4' parameter which can be calculated to be 0.929 and 0.933 for Si1 and Si2, respectively. Molecules of **24** are also connected through a coordination polymer of hydrogen bonding

triflate anions as seen in Figure 3.12 whereby there is a hydrogen bond between H28 and O401. O402 forms a hydrogen bond with an equivalent imidazole proton of the second molecule of **24** in the asymmetric unit. The second triflate anion forms hydrogen bond to one of the backbone imidazole protons, namely H2, through two of the oxygen atoms.

There is an observable increase in the Si–C bond lengths in **24** which likely results from the reduced electrophilicity of the central silicon moiety on changing from $SiBr_2$ (in **19** and **23**) to $Si(OR)_2$. The alkoxide substituent has additional lone pairs of electrons which may contribute to multiple bonding by conjugation into Si–C and Si–O σ^* orbitals. The Si1–C3 and Si1–C30 bond lengths (and the corresponding bond lengths in the second molecule in the asymmetric unit) can be measured to be 1.882(4) and 1.874(4) Å (and 1.872(4) and 1.859(4) Å). The Si–O bond lengths were measured to be 1.606(3) and 1.620(3) Å (and 1.604(4) and 1.614(4) Å). These distances are well within the range expected from the sum of covalent radii for silicon and oxygen (Σr_{cov} = 1.77 Å).[9] The Si–O bond lengths observed in **24** are also shorter than other Si–O bond lengths that have been observed in similar complexes based on a CSD search for $R_2Si(OR)_2$ (Mean = 1.628 Å, Standard deviation = 0.022).

Finally, analysis by ESI-MS in DCM reveals two mass envelopes at 1257.4570 and 554.2574 which can be assigned to the monocationic $[(aIPr)_2Si(OCH_2CH_2CH_2CH_2Br)_2(OTf)]^+$ (Calcd 1257.4547) and the dicationic $[(aIPr)_2Si(OCH_2CH_2CH_2CH_2Br)_2]^{2+}$ (Calcd 554.2511), respectively. As expected, the peaks in the mass envelope corresponding to the dication, **24**, are each separated by half a mass unit.

Using a similar methodology to that employed for the synthesis of **23**, addition of two equivalents of $[H(OEt_2)_2][B(3,5\text{-}\{CF_3\}_2C_6H_3)_4]$ to a solution of **20** in diethyl ether allows for the protonation of both carbene moieties and the generation of the dication $[(aIPr)_2GeCl_2]^{2+}$ (**25**) as the $[B(3,5\text{-}\{CF_3\}_2C_6H_3)_4]$ salt. [**25**]$[B(3,5\text{-}\{CF_3\}_2C_6H_3)_4]_2$ can be dissolved in THF

(and d_8-THF) without decomposition and no coordination and ring opening of the THF solvent is observed, consistent with the reduced oxophilic character of germanium with respect to silicon. Instead, [**25**][B(3,5-{CF_3}$_2$$C_6H_3$)$_4$]$_2$ is indefinitely stable as a THF solution (and indeed as a solid when stored under inert atmosphere). Analysis by ^{1}H NMR spectroscopy in d_8-THF reveals a similar set of resonances as those observed for **23**. Notably, the acidic imidazole proton can be observed at 10.25 ppm which is accompanied by a resonance at 8.35 ppm due to the alkenic imidazole proton. Similarly, the C2 carbon, protonated alkenic imidazole carbon and the germanium bound carbon can be identified in the ^{13}C{^{1}H} NMR spectrum at 146.1, 135.8 and 131.6 ppm, respectively.

Slow diffusion of hexane into a crude diethyl ether reaction mixture results in the formation of a colourless oil over 24 hours. When left to stand, colourless crystals spontaneously grow from the oil and these crystals were identified by single crystal X-ray diffraction as [**25**][B(3,5-{CF_3}$_2$$C_6H_3$)$_4$]$_2$·2$Et_2O$ (Figure 3.13). The molecular structure of [**25**]·2Et_2O can be seen to be geometrically similar to that observed for **21** in that the backbone imidazole proton of one aIPr ligand is directed towards the open face of the aromatic ring of an adjacent Dipp group, clearly a favourable interaction in the absence of any coordinating species such as triflate anions. Regardless, the acidic C2 protons still form hydrogen bonding interactions with two molecules of relatively non-coordinating diethyl ether solvent molecules. Analysis of the ^{1}H and ^{13}C{^{1}H} NMR spectrum of **25** in d_8-THF reveal a larger than expected number of resonances, just like that observed for compounds **6** and **7**. This is an effect of the restricted rotation about the N–Dipp bond and a strong hydrogen bonding interaction between the solvent and the acidic imidazole proton may result in the increase in steric bulk which hinders N–Dipp rotation.

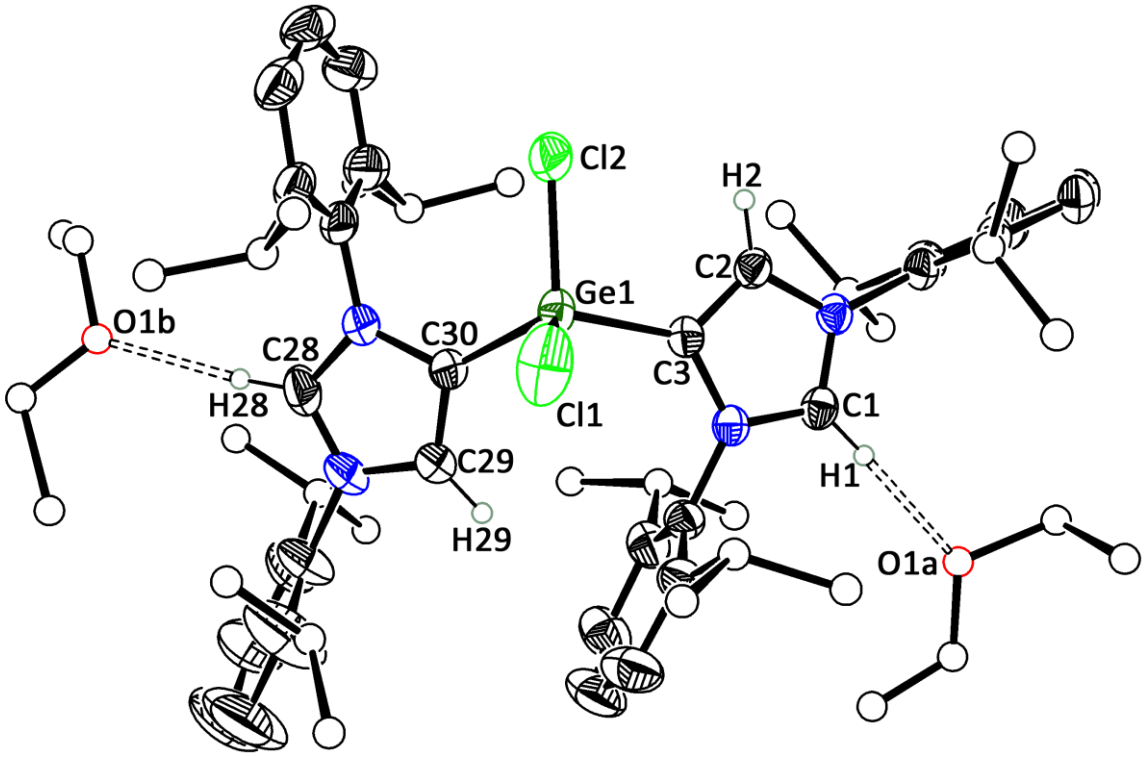

Figure 3.13: Structure of dication [**25**]·2Et_2O in [**25**][B(3,5-{CF_3}$_2C_6H_3$)$_4$]·2Et_2O. Anisotropic displacement ellipsoids pictured are set at 50% probability. Hydrogen atoms (with the exception of the imidazole protons labelled H1, H2, H28 and H29) have been omitted for clarity. Atoms of the ^{i}Pr groups, diethyl ether molecules and hydrogen atoms are pictured as spheres of arbitrary radii.

The geometry about the germanium centre is slightly distorted from tetrahedral, much like that observed for the silicon compounds **23** and **24**, and the τ_4' parameter can be calculated to be 0.892. There is a marginal increase in Ge–C bond lengths in **25** when compared to the neutral starting material, **20**, (1.925(4) and 1.930(4) Å). This is in line with the slight increase in Si–C bond lengths observed on protonation of **19**. There is however, a noticeable contraction in the Ge–Cl distances on protonation, the measured Ge1–Cl1 and Ge1–Cl2 distances in **25** are 2.089(2) and 2.093(2) Å.

Finally, protonation of **21** with two equivalents of triflic acid or [$H(OEt_2)_2$][B(3,5-{CF_3}$_2C_6H_3$)$_4$] in THF affords the dicationic species [(aIPr)$_2GeBr_2$]$^{2+}$ (**26**) as either the triflate or [B(3,5-{CF_3}$_2C_6H_3$)$_4$] salt, respectively. **26** has been characterised by ^{1}H and ^{13}C{^{1}H} NMR spectroscopy in CD_2Cl_2 and d_8-THF. The C2 proton and backbone

imidazole protons in **26** give rise to resonances at 9.70 and 8.04 ppm in CD_2Cl_2 and 10.21 and 8.25 ppm in d_8-THF showing a clear solvent dependence on the chemical shift of the acidic C2 proton.

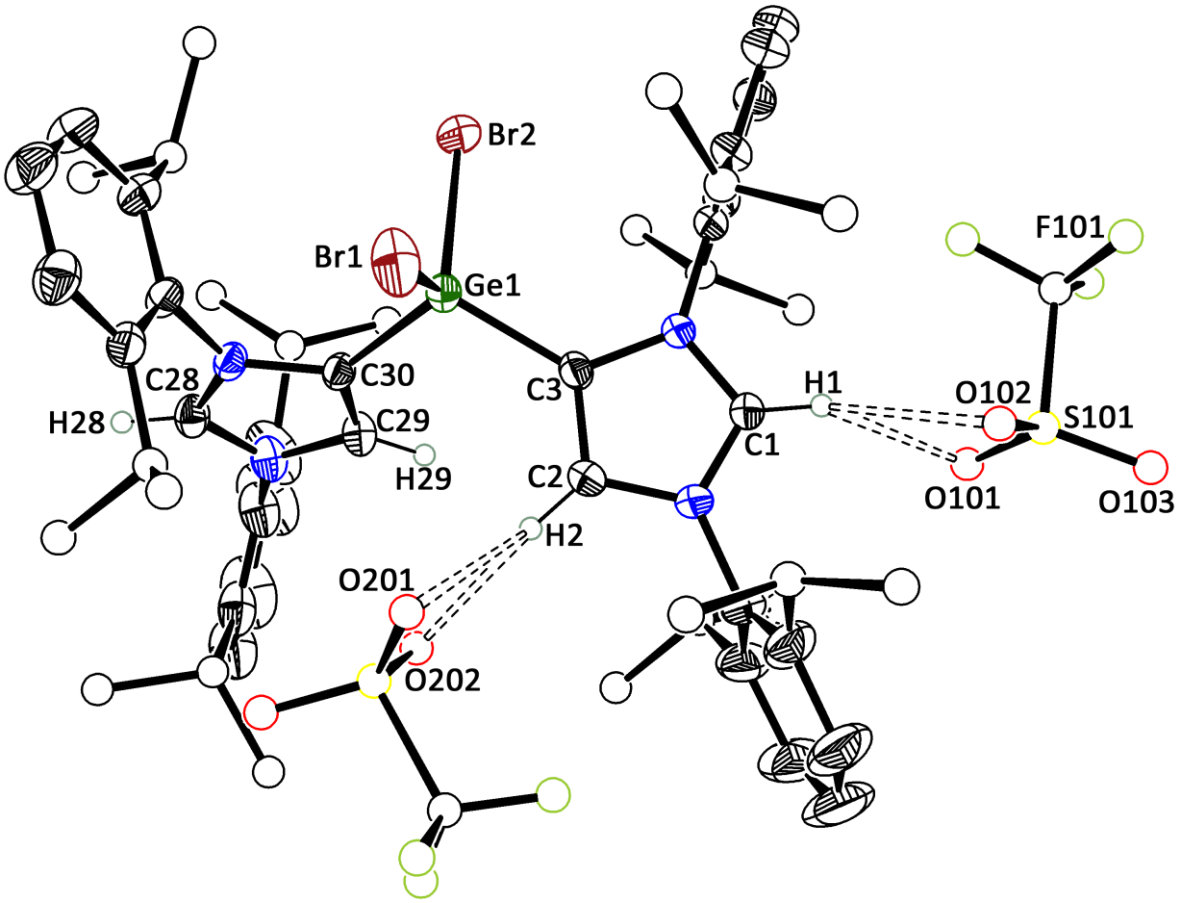

Figure 3.14: Molecular structure of [**26**][OTf]$_2$. Anisotropic displacement ellipsoids pictured are set at 50% probability. Hydrogen atoms (with the exception of the imidazole protons labelled H1, H2, H28 and H29) have been omitted for clarity. Atoms of the ^{i}Pr groups, the triflate anions and hydrogen atoms are pictured as spheres of arbitrary radii.

Similarly, the equivalent carbon resonances can be observed at 143.6 and 133.9 ppm in CD_2Cl_2 and 145.8 and 135.3 ppm in d_8-THF. The germanium bound carbon resonance cannot be observed for [**26**][OTf]$_2$ in CD_2Cl_2, however, a very broad resonance can be observed at 132.0 ppm for the germanium bound carbon of [**26**][B(3,5-{CF_3}$_2$$C_6H_3$)$_4$]$_2$ in d_8-THF.

Despite attempts to crystallise **26** as the [B(3,5-{CF_3}$_2$$C_6H_3$)$_4$]$^-$ salt, only formation of an oil was observed upon layering a THF solution with hexane. Single crystals of [**26**][OTf]$_2$·THF

suitable for single crystal X-ray diffraction were grown by slow diffusion of hexane into a THF solution and is likely favoured due to reduced flexibility of the triflate anion with respect to $[B(3,5\text{-}\{CF_3\}_2C_6H_3)_4]^-$ and the ability to form a network of hydrogen bonds to **26**. Each triflate anion forms two hydrogen bonds the imidazole protons of one of the aIPr ligands (Figure 3.14) and one triflate anion (that hydrogen bonds to H1) also forms a third hydrogen bond to the H28 proton of another molecule of **26** through O103 forming a hydrogen bonded polymer in the solid state.

The geometry about the germanium atom in **26** is almost perfectly tetrahedral as determined by the τ_4' parameter which was calculated to be 0.958. The Ge1–C3 and Ge1–C30 bond lengths (1.928(3) and 1.934(3) Å, respectively) are very similar to those observed for **25**. Similar to what was observed for **25**, there is also a noticeable decrease in the Ge–Br bond lengths upon protonation of the carbene moieties, the Ge1–Br1 and Ge1–Br2 bond lengths were measured to be 2.271(5) and 2.272(5) Å, respectively. Finally, the formation of the dicationic species, **26**, was further evidenced through ESI-MS which displayed a mass envelope at 505.2839 that can be assigned to $[(aIPr)_2GeBr_2]^{2+}$ (Calcd 505.1660). As with **23**, partial hydrolysis due to the high dilution required for analysis, results in the formation of $[(aIPr)_2GeBr(OH)]^{2+}$ and $[(aIPr)_2Ge(OH)_2]^{2+}$ as determined by the presence of mass envelopes at 473.3232 (Calcd 473.2088) and 442.3669 (Calcd 442.2513), respectively.

3.3.3 Carboxylation of $(aIPr:)_2EX_2$

Addition of CO_2 to an NHC results in the formation of an imidazolium carboxylate. Such species have unique properties and have been used in a range of ionic liquids and investigated in carbon dioxide absorption.[29,30] It has been shown possible for NHCs to capture CO_2 in the solid state with the formation of the imidazolium carboxylate and similarly, the reversible process has also been shown possible by heating the appropriate imidazolium carboxylate in

the solid state.[31,32] Likewise, synthesis of abnormal NHC adducts with carbon dioxide has also been achieved.[33,34] There is clear interest in the reversible bonding of carbon dioxide as a method of fixing this greenhouse gas with the aim of removing it from the atmosphere and generating useful, energy rich products.[35]

In light of the interest of NHC reactivity with carbon dioxide, we sought to synthesise the imidazolium carboxylates of **19**–**21**. Solutions in d_8-toluene prepared in a dinitrogen glovebox were added to an NMR tube with a gas-tight valve and degassed via three freeze-pump-thaw cycles on a Schlenk line. Approximately one atmosphere of CO_2 was added to the NMR tube and the samples analysed by multi-element NMR spectroscopy. In all samples, a shift of the NMR resonances in the ^{1}H and $^{13}C\{^{1}H\}$ NMR spectra provide evidence for the formation of the imidazolium carboxylates $(aIPr{\cdot}CO_2)_2SiBr_2$ (**27**), $(aIPr{\cdot}CO_2)_2GeCl_2$ (**28**) and $(aIPr{\cdot}CO_2)_2GeBr_2$ (**29**).

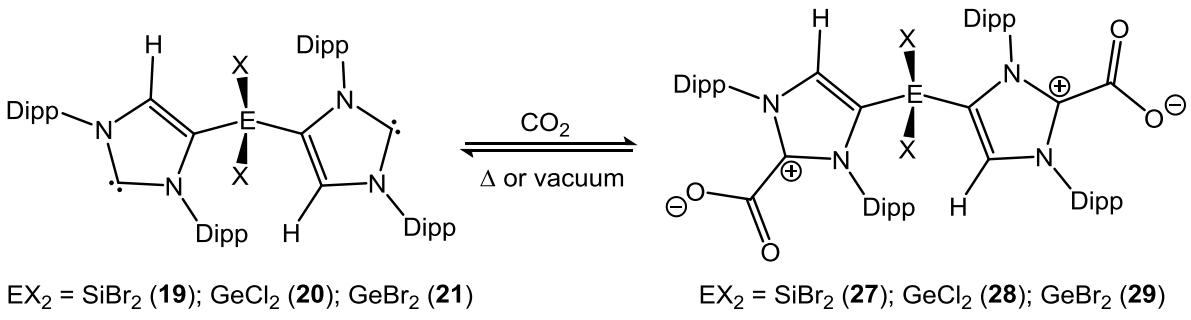

EX_2 = $SiBr_2$ (**19**); $GeCl_2$ (**20**); $GeBr_2$ (**21**)

EX_2 = $SiBr_2$ (**27**); $GeCl_2$ (**28**); $GeBr_2$ (**29**)

Scheme 3.7: Reversible carboxylation of $(aIPr:)_2EX_2$.

The general pattern of the ^{1}H NMR spectra of **27**–**29** resemble those of the starting materials **19**–**21** whereby the difference in chemical shifts of the resonances are within approximately 0.2 ppm. Table 3.1 provides a comparison of the chemical shifts of the diagnostic imidazole and methine proton resonances for **19**–**21** and **27**–**29** in d_8-toluene. A single resonance can be observed in the $^{29}Si\{^{1}H\}$ NMR spectrum of **27** at –38.6 ppm which is very similar to **19** in

d_8-THF or C_6D_6 which is to be expected as there in no change in the immediate environment of the silicon atom.

Compound	NCC*H*N δ (ppm)	$C_6H_3\{CH(CH_3)_2\}_2$ δ (ppm)
19	7.33	2.84, 2.81
27	7.23	2.77, 2.71
20	6.85	2.81, 2.78
28	6.79	2.77, 2.74
21	6.90	2.82, 2.80
29	6.83	2.75, 2.73

Table 3.1: Comparison of chemical shifts of selected resonances in the ^{1}H NMR spectra of **19**–**21** and **27**–**29** in d_8-toluene.

Subsequent attempts to synthesise and isolate solid samples of **27**–**29** by the addition of carbon dioxide to toluene solutions of **19**–**21** followed by removal of the solvent in vacuo were unsuccessful. Analysis of the isolated solid revealed the products to be the starting materials **19**–**21**. Similarly, evaporation of the solvent from the samples used for analysis by NMR spectroscopy followed by dissolution in further d_8-toluene reveals only starting material. These results suggest the presence of an equilibrium between the free carbene and carbon dioxide in solution with that of the imidazolium carboxylate products **27**–**29** (Scheme 3.7). This explanation is further substantiated through analysis of the $^{13}C\{^1H\}$ NMR spectra of all species in d_8-toluene. A small but significant change in the chemical shift of all resonances can be observed upon addition of carbon dioxide, however, in no samples could the resonances for the carbons involved in bond formation be observed (i.e. the carbene carbon and that of bound or even free carbon dioxide in solution). It can be concluded that the equilibrium that exists between the free species and the imidazolium carboxylates is in neither fast nor slow chemical exchange whereby either an average of the two chemical shifts would be observed as a single resonance or each separate species would be observed as two

resonances (i.e. one for the starting material and one for that of the imidazolium carboxylate). The rate of chemical exchange between the two states must have a rate that is approximately equal to the difference in chemical shifts of the starting materials and products, hence, these resonances are at (or near to) the coalescence point, coupled with the poor intensity which is characteristic of quaternary carbons, results in the lack of observable resonances. All other ^{13}C resonances have a small change in chemical shift and so the rate of exchange is much greater and the resonances have a relatively narrow line width.

Dynamic processes can often be studied by variable temperature NMR spectroscopy and an increase or decrease in temperature with either an increase or decrease in the rate constant for the reaction thereby allows for the system to either exist in fast or slow chemical exchange. However, in this equilibrium, increasing the temperature not only likely increases the rate constant for the reaction, but more importantly, it shifts the position the equilibrium and upon increasing the temperature of a sample of **27** in d_8-toluene to only 338 K, **19** was identified by ^{1}H and $^{13}C\{^{1}H\}$ NMR spectroscopy (Figure 3.15). Further evidence for the dynamic process described comes from the appearance of the carbene resonance (for **19**) at 219.8 ppm when heated to 338 K. Similarly, a resonance for free CO_2 in solution could also be observed at 125.9 ppm, the formation of free CO_2 being an entropic driving force for the dissociation. By extension, cooling a sample of **27** in d_8-toluene from 298 K to 238 K resulted in a progressive change in the chemical shift of the resonances in the ^{1}H NMR spectra indicating a continuous shift in the position of the equilibrium towards that of the product, **27**. Unfortunately, the insolubility of **27** at this temperature precluded analysis by $^{13}C\{^{1}H\}$ NMR spectroscopy.

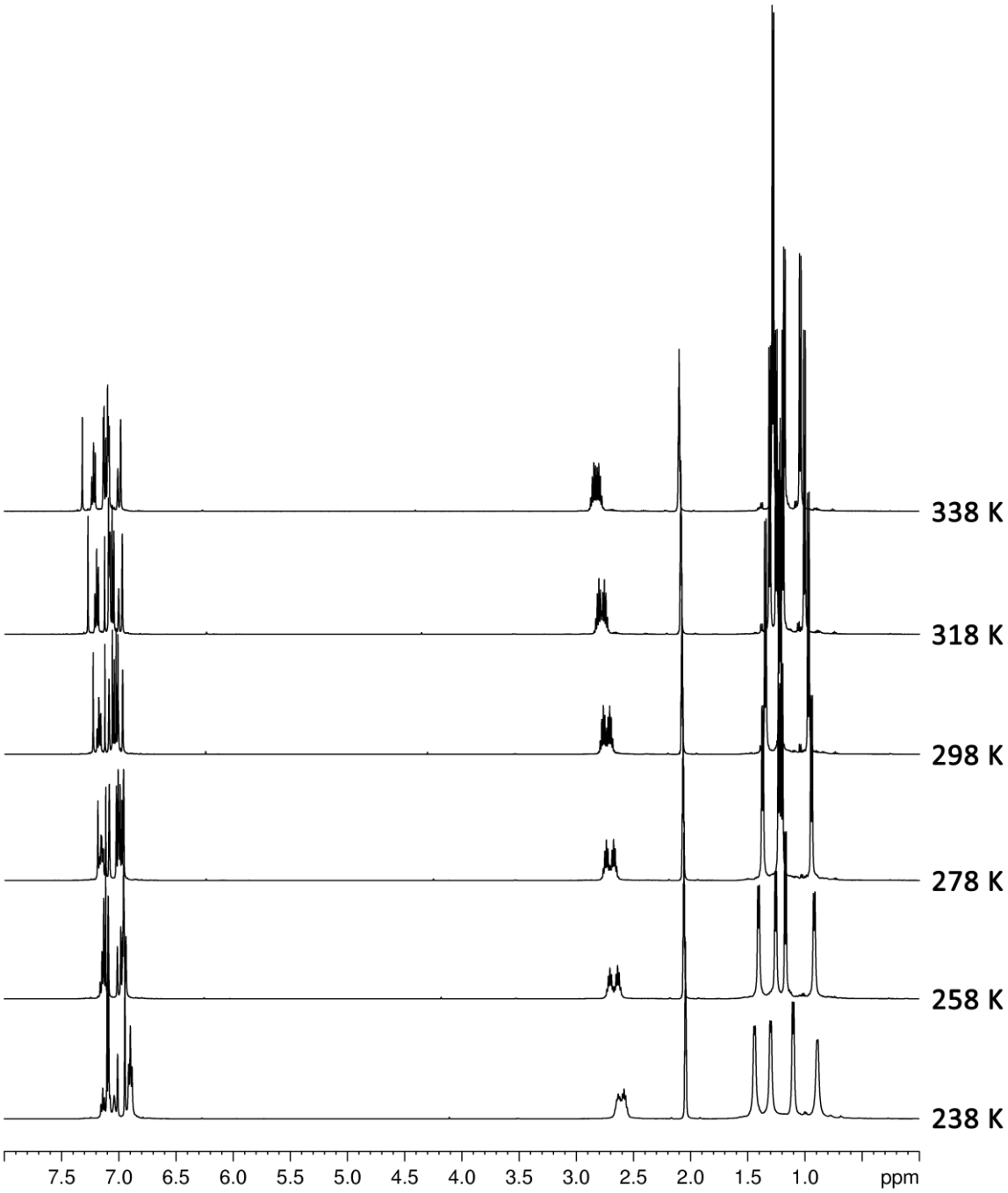

Figure 3.15: Variable temperature ^{1}H NMR at 20 K intervals from 238 K to 338 K revealing the equilibrium between **19** and **27** in d_8-toluene.

In light of the previous results which afforded the starting materials under vacuum, it was determined that the pressure of carbon dioxide also effects the position of the equilibrium. It was possible to observe a constant change in the chemical shift of the resonances in the ^{1}H NMR spectrum of **27** by addition of varying pressures of carbon dioxide to a d_8-toluene

solution of **19** (Figure 3.16). A higher pressure results in a shift towards that of **27** and by applying a partial vacuum, it was possible to revert back towards **19**. Indeed, under dynamic vacuum, and with removal of the solvent, it was possible to remove all dissolved carbon dioxide to afford the starting material.

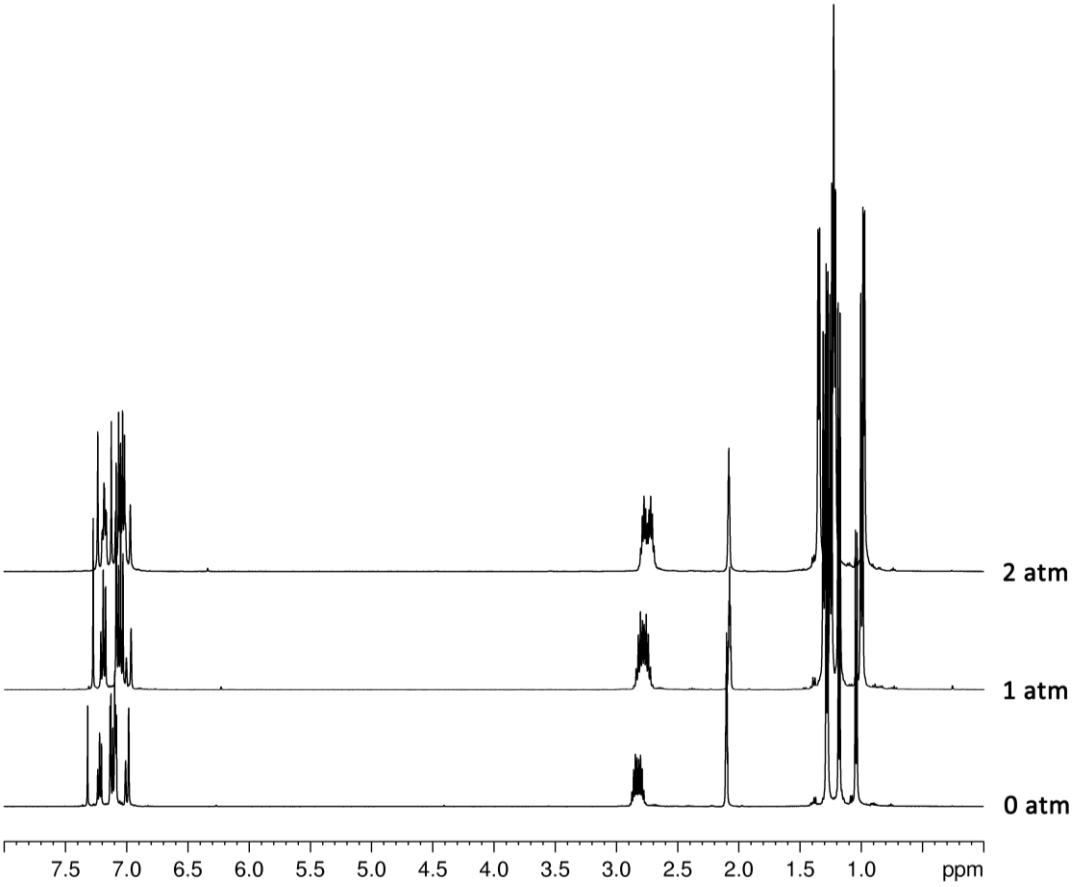

Figure 3.16: ^{1}H NMR of **19** in d_8-toluene and upon addition of 1 and 2 atm of carbon dioxide.

The reason why carbon dioxide is reversibly bound to the carbene moiety in **19**–**21** is a result of both steric and electronic contributions. It has been shown by Louie and co-workers that the bulky imidazolium carboxylate IPr·CO_2 would lose carbon dioxide between 136 and 164 °C in the solid state as determined by thermogravimetric analysis. The less bulky IMes·CO_2 had a higher thermal stability, losing CO_2 at temperatures above 187 °C and I^{i}Pr·CO_2 was stable up to its decomposition temperature of 160 °C.[32] **27**–**29** are functionalised versions of IPr·CO_2 whereby the backbone of the imidazole has been appended with an

inductively electron withdrawing EX_2R moiety. This electron withdrawing effect reduces the binding strength of the C2 position, hence, we can observe reversible carbon dioxide adduct formation at room temperature.

Given the insolubility of **27** in d_8-toluene at low temperatures, it was possible to grow single crystals of **27**·3toluene suitable for single crystal X-ray diffraction by leaving a toluene solution of **27** (formed by addition of carbon dioxide to a degassed solution of **19** in a Schlenk flask) to stand at –80 °C (Figure 3.17).

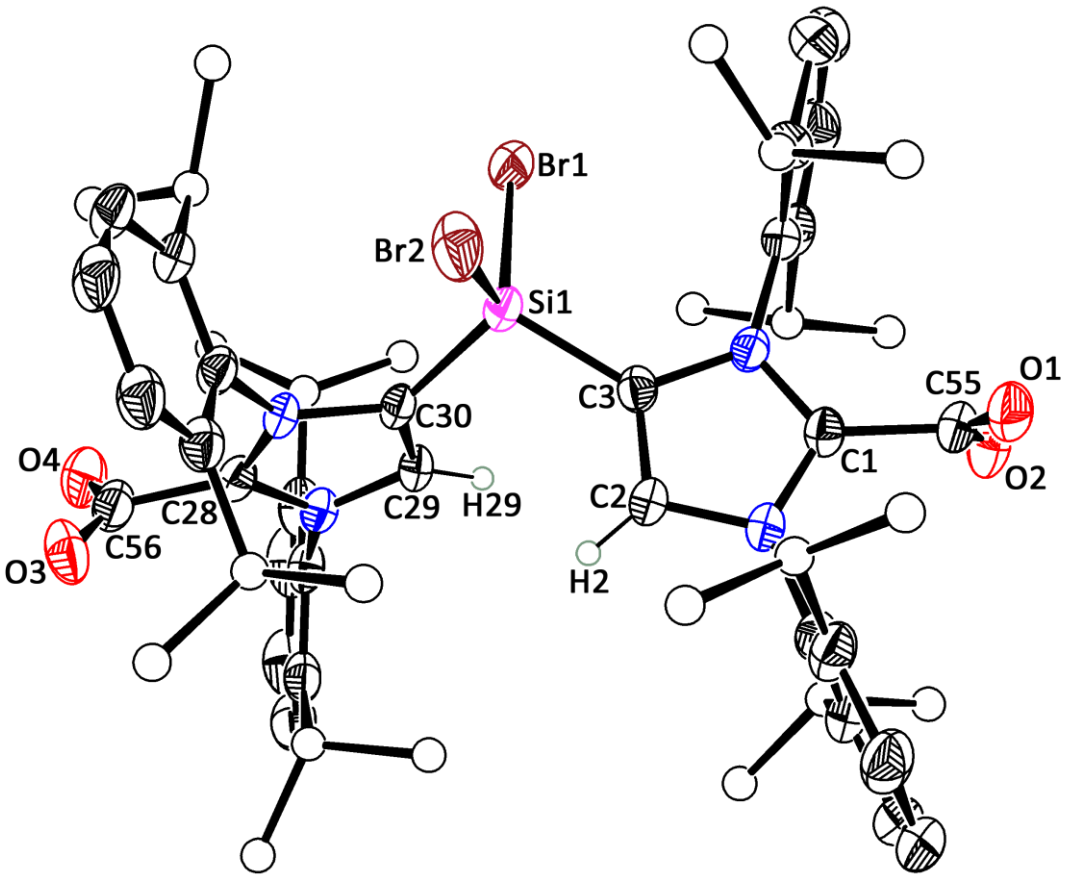

Figure 3.17: Molecular structure of **27**. Anisotropic displacement ellipsoids pictured are set at 50% probability. Hydrogen atoms (with the exception of the imidazole protons labelled H2 and H29) have been omitted for clarity. Atoms of the ^{i}Pr groups, H2 and H29 are pictured as spheres of arbitrary radii.

Attempts to grown single crystals of **28** and **29** by the same method were unsuccessful, however, single crystals of **28**·$3C_6D_6$ were fortuitously obtained on standing of a C_6D_6

solution of **20** and carbon dioxide (Figure 3.18). The poor solubility of **28** in C_6D_6 is likely due to the zwitterionic character of **28** and the non-polar nature of the solvent.

Analysis of the molecular structure of **27** by single crystal X-ray diffraction reveals that it crystallises in the *Pn* space group. The structure shows the presence of two coordinated carbon dioxide molecules which have formed an adduct with the carbene moieties of **19**. The geometry about the silicon atom remains unaffected by coordination of two carbon dioxide molecules and the τ_4' parameter (0.901) reveals a similar, slightly distorted tetrahedral geometry to that observed for **19**. Likewise, the Si1–C3 and Si1–C30 bond lengths remain very similar at 1.844(5) and 1.850(5) Å, respectively, and the Si–Br bond lengths are slightly shorter than those observed for **19** at 2.187(2) and 2.183(2) Å. The formation of the carboxylate anion results in a trigonal planar geometry about the carbon atom from the carbon dioxide molecule ($\Sigma_{\text{bond angles}}$ = 360.0° for both C55 and C56). The O1–C55–O2 and O3–C56–O4 bond angles are widest of the three bond angles about each carbon atom at 132.6(5)° and 134.5(5)°, respectively, which is to be expected due to electrostatic repulsion between the two oxygen atoms which bear significant negative charge. Finally, the C1–C55 and C28–C56 bond lengths were measured to be 1.548(6) and 1.549(6) Å, respectively. Despite the weak adduct formed between the carbene and carbon dioxide, these bond lengths are average for bond lengths observed for unsaturated, uncoordinated imidazolium carboxylate complexes that have been structurally characterised based on a search of the CSD (Mean = 1.538 Å, Standard deviation = 0.016). These bond lengths are notably longer than that observed for IPr·CO_2 which has a C–C bond length of 1.511(4) Å and this may suggest why binding of CO_2 in **27** is weaker than that of IPr·CO_2.[32]

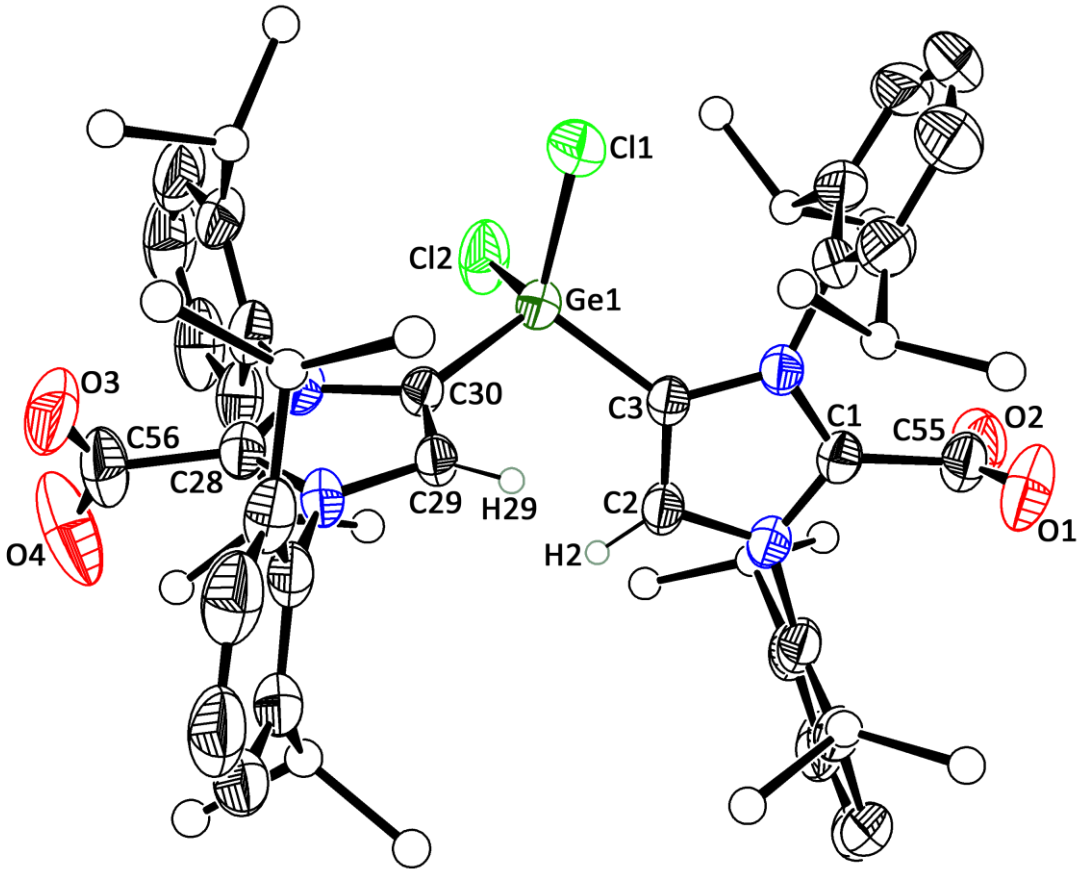

Figure 3.18: Molecular structure of **28**. Anisotropic displacement ellipsoids pictured are set at 50% probability. Hydrogen atoms (with the exception of the imidazole protons labelled H2 and H29) have been omitted for clarity. Atoms of the ^{i}Pr groups, H2 and H29 are pictured as spheres of arbitrary radii.

The geometry about the germanium centre in **28** is much like that of the precursor, **20**, whereby a slight distortion from tetrahedral is observed (τ_4' = 0.944) and the Ge–C bond lengths are very similar to those in **20** at 1.927(3) and 1.940(3) Å. A decrease in the Ge–Cl bond lengths is similar to that seen in previous compounds upon reaction of the carbene moiety. The Ge1–Cl1 and Ge1–Cl2 bond lengths were measured to be 2.103(2) and 2.110(2) Å, respectively. As in the structure of **27**, the geometry about both carboxylate carbons is trigonal planar ($\Sigma_{\text{bond angles}}$ = 360.0° for both C55 and C56) and again, a wider bond angle is observed for O1–C55–O2 and O3–C56–O4 at 132.2(4) and 132.0(5)°, respectively. There is a similar increased bond length of C1–C58 and C28–C56 (1.522(5) and 1.543(5) Å, respectively) relative to that observed in IPr·CO_2.

3.3.4 Further chemistry of (aIPr:)$_2$GeCl$_2$

The reactivity described thus far involves the addition of an electrophilic reagent to the carbene moieties of **18**–**21**. Naturally, the option for adding nucleophilic or electron rich reagents also exists as such species should react with the EX_2 moieties of **18**–**21**. Addition of two equivalents of methyllithium in diethyl ether to a diethyl ether solution of **20** results in the formation of (aIPr:)$_2$GeMe$_2$ (**30**) as determined by ^{1}H and ^{13}C{^{1}H} NMR spectroscopy (Scheme 3.8). The spectra for **30** are similar to that of **20** in C_6D_6 whereby the characteristic backbone imidazole resonance appears at 7.10 ppm and two septet resonances at 2.99 and 2.83 ppm can be assigned to the methine protons. The most diagnostic resonance attributable to **30** is the of the two germanium bound methyl groups which give rise to a singlet resonance at –0.10 ppm which integrates to six protons giving conclusive evidence for the presence of the two methyl groups in **30**. Likewise, the ^{13}C{^{1}H} NMR spectrum of **30** reveals the three imidazole resonances attributable to the carbene carbon, germanium bound carbon and protonated alkenic carbon at 223.6, 130.9 and 130.0 ppm along with a resonance at –0.5 ppm which can be assigned to the germanium bound methyl carbon atoms. Analysis of a solid sample of **30** by electron ionisation mass spectrometry (EI-MS) reveals the molecular ion at 878.4138, $[(aIPr:)_2GeMe_2]^+$ (Clacd. 878.5282), at 4% intensity due to the extensive fragmentation that occurs through this method of ionisation.

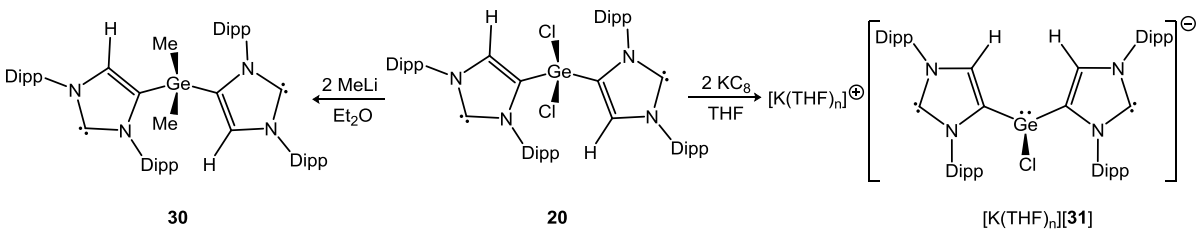

Scheme 3.8: Reaction of **20** with two equivalents of either methyl lithium or potassium intercalated graphite.

Given the precedence for heavier group 14 elements to also form compounds in the +2 oxidation state, we sought to reduce **20** using two equivalents of KC_8 (amongst other reducing agents) with the aim of accessing the germanium(II) species $(aIPr:)_2Ge$. These reactions were unsuccessful, however, it was possible to synthesise the germanium(II) anion, $[(aIPr:)_2GeCl]^-$, by addition of two equivalents of KC_8 to **20** in THF, followed by filtration of the reaction solution into an ampoule containing 2,2,2-crypt (Scheme 3.8). Slow diffusion of hexane into the THF solution allowed for the growth of single crystals of [K(2,2,2-crypt)][$(aIPr:)_2GeCl$]·THF·hexane ([K(2,2,2-crypt)][**31**]·THF·hexane) suitable for single crystal X-ray diffraction.

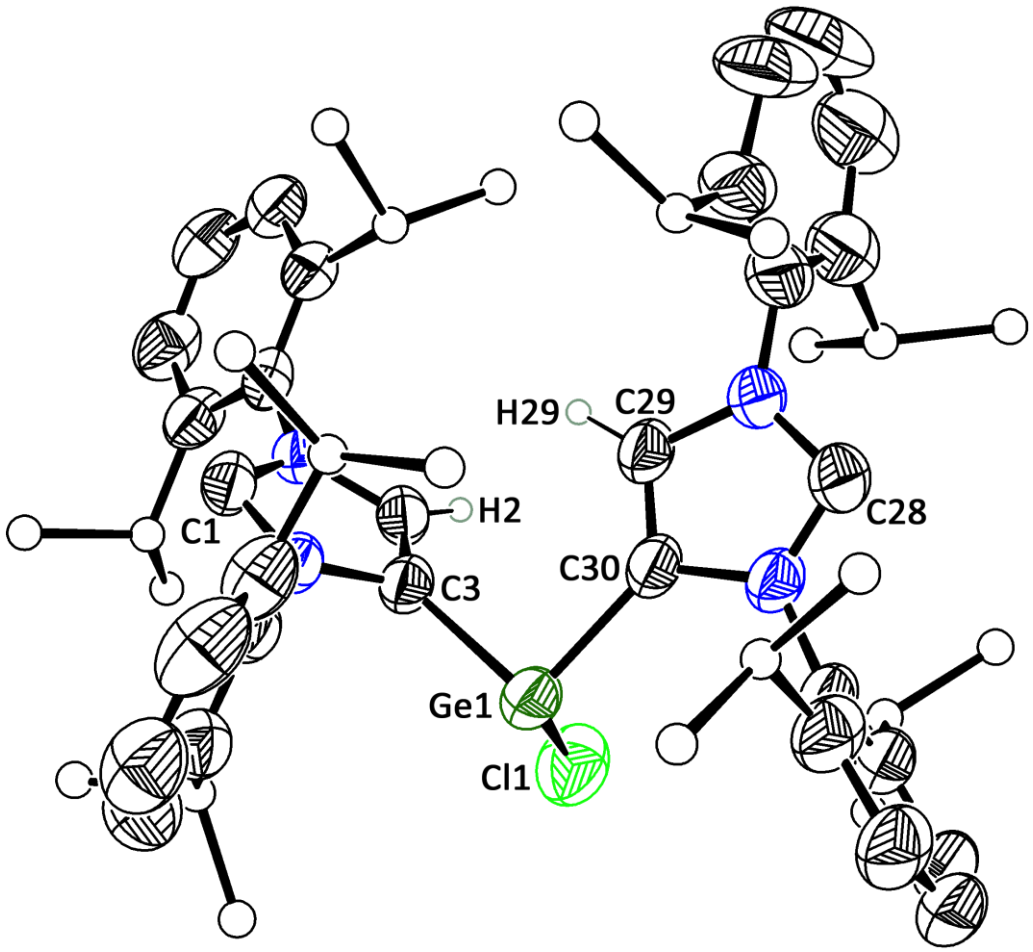

Figure 3.19: Structure of anion **31** in [K(2,2,2-crypt)][**31**]·THF·hexane. Anisotropic displacement ellipsoids pictured are set at 50% probability. Hydrogen atoms (with the exception of the imidazole protons labelled H2 and H29) have been omitted for clarity. Atoms of the ^{i}Pr groups, H2 and H29 are pictured as spheres of arbitrary radii.

The diagnostic backbone imidazole proton gives rise to a singlet resonance at 6.86 ppm in the ^{1}H NMR spectrum of **31** in d_8-THF. This is similar to that observed for other anionic, bis(aIPr:)–group 14 species such as the ions **6**–**10**. An identical doubling of certain resonances in the ^{1}H NMR spectrum is also observed (i.e. four septet methine resonances and 12 doublet methyl resonances).

Analysis of the crystals by single crystal X-ray diffraction provides unambiguous evidence for the formation of a germanium(II) species which has retained a chloride ligand (Figure 3.19) and therefore bears a negative charge and is accompanied by single counter cation, $[K(2,2,2\text{-crypt})]^+$. The geometry about the germanium centre is trigonal pyramidal, as expected for a three coordinate, anionic germanium(II) species ($\Sigma_{\text{bond angles}}$ = 282.9°) which has a stereochemically active lone pair of electrons. There is a significant increase in the Ge1–C3 and Ge1–C30 bond lengths (2.025(7) and 2.036(6) Å) of approximately 0.11 Å upon formation of **31**. This can be explained by the reduced electrophilicity of the germanium centre upon addition of two electrons. Similarly, there is an increase in the Ge–Cl bond length of approximately 0.14 Å to 2.283(3) Å which is due to identical reasons. Clearly, the electrophilicity of the proposed germylene, (aIPr:)Ge, is sufficiently great enough such that binding of a chloride anion outweighs the enthalpic gain of precipitation as KCl.

3.4 Synthesis of novel tin compounds

3.4.1 Reactivity of $[K(aIPr:)]_\infty$ with SnX_4 (X = Cl, Br)

Following a similar synthetic procedure which afforded **18**–**21**, addition of $SnCl_4$ to two equivalents of $[K(aIPr:)]_\infty$ suspended in hexane affords a novel species. Allowing the reaction solution to stir overnight, followed by filtration and evaporation of the solvent affords $(aIPr:)_2SnCl_2$ (**32**) in 52% yield. **32** was characterised by ^{1}H NMR spectroscopy whereby the

diagnostic backbone imidazole proton was found to resonate at 6.34 ppm in d_8-THF and most notably, satellites due to coupling to ^{117}Sn and ^{119}Sn spin $^1/_2$ nuclei with a coupling constant of 6 Hz. The difference in coupling constant to the two different tin nuclei is too small for separate satellite resonances to be observed. As expected, two septet methine resonances are apparent at 2.57 and 2.54 ppm. Interestingly, the three imidazole carbons can be observed in the $^{13}C\{^1H\}$ NMR spectrum of **32** in d_8-THF and the carbene carbon, protonated alkenic imidazole carbon and the tin bound carbon can be observed at 226.4, 131.8 and 127.7 ppm, respectively, and all display coupling to ^{117}Sn and ^{119}Sn nuclei with intensities proportional to their natural abundance (Natural abundance of ^{117}Sn = 7.61%, $\gamma = -9.589\times10^7$ rad·s^{-1}·T^{-1}; Natural abundance of ^{119}Sn = 8.58%, $\gamma = -10.014\times10^7$ rad·s^{-1}·T^{-1}).[36] Coupling to ^{115}Sn, which is a spin $^1/_2$ nucleus, is also possible but due to its low natural abundance (0.34%), cannot be observed. The three bond coupling constant between the carbene carbon and tin nuclei is too small to observe distinct satellites for each nuclei and a single constant of 23 Hz can be measured. The two bond coupling between the protonated imidazole carbon and the two tin nuclei can be observed as distinct resonances with a coupling constant of 152 Hz and 159 Hz, both are greater than the three bond coupling constant as expected. The larger coupling constant can be assigned to that of the ^{13}C–^{119}Sn coupling and the ratio of the two coupling constants is equal to the ratio of the two gyromagnetic ratios (1.046 and 1.044, respectively). To the same effect, the one bond coupling constant between the tin bound carbon and the two tin nuclei are the largest at 724 Hz and 758 Hz, respectively, where the ratio of the two values can be calculated to be 1.047. Finally, a single resonance at –120.2 ppm was observed in the $^{119}Sn\{^1H\}$ NMR spectrum of **32** in d_8-THF.

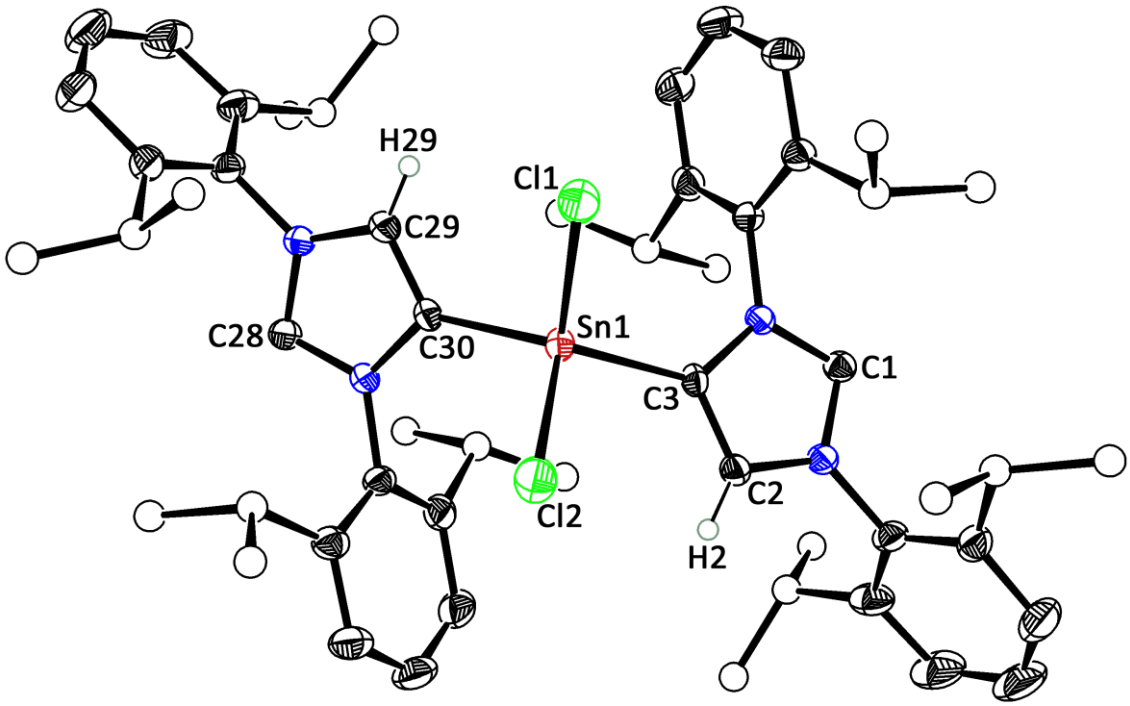

Figure 3.20: Molecular structure of **32**. Anisotropic displacement ellipsoids pictured are set at 50% probability. Hydrogen atoms (with the exception of the imidazole protons labelled H2 and H29) have been omitted for clarity. Atoms of the ^{i}Pr groups, H2 and H29 are pictured as spheres of arbitrary radii.

32 can be crystallised from a concentrated hexane solution at 4 °C and analysis by single crystal X-ray diffraction reveals that **32** crystallises isomorphous with **20** in the space group *P*1 whereby the unit cell parameters are very similar for the two crystals (Figure 3.20). The tin centre is significantly distorted from tetrahedral as indicated by the τ_4' parameter which can be calculated to be 0.810. This is mainly due to the splaying of the two aIPr: ligands which have a large C3–Sn1–C30 bond angle of 127.8(2)° (cf. 125.4(2)° for **20**) in this conformation. The Sn1–C3 and Sn1–C30 bond lengths (2.097(2) and 2.103(3) Å, respectively) are within the range expected based on the sum of covalent radii (Σr_{cov} = 2.12 Å).[31] These distances are also in line with the increase expected on changing the group 14 element from germanium (in **20**) to tin (Δr_{cov} = 0.19 Å) whereby the E–C bond lengths have increased by approximately 0.18 Å. Likewise, an increase in the E–Cl bond lengths of approximately 0.17 Å to 2.316(1) and 2.319(1) Å is in line with the increase in the covalent radius of the group 14 element.

The synthesis of **32** is not as general as the synthesis of **18**–**21**, attempts to synthesise **32** by the addition of $SnCl_4$ to two equivalents of $[K(aIPr:)]_\infty$ in THF did not afford **32** in any appreciable yield. Instead, the anionic species, $[(aIPr:)_3SnCl_2]^-$ (**33**), was observed which can be specifically targeted by reaction of the reagents in a 1 : 3 ratio (Scheme 3.9). Similarly, equivalent reactions with either $[Li(aIPr:)]_\infty$ or $[K(aIPr:)]_\infty$ with $SnBr_4$ resulted in the reduction of the tin centre and bromination of the backbone of the imidazole. This redox chemistry results in the formation of a large mixture of species from which no useful products could be isolated as compositionally pure samples. This reactivity is to be expected based upon the lower reduction potential of $SnBr_4$ relative to $SiBr_4$ or $GeBr_4$ and $SnCl_4$ (i.e. the precedence of the +2 oxidation increases down group 14 and the oxidation potential of chlorine is greater than that of bromine).

Addition of $SnCl_4$ in THF to a suspension of three equivalents of $[K(aIPr:)]_\infty$ in THF, followed by 2,2,2-crypt, allows for the synthesis of **33** and isolation as the $[K(2,2,2\text{-crypt})]^+$ salt. **33** consists of a five-coordinate tin centre bonded to three aIPr: ligands in a trigonal planar arrangement and two axial chloride ligands (affording an overall, trigonal bipyramidal complex). The trigonal planar arrangement of the aIPr: ligands is similar to that observed in the anionic mercury complex $[(aIPr:)_3Hg]^-$, **15**. A similar ^1H NMR spectrum of **33** in d_8-THF arises as a result and the imidazole proton can be observed at 4.66 ppm, highly upfield relative to other aIPr: complexes. This results from the proximity of the imidazole proton over the face of an aromatic ring of an adjacent Dipp group. As expected, two septet methine resonances are all observed at 3.04 and 2.74 ppm. **33** was also characterised by $^{13}C\{^1H\}$ NMR spectroscopy whereby three imidazole resonances were observed at 217.0, 142.8 and 128.4 ppm for the carbene carbons, tin bound carbon atoms and protonated imidazole carbons, respectively. As in the $^{13}C\{^1H\}$ NMR spectrum of **32**, satellite resonances can be observed for the carbene carbons and the tin bound carbon atoms of **33**. The three bond coupling

constant (to both ^{117}Sn and ^{119}Sn) was found to be very similar at 23 Hz and the one bond coupling constants for the ^{13}C–^{117}Sn and ^{13}C–^{119}Sn coupling are 1041 Hz and 1090 Hz, respectively. Again, the ratio of the coupling constants (1.047) is as expected. Finally, a single resonance was observed in the ^{119}Sn{^{1}H} NMR spectrum at –389.1 ppm which is downfield relative to that of **32** as expected for a formal addition of an anionic, aIPr: ligand.

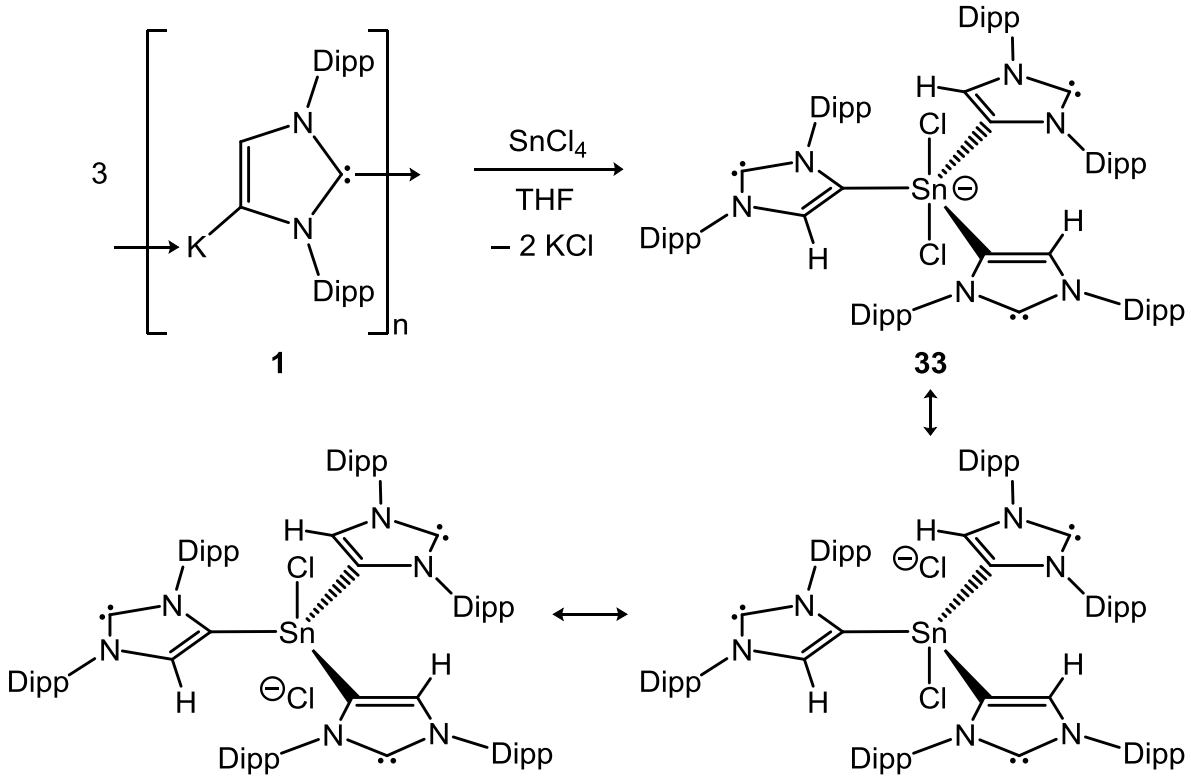

Scheme 3.9: Synthesis and resonance structures of **33** which describe the three-centre-four-electron bonding.

Analysis of the molecular structure of **33** by single crystal X-ray diffraction unambiguously confirms the trigonal bipyramidal structure whereby the two chloride ligands occupy the axial positions. The tin centre can be described as hypervalent due to the apparent presence more than eight electrons in the valence shell. As illustrated in the resonance structures in Scheme 3.9, the two axial chloride ligands can be considered to form a three-centre-four-electron bond whereby the formal bond order of each Sn–Cl bond can be considered to be $^{1}/_{2}$ and the highest occupied molecular orbital (HOMO) is an in phase set of

p orbitals localised equally on the terminal chloride ions.[37] The five-coordinate complex can be described by a τ_5 parameter which gives a numerical value to quantify the structure somewhere between a trigonal pyramidal ($\tau_5 = 1$) and square pyramidal geometry ($\tau_5 = 0$).[38]

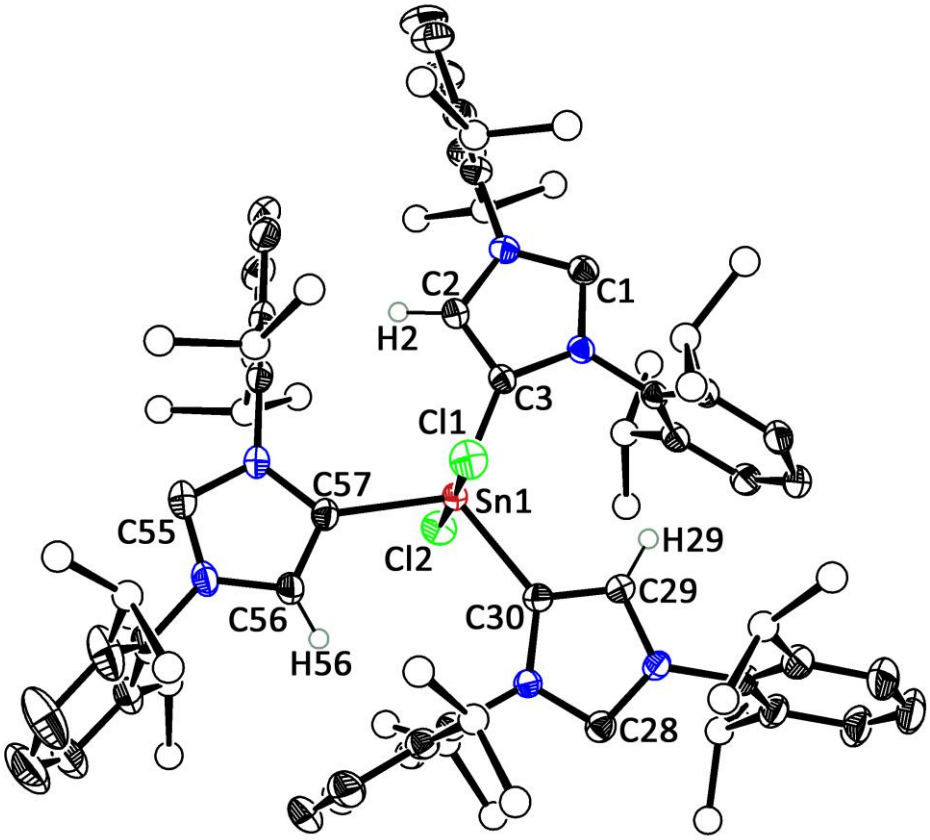

Figure 3.21: Structure of anion **33** in [K(2,2,2-crypt)][**33**]·2THF. Anisotropic displacement ellipsoids pictured are set at 50% probability. Hydrogen atoms (with the exception of the imidazole protons labelled H2, H29 and H56) have been omitted for clarity. Atoms of the ^{i}Pr groups, H2, H29 and H56 are pictured as spheres of arbitrary radii.

The τ_5 parameter of **33**, 0.964, confirms the trigonal bipyramidal geometry (Figure 3.21). The three aIPr: ligands lie almost perfectly in a trigonal planar arrangement (C3–Sn1–C30 = 119.4(1)°, C30–Sn1–C57 = 119.9(1)° and C57–Sn1–C3 = 120.6(1)°; $\Sigma_{\text{bond angles}}$ = 360.0°). Likewise, the axial chloride ligands lie in an almost perfectly linear geometry about the tin centre (Cl1–Sn1–Cl2 = 178.4(1)°). The three Sn–C bond lengths are all similar (2.163(2), 2.158(2) and 2.159(2) Å) and are slightly longer than that expected based on the sum of covalent radii (2.12 Å). In all likelihood, this results from the anionic character

of **33** which reduces the electrophilicity of the tin centre and reduces the Sn–C bond strength. Likewise, a substantial increase in the Sn–Cl bond lengths (2.543(1) and 2.515(1) Å) is observed in **33** relative to **32** (approximately 0.21 Å longer) which is in line with the three-centre-four-electron bonding model. Finally, analysis by ESI-MS reveals a mass envelope at 1351.2 in the negative ion mode which can be assigned to **33** (Calcd 1351.7).

The increased stability of tin(II) relative to the lighter group 14 elements in the +2 oxidation state prompted us to reduce **33** with two equivalents of KC_8 in THF (Scheme 3.10). The reaction results in elimination of two equivalents of KCl and the formation of the trigonal pyramidal, homoleptic anionic complex $[(aIPr:)_3Sn]^-$ (**34**). It was also possible to synthesise **34** by addition of $SnCl_4$ to three equivalents of $[K(aIPr:)]_\infty$ in THF (as in the synthesis if **33**) followed by addition of two equivalents of KC_8 to the reaction mixture. Filtration of the solvent into a Schlenk flask containing 18-crown-6 allows for the isolation of **34** as the $[K(18\text{-crown-6})(THF)_2]^+$ salt.

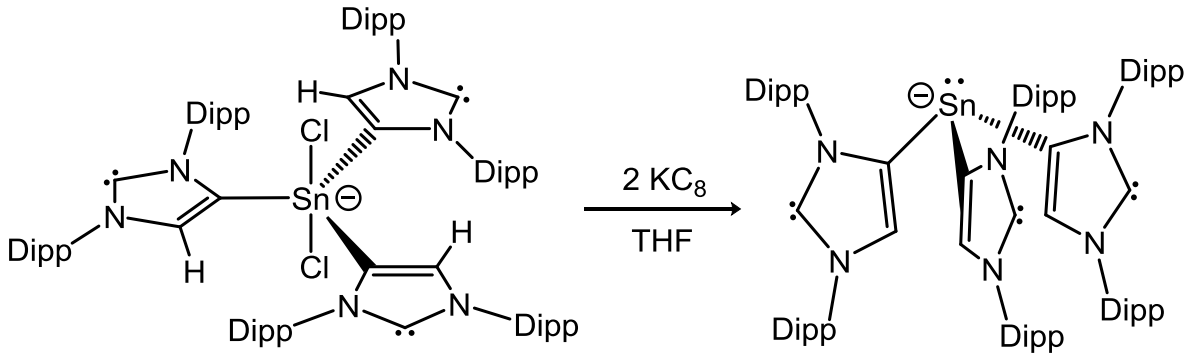

Scheme 3.10: Synthesis of **34** by reduction of **33** with two equivalents of KC_8.

Analysis of the ^1H NMR spectrum of **34** in d_8-THF reveals the backbone imidazole resonance at 6.70 ppm. The restricted rotation about the N–Dipp bond results in the presence of four septet methine resonances at 3.02, 2.94, 2.86 and 2.62 ppm along with eight doublet methyl resonances. Unexpectedly, satellites can be observed either side of the most downfield methyl

resonance at 0.52 ppm which likely results from the proximity of the methyl group to the tin atom through space; the dipolar coupling constant is 88 Hz.

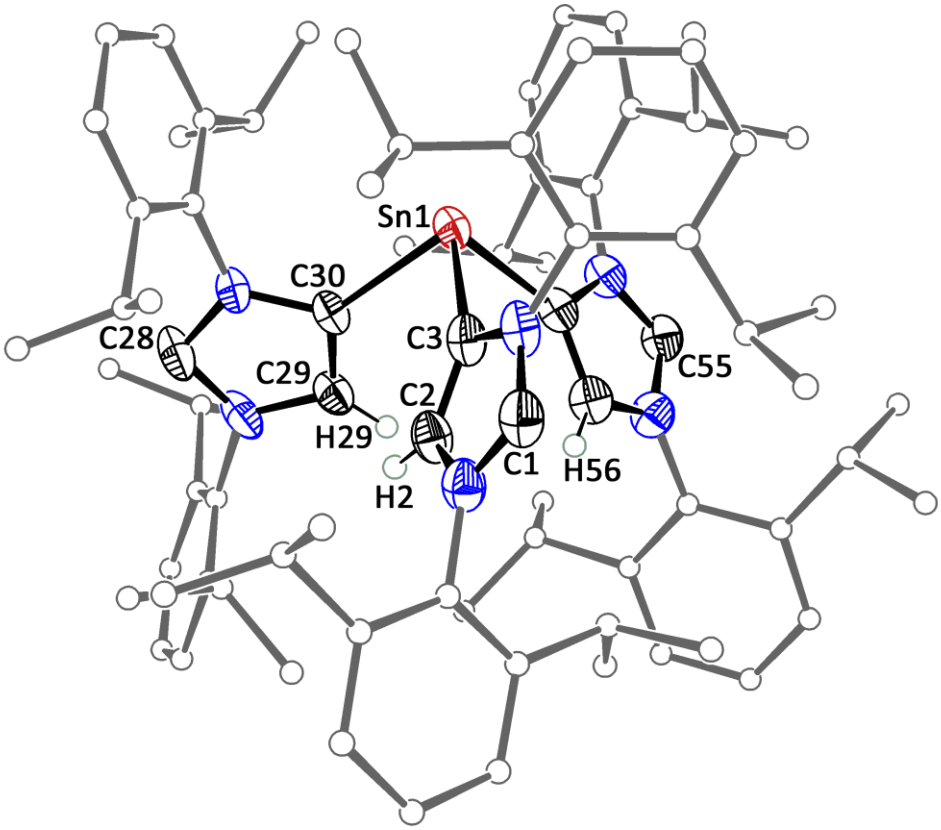

Figure 3.22: Structure of anion **34** in [K(2,2,2-crypt)][**34**]. Anisotropic displacement ellipsoids pictured are set at 50% probability. Hydrogen atoms (with the exception of the imidazole protons labelled H2, H29 and H56) have been omitted for clarity. Atoms of the Dipp groups, H2, H29 and H56 are pictured as spheres of arbitrary radii.

The carbene carbon resonance can be observed at 220.2 ppm in the $^{13}C\{^{1}H\}$ NMR spectrum along with resonances at 150.7 and 129.6 ppm which result from the tin bound imidazole carbon and the protonated imidazole carbon atoms, respectively. However, no satellites due to coupling to the ^{117}Sn or ^{119}Sn nuclei was observed for these resonances. A dipolar coupling to the most downfield methyl carbon resonance at 22.1 ppm of 50 Hz can be observed. A single resonance in the $^{119}Sn\{^{1}H\}$ NMR spectrum was observed for **34** at –352.8 ppm.

Single crystals of [K(2,2,2-crypt)][**34**] suitable for analysis by single crystal X-ray diffraction were grown by slow diffusion of hexane into a THF solution (Figure 3.22). Crystals of **34** as the $[K(18\text{-crown-6})(THF)_2]^+$ salt were grown by the same method, however, analysis of these pale pink cubic crystals by single crystal X-ray diffraction suggested a unit cell where a = 49.5490(4) Å and a suggested space group of $Pn\bar{3}n$. Even using synchrotron radiation at Diamond Light Source, there was not enough high angle data to afford a solution and periodic disorder is apparent by the presence of systematic diffuse scattering between reflections. Regardless, NMR data for **34** is identical for both salts and confirms the formation of **34**.

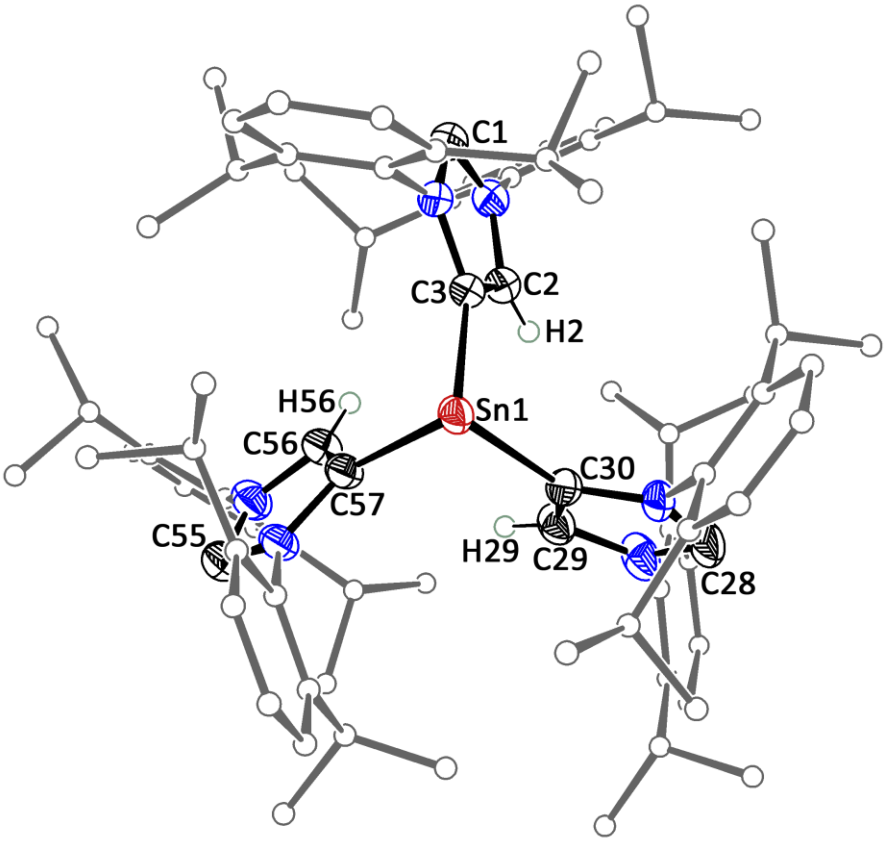

Figure 3.23: Structure of anion **34** as viewed down the C_3 rotation axis. Anisotropic displacement ellipsoids pictured are set at 50% probability. Hydrogen atoms (with the exception of the imidazole protons labelled H2, H29 and H56) have been omitted for clarity. Atoms of the Dipp groups, H2, H29 and H56 are pictured as spheres of arbitrary radii.

Analysis of the molecular structure unambiguously reveals the homoleptic, trigonal pyramidal anion, $[(aIPr:)_3Sn]^-$. The trigonal pyramidal geometry is clear from the sum of bond angles

about the tin centre (272.1°). The three aIPr: ligands are bonded equally to the tin centre where the Sn1–C3, Sn1–C30 and Sn1–C57 bond lengths were measured to be 2.234(5), 2.241(5) and 2.241(5) Å, respectively. These distances are a substantial increase on the Sn–C bond lengths observed for **33** by approximately 0.08 Å. This is expected based upon the reduction in oxidation state of the tin centre coupled with the increase steric clash between the ligands on being forced to adopt a trigonal pyramidal arrangement. The presence of a C_3 rotation axis is illustrated in Figure 3.23 and as a result of the substantial steric bulk of the ligands, restricted rotation about a number of bonds results in the complexity observed in the ^{1}H and $^{13}C\{^{1}H\}$ NMR spectra. The molecular structure also reveals how one methyl group of each ligand is forced to reside in the direction of the tin centre. As a result, dipolar coupling can be observed between this carbon (which is downfield shifted due to its proximity to the metal centre) and the tin atom.

3.4.2 Isomerisation of (IPr)SnX_4 (X = Cl, Br) with additional IPr

With the aim of synthesising (IPr)$SnBr_4$ for structural comparison, it was discovered that isomerisation of the IPr ligand can occur, likely promoted by free IPr in solution, much like what was observed in the attempted synthesis of (IPr)$GeBr_4$. Similar to (IPr)$GeCl_4$, the (IPr)$SnCl_4$ adduct has already been synthesised and structurally characterised.[39] It was determined that upon addition of two equivalents of IPr to a THF solution of either $SnCl_4$ or $SnBr_4$ will promote isomerisation of the ligand as was the case in the synthesis of **19** and **21**. However, even in the presence of additional IPr, the final product that crystallises from solution is (aIPr)$_2SnCl_4$ (**35**) or (aIPr)$_2SnBr_4$ (**36**), respectively, after heating at 65 °C whereby both equivalents of IPr have isomerised to afford two aIPr ligands, abnormally bonded to the tin centre (Scheme 3.11). Unlike the synthesis of **19** and **21**, by addition of four equivalents

of IPr, any excess IPr does not deprotonate **35** or **36** and the products are the zwitterionic species which crystallise from the THF reaction solvent.

A combination of the ability of tin to form hypervalent complexes (i.e. retain all four coordinating halide ligands along with two new aIPr ligands) coupled with the reduced electronegativity of tin with respect to germanium or silicon reduces the acidity of the C2 imidazolium proton. Therefore, the hypothetical $(aIPr)_2EBr_4$ (E = Si or Ge) is sufficiently acidic to be deprotonated by free IPr in solution which resulted in precipitation of the ionic salt, [IPrH]Br·THF.

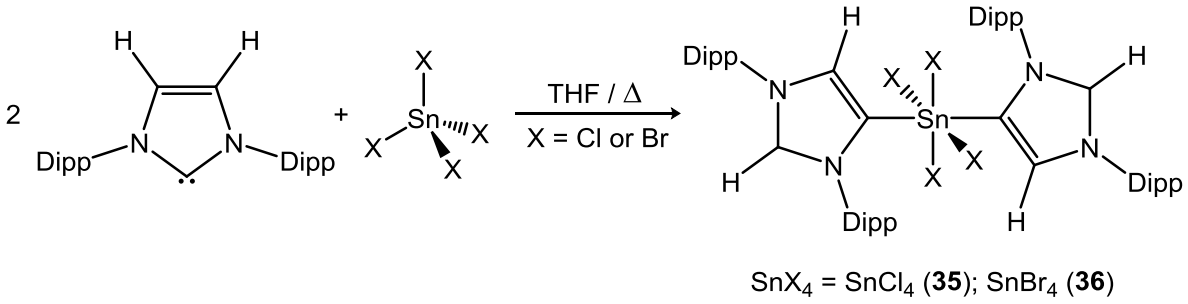

Scheme 3.11: Isomerisation of two equivalents of IPr in the coordination sphere of tin tetrachloride or tin tetrabromide to afford **35** and **36**.

Finally, it is interesting to note that reaction of alkali metals salts of aIPr: result in reduction of $SnBr_4$, however, under these reaction conditions, the formation of an aIPr ligand bonded to an $SnBr_4$ moiety was possible and no reduction chemistry was observed. **36** was isolated in an 80% crystalline yield under these conditions (**35** was also isolated in 92% crystalline yield indicating the effectiveness of the isomerisation). It was however possible to crystallise $(IPr)SnBr_4$ (See Appendix A, Figure A.5) upon diffusion of hexane into a reaction mixture of one equivalent of IPr with $SnBr_4$ prior to isomerisation.

Analysis of the ^{1}H NMR spectra of **35** and **36** in d_8-THF reveal the presence of the C2 proton as a doublet resonance at 8.75 and 8.74 ppm, respectively, both with a coupling constant of

2 Hz. The other doublet with a 2 Hz coupling constant can be observed at 8.30 and 8.68 ppm due to the backbone imidazole proton in **35** and **36**, respectively. Additionally, satellites due to coupling to the ^{117}Sn and ^{119}Sn nuclei are also observed. The coupling constants were observed to be very similar at 18 Hz, 19 Hz, 17 Hz and 21 Hz, respectively, for these resonances. Likewise, in the $^{13}C\{^{1}H\}$ spectra, resonances attributable to the three imidazole carbons were also found to have satellites due to coupling to the tin nuclei (Table 3.2).

Resonance	$(aIPr)_2SnCl_4$ (**35**)	$(aIPr)_2SnBr_4$ (**36**)
NC*C*HN Chemical shift (δ)	161.0	153.2
^{117}Sn / ^{119}Sn Coupling constant (Hz)	1394 / 1459	1272 / 1332
H*C*N$_2$ Chemical shift (δ)	137.6	137.3
^{117}Sn / ^{119}Sn Coupling constant (Hz)	47	42
NC*C*HN Chemical shift (δ)	132.5	131.0
^{117}Sn / ^{119}Sn Coupling constant (Hz)	141 / 148	157 / 164

Table 3.2: Comparison of chemical shifts of the imidazole carbon resonances in the $^{13}C\{^{1}H\}$ NMR spectra of **35** and **36** in d_8-THF.

35 and **36** were also characterised by a single resonance shifted highly downfield in the $^{119}Sn\{^{1}H\}$ NMR spectrum in d_8-THF at –602.7 and –969.2 ppm, respectively.

Both **35** and **36** are sparingly soluble in THF and thus upon forming in the THF reaction solvent, they both readily crystallise due to their zwitterionic character. Single crystals suitable for single crystal X-ray diffraction of both were obtained from the reaction solution. However, higher quality crystals of **35**·hexane were obtained by slow diffusion of hexane into a saturated THF solution and higher quality crystals of **36**·$3C_6H_6$ were fortuitously obtained upon attempted dissolution of a sample of **36** in benzene.

Analysis of the molecular structure of **35** unambiguously reveals the presence of two aIPr ligands, *trans* to one another, coordinated via the abnormal backbone imidazole carbon to a square planar $SnCl_4$ moiety (Figure 3.24). The result is a distorted octahedral, zwitterionic compound whereby the hypervalent tin centre can again be described by a combination of three-centre-four-electron bonds. The square planar arrangement of the chloride ligands can be described by the τ_4' parameter which can be calculated to be 0.074. This value indicates very little deviation from a perfect square planar arrangement which would be zero.

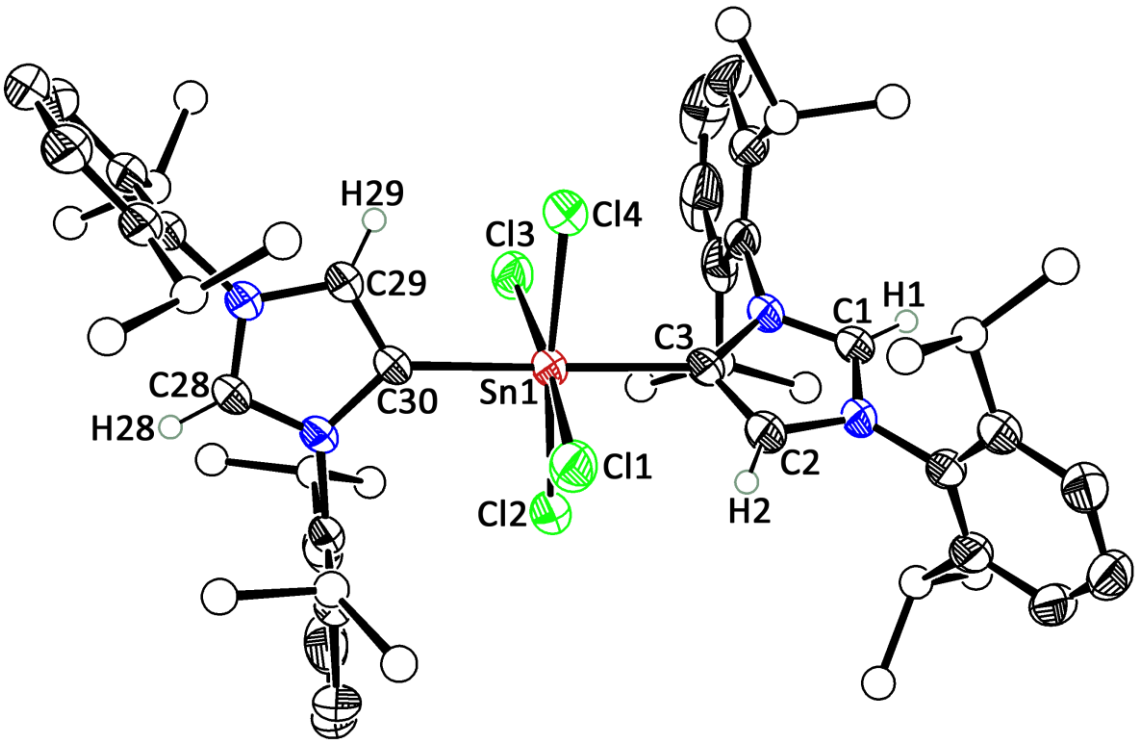

Figure 3.24: Molecular structure of **35**. Anisotropic displacement ellipsoids pictured are set at 50% probability. Hydrogen atoms (with the exception of the imidazole protons labelled H1, H2, H28 and H29) have been omitted for clarity. Atoms of the ^{i}Pr groups and hydrogen atoms are pictured as spheres of arbitrary radii.

Similarly, the *trans* arrangement of the two aIPr ligands is evidenced by the C3–Sn1–C30 bond angle which is near linear at 175.4(2)°. The two ligands do not lie in the same plane nor perpendicular to one another, and indeed, the torsion between the two imidazole rings

(C2–C3–C30–C29 = 125.8°) results from the minimisation of the steric clash between the bulky Dipp substituents and the chloride ligands.

Consistent with a hypervalent tin centre, the four Sn–Cl bond lengths are relatively long at 2.487(2), 2.455(2), 2.455(2) and 2.490(2) Å. Likewise, the Sn1–C3 and Sn1–C30 bond lengths are long at 2.192(4) and 2.195(4) Å, however shorter than those observed for **34**.

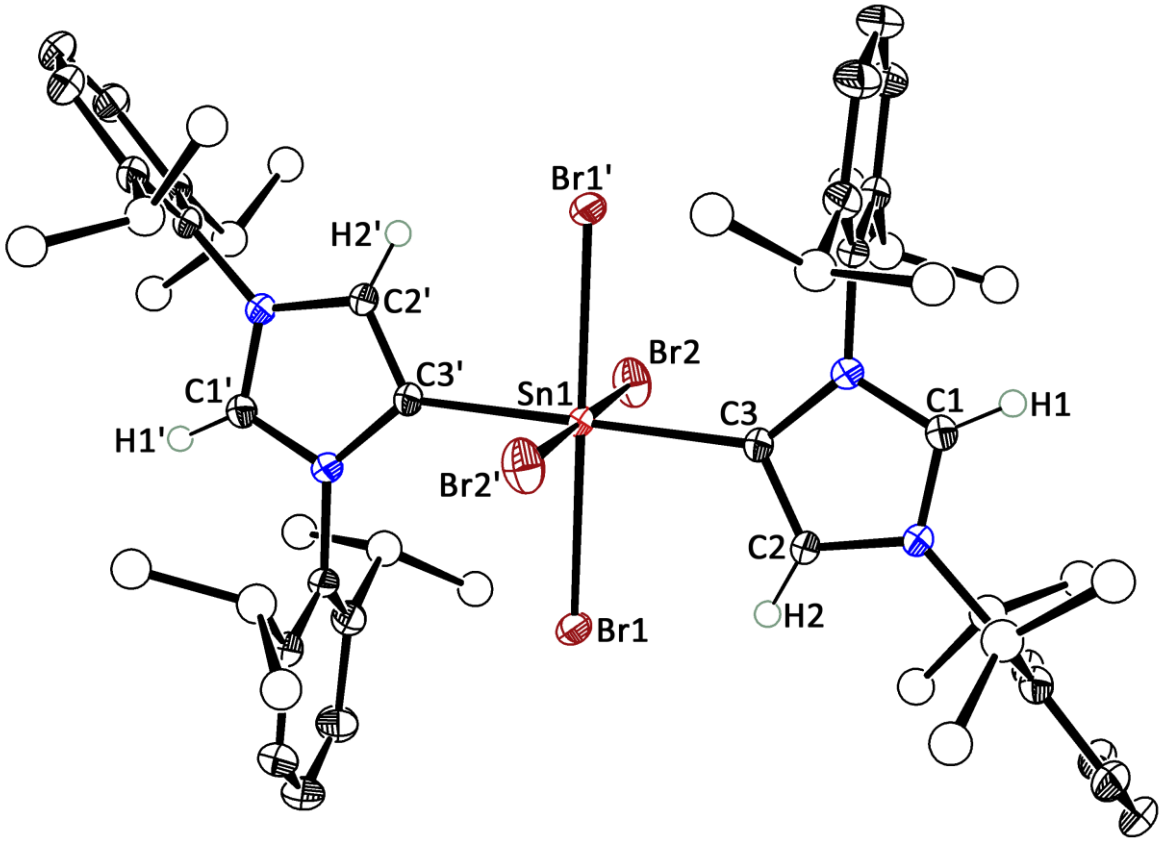

Figure 3.25: Molecular structure of **36**. Anisotropic displacement ellipsoids pictured are set at 50% probability. Hydrogen atoms (with the exception of the imidazole protons labelled H1, H2, H1' and H2') have been omitted for clarity. Atoms of the ^{i}Pr groups and hydrogen atoms are pictured as spheres of arbitrary radii. Symmetry operation: *–x*, *–y*, *–z*.

36·3C_6H_6 crystallises in the $P\bar{1}$ space group with the tin atom residing on a centre of inversion (Figure 3.25). The two aIPr ligands and two sets of the bromide ligands are related by this inversion symmetry. Analysis of the molecular structure of **36**·3C_6H_6 reveals the presence of two aIPr: ligands whose imidazole rings lie in the same plane and are also related by a C_2

rotation axis which passes through the Br2–Sn1–Br2' bonds (C2–C3–C3'–C2' = 180.0°). Similarly, the C3–Sn1–C3', Br1–Sn1–Br1' and Br2–Sn1–Br2' bond angles are 180.0° by symmetry. The square planar arrangement is only slightly distorted due to the Br1–Sn1–Br2 bond angle of 89.4(1)°. The Sn1–Br1 and Sn1–Br2 bond lengths (2.635(1) and 2.620(1) Å) are marginally longer than that expected based on the sum of covalent radii of tin and bromine (Σr_{cov} = 2.59 Å).[9] The increase in Sn–X bond lengths on changing from chlorine to bromine by approximately 0.15 Å is in line with that expected based on the larger covalent radius of bromine relative to chlorine (Δr_{cov} = 0.18 Å). The Sn1–C3 is marginally longer in **36** than in **35** (2.242(2) Å). Finally, analysis of a sample of **36** in DCM by ESI-MS reveals a mass envelope at 1135.2164 which can be ascribed to **36** having lost a bromide ion during analysis to form the cation, $[(aIPr)_2SnBr_3]^+$ (Calcd 1135.2309).

3.4.3 Halide abstraction from $(aIPr)_2SnX_4$ (X = Cl, Br)

Having determined that **36** may spontaneously lose a bromide ion under ESI-MS analytical conditions, we sought to chemically abstract halide ions from **35** and **36**, thereby generating cationic species similar to those accessed through protonation of **19**–**21**. Due to the hypervalent nature of **35** and **36**, and the formal bond order of $^1/_2$ for the Sn–X bonds, it would be reasonable to assume that facile halide abstraction of two ligands should be possible in order to access the four coordinate, dicationic species, $[(aIPr)_2SnCl_2]^{2+}$ (**37**) and $[(aIPr)_2SnBr_2]^{2+}$ (**38**). Indeed, addition of two equivalents of either $AlCl_3$ or $AlBr_3$ to a CD_2Cl_2 solution of **35** or **36**, respectively, results in quantitative halide abstraction to afford **37** and **38** as determined by ^{1}H, ^{27}Al and ^{119}Sn{^{1}H} NMR spectroscopy. The ^{1}H NMR spectrum of **37** in CD_2Cl_2 reveals two broad resonances at 8.79 and 7.89 ppm which can be assigned to the C2 proton and the imidazole backbone proton, respectively. Due to the broad nature of the resonances, coupling to the NMR active tin nuclei could not be observed. The C2 carbon

resonance and the protonated alkenic imidazole carbon also gave rise to very broad resonances in the $^{13}C\{^{1}H\}$ NMR spectrum whilst the tin bound imidazole carbon could not be identified. In contrast, analysis of **38** in CD_2Cl_2 reveals two sharp resonances at 8.98 and 7.69 ppm which can be assigned to the C2 proton and backbone imidazole proton, respectively. Coupling to the ^{117}Sn and ^{119}Sn nuclei can be observed as a single set of satellites around the 8.98 ppm resonance with a coupling constant of 15 Hz. Similar magnitude one, two and three bond coupling constants were observed in the $^{13}C\{^{1}H\}$ NMR spectrum of **38** when compared to **35** and **36**. The C2 carbon (which resonates at 142.0 ppm) is accompanied by satellites with a 31 Hz coupling constant. The protonated backbone imidazole carbon at 135.6 ppm gives rise to two satellites due to coupling to ^{117}Sn and ^{119}Sn nuclei with coupling constant of 115 Hz and 119 Hz. The tin bound imidazole carbon exhibits the largest coupling with constants of 869 Hz and 909 Hz for **38**. Both **37** and **38** were characterised by a single resonance in the $^{119}Sn\{^{1}H\}$ NMR spectrum at –142.9 and –265.3 ppm which is significantly upfield shifted when compared to the starting materials **35** and **36**, respectively. Finally, analysis of the ^{27}Al NMR spectra reveal a single resonance at 103.4 and 80.7 ppm which can be assigned to the four coordinate $[AlCl_4]^-$ and $[AlBr_4]^-$ anions, respectively.

Despite numerous attempts to obtain single crystals of both **37** and **38**, only crystals suitable for single crystal X-ray diffraction of [**37**][$AlCl_4$]$_2$·DFB were obtained by slow diffusion of hexane into a DFB solution of [**37**][$AlCl_4$]$_2$. Analysis of the molecular structure of [**37**][$AlCl_4$]$_2$ reveals the presence of the dication, **37**, bearing two aIPr ligands which lie approximately in the same plane (Figure 3.26). Two $[AlCl_4]^-$ anions lie above and below this plane and one of the chloride ligands of an $[AlCl_4]^-$ anion has a close contact to the tin centre which is within the range of the sum of van der Waals radii for tin and chlorine (Sn1–Al3 = 3.606 Å; $\Sigma r_{\text{van der Waals}}$ = 4.09 Å).[40] The opposite chloride is too far for any interaction to be invoked in the solid state (Sn1–Al7 = 4.691 Å). It may however be possible

that in solution, this contact remains in solution and a dynamic process involving exchange of chloride ligands between **37** and the $[AlCl_4]^-$ anions may give rise to the broad resonances observed in the ^1H NMR spectrum.

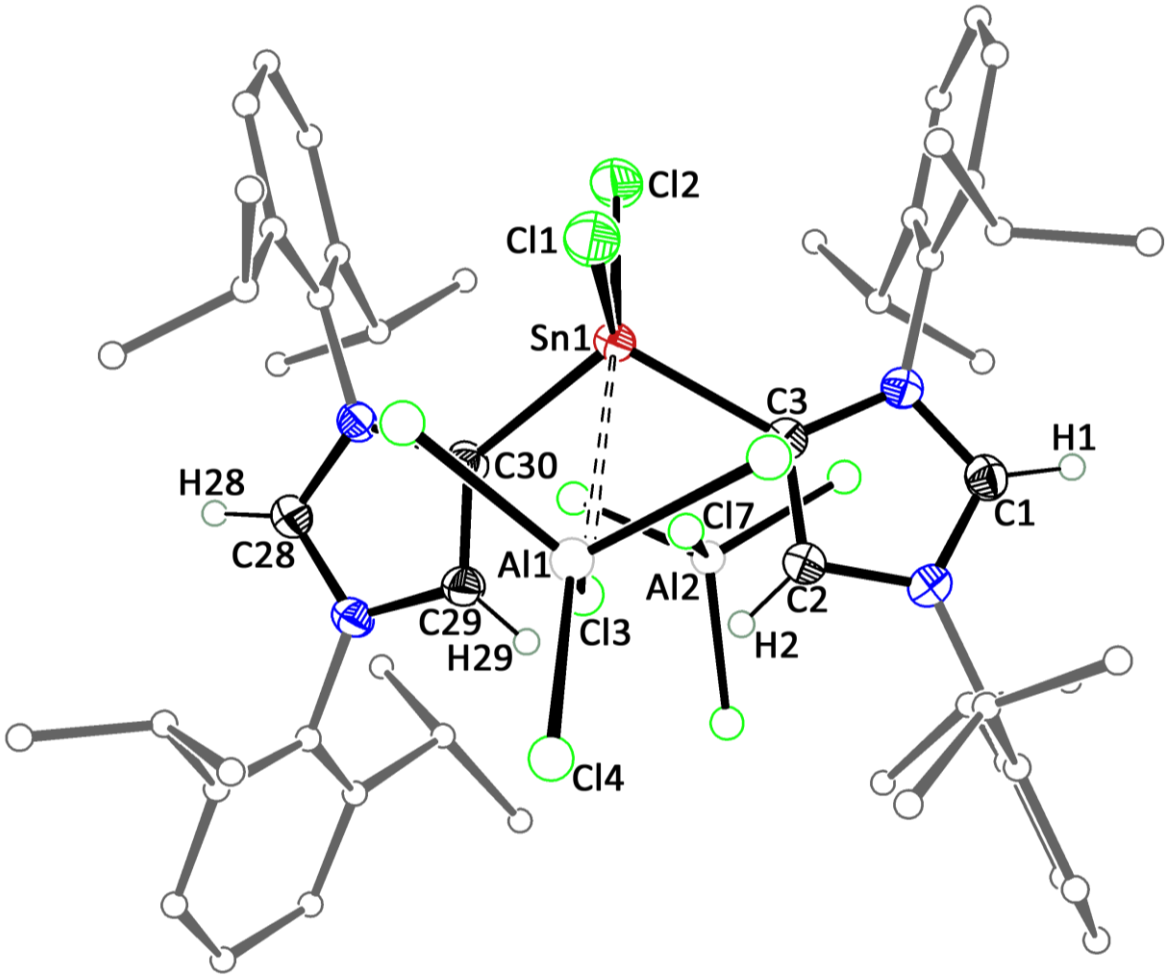

Figure 3.26: Molecular structure of [**37**][$AlCl_4$]$_2$. Anisotropic displacement ellipsoids pictured are set at 50% probability. Hydrogen atoms (with the exception of the imidazole protons labelled H1, H2, H28 and H29) have been omitted for clarity. Atoms of the Dipp groups, the tetrachloroaluminate anions and hydrogen atoms are pictured as spheres of arbitrary radii.

Despite the packing of the $[AlCl_4]^-$ anions, the geometry about the tin centre is approximately tetrahedral indicating the weak interaction with Cl3 (τ_4' = 0.942). The Sn1–Cl1 and Sn1–Cl2 bond lengths of 2.288(1) and 2.291(1) Å are shorter than those observed in the neutral, four-coordinate compound (aIPr:)$_2$SnCl$_2$, **32**. It can be considered that upon protonation of **32**, there is an increased interaction between the tin centre and the chloride ligands. The

Sn1–C3 and Sn1–C30 bond lengths are identical at 2.126(3) Å and are marginally longer than those observed in **32**.

3.5 Conclusions

This chapter has described the reactivity of $[Li(aIPr:)]_\infty$ and $[K(aIPr:)]_\infty$ with mercury dichloride and EX_4 (E = Si, Ge; X = Cl, Br) resulting in the formation of a variety of neutral, novel main group species bearing aIPr: ligands, **14** and **18**–**21**. These ligands contain unquenched carbene functionality, the availability of which was subsequently demonstrated by the addition of an acid to afford protonation of both carbene moieties affording highly Lewis acidic, dicationic complexes, **16** and **23**–**26**. Additionally, the reactivity of both carbene moieties in **19**–**21** towards carbon dioxide (affording **27**–**29**) was shown to be readily reversible under standard conditions and that the carboxylated products were isolated as crystalline precipitates upon cooling a toluene solution to –80 °C. The reactivity of $(aIPr:)_2GeCl_2$ was also investigated towards electron rich reagents, such as MeLi and KC_8, affording reactivity at the electrophilic $GeCl_2$ moiety to yield either the methylated species, **30**, or an anionic, germanium(II) species, **31**, both **30** and **31** retaining their aIPr: ligands.

Finally, the reactivity of $[K(aIPr:)]_\infty$ was also investigated towards $SnCl_4$ and $SnBr_4$. $SnBr_4$ was found to be easily reduced affording an intractable mixture of products, however, the larger size of the tin atom, with respect to silicon and germanium, was found to allow for the coordination of more than four ligands and the isolation of novel, hypervalent tin compounds using $SnCl_4$. A trigonal, bipyramidal anion bearing three aIPr: ligands in a trigonal planar arrangement, $[(aIPr:)_3SnCl_2]^-$ (**33**), was isolated from the reaction of $[K(aIPr:)]_\infty$ with $SnCl_4$ in THF. Subsequent reduction cleanly affords the homoleptic tin(II) anion $[(aIPr:)_3Sn]^-$ (**34**). Attempts to synthesise the normal IPr complexes of the group 14 tetrabromides reveals the

facile isomerisation of IPr resulting in the formation of **19**, **21** and the novel hypervalent tin species, $(aIPr)_2SnX_4$, where X = Cl (**35**) or Br (**36**).

3.6 References

(1) Uzelac, M.; Hernán-Gómez, A.; Armstrong, D. R.; Kennedy, A. R.; Hevia, E. *Chem. Sci.* **2015**, *6* (10), 5719–5728.

(2) Uzelac, M.; Kennedy, A. R.; Hernán-Gómez, A.; Fuentes, M. Á.; Hevia, E. *Z. Anorg. Allg. Chem.* **2016**, *642* (22), 1241–1244.

(3) Chen, M.; Wang, Y.; Gilliard, Jr., R. J.; Wei, P.; Schwartz, N. A.; Robinson, G. H. *Dalton Trans.* **2014**, *43* (38), 14211–14214.

(4) Marion, N.; Escudero-Adán, E. C.; Benet-Buchholz, J.; Stevens, E. D.; Fensterbank, L.; Malacria, M.; Nolan, S. P. *Organometallics* **2007**, *26* (13), 3256–3259.

(5) Wang, Y.; Xie, Y.; Wei, P.; Schaefer, H. F.; Robinson, G. H. *Dalton Trans.* **2016**, *45* (14), 5941–5944.

(6) Ghadwal, R. S.; Reichmann, S. O.; Carl, E.; Herbst-Irmer, R. *Dalton Trans.* **2014**, *43* (36), 13704–13710.

(7) Wang, Y.; Hickox, H. P.; Wei, P.; Robinson, G. H. *Dalton Trans.* **2017**, *46* (17), 5508–5512.

(8) Spek, A. L. *Acta Cryst.* **2015**, *C71*, 9–18.

(9) Cordero, B.; Gómez, V.; Platero-Prats, A. E.; Revés, M.; Echeverría, J.; Cremades, E.; Barragán, F.; Alvarez, S. *Dalton Trans.* **2008**, 2832–2838.

(10) Brookhart, M.; Grant, B.; Volpe, A. F. *Organometallics* **1992**, *11* (11), 3920–3922.

(11) Wanzlick, H. W. *Angew. Chem. Int. Ed.* **1962**, *1* (2), 75–80.

(12) Wanzlick, H.-W.; Schönherr, H.-J. *Angew. Chem. Int. Ed. Engl.* **1968**, *7* (2), 141–142.

(13) Luger, P.; Ruban, G. *Acta Cryst.* **1971**, *B27*, 2276–2279.

(14) Nishida, H.; Takada, N.; Yoshimura, M.; Sonoda, T.; Kobayashi, H. *Bull. Chem. Soc. Jpn.* **1984**, *57* (9), 2600–2604.

(15) Yakelis, N. A.; Bergman, R. G. *Organometallics* **2005**, *24* (14), 3579–3581.

(16) Pelz, S.; Mohr, F. *Organometallics* **2011**, *30* (3), 383–385.

(17) Wang, H. M. J.; Lin, I. J. B. *Organometallics* **1998**, *17* (5), 972–975.

(18) Citadelle, C. A.; Nouy, E. L.; Bisaro, F.; Slawin, A. M. Z.; Cazin, C. S. J. *Dalton Trans.* **2010**, *39* (19), 4489–4491.

(19) Berglund, M.; Wieser, M. E. *Pure Appl. Chem.* **2011**, *83* (2), 397–410.

(20) Uhlig, F.; Marsmann, H. C. *^{29}Si NMR Some Practical Aspects, Gelest Inc.* **2008**.

(21) Asay, M.; Inoue, S.; Driess, M. *Angew. Chem. Int. Ed.* **2011**, *50* (41), 9589–9592.

(22) Braddock-Wilking, J.; Zhang, Y.; Corey, J. Y.; Rath, N. P. *J. Organomet. Chem.* **2008**, *693* (7), 1233–1242.

(23) Wang, Y.; Xie, Y.; Wei, P.; King, R. B.; Schaefer III, H. F.; Schleyer, P. v. R.; Robinson, G. H. *Science* **2008**, *321* (5892), 1069–1071.

(24) Ghadwal, R. S.; Sen, S. S.; Roesky, H. W.; Tavcar, G.; Merkel, S.; Stalke, D. *Organometallics* **2009**, *28* (21), 6374–6377.

(25) Filippou, A. C.; Chernov, O.; Schnakenburg, G. *Angew. Chem. Int. Ed.* **2009**, *48* (31), 5687–5690.

(26) Fritzsche, R.; Seidel, F.; Rüffer, T.; Buschbeck, R.; Jakob, A.; Freitag, H.; Zahn, D. R. T.; Lang, H.; Mehring, M. *J. Organomet. Chem.* **2014**, *755*, 86–92.

(27) Koenig, B.; Roedel, M.; Bubenitschek, P.; Jones, P. G.; Thondorf, I. *J. Org. Chem.* **1995**, *60* (23), 7406–7410.

(28) Cole, M. L.; Jones, C.; Junk, P. C. *New J. Chem.* **2002**, *26* (10), 1296–1303.

(29) Brulé, E.; Guérineau, V.; Vermaut, P.; Prima, F.; Balogh, J.; Maron, L.; Slawin, A. M. Z.; Nolan, S. P.; Thomas, C. M. *Polym. Chem.* **2013**, *4* (8), 2414–2423.

(30) Cheek, G. T.; Roeper, D. F.; Pearson, W.; O'Grady, W. E. *ECS Trans.* **2014**, *64* (4), 161–169.

(31) Vogt, M.; Bennett, J. E.; Huang, Y.; Wu, C.; Schneider, W. F.; Brennecke, J. F.; Ashfeld, B. L. *Chem. Eur. J.* **2013**, *19* (34), 11134–11138.

(32) Duong, H. A.; Tekavec, T. N.; Arif, A. M.; Louie, J. *Chem. Commun.* **2004**, 112–113.

(33) Vogt, M.; Wu, C.; Oliver, A. G.; Meyer, C. J.; Schneider, W. F.; Ashfeld, B. L. *Chem. Commun.* **2013**, *49* (98), 11527–11529.

(34) Kelemen, Z.; Péter-Szabó, B.; Székely, E.; Hollóczki, O.; Firaha, D. S.; Kirchner, B.; Nagy, J.; Nyulászi, L. *Chem. Eur. J.* **2014**, *20* (40), 13002–13008.

(35) Liu, Q.; Wu, L.; Jackstell, R.; Beller, M. *Nat. Commun.* **2015**, *6* (5933), 1–15.

(36) NMR Periodic Table: Tin NMR, *http://triton.iqfr.csic.es/guide/eNMR/chem/Sn.html*.

(37) Green, M. L. H.; Parkin, G. *Dalton Trans.* **2016**, *45* (47), 18784–18795.

(38) Addison, A. W.; Rao, T. N.; Reedijk, J.; Rijn, J. v.; Verschoor, G. C. *J. Chem. Soc., Dalton Trans.* **1984**, 1349–1356.

(39) Ibrahim Al-Rafia, S. M.; Lummis, P. A.; Swarnakar, A. K.; Deutsch, K. C.; Ferguson, M. J.; McDonald, R.; Rivard, E. *Aust. J. Chem.* **2013**, *66* (10), 1235–1245.

(40) Batsanov, S. S. *Russ. Chem. Bull.* **1995**, *44* (1), 18–23.

Chapter 4

Synthesis of IPr and aIPr complexes of group 15 bromides

4.1 Introduction and objectives

4.1.1 Isomerisation of IPr affording aIPr complexes of main group elements

There have been multiple reports that describe the isomerisation of NHCs resulting in the formation of abnormally bonded NHC complexes of the main group elements. Some of these examples have already been addressed in Chapter 1 (See Section 1.6.1.2) and are the result of deprotonation of the backbone imidazole proton of a coordinated NHC by a free NHC in solution. Free NHC can be generated either by the simple addition of multiple equivalents of an NHC to the reaction, or upon thermal treatment of a solution of an adduct which can break the NHC–E bond. Coordination of NHCs to main group complexes results in an increase in the acidity of the imidazole protons, thereby facilitating the deprotonation and subsequent rearrangement of the NHC to afford the abnormally bonded isomer. As a result, multiple examples of isomerisation of NHCs have been discovered upon coordination to group 13 elements which are known to be highly Lewis acidic.[1–4]

By using THF as a reaction solvent, Dagorne and co-workers were able to demonstrate that the normal I^{t}Bu adducts of EMe_3 (E = Al, Ga, In) and $AlCl_3$ rapidly and quantitatively afforded the abnormal adducts (aI^{t}Bu)EMe_3 and (aI^{t}Bu)$AlCl_3$ at room temperature.[5] THF was found to accelerate the reaction by the formation of a donor–acceptor adduct with the main group reagents which liberates free I^{t}Bu. Further evidence for the presence of free I^{t}Bu in solution, even in the absence of THF, comes from the dissolution of analytically pure (I^{t}Bu)$AlCl_3$ in CH_2Cl_2 which slowly generates the protonated imidazolium salt, [I^{t}BuH][$AlCl_4$], which must result from the formation of free I^{t}Bu in solution which subsequently deprotonates CH_2Cl_2.

aNHC complexes of the group 14 elements have also been synthesised by addition of the NHC to a sufficiently electrophilic reagent such as $Sn(OTf)_2$ or even Ph_2SiCl_2.[6,7] Addition of

two equivalents of I^{i}Pr to Ph_2SiCl_2 followed heating to 66 °C in THF allows for the isomerisation of both equivalents of I^{i}Pr and the isolation of $[(aI^{i}Pr)_2SiPh_2]^{2+}$ as the chloride salt (Figure 4.1).

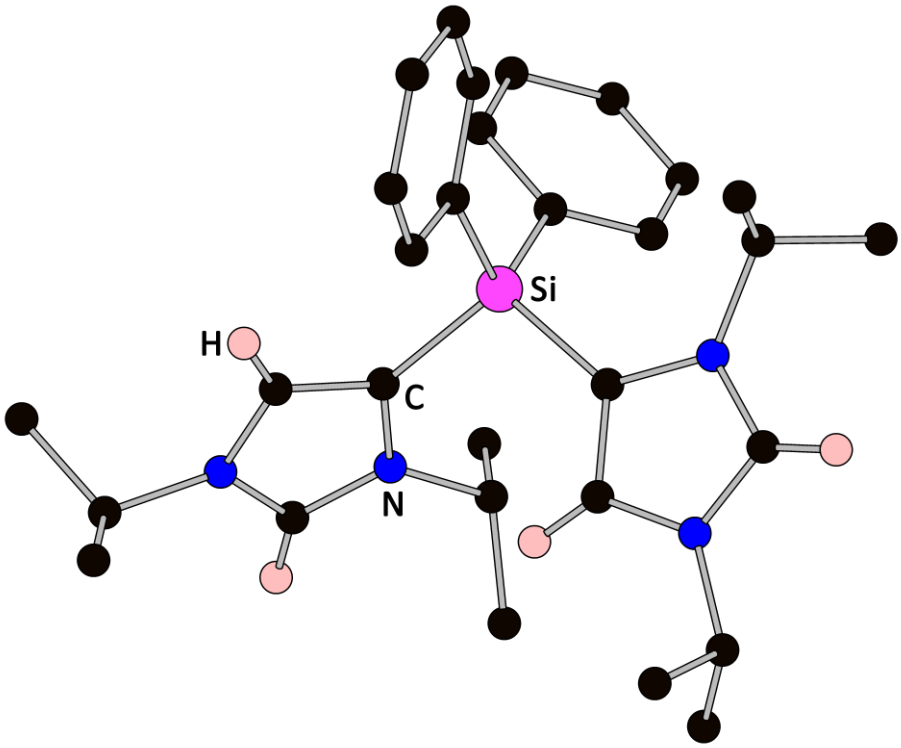

Figure 4.1: Ball and stick model of $[(aI^{i}Pr)_2SiPh_2]^{2+}$. Hydrogen atoms (with the exception of the imidazole protons) have been omitted for clarity.

Finally, isomerisation has also been observed in group 15 species. Auto-ionisation of SbF_3 accompanied by the rearrangement of IPr resulted in the formation of $[(IPr)(aIPr)SbF_2]^{+}[SbF_4]^{-}$ upon heating a toluene solution of TMEDA·SbF_3 with two equivalents of IPr at 60 °C for 16 hours.[8] Similarly, Weigand and co-workers (who have worked extensively on the use of NHCs as stabilising ligands in the synthesis of cationic phosphorus species)[9] demonstrated the normal to abnormal rearrangement is not limited to NHCs with a protonated, alkenic backbone. The bis(chlorinated) NHC, 1,3-bis(diisopropylphenyl)-4,5-dichloroimidazol-2-ylidene, which is itself formed by the reaction of IPr with CCl_4 which proceeds via the deprotonation of the imidazole backbone,

was shown to undergo isomerisation upon addition in excess to Ph_2PCl and Me_3SiOTf.[10] The adduct of the NHC with the cationic $[PPh_2]^+$ moiety can be isolated as the triflate salt as an analytically pure material. Addition of a third of an equivalent of the NHC promotes the isomerisation of the chlorinated NHC adduct, presumably via an equivalent reaction mechanism via the formal migration of Cl^+, as opposed to H^+, to afford the abnormal isomer, again as the triflate salt (Figure 4.2).

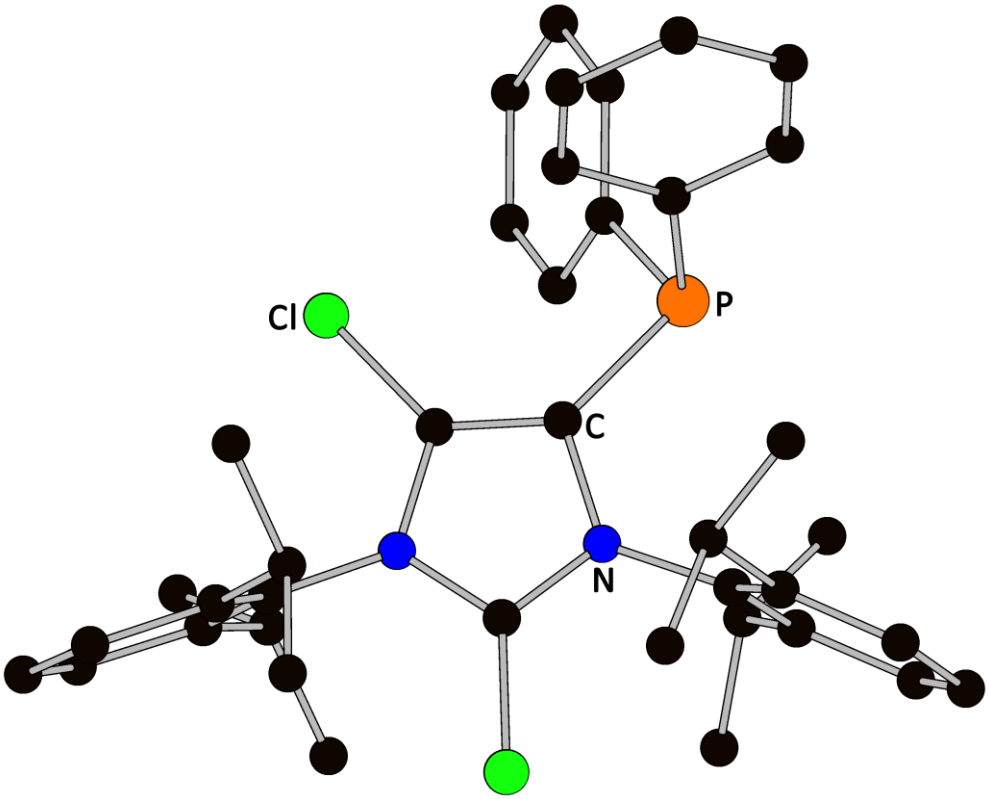

Figure 4.2: Ball and stick model of $[(a^{Cl_2}IPr)PPh_2]^+$. Hydrogen atoms have been omitted for clarity.

4.1.2 Chapter outline

Recent developments have enabled the synthesis of main group complexes bearing aNHC ligands by a base promoted mechanism, usually through the addition of multiple equivalents of the NHC and by heating NHC complexes of main group elements which affords free NHC in solution. This chapter will discuss the synthesis of normal IPr adducts of the group 15

tribromides along with the isomerisation of the ligand induced by both excess NHC and upon heating solutions of the adducts in THF. Cationic complexes with supporting IPr and aIPr ligands have also been synthesised by bromide abstraction from both the normal and abnormal species. The synthesis and reactivity of these complexes will also be discussed.

4.2 Synthesis of IPr adducts with EBr_3 (E = P, As, Sb, Bi)

The addition of one equivalent of EBr_3 (E = P, As, Sb, Bi) to a diethyl ether solution of IPr allows for the formation of the 1 : 1 adducts, (IPr)EBr_3 (E = P, **39**; As, **40**; Sb, **41**; Bi, **42**). **40**–**42** precipitate from the reaction solution instantaneously and can be isolated as pale to bright yellow solids in high yields. Conversely, **39** is soluble in the reaction solvent and can be isolated as a yellow, crystalline precipitate in greater than 50% yield by filtration of the reaction mixture, concentration and cooling to –35 °C.[11] Appropriate dilution of both IPr and PBr_3 in diethyl ether is required for the synthesis so as to avoid a large concentration of either species upon the rapid addition of one solution to the other. A high concentration of IPr results in the formation of a white precipitate and a bright orange solution containing a reduced phosphorus species which will be discussed in Chapter 5.

39–**42** were characterised by ^{1}H and $^{13}C\{^{1}H\}$ NMR spectroscopy in d_8-THF revealing a symmetric IPr ligand; chemical shifts of the diagnostic resonances are provided in Table 4.1.

Compound	N(C*H*)$_2$N δ (ppm)	C$_6$H$_3${C*H*(CH$_3$)$_2$}$_2$ δ (ppm)	*C*N$_2$ δ (ppm)
39	7.98	3.30	149.2
40	7.99	3.24	149.4
41	7.92	3.21	156.2
42	7.79	3.16	194.9

Table 4.1: Comparison of chemical shifts of selected resonances in the ^{1}H and $^{13}C\{^{1}H\}$ NMR spectra of **39**–**42** in d_8-THF.

Additionally, **39** was characterised by a single resonance at 24.8 ppm in the ^{31}P NMR spectrum which is significantly upfield shifted compared to that of the PBr_3 precursor (231.2 ppm) and is in line with that observed for other NHC adducts of phosphorus trihalides (cf. (IPr)PCl_3: 16.9 ppm).[12] Similarly, the carbene resonance appears as a doublet due to coupling to the NMR active ^{31}P nucleus with a coupling constant of 176 Hz. Likewise, a three bond coupling to the alkenic imidazole carbons was also observed with a significantly reduced coupling constant of 4 Hz. Finally, the carbene resonance in **42** was significantly broadened due to coupling to the 100% abundant, quadrupolar (I = $^9/_2$) ^{209}Bi nucleus.[13]

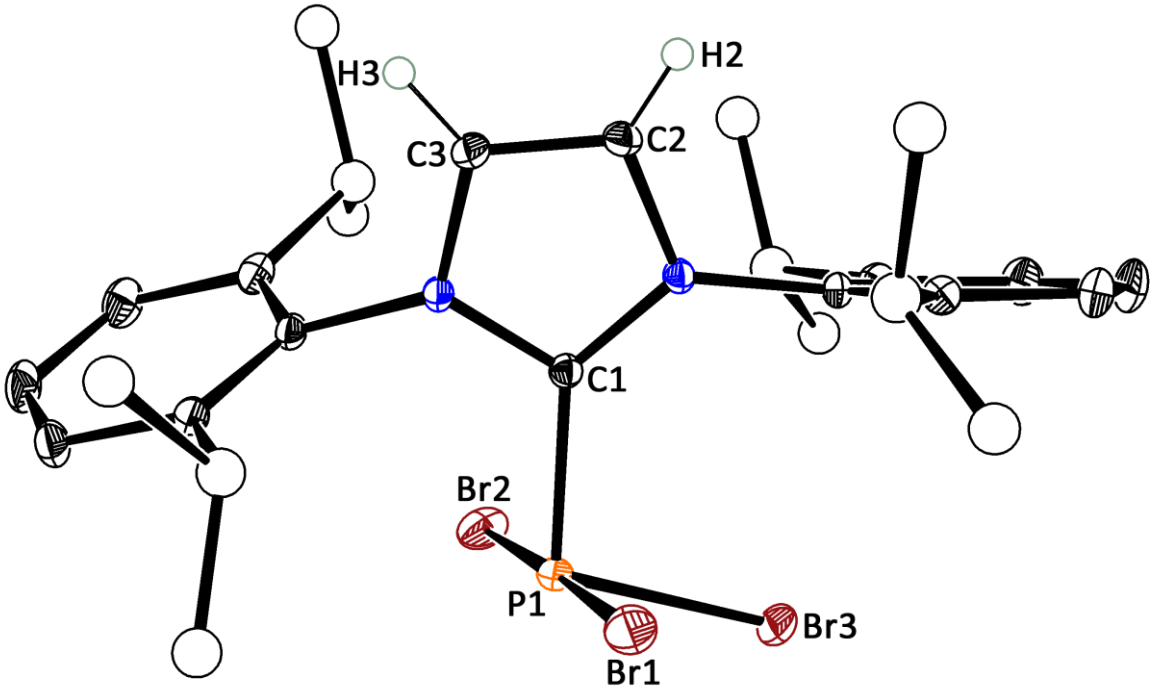

Figure 4.3: Molecular structure of **39**. Anisotropic displacement ellipsoids pictured are set at 50% probability. Hydrogen atoms (with the exception of the imidazole protons labelled H2 and H3) have been omitted for clarity. Atoms of the ^{i}Pr groups, H2 and H3 are pictured as spheres of arbitrary radii.

Single crystals of **39** suitable for single crystal X-ray diffraction were obtained from a saturated diethyl ether solution at –35 °C revealing a disphenoidal (or seesaw) geometry about the central phosphorus atom whereby the IPr ligand occupies an equatorial position (Figure 4.3).

The four coordinate disphenoidal geometry can be described by the τ_4' parameter which is 0.322 (cf. 0.237 for a perfect disphenoidal geometry where $\alpha = 120°$ and $\beta = 180°$). The geometry of the PBr_3 group has been distorted from trigonal pyramidal to a planar, T-shaped geometry as evidenced by the Br1–P1–Br2 bond angle (178.5(1)°) and the sum of bond angles about the phosphorus centre ($\Sigma_{\text{bond angles}} = 359.5°$).

The P1–C1 bond length of 1.872(2) Å is nearly identical to that observed for the similar $(IPr)PCl_3$ adduct species (1.871(11) Å) and both are marginally longer than that expected based on the sum of covalent radii ($\Sigma r_{\text{cov}} = 1.80$ Å).[14] However, this is reasonable considering the donor–acceptor nature of the bonding affording a hypervalent phosphorus centre. The hypervalent nature is also evident in the P–Br distances which are notably longer to the axial bromine atoms (2.475(1) and 2.545(1) Å) than that observed for the equatorial P1–Br3 bond length (2.232(1) Å). The linear Br1–P1–Br2 moiety can be described by a three-centre-four-electron bonding model as a result of the donation of the carbene lone pair of electrons into a P–Br σ* orbital which explains the significantly longer P–Br bond lengths (Figure 4.4).[15] The latter P1–Br3 bond length is within the range expected based on the sum of covalent radii ($\Sigma r_{\text{cov}} = 2.27$ Å).

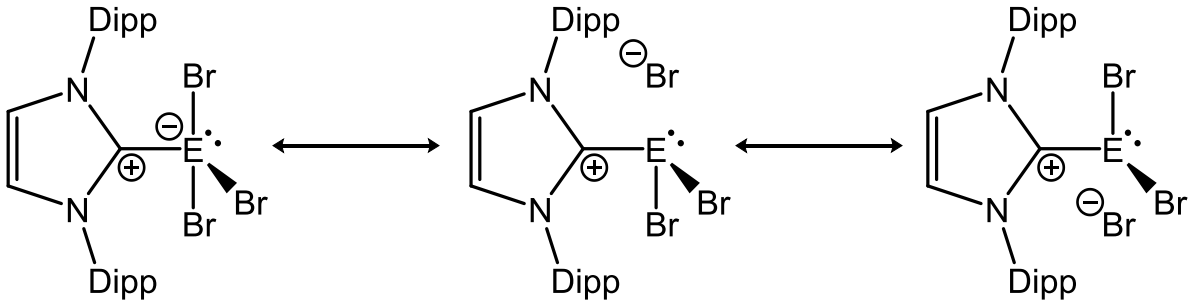

Figure 4.4: Different resonance structures for $(IPr)EBr_3$.

40 is isostructural with **39** and exhibits a disphenoidal geometry about the arsenic centre as described by the τ_4' parameter which is 0.342 (Figure 4.5). Likewise, the geometry about the

$AsBr_3$ group has been distorted from trigonal pyramidal to a planar, T-shaped geometry whereby the Br1–As1–Br2 bond angle is 177.1(1)° and the sum of bond angles about the arsenic centre is 359.7°.

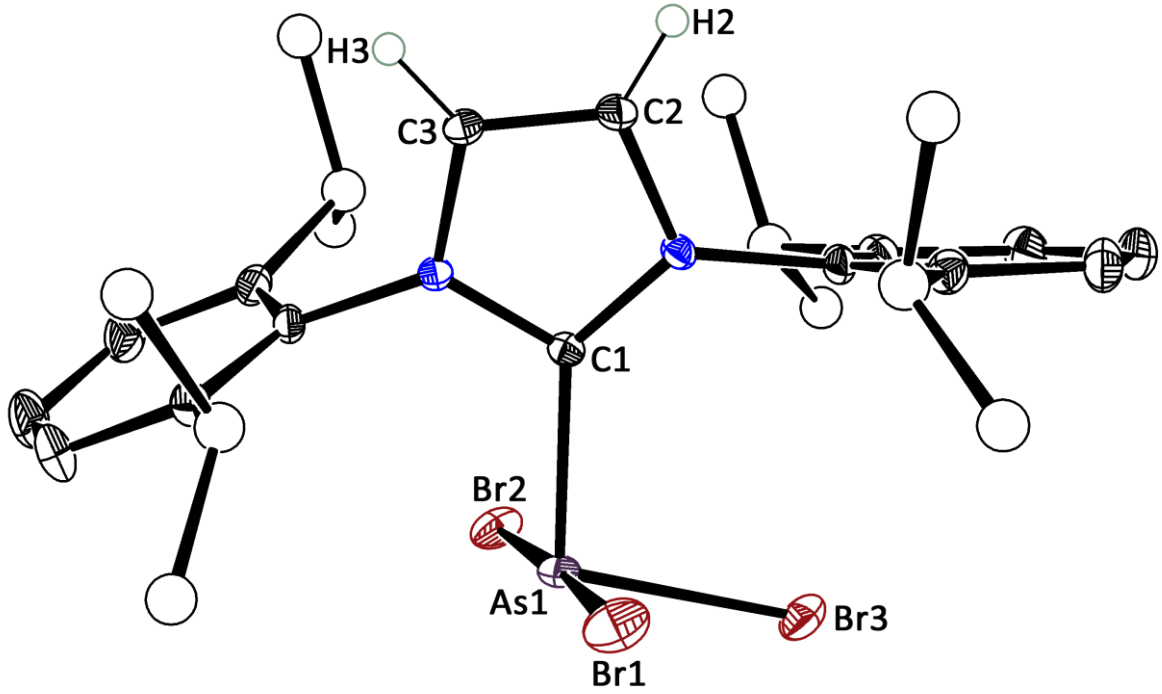

Figure 4.5: Molecular structure of **40**. Anisotropic displacement ellipsoids pictured are set at 50% probability. Hydrogen atoms (with the exception of the imidazole protons labelled H2 and H3) have been omitted for clarity. Atoms of the ^{i}Pr groups, H2 and H3 are pictured as spheres of arbitrary radii.

The As1–C1 bond length (2.011(2) Å) is approximately 0.14 Å longer than that observed for the P–C bond length in **39** as expected based on the difference in covalent radii of phosphorus and arsenic (Δr_{cov} = 0.12 Å).[14] The As1–C1 bond length in **39** is similar to that observed in (IPr)$AsCl_3$ (2.018(3) Å). An increase in the axial As1–Br1 and As1–Br2 bond lengths (2.565(1) and 2.619(1) Å, respectively) of approximately 0.08 Å is observed relative to the equivalent P–Br bonds. This reduced increase is likely a result of the particularly long P–Br bonds observed in **39** due to the large degree of steric clash between the ligands and the axial bromine substituents. The equatorial As1–Br3 bond length (2.374(1) Å) is approximately 0.14 Å longer than the equivalent bond in **39** in line with the larger covalent radius of arsenic.

The axial As–Br bonds are notably longer than that of the equatorial bond due to the three-centre-four-electron bonding nature.

Single crystals of **41**·2THF were grown from a saturated THF solution of **41** at –25 °C. Analysis of the molecular structure reveals a similar disphenoidal geometry about the antimony centre with respect to the IPr and bromine ligands (Figure 4.6). However, there is also a close contact observed between the antimony centre and that of a THF molecule *trans* to the IPr ligand resulting in a five coordinate centre in a square based pyramidal geometry.

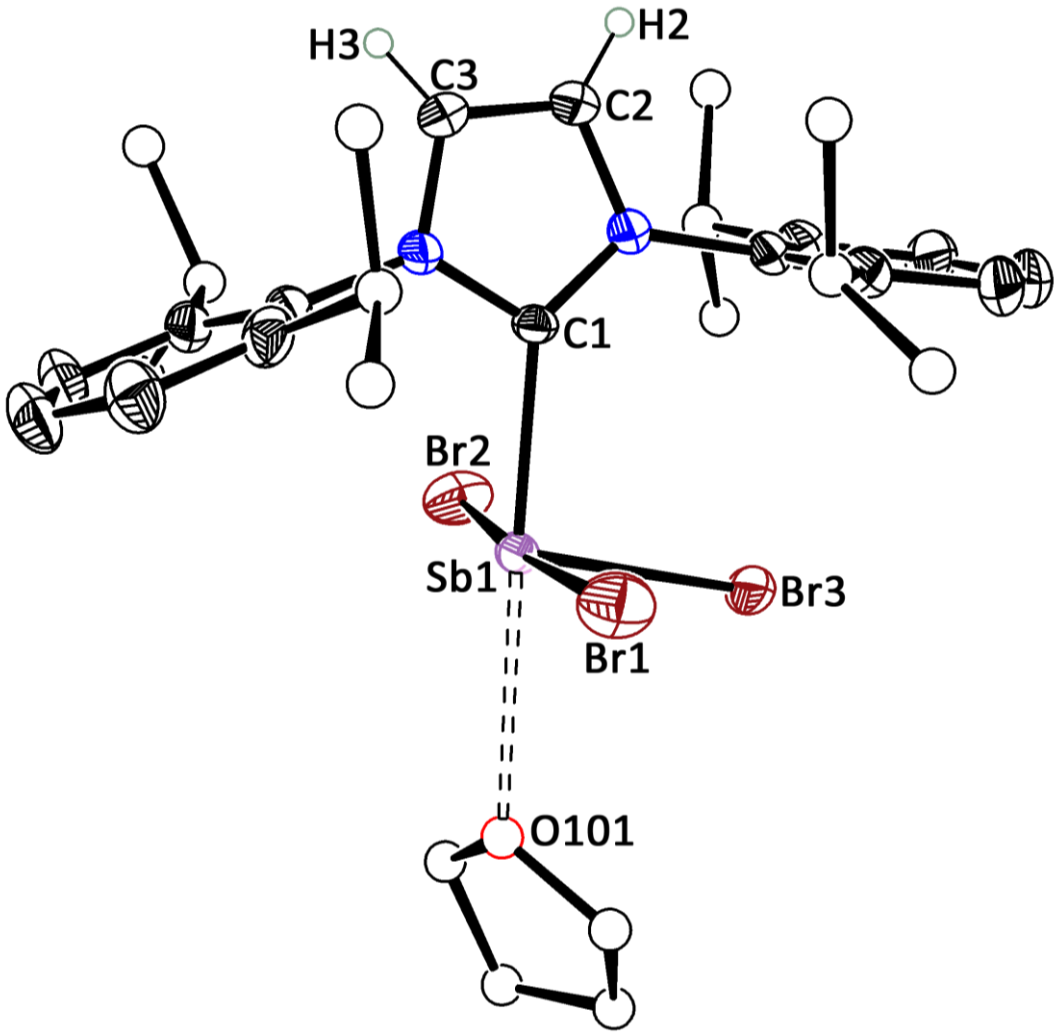

Figure 4.6: Molecular structure of **41**·THF. Anisotropic displacement ellipsoids pictured are set at 50% probability. Hydrogen atoms (with the exception of the imidazole protons labelled H2 and H3) have been omitted for clarity. Atoms of the ^{i}Pr groups, the THF molecule, H2 and H3 are pictured as spheres of arbitrary radii.

The second THF molecule is free and shows no close contacts with **41**. The geometry can be described by the τ_5 parameter which can be calculated to be 0.010 which is almost exactly what would be expected of a true square based pyramidal geometry. The close contact observed with the THF molecule in the solid state can be explained by the increase in Lewis acidity of the group 15 centre. The reduction in hybridisation of s and p orbitals results in the lone pair of electrons occupying an orbital of greater s character (hence the reduced basicity and stereochemical influence) whilst bonding orbitals are formed using a greater contribution from the p orbitals. Therefore, donation of a pair of electrons from a coordinating THF molecule into the σ* of the Sb–C bond becomes a favourable interaction. The antimony lone pair of electrons is likely directed towards a position *trans* to Br3. The Sb1–O101 distance of 2.904(4) Å is significantly greater than that of a two-centre-two-electron Sb–O covalent bond (Σr_{cov} = 2.05 Å).[14] However, this distance is shorter than the sum of van der Waals radii of antimony and oxygen (3.35 Å)[16] hence a bonding interaction is clearly evident.

The Sb1–C1 bond length (2.268(3) Å) is approximately 0.26 Å longer than the As–C bond present in **40** which is marginally longer than that expected purely based on the larger covalent radius of antimony compared to arsenic (Δr_{cov} = 0.20 Å) and may be the result of the donation of electron density into the Sb–C σ* orbital by the THF molecule reducing the IPr–Sb bonding interaction. There are no other structurally authenticated NHC adducts of antimony trihalides reported in the chemical literature for bond metric data comparison. As was the case in **39** and **40**, bonds to the two axial bromine atoms are approximately 0.22 Å longer than that to the equatorial bromine atom (2.727(1), 2.729(1) and 2.508(1) Å, respectively) and the latter is with the range expected for an Sb–Br bond (Σr_{cov} = 2.59 Å).

Bright yellow crystals of [(IPr)$BiBr_2$(μ-Br)]$_2$·THF ([**42**]$_2$·THF) suitable for single crystal X-ray diffraction were grown by slow diffusion of hexane into a THF solution of **42**. The

structure of **42** differs significantly from that of **41**. Dimerisation of **42** is a result of donation of electron density from an apical bromine atom of one molecule into the σ* of the Bi–C bond of another molecule resulting in the formation of two bromide bridges (Figure 4.7). The square based pyramidal geometry about both Bi1 and Bi2 can be described by the τ_5 parameter which can be calculated as 0.091 and 0.198, respectively. The molecular structure does not contain any symmetry elements as a result of the butterfly shape afforded by the Bi1–Br3–Bi2–Br6 ring.

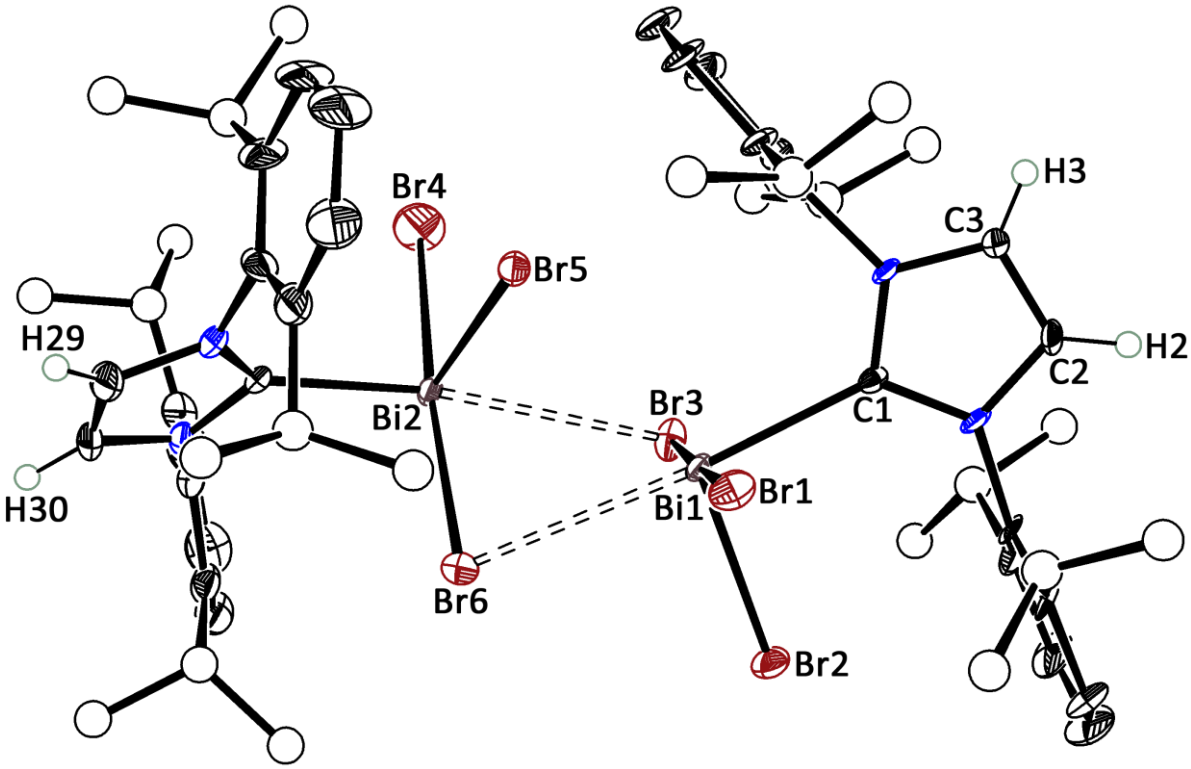

Figure 4.7: Molecular structure of [**42**]$_2$. Anisotropic displacement ellipsoids pictured are set at 50% probability. Hydrogen atoms (with the exception of the imidazole protons labelled H2, H3, H29 and H30) have been omitted for clarity. Atoms of the ^{i}Pr groups and hydrogen atoms are pictured as spheres of arbitrary radii.

The angles within the ring are all smaller than 90° which results in a buckling of the ring ($\Sigma_{\text{internal angles}}$ = 329.7°). This is in contrast to the molecular structure observed for [(IPr)$BiCl_2$(μ-Cl)]$_2$ whereby the Bi_2Cl_2 moiety is planar and there is a centre of inversion.[17] The only apparent reason for the structural distortion from a planar geometry is a result of the

close contact observed between Bi1 and Br5. The distance at 3.389(1) Å is significantly greater than the sum of covalent radii for bismuth and bromine (2.68 Å) however, is within the sum of van der Waals radii (3.70 Å) which is evidence of a bonding interaction. The Bi1–C1 and Bi2–C28 bond lengths are very similar at 2.417(6) and 2.399(6) Å which is line that that observed for the only other structurally characterised NHC–BiX_3 species, $[(IPr)BiCl_2(\mu\text{-}Cl)]_2$, which has a Bi–C bond length of 2.389(8) Å.[17]

As was the case for **39**–**41**, the 'axial' bromine atoms (Br1, Br3, Br4 and Br6) have a notably longer bond length to the bismuth atoms than the 'equatorial' bromine atoms (Br2 and Br5). Additionally, the Bi1–Br3 and Bi2–Br6 are slightly lengthened (2.850(1) and 2.855(1) Å, respectively) relative to the other axial bond (Bi1–Br1 (2.792(1) Å) and Bi2–Br4 (2.759(1) Å), respectively) as a result of dimerisation and donation of electron density from the bromine atoms into the σ* of the opposite Bi–C bond. As expected, the 'equatorial' Bi1–Br2 and Bi2–Br5 bond lengths (2.619(1) and 2.606(1) Å, respectively) are within the range expected for a covalent Bi–Br single bond. Finally, as expected, the distances between the bridging bromine atoms and that of the opposite bismuth centre are significantly longer than all other Bi–Br bond lengths. The Bi1–Br6 and Bi2–Br3 distances are 3.255(1) and 3.287(1) Å, respectively, and are well within the sum of van der Waals radii for bismuth and bromine.

4.3 Bromide abstraction from (IPr)EBr_3

The formation of an adduct between EBr_3 and the strong two electron sigma donor, IPr, results in a weakening of the E–Br bonds (Figure 4.4). The steric bulk of the IPr ligand also reduces the nucleophilicity of the element centre, hence, we sought to abstract one of the coordinating bromide ligands with the use of the highly Lewis acidic reagent, $AlBr_3$, thereby generating an $[AlBr_4]^-$ counter anion. Indeed, addition of one equivalent of $AlBr_3$ to **39**–**42** allows

for the synthesis of [(IPr)EBr$_2$][AlBr$_4$] (E = P, [**43**][AlBr$_4$]; As, [**44**][AlBr$_4$]; Sb, [**45**][AlBr$_4$]; Bi, [**46**][AlBr$_4$]). The reaction must be carried out in a non-coordinating solvent and DCM is an ideal choice. All products can be isolated in greater than 79% crystalline yield and crude NMR spectra reveal quantitative formation of the cationic species. Analysis of the crystalline samples by ^{1}H and ^{13}C{^{1}H} NMR spectroscopy in CD_2Cl_2 reveals a symmetric IPr ligand with a change in the chemical shift of the resonances indicating the formation of the cationic species **43**–**46** (Table 4.2).

Compound	N(C***H***)$_2$N δ (ppm)	C$_6$H$_3${C***H***(CH$_3$)$_2$}$_2$ δ (ppm)	***C***N$_2$ δ (ppm)
43	7.98	2.37	139.4
44	7.93	2.42	141.7
45	7.78	2.50	150.3
46	7.69	2.55	191.3

Table 4.2: Comparison of chemical shifts of selected resonances in the ^{1}H and ^{13}C{^{1}H} NMR spectra of **43**–**46** in CD_2Cl_2.

There is a definitive trend for the carbene resonance to be shifted upfield relative to that of the starting materials for **43**–**46** (Δδ = 9.8, 7.7, 5.9 and 3.6 ppm, respectively). The reduction in the difference in chemical shifts (Δδ) of the carbene resonance from P to Bi is consistent with the weaker bonding interaction between the carbene carbon and the progressively heavier (and larger) group 15 elements. This also has the effect of a general downfield shift of the carbene resonance in both sets of **39**–**42** and **43**–**46** due to the greater carbenic character retained by the ligand due to poorer orbital overlap with the heavier elements.

Providing greatest evidence for the formation of the three-coordinate, cationic centres is the upfield shift of the singlet resonance in the ^{31}P NMR spectrum of **43** (87.5 ppm). This is approximately in the same range as a similar IPr stabilised, cationic phosphorus species, [(IPr)PCl$_2$]OTf, which displays a resonance at 113.8 ppm in CD_3CN.[18] The one bond coupling

between the carbene carbon and the phosphorus atom is apparent as a doublet in the $^{13}C\{^{1}H\}$ NMR spectrum of **43** with a coupling constant of 136 Hz. Finally, all products gives rise to a relatively sharp singlet resonance in the ^{27}Al NMR spectrum between 80.8 and 81.1 ppm which results from the tetrahedral $[AlBr_4]^-$ anion.

Additional evidence for the formation of the cationic species comes from analysis by positive-ion mode ESI-MS which reveals a single mass envelope which can be ascribed to the molecular ion for each sample in DCM. Analysis of **43**–**46** reveals a mass envelope at 579.1361 for $[(IPr)PBr_2]^+$ (Calcd 579.0959), 623.0908 for $[(IPr)AsBr_2]^+$ (Calcd 623.0437), 669.1093 for $[(IPr)SbBr_2]^+$ (Calcd 669.0266) and 757.1798 for $[(IPr)BiBr_2]^+$ (Calcd 757.1025), respectively.

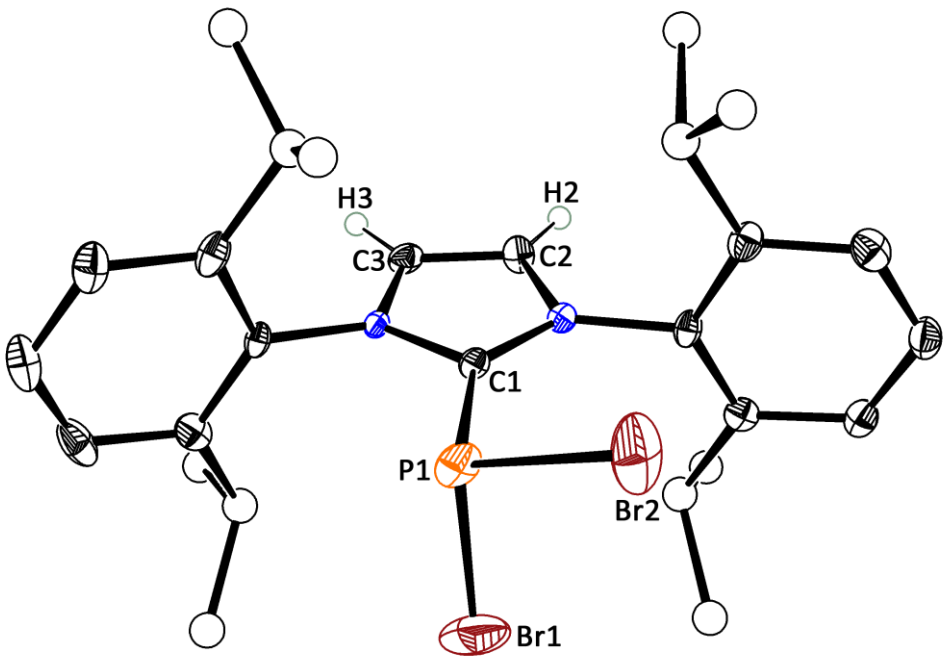

Figure 4.8: Structure of cation **43** in [**43**][$AlBr_4$]·$^1/_2$DCM. Anisotropic displacement ellipsoids pictured are set at 50% probability. Hydrogen atoms (with the exception of the imidazole protons labelled H2 and H3) have been omitted for clarity. Atoms of the ^{i}Pr groups, H2 and H3 are pictured as spheres of arbitrary radii.

Colourless to pale yellow crystals containing **43**–**46** were grown by slow diffusion of hexane into DCM solutions. Analysis of **43** by single crystal X-ray diffraction unambiguously confirms the presence of the cationic species along with an $[AlBr_4]^-$ counter anion. The molecular structure of **43** consists of a three-coordinate phosphorus centre in a trigonal pyramidal geometry ($\Sigma_{\text{bond angles}} = 305.5°$) (Figure 4.8). **43** is isoelectronic with the previously reported, neutral silicon(II) species, $(IPr)SiBr_2$.[19] The P1–C1 bond distance was measured to be 1.841(7) Å which has decreased upon bromide abstraction. The reduced electron donation to the phosphorus centre results in a greater bonding interaction between IPr and the $[PBr_2]^+$ moiety than with PBr_3. The P1–Br1 and P1–Br2 bond distances were 2.215(3) and 2.154(3) Å, respectively, and both are shorter than the equatorial P–Br bond length observed in **39** which is consistent with the increased bonding between the remaining bromide ligands and the phosphorus atom upon abstraction of one of the bromide ligands.

Analysis of the molecular structure of **44** (Figure 4.9) reveals a trigonal pyramidal geometry about the arsenic centre much like that observed for **43**. However, an additional close contact between the arsenic centre and a bromide ligand of the $[AlBr_4]^-$ anion is present in the solid state giving rise to a four-coordinate arsenic centre in a distorted, disphenoidal geometry which can be quantified by the τ_4' parameter (0.439). The bromide of the counter anion lies *trans* to the IPr ligand by donation of electron density into the σ* of the As–C bond (as opposed to the σ* of either As–Br bonds). In all likelihood, this results from the increased steric bulk of the tetrabromoaluminate anion when compared to the bromide ion itself and this prevents coordination *trans* to a bound bromide ligand. Correspondingly, the As–Br distance is quite long at 3.651(1) Å which is marginally outside the calculated value for the sum of van der Waals radii (3.60 Å).[16] The As1–C1 bond length (2.008(3) Å) is not statistically different to that found in **40**. However, a notable reduction in the As–Br bond lengths of approximately 0.05 Å is observed upon bromide abstraction (2.317(1) and 2.325(1) Å).

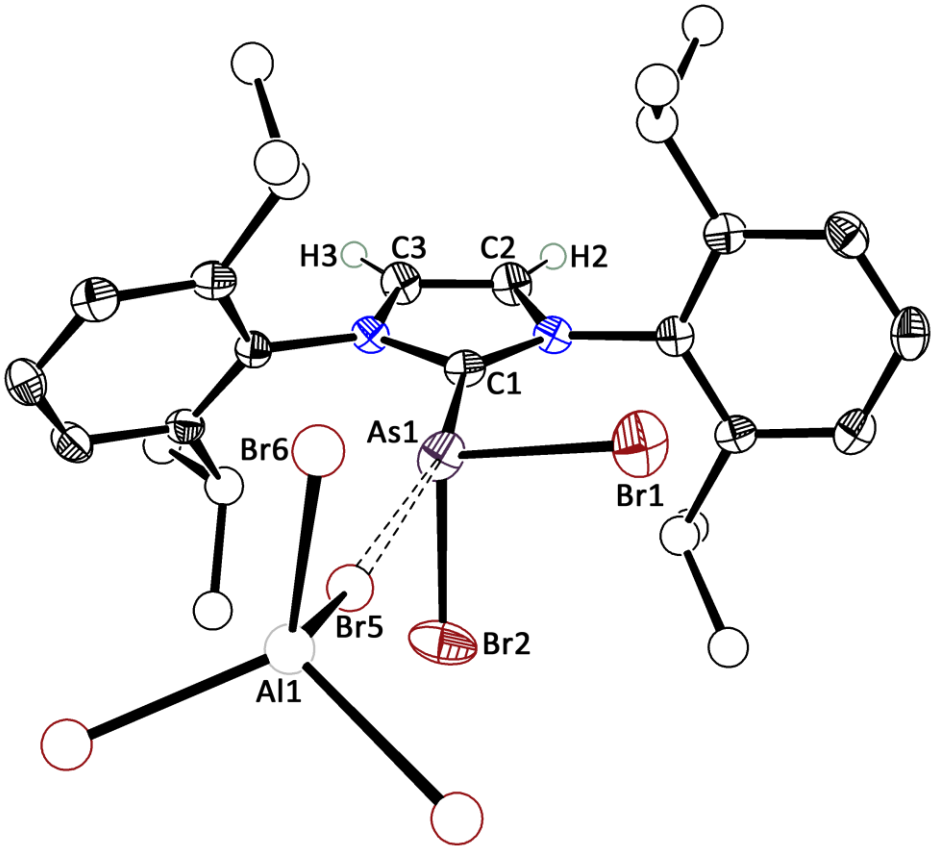

Figure 4.9: Molecular structure of [**44**][$AlBr_4$]. Anisotropic displacement ellipsoids pictured are set at 50% probability. Hydrogen atoms (with the exception of the imidazole protons labelled H2 and H3) have been omitted for clarity. Atoms of the ^{i}Pr groups, the tetrabromoaluminate anion, H2 and H3 are pictured as spheres of arbitrary radii.

The molecular structures of both **45** and **46** also reveal a close contact between the group 15 element and a bromide ligand of the $[AlBr_4]^-$ anion (Figure 4.10 and 4.11). This gives rise to a four-coordinate centre with a distorted disphenoidal geometry which can be quantified by the τ_4' parameter (0.444 for **45** and 0.443 for **46**). Both distances to the bromide ligand of the tetrabromoaluminate anion are very long at approximately 3.657(1) and 3.599(1) Å for **45** and **46**, respectively, which are approximately the same as the sum of van der Waals radii for antimony and bromine (3.65 Å) and bismuth and bromine (3.70 Å). The Sb1–C1 and Bi1–C1 bond distances of 2.219(3) and 2.340(4) Å, respectively, are slightly shorter than that observed in **41** and **42**, consistent with increased bonding character between the ligand and the group 15 element upon bromide abstraction.

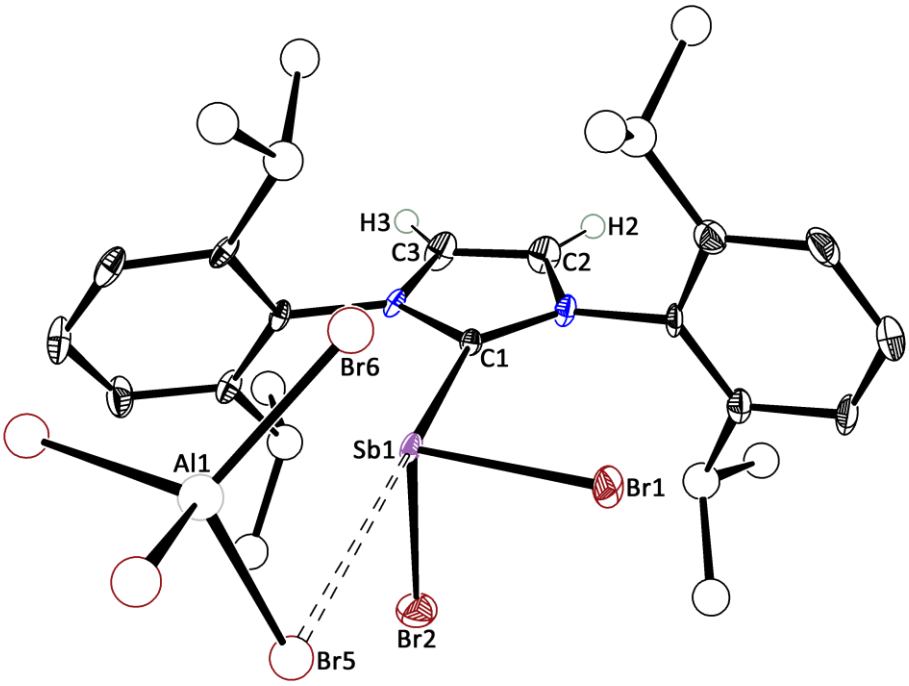

Figure 4.10: Molecular structure of [**45**][$AlBr_4$]. Anisotropic displacement ellipsoids pictured are set at 50% probability. Hydrogen atoms (with the exception of the imidazole protons labelled H2 and H3) have been omitted for clarity. Atoms of the ^{i}Pr groups, the tetrabromoaluminate anion, H2 and H3 are pictured as spheres of arbitrary radii.

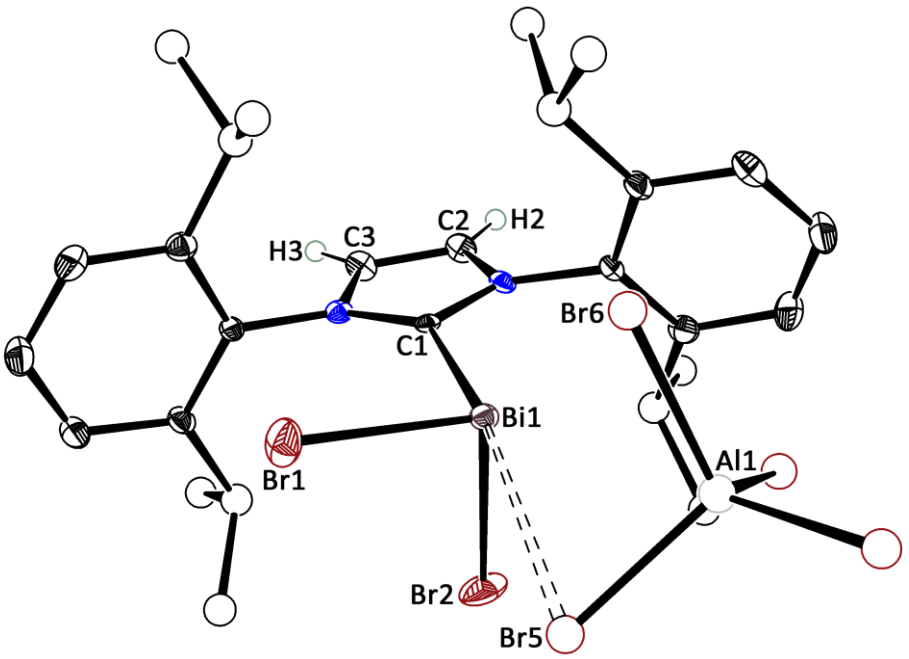

Figure 4.11: Molecular structure of [**46**][$AlBr_4$]. Anisotropic displacement ellipsoids pictured are set at 50% probability. Hydrogen atoms (with the exception of the imidazole protons labelled H2 and H3) have been omitted for clarity. Atoms of the ^{i}Pr groups, the tetrabromoaluminate anion, H2 and H3 are pictured as spheres of arbitrary radii.

The Sb1–Br1 and Sb1–Br2 bond lengths in **45** and Bi1–Br1 and Bi1–Br2 bond lengths in **46** are marginally shorter at 2.485(1) and 2.488(1) Å and 2.575(1) and 2.582(1) Å, respectively, when compared to the starting materials, **41** and **42**, respectively. Finally, a reduction in the two C–E–Br bond angles was also observed upon descending the group 15 elements (Table 4.3) as a result of the reduced hybridisation between s and p orbitals and increased contribution from the element p orbitals in bonding.

Cation	C–E–Br bond angles (°)
43	98.8(3), 104.4(3)
44	95.8(1), 100.0(1)
45	89.5(1), 97.5(1)
46	88.4(1), 96.5(1)

Table 4.3: Comparison of the two C–E–Br bond angles present in cations **43**–**46** (E = P, As, Sb, Bi).

4.4 Synthesis of aIPr adducts with EBr_3 (E = Sb, Bi)

During the synthesis of (IPr)EBr_3 it is vital that there be no excess of IPr in solution for an extended period of time with the adduct. As discussed previously, the presence of excess IPr allows for the isomerisation of the coordinated IPr ligand via a proton shuttling mechanism. Carrying out the reaction in diethyl ether allows for the precipitation and isolation of **40**–**42** in high yield. Conversely, if the reaction is carried out in THF, it is possible to observe isomerised products along with small amounts of [IPrH]Br. Ultimately, it was determined that by heating a THF solution of analytically pure **41** or **42** (obtained as a precipitate from diethyl ether) at 75 °C allows for the isomerisation of the IPr ligand affording (aIPr)$SbBr_3$ (**47**) and (aIPr)$BiBr_3$ (**48**) in essentially quantitative yields after three days and one day, respectively (when the reaction was carried out and monitored in d_8-THF) and isolated in greater than 60% crystalline yields upon diffusion of hexane into the reaction solution. This reaction likely

proceeds via the breaking of the E–C bond generating free IPr in solution, which upon heating allows for the facile deprotonation of a coordinated IPr ligand which has increased in acidity due to the inductively electron withdrawing EBr_3 group and a general proposed mechanism is given in Scheme 4.1 which clearly illustrates the catalytic nature of IPr in the transformation.

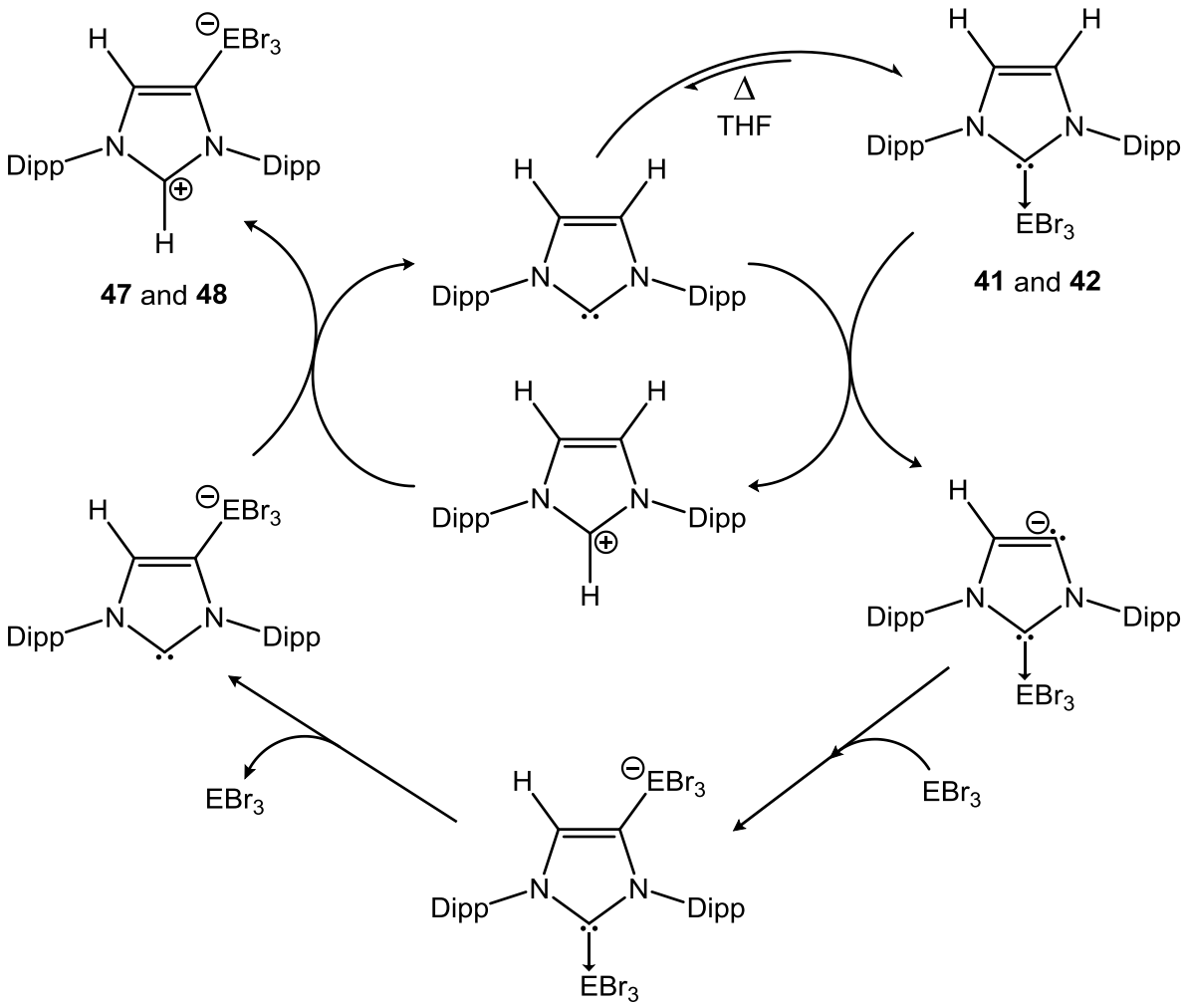

Scheme 4.1: Proposed mechanism for the isomerisation of IPr coordinated to group 15 tribromides upon heating in THF thereby generating **47** and **48**.

Isomerisation results in an asymmetric ligand environment which results in a doubling of a number of the resonances in the ^{1}H and $^{13}C\{^{1}H\}$ NMR spectra. Diagnostically, the presence of a downfield doublet resonance which results from the imidazolium proton bonded to the

C2 carbon indicates isomerisation of the ligand, along with a second doublet resonance of equal intensity arising from the remaining alkenic, imidazole proton. A comparison of selected ^{1}H and ^{13}C{^{1}H} NMR data for **47** and **48** in d_8-THF is provided in Table 4.4.

Compound	***H*CN$_2$ δ (ppm)**	**NCC*H*N δ (ppm)**	**C$_6$H$_3${C*H*(CH$_3$)$_2$}$_2$ δ (ppm)**	**N*C*CHN δ (ppm)**
47	9.37	8.37	3.06, 2.64	148.4
48	9.36	8.46	3.00, 2.57	191.8

Table 4.4: Comparison of chemical shifts for selected resonances in the ^{1}H and ^{13}C{^{1}H} NMR spectra of **47** and **48** in d_8-THF.

Single crystals of both aIPr complexes of antimony tribromide and bismuth tribromide, **47** and **48** respectively, were grown by slow diffusion of hexane into a THF solution. Analysis of the molecular structure reveals a dimeric structure of the form [(aIPr)EBr$_2$(μ-Br)]$_2$ which contains two bridging bromide ligands (Figure 4.12 and 4.13).

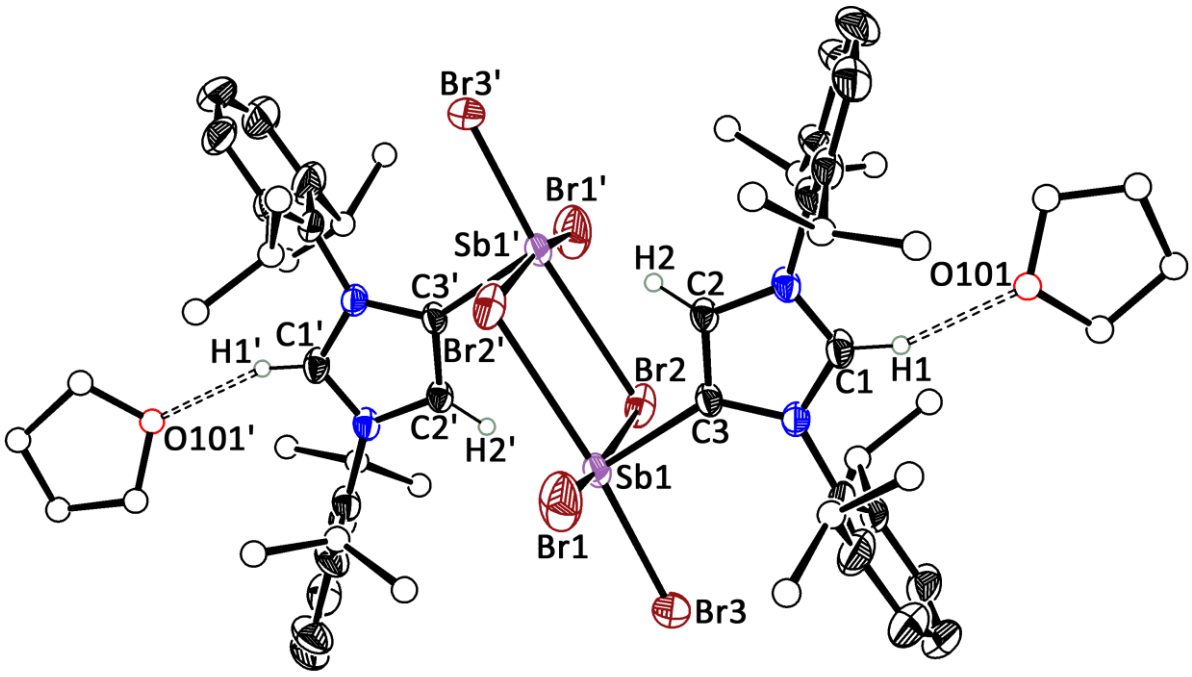

Figure 4.12: Molecular structure of [**47**]$_2$·2THF. Anisotropic displacement ellipsoids pictured are set at 50% probability. Hydrogen atoms (with the exception of the imidazole protons labelled H1, H2, H1' and H2') have been omitted for clarity. Atoms of the ^{i}Pr groups, the THF molecules and hydrogen atoms are pictured as spheres of arbitrary radii. Symmetry operation: 1–*x*, 2–*y*, 1–*z*.

47 crystallises as a dimer in the $P\bar{1}$ space group with a centre of inversion at the centre of the Sb1–Br2–Sb1'–Br2' rhombus. There are also two THF molecules which are hydrogen bonded to the acidic imidazolium protons, much like that observed for the aIPr species which were synthesised by protonation of the aIPr: precursor compounds in Chapter 3. The central Sb_2Br_6 moiety is approximately planar with a root-mean-square deviation from planarity of 0.143 Å. This structure results from the formation of two bridging bromides (Br2 and Br2') which form due to the donation of electron density into the σ* of the Sb1–Br3 bond. The central Sb1–Br2–Sb1'–Br2' moiety is approximately square with Sb1–Br2–Sb1' and Br2–Sb1–Br2' angles of 96.4(1)° and 83.6(1)°, respectively.

Unlike the dimeric structure observed for $[(IPr)BiBr_3]_2$ which formed a dimer due to donation of electron density into the Bi–C σ* orbital, in **47**, the stronger electron donating ability of the imidazole backbone of the aIPr ligand, coupled with the reduced steric bulk from only one flanking N–Dipp group results in a shorter, stronger Sb–C bond. As a result, the energy of the σ* is raised and correspondingly, the LUMO becomes that of the Sb–Br σ*. This type of bonding motif has been seen in a handful of complexes bearing formally anionic carbon based ligands such as methyl and phenyl groups and have been isolated as both the *cis* and *trans* isomers.[20,21] Only the *trans* isomer is observed upon crystallisation of **47** due to the large steric bulk of the aIPr ligand.

The geometry about the antimony atom can be described as a five-coordinate, square based pyramidal geometry which can be quantified by the τ_5 parameter which is 0.064. The lone pair of electrons on the antimony atom are stereochemically active and occupy a position *trans* to the aIPr ligand. The Sb1–C3 bond length is shorter than those in **41** and **45** at 2.182(3) Å as expected, due to the greater nucleophilicity of the backbone imidazole carbon. Similarly, the terminal Sb–Br bond lengths were measured to be 2.574(1) and 2.627(1) Å which is

approximately equal to or longer than previously discussed Sb–Br single bonds. The Sb–Br distances between the antimony centre and the two bridging bromide ligands are significantly longer at 2.976(1) and 3.129(1) Å, however, well within the range of the sum of van der Waals radii.

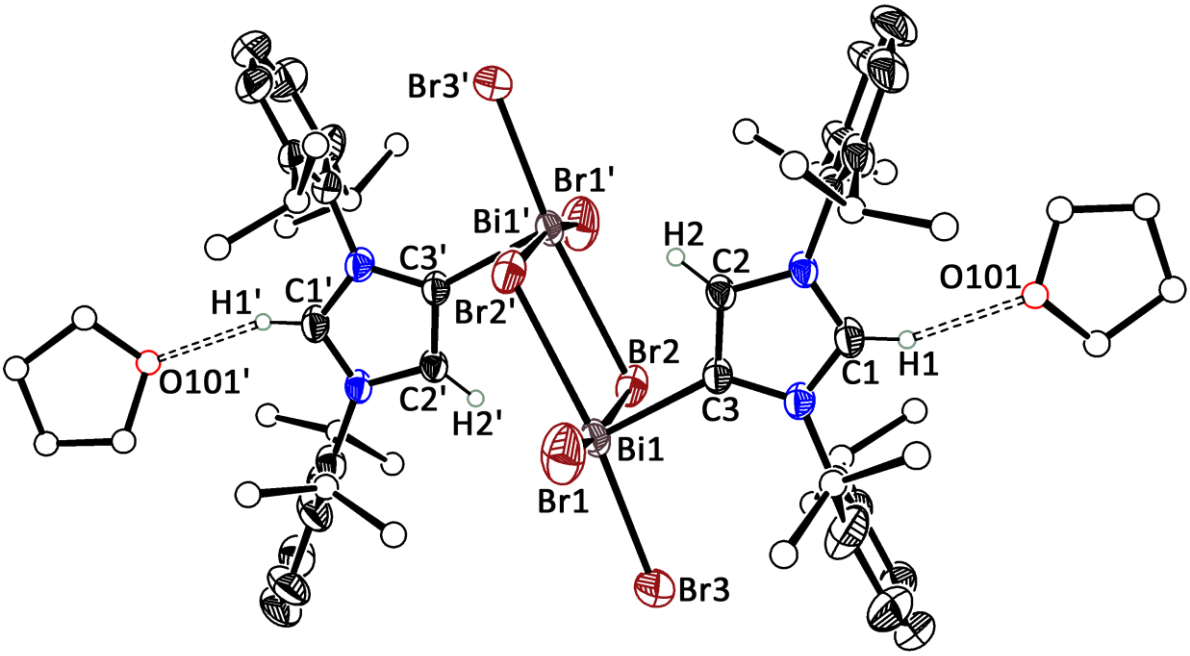

Figure 4.13: Molecular structure of [**48**]$_2$·2THF. Anisotropic displacement ellipsoids pictured are set at 50% probability. Hydrogen atoms (with the exception of the imidazole protons labelled H1, H2, H1' and H2') have been omitted for clarity. Atoms of the ^{i}Pr groups, the THF molecules and hydrogen atoms are pictured as spheres of arbitrary radii. Symmetry operation: 1–*x*, 2–*y*, 1–*z*.

Equivalent single crystals containing a dimeric structure of **48** were obtained and again, the two monomeric units are related by inversion symmetry in the $P\bar{1}$ space group. The Bi_2Br_6 moiety is approximately planar with a root-mean-square deviation from planarity of 0.137 Å. The central Bi1–Br2–Bi1'–Br2' is approximately square where the two internal angles Bi1–Br2–Bi1' and Br2–Bi1–Br2' are 97.9(1)° and 82.0(1)°, respectively. The Bi1–C3 bond length at 2.279(6) Å is shorter than those observed in **42** and **46** as expected. As in **47**, the terminal Bi–Br bonds are shorter than those to the bridging bromides at 2.677(2) and 2.705(2) Å which are slightly longer than that expected for a single Bi–Br bond. Those to the

bridging bromides are significantly longer, as expected, at 3.030(2) and 3.072(1) Å and these distances are again, well within the sum of van der Waals radii for bismuth and bromine indicating reasonable interaction.

48 is also readily soluble in DCM, and single crystals containing a tetrameric structure was obtained by diffusion of hexane into a DCM solution and analysed by single crystal X-ray diffraction (Figure 4.14).

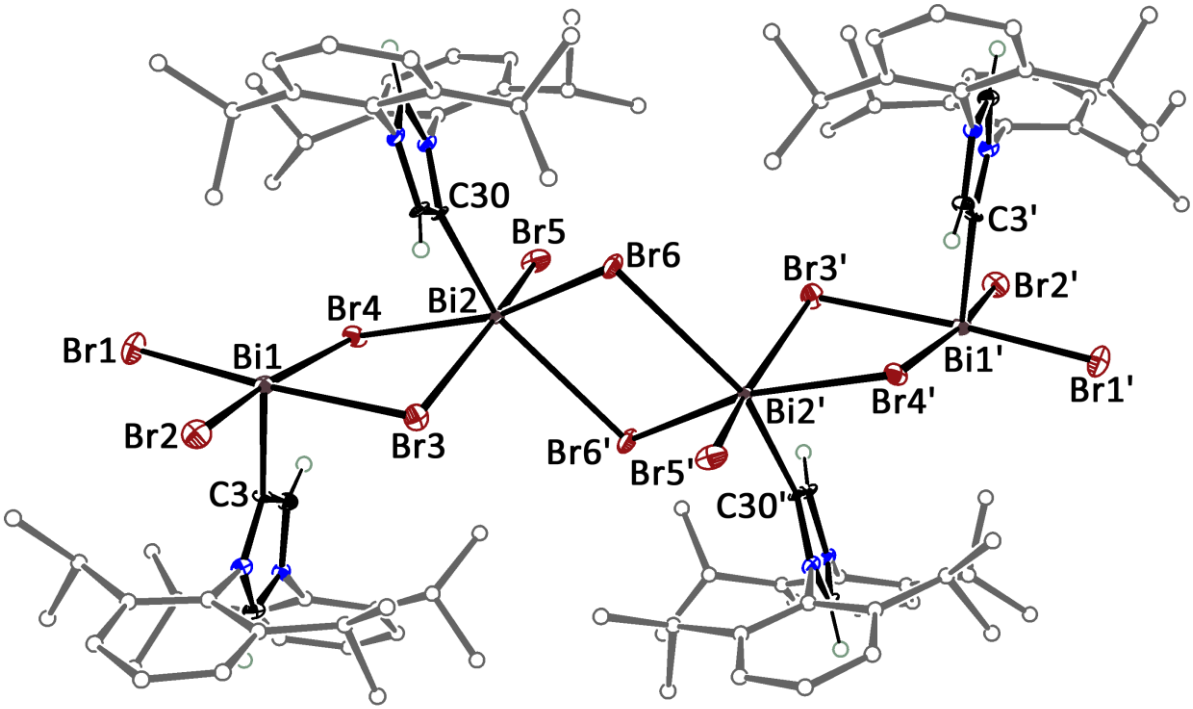

Figure 4.14: Molecular structure of [**48**]$_4$. Anisotropic displacement ellipsoids pictured are set at 50% probability. Hydrogen atoms (with the exception of the imidazole protons) have been omitted for clarity. Atoms of the Dipp groups and hydrogen atoms are pictured as spheres of arbitrary radii. Symmetry operation: 2–*x*, –*y*, 1–*z*.

The Bi_2Br_6 moiety of one dimer has been significantly distorted on formation of the tetramer as indicated by the root-mean-square deviation from planarity of 0.496 Å. Bi1 retains a square based pyramidal structure with τ_5 value of 0.043. Tetramisation occurs by a similar means as that observed in $[(IPr)BiBr_3]_2$ whereby the formation of a second bridged bromide ligand to Bi2 is a result of donation of electron density, approximately into the σ* of the Bi–C bond.

However, there is significant structural distortion due to the presence of the stereochemically active lone pair which occupies a similar area in space as the Bi–C σ*. The reduced hybridisation of s and p orbitals on bismuth results in the lone pair having significant s character, which allows for the distortion as the lone pair has little directionality. The Bi2–Br6' distance is significantly longer than other Bi–Br bonds at 3.397(1) Å, however, remains shorter than the sum of van der Waals radii (3.70 Å). Otherwise, all other bond metric data to not change by any appreciable degree.

4.5 Bromide abstraction from (aIPr)EBr_3

With the aim of synthesising the three-coordinate cationic group 15 dibromide species bearing an abnormally bonded IPr ligand, as opposed to normal IPr ligands (See Section 4.3) we sought to react **47** and **48** with Na[B(3,5-{CF_3}$_2$$C_6H_3$)$_4$] in order to abstract a bromide ligand by the favourable precipitation of NaBr. Accordingly, addition of one equivalent of the sodium salt with either **47** or **48** in DCM results in immediate precipitation of NaBr (as determined by the absence of a resonance in the ^{23}Na NMR spectrum) and the formation of the cationic species $[(aIPr)SbBr_2]^+$ (**49**) and $[(aIPr)BiBr_2]^+$ (**50**).

Evidence for bromide abstraction and the formation of a cationic complex comes from the observable shifts in the resonances in the ^{1}H and ^{13}C{^{1}H} NMR spectra in CD_2Cl_2 coupled with the appearance of resonances attributable with the $[B(3,5\text{-}\{CF_3\}_2C_6H_3)_4]^-$ anion. A comparison of chemical shifts for selected resonances is provided in Table 4.5.

Compound	*H*CN$_2$ δ (ppm)	NCC*H*N δ (ppm)	C$_6$H$_3${C*H*(CH$_3$)$_2$}$_2$ δ (ppm)	NC*C*HN δ (ppm)
49	8.52	8.08	2.43, 2.35	141.3
50	8.49	8.23	2.51, 2.36	181.8

Table 4.5: Comparison of chemical shifts for selected resonances in the ^{1}H and ^{13}C{^{1}H} NMR spectra of **49** and **50** in CD_2Cl_2.

More conclusive evidence for the formation of the cationic species, **49** and **50**, comes from analysis of the samples by ESI-MS in DCM. Analysis of **49** by ESI-MS reveals a mass envelope at 669.8062 which can be ascribed to the molecular ion $[(aIPr)SbBr_2]^+$ (Calcd 669.0266). Similarly, analysis of **50** by ESI-MS reveals a mass envelope at 757.1990 which can be ascribed to the molecular ion $[(aIPr)BiBr_2]^+$ (Calcd 757.1025).

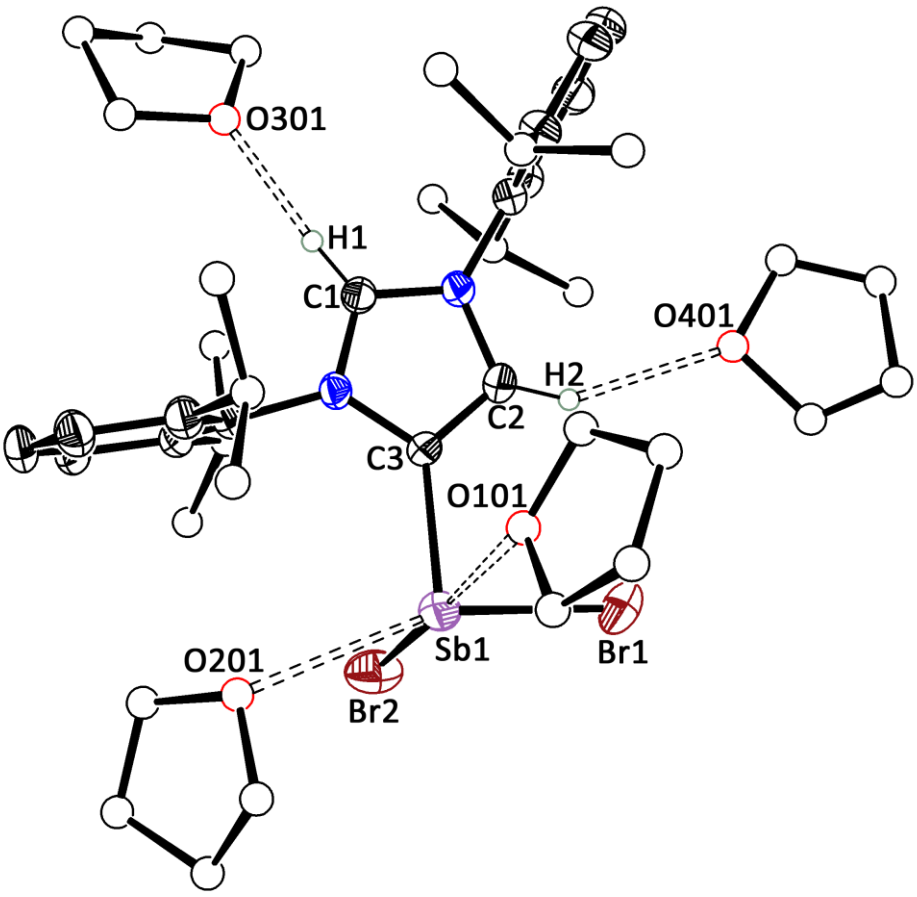

Figure 4.15: Structure of cation **49**·4THF in [**49**][B(3,5-{CF$_3$}$_2$C$_6$H$_3$)$_4$]·4THF. Anisotropic displacement ellipsoids pictured are set at 50% probability. Hydrogen atoms (with the exception of the imidazole protons labelled H1 and H2) have been omitted for clarity. Atoms of the ^{i}Pr groups, the THF molecules, H1 and H2 are pictured as spheres of arbitrary radii.

Both **49** and **50** were crystallised from THF with two molecules of THF coordinated to the group 15 element centre along with two additional molecules of THF which hydrogen bond to the protons of the imidazole rings (Figure 4.15 and 4.16). The coordination of the aIPr ligand and the two bromide ligands result in a trigonal pyramidal geometry as expected for both **49** and **50** and the coordination of two additional molecules of THF by donation of electron density into the two E–Br σ* orbitals affords a distorted, square based pyramidal structure which can be quantified by the τ_5 value which is 0.277 for **49**·4THF.

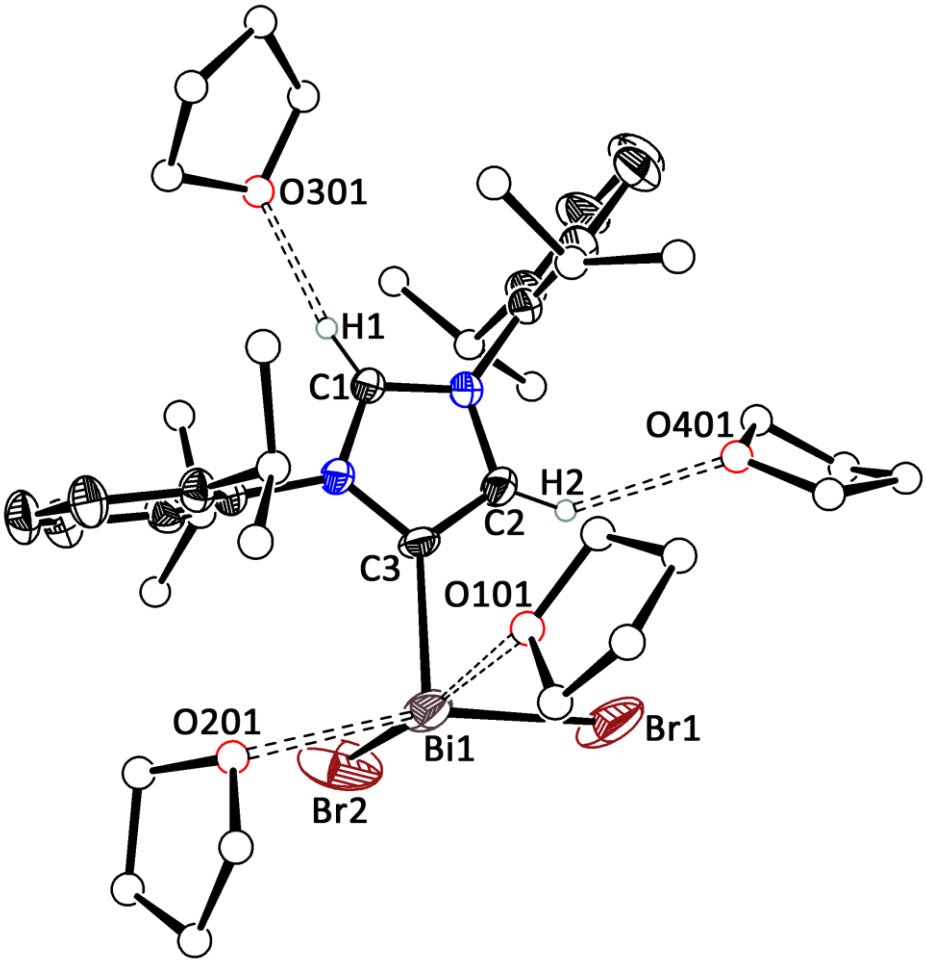

Figure 4.16: Structure of cation **50**·4THF in [**50**][B(3,5-{CF_3}$_2$$C_6H_3$)$_4$]·$^5/_2$THF. Anisotropic displacement ellipsoids pictured are set at 50% probability. Hydrogen atoms (with the exception of the imidazole protons labelled H1 and H2) have been omitted for clarity. Atoms of the ^{i}Pr groups, the THF molecules, H1 and H2 are pictured as spheres of arbitrary radii.

The longer bonds between the ligands and the bismuth centre in **50**·4THF results in reduced steric clash which allows for greater square based pyramidal character as determined by the τ_5 value which is 0.148. The Sb1–C3 bond length was measured to be 2.184(3) Å which is significantly shorter than previously discussed Sb–C bond lengths due to the greater nucleophilicity of the backbone imidazole carbon coupled with the increase in electrophilicity of the antimony centre upon bromide abstraction. Likewise, the Bi1–C3 bond length at 2.291(4) Å is notably shorter than previously discussed Bi–C bond lengths due to the same reasoning. Analogous arguments also explain the short Sb–Br bond lengths (2.525(1) and 2.526(1) Å) and Bi–Br bond lengths (2.635(2) and 2.653(1) Å) in **49** and **50**, respectively.

4.6 Synthesis of bis(aIPr) adducts with EBr_3 (E = Sb, Bi)

The addition of a second equivalent of IPr to (IPr)$SbBr_3$ (or simply the addition of two equivalents of IPr to $SbBr_3$) followed by heating in THF results in the isomerisation of both equivalents of IPr and the resulting complex bears two abnormally bonded IPr ligands (Scheme 4.2).

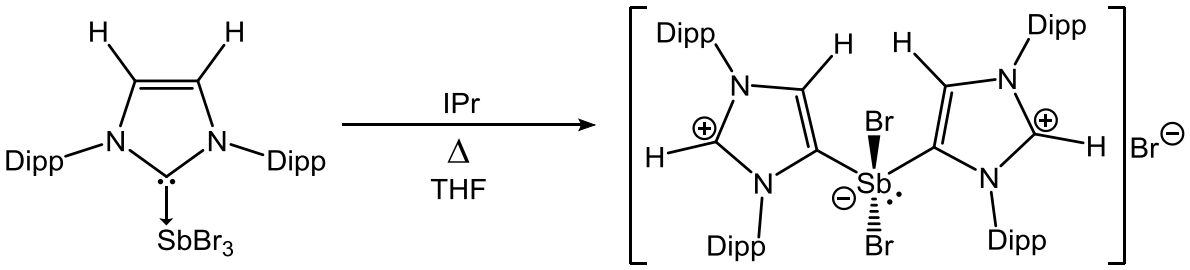

Scheme 4.2: Reaction scheme for synthesis of [**51**]Br by heating a THF solution of two equivalents of IPr with $SbBr_3$.

During the reaction, colourless crystals of the product form in the reaction flask, the insolubility a result of the ionic nature of the product which has liberated a bromide ion in place of the second aIPr ligand affording [$(aIPr)_2SbBr_2$]Br ([**51**]Br). The molecular structure

of **51** was determined by single crystal X-ray diffraction and reveals a four-coordinate antimony centre coordinated by two aIPr ligands and two bromide ligands (Figure 4.17).

Reaction of [**51**]Br with either $AlBr_3$ or Na[B(3,5-{CF_3}$_2$$C_6H_3$)$_4$] in DCM allows for isolation of **51** as the $[AlBr_4]^-$ or $[B(3,5\text{-}\{CF_3\}_2C_6H_3)_4]^-$ salts, respectively. The formation of $[(aIPr)_2SbBr_2]^+$ was further evidenced by the presence of a mass envelope at 1057.4980 (Calcd 1057.3142) upon analysis of a sample of [**51**][B(3,5-{CF_3}$_2$$C_6H_3$)$_4$] by ESI-MS in DCM.

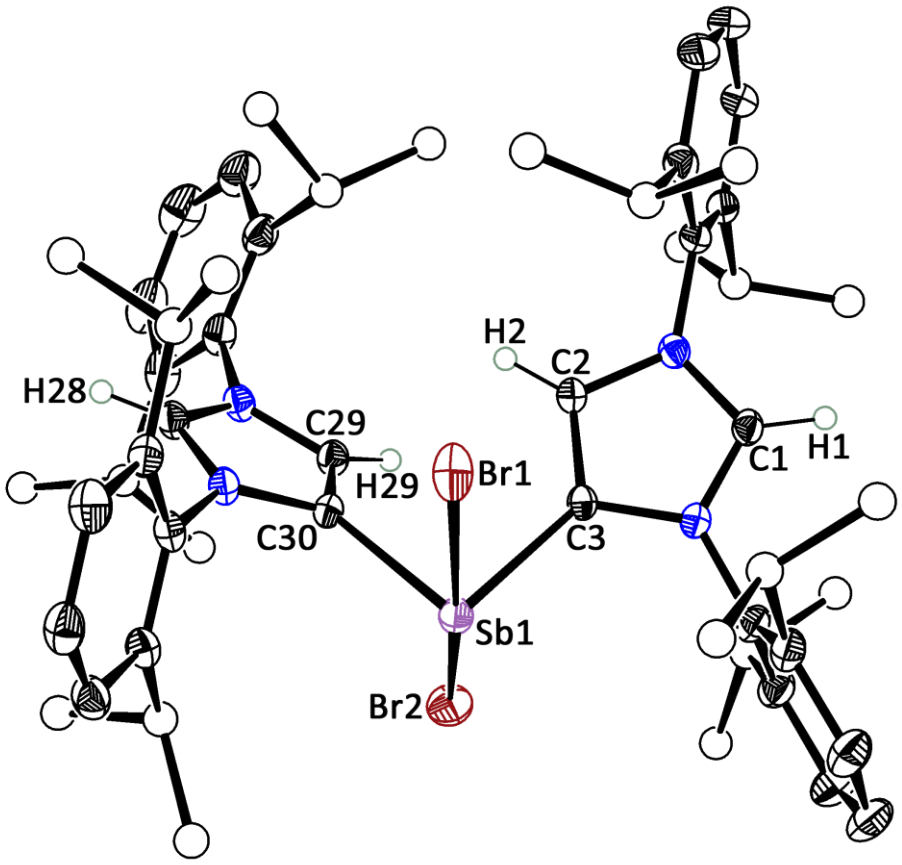

Figure 4.17: Molecular structure of **51**. Anisotropic displacement ellipsoids pictured are set at 50% probability. Hydrogen atoms (with the exception of the imidazole protons labelled H1, H2, H28 and H29) have been omitted for clarity. Atoms of the ^{i}Pr groups, the THF molecules and hydrogen atoms are pictured as spheres of arbitrary radii.

Equivalent reactions with $BiBr_3$ do not give rise to isomerisation of the second equivalent of IPr. Extended heating at temperatures up to 100 °C in d_8-THF reveal the presence of only (aIPr)$BiBr_3$ (**48**) and free IPr. It may be that the acidity of the backbone proton of the

coordinated IPr ligand is not sufficiently great enough to be abstracted by free IPr. An alternative mechanism relies on the autoionisation of IPr upon heating, generating small quantities of both $[IPrH]^+$ and $[aIPr:]^-$ which may give rise to free aIPr and then proceed to react with other electrophiles in solution such as EBr_3. It may then be the case that there is no favourable energy gain on forming an additional aIPr–Bi bond due to the inherent weakness of Bi–C bonds, hence any free, uncoordinated aIPr in solution would favourably isomerise to give IPr.

It is also worth noting, that upon addition of IPr to $(IPr)AsBr_3$ (or indeed on prolonged standing of a THF solution of $(IPr)AsBr_3$) isomerisation of one IPr ligand was observed resulting in the formation of pale pink crystals of $[(IPr)(aIPr)AsBr_2]Br$, (See Appendix A, Figure A.6), the structure of which was determined by single crystal X-ray diffraction. This species could not be isolated as a pure material due to the concomitant crystallisation of [IPrH]Br and attempts to drive the reaction to completion by heating the reaction solution resulted in similar redox chemistry as observed for the phosphorus samples discussed in Chapter 5.

All salts of **51** may be crystallised by slow diffusion of hexane into THF or DCM solutions and the bond metric data observed for **51** in all samples are similar, consequently only that of [**51**]Br will be discussed. Analysis of the molecular structure of **51** reveals a four-coordinate antimony centre in a disphenoidal geometry with a τ_4' parameter of 0.380. The two aIPr ligands occupy an equatorial position forming two single Sb–C bonds (2.158(2) and 2.163(2) Å, cf. 2.165(3) Å for the only other structurally characterised aIPr complex of antimony, $[(IPr)(aIPr)SbF_2]^+$)[8] whilst the two bromide ligands occupy the axial positions and form part of a three-centre-four-electron bonding motif with the central antimony atom. As expected, the Sb–Br bond lengths are quite long at 2.717(1) and 2.742(1) Å due to the reduced

bonding character between the antimony and the bromide ligands. The stereochemically active lone pair of electrons residing on the antimony centre occupies an equatorial position.

Finally, with the aim of investigating the possibility of the abstraction of a bromide ion from the cationic species, addition of two equivalents of Na[B(3,5-{CF_3}$_2$$C_6H_3$)$_4$] to [**51**]Br in DCM resulted in the immediate precipitation of two equivalents of NaBr (as determined by the absence of a resonance in the ^{23}Na NMR spectrum when monitored in CD_2Cl_2). The resulting dicationic species, [(aIPr)$_2$SbBr]$^{2+}$ (**52**), was isolated as a colourless, amorphous solid in 76% yield by removal of the solvent in vacuo after filtration from the NaBr. Analysis of **52** by ESI-MS in DCM reveals a mass envelope at 489.2816 (Calcd 489.1976) which can be ascribed to the dication, **52**, and exhibits an isotopic distribution whereby the peaks are separated by half a mass unit as a result of the dicationic charge. The ^{1}H NMR spectrum reveals a shift in the chemical shift of all resonances and the presence of the two imidazole proton resonances as two coupled doublets at 8.62 and 7.73 ppm. Consistent with that observed for other species bearing two aIPr or aIPr: ligands, restricted rotation about the N–Dipp bonds results in the doubling of a number of resonances in the ^{1}H and ^{13}C{^{1}H} NMR spectra. Finally, the protonated C2 carbon, antimony bound carbon and the protonated alkenic imidazole carbon were found in the ^{13}C{^{1}H} NMR spectrum at 140.9, 135.7 and 135.4 ppm. Slow diffusion of hexane into DCM or THF solutions results in the formation of a colourless oil which on standing for over two months gave rise to small colourless crystals suitable for single crystal X-ray diffraction. Analysis of the data reveals evidence for the dication, **52** (See Appendix A, Figure A.7), however this is accompanied with a disordered dicationic species (based to the number of [B(3,5-{CF_3}$_2$$C_6H_3$)$_4$]$^-$ anions in the unit cell) which lies on an inversion centre and cannot be accurately identified.

4.7 Conclusions

This chapter has described the synthesis of normal IPr complexes with the group 15 bromides, EBr_3 (E = P, As, Sb, Bi), **39**–**42**. Subsequent bromide abstraction with the use of the Lewis acid, $AlBr_3$, resulted in the formation of the cationic dibromide complexes **43**–**46** as $[AlBr_4]^-$ salts. The isomerisation of the IPr ligand in (IPr)$SbBr_3$ and (IPr)$BiBr_3$ was investigated by heating THF solutions of the reagents affording the abnormal complexes **47** and **48** which were crystallised as dimeric structures. **48** was also reproducibly crystallised as a tetramer by slow diffusion of hexane into a DCM solution. Similar bromide abstraction of these complexes, making use of the sodium salt of a non-coordinating anion $Na[B(3,5\text{-}\{CF_3\}_2C_6H_3)_4]$, affords the aIPr complexes of antimony and bismuth dibromide cations, **49** and **50** by precipitation of NaBr. Finally, the isomerisation of two equivalents of IPr upon addition to $SbBr_3$ and $BiBr_3$ and heating in THF was investigated. Upon reaction with $SbBr_3$, isomerisation of both ligands was observed to form the hypervalent species $[(aIPr)_2SbBr_2]^+$ (**51**) and bromide abstraction afforded the dicationic species, **52**. Conversely, isomerisation of a second IPr ligand was not observed in the coordination sphere of bismuth affording only **50** and free IPr.

4.8 References

(1) Kolychev, E. L.; Bannenberg, T.; Freytag, M.; Daniliuc, C. G.; Jones, P. G.; Tamm, M. *Chem. Eur. J.* **2012**, *18* (52), 16938–16946.

(2) Ganesamoorthy, C.; Bläser, D.; Wölper, C.; Schulz, S. *Organometallics* **2015**, *34* (12), 2991–2996.

(3) Winkler, A.; Freytag, M.; Jones, P. G.; Tamm, M. *J. Organomet. Chem.* **2015**, *775*, 164–168.

(4) Uzelac, M.; Hernán-Gómez, A.; Armstrong, D. R.; Kennedy, A. R.; Hevia, E. *Chem. Sci.* **2015**, *6* (10), 5719–5728.

(5) Schnee, G.; Nieto Faza, O.; Specklin, D.; Jacques, B.; Karmazin, L.; Welter, R.; Silva López, C.; Dagorne, S. *Chem. Eur. J.* **2015**, *21* (49), 17959–17972.

(6) Turbervill, R. S. P.; Goicoechea, J. M. *Aust. J. Chem.* **2013**, *66* (10), 1131–1137.

(7) Schneider, H.; Schmidt, D.; Radius, U. *Chem. Eur. J.* **2015**, *21* (7), 2793–2797.

(8) Ališ, B.; Štefančič, A.; Tavčar, G. *Dalton Trans.* **2017**, *46* (10), 3338–3346.

(9) Schwedtmann, K.; Holthausen, M. H.; Feldmann, K.-O.; Weigand, J. J. *Angew. Chem. Int. Ed.* **2013**, *52* (52), 14204–14208.

(10) Schwedtmann, K.; Schoemaker, R.; Hennersdorf, F.; Bauzá, A.; Frontera, A.; Weiss, R.; Weigand, J. J. *Dalton Trans.* **2016**, *45* (28), 11384–11396.

(11) Waters, J. B.; Everitt, T. A.; Myers, W. K.; Goicoechea, J. M. *Chem. Sci.* **2016**, *7* (12), 6981–6987.

(12) Wang, Y.; Xie, Y.; Abraham, M. Y.; Gilliard, Jr., R. J.; Wei, P.; Schaefer III, H. F.; Schleyer, P. v. R.; Robinson, G. H. *Organometallics* **2010**, *29* (21), 4778–4780.

(13) Berglund, M.; Wieser, M. E. *Pure Appl. Chem.* **2011**, *83* (2), 397–410.

(14) Cordero, B.; Gómez, V.; Platero-Prats, A. E.; Revés, M.; Echeverría, J.; Cremades, E.; Barragán, F.; Alvarez, S. *Dalton Trans.* **2008**, 2832–2838.

(15) Green, M. L. H.; Parkin, G. *Dalton Trans.* **2016**, *45* (47), 18784–18795.

(16) Batsanov, S. S. *Russ. Chem. Bull.* **1995**, *44* (1), 18–23.

(17) Aprile, A.; Corbo, R.; Tan, K. V.; Wilson, D. J. D.; Dutton, J. L. *Dalton Trans.* **2013**, *43* (2), 764–768.

(18) Henne, F. D.; Schnöckelborg, E.-M.; Feldmann, K.-O.; Grunenberg, J.; Wolf, R.; Weigand, J. J. *Organometallics* **2013**, *32* (22), 6674–6680.

(19) Filippou, A. C.; Chernov, O.; Schnakenburg, G. *Angew. Chem. Int. Ed.* **2009**, *48* (31), 5687–5690.

(20) Breunig, H. J.; Denker, M.; Lork, E. *Z. Anorg. Allg. Chem.* **1999**, *625* (1), 117–120.

(21) Althaus, H.; Breunig, H. J.; Lork, E. *Chem. Commun.* **1999**, 1971–1972.

Chapter 5

Redox chemistry of IPr complexes of group 15 bromides

5.1 Introduction and objectives

5.1.1 Reduction of NHC stabilised main group compounds

As discussed in Chapter 1, Section 1.4, NHCs have recently found use as ligands in the synthesis of compounds exhibiting multiple bonds between main group elements. With the use of NHCs (predominantly IPr due to the ease of synthesis and reasonable steric bulk), compounds containing main group element diatomics in a formally zero oxidation state have recently been synthesised, i.e. $(IPr)_2E_2$ (E = B, Si, Ge, Sn, P, As).[1–6] These were accessed by reduction of the IPr adduct of the group 14 dichlorides or group 15 trichlorides in poor to reasonable yields with the exception of $(IPr)_2B_2$ which was accessed by reduction of $(IPr)_2B_2Br_4$ which has a pre-existing B–B bond which likely explains the higher yield obtained in the reduction. Reduction of the other precursors with typically KC_8 or a magnesium(I) species, $[Mg\{N(Ar)CMe\}_2CH]_2$, results in a mixture of products and product yields as low as 5% which indicates the uncontrolled reactivity that takes place upon reduction.

Reduction is not restricted to NHC adducts of the main group halides. It was found that addition of a magnesium(I) reducing agent to the IPr adduct of alane, $(IPr)AlH_3$, results in the formation of the corresponding magnesium(II) hydride and the aluminium(II) species, $(IPr)_2Al_2H_4$, which is an IPr stabilised dialane(4) (Figure 5.1).[7]

Similarly, alternative reduction methods are being investigated and employed in the synthesis of main group elements which exhibit multiple bonding stabilised by the coordination of NHCs. Grützmacher and co-workers have utilised the IPr and SIPr stabilised parent phosphinidene, (IPr)PH and (SIPr)PH, respectively, which contain an NHC supported phosphorus atom in a formal –1 oxidation state. Addition of two equivalents of (IPr)PH to PCl_3 or $AsCl_3$ in the presence of a base results in the formation of IPr stabilised chains of

P–P–P and P–As–P as cationic species which can subsequently be reduced to the neutral radical species by magnesium metal.[8] Similarly, addition of two equivalents of (SIPr)PH to $HgCl_2$ along with DBU as a base affords the bis(phosphinidene)mercury complex, $[(SIPr)P]_2Hg$.[9]

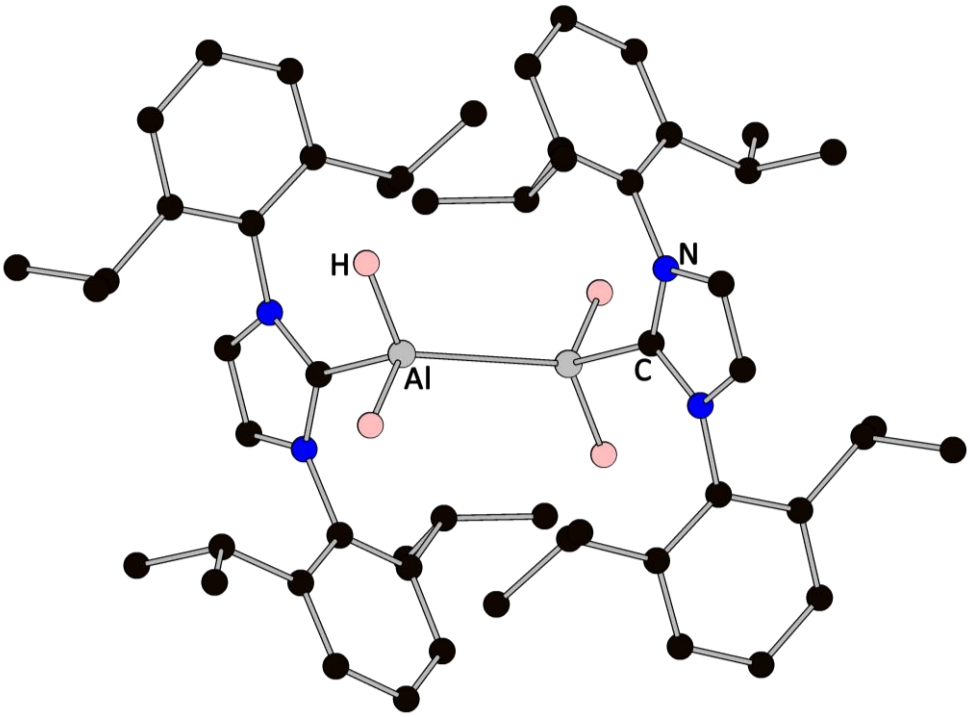

Figure 5.1: Ball and stick model of $(IPr)_2Al_2H_4$. Hydrogen atoms (with the exception of the Al_2H_4 protons) have been omitted for clarity.

5.1.2 Oxidation of IPr stabilised main group diatomics

As discussed in Chapter 1, Section 1.5, chemical oxidation of the aforementioned main group diatomic species has allowed for the synthesis of the oxidised products as stable and persistent radical cations and diamagnetic dications, namely those of diphosphorus and diarsenic.[10,11] Similarly, oxidation by dry oxygen gas, as opposed to the ferrocenium cation, trityl cation or gallium trichloride used in the previous examples, resulted in the formation of novel main group oxides of the heavier elements such as P_2O_4 and Si_2O_3 stabilised by IPr. These species would otherwise normally oligomerise in the absence of the ligand.[12–14] Finally, oxidation has

also been achieved by addition of $C_2H_4X_2$ (X = Br, I) to $(IPr)_2Si_2$ resulting in the formal oxidation from silicon(0) to silicon(I) in $(IPr)_2Si_2X_2$ with loss of C_2H_4.[15] Iodide abstraction with the use of the lithium salt of a non-coordinating borate anion resulted in the formation of the novel disilicon(I) salt, $[(IPr)_2Si_2I][B(C_6F_5)_4]$ (Figure 5.2).

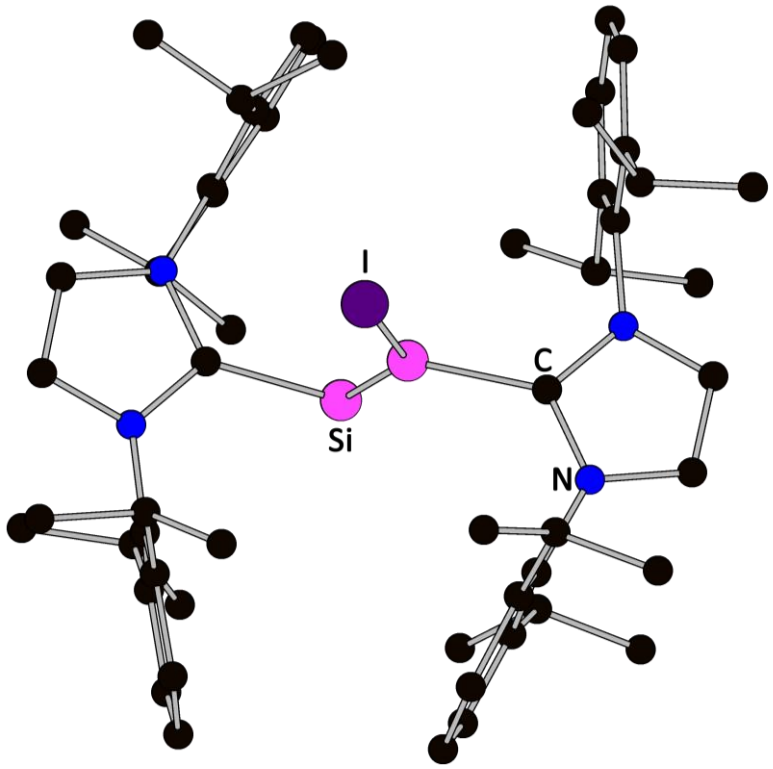

Figure 5.2: Ball and stick model of $[(IPr)_2Si_2I]^+$. Hydrogen atoms have been omitted for clarity.

5.1.3 Chapter outline

All known reported routes to main group diatomic species stabilised by the coordination of NHC ligands require the use of strong reducing agents such as KC_8, sodium napthalenide or a highly reactive magnesium(I) compound. These reactions result in a relatively uncontrolled reduction of the precursor reagents and typically afford low yields of the target products. In order to access novel oxidation states of the main group elements in this bonding motif, full reduction to the zero oxidation state has been employed followed by chemical oxidation, however this is an ineffective synthetic methodology. A logical route to such species would

be with the use of milder reducing agents affording a stepwise reduction from a high to low oxidation state via a controlled reaction mechanism. This chapter will discuss a stepwise approach in the reduction of (IPr)PBr_3 to afford high yields of novel intermediate species which likely form in the synthesis of the diphosphorus species, $(IPr)_2P_2$, with the use of mild and organic solvent soluble reducing agents.

5.2 Reductive coupling of (IPr)PBr_3

5.2.1 Synthesis of [$(IPr)_2P_2Br_3$]Br ([53]Br)

With the aim of synthesising the abnormal isomer of (IPr)PBr_3, we sought to heat a THF solution of **39** to induce isomerisation of the IPr ligand as discussed in Chapter 4. Interestingly, when a THF solution of **39** was heated to 55 °C, large dark red crystals slowly begin to form in the reaction flask. The reaction is complete after heating for three days as evidenced by ^{31}P NMR spectroscopy which reveals consumption of the starting material. The crystals formed were determined to be [$(IPr)_2P_2Br_3$]Br ([**53**]Br) which arises from the reductive coupling of two equivalents of **39** along with a formal loss of bromine (Scheme 5.1) which is a highly unique and novel reaction given the absence of an external reducing agent.[16] Under the reaction conditions, bromine is observed to react rapidly with THF affording brominated organic species such as 1,4-dibromobutane as determined by GC-MS, presumably via a radical based mechanism. The by-products were confirmed to form in a control experiment whereby bromine was heated to 55 °C in THF and the solution analysed by GC-MS. The reductive coupling was also observed to take place in the solid state; a solid sample of **39** was heated to 140 °C and held at this temperature for ten hours upon thermogravimetric analysis revealing approximately 11% reduction in mass (the formal loss of half an equivalent of bromine would give rise to a 12.1% reduction in mass).

The reduction process is facilitated by the strong electron donation of the IPr ligand to the phosphorus centre in **39** which significantly weakens the P–Br bonds. Crystallisation of [**53**]Br from the reaction mixture results from initial coupling of the reduced phosphorus centres, possibly via a radical based mechanism, followed by bromide elimination and the formation of a bromide bridged species. The electronic and steric stabilisation afforded by the two IPr ligands serve to stabilise what can be described as a cyclic bromonium ion, or conversely, the dicationic species, $[(IPr)_2P_2Br_2]^{2+}$, which forms a strong electrostatic interaction with a bromide ion.

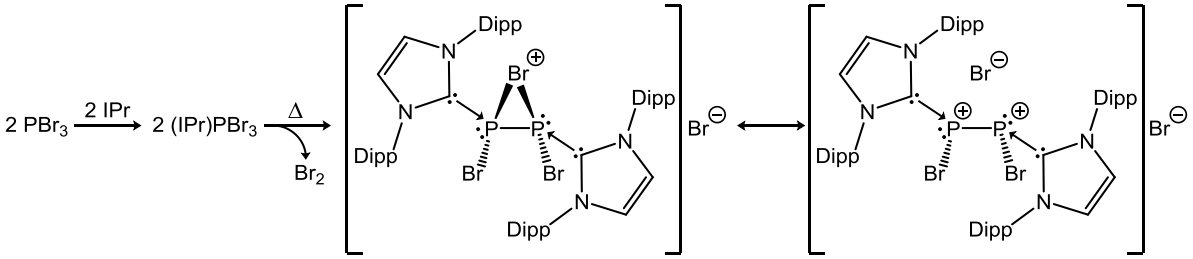

Scheme 5.1: Thermally induced reductive coupling of **39** affording $[(IPr)_2P_2Br_3]Br$, [**53**]Br.

The elimination of the bromide ion and the formation of a salt results in an ionic species which is insoluble in THF and crystallises from solution. The formation of **53** was evidenced by analysis of the ^{1}H, $^{13}C\{^{1}H\}$ and ^{31}P NMR spectra of the red crystals upon dissolution in CD_2Cl_2. The ^{1}H NMR spectrum reveals a high degree of restricted rotation on the NMR timescale. Each ligand is equivalent, however, restricted rotation about the N–Dipp and P–C bonds give rise to many resonances in the ^{1}H and $^{13}C\{^{1}H\}$ NMR spectra. The diagnostic imidazole protons give rise to two separate doublet resonances with a coupling constant of 2 Hz at 7.55 and 7.43 ppm. Similarly, four septet methine resonances and eight doublet methyl resonances are observed as a result. The carbene carbons give rise to a complex multiplet resonance in an AA'XX' coupling pattern centred at 150.2 ppm. Finally, a single resonance is observed in the ^{31}P NMR spectrum, indicating the equivalence of the two phosphorus atoms,

at –27.3 ppm. The formation of the ionic species was further corroborated by the presence of a mass envelope at 1079.2753 in the ESI-MS which can be assigned to **53** (Calcd 1079.2739).

The molecular structure of **53** was unambiguously determined through single crystal X-ray diffraction (Figure 5.3) and reveals a planar $[P_2Br_3]^+$ moiety with a root-mean-square deviation from planarity of 0.018 Å in which one of the bromine atoms bridges the P–P bond.

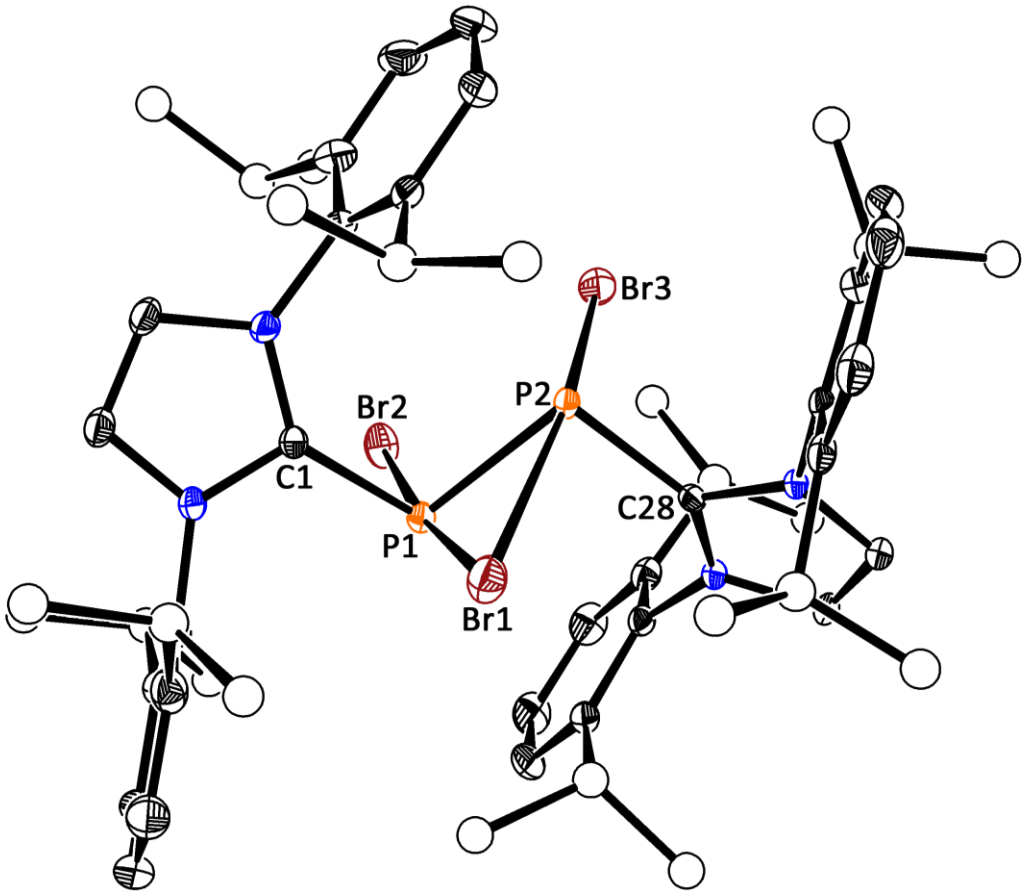

Figure 5.3: Structure of cation **53** in [**53**]Br·3THF. Anisotropic displacement ellipsoids pictured are set at 50% probability. Hydrogen atoms have been omitted for clarity. Atoms of the ^{i}Pr groups are pictured as spheres of arbitrary radii.

The two IPr ligands lie on opposite faces of the $[P_2Br_3]^+$ moiety resulting in a distorted, disphenoidal geometry about each phosphorus centre which can be described by the τ_4' values of 0.397 and 0.436 for P1 and P2, respectively. The P–C bond lengths were measured to be 1.860(3) and 1.866(3) Å which are not significantly different to those of the precursor

(cf. 1.872(2) Å in **39**). The P–P distance of 2.252(1) Å is long but consistent with a formal P–P single bond (Σr_{cov} = 2.14 Å)[17] and very similar to that observed in the chloride analogue $[(IPr)_2P_2Cl_3]^+$ (**54**) (2.242(1) Å) synthesised by Weigand and co-workers (Figure 5.4).[18] The bridging bromide is found to be largely equidistant between the two phosphorus atoms (P1–Br1 = 2.667(1) Å and P2–Br1 = 2.810(1) Å) and these distances are notably longer than those observed to the terminal bromide ligands (P1–Br2 = 2.349(1) Å and P2–Br3 = 2.288(1) Å). The cyclic structure present in **53** allows for the interpretation as a phosphorus containing analogue of a bromonium ion given the diagonal relationship between a phosphorus atom and that of a methine group. However, previous computational analysis of the chloride analogue indicates an interaction between the two phosphorus centres and the bridging chloride is more consistent with that of an electrostatic interaction between the chloride ion and the dicationic $[(IPr)_2P_2Cl_2]^{2+}$.[18] This conclusion was made on the basis of the low Wiberg bond indices between the phosphorus atoms and the bridging chloride (0.25), the relatively high negative charge associated with the bridging chloride and an AIM topological analysis. **53** could be accessed through the use of KC_8 as a reducing agent, however over reduction was a significant issue giving rise to a mixture of products. Our synthetic route represents a unique methodology in order to access low valent phosphorus species, and presumably arises due to the weaker oxidative character of bromine relative to chlorine.

Exchange of the uncoordinated bromide for that of a non-coordinating anion, namely $[B(3,5\text{-}\{CF_3\}_2C_6H_3)_4]^-$, was possible by the addition of $Na[B(3,5\text{-}\{CF_3\}_2C_6H_3)_4]$ to [**53**]Br in THF. Whereas **53** is insoluble in ethereal solvents as the bromide salt, the $[B(3,5\text{-}\{CF_3\}_2C_6H_3)_4]^-$ salt is notably more soluble in common organic solvents. [**53**][$B(3,5\text{-}\{CF_3\}_2C_6H_3)_4$] was crystallographically characterised and the bond metric data are comparable to the observed for [**53**]Br.

It was noted that upon standing of a DCM solution of [**53**]Br, a new resonance in the ^{31}P NMR spectrum could be observed at –35.4 ppm which can be assigned to **54**. Heating a DCM solution to 60 °C overnight allowed for full conversion via an unknown mechanism. This was also true of a sample of [**53**][B(3,5-{CF_3}$_2$$C_6H_3$)$_4$] indicating that the free bromide ion was not involved.

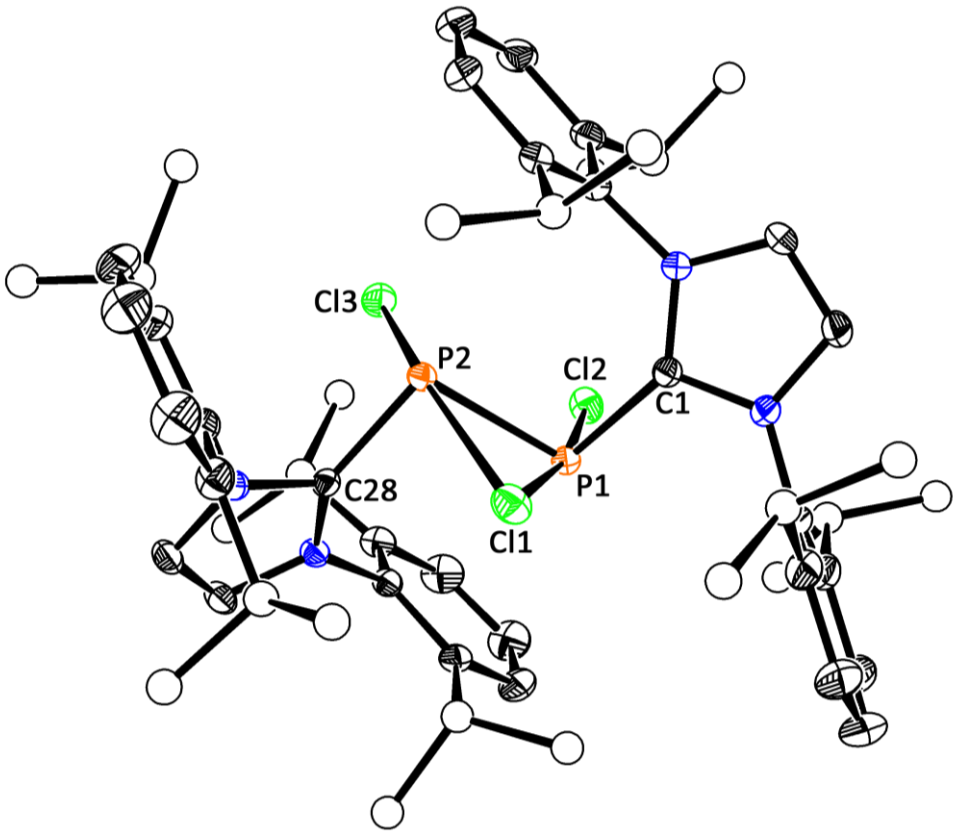

Figure 5.4: Structure of cation **54** in [**54**]Br·4DCM. Anisotropic displacement ellipsoids pictured are set at 50% probability. Hydrogen atoms have been omitted for clarity. Atoms of the ^{i}Pr groups are pictured as spheres of arbitrary radii.

Ultimately, the stronger P–Cl bonds are a driving force for the transformation and **54** was identified by ESI-MS which displays a mass envelope at 945.4067 (Calcd 945.4267). Single crystals of [**54**]Br·4DCM suitable for analysis by single crystal X-ray diffraction were grown by slow diffusion of hexane into a crude reaction mixture and confirms the formation of **54** (Figure 5.4).

5.2.2 Bromide abstraction from 53 and 54

We sought to synthesise the phosphorus(II) dication through abstraction of the bridging bromide ion in **53**. Addition of Na[B(3,5-{CF_3}$_2$$C_6H_3$)$_4$] to [**53**][B(3,5-{$CF_3$}$_2$$C_6H_3$)$_4$] in THF did not afford any reaction due to solvation of the alkali metal cation, however, using DFB as a reaction solvent resulted in the immediate elimination of NaBr and the formation of the novel dicationic species, [(IPr)$_2$$P_2$$Br_2$]$^{2+}$ (**55**) as the [B(3,5-{CF_3}$_2$$C_6H_3$)$_4$]$^-$ salt (Figure 5.5). Interestingly, the product reveals an anticlinal arrangement of the bromine atoms with the IPr ligands in antiperiplanar positions and there exists a centre of inversion along the centre of the P–P bond rendering the two phosphorus centres enantiomeric (1*S*,2*R*). At no point was evidence obtained for the formation of the stereoisomers 1*R*,2*R* or 1*S*,2*S* (Scheme 5.2).

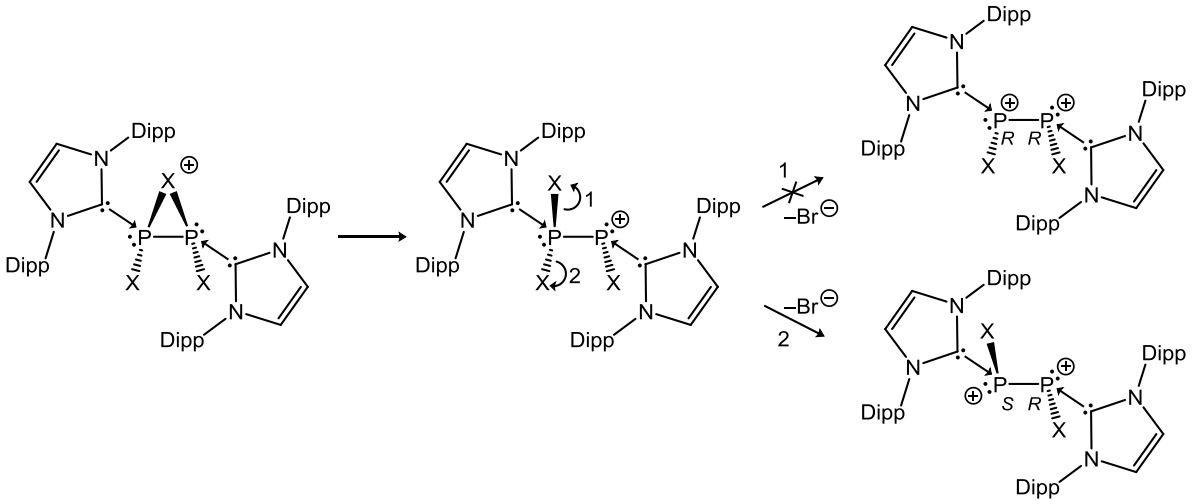

Scheme 5.2: Possible stereochemical outcomes from halide abstraction from **53** and **54**.

This observation reveals that it is a terminal bromide ligand that is lost on bromide abstraction as removal of the bridging bromide ligand can only afford the 1*R*,2*R*/1*S*,2*S* enantiomeric pair as inversion at one of the phosphorus centres is highly unlikely due to the high barrier to inversion (typically >80 kJ·mol^{-1}).[19–22] The reaction possibly proceeds via a mechanism whereby the bridging bromide adopts a terminal position and the bromide *trans* to it is lost.

Density functional theory (DFT) level calculations carried out by Prof. Jose Goicoechea reveal that the 1*S*,2*R* isomer is 29.0 kJ·mol^{-1} more stable than the 1*R*,2*R* stereoisomer indicating that this may well be a thermodynamically favoured phenomenon. The equivalent chloride abstraction from **54** results in an analogous results forming $[(IPr)_2P_2Cl_2]^{2+}$ (**56**) as the $[B(3,5\text{-}\{CF_3\}_2C_6H_3)_4]$ salt (Figure 5.6).

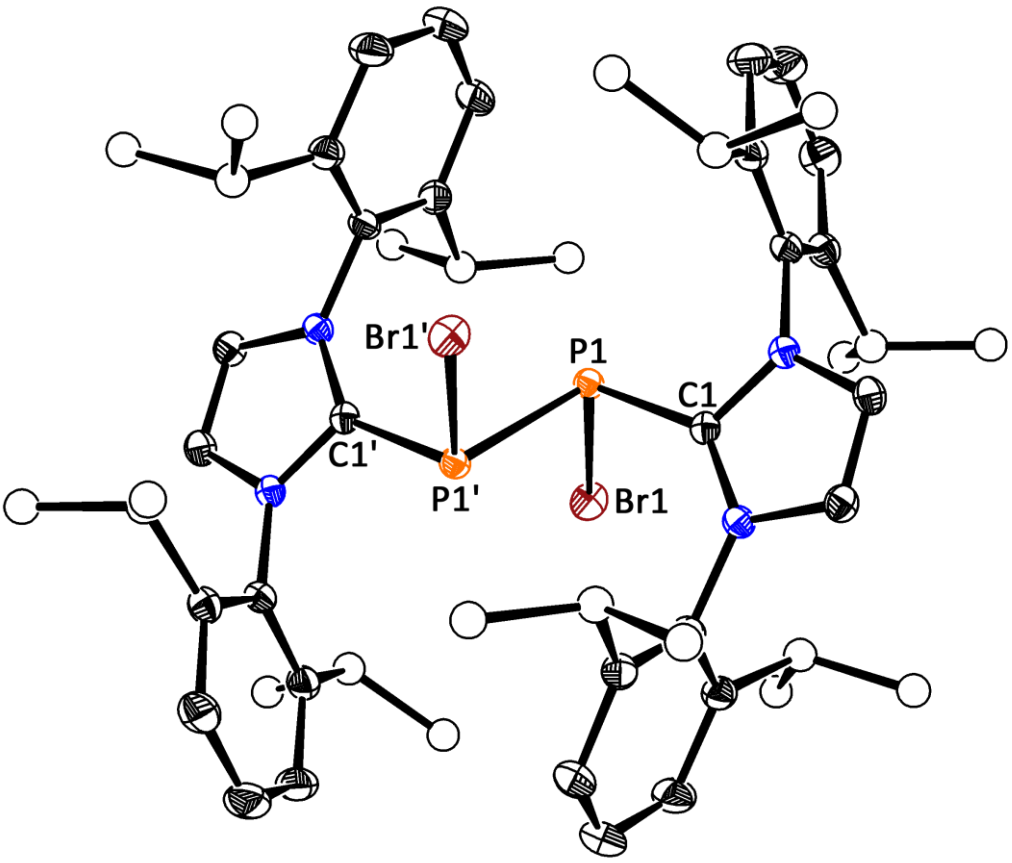

Figure 5.5 Structure of dication **55** in [**55**][B(3,5-{CF_3}$_2$$C_6H_3$)$_4$]$_2$·2DFB. Anisotropic displacement ellipsoids pictured are set at 50% probability. Hydrogen atoms have been omitted for clarity. Atoms of the ^{i}Pr groups are pictured as spheres of arbitrary radii. Symmetry operation: 1–*x*, 1–*y*, 2–*z*.

Single crystals of [**55**][B(3,5-{CF_3}$_2$$C_6H_3$)$_4$]$_2$·2DFB and [**55**][B(3,5-{CF_3}$_2$$C_6H_3$)$_4$]$_2$·$^3/_2$DCM were grown by slow diffusion of hexane into a DFB and DCM solution, respectively, and both solvates exhibit comparable bond metric data. For clarity, only **55** from [**55**][B(3,5-{CF_3}$_2$$C_6H_3$)$_4$]$_2$·2DFB will be discussed. Similarly, single crystals of [**56**][B(3,5-{CF_3}$_2$$C_6H_3$)$_4$]$_2$·DFB were grown by slow diffusion of hexane into a DFB solution

and analysis by single crystal X-ray diffraction unambiguously confirms the anticlinal arrangement of the halide ligands.

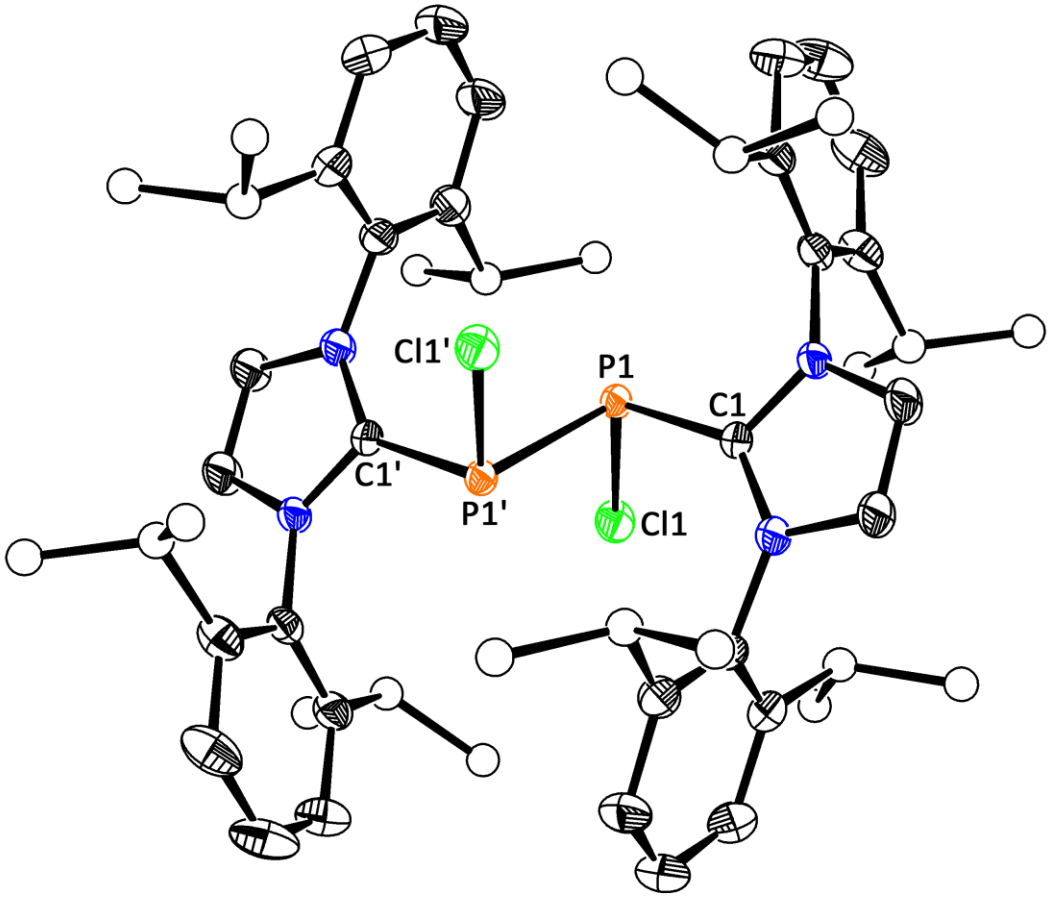

Figure 5.6 Structure of dication **56** in [**56**][B(3,5-{CF_3}$_2$$C_6H_3$)$_4$]$_2$·DFB Anisotropic displacement ellipsoids pictured are set at 50% probability. Hydrogen atoms have been omitted for clarity. Atoms of the ^{i}Pr groups are pictured as spheres of arbitrary radii. Symmetry operation: 1–*x*, 2–*y*, 1–*z*.

Halide abstraction affords two, three-coordinate phosphorus centres in both **55** and **56** where each is related by inversion symmetry. The geometry is evident from the sum of bond angles about the phosphorus atom which are 295.7° and 294.7°, respectively, which is expected for a pyramidal phosphorus centre possessing a stereochemically active lone pair of electrons. The P–P bond distances in **55** and **56** were measured to be 2.240(2) and 2.243(2) Å, respectively, which are marginally shorter than those observed in the precursors. There is a reasonable decrease in the P–C bond distances by approximately 0.02 Å upon bromide abstraction (1.843(2) Å in **55** and 1.838(3) Å in **56**) which is as expected due to greater σ

donation from IPr upon loss of a ligand. However, the P–X bond distances are more dramatically affected, a reduction of approximately 0.11 and 0.07 Å is observed for **55** (2.211(1) Å) and **56** (2.062(1) Å), respectively. Given the very small changes in the P–P and P–C distances, the description of **54** and **55** as dicationic species bearing a bridging bromide ion is more appropriate (as opposed to a halonium ion). **55** is isoelectronic with the neutral silicon(I) species previously reported by Filippou and co-workers, $(IPr)_2Si_2Br_2$, and it is worth noting that only the *RR*/*SS* stereoisomers were observed for this species.[15]

The formation of the dicationic species was further confirmed by the presence of a mass envelope at 499.1745 for **54** (Calcd 499.1787) and at 455.3389 for **55** (Calcd 455.2290). The peaks in the mass envelope are separated by half a mass unit as a result of the dicationic charge of the molecular ion.

5.2.3 Further reduction

Given the ease with which $(IPr)PBr_3$ (**39**) could be reduced to $[(IPr)_2P_2Br_3]Br$ (**53**) by a thermally induced reductive coupling, we sought to reduce **53** further with the use of mild reducing agents exploiting the relative weakness of the P–Br bonds. A two electron reduction upon addition of one equivalent of $SnBr_2$ in THF results in the formation of $[(IPr)_2P_2Br]^+$ (**57**) and $[SnBr_5(THF)]^-$ (Scheme 5.3) as a deep red solution.

When the reaction was monitored by ^{31}P NMR spectroscopy, near quantitative conversion of **53** to **57** was evidenced by the appearance of two doublets at 145.4 and –7.6 ppm with a one bond coupling constant of 391 Hz. The magnitude of the coupling constant is also indicative of multiple bonding character as represented by one resonance form in Scheme 5.3. The two inequivalent phosphorus environments and their chemical shifts are consistent with the formation of **57** whereby the highest frequency resonance (145.4 ppm) can be attributed to

the two-coordinate phosphorus atom. **57** can be interpreted as either a phosphorus(I) dimer or as a mixed valence phosphorus(II)/phosphorus(0) species depending on which resonance structure is invoked.

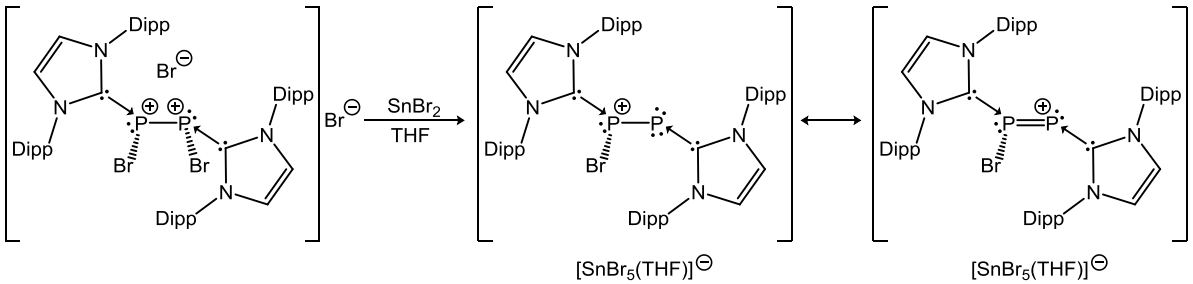

Scheme 5.3: Reduction of [**53**]Br with $SnBr_2$ to afford [**57**][$SnBr_5$(THF)].

Variable temperature NMR studies reveal fluxional behaviour that leads to exchange of the heterotopic phosphorus nuclei. A similar fluxionality was observed for a similar silicon(I) species, $[(IPr)_2Si_2I]^+$, reported by Filippou and co-workers (Figure 5.2). At 338 K, the two resonances in the ^{31}P NMR spectrum broaden beyond recognition, although on cooling to 208 K, the two doublets progressively sharpen due to the decreasing rate of exchange of the bromide ligand between the two phosphorus centres. At 208 K, the ^{1}H NMR spectrum reveals two distinct IPr environments whereby only one IPr ligand has restricted rotation about the P–C bond and this is evident from the diagnostic imidazole proton resonances. One IPr ligand displays two distinct singlets at 8.24 and 8.20 ppm which each integrate to one proton, demonstrating the asymmetry of the ligand. A third resonance at 7.80 ppm is attributed to the imidazole protons of the second IPr ligand and integrates to two protons. Likewise, the $^{13}C\{^{1}H\}$ NMR spectrum at 208 K reveals two doublet of doublet resonances at 164.2 and 150.6 ppm which can be assigned to the two separate carbene carbons. The one bond $^{13}C–^{31}P$ coupling constant can be measured to be 118 and 85 Hz, respectively, indicating a greater degree of multiple bonding between the carbene carbon and the two-coordinate phosphorus atom. The chlorine containing analogue of **57**, $[(IPr)_2P_2Cl]^+$ has previously been reported by

Wolf and Weigand via reduction of [(IPr)PCl_2][OTf] with an organometallic iron reducing agent to afford a mixture of products.[18] Analysis by ESI-MS in DCM reveals the molecular ion at 919.5514 (Calcd 919.4354).

[**57**][$SnBr_5$(THF)] was crystallised by slow diffusion of hexane into a THF reaction mixture, however, the presence of [$SnBr_5$(THF)]$^-$ in solution can result in an equilibrium with $SnBr_4$ and $[SnBr_6]^{2-}$. The Lewis acidic $SnBr_4$ can act to abstract a bromide ion from **57** giving rise to the dicationic species, $[(IPr)_2P_2]^{2+}$ as the hexabromostannate salt when solutions are allowed to stand for prolonged periods of time. The presence of this dication, which has been previously reported by Bertrand and co-workers,[10] was evidenced by the appearance of a resonance at 442.6 ppm in the ^{31}P NMR spectrum. Halide abstraction can be circumvented by the addition of half an equivalent of IPr in order to sequester $SnBr_4$ as the Lewis acid–base adduct (IPr)$SnBr_4$ resulting in the crystallisation of [**57**]$_2$[$SnBr_6$]·THF (Figure 5.7). Two molecules of **57** are present in the asymmetric unit and bond metric data are comparable for both cations. For clarity, only one will be discussed. The P–P bond distance (2.096(2) Å) is notably shorter than that observed in **53** and **55** and is of comparable magnitude to literature reported values for species containing a P=P double bond. This indicates that there is significant contribution to bonding from the resonance structure carrying a formal positive charge on the two-coordinate phosphorus atom. Computed Hirshfeld charges show that the greatest degree of positive charge accumulates on the phosphorus atom bonded to the bromine atom (0.143) indicating both resonance structures must contribute significantly. The P–C bond lengths (1.847(5) and 1.845(5) Å) are not appreciably different from those observed in **53**, whereas the P–Br bond length has increased by approximately 0.12 Å to 2.443(1) Å indicating a weak interaction providing justification for the observation of further bromide abstraction upon standing in solution.

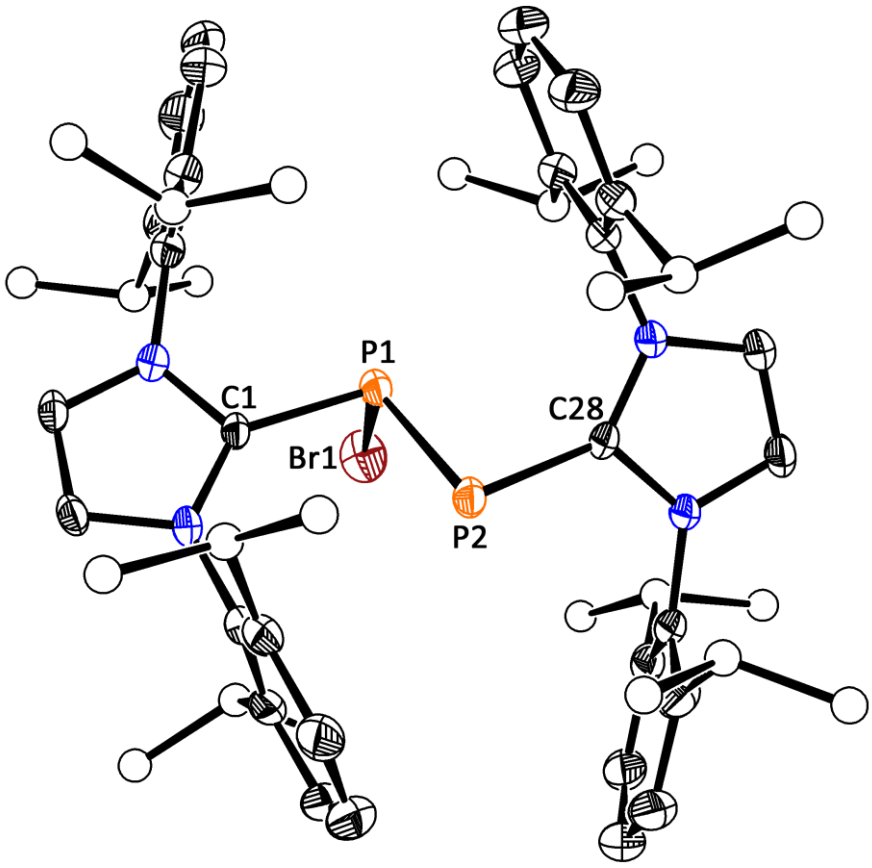

Figure 5.7 Structure of cation **57** in [**57**]$_2$[SnBr$_6$]·THF. Anisotropic displacement ellipsoids pictured are set at 50% probability. Hydrogen atoms have been omitted for clarity. Atoms of the ^{i}Pr groups are pictured as spheres of arbitrary radii.

By making use of a stronger reducing agent such as tetrakis(dimethylamino)ethylene (TDAE), a three electron reduction of **53** affords the known radical cation [(IPr)$_2$P$_2$]$^{\bullet+}$ (**58**) which could be isolated as the [B(3,5-{CF$_3$}$_2$C$_6$H$_3$)$_4$] salt (Scheme 5.4). Addition of one and half equivalents of TDAE to [**53**][B(3,5-{CF$_3$}$_2$C$_6$H$_3$)$_4$] yields the radical cation, **58**, in quantitative yield with concomitant elimination of [TDAE][Br]$_2$ in THF. Addition of an excess of TDAE has no effect and no further reduction is observed. **58** has been synthesised previously by chemical oxidation of (IPr)$_2$P$_2$ with [CPh$_3$][B(C$_6$F$_5$)$_4$].[10] **58** was structurally authenticated by single crystal X-ray diffraction as [**58**][B(3,5-{CF$_3$}$_2$C$_6$H$_3$)$_4$] and the bond metric data are consistent with that reported by Bertrand and co-workers for [**58**][B(C$_6$F$_5$)$_4$].

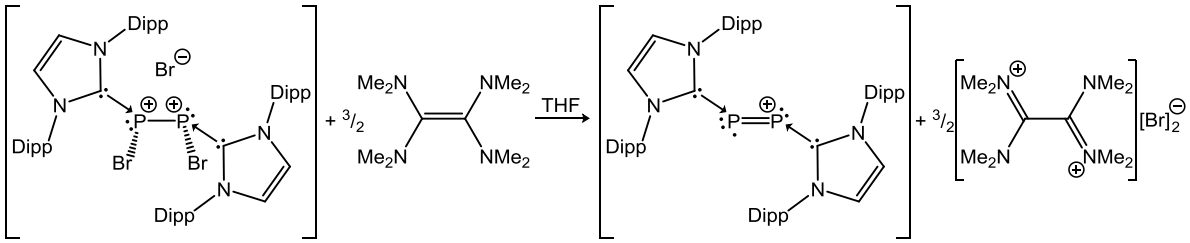

Scheme 5.4: Reduction of **53** with one and half equivalents of TDAE to afford **58**.

The P–P bond length of 2.111(1) Å is indicative of multiple bonding character similar to that observed in **57**. There is a marginal decrease in the P–C bond lengths (1.795(2) and 1.824(2) Å) which is again indicative of multiple bonding, an increase in the π backbonding from the central P_2 moiety to the carbene carbon of the ligands as a results of the addition of an extra electron. The formation of **58** as the only cationic species was further evidenced by the presence of a single mass envelope at 838.5018 (Calcd 838.5227).

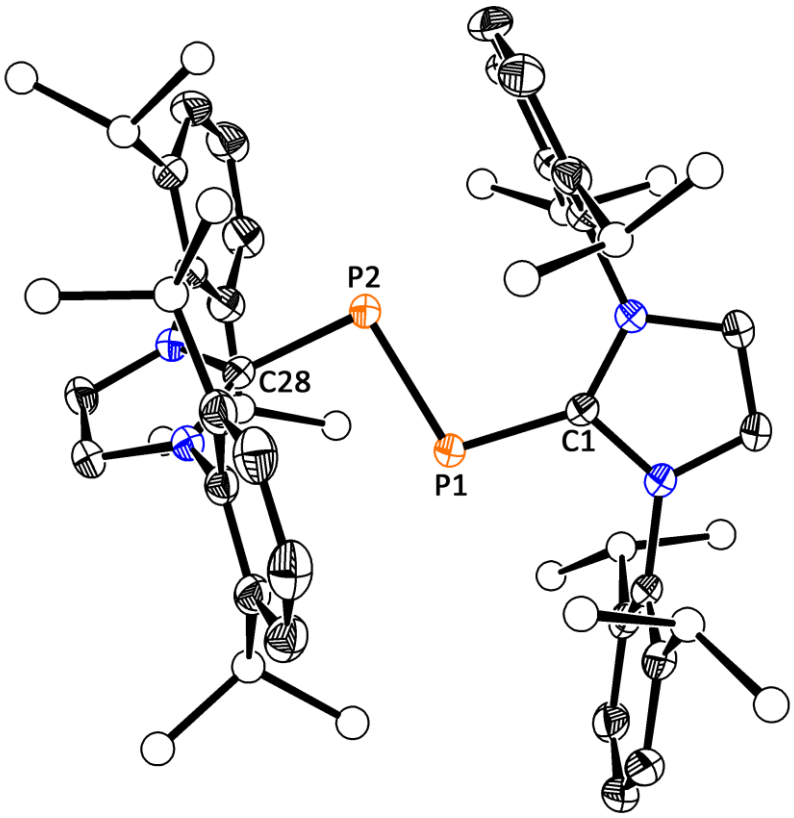

Figure 5.8 Structure of cation **58** in [**58**][B(3,5-{CF_3}$_2$$C_6H_3$)$_4$]. Anisotropic displacement ellipsoids pictured are set at 50% probability. Hydrogen atoms have been omitted for clarity. Atoms of the ^{i}Pr groups are pictured as spheres of arbitrary radii.

Room temperature X-band (v = 9.3761 GHz) electron paramagnetic resonance (EPR) spectroscopy carried out by Dr. William Myers on a 100 μM solution of [**58**][B(3,5-{CF_3}$_2$$C_6H_3$)$_4$] in fluorobenzene revels that the predominant spin density is located on the ^{31}P nuclei giving rise to a 1 : 2 : 1 hyperfine pattern (g_{iso} = 2.0090 (+/– 0.0001); as previously reported by Bertrand and co-workers). The isotropic hyperfine splitting for the ^{31}P nuclei, A_{iso}(^{31}P), is 126 MHz. The hyperfine interactions of the four ^{14}N atoms of the imidazole groups are resolved as a nine-peak pattern on the central peak. The ^{14}N isotropic hyperfine splitting, A_{iso}(^{14}N), is 4 MHz (full details of the EPR spectrum are provided in Appendix B).

5.3 Reduction of (IPr)AsBr$_3$

5.3.1 Synthesis of [(IPr)$_2$As$_2$Br$_3$]Br ([59]Br)

Attempts to heat a THF solution (IPr)AsBr$_3$ (**40**) to afford similar reactivity observed for (IPr)PBr$_3$ did not give rise to [(IPr)$_2$As$_2$Br$_3$]Br ([**59**]Br) as a major product. A mixture of products form from which [(IPr)(aIPr)AsBr$_2$]Br crystallises from solution as previously discussed in Chapter 4, Section 4.6. The As–C and As–Br bonds in **40** are of comparable strength such that upon heating both bonds are just as likely to cleave giving rise to a mixture of products through the isomerisation of the IPr ligand and reduction of the arsenic centres. Utilising the high reduction potential of TDAE coupled with its high solubility in organic solvents including DCM, we sought to reduce **40** with TDAE to afford [(IPr)$_2$As$_2$Br$_3$]Br, ([**59**]Br). Addition of half an equivalent of TDAE to a DCM solution of **40** immediately gives rise to an orange colour which gradually becomes green and over five minutes gives rise to a deep pink solution and colourless precipitate. The colourless precipitate, [TDAE][Br]$_2$, is insoluble in DCM and can be filtered from the reaction mixture which contains [**59**]Br. Analysis by ^{1}H and ^{13}C{^{1}H} NMR spectroscopy reveals restricted rotation identical to that

observed in the phosphorus-containing analogue. Two distinct imidazole resonances were observed at 7.58 and 7.42 ppm in the ^{1}H NMR spectrum each of which integrates to two protons due to restricted As–C bond rotation. A single resonance attributable to the carbene carbon appears at 150.1 ppm in the $^{13}C\{^{1}H\}$ NMR spectrum and two distinct backbone imidazole carbon resonances can be observed at 128.7 and 126.9 ppm.

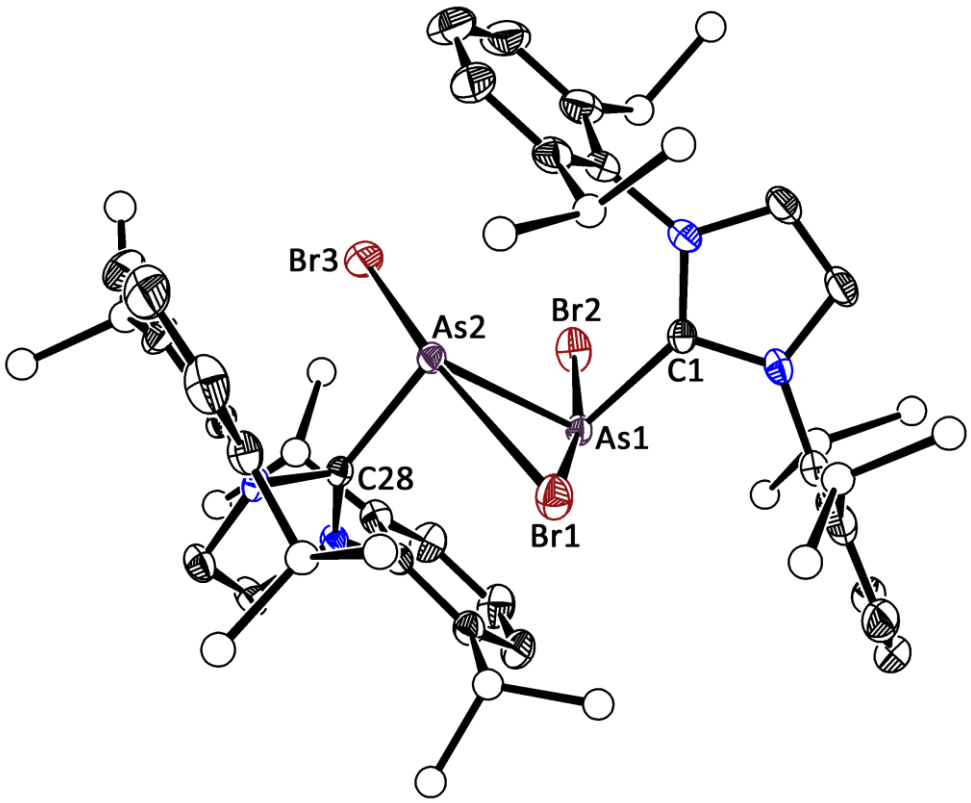

Figure 5.9 Structure of cation **59** in [**59**]Br·3DCM. Anisotropic displacement ellipsoids pictured are set at 50% probability. Hydrogen atoms have been omitted for clarity. Atoms of the ^{i}Pr groups are pictured as spheres of arbitrary radii.

Analysis of [**59**]Br by ESI-MS in DCM reveals a single mass envelope at 1167.3397 corresponding to the molecular ion **59** (Calcd 1167.1696). Single crystals of $[(IPr)_2As_2Br_3]Br\cdot 3DCM$ suitable for single crystal X-ray diffraction were grown by slow diffusion of hexane into a DCM solution and reveals a planar $[As_2Br_3]^{+}$ moiety (root-mean-square deviation from planarity = 0.034 Å) coordinated by two IPr ligands residing on opposite faces of the plane. The structure again gives rise to a distorted,

disphenoidal geometry about the arsenic atoms as indicated by the τ_4' values of 0.369 and 0.381. The As–C bond lengths were measured to be 1.992(3) and 1.997(3) Å which are approximately 0.13 Å longer than those in **53**. This is in line with the larger covalent radius of arsenic when compared with phosphorus (Δr_{cov} = 0.12 Å).[17] Likewise, there is a long As–As bond at 2.477(1) Å which is consistent with a single bond. The bridging bromide is largely equidistant between As1 and As2 (2.803(1) and 2.865(1) Å, respectively) whilst the As–Br bonds to the terminal bromine atoms (Br2 and Br3) are significantly shorter at 2.431(1) and 2.389(1) Å, respectively.

5.3.2 Bromide abstraction from 59

As with the synthesis of both **55** and **56**, addition of two equivalents of Na[B(3,5-{CF_3}$_2$$C_6H_3$)$_4$] to a DFB solution of [**59**]Br gives rise to a bright yellow solution and a colourless precipitate (NaBr). The reaction affords an analogous dicationic arsenic(II) species, $[(IPr)_2As_2Br_2]^{2+}$ (**60**) which can be isolated in 85% crystalline yield upon filtration of the reaction solution and slow diffusion of hexane into the reaction mixture. Similarly, only evidence for the formation of the 1*R*/2*S* isomer was observed indicating an identical reaction mechanism whereby one of the original terminal bromide ligands is the one that is ultimately lost. Analysis of the molecular structure reveals a trigonal pyramidal geometry about the arsenic centre which is to be expected due to the presence of a stereochemically active lone pair of electrons. A centre of inversion which lies along the As–As bond renders each half of the molecule equivalent by symmetry and the As–C bond distance can be measured to be 2.026(3) Å which is marginally longer than those observed in the precursor, **59**.

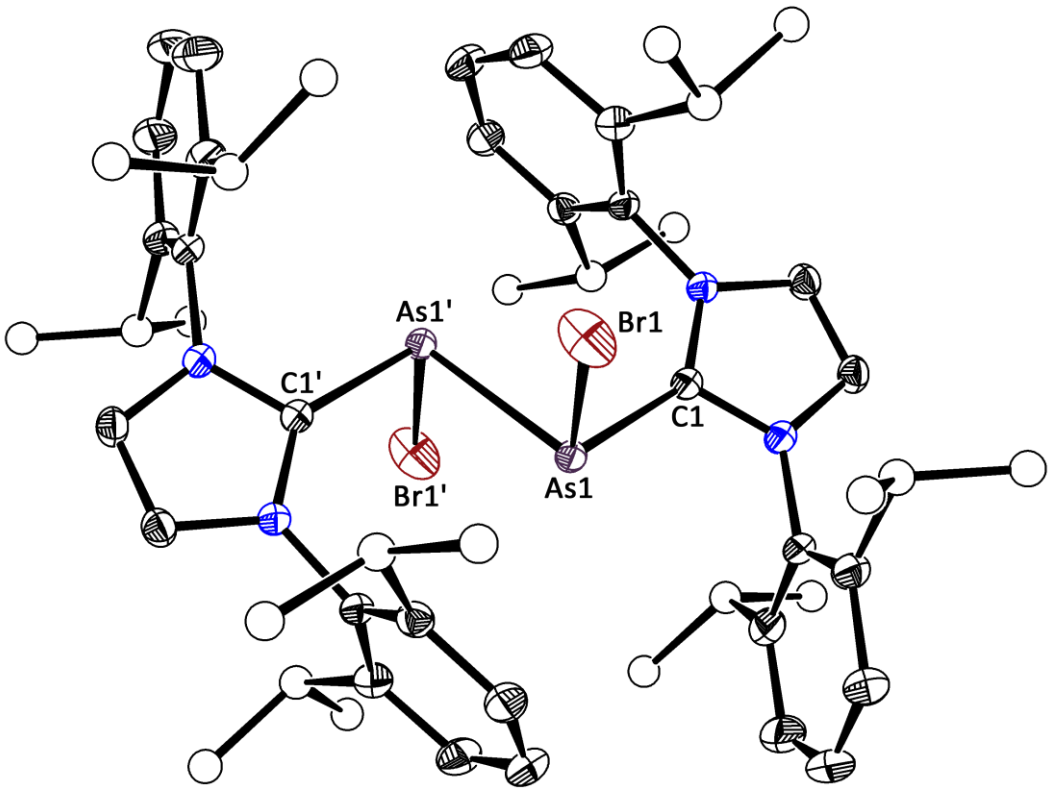

Figure 5.10 Structure of dication **60** in [**60**][B(3,5-{CF_3}$_2$$C_6H_3$)$_4$]$_2$·2DFB. Anisotropic displacement ellipsoids pictured are set at 50% probability. Hydrogen atoms have been omitted for clarity. Atoms of the ^{i}Pr groups are pictured as spheres of arbitrary radii. Symmetry operation: *–x*, 1*–y*, 1*–z*.

The As–As bond length at 2.444(2) Å is notably shorter than that of the precursor, however still in line with that expected for a single bond. Unlike the change in P–Br bond lengths observed on bromide abstraction from **53**, the As–Br bond length at 2.357(2) Å does not change significantly from those observed for the bond distances to the terminal bromide in **59**.

5.4 Conclusions

This chapter has described the facile reduction of (IPr)PBr_3 as a result of the strong σ donating properties of IPr which greatly alters the reduction potential of PBr_3. By heating a THF solution of (IPr)PBr_3, this gives rise to a reduced phosphorus(II) species, $[(IPr)_2P_2Br_3]^+$ (**53**) and represents a unique methodology to access low valent phosphorus compounds via a novel, NHC induced reductive coupling. This chemistry is possible by use of bromide ligands which

typically form weaker bonds to the main group elements than chloride substituents, the latter of which has been commonly employed in main group chemistry. Halide exchange was possible by heating **53** in DCM to afford the previously reported chloride analogue. Halide abstraction of both species was possible by addition of Na[B(3,5-{CF_3}$_2$$C_6H_3$)$_4$] affording the dicationic species **55** and **56** by using DFB as a reaction solvent which favours precipitation of NaBr. When the reaction was carried in THF, solvation of the alkali metal cation was sufficient to preclude NaBr precipitation. **53** was further reduced using other mild reducing agents such as $SnBr_2$ and TDAE to afford $[(IPr)_2P_2Br]^+$ and $[(IPr)_2P_2^{\bullet}]^+$, **57** and **58**, respectively. Finally, synthesis of the equivalent arsenic analogue of **53**, $[(IPr)_2As_2Br_3]^+$, **59**, was possible by reduction of $(IPr)AsBr_3$ with TDAE in DCM in a reasonable yield. An identical bromide abstraction in DFB afforded the arsenic(II) dicationic species, $[(IPr)_2As_2Br_2]^{2+}$ (**60**) via an equivalent mechanism that specifically only gives rise to the 1*R*/2*S* isomer.

5.5 References

(1) Braunschweig, H.; Dewhurst, R. D.; Hammond, K.; Mies, J.; Radacki, K.; Vargas, A. *Science* **2012**, *336* (6087), 1420–1422.

(2) Wang, Y.; Xie, Y.; Wei, P.; King, R. B.; Schaefer III, H. F.; Schleyer, P. v. R.; Robinson, G. H. *Science* **2008**, *321* (5892), 1069–1071.

(3) Sidiropoulos, A.; Jones, C.; Stasch, A.; Klein, S.; Frenking, G. *Angew. Chem. Int. Ed.* **2009**, *48* (51), 9701–9704.

(4) Jones, C.; Sidiropoulos, A.; Holzmann, N.; Frenking, G.; Stasch, A. *Chem. Commun.* **2012**, *48* (79), 9855–9857.

(5) Wang, Y.; Xie, Y.; Wei, P.; King, R. B.; Schaefer III, H. F.; Schleyer, P. v. R.; Robinson, G. H. *J. Am. Chem. Soc.* **2008**, *130* (45), 14970–14971.

(6) Abraham, M. Y.; Wang, Y.; Xie, Y.; Wei, P.; Schaefer III, H. F.; Schleyer, P. v. R.; Robinson, G. H. *Chem. Eur. J.* **2010**, *16* (2), 432–435.

(7) Bonyhady, S. J.; Collis, D.; Frenking, G.; Holzmann, N.; Jones, C.; Stasch, A. *Nat. Chem.* **2010**, *2* (10), 865–869.

(8) Tondreau, A. M.; Benkő, Z.; Harmer, J. R.; Grützmacher, H. *Chem. Sci.* **2014**, *5* (4), 1545–1554.

(9) Bispinghoff, M.; Tondreau, A. M.; Grützmacher, H.; Faradji, C. A.; Pringle, P. G. *Dalton Trans.* **2016**, *45* (14), 5999–6003.

(10) Back, O.; Donnadieu, B.; Parameswaran, P.; Frenking, G.; Bertrand, G. *Nat. Chem.* **2010**, *2* (5), 369–373.

(11) Abraham, M. Y.; Wang, Y.; Xie, Y.; Gilliard, Jr., R. J.; Wei, P.; Vaccaro, B. J.; Johnson, M. K.; Schaefer III, H. F.; Schleyer, P. v. R.; Robinson, G. H. *J. Am. Chem. Soc.* **2013**, *135* (7), 2486–2488.

(12) Wang, Y.; Xie, Y.; Wei, P.; Schaefer III, H. F.; Schleyer, P. v. R.; Robinson, G. H. *J. Am. Chem. Soc.* **2013**, *135* (51), 19139–19142.

(13) Wang, Y.; Chen, M.; Xie, Y.; Wei, P.; Schaefer III, H. F.; Schleyer, P. v. R.; Robinson, G. H. *Nat. Chem.* **2015**, *7* (6), 509–513.

(14) Wang, Y.; Chen, M.; Xie, Y.; Wei, P.; Schaefer, H. F.; Robinson, G. H. *J. Am. Chem. Soc.* **2015**, *137* (26), 8396–8399.

(15) Arz, M. I.; Geiß, D.; Straßmann, M.; Schnakenburg, G.; Filippou, A. C. *Chem. Sci.* **2015**, *6* (11), 6515–6524.

(16) Waters, J. B.; Everitt, T. A.; Myers, W. K.; Goicoechea, J. M. *Chem. Sci.* **2016**, *7* (12), 6981–6987.

(17) Cordero, B.; Gómez, V.; Platero-Prats, A. E.; Revés, M.; Echeverría, J.; Cremades, E.; Barragán, F.; Alvarez, S. *Dalton Trans.* **2008**, 2832–2838.

(18) Henne, F. D.; Schnöckelborg, E.-M.; Feldmann, K.-O.; Grunenberg, J.; Wolf, R.; Weigand, J. J. *Organometallics* **2013**, *32* (22), 6674–6680.

(19) Baechler, R. D.; Mislow, K. *J. Am. Chem. Soc.* **1970**, *92* (10), 3090–3093.

(20) Baechler, R. D.; Mislow, K. *J. Am. Chem. Soc.* **1970**, *92* (15), 4758–4759.

(21) Mislow, K.; Baechler, R. D. *J. Am. Chem. Soc.* **1971**, *93* (3), 773–774.

(22) Mislow, K.; Egan, W. *J. Am. Chem. Soc.* **1971**, *93* (7), 1805–1806.

Chapter 6

Further work and conclusions

6.1 Further work

6.1.1 Halide abstraction from group 14 NHC complexes

The research described in Chapters 4 and 5 focussed on the chemistry of the group 15 elements. Naturally, the equivalent chemistry can be investigated for the IPr adducts of the group 14 dibromides. Bromide abstraction would allow for the synthesis of cationic group 14 complexes supported by a strongly coordinating IPr ligand. Addition of IPr to $SnBr_2$ in THF allows for the isolation of the adduct (IPr)$SnBr_2$ (**61**) in 92% crystalline yield (Figure 6.1) which is structurally similar to (IPr)$GeBr_2$, described in Chapter 3, and the previously reported (IPr)$SnCl_2$.[1]

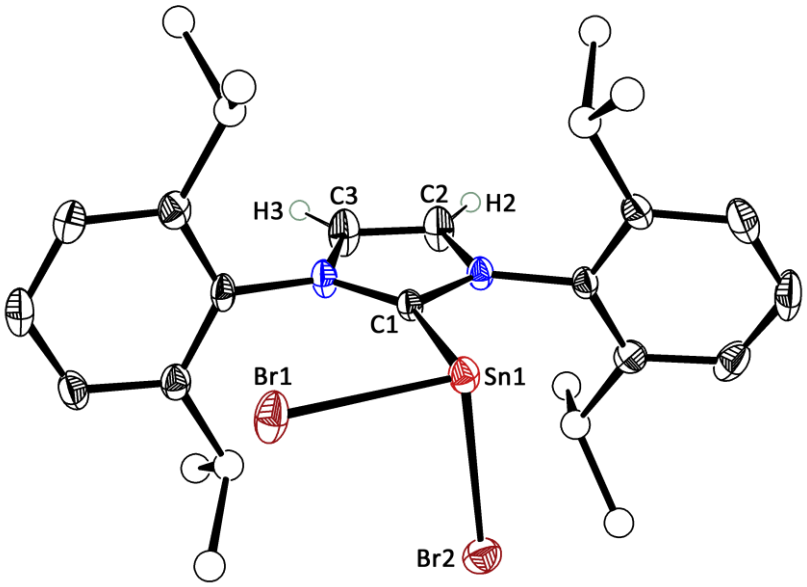

Figure 6.1: Molecular structure of **61**. Anisotropic displacement ellipsoids pictured are set at 50% probability. Hydrogen atoms (with the exception of the imidazole protons labelled H2 and H3) have been omitted for clarity. Atoms of the ^{i}Pr groups, H2 and H3 are pictured as spheres of arbitrary radii.

By increasing the Lewis acidity of the tin centre through bromide abstraction, this will reduce the reduction potential and may allow for the facile reduction and synthesis of low coordinate, low valent tin complexes. Preliminary work has demonstrated the potential for bromide

abstraction using half an equivalent of $AlBr_3$ yielding $[(IPr)_2Sn_2Br_2(\mu\text{-}Br)][AlBr_4]$ as determined by single crystal X-ray diffraction. $[(IPr)_2Sn_2Br_2(\mu\text{-}Br)]^+$ consists of what can be described as two cationic stannylene bromide moieties which are bridged by a bromide anion.

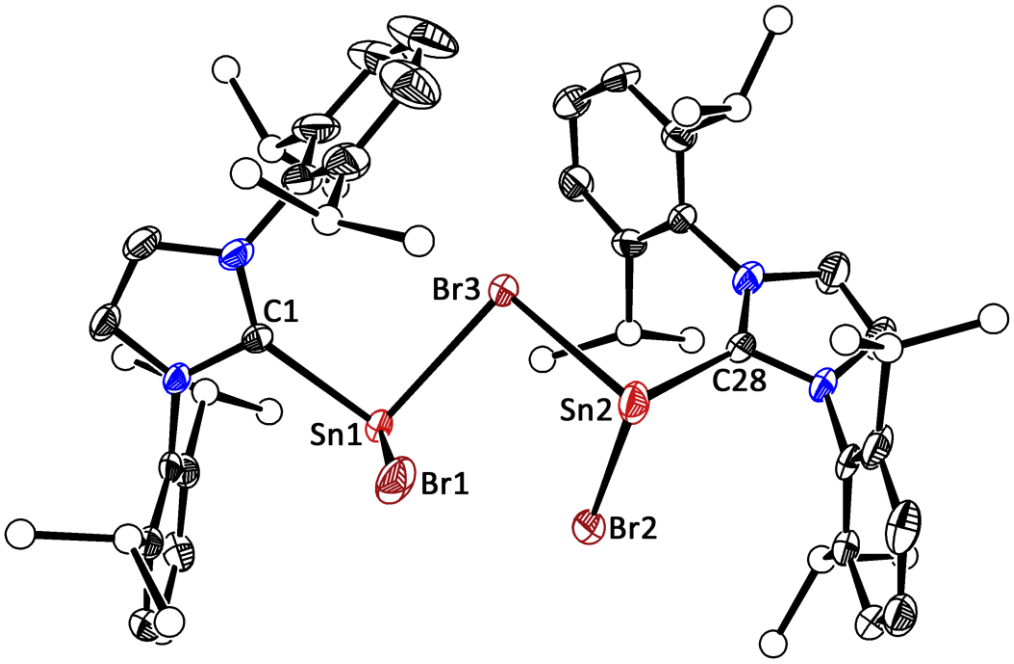

Figure 6.2: Structure of cation $[(IPr)_2Sn_2Br_2(\mu\text{-}Br)]^+$. Anisotropic displacement ellipsoids pictured are set at 50% probability. Hydrogen atoms have been omitted for clarity. Atoms of the ^{i}Pr groups are pictured as spheres of arbitrary radii.

The weaker interaction to the bridging bromide is indicated by the longer Sn–Br bond lengths. Br3 is equidistant from the two tin centres (2.772(1) and 2.723(1) Å). The terminal Sn–Br bond distances (2.577(1) and 2.581(1) Å) remain similar to those observed in the precursor, **61**.

6.1.2 Halide abstraction and redox chemistry of group 13 NHC complexes

Finally, the chemistry described in this thesis has been limited to IPr, aIPr and aIPr: complexes of group 12, 14 and 15 elements. Logically, an extension of the work described would be to investigate the chemistry of IPr complexes of the group 13 elements under similar reaction conditions. Complexes of the group 13 elements are typically Lewis acidic and by using IPr

as a neutral ligand, the synthesis of cationic group 13 halide species stabilised by NHC coordination allows for the synthesis of species with increased Lewis acidity. The possibility of reactions of such species with nucleophilic reagents may provide a method for heteronuclear bond forming processes and the synthesis of low coordinate, low valent main group species supported by NHC ligands. The addition of $AlBr_3$ to the previously reported $(IPr)BBr_3$,[2] affords the cationic species $[(IPr)BBr_2]^+$ (**62**) which consists of a three-coordinate, trigonal planar, Lewis acidic boron centre (Figure 6.3). Similar cationic dichloroborenium species have previously been described by Vidović and co-workers.[3]

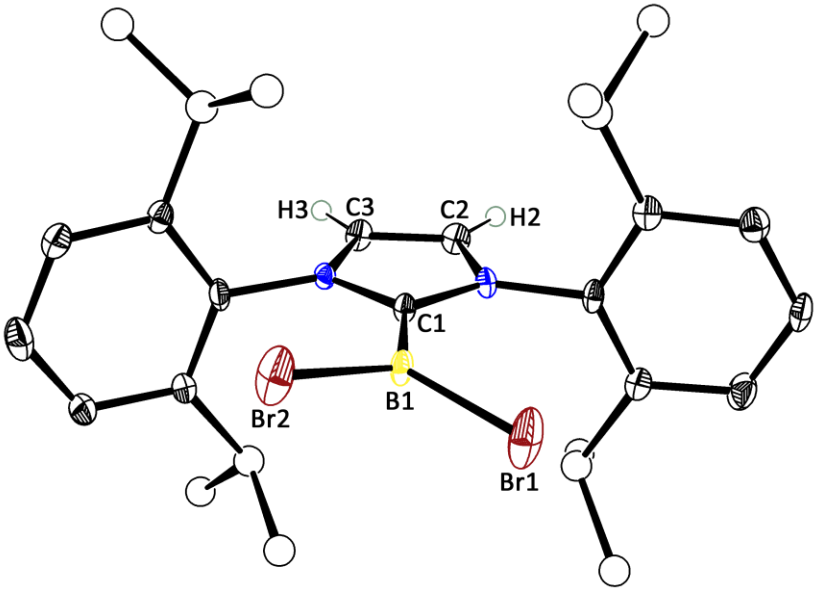

Figure 6.3: Structure of cation **62** in [**62**][$AlBr_4$]. Anisotropic displacement ellipsoids pictured are set at 50% probability. Hydrogen atoms have been omitted for clarity. Atoms of the ^{i}Pr groups are pictured as spheres of arbitrary radii.

Finally, the gallium(II) species $(IPr)_2Ga_2Br_4$ (**63**, Figure 6.4) was synthesised by addition of IPr to a THF solution of $(THF)_2Ga_2Br_4$ (which was formed by the dissolution of $Ga[GaBr_4]$ in THF).[4,5] Similarly, with the use of bromide ligands, subsequent reduction chemistry may be much easier due to the reduced reduction potential, allowing for the use of mild reducing agents and higher yields of products.

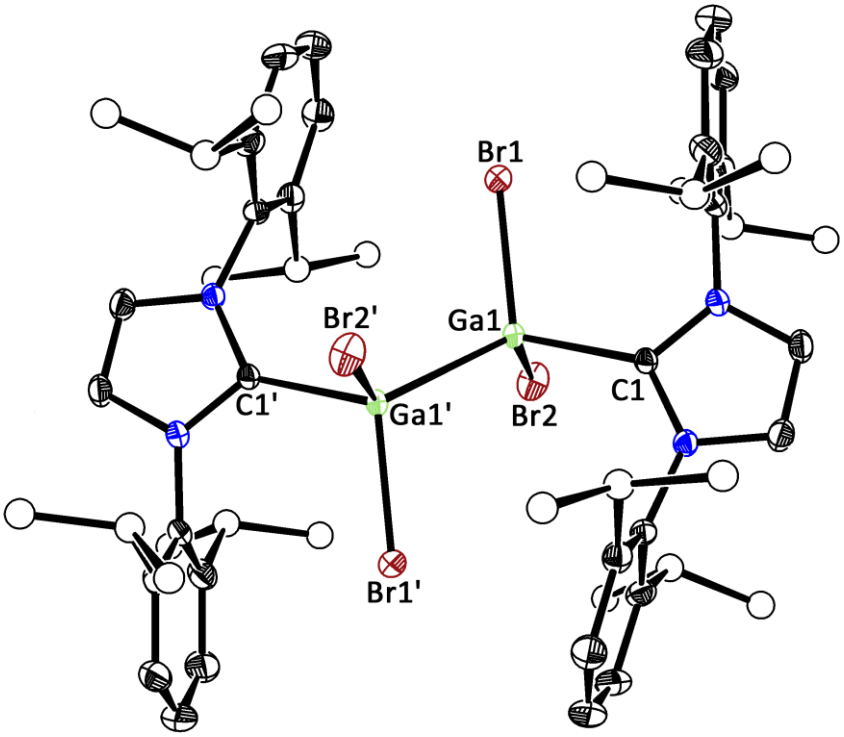

Figure 6.4: Molecular structure of **63**. Anisotropic displacement ellipsoids pictured are set at 50% probability. Hydrogen atoms have been omitted for clarity. Atoms of the ^{i}Pr groups are pictured as spheres of arbitrary radii.

6.2 Conclusions

This thesis has described the reactivity and coordination chemistry of N-heterocyclic carbene complexes of the main group elements, spanning normal and abnormal coordination modes of IPr and the synthesis of complexes bearing ditopic carbanionic ligands (aIPr:).[6] The utility of both the potassium and lithium salts of deprotonated IPr ([Li(aIPr:)]$_\infty$ and [K(aIPr:)]$_\infty$) as reagents for the synthesis of novel group 12 and group 14 species bearing aIPr: ligands has been reported.[7] [K(aIPr:)]$_\infty$ could reliably be used as a reagent in reactions with group 12 and 14 bis(trimethylsilyl)amides and tetrahalides and the chemistry of such species by making use of the unquenched carbene functionality was subsequently investigated. The use of [Li(aIPr:)]$_\infty$ in reactions with tin and lead bis(trimethylsilyl)amides gave rise to the formation

of novel distannane and plumbylene complexes which results from the deprotonation of the coordinated amide.

A reversible carboxylation process was found to take place upon addition of carbon dioxide to the bis(aIPr:) species, $(aIPr:)_2EX_2$ (E = Si, Ge; X = Cl, Br) as a result of the electron withdrawing main group moiety on the backbone of the imidazole ring which inductively withdraws electron density from the carbene thereby reducing the nucleophilicity relative to that of free IPr.

Subsequently, the isomerisation of IPr adducts with group 14 and group 15 bromides was investigated and it was discovered that such abnormally bonded complexes could be synthesised in high yields upon heating THF solutions of the adducts, or upon addition of multiple equivalents of IPr. The additional equivalents facilitate the isomerisation of the ligand by deprotonation of the complex ligand backbone. The possibility of precipitation as the imidazolium bromide or liberation of the proton gave rise to varying products. These reaction outcomes are strongly dependent of the lattice enthalpies of the resulting products and the respective bond enthalpies involved giving rise to thermodynamic control.

Finally, the discovery that heating a THF solution of $(IPr)PBr_3$ gave rise to the reductive coupling of two phosphorus centres allowed for the high yielding synthesis of a number of low coordinate, low valent phosphorus species with the use of very mild reducing agents.[8] This route provides insight into the possibility of alternative methodologies with regards to the synthesis and isolation of novel main group complexes in a variety of oxidation states via a logical and efficient synthetic methodology. Future work will involve extending these results for the design of logical synthetic routes that should give us access to heteroatomic, low coordinate, low valent main group species supported by NHC ligands.

6.3 References

(1) Thimer, K. C.; Al-Rafia, S. M. I.; Ferguson, M. J.; McDonald, R.; Rivard, E. *Chem. Commun.* **2009**, 7119–7121.

(2) Wang, Y.; Quillian, B.; Wei, P.; Wannere, C. S.; Xie, Y.; King, R. B.; Schaefer III, H. F.; Schleyer, P. v. R.; Robinson, G. H. *J. Am. Chem. Soc.* **2007**, *129* (41), 12412–12413.

(3) Muthaiah, S.; Do, D. C. H.; Ganguly, R.; Vidović, D. *Organometallics* **2013**, *32* (22), 6718–6724.

(4) Beamish, J. C.; Boardman, A.; Small, R. W. H.; Worrall, I. J. *Polyhedron* **1985**, *4* (6), 983–987.

(5) Schmidbaur, H.; Nowak, R.; Bublak, W.; Burkert, P.; Huber, B.; Müller, G. *Z. Naturforsch. B* **2014**, *42* (5), 553–556.

(6) Waters, J. B.; Goicoechea, J. M. *Coord. Chem. Rev.* **2015**, *293–294*, 80–94.

(7) Waters, J. B.; Goicoechea, J. M. *Dalton Trans.* **2014**, *43* (38), 14239–14248.

(8) Waters, J. B.; Everitt, T. A.; Myers, W. K.; Goicoechea, J. M. *Chem. Sci.* **2016**, *7* (12), 6981–6987.

Chapter 7

Experimental

7.1 General synthetic methods

All reactions and product manipulations were carried out under an inert atmosphere of argon or dinitrogen using standard Schlenk-line or glovebox techniques (MBraun UNIlab or MBraun LABmaster 130 glovebox maintained at < 0.1 ppm H_2O and < 0.1 ppm O_2).

Diethyl ether (Et_2O; puriss. p.a., ACS reagent grade, ≥99.8%, Sigma-Aldrich) and tetrahydrofuran (THF; HPLC grade, ≥99.9%, Sigma-Aldrich) were distilled from a sodium or potassium/benzophenone mixture respectively. 1,2-Difluorobenzene (DFB; 98%, Fluorochem) and fluorobenzene (C_6H_5F; 99%, Alfa Aesar) were distilled from CaH_2. Dichloromethane (DCM; HPLC grade, ≥99.8%, Sigma-Aldrich), *N*,*N*-dimethylformamide (DMF; glass distilled grade, >99.8%, Rathburn), hexane (HPLC grade, >97%, Sigma-Aldrich), toluene (HPLC grade, 99.9%, Sigma-Aldrich) were purified using an MBraun SPS-800 solvent system. C_6D_6 (99.6%, Sigma-Aldrich), CD_2Cl_2 (99.9%, Fluorochem), d_8-THF (99.5%, Fluorochem) and d_8-toluene (99.6%, Sigma-Aldrich) were dried over CaH_2, vacuum distilled and degassed before use. All dry solvents were stored under argon in gas-tight ampoules over activated 3 Å molecular sieves. Deionised water was obtained from a Millipore Milli-Q machine.

The suppliers and purification procedures for the commercially purchased chemicals are detailed in Table 7.1.

Table 7.1: Supplier and purification procedures for commercially purchased chemicals.

Reagent	Supplier	Purity	Purification
$AlCl_3$	Alfa Aesar	99.985%	Used as received
$AlBr_3$	Alfa Aesar	98%	Used as received
$AsBr_3$	Sigma-Aldrich	99%	Used as received

Bi chunks	Harrington Brothers Ltd.	Unspecified	Used as received
^{n}BuLi in hexanes	Acros Organics	2.5 M	Used as received
CO_2	BOC	Unspecified	Used as received
18-Crown-6	Alfa Aesar	99%	Dried under vacuum with heating
2,2,2-Crypt	VWR	99%	Dried under vacuum
Ga metal	Strem	99.99%	Used as received
Ge chunks	Strategic Metal Investments Ltd.	99.999%	Used as received
$GeCl_2$·dioxane	Sigma-Aldrich	Unspecified	Used as received
$GeCl_4$	Strem	99.99%	Used as received
Graphite powder, crystalline, -325 mesh	Alfa Aesar	99%	Dried under vacuum with heating
HCl in Et_2O	Alfa Aesar	2 M	Used as received
$HgBr_2$	Acros Organics	99+%	Used as received
$HgCl_2$	BDH Ltd.	99.5%	Used as received
K chunks	Strem	99.95%	Used as received
KHMDS	Sigma-Aldrich	95%	Used as received
KO^{t}Bu	Aldrich	≥98%	Used as received
LiHMDS	Aldrich	97%	Used as received
MeLi in Et_2O	Acros Organics	1.6 M	Used as received
Mg turnings	Merck	99%	Washed with dilute nitric acid and distilled water followed by Et_2O and dried thoroughly under vacuum
Na sticks	Acros Organics	99.8%	Washed with hexane and dried under vacuum
$NaBF_4$	Alfa Aesar	97%	Dried under vacuum
$PbCl_2$	Alfa Aesar	99%	Used as received
PBr_3	Aldrich	97%	Used as received
$SiBr_4$	Alfa Aesar	Unspecified	Used as received
$SiCl_4$	Aldrich	99%	Used as received

Sb shot	Aldrich	99.999%	Used as received
Sn sticks	Berkshire ores and chemicals Ltd.	Unspecified	Used as received
$SnBr_2$	Aldrich	Unspecified	Recrystallised from THF and dried thoroughly under vacuum
$SnCl_2$	Acros Organics	98%	Used as received
$SnCl_4$	Aldrich	99%	Used as received
TDAE	Fluorochem	95%	Used as received
Triflic acid	Alfa Aesar	98+%	Degassed

[IPrH]Cl[1] and [:C(N(2,6-$^{i}Pr_2C_6H_3)_2$)(CH)CLi]$_n$ ([Li(aIPr:)]$_\infty$)[2] were prepared according to literature procedures. IPr was synthesised by a modification of literature procedures.[3,4] To a suspension of [IPrH]Cl in Et_2O was added one equivalent of ^{n}BuLi (2.5 M in hexanes) slowly with stirring at ambient temperature and allowed to stir overnight. The solution was then filtered and stored at –80 °C to afford IPr as a crystalline material which was isolated by filtration and dried thoroughly under vacuum.

KC_8 was prepared by stirring potassium with eight equivalents of graphite at temperatures greater than 200 °C under argon by using a heat gun to afford a uniform bronze solid.

$Zn[N(SiMe_3)_2]_2$, $Ge[N(SiMe_3)_2]_2$, $Sn[N(SiMe_3)_2]_2$ and $Pb[N(SiMe_3)_2]_2$ were prepared according to literature procedures.[5,6]

$Na[B(3,5\text{-}\{CF_3\}_2C_6H_3)_4]$ and $[H(OEt_2)_2][B(3,5\text{-}\{CF_3\}_2C_6H_3)_4]$ were prepared according to a literature procedure.[7] Additionally, $Na[B(3,5\text{-}\{CF_3\}_2C_6H_3)_4]$ was recrystallised from a mixture of DCM and Et_2O at –35 °C and $[H(OEt_2)_2][B(3,5\text{-}\{CF_3\}_2C_6H_3)_4]$ was stored at –25 °C in an inert atmosphere glovebox.

$GeBr_4$ was prepared by refluxing germanium powder in an ampoule in bromine for two weeks. Bromine was removed in vacuo and $GeBr_4$ was redissolved in hexane and filtered from the

remaining germanium. Removal of hexane in vacuo and vacuum distillation of the low melting point solid afforded pure colourless $GeBr_4$. $BiBr_3$ was prepared by an equivalent method after heating bismuth chunks in bromine for five hours to afford a high melting point, yellow crystalline solid.

$SnBr_4$ and $SbBr_4$ were prepared by refluxing a bromine in carbon tetrachloride with an excess of the respective metal until no bromine colour remained. After filtration of the warm reaction mixture, colourless crystals of the products form on cooling which were then isolated by filtration and dried carefully under vacuum.

'$GaBr_2$' was prepared by heating gallium metal with a stoichiometric amount of $HgBr_2$ under argon in an ampoule with a heat gun to afford mercury metal and a high melting point solid. '$GaBr_2$' was extracted with toluene and the solvent removed in vacuo to afford a colourless crystalline solid.

$SnCl_4(THF)_2$ was prepared by dropwise addition of $SnCl_4$ to THF while stirring at ambient temperature to afford a colourless crystalline precipitate which was isolated by filtration and dried thoroughly under vacuum.

7.2 Syntheses of compounds

7.2.1 Chapter 2 – Synthesis of aIPr: complexes of group 12 and 14 bis(trimethylsilyl)amides

7.2.1.1 $[:C(N(2,6\text{-}^{i}Pr_2C_6H_3))_2(CH)CK]_n$ ($[K(aIPr:)]_\infty$) (1)

To a mixture of $[Li(aIPr:)]_\infty$ (2.873 g, 7.29 mmol) and KO^tBu (0.818 g, 7.29 mmol) cooled to −78 °C was added diethyl ether (50 mL) slowly under argon on a Schlenk line. The solution was stirred for 30 minutes before being warmed to room temperature and stirred for a further 60 minutes resulting in an orange solution. The solution was filtered and concentrated to

5 mL, to which THF (40 mL) and hexane (40 mL) was added while stirring to give a white precipitate and an orange solution (containing LiO^tBu). The mixture was cooled to −78 °C and filtered to yield a fine off-white powder. The solid was then washed with a further 20 mL of THF followed by 40 mL of hexane. The fine white powder was dried thoroughly under vacuum for 3 hours (1.740 g, 56% yield). Anal. Calcd for $KC_{27}H_{35}N_2$ (426.68): C 76.01%, H 8.27%, N 6.56%. Found: C 74.15%, H 8.17%, N 6.30%. The product was crystallised by slow diffusion of hexane into a saturated THF solution to yield $[:C(N(2,6\text{-}^iPr_2C_6H_3)_2)_2(CH)CK(THF)_2]_n$ as colourless crystals which were dried under an argon flow for one hour after decantation of the solvent. Anal. Calcd for $KC_{35}H_{51}N_2O_2$ (570.89): C 73.64%, H 9.00%, N 4.91%. Found: C 72.94%, H 8.46%, N 5.48%. ESI-MS, negative-ion mode (THF, 150 °C, 2.4 kV): *m/z* 389.0 (100%) $[:C(N(2,6\text{-}^iPr_2C_6H_3))_2(CH)C:]^-$, 815.1 (10%) $[(:C(N(2,6\text{-}^iPr_2C_6H_3))_2(CH)C:)_2K]^-$. ^{1}H NMR (500.30 MHz, d_8-THF): δ (ppm) 7.13 (m, 1H; *para*-Dipp), 7.09 (m, 2H; *meta*-Dipp), 7.05 (s, 3H; *meta*-Dipp and *para*-Dipp), 6.07 (s, 1H; NCC*H*N), 3.28 (sept, $^3J_{H–H}$ = 7 Hz, 2H; $C_6H_3\{CH(CH_3)_2\}_2$), 3.04 (sept, $^3J_{H–H}$ = 7 Hz, 2H; $C_6H_3\{CH(CH_3)_2\}_2$), 1.12 (d, $^3J_{H–H}$ = 7 Hz, 6H; $C_6H_3\{CH(CH_3)_2\}_2$), 1.10 (d, $^3J_{H–H}$ = 7 Hz, 6H; $C_6H_3\{CH(CH_3)_2\}_2$), 1.08 (d, $^3J_{H–H}$ = 7 Hz, 12H; $C_6H_3\{CH(CH_3)_2\}_2$). $^{13}C\{^1H\}$ NMR (125.80 MHz, d_8-THF): δ (ppm) 215.1 (CN_2), 176.3 (NCCHN), 149.5 (*ipso*-Dipp), 147.2, 146.8 (*ortho*-Dipp), 143.8 (*ipso*-Dipp), 126.8 (NCCHN), 126.5, 125.7 (*para*-Dipp), 123.0, 122.7 (*meta*-Dipp), 28.7 28.6 ($C_6H_3\{CH(CH_3)_2\}_2$), 25.5 ($C_6H_3\{CH(CH_3)_2\}_2$), 25.4, 24.5, 24.0 ($C_6H_3\{CH(CH_3)_2\}_2$). No resonance observed in ^{7}Li NMR spectrum.

7.2.1.2 [K(2,2,2-crypt)][2] (2: $[(aIPr:)Zn\{N(SiMe_3)_2\}_2]^-$)

To a suspension of $[K(aIPr:)]_\infty$ (21 mg, 0.049 mmol) in d_8-THF (500 µL) was added $Zn[N(SiMe_3)_2]_2$ (20 µL, 0.049 mmol) via microsyringe and the mixture stirred until a clear

solution remained. 2,2,2-crypt (19 mg, 0.049 mmol) was added to the solution and stirred until the solid dissolved. The solution was then transferred to an NMR tube and characterised. Slow diffusion of hexane into a saturated solution of the reaction product afforded colourless crystals of [K(2,2,2-crypt)][(aIPr:)Zn{N(SiMe$_3$)$_2$}$_2$]·THF suitable for single crystal X-ray diffraction (44 mg, 76% crystalline yield). Anal. Calcd for $C_{57}H_{107}KN_6O_6Si_4Zn$ (1189.35): C 57.59%, H 9.07%, N 7.07%. Found: C 57.60%, 8.55%, N 6.70%. ESI-MS, negative-ion mode (THF, 150 °C, 2.4 kV): *m/z* 773.9 (100%) [(aIPr:)Zn{N(SiMe$_3$)$_2$}$_2$]$^-$, 544.6 (85%) [Zn{N(SiMe$_3$)$_2$}$_3$]$^-$. ^{1}H NMR (500.30 MHz, d_8-THF): δ (ppm) 7.21 (m, 1H; *para*-Dipp), 7.13 (m, 2H; *meta*-Dipp), 7.11 (s, 3H; *meta*-Dipp and *para*-Dipp), 6.92 (s, 1H; NCC*H*N), 3.54 (s, 12H; 2,2,2-crypt), 3.50 (t, $^3J_{H–H}$ = 5 Hz, 12H; 2,2,2-crypt), 3.23 (sept, $^3J_{H–H}$ = 7 Hz, 2H; C$_6$H$_3${C*H*(CH$_3$)$_2$}$_2$), 3.03 (sept, $^3J_{H–H}$ = 7 Hz, 2H; C$_6$H$_3${C*H*(CH$_3$)$_2$}$_2$), 2.51 (t, $^3J_{H–H}$ = 5 Hz, 12H; 2,2,2-crypt), 1.28 (d, $^3J_{H–H}$ = 7 Hz, 6H; C$_6$H$_3${CH(C*H*$_3$)$_2$}$_2$), 1.16 (d, $^3J_{H–H}$ = 7 Hz, 6H; C$_6$H$_3${CH(C*H*$_3$)$_2$}$_2$), 1.10 (d, $^3J_{H–H}$ = 7 Hz, 12H; C$_6$H$_3${CH(C*H*$_3$)$_2$}$_2$), −0.08 (s, satellites $^2J_{H–^{29}Si}$ = 6 Hz, 36H; N(Si(C*H*$_3$)$_3$)$_2$). ^{13}C{^{1}H} NMR (125.82 MHz, d_8-THF): δ (ppm) 219.9 (*C*N$_2$), 152.6 (N*C*CHN), 147.5, 146.6 (*ortho*-Dipp), 145.4 (NC*C*HN), 142.0, 133.2 (*ipso*-Dipp), 127.8, 126.9 (*para*-Dipp), 123.4, 123.3 (*meta*-Dipp), 71.5, 68.6, 54.9 (2,2,2-crypt), 29.1, 28.7 (C$_6$H$_3${*C*H(CH$_3$)$_2$}$_2$), 27.1, 25.2, 24.7, 23.5 (C$_6$H$_3${CH(*C*H$_3$)$_2$}$_2$), 7.1 (N(Si(*C*H$_3$)$_3$)$_2$). ^{29}Si{^{1}H} NMR (99.31 MHz, d_8-THF): δ (ppm) −9.7 (s).

7.2.1.3 [K(18-crown-6)(THF)$_2$][3] (3: [(aIPr:)Sn{N(SiMe$_3$)$_2$}$_2$]$^-$)

To a suspension of [K(aIPr:)]$_\infty$ (65 mg, 0.152 mmol) in THF (5 mL) was added Sn[N(SiMe$_3$)$_2$]$_2$ (67 mg, 0.152 mmol) and the mixture stirred until a clear solution remained. 18-Crown-6 (40 mg, 0.152 mmol) was added to the solution and stirred until the solid dissolved. The solution was then filtered and layered with hexane to afford colourless crystals of [K(18-crown-6)(THF)$_2$][(aIPr:)Sn{N(SiMe$_3$)$_2$}$_2$]·$^1/_2$THF suitable for single crystal X-ray

diffraction (165 mg, 96% crystalline yield). Anal. Calcd for $C_{59}H_{111}KN_4O_8Si_2Sn$ (1218.52): C 58.17%, H 9.18%, N 4.60%. Found C 56.25%, H 8.74%, N 4.34%. ESI-MS, negative-ion mode (THF, 150 °C, 2.4 kV): *m/z* 826.2 (100%) $[(aIPr:)Sn\{N(SiMe_3)_2\}_2]^-$. ^{1}H NMR (500.30 MHz, d_8-THF): δ (ppm) 7.21 (m, 1H; *para*-Dipp), 7.14 (m, 3H; *meta*-Dipp and *para*-Dipp), 7.10 (m, 2H; *meta*-Dipp), 7.01 (s, 1H; NCC*H*N), 3.58 (s, 24H; 18-crown-6), 3.26 (sept, $^3J_{H–H}$ = 7 Hz, 2H; $C_6H_3\{CH(CH_3)_2\}_2$), 3.06 (sept, $^3J_{H–H}$ = 7 Hz, 2H; $C_6H_3\{CH(CH_3)_2\}_2$), 1.30 (d, $^3J_{H–H}$ = 7 Hz, 6H; $C_6H_3\{CH(CH_3)_2\}_2$), 1.17 (d, $^3J_{H–H}$ = 7 Hz, 6H; $C_6H_3\{CH(CH_3)_2\}_2$), 1.10 (d, $^3J_{H–H}$ = 7 Hz, 6H; $C_6H_3\{CH(CH_3)_2\}_2$), 1.09 (d, $^3J_{H–H}$ = 7 Hz, 6H; $C_6H_3\{CH(CH_3)_2\}_2$), 0.04 (s, satellites $^2J_{H–^{29}Si}$ = 6 Hz, 36H; $N(Si(CH_3)_3)_2$). $^{13}C\{^1H\}$ NMR (125.80 MHz, d_8-THF): δ (ppm) 218.7 (CN_2), 163.2 (NCCHN), 147.5, 147.1 (*ortho*-Dipp), 143.7, 141.7 (*ipso*-Dipp), 130.4, 127.8 (*para*-Dipp), 127.3 (NCCHN), 123.4, 123.2 (*meta*-Dipp), 71.3 (18-crown-6), 29.5, 28.6 ($C_6H_3\{CH(CH_3)_2\}_2$), 27.3, 25.5, 24.8, 23.3 ($C_6H_3\{CH(CH_3)_2\}_2$), 7.6 ($N(Si(CH_3)_3)_2$; satellites $^3J_{^{13}C–^{117/119}Sn}$ = 24 Hz, $^1J_{^{13}C–^{29}Si}$ = 53 Hz). $^{29}Si\{^1H\}$ NMR (99.32 MHz, d_8-THF): δ (ppm) –6.1 (s). $^{119}Sn\{^1H\}$ NMR (186.43 MHz, d_8-THF): δ (ppm) 10.9 (s).

7.2.1.4 [K(18-crown-6)(THF)$_2$][4] (4: [(aIPr:)Ge{N(SiMe$_3$)$_2$}$_2$]$^-$)

To a suspension of $[K(aIPr:)]_\infty$ (37 mg, 0.086 mmol) in d_8-THF (500 µL) was added $Ge[N(SiMe_3)_2]_2$ (34 mg, 0.086 mmol) and the mixture stirred until a clear solution remained. 18-Crown-6 (23 mg, 0.084 mmol) was added to the solution and stirred until the solid dissolved. The solution was then transferred to an NMR tube and characterised. The ^{1}H NMR spectrum of the crude reaction mixture collected immediately after the dissolution of the reagents is consistent with the formation of $[K(18\text{-crown-6})(THF)_2][(aIPr:)Ge\{N(SiMe_3)_2\}_2]$, however over time these resonances decrease in intensity and new resonances appear in the spectrum. Filtration of the reaction mixture afforded a colourless solution. Slow diffusion of hexane into this solution afforded colourless crystals which were identified as

[K(18-crown-6)(THF)$_2$]$_2$[(aIPr:)Ge{N(SiMe$_3$)$_2$}$_2$][(aIPr:)$_2$Ge{N(SiMe$_3$)$_2$}]·THF by single crystal X-ray diffraction. ESI-MS, negative-ion mode (THF, 150 °C, 2.4 kV): *m/z* 544.3 (100%) [(aIPr:)Ge{N(SiMe$_3$)}]$^-$ and [Ge{N(SiMe$_3$)$_2$}$_3$]$^-$, 771.6 (40%) [(aIPr:)Ge{N(SiMe$_3$)$_2$}$_2$]$^-$, 1008.9 (15%) [(aIPr:)$_2$Ge{N(SiMe$_3$)$_2$}$_2$]$^-$. ^{1}H NMR (500.30 MHz, d_8-THF): δ (ppm) 7.20 (t, $^3J_{H–H}$ = 8 Hz, 1H; *para*-Dipp), 7.14 (d,, $^3J_{H–H}$ = 8 Hz, 2H; *meta*-Dipp), 7.11 (m, 3H; *meta*-Dipp and *para*-Dipp), 6.83 (s, 1H; NCC*H*N), 3.53 (s, 24H; 18-crown-6), 3.48 (sept, $^3J_{H–H}$ = 7 Hz, 2H; C$_6$H$_3${C*H*(CH$_3$)$_2$}$_2$), 3.08 (sept, $^3J_{H–H}$ = 7 Hz, 2H; C$_6$H$_3${C*H*(CH$_3$)$_2$}$_2$), 1.32 (d, $^3J_{H–H}$ = 7 Hz, 6H; C$_6$H$_3${CH(C*H*$_3$)$_2$}$_2$), 1.16 (d, $^3J_{H–H}$ = 7 Hz, 6H; C$_6$H$_3${CH(C*H*$_3$)$_2$}$_2$), 1.12 (d, $^3J_{H–H}$ = 7 Hz, 6H; C$_6$H$_3${CH(C*H*$_3$)$_2$}$_2$), 1.06 (d, $^3J_{H–H}$ = 7 Hz, 6H; C$_6$H$_3${CH(C*H*$_3$)$_2$}$_2$), 0.03 (s, satellites $^2J_{H–^{29}Si}$ = 6 Hz, 36H; N(Si(C*H*$_3$)$_3$)$_2$). ^{13}C{^{1}H} NMR (125.80 MHz, d_8-THF): δ (ppm) 219.7 (*C*N$_2$), 157.1 (N*C*CHN), 147.5, 147.1 (*ortho*-Dipp), 142.9, 142.0 (*ipso*-Dipp), 128.3, 127.8 (*para*-Dipp), 127.0 (NC*C*HN), 123.3, 123.2 (*meta*-Dipp), 71.2 (18-crown-6), 29.9, 28.7 (C$_6$H$_3${*C*H(CH$_3$)$_2$}$_2$), 27.8, 25.5, 24.6, 22.8 (C$_6$H$_3${CH(*C*H$_3$)$_2$}$_2$), 7.5 (N(Si(*C*H$_3$)$_3$)$_2$). ^{29}Si{^{1}H} NMR (99.32 MHz, d_8-THF): δ (ppm) −5.6 (s).

7.2.1.5 [K(18-crown-6)(THF)$_2$][5] (5: [(aIPr:)Pb{N(SiMe$_3$)$_2$}$_2$]$^-$)

To a suspension of [K(aIPr:)]$_\infty$ (25 mg, 0.059 mmol) in d_8-THF (500 µL) was added Pb[N(SiMe$_3$)$_2$]$_2$ (31 mg, 0.059 mmol) and the mixture stirred until a clear solution remained. 18-Crown-6 (16 mg, 0.059 mmol) was added to the solution and stirred until the solid dissolved. The solution was then transferred to an NMR tube and characterised by multielement NMR spectroscopy. ^{1}H NMR (500.30 MHz, d_8-THF): δ (ppm) 7.05–7.22 (m, 6H; *meta*-Dipp and *para*-Dipp), 7.00 (s, 1H; NCC*H*N), 3.55 (s, 24H; 18-crown-6), 3.19 (sept, $^3J_{H–H}$ = 7 Hz, 2H; C$_6$H$_3${C*H*(CH$_3$)$_2$}$_2$), 3.06 (sept, $^3J_{H–H}$ = 7 Hz, 2H; C$_6$H$_3${C*H*(CH$_3$)$_2$}$_2$), 1.29 (d, $^3J_{H–H}$ = 7 Hz, 6H; C$_6$H$_3${CH(C*H*$_3$)$_2$}$_2$), 1.16 (d, $^3J_{H–H}$ = 7 Hz, 6H; C$_6$H$_3${CH(C*H*$_3$)$_2$}$_2$), 1.10

(d, $^{3}J_{H–H}$ = 7 Hz, 12H; $C_6H_3\{CH(CH_3)_2\}_2$), 0.12 (s, satellites $^{2}J_{H–^{29}Si}$ = 7 Hz, 36H; $N(Si(CH_3)_3)_2$). $^{13}C\{^{1}H\}$ NMR (125.80 MHz, d_8-THF): δ (ppm) 216.1 (CN_2), 147.6, 147.2 (*ortho*-Dipp), 143.4 (N*C*CHN), 135.4 (NC*C*HN), 127.9, 127.6 (*para*-Dipp), 123.4, 123.3 (*meta*-Dipp), 71.3 (18-crown-6), 29.1, 28.6 ($C_6H_3\{CH(CH_3)\}_2$), 26.9, 25.6, 24.8, 24.1 ($C_6H_3\{CH(CH_3)_2\}_2$), 7.8 ($N(Si(CH_3)_3)_2$). $^{29}Si\{^{1}H\}$ NMR (99.32 MHz, d_8-THF): δ (ppm) –9.7 (s).

7.2.1.6 [K(18-crown-6)(THF)$_2$][6] (6: [(aIPr:)$_2$Ge{N(SiMe$_3$)$_2$}]$^-$)

To a suspension of $[K(aIPr:)]_\infty$ (93 mg, 0.219 mmol) in THF (5 mL) was added $Ge[N(SiMe_3)_2]_2$ (43 mg, 0.109 mmol) and the mixture stirred until a clear solution remained. 18-Crown-6 (58 mg, 0.219 mmol) was added to the solution and stirred until the solid dissolved. The solution was then filtered and layered with hexane to afford colourless crystals of $[K(18\text{-crown-6})(THF)_2][(aIPr:)_2Ge\{N(SiMe_3)_2\}]\cdot THF$ suitable for single crystal X-ray diffraction (125 mg, 77% crystalline yield). Anal. Calcd for $C_{72}H_{112}GeKN_5O_6Si_2$ (1311.60): C 65.93%, H 8.61%, N 5.34%. Found: C 63.11%, H 8.26%, N 5.02%. ESI-MS, negative-ion mode (THF, 150 °C, 2.4 kV): m/z 1002.0 (100%) $[(aIPr:)_2Ge\{N(SiMe_3)_2\}]^-$. ^{1}H NMR (500.30 MHz, d_8-THF): δ (ppm) 7.19 (t, $^{3}J_{H–H}$ = 8 Hz, 2H; *para*-Dipp), 7.01–7.12 (m, 10H; *meta*-Dipp and *para*-Dipp), 6.93 (s, 2H; NCC*H*N), 3.48 (s, 24H; 18-crown-6), 3.06 (sept, $^{3}J_{H–H}$ = 7 Hz, 2H; $C_6H_3\{CH(CH_3)_2\}_2$), 3.04 (sept, $^{3}J_{H–H}$ = 7 Hz, 2H; $C_6H_3\{CH(CH_3)_2\}_2$), 2.99 (sept, $^{3}J_{H–H}$ = 7 Hz, 2H; $C_6H_3\{CH(CH_3)_2\}_2$), 2.87 (sept, $^{3}J_{H–H}$ = 7 Hz, 2H; $C_6H_3\{CH(CH_3)_2\}_2$), 1.25 (d, $^{3}J_{H–H}$ = 7 Hz, 6H; $C_6H_3\{CH(CH_3)_2\}_2$), 1.16 (d, $^{3}J_{H–H}$ = 7 Hz, 12H; $C_6H_3\{CH(CH_3)_2\}_2$), 1.11 (d, $^{3}J_{H–H}$ = 7 Hz, 6H; $C_6H_3\{CH(CH_3)_2\}_2$), 1.08 (d, $^{3}J_{H–H}$ = 7 Hz, 6H; $C_6H_3\{CH(CH_3)_2\}_2$), 1.00 (d, $^{3}J_{H–H}$ = 7 Hz, 6H; $C_6H_3\{CH(CH_3)_2\}_2$), 0.95 (d, $^{3}J_{H–H}$ = 7 Hz, 6H; $C_6H_3\{CH(CH_3)_2\}_2$), 0.87 (d, $^{3}J_{H–H}$ = 7 Hz, 6H; $C_6H_3\{CH(CH_3)_2\}_2$), 0.03 (s, satellites $^{2}J_{H–^{29}Si}$ = 6 Hz, 9H; $N(Si(CH_3)_3)_2$), –0.44 (s, satellites $^{2}J_{H–^{29}Si}$ = 6 Hz, 9H; $N(Si(CH_3)_3)_2$).

$^{13}C\{^{1}H\}$ NMR (125.80 MHz, d_8-THF): δ (ppm) 214.6 (*C*N_2), 154.1 (N*C*CHN), 147.7, 147.5, 147.1, 147.0 (*ortho*-Dipp), 143.2, 140.9 (*ipso*-Dipp), 128.4, 128.1 (*para*-Dipp), 127.8 (NC*C*HN), 123.9, 123.6, 123.5, 123.1 (*meta*-Dipp), 71.2 (18-crown-6), 29.5, 29.0, 28.7, 28.6 ($C_6H_3\{CH(CH_3)_2\}_2$), 26.7, 26.2, 25.6, 25.5, 25.0, 24.9, 24.2, 22.6 ($C_6H_3\{CH(CH_3)_2\}_2$), 7.2 ($N(Si(CH_3)_3)_2$), 7.1 ($N(Si(CH_3)_3)_2$). $^{29}Si\{^{1}H\}$ NMR (99.32 MHz, d_8-THF): δ (ppm) –2.6 (s), –3.5 (s).

7.2.1.7 [K(18-crown-6)(THF)$_2$][7] (7: [(aIPr:)$_2$Pb{N(SiMe$_3$)$_2$}]$^-$)

To a suspension of $[K(aIPr:)]_\infty$ (60 mg, 0.140 mmol) in THF (5 mL) was added $Pb[N(SiMe_3)_2]_2$ (37 mg, 0.077 mmol) and the mixture stirred until a clear solution remained. 18-Crown-6 (37 mg, 0.140 mmol) was added to the solution and stirred until the solid dissolved. The solution was then filtered and layered with hexane to afford colourless crystals of $[K(18\text{-crown-6})(THF)_2][(aIPr:)_2Pb\{N(SiMe_3)_2\}]\cdot THF$ suitable for single crystal X-ray diffraction (88 mg, 79% crystalline yield). Anal. Calcd for $C_{72}H_{112}KN_5O_6PbSi_2$ (1446.18): C 59.80%, H 7.81%, N 4.84%. Found: C 59.90%, H 7.59%, N 4.70%. ESI-MS, negative-ion mode (THF, 150 °C, 2.4 kV): *m/z* 1136.6 (100%) $[(aIPr:)_2Pb\{N(SiMe_3)_2\}]^-$. ^{1}H NMR (500.30 MHz, d_8-THF): δ (ppm) 7.04–7.19 (m, 12H; *meta*-Dipp and *para*-Dipp), 6.96 (s, 2H; NCC*H*N), 3.48 (s, 24H; 18-crown-6), 3.04 (sept, $^{3}J_{H–H}$ = 7 Hz, 2H; $C_6H_3\{CH(CH_3)_2\}_2$), 2.98 (sept, $^{3}J_{H–H}$ = 7 Hz, 2H; $C_6H_3\{CH(CH_3)_2\}_2$), 2.93 (sept, $^{3}J_{H–H}$ = 7 Hz, 2H; $C_6H_3\{CH(CH_3)_2\}_2$), 2.89 (sept, $^{3}J_{H–H}$ = 7 Hz, 2H; $C_6H_3\{CH(CH_3)_2\}_2$), 1.25 (d, $^{3}J_{H–H}$ = 7 Hz, 6H; $C_6H_3\{CH(CH_3)_2\}_2$), 1.13 (d, $^{3}J_{H–H}$ = 7 Hz, 6H; $C_6H_3\{CH(CH_3)_2\}_2$), 1.12 (d, $^{3}J_{H–H}$ = 7 Hz, 6H; $C_6H_3\{CH(CH_3)_2\}_2$), 1.09 (d, $^{3}J_{H–H}$ = 7 Hz, 6H; $C_6H_3\{CH(CH_3)_2\}_2$), 1.07 (d, $^{3}J_{H–H}$ = 7 Hz, 6H; $C_6H_3\{CH(CH_3)_2\}_2$), 1.02 (d, $^{3}J_{H–H}$ = 7 Hz, 6H; $C_6H_3\{CH(CH_3)_2\}_2$), 1.00 (d, $^{3}J_{H–H}$ = 7 Hz, 6H; $C_6H_3\{CH(CH_3)_2\}_2$), 0.86 (d, $^{3}J_{H–H}$ = 7 Hz, 6H; $C_6H_3\{CH(CH_3)_2\}_2$), –0.23 (s, 18H; $N(Si(CH_3)_3)_2$). $^{13}C\{^{1}H\}$ NMR (125.80 MHz, d_8-THF): δ (ppm) 217.1 (*C*N_2), 191.8 (N*C*CHN),

147.8, 147.7, 147.1, 146.9 (*ortho*-Dipp), 144.1, 142.0 (*ipso*-Dipp), 134.2 (NC*C*HN), 127.8, 127.4 (*para*-Dipp), 123.5, 123.4, 123.1, 122.7 (*meta*-Dipp), 71.3 (18-crown-6), 29.1, 28.9, 28.8, 28.6 ($C_6H_3\{CH(CH_3)_2\}_2$), 26.4, 26.3, 25.5, 25.4, 25.1, 24.9, 24.2, 23.1 ($C_6H_3\{CH(CH_3)_2\}_2$), 7.5 ($N(Si(CH_3)_3)_2$). $^{29}Si\{^1H\}$ NMR (99.32 MHz, d_8-THF): δ (ppm) –6.1 (s).

7.2.1.8 (aIPr:)(aIPr·Li(THF)$_2$)Ge{N(SiMe$_3$)$_2$} (8)

To a solution of $[Li(aIPr:)]_\infty$ (310 mg, 0.787 mmol) in THF (10 mL) was added and solution of $Ge[N(SiMe_3)_2]_2$ (155 mg, 0.393 mmol) in THF (5 mL) with stirring at ambient temperature. The green solution was allowed to stir for 30 minutes to afford a pale orange solution. The solution was then filtered and layered with hexane to afford colourless crystals of (360 mg, 79% crystalline yield). ^1H NMR (500.30 MHz, d_8-THF): δ (ppm) 7.24 (t, $^3J_{H–H}$ = 8 Hz, 2H; *para*-Dipp), 7.06–7.18 (m, 10H; *meta*-Dipp and *para*-Dipp); 6.95 (s, 2H; NCC*H*N); 3.62 (m, 8H; THF); 3.02 (sept, $^3J_{H–H}$ = 7 Hz, 2H; $C_6H_3\{CH(CH_3)_2\}_2$); 3.00 (sept, $^3J_{H–H}$ = 7 Hz, 2H; $C_6H_3\{CH(CH_3)_2\}_2$); 2.96 (sept, $^3J_{H–H}$ = 7 Hz, 2H; $C_6H_3\{CH(CH_3)_2\}_2$); 2.82 (sept, $^3J_{H–H}$ = 7 Hz, 2H; $C_6H_3\{CH(CH_3)_2\}_2$); 1.77 (m, 8H; THF); 1.27 (d, $^3J_{H–H}$ = 7 Hz, 3H; $C_6H_3\{CH(CH_3)_2\}_2$); 1.15 (d, $^3J_{H–H}$ = 7 Hz, 3H; $C_6H_3\{CH(CH_3)_2\}_2$); 1.14 (d, $^3J_{H–H}$ = 7 Hz, 3H; $C_6H_3\{CH(CH_3)_2\}_2$); 1.11 (d, $^3J_{H–H}$ = 7 Hz, 3H; $C_6H_3\{CH(CH_3)_2\}_2$); 1.10 (d, $^3J_{H–H}$ = 7 Hz, 3H; $C_6H_3\{CH(CH_3)_2\}_2$); 1.02 (d, $^3J_{H–H}$ = 7 Hz, 3H; $C_6H_3\{CH(CH_3)_2\}_2$); 0.95 (d, $^3J_{H–H}$ = 7 Hz, 3H; $C_6H_3\{CH(CH_3)_2\}_2$); 1.87 (d, $^3J_{H–H}$ = 7 Hz, 3H; $C_6H_3\{CH(CH_3)_2\}_2$); 0.05 (s, 9H; $N(Si(CH_3)_3)_2$); –0.42 (s, 9H; $N(Si(CH_3)_3)_2$).

7.2.1.9 (aIPr:)(aIPr·Li(THF)$_2$)Sn{N(SiMe$_3$)$_2$} (9)

To a solution of $[Li(aIPr:)]_\infty$ (260 mg, 0.660 mmol) in THF (10 mL) was added and solution of $Sn[N(SiMe_3)_2]_2$ (130 mg, 0.330 mmol) in THF (5 mL) with stirring at ambient temperature.

The orange solution was allowed to stir for 30 minutes to afford a pale yellow solution. The solution was then filtered and layered with hexane to afford colourless crystals (310 mg, 78% crystalline yield). ^{1}H NMR (500.30 MHz, d_8-THF): δ (ppm) 7.24 (t, $^{3}J_{H–H}$ = 8 Hz, 2H; *para*-Dipp), 7.07–7.19 (m, 10H; *meta*-Dipp and *para*-Dipp); 6.95 (s, 2H; NCC*H*N); 3.62 (m, 8H; THF); 2.95 (sept, $^{3}J_{H–H}$ = 7 Hz, 2H; $C_6H_3\{CH(CH_3)_2\}_2$); 2.94 (sept, $^{3}J_{H–H}$ = 7 Hz, 2H; $C_6H_3\{CH(CH_3)_2\}_2$); 2.91 (sept, $^{3}J_{H–H}$ = 7 Hz, 2H; $C_6H_3\{CH(CH_3)_2\}_2$); 2.82 (sept, $^{3}J_{H–H}$ = 7 Hz, 2H; $C_6H_3\{CH(CH_3)_2\}_2$); 1.77 (m, 8H; THF); 1.27 (d, $^{3}J_{H–H}$ = 7 Hz, 3H; $C_6H_3\{CH(CH_3)_2\}_2$); 1.18 (d, $^{3}J_{H–H}$ = 7 Hz, 3H; $C_6H_3\{CH(CH_3)_2\}_2$); 1.12 (d, $^{3}J_{H–H}$ = 7 Hz, 3H; $C_6H_3\{CH(CH_3)_2\}_2$); 1.10 (d, $^{3}J_{H–H}$ = 7 Hz, 3H; $C_6H_3\{CH(CH_3)_2\}_2$); 1.08 (d, $^{3}J_{H–H}$ = 7 Hz, 3H; $C_6H_3\{CH(CH_3)_2\}_2$); 1.03 (d, $^{3}J_{H–H}$ = 7 Hz, 3H; $C_6H_3\{CH(CH_3)_2\}_2$); 0.99 (d, $^{3}J_{H–H}$ = 7 Hz, 3H; $C_6H_3\{CH(CH_3)_2\}_2$); 1.85 (d, $^{3}J_{H–H}$ = 7 Hz, 3H; $C_6H_3\{CH(CH_3)_2\}_2$); –0.18 (br s, 18H; $N(Si(CH_3)_3)_2$).

7.2.1.10 (aIPr:)(aIPr·Li(THF)$_2$)Pb{N(SiMe$_3$)$_2$} (10)

To a solution of $[Li(aIPr:)]_\infty$ (286 mg, 0.726 mmol) in THF (10 mL) was added and solution of $Pb[N(SiMe_3)_2]_2$ (192 mg, 0.363 mmol) in THF (5 mL) with stirring at ambient temperature. The dark orange solution was allowed to stir for 30 minutes before being concentrated to 5 mL. With vigorous stirring, hexane (25 mL) was added to induce precipitation of the product as a pale orange crystalline powder. The solution was filtered and the solid washed again with hexane (10 mL) before being dried thoroughly under vacuum (321 mg, 68% yield). Single crystals suitable for single crystal X-ray diffraction were grown by layering a THF solution with hexane. Anal. Calcd for $C_{68}H_{104}LiN_5O_2PbSi_2$ (1293.92): C 63.12%, H 8.10%, N 5.41%. Found: C 62.90%, H 7.98%, N 5.48%. ^{1}H NMR (500.30 MHz, d_8-THF): δ (ppm) 7.10–7.27 (m, 12H; *meta*-Dipp and *para*-Dipp); 6.99 (s, 2H; NCC*H*N); 3.62 (m, 8H; THF); 2.98 (sept, $^{3}J_{H–H}$ = 7 Hz, 2H; $C_6H_3\{CH(CH_3)_2\}_2$); 2.91 (sept, $^{3}J_{H–H}$ = 7 Hz, 2H; $C_6H_3\{CH(CH_3)_2\}_2$); 2.90

(sept, $^{3}J_{H–H}$ = 7 Hz, 2H; $C_6H_3\{CH(CH_3)_2\}_2$); 2.83 (sept, $^{3}J_{H–H}$ = 7 Hz, 2H; $C_6H_3\{CH(CH_3)_2\}_2$); 1.77 (m, 8H; THF); 1.28 (d, $^{3}J_{H–H}$ = 7 Hz, 3H; $C_6H_3\{CH(CH_3)_2\}_2$); 1.14 (d, $^{3}J_{H–H}$ = 7 Hz, 3H; $C_6H_3\{CH(CH_3)_2\}_2$); 1.12 (d, $^{3}J_{H–H}$ = 7 Hz, 3H; $C_6H_3\{CH(CH_3)_2\}_2$); 1.10 (d, $^{3}J_{H–H}$ = 7 Hz, 3H; $C_6H_3\{CH(CH_3)_2\}_2$); 1.08 (d, $^{3}J_{H–H}$ = 7 Hz, 3H; $C_6H_3\{CH(CH_3)_2\}_2$); 1.03 (d, $^{3}J_{H–H}$ = 7 Hz, 3H; $C_6H_3\{CH(CH_3)_2\}_2$); 1.00 (d, $^{3}J_{H–H}$ = 7 Hz, 3H; $C_6H_3\{CH(CH_3)_2\}_2$); 1.86 (d, $^{3}J_{H–H}$ = 7 Hz, 3H; $C_6H_3\{CH(CH_3)_2\}_2$); –0.22 (s, 18H; $N(Si(CH_3)_3)_2$). $^{13}C\{^{1}H\}$ NMR (125.80 MHz, d_8-THF): δ (ppm) 210.1 (v br, fwhm = 90 Hz; *C*N_2); 192.3 (N*C*CHN); 147.7, 147.6, 147.0 146.7 (*ortho*-Dipp); 143.4, 141.1 (*ipso*-Dipp); 134.7 (NC*C*HN); 128.4, 128.1 (*para*-Dipp); 124.0, 123.9, 123.5, 123.2 (*meta*-Dipp); 68.4 (THF); 29.2, 28.9, 28.8, 28.7 ($C_6H_3\{CH(CH_3)_2\}_2$); 26.6 (THF); 26.3, 26.2, 25.32, 25.29, 25.2, 25.1, 24.4, 23.1 ($C_6H_3\{CH(CH_3)_2\}_2$); 7.4 ($N(Si(CH_3)_3)_2$). $^{207}Pb\{^{1}H\}$ NMR (104.59 MHz, d_8-THF): δ (ppm) 1619.2 (s).

7.2.1.11 (aIPr)(aIPr:)Ge{N(SiMe$_3$)$_2$} (11)

To a solution of (aIPr:)(aIPr·Li(THF)$_2$)Ge{N(SiMe$_3$)$_2$} (26 mg, 0.022 mmol) in d_8-THF (500 μL) was added and [H(OEt$_2$)$_2$][B(3,5-{CF$_3$}$_2$C$_6$H$_3$)$_4$] (23 mg, 0.022 mmol). The solution was then transferred to an NMR tube and characterised by multielement NMR spectroscopy. Single crystals of (aIPr·THF)(aIPr:)Ge{N(SiMe$_3$)$_2$} were grown from a saturated THF solution. ^{1}H NMR (500.30 MHz, d_8-THF): δ (ppm) 9.02 (d, $^{4}J_{H–H}$ = 2 Hz, 1H; *H*CN_2); 7.56 (t, $^{3}J_{H–H}$ = 8 Hz, 1H; *para*-Dipp); 7.47 (t, $^{3}J_{H–H}$ = 8 Hz, 1H; *para*-Dipp); 7.30 (d, $^{4}J_{H–H}$ = 2 Hz, 1H; *H*CN_2); 7.07–7.44 (m, 10H; *meta*-Dipp and *para*-Dipp); 3.03 (sept, $^{3}J_{H–H}$ = 7 Hz, 1H; $C_6H_3\{CH(CH_3)_2\}_2$); 2.98 (sept, $^{3}J_{H–H}$ = 7 Hz, 1H; $C_6H_3\{CH(CH_3)_2\}_2$); 2.86 (sept, $^{3}J_{H–H}$ = 7 Hz, 1H; $C_6H_3\{CH(CH_3)_2\}_2$); 2.84 (sept, $^{3}J_{H–H}$ = 7 Hz, 1H; $C_6H_3\{CH(CH_3)_2\}_2$); 2.74 (sept, $^{3}J_{H–H}$ = 7 Hz, 1H; $C_6H_3\{CH(CH_3)_2\}_2$); 2.68 (sept, $^{3}J_{H–H}$ = 7 Hz, 1H; $C_6H_3\{CH(CH_3)_2\}_2$); 2.53 (sept, $^{3}J_{H–H}$ = 7 Hz, 1H; $C_6H_3\{CH(CH_3)_2\}_2$); 2.50 (sept, $^{3}J_{H–H}$ = 7 Hz, 1H; $C_6H_3\{CH(CH_3)_2\}_2$); 1.38 (d, $^{3}J_{H–H}$ = 7 Hz, 3H; $C_6H_3\{CH(CH_3)_2\}_2$); 1.27 (d, $^{3}J_{H–H}$ = 7 Hz, 3H;

$C_6H_3\{CH(CH_3)_2\}_2$); 1.26 (d, $^3J_{H–H}$ = 7 Hz, 3H; $C_6H_3\{CH(CH_3)_2\}_2$); 1.09–1.20 (m, 27H; $C_6H_3\{CH(CH_3)_2\}_2$); 1.02 (d, $^3J_{H–H}$ = 7 Hz, 3H; $C_6H_3\{CH(CH_3)_2\}_2$); 1.01 (d, $^3J_{H–H}$ = 7 Hz, 3H; $C_6H_3\{CH(CH_3)_2\}_2$); 0.96 (d, $^3J_{H–H}$ = 7 Hz, 3H; $C_6H_3\{CH(CH_3)_2\}_2$); 0.71 (d, $^3J_{H–H}$ = 7 Hz, 3H; $C_6H_3\{CH(CH_3)_2\}_2$); 0.08 (s, 9H; $N(Si(CH_3)_3)_2$); –0.41 (s, 9H; $N(Si(CH_3)_3)_2$). $^{13}C\{^1H\}$ NMR (125.80 MHz, d_8-THF): δ (ppm) 221.2 (CN_2); 163.6 (NCCHN); 149.5 (NCCHN); 147.3, 146.8, 146.7, 146.5 (×2), 146.4, 146.3, 146.0 (*ortho*-Dipp); 145.8, 142.2, 140.3 (*ipso*-Dipp); 139.3 (HCN_2); 134.0 (*ipso*-Dipp); 132.0, 131.2 (NCCHN); 129.0, 128.2, 127.6, 127.5 (*para*-Dipp); 125.2, 125.1, 125.0, 124.8, 123.8, 123.7, 123.1, 122.3 (*meta*-Dipp); 68.0 (THF); 29.8, 29.3, 29.2, 29.1, 29.0, 28.8, 28.6, 28.5 ($C_6H_3\{CH(CH_3)_2\}_2$); 26.2 (THF); 26.2, 26.1, 25.8, 25.7, 25.4, 25.0, 24.9, 24.8, 24.7, 24.6, 24.4, 24.3, 24.2, 24.1, 23.7, 23.5 ($C_6H_3\{CH(CH_3)\}_2$); 6.6 ($N(Si(CH_3)_3)_2$); 6.5 ($N(Si(CH_3)_3)_2$). $^{29}Si\{^1H\}$ NMR (99.32 MHz, d_8-THF): δ (ppm) –0.4 (s); –1.3 (s).

7.2.1.12 (aIPr·Li(THF)$_2$)Sn{N(SiMe$_3$)(SiMe$_2$CH$_2$)}(aIPr:)Sn{N(SiMe$_3$)$_2$} (12)

To a solution of $[Li(aIPr:)]_\infty$ (240 mg, 0.609 mmol) in THF (5 mL) was added and solution of $Sn[N(SiMe_3)_2]_2$ (268 mg, 0.609 mmol) in THF (5 mL) with stirring at ambient temperature. The orange solution was allowed to stir for 30 minutes before being filtered into a large crystallisation ampoule. The solution was layered with hexane and stored at 4 °C. After a few days, yellow crystals begin to grow on the walls of the ampoule. The solution is periodically agitated to encourage mixing of the two solutions and crystallisation of the product for about two weeks until both solutions have fully mixed and no further crystallisation is observed. The yellow solution is decanted from the crystals which are then dried well under vacuum (245 mg, 54% crystalline yield). Anal. Calcd for $C_{74}H_{121}LiN_6O_2Si_4Sn_2$ (1484.50): C 59.87%, H 8.28%, N 5.66%. Found: C 59.65%, H 8.00%, N 5.56%. ^1H NMR (500.30 MHz, d_8-THF): δ (ppm) 7.11–7.27 (m, 12H; *meta*-Dipp and *para*-Dipp); 7.04 (s, 1H; NCCHN); 6.89 (s, 1H;

NCC*H*N); 3.62 (m, 8H; THF); 3.33 (sept, $^{3}J_{H–H}$ = 7 Hz, 1H; $C_6H_3\{C\mathit{H}(CH_3)_2\}_2$); 3.19 (sept, $^{3}J_{H–H}$ = 7 Hz, 1H; $C_6H_3\{C\mathit{H}(CH_3)_2\}_2$); 3.06 (sept, $^{3}J_{H–H}$ = 7 Hz, 1H; $C_6H_3\{C\mathit{H}(CH_3)_2\}_2$); 2.95 (sept, $^{3}J_{H–H}$ = 7 Hz, 1H; $C_6H_3\{C\mathit{H}(CH_3)_2\}_2$); 2.89 (sept, $^{3}J_{H–H}$ = 7 Hz, 1H; $C_6H_3\{C\mathit{H}(CH_3)_2\}_2$); 2.78–2.87 (m, 3H; $C_6H_3\{C\mathit{H}(CH_3)_2\}_2$); 1.77 (m, 8H; THF); 1.43 (d, $^{3}J_{H–H}$ = 7 Hz, 3H; $C_6H_3\{CH(C\mathit{H}_3)_2\}_2$); 1.33 (d, $^{3}J_{H–H}$ = 7 Hz, 3H; $C_6H_3\{CH(C\mathit{H}_3)_2\}_2$); 1.27 (d, $^{3}J_{H–H}$ = 7 Hz, 3H; $C_6H_3\{CH(C\mathit{H}_3)_2\}_2$); 1.26 (d, $^{3}J_{H–H}$ = 7 Hz, 3H; $C_6H_3\{CH(C\mathit{H}_3)_2\}_2$); 1.25 (d, $^{3}J_{H–H}$ = 7 Hz, 3H; $C_6H_3\{CH(C\mathit{H}_3)_2\}_2$); 1.18 (d, $^{3}J_{H–H}$ = 7 Hz, 3H; $C_6H_3\{CH(C\mathit{H}_3)_2\}_2$); 1.16 (d, $^{3}J_{H–H}$ = 7 Hz, 3H; $C_6H_3\{CH(C\mathit{H}_3)_2\}_2$); 1.12–1.16 (m, 12H; $C_6H_3\{CH(C\mathit{H}_3)_2\}_2$); 1.10 (d, $^{3}J_{H–H}$ = 7 Hz, 3H; $C_6H_3\{CH(C\mathit{H}_3)_2\}_2$); 1.06 (d, $^{3}J_{H–H}$ = 7 Hz, 3H; $C_6H_3\{CH(C\mathit{H}_3)_2\}_2$); 0.99 (d, $^{3}J_{H–H}$ = 7 Hz, 3H; $C_6H_3\{CH(C\mathit{H}_3)_2\}_2$); 0.98 (d, $^{3}J_{H–H}$ = 7 Hz, 3H; $C_6H_3\{CH(C\mathit{H}_3)_2\}_2$); 0.96 (d, $^{3}J_{H–H}$ = 7 Hz, 3H; $C_6H_3\{CH(C\mathit{H}_3)_2\}_2$); 0.53 (d, $^{2}J_{H–H}$ = 12 Hz, 1H; $N(Si(CH_3)_3)(Si(CH_3)_2C\mathit{H}_2)$); 0.41 (d, $^{2}J_{H–H}$ = 12 Hz, 1H; $N(Si(CH_3)_3)(Si(CH_3)_2C\mathit{H}_2)$); 0.13 (s, 3H; $N(Si(CH_3)_3)(Si(C\mathit{H}_3)_2CH_2)$); –0.08 (s, 3H; $N(Si(CH_3)_3)(Si(C\mathit{H}_3)_2CH_2)$); –0.20 (s, 18H; $N(Si(C\mathit{H}_3)_3)_2$); –0.23 (s, 9H; $N(Si(C\mathit{H}_3)_3)(Si(CH_3)_2CH_2)$). $^{13}C\{^{1}H\}$ NMR (125.80 MHz, d_8-THF): δ (ppm) 221.9 ($\mathit{C}N_2$); 215.7 (br, fwhm = 20 Hz; Li$\mathit{C}N_2$); 151.7 (N*C*CHN); 147.7, 147.5, 147.4, 147.3, 147.2, 147.0, 146.8, 146.2 (*ortho*-Dipp); 143.4 (*ipso*-Dipp); 143.0 (N*C*CHN); 142.8, 141.0, 140.6 (*ipso*-Dipp); 132.1, 130.9 (NC*C*HN); 128.4, 128.1 (×2), 128.0 (*para*-Dipp); 124.6, 123.9, 123.8, 123.7 (×2), 123.4, 123.3, 123.2 (*meta*-Dipp); 68.4 (THF); 29.9, 29.8, 29.1, 29.0, 28.9, 28.8, 28.7 (×2) ($C_6H_3\{\mathit{C}H(CH_3)_2\}_2$); 27.8, 26.9, 26.8 ($C_6H_3\{CH(\mathit{C}H_3)_2\}_2$); 26.6 (THF); 26.3, 26.2, 26.0, 25.9, 25.4, 25.0, 24.9, 24.8, 24.2, 24.1, 23.7, 22.9, 22.7 ($C_6H_3\{CH(\mathit{C}H_3)\}_2$); 15.2 ($Si(CH_3)_2\mathit{C}H_2$); 7.9, 7.4 ($Si(\mathit{C}H_3)_2CH_2$); 7.2 ($N(Si(\mathit{C}H_3)_3)(Si(CH_3)_2CH_2)$); 6.9 ($N(Si(\mathit{C}H_3)_3)_2$). $^{29}Si\{^{1}H\}$ NMR (99.32 MHz, d_8-THF): δ (ppm) –0.2 (s, $N(Si(CH_3)_3)(\mathit{Si}(CH_3)_2CH_2)$); –1.2 (s, $N(\mathit{Si}(CH_3)_3)(Si(CH_3)_2CH_2)$); –5.0 (s, $N(\mathit{Si}(CH_3)_3)_2$). $^{119}Sn\{^{1}H\}$ NMR (186.43 MHz, d_8-THF): δ (ppm) –12.5 (s; satellites

$^{1}J_{^{119}Sn-^{117}Sn}$ = 8613 Hz, $^{1}J_{^{119}Sn-^{119}Sn}$ = 8977 Hz); –126.2 (s; satellites $^{1}J_{^{119}Sn-^{117}Sn}$ = 8570 Hz, $^{1}J_{^{119}Sn-^{119}Sn}$ = 8996 Hz).

7.2.1.13 (aIPr·Li(THF)$_2$)Pb{N(SiMe$_3$)$_2$}(aIPr·Pb{N(SiMe$_3$)SiMe$_2$CH$_2$}) (13)

To a solution of (aIPr:)(aIPr·Li(THF)$_2$)Pb{N(SiMe$_3$)$_2$} (247 mg, 0.191 mmol) in THF (5 mL) was added a solution of Pb[N(SiMe$_3$)$_2$]$_2$ (101 mg, 0.191 mmol) in THF (5 mL) with stirring at ambient temperature. The yellow solution was allowed to stir overnight before being filtered and solution layered with hexane to afford yellow crystals suitable for single crystal X-ray diffraction (220 mg, 69% crystalline yield). ^{1}H NMR (500.30 MHz, d_8-THF, 298 K): δ (ppm) 7.22–7.30 (m, 4H; *para*-Dipp); 7.12–7.20 (m, 8H; *meta*-Dipp); 7.04 (s, 2H; NCC*H*N); 3.62 (m, 8H; THF); 2.84–2.93 (m, 4H; C$_6$H$_3${C*H*(CH$_3$)$_2$}$_2$); 2.81 (sept, $^{3}J_{H-H}$ = 7 Hz, 2H; C$_6$H$_3${C*H*(CH$_3$)$_2$}$_2$); 2.76 (sept, $^{3}J_{H-H}$ = 7 Hz, 2H; C$_6$H$_3${C*H*(CH$_3$)$_2$}$_2$); 1.77 (m, 8H; THF); 1.28 (d, $^{3}J_{H-H}$ = 7 Hz, 6H; C$_6$H$_3${CH(C*H*$_3$)$_2$}$_2$); 1.18–1.23 (m, 12H; C$_6$H$_3${CH(C*H*$_3$)$_2$}$_2$); 1.10–1.16 (m, 18H; C$_6$H$_3${CH(C*H*$_3$)$_2$}$_2$); 1.07 (d, $^{3}J_{H-H}$ = 7 Hz, 6H; C$_6$H$_3${CH(C*H*$_3$)$_2$}$_2$); 0.86 (br s, 6H; C$_6$H$_3${CH(C*H*$_3$)$_2$}$_2$); –0.21 (br s, 18H; N(Si(C*H*$_3$)$_3$)$_2$); –0.42 (br s, 6H; N(Si(CH$_3$)$_3$)(Si(C*H*$_3$)$_2$CH$_2$)); –0.54 (s, 9H; N(Si(C*H*$_3$)$_3$)(Si(CH$_3$)$_2$CH$_2$)); –1.67 (v br s, 2H; N(Si(CH$_3$)$_3$)(Si(CH$_3$)$_2$C*H*$_2$)). ^{1}H NMR (500.30 MHz, d_8-THF, 338 K): δ (ppm) 7.23–7.30 (m, 4H; *para*-Dipp); 7.14–7.21 (m, 8H; *meta*-Dipp); 7.07 (s, 2H; NCC*H*N); 3.62 (m, 8H; THF); 2.92 (sept, $^{3}J_{H-H}$ = 7 Hz, 2H; C$_6$H$_3${C*H*(CH$_3$)$_2$}$_2$); 2.88 (sept, $^{3}J_{H-H}$ = 7 Hz, 2H; C$_6$H$_3${C*H*(CH$_3$)$_2$}$_2$); 2.83 (sept, $^{3}J_{H-H}$ = 7 Hz, 2H; C$_6$H$_3${C*H*(CH$_3$)$_2$}$_2$); 2.77 (sept, $^{3}J_{H-H}$ = 7 Hz, 2H; C$_6$H$_3${C*H*(CH$_3$)$_2$}$_2$); 1.77 (m, 8H; THF); 1.30 (d, $^{3}J_{H-H}$ = 7 Hz, 6H; C$_6$H$_3${CH(C*H*$_3$)$_2$}$_2$); 1.17–1.23 (m, 12H; C$_6$H$_3${CH(C*H*$_3$)$_2$}$_2$); 1.16 (d, $^{3}J_{H-H}$ = 7 Hz, 12H; C$_6$H$_3${CH(C*H*$_3$)$_2$}$_2$); 1.13 (d, $^{3}J_{H-H}$ = 7 Hz, 6H; C$_6$H$_3${CH(C*H*$_3$)$_2$}$_2$); 1.08 (d, $^{3}J_{H-H}$ = 7 Hz, 6H; C$_6$H$_3${CH(C*H*$_3$)$_2$}$_2$); 0.87 (d, $^{3}J_{H-H}$ = 7 Hz, 6H; C$_6$H$_3${CH(C*H*$_3$)$_2$}$_2$); –0.20 (br s, 18H; N(Si(C*H*$_3$)$_3$)$_2$); –0.41 (br s, 6H; N(Si(CH$_3$)$_3$)(Si(C*H*$_3$)$_2$CH$_2$)); –0.51 (s, 9H;

N(Si(C*H*$_3$)$_3$)(Si(CH$_3$)$_2$CH$_2$)); –1.67 (br s, 2H; N(Si(CH$_3$)$_3$)(Si(CH$_3$)$_2$C*H*$_2$)). ^{1}H NMR (500.30 MHz, d_8-THF, 238 K): δ (ppm) 7.23–7.30 (m, 4H; *para*-Dipp); 7.10–7.34 (br m, 12H; *meta*-Dipp and *para*-Dipp); 7.06 (br s, 1H; NCC*H*N); 6.92 (v br s, 1H; NCC*H*N); 3.62 (m, 8H; THF); 2.56–3.00 (br m, 8H; C$_6$H$_3${C*H*(CH$_3$)$_2$}$_2$); 1.77 (m, 8H; THF); 0.97–1.35 (br m, 48H; C$_6$H$_3${CH(C*H*$_3$)$_2$}$_2$); –0.03 (br s, 9H; N(Si(C*H*$_3$)$_3$)$_2$); –0.33 (br s, 3H; N(Si(CH$_3$)$_3$)(Si(C*H*$_3$)$_2$CH$_2$)); –0.42 (br s, 9H; N(Si(C*H*$_3$)$_3$)$_2$); –0.53 (br s, 3H; N(Si(CH$_3$)$_3$)(Si(C*H*$_3$)$_2$CH$_2$)); –0.60 (s, 9H; N(Si(C*H*$_3$)$_3$)(Si(CH$_3$)$_2$CH$_2$)); –1.17 (d, $^2J_{H–H}$ = 11 Hz, 1H; N(Si(CH$_3$)$_3$)(Si(CH$_3$)$_2$C*H*$_2$)); –2.26 (d, $^2J_{H–H}$ = 11 Hz, 1H; N(Si(CH$_3$)$_3$)(Si(CH$_3$)$_2$C*H*$_2$)). ^{13}C{^{1}H} NMR (125.80 MHz, d_8-THF, 298 K): δ (ppm) 200.0 (v br, fwhm = 532 Hz; *C*N$_2$); 193.9 (br, fwhm = 104 Hz; N*C*CHN); 147.5, 147.3, 146.9, 146.4 (*ortho*-Dipp); 141.6 (br, fwhm = 31 Hz; *ipso*-Dipp); 139.0 (br, fwhm = 45 Hz; *ipso*-Dipp); 135.7 (br, fwhm = 16 Hz; NC*C*HN); 129.4 (br, fwhm = 9 Hz; *para*-Dipp); 128.9 (br, fwhm = 9 Hz; *para*-Dipp); 124.5, 124.3, 124.1, 123.8 (*meta*-Dipp); 68.4 (THF); 29.2, 29.1, 29.0, 28.9 (C$_6$H$_3${*C*H(CH$_3$)$_2$}$_2$); 26.5 (THF); multiple overlapping broad and sharp resonances obscured by solvent resonance (C$_6$H$_3${CH(*C*H$_3$)}$_2$); 14.6 (v br, fwhm = 99 Hz; N(Si(CH$_3$)$_3$)(Si(*C*H$_3$)$_2$CH$_2$)); 7.4 (br, fwhm = 9 Hz; N(Si(*C*H$_3$)$_3$)$_2$); 5.3 (N(Si(*C*H$_3$)$_3$)(Si(CH$_3$)$_2$CH$_2$)). The resonance corresponding to the (N(Si(CH$_3$)$_3$)(Si(CH$_3$)$_2$*C*H$_2$)) carbon environment cannot be observed. ^{29}Si{^{1}H} NMR (99.32 MHz, d_8-THF, 298 K): δ (ppm) –4.9 (s, N(*Si*(CH$_3$)$_3$)(Si(CH$_3$)$_2$CH$_2$)); –6.6 (s, N(*Si*(CH$_3$)$_3$)$_2$); –15.6 (s, N(Si(CH$_3$)$_3$)(*Si*(CH$_3$)$_2$CH$_2$)). ^{207}Pb{^{1}H} NMR (104.59 MHz, d_8-THF, 298 K): δ (ppm) 2840.6 (v br, fwhm = 4569 Hz; (aIPr·Li(THF)$_2$)Pb{N(SiMe$_3$)$_2$}(aIPr·*Pb*{N(SiMe$_3$)SiMe$_2$CH$_2$})); 1674.6 (v br, fwhm = 2576 Hz; (aIPr·Li(THF)$_2$)*Pb*{N(SiMe$_3$)$_2$}(aIPr·Pb{N(SiMe$_3$)SiMe$_2$CH$_2$})).

7.2.2 Chapter 3 – Synthesis of aIPr and aIPr: complexes of group 12 and 14 halides

7.2.2.1 (aIPr:)$_2$Hg (14)

To a mixture of [K(aIPr:)]$_\infty$ (500 mg, 1.173 mmol) and $HgCl_2$ (159 mg, 0.586 mmol) was added THF (25 mL) slowly under argon at –78 °C. The solution was then allowed to warm to ambient temperature to afford a pale orange solution and a viscous suspension. The mixture was stirred overnight and the suspension given enough time to settle before the solution was filtered and the solvent removed in vacuo to afford an off-white solid (327 mg, 57% yield). Colourless octahedral crystals were grown from a concentrated hexane solution at –35 °C. Anal. Calcd for $C_{54}H_{70}HgN_4$ (975.76): C 66.47%, H 7.23%, N 5.74%. Found: C 65.36%, H 7.34%, N 5.61%. EI-MS: *m/z* 387.2105 (100%) [aIPr:]$^+$ (Calcd 387.2800), 976.2751 (30%) [(aIPr:)$_2$Hg]$^+$ (Calcd 976.5318). ^{1}H NMR (500.30 MHz, d_8-THF): δ (ppm) 7.32 (t, $^3J_{H–H}$ = 8 Hz, 2H; *para*-Dipp), 7.30 (t, $^3J_{H–H}$ = 8 Hz, 2H; *para*-Dipp), 7.22 (d, $^3J_{H–H}$ = 8 Hz, 4H; *meta*-Dipp), 7.14 (d, $^3J_{H–H}$ = 8 Hz, 4H; *meta*-Dipp), 6.94 (s, 2H; NC*C*HN), 2.76 (sept, $^3J_{H–H}$ = 7 Hz, 4H; $C_6H_3\{CH(CH_3)\}_2$), 2.70 (sept, $^3J_{H–H}$ = 7 Hz, 4H; $C_6H_3\{CH(CH_3)_2\}_2$), 1.15 (d, $^3J_{H–H}$ = 7 Hz, 12H; $C_6H_3\{CH(CH_3)_2\}_2$), 1.11 (d, $^3J_{H–H}$ = 7 Hz, 12H; $C_6H_3\{CH(CH_3)_2\}_2$), 1.07 (d, $^3J_{H–H}$ = 7 Hz, 12H; $C_6H_3\{CH(CH_3)_2\}_2$), 1.00 (d, $^3J_{H–H}$ = 7 Hz, 12H; $C_6H_3\{CH(CH_3)_2\}_2$). ^{13}C{^{1}H} NMR (125.80 MHz, d_8-THF): δ (ppm) 222.4 (CN_2), 162.0 (N*C*CHN), 146.9, 146.6 (*ortho*-Dipp), 142.2, 140.0 (*ipso*-Dipp), 129.3, 129.2 (*para*-Dipp), 129.1 (NC*C*HN), 124.3, 124.0 (*meta*-Dipp), 29.3, 29.2 ($C_6H_3\{CH(CH_3)_2\}_2$), 25.4, 25.1, 24.1, 23.9 ($C_6H_3\{CH(CH_3)_2\}_2$). ^{199}Hg{^{1}H} NMR (89.54 MHz, d_8-THF): δ (ppm) –635.0 (s). ^{1}H NMR (500.30 MHz, C_6D_6): δ (ppm) 7.30 (t, $^3J_{H–H}$ = 8 Hz, 2H; *para*-Dipp), 7.20 (d, $^3J_{H–H}$ = 8 Hz, 4H; *meta*-Dipp), 7.19 (m, 2H; *para*-Dipp), 7.06 (d, $^3J_{H–H}$ = 8 Hz, 4H; *meta*-Dipp), 6.54 (s, 2H; NC*C*HN), 2.92 (sept, $^3J_{H–H}$ = 7 Hz, 4H; $C_6H_3\{CH(CH_3)_2\}_2$), 2.91 (sept, $^3J_{H–H}$ = 7 Hz, 4H; $C_6H_3\{CH(CH_3)_2\}_2$), 1.27 (d, $^3J_{H–H}$ = 7 Hz, 12H; $C_6H_3\{CH(CH_3)_2\}_2$),

1.23 (d, $^{3}J_{H–H}$ = 7 Hz, 12H; $C_6H_3\{CH(CH_3)_2\}_2$), 1.19 (d, $^{3}J_{H–H}$ = 7 Hz, 12H; $C_6H_3\{CH(CH_3)_2\}_2$), 1.04 (d, $^{3}J_{H–H}$ = 7 Hz, 12H; $C_6H_3\{CH(CH_3)_2\}_2$). $^{13}C\{^{1}H\}$ NMR (100.61 MHz, C_6D_6): δ (ppm) 222.3 (CN_2), 161.3 (NCCHN), 146.3, 146.0 (*ortho*-Dipp), 141.3, 139.1 (*ipso*-Dipp), 129.1, 129.0 (*para*-Dipp), 128.1 (NCCHN), 124.0, 123.7 (*meta*-Dipp), 28.8, 28.7 ($C_6H_3\{CH(CH_3)_2\}_2$), 25.0, 24.8, 23.7, 23.6 ($C_6H_3\{CH(CH_3)_2\}_2$). $^{199}Hg\{^{1}H\}$ NMR (89.54 MHz, C_6D_6): δ (ppm) –551.4 (s).

7.2.2.2 [K(2,2,2-crypt)][15] (15: $[(aIPr:)_3Hg]^-$)

To a mixture of $[K(aIPr:)]_\infty$ (111 mg, 0.260 mmol) and $HgCl_2$ (24 mg, 0.088 mmol) was added THF (5 mL) slowly under argon while stirring at –78 °C. The solution was then allowed to warm to ambient temperature to afford a pale orange solution and a viscous suspension. The suspension was given enough time to settle before the solution was filtered into a Schlenk containing 2,2,2-crypt (33 mg, 0.088 mmol). The solution was stirred until the 2,2,2-crypt dissolved and then layered in a crystallisation ampoule with hexane to afford colourless crystals of [K(2,2,2-crypt)][$(aIPr:)_3Hg$]. ^{1}H NMR (500.30 MHz, d_8-THF): δ (ppm) 7.31 (t, $^{3}J_{H–H}$ = 8 Hz, 3H; *para*-Dipp), 7.22 (d, $^{3}J_{H–H}$ = 8 Hz, 6H; *meta*-Dipp), 6.87 (d, $^{3}J_{H–H}$ = 8 Hz, 6H; *meta*-Dipp), 6.40 (t, $^{3}J_{H–H}$ = 8 Hz, 3H; *para*-Dipp), 4.37 (s, 3H; NCCHN), 2.97 (sept, $^{3}J_{H–H}$ = 7 Hz, 6H; $C_6H_3\{CH(CH_3)_2\}_2$), 2.71 (sept, $^{3}J_{H–H}$ = 7 Hz, 6H; $C_6H_3\{CH(CH_3)_2\}_2$), 1.34 (d, $^{3}J_{H–H}$ = 7 Hz, 18H; $C_6H_3\{CH(CH_3)_2\}_2$), 1.07 (d, $^{3}J_{H–H}$ = 7 Hz, 18H; $C_6H_3\{CH(CH_3)_2\}_2$), 1.06 (d, $^{3}J_{H–H}$ = 7 Hz, 18H; $C_6H_3\{CH(CH_3)_2\}_2$), 0.99 (d, $^{3}J_{H–H}$ = 7 Hz, 18H; $C_6H_3\{CH(CH_3)_2\}_2$). $^{13}C\{^{1}H\}$ (125.80 MHz, d_8-THF): δ (ppm) 214.4 (CN_2), 171.8 (NCCHN; satellites $^{1}J_{^{13}C–^{199}Hg}$ = 1526 Hz), 147.0, 146.7 (*ortho*-Dipp), 144.8, 141.6 (*ipso*-Dipp), 130.9 (NCCHN; satellites $^{2}J_{^{13}C–^{199}Hg}$ = 153 Hz), 127.5, 127.0 (*para*-Dipp), 123.4, 122.7 (*meta*-Dipp), 28.5, 28.3 ($C_6H_3\{CH(CH_3)_2\}_2$), 26.2, 24.4, 23.8, 23.2 ($C_6H_3\{CH(CH_3)_2\}_2$). $^{199}Hg\{^{1}H\}$ NMR (89.54 MHz, d_8-THF): δ (ppm) 14.0 (s).

7.2.2.3 [16][B(3,5-{CF_3}$_2$$C_6H_3$)$_4$]$_2$ (16: [(aIPr·Et_2O)$_2$Hg(Et_2O)]$^{2+}$)

To a mixture of (aIPr:)$_2$Hg (60 mg, 0.062 mmol) and [H(OEt_2)$_2$][B(3,5-{CF_3}$_2$$C_6H_3$)$_4$] (125 mg, 0.123 mmol) was added diethyl ether (5 mL) while stirring at ambient temperature. After 30 minutes, the pale orange solution was filtered into a crystallisation ampoule and layered with hexane to afford colourless crystals suitable for single crystal X-ray diffraction (133 mg, 74% crystalline yield). Anal. Calcd for $C_{130}H_{124}B_2F_{48}HgN_4O_3$ (2924.55): C 53.39%, H 4.27%, 1.92%. Found: C 53.31%, H 4.25%, N 1.98%. ESI-MS, positive-ion mode (DCM, 60 °C, 4.5 kV): *m*/*z* 489.2803 (100%) [(aIPr)$_2$Hg]$^{2+}$ (Calcd 489.2732), 1842.6138 (10%) [((aIPr)$_2$Hg)(B(3,5-{CF_3}$_2$$C_6H_3$)$_4$)]$^+$ (Calcd 1841.6112). ^{1}H NMR (500.30 MHz, d_8-THF): δ (ppm) 9.81 (d, $^4J_{H–H}$ = 1 Hz, 2H; *H*CN_2), 7.86 (d, $^4J_{H–H}$ = 1 Hz, 2H; NC(C*H*)N), 7.80 (br m, 16H; BC(C*H*)$_2$(CCF_3)$_2$CH), 7.71 (t, $^3J_{H–H}$ = 8 Hz, 2H; *para*-Dipp), 7.68 (t, $^3J_{H–H}$ = 8 Hz, 2H; *para*-Dipp), 7.59 (br s, 8H; BC(CH)$_2$(CCF_3)$_2$C*H*), 7.53 (d, $^3J_{H–H}$ = 8 Hz, 4H; *meta*-Dipp), 7.42 (d, $^3J_{H–H}$ = 8 Hz, 4H; *meta*-Dipp), 3.39 (q, $^3J_{H–H}$ = 7 Hz, 12H; O(C$H_2$$CH_3$)$_2$), 2.36 (sept, $^3J_{H–H}$ = 7 Hz, 4H; C_6H_3{C*H*(CH_3)$_2$}$_2$), 2.29 (sept, $^3J_{H–H}$ = 7 Hz, 4H; C_6H_3{C*H*(CH_3)$_2$}$_2$), 1.27 (d, $^3J_{H–H}$ = 7 Hz, 12H; C_6H_3{CH(C*H*$_3$)$_2$}$_2$), 1.20 (d, $^3J_{H–H}$ = 7 Hz, 12H; C_6H_3{CH(C*H*$_3$)$_2$}$_2$), 1.14 (d, $^3J_{H–H}$ = 7 Hz, 12H; C_6H_3{CH(C*H*$_3$)$_2$}$_2$), 1.12 (t, $^3J_{H–H}$ = 7 Hz, 18H; O(CH_2C*H*$_3$)$_2$), 1.05 (d, $^3J_{H–H}$ = 7 Hz, 12H; C_6H_3{CH(C*H*$_3$)$_2$}$_2$). ^{13}C{^{1}H} NMR (125.80 MHz, d_8-THF): δ (ppm) 162.8 (N*C*CHN), 162.6 (m, $^1J_{^{13}C–^{10}B}$ = 17 Hz, $^1J_{^{13}C–^{11}B}$ = 50 Hz, B*C*(CH)$_2$(CCF_3)$_2$CH), 145.7, 145.5 (*ortho*-Dipp), 142.8 (H*C*N_2), 135.4 (br s, BC(*C*H)$_2$(CCF_3)$_2$CH), 133.9 (NC*C*HN), 133.5, 133.3 (*para*-Dipp), 132.8, 130.6 (*ipso*-Dipp), 129.8 (qq, $^2J_{^{13}C–^{19}F}$ = 32 Hz, $^4J_{^{13}C–^{19}F}$ = 3 Hz, BC(CH)$_2$(*C*CF_3)$_2$CH), 126.2, 125.8 (*meta*-Dipp), 125.3 (q, $^1J_{^{13}C–^{19}F}$ = 273 Hz, BC(CH)$_2$(C*C*F_3)$_2$CH), 118.0 (br sept, $^3J_{^{13}C–^{19}F}$ = 4 Hz, BC(CH)$_2$(CCF_3)$_2$*C*H), 66.1 (O(*C*$H_2$$CH_3$)$_2$), 30.0, 29.8 ($C_6H_3${*C*H($CH_3$)$_2$}$_2$), 24.8, 24.5, 23.9, 23.3 (C_6H_3{CH(*C*H$_3$)$_2$}$_2$), 15.5 (O(CH_2*C*H$_3$)$_2$). ^{11}B NMR (128.39 MHz, d_8-THF): δ (ppm) –6.5 (s). ^{19}F NMR

(376.52 MHz, d_8-THF): δ (ppm) –63.3 (s). ^{199}Hg{^{1}H} NMR (89.54 MHz, d_8-THF): δ (ppm) –997.5 (s).

7.2.2.4 [17][B(3,5-{CF$_3$}$_2$C$_6$H$_3$)$_4$] (17: [(IPr)$_2$HgCl]$^+$)

To a mixture of IPr (348 mg, 0.897 mmol), $HgCl_2$ (122 mg, 0.448 mmol) and Na[B(3,5-{CF_3}$_2$$C_6H_3$)$_4$] (397 mg, 0.448 mmol) was added THF (15 mL) while stirring at ambient temperature to afford a pale orange solution and white precipitate. The mixture was allowed to stir overnight before filtration and removal of THF in vacuo. The solid was then washed with hexane (20 mL) and dried under vacuum (580 mg, 69% yield). Colourless crystals suitable for single crystal X-ray diffraction were grown by layering a THF solution with hexane. Anal. Calcd for $C_{86}H_{84}BClF_{24}HgN_4$ (1876.44): C 55.05%, H 4.51%, N 2.99%. Found: C 55.00%, H 4.55%, N 3.06%. ESI-MS, positive-ion mode (DCM, 60 °C, 4.5 kV): *m*/*z* 1013.5015 (100%) [(IPr)$_2$HgCl]$^+$ (Calcd 1013.5152). ^{1}H NMR (500.30 MHz, d_8-THF): δ (ppm) 7.84 (s, 4H; N(C*H*)$_2$N), 7.80 (br s, 8H; BC(C*H*)$_2$(CCF$_3$)$_2$CH), 7.58 (br s, 4H; BC(CH)$_2$(CCF$_3$)$_2$C*H*), 7.57 (t, $^3J_{H–H}$ = 8 Hz, 4H; *para*-Dipp), 7.24 (d, $^3J_{H–H}$ = 8 Hz, 8H; *meta*-Dipp), 2.56 (sept, $^3J_{H–H}$ = 7 Hz, 4H; C$_6$H$_3${C*H*(CH$_3$)$_2$}$_2$), 1.03 (d, $^3J_{H–H}$ = 7 Hz, 12H; C$_6$H$_3${C*H*(CH$_3$)$_2$}$_2$), 0.98 (d, $^3J_{H–H}$ = 7 Hz, 12H; C$_6$H$_3${C*H*(CH$_3$)$_2$}$_2$). ^{13}C{^{1}H} NMR (125.80 MHz, d_8-THF): δ (ppm) 182.3 (*C*N$_2$; satellites $^1J_{^{13}C–^{199}Hg}$ = 2644 Hz), 163.0 (m, $^1J_{^{13}C–^{10}B}$ = 17 Hz, $^1J_{^{13}C–^{11}B}$ = 50 Hz, B*C*(CH)$_2$(CCF$_3$)$_2$CH), 146.7 (*ortho*-Dipp), 135.8 (br s, BC(*C*H)$_2$(CCF$_3$)$_2$CH), 134.0 (*ipso*-Dipp), 132.7 (*para*-Dipp), 130.2 (qq, $^2J_{^{13}C–^{19}F}$ = 32 Hz, $^4J_{^{13}C–^{19}F}$ = 3 Hz, BC(CH)$_2$(*C*CF$_3$)$_2$CH), 128.8 (N(*C*H)$_2$N; satellites $^3J_{^{13}C–^{199}Hg}$ = 75 Hz), 126.1 (*meta*-Dipp), 125.7 (q, $^1J_{^{13}C–^{19}F}$ = 273 Hz, BC(CH)$_2$(C*C*F$_3$)$_2$CH), 118.4 (br sept, $^3J_{^{13}C–^{19}F}$ = 4 Hz, BC(CH)$_2$(CCF$_3$)$_2$*C*H), 29.7 (C$_6$H$_3${*C*H(CH$_3$)$_2$}$_2$), 25.6, 24.3 (C$_6$H$_3${CH(*C*H$_3$)$_2$}$_2$). ^{11}B NMR (128.39 MHz, d_8-THF): δ (ppm) –6.5 (s). ^{19}F NMR

(376.52 MHz, d_8-THF): δ (ppm) –63.3 (s). ^{199}Hg{^{1}H} NMR (89.54 MHz, d_8-THF): δ (ppm) –700.2 (s).

7.2.2.5 (aIPr:)$_2$SiCl$_2$ (18)

To a suspension of [K(aIPr:)]$_\infty$ (700 mg, 1.642 mmol) in hexane (25 mL) was added a solution of $SiCl_4$ (140 mg, 0.821 mmol) in hexane (5 mL) while stirring at ambient temperature. The pale orange suspension was then allowed to stir overnight. The solution was then filtered and the solvent removed in vacuo to afford a fine, off-white solid (460 mg, 64% yield). Colourless crystals suitable for single crystal X-ray diffraction were grown from a concentrated hexane solution at 4 °C. ^{1}H NMR (500.30 MHz, d_8-THF): δ (ppm) 7.52 (s, 2H; NCC*H*N); 7.39 (t, $^3J_{H–H}$ = 8 Hz, 2H; *para*-Dipp); 7.34 (t, $^3J_{H–H}$ = 8 Hz, 2H; *para*-Dipp); 7.27 (d, $^3J_{H–H}$ = 8 Hz, 4H; *meta*-Dipp); 7.21 (d, $^3J_{H–H}$ = 8 Hz, 4H; *meta*-Dipp); 2.71 (sept, $^3J_{H–H}$ = 7 Hz, 4H; $C_6H_3\{CH(CH_3)_2\}_2$); 2.61 (sept, $^3J_{H–H}$ = 7 Hz, 4H; $C_6H_3\{CH(CH_3)_2\}_2$); 1.21 (d, $^3J_{H–H}$ = 7 Hz, 12H; $C_6H_3\{CH(CH_3)_2\}_2$); 1.13 (d, $^3J_{H–H}$ = 7 Hz, 12H; $C_6H_3\{CH(CH_3)_2\}_2$); 1.12 (d, $^3J_{H–H}$ = 7 Hz, 12H; $C_6H_3\{CH(CH_3)_2\}_2$); 1.08 (d, $^3J_{H–H}$ = 7 Hz, 12H; $C_6H_3\{CH(CH_3)_2\}_2$). ^{13}C{^{1}H} NMR (125.80 MHz, d_8-THF): δ (ppm) 225.9 (CN_2); 147.2, 146.5 (*ortho*-Dipp); 138.8, 138.4 (*ipso*-Dipp); 136.3 (NC*C*HN; satellites $^2J_{^{13}C–^{29}Si}$ = 16 Hz); 130.1, 130.0 (*para*-Dipp); 126.6 (N*C*CHN; satellites $^1J_{^{13}C–^{29}Si}$ = 113 Hz); 124.4, 124.0 (*meta*-Dipp); 29.9, 29.4 ($C_6H_3\{CH(CH_3)_2\}_2$); 26.2, 24.9, 24.1, 22.5 ($C_6H_3\{CH(CH_3)_2\}_2$). ^{29}Si{^{1}H} NMR (99.31 MHz, d_8-THF): δ (ppm) –18.1 (s). ^{1}H NMR (500.30 MHz, C_6D_6): δ (ppm) 7.34 (s, 2H; NCC*H*N); 7.24 (m, 4H; *para*-Dipp); 7.14 (d, $^3J_{H–H}$ = 8 Hz, 4H; *meta*-Dipp); 7.11 (d, $^3J_{H–H}$ = 8 Hz, 4H; *meta*-Dipp); 2.89 (sept, $^3J_{H–H}$ = 7 Hz, 4H; $C_6H_3\{CH(CH_3)_2\}_2$); 2.85 (sept, $^3J_{H–H}$ = 7 Hz, 4H; $C_6H_3\{CH(CH_3)_2\}_2$); 1.32 (d, $^3J_{H–H}$ = 7 Hz, 12H; $C_6H_3\{CH(CH_3)_2\}_2$); 1.27 (d, $^3J_{H–H}$ = 7 Hz, 12H; $C_6H_3\{CH(CH_3)_2\}_2$); 1.19 (d, $^3J_{H–H}$ = 7 Hz, 12H; $C_6H_3\{CH(CH_3)_2\}_2$); 1.05 (d, $^3J_{H–H}$ = 7 Hz, 12H; $C_6H_3\{CH(CH_3)_2\}_2$). ^{13}C{^{1}H} NMR (125.80 MHz, C_6D_6): δ (ppm)

226.6 (*C*N_2); 146.6, 145.9 (*ortho*-Dipp); 138.1, 137.7 (*ipso*-Dipp); 135.3 (NC*C*HN); 129.7, 129.5 (*para*-Dipp); 126.4 (N*C*CHN); 123.9, 123.6 (*meta*-Dipp); 29.4, 28.8 ($C_6H_3\{CH(CH_3)_2\}_2$); 25.9, 24.6, 23.7, 22.2 ($C_6H_3\{CH(CH_3)_2\}_2$). $^{29}Si\{^1H\}$ NMR (99.31 MHz, C_6D_6): δ (ppm) –18.0 (s).

7.2.2.6 (aIPr:)$_2$SiBr$_2$ (19)

To a suspension of $[Li(aIPr:)]_\infty$ (2.439 mg, 6.190 mmol) in hexane (50 mL) was added a solution of $SiBr_4$ (1076 mg, 3.095 mmol) in hexane (10 mL) while stirring at ambient temperature. The pale orange suspension was then allowed to stir overnight. The solution was then filtered and the solvent concentrated to approximately 10 mL to promote crystallisation which may occur spontaneously at room temperature. Crystallisation may be induced by sonication or by cooling the solution in a –80 °C freezer. The orange solution was then filtered from the colourless crystals which were then dried under vacuum (1.583 g, 53% crystalline yield). Alternatively, a solution of $SiBr_4$ (1.080 g, 3.106 mmol) in THF (5 mL) was added to a solution of IPr (4.821 g, 4.821 mmol) in THF (40 mL) while stirring in an ampoule. The orange solution was then heated to 65 °C and stirred for four days to afford a precipitate. The solution was then filtered and the solvent removed in vacuo to afford an off-white solid. The product was then extracted with toluene (30 mL) to afford an off-white solid (1.414 g, 47% yield). Anal. Calcd for $C_{54}H_{70}Br_2N_4Si$ (963.06): C 67.35%, H 7.33%, N 5.82%. Found: C 66.08%, H 7.52%, N 5.69%. ^1H NMR (500.30 MHz, d_8-THF): δ (ppm) 7.47 (s, 2H; NCC*H*N); 7.39 (t, $^3J_{H–H}$ = 8 Hz, 2H; *para*-Dipp); 7.33 (t, $^3J_{H–H}$ = 8 Hz, 2H; *para*-Dipp); 7.27 (d, $^3J_{H–H}$ = 8 Hz, 4H; *meta*-Dipp); 7.21 (d, $^3J_{H–H}$ = 8 Hz, 4H; *meta*-Dipp); 2.71 (sept, $^3J_{H–H}$ = 7 Hz, 4H; $C_6H_3\{CH(CH_3)_2\}_2$); 2.64 (sept, $^3J_{H–H}$ = 7 Hz, 4H; $C_6H_3\{CH(CH_3)_2\}_2$); 1.24 (d, $^3J_{H–H}$ = 7 Hz, 12H; $C_6H_3\{CH(CH_3)_2\}_2$); 1.13 (d, $^3J_{H–H}$ = 7 Hz, 12H; $C_6H_3\{CH(CH_3)_2\}_2$); 1.12 (d, $^3J_{H–H}$ = 7 Hz, 12H; $C_6H_3\{CH(CH_3)_2\}_2$); 1.08 (d, $^3J_{H–H}$ = 7 Hz, 12H;

$C_6H_3\{CH(CH_3)_2\}_2$). $^{13}C\{^1H\}$ NMR (125.80 MHz, d_8-THF): δ (ppm) 221.2 (*C*N_2); 147.4, 146.5 (*ortho*-Dipp); 138.7, 138.4 (*ipso*-Dipp); 136.1 (NC*C*HN); 130.1, 130.0 (*para*-Dipp); 126.4 (N*C*CHN); 124.4, 124.0 (*meta*-Dipp); 30.0, 29.0 ($C_6H_3\{CH(CH_3)_2\}_2$); 26.3, 24.9, 24.1, 22.6 ($C_6H_3\{CH(CH_3)_2\}_2$). $^{29}Si\{^1H\}$ NMR (99.32 MHz, d_8-THF): δ (ppm) –38.9 (s). ^1H NMR (500.30 MHz, C_6D_6): δ (ppm) 7.37 (s, 2H; NCC*H*N); 7.25 (t, $^3J_{H–H}$ = 8 Hz, 2H; *para*-Dipp); 7.24 (t, $^3J_{H–H}$ = 8 Hz, 2H; *para*-Dipp); 7.15 (d, $^3J_{H–H}$ = 8 Hz, 4H; *meta*-Dipp); 7.11 (d, $^3J_{H–H}$ = 8 Hz, 4H; *meta*-Dipp); 2.90 (sept, $^3J_{H–H}$ = 7 Hz, 4H; $C_6H_3\{CH(CH_3)_2\}_2$); 2.88 (sept, $^3J_{H–H}$ = 7 Hz, 4H; $C_6H_3\{CH(CH_3)_2\}_2$); 1.33 (d, $^3J_{H–H}$ = 7 Hz, 12H; $C_6H_3\{CH(CH_3)_2\}_2$); 1.30 (d, $^3J_{H–H}$ = 7 Hz, 12H; $C_6H_3\{CH(CH_3)_2\}_2$); 1.19 (d, $^3J_{H–H}$ = 7 Hz, 12H; $C_6H_3\{CH(CH_3)_2\}_2$); 1.05 (d, $^3J_{H–H}$ = 7 Hz, 12H; $C_6H_3\{CH(CH_3)_2\}_2$). $^{13}C\{^1H\}$ NMR (125.80 MHz, C_6D_6): δ (ppm) 226.8 (*C*N_2); 146.8, 145.9 (*ortho*-Dipp); 138.0, 137.6 (*ipso*-Dipp); 135.1 (NC*C*HN); 129.7, 129.5 (*para*-Dipp); 126.2 (N*C*CHN); 123.9, 123.6 (*meta*-Dipp); 29.4, 28.8 ($C_6H_3\{CH(CH_3)_2\}_2$); 26.0, 24.5, 23.8, 22.3 ($C_6H_3\{CH(CH_3)_2\}_2$). $^{29}Si\{^1H\}$ NMR (99.32 MHz, C_6D_6): δ (ppm) –36.9 (s).

7.2.2.7 (aIPr:)$_2$GeCl$_2$ (20)

To a suspension of $[K(aIPr:)]_\infty$ (1.459 g, 3.423 mmol) in hexane (50 mL) was added a solution of $GeCl_4$ (367 mg, 1.712 mmol) in hexane (10 mL) while stirring at ambient temperature. The pale orange suspension was then allowed to stir overnight. The solution was then filtered and the solvent removed in vacuo to afford a fine, off-white solid (858 mg, 55% yield). Colourless crystals suitable for single crystal X-ray diffraction were grown from a 1 : 1 mixture of hexane and toluene at –35 °C. Anal. Calcd for $C_{54}H_{70}Cl_2GeN_4$ (918.71): C 70.60%, H 7.68%, N 6.10%. Found: C 70.58%, H 7.80%, N 5.96%. EI-MS: *m/z* 186.1263 (58%) $[Dipp–(CH)=(CH)]^+$ (Calcd 187.1487), 387.2635 (100%) $[aIPr:]^+$ (Calcd 387.2800), 918.2744 (3%) $[(aIPr:)_2GeCl_2]^+$ (Calcd 918.4189). ^1H NMR (500.30 MHz, C_6D_6): δ (ppm) 7.26 (t,

$^{3}J_{H–H}$ = 8 Hz, 2H; *para*-Dipp); 7.11–7.17 (m, 10H; *meta*-Dipp and *para*-Dipp); 6.88 (s, 2H; NCC*H*N); 2.87 (sept, $^{3}J_{H–H}$ = 7 Hz, 4H; $C_6H_3\{CH(CH_3)_2\}_2$); 2.83 (sept, $^{3}J_{H–H}$ = 7 Hz, 4H; $C_6H_3\{CH(CH_3)_2\}_2$); 1.29 (d, $^{3}J_{H–H}$ = 7 Hz, 12H; $C_6H_3\{CH(CH_3)_2\}_2$); 1.28 (d, $^{3}J_{H–H}$ = 7 Hz, 12H; $C_6H_3\{CH(CH_3)_2\}_2$); 1.21 (d, $^{3}J_{H–H}$ = 7 Hz, 12H; $C_6H_3\{CH(CH_3)_2\}_2$); 1.16 (d, $^{3}J_{H–H}$ = 7 Hz, 12H; $C_6H_3\{CH(CH_3)_2\}_2$). $^{13}C\{^{1}H\}$ NMR (125.80 MHz, C_6D_6): δ (ppm) 225.9 (CN_2); 146.9, 145.9 (*ortho*-Dipp); 137.9, 137.6 (*ipso*-Dipp); 132.3 (NC*C*HN); 129.9, 129.5 (*para*-Dipp); 127.0 (N*C*CHN); 123.9, 123.8 (*meta*-Dipp); 29.3, 28.8 ($C_6H_3\{CH(CH_3)_2\}_2$); 25.8, 24.8, 23.7, 22.4 ($C_6H_3\{CH(CH_3)_2\}_2$).

7.2.2.8 (aIPr:)$_2$GeBr$_2$ (21)

To a suspension of [Li(aIPr:)]$_\infty$ (2.109 g, 5.353 mmol) in hexane (40 mL) was added a solution of $GeBr_4$ (1.050 g, 2.676 mmol) in hexane (10 mL) while stirring at ambient temperature. The pale orange suspension was then allowed to stir overnight. The solution was then filtered and the solvent concentrated to approximately 10 mL to promote crystallisation which may occur spontaneously at room temperature. Crystallisation may be induced by sonication or by cooling the solution in a –80 °C freezer. The orange solution was then filtered from the colourless crystals and the solid dried under vacuum (1.534 g, 57% crystalline yield). The solvent from the filtrate was removed in vacuo to afford the remainder of the product as an amorphous off-white solid (653 mg, 81% combined yield). Alternatively, a solution of $GeBr_4$ (1.005 g, 2.562 mmol) in THF (5 mL) was added to a solution of IPr (3.976 g, 10.247 mmol) in THF (40 mL) while stirring in an ampoule. A precipitate immediately began to form from the solution and the mixture was then heated to 65 °C and stirred for four days to afford a white crystalline precipitate of the imidazolium bromide which can be recovered and recycled. The pale orange solution was then filtered and the solvent removed in vacuo to afford an off-white solid. The product was then extracted with toluene (30 mL) to afford an off-white

solid (1.560 g, 60% yield). Colourless crystals suitable for single crystal X-ray diffraction were grown from toluene at –35 °C. Anal. Calcd for $C_{54}H_{70}Br_2GeN_4$ (1007.61): C 64.37%, H 7.00%, N 5.56%. Found: C 64.03%, H 7.24%, N 5.48%. ^{1}H NMR (500.30 MHz, d_8-THF): δ (ppm) 7.40 (t, $^3J_{H–H}$ = 8 Hz, 2H; *para*-Dipp); 7.26–7.30 (m, 6H; *meta*-Dipp and *para*-Dipp); 7.21 (d, $^3J_{H–H}$ = 8 Hz, 4H; *meta*-Dipp); 7.15 (s, 2H; NCC*H*N); 2.68 (sept, $^3J_{H–H}$ = 7 Hz, 4H; $C_6H_3\{CH(CH_3)_2\}_2$); 2.65 (sept, $^3J_{H–H}$ = 7 Hz, 4H; $C_6H_3\{CH(CH_3)_2\}_2$); 1.24 (d, $^3J_{H–H}$ = 7 Hz, 12H; $C_6H_3\{CH(CH_3)_2\}_2$); 1.14 (d, $^3J_{H–H}$ = 7 Hz, 12H; $C_6H_3\{CH(CH_3)_2\}_2$); 1.13 (d, $^3J_{H–H}$ = 7 Hz, 12H; $C_6H_3\{CH(CH_3)_2\}_2$); 1.12 (d, $^3J_{H–H}$ = 7 Hz, 12H; $C_6H_3\{CH(CH_3)_2\}_2$). $^{13}C\{^1H\}$ NMR (125.80 MHz, d_8-THF): δ (ppm) 226.5 (CN_2); 147.5, 146.5 (*ortho*-Dipp); 138.4, 138.3 (*ipso*-Dipp); 132.7 (NC*C*HN); 130.3, 130.0 (*para*-Dipp); 127.1 (N*C*CHN); 124.4, 124.3 (*meta*-Dipp); 29.9, 29.4 ($C_6H_3\{CH(CH_3)_2\}_2$); 26.1, 25.0, 24.1, 22.7 ($C_6H_3\{CH(CH_3)_2\}_2$). ^{1}H NMR (500.30 MHz, C_6D_6): δ (ppm) 7.26 (t, $^3J_{H–H}$ = 8 Hz, 2H; *para*-Dipp); 7.11–7.17 (m, 10H; *meta*-Dipp and *para*-Dipp); 6.93 (s, 2H; NCC*H*N); 2.89 (sept, $^3J_{H–H}$ = 7 Hz, 4H; $C_6H_3\{CH(CH_3)_2\}_2$); 2.85 (sept, $^3J_{H–H}$ = 7 Hz, 4H; $C_6H_3\{CH(CH_3)_2\}_2$); 1.30 (d, $^3J_{H–H}$ = 7 Hz, 24H; $C_6H_3\{CH(CH_3)_2\}_2$); 1.21 (d, $^3J_{H–H}$ = 7 Hz, 12H; $C_6H_3\{CH(CH_3)_2\}_2$); 1.12 (d, $^3J_{H–H}$ = 7 Hz, 12H; $C_6H_3\{CH(CH_3)_2\}_2$). $^{13}C\{^1H\}$ NMR (125.80 MHz, C_6D_6): δ (ppm) 225.8 (CN_2); 147.0, 145.9 (*ortho*-Dipp); 137.8, 137.7 (*ipso*-Dipp); 132.0 (NC*C*HN); 129.8, 129.5 (*para*-Dipp); 126.8 (N*C*CHN); 124.0, 123.9 (*meta*-Dipp); 29.3, 28.8 ($C_6H_3\{CH(CH_3)_2\}_2$); 25.8, 24.7, 23.8, 22.5 ($C_6H_3\{CH(CH_3)_2\}_2$).

7.2.2.9 (IPr)GeBr$_2$ (22)

To a mixture of IPr (175 mg, 0.451 mmol) and $GeBr_4$ (177 mg, 0.451 mmol) was added diethyl ether (15 mL) while stirring at ambient temperature to immediately afford a colourless precipitate. The mixture was stirred for one hour before the solution was filtered and cooled to –35 °C to afford large colourless crystals (95 mg, 68% crystalline yield). ^{1}H NMR

(500.30 MHz, d_8-THF): δ (ppm) 7.67 (s, 2H; NC*H*$_2$N); 7.50 (t, $^3J_{H–H}$ = 8 Hz, 2H; *para*-Dipp); 7.33 (d, $^3J_{H–H}$ = 8 Hz, 4H; *meta*-Dipp); 2.76 (sept, $^3J_{H–H}$ = 7 Hz, 4H; C$_6$H$_3${C*H*(CH$_3$)$_2$}$_2$); 1.37 (d, $^3J_{H–H}$ = 7 Hz, 12H; C$_6$H$_3${CH(C*H*$_3$)$_2$}$_2$); 1.16 (d, $^3J_{H–H}$ = 7 Hz, 12H; C$_6$H$_3${CH(C*H*$_3$)$_2$}$_2$). ^{13}C{^{1}H} NMR (125.80 MHz, d_8-THF): δ (ppm) 169.1 (*C*N$_2$); 146.8 (*ortho*-Dipp); 134.4 (*ipso*-Dipp); 131.8 (*para*-Dipp); 126.9 (NC*C*HN); 125.0 (*meta*-Dipp); 30.1 (C$_6$H$_3${*C*H(CH$_3$)$_2$}$_2$); 26.0, 23.5 (C$_6$H$_3${CH(*C*H$_3$)$_2$}$_2$).

7.2.2.10 [23][OTf]$_2$ (23: [(aIPr)$_2$SiBr$_2$]$^{2+}$)

To a stirring solution of (aIPr:)$_2$SiBr$_2$ (250 mg, 0.260 mmol) in DFB (5 mL) was added HOTf (46 μL, 0.520 mmol) via microsyringe. The initially pale yellow solution instantly turned colourless and the solution was allowed to stir for a further 30 minutes before the volatiles were removed in vacuo to afford a fine white powder (285 mg, 87% yield). Crystals suitable for single crystal X-ray diffraction were grown by layering a DCM solution with hexane. ESI-MS, positive ion mode (DCM, 60 °C, 4.5 kV): *m*/*z* 987.5142 (100%) [(aIPr)$_2$Si(OH)$_2$(OTf)]$^+$ (Calcd 987.5096), 919.4720 (13%) [(aIPr)$_2$Si(OH)$_2$Br]$^+$ (Calcd 919.4743), 873.5179 (13%) [(aIPr)$_2$Si(OH)$_2$Cl]$^+$ (Calcd 873.5264), 461.3559 (20%) [(aIPr)$_2$Si(OH)$_2$(CH$_2$Cl$_2$)]$^{2+}$ (Calcd 461.2552). ^{1}H NMR (500.30 MHz, CD$_2$Cl$_2$): δ (ppm) 9.84 (s, 2H; *H*CN$_2$); 8.40 (s, 2H; NCC*H*N); 7.63 (t, $^3J_{H–H}$ = 8 Hz, 4H; *para*-Dipp); 7.37 (d, $^3J_{H–H}$ = 8 Hz, 8H; *meta*-Dipp); 2.35 (sept, $^3J_{H–H}$ = 7 Hz, 4H; C$_6$H$_3${C*H*(CH$_3$)$_2$}$_2$); 2.29 (sept, $^3J_{H–H}$ = 7 Hz, 4H; C$_6$H$_3${C*H*(CH$_3$)$_2$}$_2$); 1.29 (d, $^3J_{H–H}$ = 7 Hz, 12H; C$_6$H$_3${CH(C*H*$_3$)$_2$}$_2$); 1.17 (d, $^3J_{H–H}$ = 7 Hz, 24H; C$_6$H$_3${CH(C*H*$_3$)$_2$}$_2$); 1.14 (d, $^3J_{H–H}$ = 7 Hz, 12H; C$_6$H$_3${CH(C*H*$_3$)$_2$}$_2$). ^{13}C{^{1}H} NMR (125.80 MHz, CD$_2$Cl$_2$): δ (ppm) 146.0, 145.1 (*ortho*-Dipp); 144.9 (H*C*N$_2$); 137.2 (NC*C*HN); 133.5, 132.9 (*para*-Dipp); 129.4, 129.3 (*ipso*-Dipp); 127.0 (N*C*CHN); 125.4, 125.3 (*meta*-Dipp); 120.7 (q, $^1J_{^{13}C–^{19}F}$ = 320 Hz); 29.9, 29.7 (C$_6$H$_3${*C*H(CH$_3$)$_2$}$_2$); 26.0,

24.5, 24.0, 22.5 ($C_6H_3\{CH(CH_3)_2\}_2$). $^{29}Si\{^1H\}$ NMR (99.32 MHz, CD_2Cl_2): δ (ppm) –42.6 (s).

7.2.2.11 [24][OTf]$_2$ (24: [(aIPr)$_2$Si(OCH$_2$CH$_2$CH$_2$CH$_2$Br)$_2$]$^{2+}$)

To a stirring solution of (aIPr:)$_2$SiBr$_2$ (308 mg, 0.320 mmol) in THF (5 mL) was added HOTf (56 μL, 0.640 mmol) via microsyringe. The initially pale yellow solution instantly turned colourless and the solution was allowed to stir for a further 30 minutes before the volatiles were removed in vacuo to afford a fine white powder (343 mg, 85% yield). Single crystals suitable for single crystal X-ray diffraction were grown by layering a THF solution with hexane. ESI-MS, positive ion mode (DCM, 60 °C, 4.5 kV): *m*/*z* 1257.4570 (100%) $[(aIPr)_2Si(OCH_2CH_2CH_2CH_2Br)_2(OTf)]^+$ (Calcd 1257.4547), 554.2574 (17%) $[(aIPr)_2Si(OCH_2CH_2CH_2CH_2Br)_2]^{2+}$ (Calcd 554.2511), ^1H NMR (500.30 MHz, CD_2Cl_2): δ (ppm) 9.57 (s, 2H; *H*CN$_2$); 8.10 (s, 2H; NCC*H*N); 7.63 (t, $^3J_{H–H}$ = 8 Hz, 4H; *para*-Dipp); 7.41 (d, $^3J_{H–H}$ = 8 Hz, 4H; *meta*-Dipp); 7.38 (d, $^3J_{H–H}$ = 8 Hz, 4H; *meta*-Dipp); 3.24–3.29 (m, 8H; OC*H*$_2$CH$_2$CH$_2$C*H*$_2$Br); 2.34 (sept, $^3J_{H–H}$ = 7 Hz, 4H; $C_6H_3\{CH(CH_3)_2\}_2$); 2.28 (sept, $^3J_{H–H}$ = 7 Hz, 4H; $C_6H_3\{CH(CH_3)_2\}_2$); 1.45–1.53 (m, 4H; OCH$_2$C*H*$_2$CH$_2$CH$_2$Br); 1.30 (d, $^3J_{H–H}$ = 7 Hz, 12H; $C_6H_3\{CH(CH_3)_2\}_2$); 1.18–1.27 (m, 4H; OCH$_2$CH$_2$C*H*$_2$CH$_2$Br); 1.19 (d, $^3J_{H–H}$ = 7 Hz, 12H; $C_6H_3\{CH(CH_3)_2\}_2$); 1.18 (d, $^3J_{H–H}$ = 7 Hz, 12H; $C_6H_3\{CH(CH_3)_2\}_2$); 1.17 (d, $^3J_{H–H}$ = 7 Hz, 12H; $C_6H_3\{CH(CH_3)_2\}_2$). $^{13}C\{^1H\}$ NMR (125.80 MHz, CD_2Cl_2): δ (ppm) 145.6, 146.0 (*ortho*-Dipp); 143.9 (H*C*N$_2$); 136.6 (NC*C*HN); 133.1, 132.9 (*para*-Dipp); 130.9, 130.3 (*ipso*-Dipp); 129.3 (N*C*CHN); 125.4, 125.3 (*meta*-Dipp); 120.7 (q, $^1J_{^{13}C–^{19}F}$ = 320 Hz); 65.1 (O*C*H$_2$CH$_2$CH$_2$CH$_2$Br); 33.5 (OCH$_2$CH$_2$CH$_2$*C*H$_2$Br); 30.3 (OCH$_2$C*H*$_2$CH$_2$CH$_2$Br); 29.8, 29.7 ($C_6H_3\{CH(CH_3)_2\}_2$); 28.6 (OCH$_2$CH$_2$C*H*$_2$CH$_2$Br); 25.8, 24.5, 24.0, 23.0 ($C_6H_3\{CH(CH_3)_2\}_2$). $^{29}Si\{^1H\}$ NMR (99.32 MHz, CD_2Cl_2): δ (ppm) –56.9 (s). ^{19}F NMR (376.54 MHz, CD_2Cl_2): δ (ppm) –79.2 (s).

7.2.2.12 [25][B(3,5-{CF_3}$_2$$C_6H_3$)$_4$]$_2$ (25: [(aIPr)$_2$$GeCl_2$]$^{2+}$)

To a mixture of (aIPr:)$_2$$GeCl_2$ (50 mg, 0.054 mmol) and [H(OEt_2)$_2$][B(3,5-{CF_3}$_2$$C_6H_3$)$_4$] (110 mg, 0.109 mmol) was added diethyl ether (5 mL) while stirring at ambient temperature. The solution was stirred for 30 minutes then filtered into a crystallisation ampoule and layered with hexane to afford colourless crystals of [**25**][B(3,5-{CF_3}$_2$$C_6H_3$)$_4$]$_2$·2$Et_2O$ suitable for single crystal X-ray diffraction (92 mg, 0.031 mmol, 58% crystalline yield). ^{1}H NMR (500.30 MHz, d_8-THF): δ (ppm) 10.25 (s, 2H; *H*CN_2); 8.35 (s, 2H; NCC*H*N); 7.81 (s, 16H; BC(C*H*)$_2$(CCF_3)$_2$CH); 7.74 (t, $^3J_{H–H}$ = 8 Hz, 2H; *para*-Dipp); 7.72 (t, $^3J_{H–H}$ = 8 Hz, 2H; *para*-Dipp); 7.59 (s, 8H; BC(CH)$_2$(CCF_3)$_2$C*H*); 7.54–7.59 (m, 8H; *meta*-Dipp); 2.44 (sept, $^3J_{H–H}$ = 7 Hz, 2H; C_6H_3{C*H*(CH_3)$_2$}$_2$); 2.35 (sept, $^3J_{H–H}$ = 7 Hz, 2H; C_6H_3{C*H*(CH_3)$_2$}$_2$); 2.34 (sept, $^3J_{H–H}$ = 7 Hz, 2H; C_6H_3{C*H*(CH_3)$_2$}$_2$); 2.29 (sept, $^3J_{H–H}$ = 7 Hz, 2H; C_6H_3{C*H*(CH_3)$_2$}$_2$); 1.39 (d, $^3J_{H–H}$ = 7 Hz, 6H; C_6H_3{CH(C*H*$_3$)$_2$}$_2$); 1.35 (d, $^3J_{H–H}$ = 7 Hz, 6H; C_6H_3{CH(C*H*$_3$)$_2$}$_2$); 1.30 (d, $^3J_{H–H}$ = 7 Hz, 6H; C_6H_3{CH(C*H*$_3$)$_2$}$_2$); 1.28 (d, $^3J_{H–H}$ = 7 Hz, 6H; C_6H_3{CH(C*H*$_3$)$_2$}$_2$); 1.24 (d, $^3J_{H–H}$ = 7 Hz, 6H; C_6H_3{CH(C*H*$_3$)$_2$}$_2$); 1.23 (d, $^3J_{H–H}$ = 7 Hz, 6H; C_6H_3{CH(C*H*$_3$)$_2$}$_2$); 1.19 (d, $^3J_{H–H}$ = 7 Hz, 6H; C_6H_3{CH(C*H*$_3$)$_2$}$_2$); 1.18 (d, $^3J_{H–H}$ = 7 Hz, 6H; C_6H_3{CH(C*H*$_3$)$_2$}$_2$). ^{13}C{^{1}H} NMR (125.80 MHz, d_8-THF): δ (ppm) 163.0 (m, $^1J_{^{13}C–^{11}B}$ = 50 Hz, $^1J_{^{13}C–^{10}B}$ = 17 Hz; B*C*(CH)$_2$(CCF_3)$_2$CH); 146.8, 146.6 (*ortho*-Dipp); 146.1 (H*C*N_2); 145.9, 145.8 (*ortho*-Dipp); 135.8 (×2) (BC(*C*H)$_2$(CCF_3)$_2$CH and NC*C*HN); 134.6, 134.4 (*para*-Dipp); 131.6 (N*C*CHN); 130.5 (*ipso*-Dipp); 130.2 (qq, $^2J_{^{13}C–^{19}F}$ = 31 Hz, $^4J_{^{13}C–^{19}F}$ = 2 Hz; BC(CH)$_2$(*C*CF_3)$_2$CH); 130.1 (*ipso*-Dipp); 126.6, 126.5, 126.4 (×2) (*meta*-Dipp); 125.7 (q, $^1J_{^{13}C–^{19}F}$ = 271 Hz; BC(CH)$_2$(C*C*F_3)$_2$CH); 118.4 (sept, $^3J_{^{13}C–^{19}F}$ = 4 Hz; BC(CH)$_2$(CCF_3)$_2$*C*H); 30.8, 30.7, 30.5 (×2) (C_6H_3{*C*H(CH_3)$_2$}$_2$); 26.4, 26.0, 25.0, 24.8, 24.1, 23.9, 22.7, 22.4 (C_6H_3{CH(*C*H_3)$_2$}$_2$).

7.2.2.13 [26][OTf]$_2$ (26: [(aIPr)$_2$GeBr$_2$]$^{2+}$)

To a stirring solution of (aIPr:)$_2$GeBr$_2$ (140 mg, 0.139 mmol) in THF (5 mL) was added HOTf (25 μL, 0.278 mmol) via microsyringe. The colourless solution was allowed to stir for a further 30 minutes before the volatiles were removed in vacuo to afford a fine white powder (144 mg, 79% yield). Single crystals suitable for single crystal X-ray diffraction were grown by layering a THF solution with hexane. Anal. Calcd for $C_{56}H_{72}Br_2F_6GeN_4O_6S_2$ (1307.76): C 51.43%, H 5.55%, N 4.28%. Found: C 52.14%, H 5.80%, N 4.24%. ESI-MS, positive ion mode (DCM, 60 °C, 4.5 kV): *m*/*z* 1033.4619 (100%) $[(aIPr)_2Ge(OH)_2(OTf)]^+$ (Calcd 1033.4552), 963.4362 (51%) $[(aIPr)_2Ge(OH)_2Br]^+$ (Calcd 963.4210), 919.4523 (38%) $[(aIPr)_2Ge(OH)_2Cl]^+$ (Calcd 919.4716). ^{1}H NMR (500.30 MHz, CD_2Cl_2): δ (ppm) 9.70 (s, 2H; *H*CN$_2$); 8.04 (s, 2H; NCC*H*N); 7.64 (t, $^3J_{H–H}$ = 8 Hz, 2H; *para*-Dipp); 7.58 (t, $^3J_{H–H}$ = 8 Hz, 2H; *para*-Dipp); 7.39 (d, $^3J_{H–H}$ = 8 Hz, 4H; *meta*-Dipp); 7.38 (d, $^3J_{H–H}$ = 8 Hz, 4H; *meta*-Dipp); 2.46 (sept, $^3J_{H–H}$ = 7 Hz, 4H; C$_6$H$_3${C*H*(CH$_3$)$_2$}$_2$); 2.31 (sept, $^3J_{H–H}$ = 7 Hz, 4H; C$_6$H$_3${C*H*(CH$_3$)$_2$}$_2$); 1.31 (d, $^3J_{H–H}$ = 7 Hz, 12H; C$_6$H$_3${CH(C*H*$_3$)$_2$}$_2$); 1.23 (d, $^3J_{H–H}$ = 7 Hz, 12H; C$_6$H$_3${CH(C*H*$_3$)$_2$}$_2$); 1.20 (d, $^3J_{H–H}$ = 7 Hz, 12H; C$_6$H$_3${CH(C*H*$_3$)$_2$}$_2$); 1.15 (d, $^3J_{H–H}$ = 7 Hz, 12H; C$_6$H$_3${CH(C*H*$_3$)$_2$}$_2$). ^{13}C{^{1}H} NMR (125.80 MHz, CD_2Cl_2): δ (ppm) 146.3, 145.1 (*ortho*-Dipp); 143.6 (H*C*N$_2$); 133.9 (NC*C*HN); 133.6, 133.0 (*para*-Dipp); 129.4, 129.3 (*ipso*-Dipp); 125.5, 125.3 (*meta*-Dipp); 120.7 (q, $^1J_{^{13}C–^{19}F}$ = 320 Hz); 29.9, 29.6 (C$_6$H$_3${*C*H(CH$_3$)$_2$}$_2$); 26.0, 24.5, 24.0, 22.7 (C$_6$H$_3${CH(*C*H$_3$)$_2$}$_2$). The N*C*CHN could not be observed.

7.2.2.14 [26][B(3,5-{CF$_3$}$_2$C$_6$H$_3$)$_4$]$_2$ (26: [(aIPr)$_2$GeBr$_2$]$^{2+}$)

To a mixture of (aIPr:)$_2$GeBr$_2$ (66 mg, 0.066 mmol) and [H(OEt$_2$)$_2$][B(3,5-{CF$_3$}$_2$C$_6$H$_3$)$_4$] (132 mg, 0.131 mmol) was added THF (5 mL) while stirring at ambient temperature. The solution was stirred for 30 minutes then filtered into a crystallisation ampoule and layered

with hexane. The product initially formed a colourless oil which after a few weeks spontaneously gave rise to colourless crystals suitable for analysis by single crystal X-ray diffraction (91 mg, 51% crystalline yield). Anal. Calcd for $C_{118}H_{94}B_2Br_2F_{48}GeN_4$ (2734.03): C 51.84%, H 3.47%, N 2.05%. Anal. Calcd for $C_{118}H_{94}B_2Br_2F_{48}GeN_4(C_4H_8O)_6$ (3166.67): C 53.86%, H 4.52%, N 1.77%. Found: C 54.09%, H 4.31%, N 1.86%. ESI-MS, positive ion mode (DCM, 60 °C, 4.5 kV): *m*/*z* 1873.8215 (1%) $[(aIPr)_2GeBr_2(B(3,5\text{-}\{CF_3\}_2C_6H_3)_4)]^+$ (Calcd 1873.4000), 1809.8859 (1%) $[(aIPr)_2GeBr(OH)(B(3,5\text{-}\{CF_3\}_2C_6H_3)_4)]^+$ (Calcd 1809.4852), 1747.9815 (1%) $[(aIPr)_2Ge(OH)_2(B(3,5\text{-}\{CF_3\}_2C_6H_3)_4)]^+$ (Calcd 1747.5701), 505.2839 (29%) $[(aIPr)_2GeBr_2]^{2+}$ (Calcd 505.1660), 473.3232 (84%) $[(aIPr)_2GeBr(OH)]^{2+}$ (Calcd 473.2088), 442.3669 (100%) $[(aIPr)_2Ge(OH)_2]^{2+}$ (Calcd 442.2513). ^{1}H NMR (500.30 MHz, d_8-THF): δ (ppm) 10.21 (s, 2H; *H*CN$_2$); 8.25 (s, 2H; NCC*H*N); 7.80 (s, 16H; BC(C*H*)$_2$(CCF$_3$)$_2$CH); 7.74 (t, $^3J_{H–H}$ = 8 Hz, 2H; *para*-Dipp); 7.71 (t, $^3J_{H–H}$ = 8 Hz, 2H; *para*-Dipp); 7.58 (s, 8H; BC(CH)$_2$(CCF$_3$)$_2$C*H*); 7.54–7.58 (m, 8H; *meta*-Dipp); 2.42 (br m, 2H; C$_6$H$_3${C*H*(CH$_3$)$_2$}$_2$); 2.32 (br m, 2H; C$_6$H$_3${C*H*(CH$_3$)$_2$}$_2$); 1.37 (br d, $^3J_{H–H}$ = 7 Hz, 6H; C$_6$H$_3${CH(C*H*$_3$)$_2$}$_2$); 1.27 (d, $^3J_{H–H}$ = 7 Hz, 6H; C$_6$H$_3${CH(C*H*$_3$)$_2$}$_2$); 1.23 (d, $^3J_{H–H}$ = 7 Hz, 6H; C$_6$H$_3${CH(C*H*$_3$)$_2$}$_2$); 1.18 (d, $^3J_{H–H}$ = 7 Hz, 6H; C$_6$H$_3${CH(C*H*$_3$)$_2$}$_2$). ^{13}C{^{1}H} NMR (125.80 MHz, d_8-THF): δ (ppm) 163.0 (m, $^1J_{^{13}C–^{11}B}$ = 50 Hz, $^1J_{^{13}C–^{10}B}$ = 17 Hz; B*C*(CH)$_2$(CCF$_3$)$_2$CH); 146.7, 145.9 (*ortho*-Dipp); 145.8 (H*C*N$_2$); 135.8 (BC(*C*H)$_2$(CCF$_3$)$_2$CH); 135.3 (NC*C*HN); 134.5, 134.4 (*para*-Dipp); 132.0 (v br, N*C*CHN); 130.5 (*ipso*-Dipp); 130.2 (qq, $^2J_{^{13}C–^{19}F}$ = 31 Hz, $^4J_{^{13}C–^{19}F}$ = 2 Hz; BC(CH)$_2$(*C*CF$_3$)$_2$CH); 130.1 (*ipso*-Dipp); 126.6, 126.4 (*meta*-Dipp); 125.7 (q, $^1J_{^{13}C–^{19}F}$ = 271 Hz; BC(CH)$_2$(C*C*F$_3$)$_2$CH); 118.4 (sept, $^3J_{^{13}C–^{19}F}$ = 4 Hz; BC(CH)$_2$(CCF$_3$)$_2$*C*H); 30.8, 30.5 (C$_6$H$_3${*C*H(CH$_3$)$_2$}$_2$); 26.2, 24.8, 24.0, 22.6 (C$_6$H$_3${CH(*C*H$_3$)$_2$}$_2$).

7.2.2.15 (aIPr·CO_2)$_2$$SiBr_2$ (27)

(aIPr:)$_2$$SiBr_2$ (26 mg, 0.027 mmol) was dissolved in d_8-toluene (500 µL) in an NMR tube fitted with a gas-tight valve. The solution was degassed by three freeze-pump-thaw cycles on a Schlenk line and then filled with CO_2 (1 atm). Crystals suitable for single crystal X-ray diffraction were grown from toluene at –80 °C. ^{1}H NMR (500.30 MHz, d_8-toluene): δ (ppm) 7.23 (s, 2H; NCC*H*N); 7.18 (t, $^3J_{H–H}$ = 8 Hz, 4H; *para*-Dipp); 7.05 (d, $^3J_{H–H}$ = 8 Hz, 4H; *meta*-Dipp); 7.02 (d, $^3J_{H–H}$ = 8 Hz, 4H; *meta*-Dipp); 2.77 (sept, $^3J_{H–H}$ = 7 Hz, 4H; C_6H_3{C*H*$(CH_3)_2$}$_2$); 2.71 (sept, $^3J_{H–H}$ = 7 Hz, 4H; C_6H_3{C*H*$(CH_3)_2$}$_2$); 1.35 (d, $^3J_{H–H}$ = 7 Hz, 12H; C_6H_3{CH(C*H*$_3)_2$}$_2$); 1.23 (d, $^3J_{H–H}$ = 7 Hz, 12H; C_6H_3{CH(C*H*$_3)_2$}$_2$); 1.22 (d, $^3J_{H–H}$ = 7 Hz, 12H; C_6H_3{CH(C*H*$_3)_2$}$_2$); 0.97 (d, $^3J_{H–H}$ = 7 Hz, 12H; C_6H_3{CH(C*H*$_3)_2$}$_2$). ^{13}C{^{1}H} NMR (125.80 MHz, C_6D_6): δ (ppm) 146.7, 145.7 (*ortho*-Dipp); 136.2, 136.0 (*ipso*-Dipp); 134.6 (NC*C*HN); 130.3, 130.0 (*para*-Dipp); 125.9 (N*C*CHN); 124.0, 123.8 (*meta*-Dipp); 29.5, 29.0 (C_6H_3{*C*H$(CH_3)_2$}$_2$); 25.7, 24.2, 23.9, 22.6 (C_6H_3{CH(*C*H$_3)_2$}$_2$). The resonances corresponding to the *C*N_2 and *C*O_2 carbon environments could not be observed. ^{29}Si{^{1}H} NMR (99.32 MHz, d_8-toluene): δ (ppm) –38.6 (s).

7.2.2.16 (aIPr·CO_2)$_2$$GeCl_2$ (28)

(aIPr:)$_2$$GeCl_2$ (10 mg, 0.010 mmol) was dissolved in d_8-toluene (500 µL) or C_6D_6 (500 µL) in an NMR tube fitted with a gas-tight valve. The solution was degassed by three freeze-pump-thaw cycles on a Schlenk line and then filled with CO_2 (1 atm). Upon standing, colourless crystals suitable for single crystal X-ray diffraction were obtained. ^{1}H NMR (500.30 MHz, d_8-toluene): δ (ppm) 7.22 (t, $^3J_{H–H}$ = 8 Hz, 2H; *para*-Dipp); 7.04–7.10 (m, 10H; *meta*-Dipp and *para*-Dipp,); 6.79 (s, 2H; NCC*H*N); 2.77 (sept, $^3J_{H–H}$ = 7 Hz, 4H; C_6H_3{C*H*$(CH_3)_2$}$_2$); 2.74 (sept, $^3J_{H–H}$ = 7 Hz, 4H; C_6H_3{C*H*$(CH_3)_2$}$_2$); 1.25 (d, $^3J_{H–H}$ = 7 Hz, 12H; C_6H_3{CH(C*H*$_3)_2$}$_2$); 1.23 (d, $^3J_{H–H}$ = 7 Hz, 12H; C_6H_3{CH(C*H*$_3)_2$}$_2$); 1.17 (d,

$^{3}J_{H–H}$ = 7 Hz, 12H; $C_6H_3\{CH(CH_3)_2\}_2$); 1.07 (d, $^{3}J_{H–H}$ = 7 Hz, 12H; $C_6H_3\{CH(CH_3)_2\}_2$). $^{13}C\{^{1}H\}$ NMR (125.80 MHz, d_8-toluene): δ (ppm) 146.8, 145.8 (*ortho*-Dipp); 137.1, 136.9 (*ipso*-Dipp); 132.1 (NC*C*HN); 130.0, 129.7 (*para*-Dipp); 126.9 (N*C*CHN); 123.9, 123.8 (*meta*-Dipp); 29.3, 28.9 ($C_6H_3\{CH(CH_3)_2\}_2$); 25.6, 24.6, 23.7, 22.5 ($C_6H_3\{CH(CH_3)_2\}_2$). The resonances corresponding to the CN_2 and CO_2 carbon environments could not be observed. ^{1}H NMR (500.30 MHz, C_6D_6): δ (ppm) 7.22 (t, $^{3}J_{H–H}$ = 8 Hz, 2H; *para*-Dipp); 7.04–7.08 (m, 10H; *meta*-Dipp and *para*-Dipp,); 6.70 (s, 2H; NCC*H*N); 2.78 (sept, $^{3}J_{H–H}$ = 7 Hz, 4H; $C_6H_3\{CH(CH_3)_2\}_2$); 2.73 (sept, $^{3}J_{H–H}$ = 7 Hz, 4H; $C_6H_3\{CH(CH_3)_2\}_2$); 1.34 (d, $^{3}J_{H–H}$ = 7 Hz, 12H; $C_6H_3\{CH(CH_3)_2\}_2$); 1.25 (d, $^{3}J_{H–H}$ = 7 Hz, 12H; $C_6H_3\{CH(CH_3)_2\}_2$); 1.22 (d, $^{3}J_{H–H}$ = 7 Hz, 12H; $C_6H_3\{CH(CH_3)_2\}_2$); 1.06 (d, $^{3}J_{H–H}$ = 7 Hz, 12H; $C_6H_3\{CH(CH_3)_2\}_2$). $^{13}C\{^{1}H\}$ NMR (125.80 MHz, C_6D_6): δ (ppm) 146.7, 145.6 (*ortho*-Dipp); 135.5, 135.4 (*ipso*-Dipp); 132.0 (NC*C*HN); 130.6, 130.3 (*para*-Dipp); 126.8 (N*C*CHN); 124.3, 124.2 (*meta*-Dipp); 29.5, 29.1 ($C_6H_3\{CH(CH_3)_2\}_2$); 25.5, 24.4, 23.9, 22.9 ($C_6H_3\{CH(CH_3)_2\}_2$). The resonances corresponding to the CN_2 and CO_2 carbon environments could not be observed.

7.2.2.17 (aIPr·CO_2)$_2$$GeBr_2$ (29)

(aIPr:)$_2$$GeBr_2$ (18 mg, 0.018 mmol) was dissolved in d_8-toluene (500 μL) in an NMR tube fitted with a gas-tight valve. The solution was degassed by three freeze-pump-thaw cycles on a Schlenk line and then filled with CO_2 (1 atm). ^{1}H NMR (500.30 MHz, d_8-toluene): δ (ppm) 7.21 (t, $^{3}J_{H–H}$ = 8 Hz, 2H; *para*-Dipp); 7.05–7.11 (m, 8H; *meta*-Dipp and *para*-Dipp); 6.83 (s, 2H; NCC*H*N); 2.75 (sept, $^{3}J_{H–H}$ = 7 Hz, 4H; $C_6H_3\{CH(CH_3)_2\}_2$); 2.73 (sept, $^{3}J_{H–H}$ = 7 Hz, 4H; $C_6H_3\{CH(CH_3)_2\}_2$); 1.29 (d, $^{3}J_{H–H}$ = 7 Hz, 12H; $C_6H_3\{CH(CH_3)_2\}_2$); 1.25 (d, $^{3}J_{H–H}$ = 7 Hz, 12H; $C_6H_3\{CH(CH_3)_2\}_2$); 1.21 (d, $^{3}J_{H–H}$ = 7 Hz, 12H; $C_6H_3\{CH(CH_3)_2\}_2$); 1.07 (d, $^{3}J_{H–H}$ = 7 Hz, 12H; $C_6H_3\{CH(CH_3)_2\}_2$). $^{13}C\{^{1}H\}$ NMR (125.80 MHz, d_8-toluene): δ (ppm) 146.9, 145.7 (*ortho*-Dipp); 136.4 (×2) (br, *ipso*-Dipp); 131.6 (NC*C*HN); 130.2, 129.9

(*para*-Dipp); 126.6 (N*C*CHN); 124.0, 123.9 (*meta*-Dipp); 29.4, 28.9 ($C_6H_3\{CH(CH_3)_2\}_2$); 25.6, 24.4, 23.9, 22.7 ($C_6H_3\{CH(CH_3)_2\}_2$). The resonances corresponding to the CN_2 and CO_2 carbon environments could not be observed.

7.2.2.18 (aIPr:)$_2$GeMe$_2$ (30)

MeLi (100 μL, 1.6 M in Et_2O, 0.160 mmol) was added to a suspension of (aIPr:)$_2$GeCl$_2$ (74 mg, 0.080 mmol) in diethyl ether (5 mL) while stirring at ambient temperature. On addition, the cloudy suspension instantly turned clear and a white precipitate was evolved over a one hour period. The pale yellow solution was filtered from the precipitate and dried thoroughly under vacuum yielding an off-white powder (29 mg, 0.030 mmol, 41% yield). EI-MS: *m/z* 186.1262 (81.0%) [Dipp–(CH)=(CH)]$^+$ (Calcd 187.1487), 387.2700 (100%) [aIPr:]$^+$ (Calcd 387.2800), 878.4138 (4%) [(aIPr:)$_2$GeMe$_2$]$^+$ (Calcd 878.5282). ^{1}H NMR (500.30 MHz, C_6D_6): δ (ppm) 7.26 (t, $^3J_{H–H}$ = 8 Hz, 2H; *para*-Dipp); 7.24 (t, $^3J_{H–H}$ = 8 Hz, 2H; *para*-Dipp); 7.14 (d, $^3J_{H–H}$ = 8 Hz, 4H; *meta*-Dipp); 7.13 (d, $^3J_{H–H}$ = 8 Hz, 4H; *meta*-Dipp); 7.10 (s, 2H; NCC*H*N); 2.99 (sept, $^3J_{H–H}$ = 7 Hz, 4H; $C_6H_3\{CH(CH_3)_2\}_2$); 2.83 (sept, $^3J_{H–H}$ = 7 Hz, 4H; $C_6H_3\{CH(CH_3)_2\}_2$); 1.35 (d, $^3J_{H–H}$ = 7 Hz, 12H; $C_6H_3\{CH(CH_3)_2\}_2$); 1.23 (d, $^3J_{H–H}$ = 7 Hz, 12H; $C_6H_3\{CH(CH_3)_2\}_2$); 1.21 (d, $^3J_{H–H}$ = 7 Hz, 12H; $C_6H_3\{CH(CH_3)_2\}_2$); 1.09 (d, $^3J_{H–H}$ = 7 Hz, 12H; $C_6H_3\{CH(CH_3)_2\}_2$); –0.10 (s, 6H; Ge(CH_3)$_2$). ^{13}C{^{1}H} NMR (125.80 MHz, C_6D_6): δ (ppm) 223.6 (CN_2); 146.6, 146.1 (*ortho*-Dipp); 139.7, 138.6 (*ipso*-Dipp); 130.9 (N*C*CHN); 130.0 (NC*C*HN); 129.3, 129.0 (*para*-Dipp); 123.8, 123.5 (*meta*-Dipp); 29.1, 28.7 ($C_6H_3\{CH(CH_3)_2\}_2$); 26.2, 24.7, 23.8, 22.1 ($C_6H_3\{CH(CH_3)_2\}_2$); –0.5 (Ge(CH_3)$_2$).

7.2.2.19 [K(2,2,2-crypt)][31] (31: [(aIPr:)$_2$GeCl]$^-$)

To a mixture of (aIPr:)$_2$GeCl$_2$ (65 mg, 0.071 mmol) and KC_8 (19 mg, 0.142 mmol) was added THF (5 mL) while stirring at ambient temperature. The suspension was allowed to stir overnight before the clear solution was filtered from the graphite into a crystallisation ampoule containing 2,2,2-crypt (53 mg, 0.142 mmol) before the solution was layered with hexane to afford colourless crystals (39 mg, 42% crystalline yield). ^{1}H NMR (500.30 MHz, d_8-THF): δ (ppm) 7.29 (t, $^3J_{H–H}$ = 8 Hz, 2H; *para*-Dipp); 7.00–7.15 (m, 10H; *meta*-Dipp and *para*-Dipp); 6.86 (s, 2H; NCC*H*N); 3.49 (s, 12H, 2,2,2-crypt); 3.45 (t, $^3J_{H–H}$ = 5 Hz, 12H; 2,2,2-crypt); 3.06 (sept, $^3J_{H–H}$ = 7 Hz, 4H; $C_6H_3\{CH(CH_3)_2\}_2$); 3.05 (sept, $^3J_{H–H}$ = 7 Hz, 4H; $C_6H_3\{CH(CH_3)_2\}_2$); 2.92 (sept, $^3J_{H–H}$ = 7 Hz, 4H; $C_6H_3\{CH(CH_3)_2\}_2$); 2.85 (sept, $^3J_{H–H}$ = 7 Hz, 4H; $C_6H_3\{CH(CH_3)_2\}_2$); 2.46 (t, $^3J_{H–H}$ = 5 Hz, 12H; 2,2,2-crypt); 1.24 (d, $^3J_{H–H}$ = 7 Hz, 6H; $C_6H_3\{CH(CH_3)_2\}_2$); 1.13 (d, $^3J_{H–H}$ = 7 Hz, 6H; $C_6H_3\{CH(CH_3)_2\}_2$); 1.10 (d, $^3J_{H–H}$ = 7 Hz, 12H; $C_6H_3\{CH(CH_3)_2\}_2$); 1.04 (d, $^3J_{H–H}$ = 7 Hz, 12H; $C_6H_3\{CH(CH_3)_2\}_2$); 1.03 (d, $^3J_{H–H}$ = 7 Hz, 12H; $C_6H_3\{CH(CH_3)_2\}_2$); 1.00 (d, $^3J_{H–H}$ = 7 Hz, 12H; $C_6H_3\{CH(CH_3)_2\}_2$); 0.97 (d, $^3J_{H–H}$ = 7 Hz, 12H; $C_6H_3\{CH(CH_3)_2\}_2$).

7.2.2.21 (aIPr:)$_2$SnCl$_2$ (32)

To a suspension of [K(aIPr:)]$_\infty$ (1.374 g, 3.224 mmol) in hexane (30 mL) was added a solution of $SnCl_4$ (420 mg, 1.612 mmol) in hexane (10 mL) while stirring at ambient temperature. The pale orange suspension was then allowed to stir overnight. The solution was then filtered and the solvent removed in vacuo to afford an off-white solid (484 mg, 52% yield). Colourless crystals suitable for single crystal X-ray diffraction were grown from a concentrated hexane solution at 4 °C. ^{1}H NMR (500.30 MHz, d_8-THF): δ (ppm) 7.40 (t, $^3J_{H–H}$ = 8 Hz, 2H; *para*-Dipp); 7.27 (d, $^3J_{H–H}$ = 8 Hz, 4H; *meta*-Dipp); 7.14 (m, 6H; *meta*-Dipp and *para*-Dipp); 6.34 (s, satellites $^3J_{H–^{117/119}Sn}$ = 6 Hz, 2H; NCC*H*N); 2.57 (sept, $^3J_{H–H}$ = 7 Hz, 4H;

$C_6H_3\{CH(CH_3)_2\}_2$); 2.54 (sept, $^3J_{H–H}$ = 7 Hz, 4H; $C_6H_3\{CH(CH_3)_2\}_2$); 1.15 (d, $^3J_{H–H}$ = 7 Hz, 12H; $C_6H_3\{CH(CH_3)_2\}_2$); 1.12 (d, $^3J_{H–H}$ = 7 Hz, 12H; $C_6H_3\{CH(CH_3)_2\}_2$); 1.06 (d, $^3J_{H–H}$ = 7 Hz, 24H; $C_6H_3\{CH(CH_3)_2\}_2$). $^{13}C\{^1H\}$ NMR (125.80 MHz, d_8-THF): δ (ppm) 226.4 (CN_2; satellites $^3J_{^{13}C–^{117/119}Sn}$ = 23 Hz); 146.8, 146.2 (*ortho*-Dipp); 139.3, 138.1 (*ipso*-Dipp); 131.8 (NC*C*HN; satellites $^2J_{^{13}C–^{117}Sn}$ = 152 Hz, $^2J_{^{13}C–^{119}Sn}$ = 159 Hz); 129.6, 129.5 (*para*-Dipp); 127.7 (N*C*CHN; satellites $^1J_{^{13}C–^{117}Sn}$ = 724 Hz, $^1J_{^{13}C–^{119}Sn}$ = 758 Hz); 124.1, 123.9 (*meta*-Dipp); 29.3, 29.0 ($C_6H_3\{CH(CH_3)_2\}_2$); 26.3, 25.8, 23.6, 22.5 ($C_6H_3\{CH(CH_3)_2\}_2$). $^{119}Sn\{^1H\}$ NMR (186.43 MHz, d_8-THF): δ (ppm) –120.2 (s).

7.2.2.21 [K(2,2,2crypt)][33] (33: $[(aIPr:)_3SnCl_2]^-$)

To a suspension of $[K(aIPr:)]_\infty$ (154 mg, 0.360 mmol) in THF (5 mL) was added a solution of $SnCl_4(THF)_2$ (50 mg, 0.120 mmol) in THF (5 mL) rapidly while stirring at ambient temperature. After 30 minutes, 2,2,2-crypt (136 mg, 0.360 mmol) was added to the reaction mixture and the suspension was allowed to stir overnight before the orange solution was filtered from the precipitate. The solution was concentrated to 5 mL before it was layered with hexane to afford large colourless crystals of $[K(2,2,2\text{-crypt})][(aIPr:)_3SnCl_2]\cdot 2THF$ (91 mg, 40% crystalline yield). Anal. Calcd for $C_{99}H_{141}Cl_2KN_8O_6Sn$ (1767.95): C 67.26%, H 8.04%, N 6.34%. Anal. Calcd for $C_{107}H_{157}Cl_2KN_8O_8Sn$ (1912.16): C 67.21%, H 8.28%, N 5.86%. Found: C 65.40%, H 8.24%, N 5.76%. ESI-MS, negative-ion mode (DMF, 150 °C, 2.4 kV): *m/z* 1351.2 (100%) $[(aIPr:)_3SnCl_2]^-$ (Calcd 1351.7). ^1H NMR (500.30 MHz, d_8-THF): δ (ppm) 7.31 (t, $^3J_{H–H}$ = 8 Hz, 3H; *para*-Dipp); 7.21 (d, $^3J_{H–H}$ = 8 Hz, 6H; *meta*-Dipp); 6.82 (d, $^3J_{H–H}$ = 8 Hz, 6H; *meta*-Dipp); 6.25 (t, $^3J_{H–H}$ = 8 Hz, 3H; *para*-Dipp); 4.66 (s, 3H; NCC*H*N); 3.51 (s, 12H; 2,2,2-crypt); 3.48 (t, $^3J_{H–H}$ = 4 Hz, 12H; 2,2,2-crypt); 3.04 (sept, $^3J_{H–H}$ = 7 Hz, 6H; $C_6H_3\{CH(CH_3)_2\}_2$); 2.74 (sept, $^3J_{H–H}$ = 7 Hz, 6H; $C_6H_3\{CH(CH_3)_2\}_2$); 2.48 (t, $^3J_{H–H}$ = 4 Hz, 12H; 2,2,2-crypt); 1.30 (d, $^3J_{H–H}$ = 7 Hz, 18H; $C_6H_3\{CH(CH_3)_2\}_2$); 1.20 (d,

$^{3}J_{H–H}$ = 7 Hz, 18H; $C_6H_3\{CH(CH_3)_2\}_2$); 1.04 (d, $^{3}J_{H–H}$ = 7 Hz, 18H; $C_6H_3\{CH(CH_3)_2\}_2$); 0.95 (d, $^{3}J_{H–H}$ = 7 Hz, 18H; $C_6H_3\{CH(CH_3)_2\}_2$). $^{13}C\{^{1}H\}$ NMR (125.80 MHz, d_8-THF): δ (ppm) 217.0 (CN_2; satellites $^{3}J_{^{13}C–^{117/119}Sn}$ = 25 Hz); 149.1, 147.3 (*ortho*-Dipp); 142.8 (NCCHN; satellites $^{1}J_{^{13}C–^{117}Sn}$ = 1041 Hz, $^{1}J_{^{13}C–^{119}Sn}$ = 1090 Hz); 142.6, 140.8 (*ipso*-Dipp); 128.4 (NCCHN); 128.2, 128.1 (*para*-Dipp); 123.8, 123.3 (*meta*-Dipp); 71.4, 68.6, 55.0 (2,2,2-crypt); 29.1, 28.7 ($C_6H_3\{CH(CH_3)_2\}_2$); 27.1 (×2), 23.9 (×2) ($C_6H_3\{CH(CH_3)_2\}_2$). $^{119}Sn\{^{1}H\}$ NMR (186.43 MHz, d_8-THF): δ (ppm) –389.1 (s).

7.2.2.22 [K(18-crown-6)(THF)$_2$][34] (34: [(aIPr:)$_3$Sn]$^-$)

To a suspension of $[K(aIPr:)]_\infty$ (72 mg, 0.168 mmol) in THF (5 mL) was added a solution of $SnCl_4(THF)_2$ (22 mg, 0.056 mmol) in THF (5 mL) rapidly while stirring at ambient temperature. KC_8 (15 mg, 0.111 mmol) was added to the stirring suspension and allowed to stir overnight before being filtered into a Schlenk tube containing 18-crown-6 (15 mg, 0.056 mmol). Once all of the crown ether had dissolved, the clear solution was layered with hexane to afford large pale pink cubic crystals unsuitable for single crystal X-ray diffraction (35 mg, 40% crystalline yield). The supernatant was then decanted and the crystals subsequently dried thoroughly under vacuum. Crystals of [K(2,2,2-crypt)][(aIPr:)$_3$Sn] suitable for analysis by single crystal X-ray diffraction were synthesised by the same method with 2,2,2-crypt employed in place of 18-crown-6. Anal. Calcd for $C_{101}H_{145}KN_6O_8Sn$ (1729.08): C 70.16%, H 8.45%, N 4.86%. Found: C 68.54%, H 8.50%, N 4.68%. ESI-MS, negative-ion mode (DMF, 150 °C, 2.4 kV): *m/z* 1281.9 (100%) $[(aIPr:)_3Sn]^-$ (Calcd 1281.7). ^{1}H NMR (500.30 MHz, d_8-THF): δ (ppm) 6.89–7.20 (m, 12H; *meta*-Dipp and *para*-Dipp); 6.70 (s, 3H; NCCHN); 3.52 (s, 24H; 18-crown-6); 3.02 (sept, $^{3}J_{H–H}$ = 7 Hz, 3H; $C_6H_3\{CH(CH_3)_2\}_2$); 2.94 (sept, $^{3}J_{H–H}$ = 7 Hz, 3H; $C_6H_3\{CH(CH_3)_2\}_2$); 2.86 (sept, $^{3}J_{H–H}$ = 7 Hz, 3H; $C_6H_3\{CH(CH_3)_2\}_2$); 2.62 (sept, $^{3}J_{H–H}$ = 7 Hz, 3H; $C_6H_3\{CH(CH_3)_2\}_2$); 1.23

(d, $^{3}J_{H–H}$ = 7 Hz, 6H; $C_6H_3\{CH(CH_3)_2\}_2$); 1.13 (d, $^{3}J_{H–H}$ = 7 Hz, 6H; $C_6H_3\{CH(CH_3)_2\}_2$); 1.10 (d, $^{3}J_{H–H}$ = 7 Hz, 6H; $C_6H_3\{CH(CH_3)_2\}_2$); 0.99 (d, $^{3}J_{H–H}$ = 7 Hz, 6H; $C_6H_3\{CH(CH_3)_2\}_2$); 0.86 (d, $^{3}J_{H–H}$ = 7 Hz, 6H; $C_6H_3\{CH(CH_3)_2\}_2$); 0.78 (d, $^{3}J_{H–H}$ = 7 Hz, 6H; $C_6H_3\{CH(CH_3)_2\}_2$); 0.71 (d, $^{3}J_{H–H}$ = 7 Hz, 6H; $C_6H_3\{CH(CH_3)_2\}_2$); 0.52 (d, $^{3}J_{H–H}$ = 7 Hz, 6H; $C_6H_3\{CH(CH_3)_2\}_2$; satellites $D^{1}_{H–^{117/119}Sn}$ = 88 Hz). $^{13}C\{^{1}H\}$ NMR (125.80 MHz, d_8-THF): δ (ppm) 220.2 (CN_2); 150.7 (NCCHN); 148.0, 147.1, 146.9, 146.7 (*ortho*-Dipp); 143.4, 142.0 (*ipso*-Dipp); 129.6 (NCCHN); 127.8, 127.1 (*para*-Dipp); 123.4 (×2), 123.1, 122.9 (*meta*-Dipp); 71.3 (18-crown-6); 29.2, 28.9, 28.7, 28.6 ($C_6H_3\{CH(CH_3)_2\}_2$); 27.0, 26.4, 26.2, 25.8, 24.2, 23.9, 23.7 ($C_6H_3\{CH(CH_3)_2\}_2$); 22.1 ($C_6H_3\{CH(CH_3)_2\}_2$; satellites $D^{13}_{C–^{117/119}Sn}$ = 50 Hz). $^{119}Sn\{^{1}H\}$ NMR (186.43 MHz, d_8-THF): δ (ppm) –352.8 (s).

7.2.2.23 $(aIPr)_2SnCl_4$ (35)

To a solution of IPr (1.794 g, 4.624 mmol) in THF (25 mL) was added a solution of $SnCl_4(THF)_2$ (934 mg, 2.312 mmol) in THF (10 mL) while stirring at ambient temperature. The pale orange solution was then heated to 65 °C for three days without stirring. The initial microcrystalline material that precipitates from solution slowly gives rise to large colourless crystals suitable for single crystal X-ray diffraction. The solution is then decanted from the crystals and cooled to –80 °C to obtain a second crop of crystals (2.204 g, 92% total crystalline yield). Anal. Calcd for $C_{54}H_{72}Cl_4N_4Sn$ (1037.70): C 62.50%, H 6.99%, N 5.40%. Found: C 62.32%, H 7.08%, N 5.34%. ^{1}H NMR (500.30 MHz, d_8-THF): δ (ppm) 8.75 (d, $^{4}J_{H–H}$ = 2 Hz, 2H; HCN_2; satellites $^{4}J^{1}_{H–^{117/119}Sn}$ = 18 Hz), 8.30 (d, $^{4}J_{H–H}$ = 2 Hz, 2H; NCCHN; satellites $^{3}J^{1}_{H–^{117/119}Sn}$ = 19 Hz), 7.51 (t, $^{3}J_{H–H}$ = 8 Hz, 2H; *para*-Dipp); 7.36 (d, $^{3}J_{H–H}$ = 8 Hz, 4H; *meta*-Dipp); 7.31 (t, $^{3}J_{H–H}$ = 8 Hz, 2H; *para*-Dipp); 7.17 (d, $^{3}J_{H–H}$ = 8 Hz, 4H; *meta*-Dipp); 3.07 (sept, $^{3}J_{H–H}$ = 7 Hz, 4H; $C_6H_3\{CH(CH_3)_2\}_2$); 2.59 (sept, $^{3}J_{H–H}$ = 7 Hz, 4H; $C_6H_3\{CH(CH_3)_2\}_2$); 1.37 (d, $^{3}J_{H–H}$ = 7 Hz, 12H; $C_6H_3\{CH(CH_3)_2\}_2$); 1.23 (d, $^{3}J_{H–H}$ = 7 Hz,

12H; $C_6H_3\{CH(CH_3)_2\}_2$); 1.17 (d, $^3J_{H–H}$ = 7 Hz, 12H; $C_6H_3\{CH(CH_3)_2\}_2$); 1.01 (d, $^3J_{H–H}$ = 7 Hz, 12H; $C_6H_3\{CH(CH_3)_2\}_2$). $^{13}C\{^1H\}$ NMR (125.80 MHz, d_8-THF): δ (ppm) 161.0 (N*C*CHN; $^1J_{^{13}C–^{117}Sn}$ = 1394 Hz, $^1J_{^{13}C–^{119}Sn}$ = 1459 Hz); 147.6, 146.9 (*ortho*-Dipp); 137.6 (H*C*N_2; satellites $^3J_{^{13}C–^{117/119}Sn}$ = 47 Hz); 135.4, 132.6 (*ipso*-Dipp); 132.5 (NC*C*HN; satellites $^1J_{^{13}C–^{117}Sn}$ = 141 Hz, $^1J_{^{13}C–^{119}Sn}$ = 148 Hz); 131.9, 130.6 (*para*-Dipp); 125.1, 124.1 (*meta*-Dipp); 29.6, 29.3 ($C_6H_3\{CH(CH_3)_2\}_2$); 26.7, 25.0, 24.6, 23.7 ($C_6H_3\{CH(CH_3)_2\}_2$). $^{119}Sn\{^1H\}$ NMR (186.43 MHz, d_8-THF): δ (ppm) –602.7 (s).

7.2.2.24 $(aIPr)_2SnBr_4$ (36)

To a solution of IPr (2.010 g, 5.180 mmol) in THF (25 mL) was added a solution of $SnBr_4$ (1.135 g, 2.590 mmol) in THF (10 mL) while stirring at ambient temperature. The pale orange solution was then heated to 65 °C for 3 days without stirring. The initial microcrystalline material that precipitates from solution slowly gives rise to large colourless crystals suitable for single crystal X-ray diffraction. The solution is then decanted from the crystals and cooled to –80 °C to obtain a second crop of crystals (2.527 g, 80% total crystalline yield). Anal. Calcd for $C_{54}H_{72}Br_4N_4Sn$ (1215.50): C 53.36%, H 5.97%, N 4.61%. Found: C 53.64%, H 6.16%, N 4.53%. ESI-MS, positive-ion mode (DCM, 60 °C, 4.5 kV): *m*/*z* 1135.2164 (100%) $[(aIPr)_2SnBr_3]^+$ (Calcd 1135.2309). ^1H NMR (500.30 MHz, d_8-THF): δ (ppm) 8.74 (d, $^4J_{H–H}$ = 2 Hz, 2H; *H*CN_2; satellites $^4J_{^1H–^{117/119}Sn}$ = 17 Hz), 8.68 (d, $^4J_{H–H}$ = 2 Hz, 2H; NCC*H*N; satellites $^3J_{^1H–^{117/119}Sn}$ = 21 Hz), 7.52 (t, $^3J_{H–H}$ = 8 Hz, 2H; *para*-Dipp); 7.37 (d, $^3J_{H–H}$ = 8 Hz, 4H; *meta*-Dipp); 7.33 (t, $^3J_{H–H}$ = 8 Hz, 2H; *para*-Dipp); 7.19 (d, $^3J_{H–H}$ = 8 Hz, 4H; *meta*-Dipp); 3.21 (sept, $^3J_{H–H}$ = 7 Hz, 4H; $C_6H_3\{CH(CH_3)_2\}_2$); 2.60 (sept, $^3J_{H–H}$ = 7 Hz, 4H; $C_6H_3\{CH(CH_3)_2\}_2$); 1.40 (d, $^3J_{H–H}$ = 7 Hz, 12H; $C_6H_3\{CH(CH_3)_2\}_2$); 1.24 (d, $^3J_{H–H}$ = 7 Hz, 12H; $C_6H_3\{CH(CH_3)_2\}_2$); 1.18 (d, $^3J_{H–H}$ = 7 Hz, 12H; $C_6H_3\{CH(CH_3)_2\}_2$); 1.00 (d, $^3J_{H–H}$ = 7 Hz, 12H; $C_6H_3\{CH(CH_3)_2\}_2$). $^{13}C\{^1H\}$ NMR (125.80 MHz, d_8-THF): δ (ppm) 153.2

(N*C*CHN; satellites $^{1}J_{^{13}C-^{117}Sn}$ = 1272 Hz, $^{1}J_{^{13}C-^{119}Sn}$ = 1332 Hz); 147.9, 146.8 (*ortho*-Dipp); 137.3 (H*C*N_2; satellites $^{3}J_{^{13}C-^{117/119}Sn}$ = 42 Hz); 135.1, 132.6 (*ipso*-Dipp); 132.0 (*para*-Dipp); 131.0 (NC*C*HN; satellites $^{2}J_{^{13}C-^{117}Sn}$ = 157 Hz, $^{2}J_{^{13}C-^{119}Sn}$ = 164 Hz); 130.9 (*para*-Dipp); 125.2, 124.4 (*meta*-Dipp); 29.6, 29.2 ($C_6H_3\{CH(CH_3)_2\}_2$); 26.6, 25.3, 24.3, 24.0 ($C_6H_3\{CH(CH_3)_2\}_2$). $^{119}Sn\{^{1}H\}$ NMR (186.43 MHz, d_8-THF): δ (ppm) –969.2 (s).

7.2.2.25 [37][AlCl$_4$]$_2$ (37: [(aIPr)$_2$SnCl$_2$]$^{2+}$)

To a mixture of (aIPr)$_2$SnCl$_4$ (232 mg, 0.224 mmol) and $AlCl_3$ (60 mg, 0.448 mmol) was added DCM (5 mL) rapidly while stirring at ambient temperature to afford a pale orange solution and precipitate. The solution was stirred for 30 minutes before the solution was filtered and layered with hexane to afford colourless crystals suitable which were subsequently dried thoroughly under vacuum (237 mg, 81% crystalline yield). Colourless crystals of [(aIPr)$_2$SnCl$_2$][AlCl$_4$]$_2$·DFB suitable for single crystal X-ray diffraction were grown by slow diffusion of hexane into a DFB solution. Anal Calcd for $C_{54}H_{72}Al_2Cl_{10}N_4Sn$ (1304.38): C 49.72%, H 5.56%, N 4.30%. Anal Calcd for $C_{55}H_{74}Al_2Cl_{12}N_4Sn$ (1389.31): C 47.55%, H 5.37%, N 4.03%. Found: C 48.51%, H 5.54%, N 4.12%. ESI-MS, positive-ion mode (DCM, 60 °C, 4.5 kV): *m*/*z* 1135.39476 (100%) [(aIPr)$_2$SnCl$_2$][AlCl$_4$]$^+$ (Calcd 1135.2691). ^{1}H NMR (500.30 MHz, CD_2Cl_2): δ (ppm) 8.79 (br s, 2H; *H*CN_2); 7.89 (v br s, 2H; NCC*H*N); 7.68 (t, $^{3}J_{H-H}$ = 8 Hz, 2H; *para*-Dipp); 7.63 (t, $^{3}J_{H-H}$ = 8 Hz, 2H; *para*-Dipp); 7.44 (d, $^{3}J_{H-H}$ = 8 Hz, 4H; *meta*-Dipp); 7.42 (d, $^{3}J_{H-H}$ = 8 Hz, 4H; *meta*-Dipp); 2.44 (br sept, $^{3}J_{H-H}$ = 7 Hz, 4H; $C_6H_3\{CH(CH_3)_2\}_2$); 2.32 (sept, $^{3}J_{H-H}$ = 7 Hz, 4H; $C_6H_3\{CH(CH_3)_2\}_2$); 1.32 (d, $^{3}J_{H-H}$ = 7 Hz, 24H; $C_6H_3\{CH(CH_3)_2\}_2$); 1.21 (d, $^{3}J_{H-H}$ = 7 Hz, 12H; $C_6H_3\{CH(CH_3)_2\}_2$); 1.15 (d, $^{3}J_{H-H}$ = 7 Hz, 12H; $C_6H_3\{CH(CH_3)_2\}_2$). $^{13}C\{^{1}H\}$ NMR (125.80 MHz, CD_2Cl_2): δ (ppm) 146.1, 145.2 (*ortho*-Dipp); 141.4 (br s; H*C*N_2); 135.9 (v br s; NC*C*HN); 134.1, 133.5 (*ipso*-Dipp); 129.9, 128.9 (*para*-Dipp); 126.0, 125.7 (*meta*-Dipp);

29.8, 29.6 ($C_6H_3\{CH(CH_3)_2\}_2$); 26.7, 25.0, 24.2, 22.7 ($C_6H_3\{CH(CH_3)_2\}_2$). The N*C*CHN resonance could not be observed. $^{119}Sn\{^1H\}$ NMR (186.43 MHz, CD_2Cl_2): δ (ppm) –142.9 (s). ^{27}Al NMR (104.27 MHz, CD_2Cl_2): δ (ppm) 103.4 (s).

7.2.2.26 $[38][AlBr_4]_2$ (38: $[(aIPr)_2SnBr_2]^{2+}$)

To a suspension of $(aIPr)_2SnBr_4$ (52 mg, 0.043 mmol) in CD_2Cl_2 (500 μL) was added $AlBr_3$ (23 mg, 0.086 mmol) to afford a colourless solution which was then analysed by multinuclear NMR spectroscopy. ^1H NMR (500.30 MHz, CD_2Cl_2): δ (ppm) 8.98 (s, 2H; *H*CN_2; satellites $^4J_{^1H–^{117/119}Sn}$ = 15 Hz); 7.70 (t, $^3J_{H–H}$ = 8 Hz, 2H; *para*-Dipp); 7.69 (s, 2H; NCC*H*N); 7.65 (t, $^3J_{H–H}$ = 8 Hz, 2H; *para*-Dipp); 7.45 (d, $^3J_{H–H}$ = 8 Hz, 8H; *meta*-Dipp); 2.35 (sept, $^3J_{H–H}$ = 7 Hz, 4H; $C_6H_3\{CH(CH_3)_2\}_2$); 2.26 (sept, $^3J_{H–H}$ = 7 Hz, 4H; $C_6H_3\{CH(CH_3)_2\}_2$); 1.34 (d, $^3J_{H–H}$ = 7 Hz, 12H; $C_6H_3\{CH(CH_3)_2\}_2$); 1.32 (d, $^3J_{H–H}$ = 7 Hz, 12H; $C_6H_3\{CH(CH_3)_2\}_2$); 1.23 (d, $^3J_{H–H}$ = 7 Hz, 12H; $C_6H_3\{CH(CH_3)_2\}_2$); 1.21 (d, $^3J_{H–H}$ = 7 Hz, 12H; $C_6H_3\{CH(CH_3)_2\}_2$). $^{13}C\{^1H\}$ NMR (125.80 MHz, CD_2Cl_2): δ (ppm) 145.8, 144.9 (*ortho*-Dipp); 142.0 (H*C*N_2; satellites $^3J_{^{13}C–^{117/119}Sn}$ = 31 Hz); 135.6 (NC*C*HN; satellites $^2J_{^{13}C–^{117}Sn}$ = 115 Hz, $^2J_{^{13}C–^{119}Sn}$ = 119 Hz); 134.5, 133.7 (*para*-Dipp); 130.7 (NC*C*HN; satellites $^1J_{^{13}C–^{117}Sn}$ = 869 Hz, $^1J_{^{13}C–^{119}Sn}$ = 909 Hz); 129.6, 128.8 (*ipso*-Dipp); 126.3, 125.8 (*meta*-Dipp); 29.9, 29.8 ($C_6H_3\{CH(CH_3)_2\}_2$); 26.3, 25.0, 24.3, 23.3 ($C_6H_3\{CH(CH_3)_2\}_2$). $^{119}Sn\{^1H\}$ NMR (186.43 MHz, CD_2Cl_2): δ (ppm) –265.3 (s). ^{27}Al NMR (104.27 MHz, CD_2Cl_2): δ (ppm) 80.7 (s).

7.2.3 Chapter 4 – Synthesis of IPr and aIPr complexes of group 15 bromides

7.2.3.1 $(IPr)PBr_3$ (39)

To a solution of IPr (519 mg, 1.338 mmol) in diethyl ether (25 mL) was added a solution of PBr_3 (362 mg, 1.338 mmol) in diethyl ether (25 mL) rapidly while stirring at ambient

temperature to afford a yellow solution and a fine white precipitate. The mixture was stirred for one hour before the solution was filtered and the solution concentrated to 10 mL and cooled to –35 °C overnight to afford yellow crystals which were subsequently filtered and dried thoroughly under vacuum (460 mg, 52% crystalline yield). Yellow crystals suitable for single crystal X-ray diffraction were grown by layering a THF solution with hexane. Anal. Calcd for $C_{27}H_{36}Br_3N_2P$ (659.27): C 49.19%, H 5.50%, N 4.25%. Found: C 49.98%, H 5.79%, N 4.18%. ^{1}H NMR (500.30 MHz, d_8-THF): δ (ppm) 7.98 (s, 2H; N(C*H*)$_2$N); 7.55 (t, $^3J_{H–H}$ = 8 Hz, 2H; *para*-Dipp); 7.38 (d, $^3J_{H–H}$ = 8 Hz, 4H; *meta*-Dipp); 3.30 (sept, $^3J_{H–H}$ = 7 Hz, 4H; $C_6H_3\{CH(CH_3)_2\}_2$; 1.44 (d, $^3J_{H–H}$ = 7 Hz, 12H; $C_6H_3\{CH(CH_3)_2\}_2$); 1.12 (d, $^3J_{H–H}$ = 7 Hz, 12H; $C_6H_3\{CH(CH_3)_2\}_2$). $^{13}C\{^1H\}$ NMR (125.80 MHz, d_8-THF): δ (ppm) 149.2 (d, $^1J_{^{13}C–^{31}P}$ = 176 Hz; *C*N$_2$); 148.0 (*ortho*-Dipp); 133.6 (*ipso*-Dipp); 132.7 (*para*-Dipp); 128.6 (d, $^3J_{^{13}C–^{31}P}$ = 4 Hz; N(*C*H)$_2$N); 125.5 (*meta*-Dipp); 30.4 ($C_6H_3\{CH(CH_3)_2\}_2$); 26.6, 23.9 ($C_6H_3\{CH(CH_3)_2\}_2$). ^{31}P NMR (202.38 MHz, d_8-THF): δ (ppm) 24.8 (s).

7.2.3.2 (IPr)AsBr$_3$ (40)

To a suspension of IPr (2.668 g, 6.875 mmol) in diethyl ether (30 mL) was added a solution of $AsBr_3$ (2.163 g, 6.875 mmol) in diethyl ether (5 mL) rapidly while stirring at ambient temperature to afford a pale yellow solution and pale yellow precipitate. The mixture was stirred for one hour before the solution was filtered from the precipitate and the pale yellow solid dried thoroughly under vacuum (4.601 g, 95% yield). Pale yellow crystals suitable for single crystal X-ray diffraction were grown by slow diffusion of hexane into a THF solution. Anal. Calcd for $C_{27}H_{36}AsBr_3N_2$ (703.22): C 46.12%, H 5.16%, N 3.98%. Found: C 46.39%, H 5.29%, N 3.98%. ^{1}H NMR (500.30 MHz, d_8-THF): δ (ppm) 7.99 (s, 2H; N(C*H*)$_2$N); 7.56 (t, $^3J_{H–H}$ = 8 Hz, 2H; *para*-Dipp); 7.39 (d, $^3J_{H–H}$ = 8 Hz, 4H; *meta*-Dipp); 3.24 (sept, $^3J_{H–H}$ = 7 Hz, 4H; $C_6H_3\{CH(CH_3)_2\}_2$); 1.45 (d, $^3J_{H–H}$ = 7 Hz, 12H; $C_6H_3\{CH(CH_3)_2\}_2$); 1.12

(d, $^{3}J_{H–H}$ = 7 Hz, 12H; $C_6H_3\{CH(CH_3)_2\}_2$). $^{13}C\{^{1}H\}$ NMR (125.80 MHz, d_8-THF): δ (ppm) 149.4 (*C*N_2); 148.0 (*ortho*-Dipp); 133.3 (*ipso*-Dipp); 132.8 (*para*-Dipp); 128.9 (N(*C*H)$_2$N); 125.5 (*meta*-Dipp); 30.3 ($C_6H_3\{CH(CH_3)_2\}_2$); 26.7, 23.9 ($C_6H_3\{CH(CH_3)_2\}_2$).

7.2.3.3 (IPr)$SbBr_3$ (41)

To a suspension of IPr (536 mg, 1.383 mmol) in diethyl ether (15 mL) was added a solution of $SbBr_3$ (500 mg, 1.383 mmol) in diethyl ether (5 mL) rapidly while stirring at ambient temperature to afford a pale yellow solution and pale yellow precipitate. The mixture was stirred for one hour before the solution was filtered from the precipitate and the pale yellow solid dried thoroughly under vacuum (838 mg, 81% yield). Pale yellow crystals of (IPr)$SbBr_3$·2THF suitable for single crystal X-ray diffraction were grown from a saturated THF solution at –25 °C. Anal. Calcd for $C_{27}H_{36}Br_3N_2Sb$ (750.06): C 43.24%, H 4.84%, N 3.74%. Found: C 42.80%, H 4.81%, N 3.70%. ^{1}H NMR (500.30 MHz, d_8-THF): δ (ppm) 7.92 (s, 2H; N(C*H*)$_2$N); 7.56 (t, $^{3}J_{H–H}$ = 8 Hz, 2H; *para*-Dipp); 7.39 (d, $^{3}J_{H–H}$ = 8 Hz, 4H; *meta*-Dipp); 3.21 (sept, $^{3}J_{H–H}$ = 7 Hz, 4H; $C_6H_3\{CH(CH_3)_2\}_2$); 1.45 (d, $^{3}J_{H–H}$ = 7 Hz, 12H; $C_6H_3\{CH(CH_3)_2\}_2$); 1.12 (d, $^{3}J_{H–H}$ = 7 Hz, 12H; $C_6H_3\{CH(CH_3)_2\}_2$). $^{13}C\{^{1}H\}$ NMR (125.80 MHz, d_8-THF): δ (ppm) 156.2 (*C*N_2); 148.0 (*ortho*-Dipp); 133.7 (*ipso*-Dipp); 132.7 (*para*-Dipp); 128.5 (N(*C*H)$_2$N); 125.4 (*meta*-Dipp); 30.1 ($C_6H_3\{CH(CH_3)_2\}_2$); 26.8, 24.0 ($C_6H_3\{CH(CH_3)_2\}_2$).

7.2.3.4 (IPr)$BiBr_3$ (42)

To a suspension of IPr (754 mg, 1.943 mmol) in diethyl ether (30 mL) was added a solution of $BiBr_3$ (872 mg, 1.943 mmol) in diethyl ether (10 mL) rapidly while stirring at ambient temperature to afford a yellow solution and bright yellow precipitate. The mixture was stirred for one hour before the solution was filtered from the precipitate and the yellow solid dried

thoroughly under vacuum (1.460 g, 90% yield). Yellow crystals of $[(IPr)BiBr_2(\mu\text{-}Br)]_2\cdot THF$ suitable for single crystal X-ray diffraction were grown by slow diffusion of hexane into a THF solution. Anal. Calcd for $C_{27}H_{36}BiBr_3N_2$ (837.28): C 38.73%, H 4.33%, N 3.35%. Found: C 38.60%, H 4.62%, N 3.35%. ^{1}H NMR (500.30 MHz, d_8-THF): δ (ppm) 7.79 (s, 2H; N(C*H*)$_2$N); 7.50 (t, $^3J_{H–H}$ = 8 Hz, 2H; *para*-Dipp); 7.34 (d, $^3J_{H–H}$ = 8 Hz, 4H; *meta*-Dipp); 3.16 (sept, $^3J_{H–H}$ = 7 Hz, 4H; $C_6H_3\{CH(CH_3)_2\}_2$); 1.46 (d, $^3J_{H–H}$ = 7 Hz, 12H; $C_6H_3\{CH(CH_3)_2\}_2$); 1.11 (d, $^3J_{H–H}$ = 7 Hz, 12H; $C_6H_3\{CH(CH_3)_2\}_2$). $^{13}C\{^1H\}$ NMR (125.80 MHz, d_8-THF): δ (ppm) 194.9 (v br, *C*N$_2$); 147.7 (*ortho*-Dipp); 135.2 (*ipso*-Dipp); 132.0 (*para*-Dipp); 128.7 (N(*C*H)$_2$N); 125.2 (*meta*-Dipp); 30.0 ($C_6H_3\{CH(CH_3)_2\}_2$); 26.7, 24.3 ($C_6H_3\{CH(CH_3)_2\}_2$).

7.2.3.5 [43][AlBr$_4$] (43: [(IPr)PBr$_2$]$^+$)

To a mixture of (IPr)PBr$_3$ (166 mg, 0.252 mmol) and AlBr$_3$ (67 mg, 0.252 mmol) was added DFB (5 mL) while stirring at ambient temperature to afford a colourless solution. The mixture was stirred for 30 minutes before the solution was filtered and layered with hexane to afford colourless crystals which were subsequently dried thoroughly under vacuum (190 mg, 82% yield). Colourless crystals of $[(IPr)PBr_2][AlBr_4]\cdot{}^1/_2DCM$ suitable for single crystal X-ray diffraction were grown by slow diffusion of hexane into a DCM solution. Anal. Calcd for $C_{27}H_{36}AlBr_6N_2P$ (925.97): C 35.02%, H 3.92%, N 3.03%. Found: C 35.62%, H 4.03%, N 3.06%. ESI-MS, positive ion mode (DCM, 60 °C, 4.5 kV): *m*/*z* 579.1361 (100%) $[(IPr)PBr_2]^+$ (Calcd 579.0959). ^{1}H NMR (500.30 MHz, CD_2Cl_2): δ (ppm) 7.98 (s, 2H; N(C*H*)$_2$N); 7.74 (t, $^3J_{H–H}$ = 8 Hz, 2H; *para*-Dipp); 7.45 (d, $^3J_{H–H}$ = 8 Hz, 4H; *meta*-Dipp); 2.37 (sept, $^3J_{H–H}$ = 7 Hz, 4H; $C_6H_3\{CH(CH_3)_2\}_2$); 1.38 (d, $^3J_{H–H}$ = 7 Hz, 12H; $C_6H_3\{CH(CH_3)_2\}_2$); 1.26 (d, $^3J_{H–H}$ = 7 Hz, 12H; $C_6H_3\{CH(CH_3)_2\}_2$). $^{13}C\{^1H\}$ NMR (125.80 MHz, CD_2Cl_2): δ (ppm) 145.6 (d, $^4J_{^{13}C–^{31}P}$ = 1 Hz; *ortho*-Dipp); 139.4 (d, $^1J_{^{13}C–^{31}P}$ = 136 Hz; *C*N$_2$); 134.0 (*para*-Dipp); 130.3 (d, $^3J_{^{13}C–^{31}P}$ = 3 Hz; N(*C*H)$_2$N); 129.5 (d, $^4J_{^{13}C–^{31}P}$ = 2 Hz; *ipso*-Dipp); 125.9

(*meta*-Dipp); 30.2 ($C_6H_3\{CH(CH_3)_2\}_2$); 26.3, 22.8 ($C_6H_3\{CH(CH_3)_2\}_2$). ^{31}P NMR (202.38 MHz, CD_2Cl_2): δ (ppm) 87.5 (s). ^{27}Al NMR (104.27 MHz, CD_2Cl_2): δ (ppm) 80.9 (s).

7.2.3.6 [44][AlBr$_4$] (44: [(IPr)AsBr$_2$]$^+$)

To a mixture of (IPr)$AsBr_3$ (197 mg, 0.280 mmol) and $AlBr_3$ (75 mg, 0.280 mmol) was added DCM (5 mL) while stirring at ambient temperature to afford a pale yellow solution. The mixture was stirred for 30 minutes before the solution was filtered and layered with hexane to afford colourless crystals suitable for single crystal X-ray diffraction (247 mg, 91% crystalline yield). Anal. Calcd for $C_{27}H_{36}AlAsBr_6N_2$ (969.91): C 33.44%, H 3.74%, N 2.89%. Found: C 33.74%, H 3.70%, N 2.90%. ESI-MS, positive ion mode (DCM, 60 °C, 4.5 kV): *m*/*z* 623.0908 (100%) $[(IPr)AsBr_2]^+$ (Calcd 623.0437). ^1H NMR (500.30 MHz, CD_2Cl_2): δ (ppm) 7.93 (s, 2H; $N(CH)_2N$); 7.74 (t, $^3J_{H–H}$ = 8 Hz, 2H; *para*-Dipp); 7.48 (d, $^3J_{H–H}$ = 8 Hz, 4H; *meta*-Dipp); 2.42 (sept, $^3J_{H–H}$ = 7 Hz, 4H; $C_6H_3\{CH(CH_3)_2\}_2$); 1.38 (d, $^3J_{H–H}$ = 7 Hz, 12H; $C_6H_3\{CH(CH_3)_2\}_2$); 1.27 (d, $^3J_{H–H}$ = 7 Hz, 12H; $C_6H_3\{CH(CH_3)_2\}_2$). $^{13}C\{^1H\}$ NMR (125.80 MHz, CD_2Cl_2): δ (ppm) 145.8 (*ortho*-Dipp); 141.7 (CN_2); 134.1 (*para*-Dipp); 129.8 ($N(CH)_2N$); 129.5 (*ipso*-Dipp); 126.0 (*meta*-Dipp); 30.1 ($C_6H_3\{CH(CH_3)_2\}_2$); 26.3, 23.0 ($C_6H_3\{CH(CH_3)_2\}_2$). ^{27}Al NMR (104.27 MHz, CD_2Cl_2): δ (ppm) 80.8 (s).

7.2.3.7 [45][AlBr$_4$] (45: [(IPr)SbBr$_2$]$^+$)

To a mixture of (IPr)$SbBr_3$ (138 mg, 0.184 mmol) and $AlBr_3$ (49 mg, 0.184 mmol) was added DCM (5 mL) while stirring at ambient temperature to afford a colourless solution. The mixture was stirred for 30 minutes before the solution was filtered and layered with hexane to afford colourless crystals of $[(IPr)SbBr_2][AlBr_4]\cdot{}^1/_2DCM$ suitable for single crystal X-ray diffraction (147 mg, 79% crystalline yield). Anal. Calcd for $C_{27}H_{36}AlBr_6N_2Sb$ (1016.75): C 31.90%, H 3.57%, N 2.76%. Found: C 33.52%, H 3.82%, N 2.86%. ESI-MS, positive ion

mode (DCM, 60 °C, 4.5 kV): *m*/*z* 669.1093 (100%) $[(IPr)SbBr_2]^+$ (Calcd 669.0266). ^1H NMR (500.30 MHz, CD_2Cl_2): δ (ppm) 7.78 (s, 2H; N(C*H*)$_2$N); 7.71 (t, $^3J_{H–H}$ = 8 Hz, 2H; *para*-Dipp); 7.46 (d, $^3J_{H–H}$ = 8 Hz, 4H; *meta*-Dipp); 2.50 (sept, $^3J_{H–H}$ = 7 Hz, 4H; $C_6H_3\{CH(CH_3)_2\}_2$); 1.39 (d, $^3J_{H–H}$ = 7 Hz, 12H; $C_6H_3\{CH(CH_3)_2\}_2$); 1.23 (d, $^3J_{H–H}$ = 7 Hz, 12H; $C_6H_3\{CH(CH_3)_2\}_2$). $^{13}C\{^1H\}$ NMR (125.80 MHz, CD_2Cl_2): δ (ppm) 150.3 (*C*N$_2$); 146.0 (*ortho*-Dipp); 133.9 (*para*-Dipp); 130.5 (*ipso*-Dipp); 129.1 (N(*C*H)$_2$N); 125.9 (*meta*-Dipp); 30.0 ($C_6H_3\{CH(CH_3)_2\}_2$); 26.3, 23.2 ($C_6H_3\{CH(CH_3)_2\}_2$). ^{27}Al NMR (104.27 MHz, CD_2Cl_2): δ (ppm) 80.9 (s).

7.2.3.8 [46][AlBr$_4$] (46: [(IPr)BiBr$_2$]$^+$)

To a mixture of $(IPr)BiBr_3$ (225 mg, 0.269 mmol) and $AlBr_3$ (72 mg, 0.269 mmol) was added DCM (5 mL) while stirring at ambient temperature to afford a pale yellow solution and pale yellow precipitate. The mixture was stirred for 30 minutes before the volatiles were removed in vacuo and the yellow solid dried thoroughly under vacuum (261 mg, 88% yield). Pale yellow crystals of $[(IPr)BiBr_2][AlBr_4]\cdot{}^1/_2DCM$ suitable for single crystal X-ray diffraction were grown by slow diffusion of hexane into a DCM solution. ESI-MS, positive ion mode (DCM, 60 °C, 4.5 kV): *m*/*z* 757.1798 (100%) $[(IPr)BiBr_2]^+$ (Calcd 757.1025). ^1H NMR (500.30 MHz, CD_2Cl_2): δ (ppm) 7.69 (s and t, $^3J_{H–H}$ = 8 Hz, 2H; N(C*H*)$_2$N and *para*-Dipp); 7.46 (d, $^3J_{H–H}$ = 8 Hz, 4H; *meta*-Dipp); 2.55 (sept, $^3J_{H–H}$ = 7 Hz, 4H; $C_6H_3\{CH(CH_3)_2\}_2$); 1.41 (d, $^3J_{H–H}$ = 7 Hz, 12H; $C_6H_3\{CH(CH_3)_2\}_2$); 1.21 (d, $^3J_{H–H}$ = 7 Hz, 12H; $C_6H_3\{CH(CH_3)_2\}_2$). $^{13}C\{^1H\}$ NMR (125.80 MHz, CD_2Cl_2): δ (ppm) 191.3 (*C*N$_2$); 145.9 (*ortho*-Dipp); 133.6 (*para*-Dipp); 131.4 (*ipso*-Dipp); 129.1 (N(*C*H)$_2$N); 125.9 (*meta*-Dipp); 29.8 ($C_6H_3\{CH(CH_3)_2\}_2$); 26.3, 23.6 ($C_6H_3\{CH(CH_3)_2\}_2$). ^{27}Al NMR (104.27 MHz, CD_2Cl_2): δ (ppm) 81.1 (s).

7.2.3.9 (aIPr)$SbBr_3$ (47)

To a solution of IPr (510 mg, 1.314 mmol) in an ampoule in THF (5 mL) was added a solution of $SbBr_3$ (475 mg, 1.314 mmol) in THF (5 mL) rapidly while stirring at ambient temperature to afford a colourless solution. The ampoule was then closed and the solution heated to 75 °C for three days before the solution was filtered and layered with hexane and allowed to diffuse slowly over one week to afford large colourless crystals of $[(aIPr)SbBr_2(\mu\text{-}Br)]_2 \cdot 2THF$ suitable for single crystal X-ray diffraction. The supernatant was then decanted and the crystals dried thoroughly under vacuum (626 mg, 63% crystalline yield). Anal. Calcd for $C_{27}H_{36}Br_3N_2Sb$ (750.06): C 43.24%, H 4.84%, N 3.74%. Found: C 43.65%, H 5.14%, N 3.36%. ^{1}H NMR (500.30 MHz, d_8-THF): δ (ppm) 9.37 (s, 1H; *H*CN$_2$); 8.37 (s, 1H; NCC*H*N); 7.63 (t, $^3J_{H–H}$ = 8 Hz, 1H; *para*-Dipp); 7.59 (t, $^3J_{H–H}$ = 8 Hz, 1H; *para*-Dipp); 7.47 (d, $^3J_{H–H}$ = 8 Hz, 2H; *meta*-Dipp); 7.42 (d, $^3J_{H–H}$ = 8 Hz, 2H; *meta*-Dipp); 3.06 (sept, $^3J_{H–H}$ = 7 Hz, 2H; $C_6H_3\{CH(CH_3)_2\}_2$); 2.64 (sept, $^3J_{H–H}$ = 7 Hz, 2H; $C_6H_3\{CH(CH_3)_2\}_2$); 1.44 (d, $^3J_{H–H}$ = 7 Hz, 6H; $C_6H_3\{CH(CH_3)_2\}_2$); 1.30 (d, $^3J_{H–H}$ = 7 Hz, 6H; $C_6H_3\{CH(CH_3)_2\}_2$); 1.23 (d, $^3J_{H–H}$ = 7 Hz, 6H; $C_6H_3\{CH(CH_3)_2\}_2$); 1.11 (d, $^3J_{H–H}$ = 7 Hz, 6H; $C_6H_3\{CH(CH_3)_2\}_2$). ^{13}C{^{1}H} NMR (125.80 MHz, d_8-THF): δ (ppm) 148.4 (N*C*CHN); 147.3, 146.7 (*ortho*-Dipp); 140.1 (H*C*N$_2$); 135.6 (NC*C*HN); 132.9, 132.8 (*para*-Dipp); 132.3, 131.8 (*ipso*-Dipp); 125.6, 125.5 (*meta*-Dipp); 29.9, 29.8 ($C_6H_3\{CH(CH_3)_2\}_2$); 27.0, 24.8, 24.7, 23.6 ($C_6H_3\{CH(CH_3)_2\}_2$).

7.2.3.10 (aIPr)$BiBr_3$ (48)

To a solution of IPr (258 mg, 0.665 mmol) in an ampoule in THF (5 mL) was added a solution of $BiBr_3$ (298 mg, 0.665 mmol) in THF (5 mL) rapidly while stirring at ambient temperature to afford a yellow solution. The ampoule was then closed and the solution heated to 75 °C overnight before the very pale yellow solution was layered with hexane to immediately afford

colourless crystals. The supernatant was then decanted and the crystals dried thoroughly under vacuum (343 mg, 62% crystalline yield). Crystals of the dimer [(aIPr)$BiBr_2$(μ-Br)]$_2$·2THF suitable for single crystal X-ray diffraction were grown by slow diffusion of hexane into a THF solution. Crystals of the tetramer [(aIPr)$BiBr_2$(μ-Br)][(aIPr)$BiBr$(μ-$Br)_2$]$_2$·2DCM were grown by slow diffusion of hexane into a DCM solution. Anal. Calcd for $C_{27}H_{36}BiBr_3N_2$ (837.28): C 38.73%, H 4.33%, N 3.35%. Anal. Calcd for $C_{31}H_{44}BiBr_3N_2O$ (909.39): C 40.94%, H 4.88%, N 3.08%. Found: C 40.08%, H 4.69%, N 3.06%. ^{1}H NMR (500.30 MHz, d_8-THF): δ (ppm) 9.36 (d, $^4J_{H–H}$ = 2 Hz, 1H; *H*CN_2); 8.46 (d, $^4J_{H–H}$ = 2 Hz, 1H; NCC*H*N); 7.60 (t, $^3J_{H–H}$ = 8 Hz, 1H; *para*-Dipp); 7.49 (t, $^3J_{H–H}$ = 8 Hz, 1H; *para*-Dipp); 7.43 (d, $^3J_{H–H}$ = 8 Hz, 2H; *meta*-Dipp); 7.32 (d, $^3J_{H–H}$ = 8 Hz, 2H; *meta*-Dipp); 3.00 (sept, $^3J_{H–H}$ = 7 Hz, 2H; C_6H_3{C*H*$(CH_3)_2$}$_2$); 2.57 (sept, $^3J_{H–H}$ = 7 Hz, 2H; C_6H_3{C*H*$(CH_3)_2$}$_2$); 1.44 (d, $^3J_{H–H}$ = 7 Hz, 6H; C_6H_3{CH(C*H*$_3)_2$}$_2$); 1.26 (d, $^3J_{H–H}$ = 7 Hz, 6H; C_6H_3{CH(C*H*$_3)_2$}$_2$); 1.21 (d, $^3J_{H–H}$ = 7 Hz, 6H; C_6H_3{CH(C*H*$_3)_2$}$_2$); 1.08 (d, $^3J_{H–H}$ = 7 Hz, 6H; C_6H_3{CH(C*H*$_3)_2$}$_2$). ^{13}C{^{1}H} NMR (125.80 MHz, d_8-THF): δ (ppm) 191.8 (v br, N*C*CHN); 147.5, 146.7 (*ortho*-Dipp); 141.8 (H*C*N_2); 141.0 (NC*C*HN); 134.0 (*ipso*-Dipp); 132.6, 132.0 (*para*-Dipp); 131.9 (*ipso*-Dipp); 125.5, 125.0 (*meta*-Dipp); 29.8 (×2) (C_6H_3{*C*H$(CH_3)_2$}$_2$); 26.7, 25.2, 24.5, 23.9 (C_6H_3{CH(*C*H$_3)_2$}$_2$). ^{1}H NMR (500.30 MHz, CD_2Cl_2): δ (ppm) 8.53 (d, $^4J_{H–H}$ = 2 Hz, 1H; *H*CN_2); 8.20 (d, $^4J_{H–H}$ = 2 Hz, 1H; NCC*H*N); 7.58 (t, $^3J_{H–H}$ = 8 Hz, 2H; *para*-Dipp); 7.37 (d, $^3J_{H–H}$ = 8 Hz, 2H; *meta*-Dipp); 7.35 (d, $^3J_{H–H}$ = 8 Hz, 2H; *meta*-Dipp); 2.85 (sept, $^3J_{H–H}$ = 7 Hz, 2H; C_6H_3{C*H*$(CH_3)_2$}$_2$); 2.46 (sept, $^3J_{H–H}$ = 7 Hz, 2H; C_6H_3{C*H*$(CH_3)_2$}$_2$); 1.44 (d, $^3J_{H–H}$ = 7 Hz, 6H; C_6H_3{CH(C*H*$_3)_2$}$_2$); 1.28 (d, $^3J_{H–H}$ = 7 Hz, 6H; C_6H_3{CH(C*H*$_3)_2$}$_2$); 1.19 (d, $^3J_{H–H}$ = 7 Hz, 6H; C_6H_3{CH(C*H*$_3)_2$}$_2$); 1.05 (d, $^3J_{H–H}$ = 7 Hz, 6H; C_6H_3{CH(C*H*$_3)_2$}$_2$). ^{13}C{^{1}H} NMR (125.80 MHz, CD_2Cl_2): δ (ppm) 188.1 (br, N*C*CHN); 146.8, 145.8 (*ortho*-Dipp); 141.6 (H*C*N_2); 138.4 (NC*C*HN); 132.4 (*ipso*-Dipp); 132.3, 132.1 (*para*-Dipp);

130.2 (*ipso*-Dipp); 125.1, 124.8 (*meta*-Dipp); 29.4, 29.3 ($C_6H_3\{CH(CH_3)_2\}_2$); 26.7, 25.0, 24.4, 23.4 ($C_6H_3\{CH(CH_3)_2\}_2$).

7.2.3.11 [49][B(3,5-{CF_3}$_2$$C_6H_3$)$_4$] (49: [(aIPr)$SbBr_2$]$^+$)

To a mixture of (aIPr)$SbBr_3$ (82 mg, 0.109 mmol) and Na[B(3,5-{CF_3}$_2$$C_6H_3$)$_4$] (97 mg, 0.109 mmol) was added DCM (5 mL) rapidly while stirring at ambient temperature to afford a colourless solution and colourless precipitate. The solution was stirred for one hour then filtered and the volatiles removed in vacuo to afford a colourless solid. The solid was then dissolved in THF, filtered, then layered with hexane to afford colourless crystals of [(aIPr)$SbBr_2$(THF)$_2$][B(3,5-{CF_3}$_2$$C_6H_3$)$_4$]·2THF suitable for single crystal X-ray diffraction. (122 mg, 73% crystalline yield). Anal. Calcd for $C_{59}H_{48}BBr_2F_{24}N_2Sb$ (1533.37): C 46.21%, H 3.16%, N 1.83%. Anal. Calcd for $C_{67}H_{64}BBr_2F_{24}N_2O_2Sb$ (1677.58): C 47.97%, H 3.85%, N 1.67%. Found: C 47.88%, H 3.46%, N 1.92%. ESI-MS, positive ion mode (DCM, 60 °C, 4.5 kV): *m*/*z* 669.0862 (100%) [(aIPr)$SbBr_2$]$^+$ (Calcd 669.0266), 625.12914 (37%) [(aIPr)SbBr(OH)(OH_2)]$^+$ (Calcd 625.1211), 607.1596 (88%) [(aIPr)SbBr(OH)]$^+$ (Calcd 607.1106), 581.1702 (4%) [(aIPr)Sb(OH)$_2$(OH_2)$_2$]$^+$ (Calcd 581.2183), 563.2008 (27%) [(aIPr)Sb(OH)$_2$(OH_2)]$^+$ (Calcd 563.2077), 543.2307 (15%) [(aIPr)Sb(OH)$_2$]$^+$ (Calcd 543.1966). ^{1}H NMR (500.30 MHz, CD_2Cl_2): δ (ppm) 8.52 (d, $^4J_{H–H}$ = 2 Hz, 1H; *H*CN_2); 8.08 (d, $^4J_{H–H}$ = 2 Hz, 1H; NCC*H*N); 7.72 (m, 9H; BC(C*H*)$_2$(CCF_3)$_2$CH and *para*-Dipp); 7.68 (t, $^3J_{H–H}$ = 8 Hz, 1H; *para*-Dipp); 7.56 (s, 4H; BC(CH)$_2$(CCF_3)$_2$C*H*); 7.50 (d, $^3J_{H–H}$ = 8 Hz, 2H; *meta*-Dipp); 7.45 (d, $^3J_{H–H}$ = 8 Hz, 2H; *meta*-Dipp); 2.43 (sept, $^3J_{H–H}$ = 7 Hz, 2H; $C_6H_3\{CH(CH_3)_2\}_2$); 2.35 (sept, $^3J_{H–H}$ = 7 Hz, 2H; $C_6H_3\{CH(CH_3)_2\}_2$); 1.39 (d, $^3J_{H–H}$ = 7 Hz, 6H; $C_6H_3\{CH(CH_3)_2\}_2$); 1.31 (d, $^3J_{H–H}$ = 7 Hz, 6H; $C_6H_3\{CH(CH_3)_2\}_2$); 1.23 (d, $^3J_{H–H}$ = 7 Hz, 6H; $C_6H_3\{CH(CH_3)_2\}_2$); 1.17 (d, $^3J_{H–H}$ = 7 Hz, 6H; $C_6H_3\{CH(CH_3)_2\}_2$). ^{13}C{^{1}H} NMR (125.80 MHz, CD_2Cl_2): δ (ppm) 162.2 (m, $^1J_{^{13}C–^{11}B}$ = 50 Hz, $^1J_{^{13}C–^{10}B}$ = 17 Hz;

B*C*(CH)$_2$(CCF$_3$)$_2$CH); 145.5, 145.2 (*ortho*-Dipp); 141.3 (N*C*CHN); 139.5 (H*C*N$_2$); 135.2 (BC(*C*H)$_2$(CCF$_3$)$_2$CH and NC*C*HN); 134.6, 133.6 (*para*-Dipp); 129.3 (qq, $^2J_{^{13}C-^{19}F}$ = 31 Hz, $^4J_{^{13}C-^{19}F}$ = 2 Hz; BC(CH)$_2$(*C*CF$_3$)$_2$CH); 129.3, 129.2 (*ipso*-Dipp); 126.5, 125.8 (*meta*-Dipp); 125.1 (q, $^1J_{^{13}C-^{19}F}$ = 271 Hz; BC(CH)$_2$(C*C*F$_3$)$_2$CH); 117.9 (sept, $^3J_{^{13}C-^{19}F}$ = 4 Hz; BC(CH)$_2$(CCF$_3$)$_2$*C*H); 30.0, 29.8 (C$_6$H$_3${*C*H(CH$_3$)$_2$}$_2$); 26.4, 24.6, 24.1, 23.0 (C$_6$H$_3${CH(*C*H$_3$)$_2$}$_2$). ^{11}B NMR (128.39 MHz, CD$_2$Cl$_2$): δ (ppm) –6.6 (s). ^{19}F NMR (376.54 MHz, CD$_2$Cl$_2$): δ (ppm) –62.8 (s).

7.2.3.12 [50][B(3,5-{CF$_3$}$_2$C$_6$H$_3$)$_4$] (50: [(aIPr)BiBr$_2$]$^+$)

To a mixture of (aIPr)BiBr$_3$ (40 mg, 0.048 mmol) and Na[B(3,5-{CF$_3$}$_2$C$_6$H$_3$)$_4$] (42 mg, 0.048 mmol) was added DCM (5 mL) rapidly while stirring at ambient temperature to afford a pale yellow solution and colourless precipitate. The solution was stirred for one hour then filtered and the volatiles removed in vacuo to afford a colourless solid. The solid was then dissolved in THF, filtered, then layered with hexane to afford colourless crystals of [(aIPr)BiBr$_2$(THF)$_2$][B(3,5-{CF$_3$}$_2$C$_6$H$_3$)$_4$]·2THF suitable for single crystal X-ray diffraction. (55 mg, 71% crystalline yield). Anal. Calcd for C$_{59}$H$_{48}$BBiBr$_2$F$_{24}$N$_2$ (1620.59): C 43.73%, 2.99%, 1.73%. Anal. Calcd for C$_{67}$H$_{64}$BBiBr$_2$F$_{24}$N$_2$O$_2$ (1764.80): C 45.60%, H 3.66%, N 1.59%. Found: C 45.20%, H 3.18%, N 1.74%. ESI-MS, positive ion mode (DCM, 60 °C, 4.5 kV): *m*/*z* 757.1990 (100%) [(aIPr)BiBr$_2$]$^+$ (Calcd 757.1025). ^{1}H NMR (500.30 MHz, CD$_2$Cl$_2$): δ (ppm) 8.49 (d, $^4J_{H-H}$ = 2 Hz, 1H; *H*CN$_2$); 8.23 (d, $^4J_{H-H}$ = 2 Hz, 1H; NCC*H*N); 7.73 (m, 9H; BC(C*H*)$_2$(CCF$_3$)$_2$CH and *para*-Dipp); 7.66 (t, $^3J_{H-H}$ = 8 Hz, 1H; *para*-Dipp); 7.56 (s, 4H; BC(CH)$_2$(CCF$_3$)$_2$C*H*); 7.50 (d, $^3J_{H-H}$ = 8 Hz, 2H; *meta*-Dipp); 7.44 (d, $^3J_{H-H}$ = 8 Hz, 2H; *meta*-Dipp); 2.51 (sept, $^3J_{H-H}$ = 7 Hz, 2H; C$_6$H$_3${C*H*(CH$_3$)$_2$}$_2$); 2.36 (sept, $^3J_{H-H}$ = 7 Hz, 2H; C$_6$H$_3${C*H*(CH$_3$)$_2$}$_2$); 1.40 (d, $^3J_{H-H}$ = 7 Hz, 6H; C$_6$H$_3${CH(C*H*$_3$)$_2$}$_2$); 1.31 (d, $^3J_{H-H}$ = 7 Hz, 6H; C$_6$H$_3${CH(C*H*$_3$)$_2$}$_2$); 1.23 (d, $^3J_{H-H}$ = 7 Hz, 6H; C$_6$H$_3${CH(C*H*$_3$)$_2$}$_2$); 1.16 (d, $^3J_{H-H}$ = 7 Hz, 6H;

$C_6H_3\{CH(CH_3)_2\}_2$). $^{13}C\{^1H\}$ NMR (125.80 MHz, CD_2Cl_2): δ (ppm) 181.8 (v br, N*C*CHN); 162.2 (m, $^1J_{^{13}C-^{11}B}$ = 50 Hz, $^1J_{^{13}C-^{10}B}$ = 17 Hz; B*C*$(CH)_2(CCF_3)_2CH$); 145.5, 145.3 (*ortho*-Dipp); 141.2 (NC*C*HN); 140.5 (H*C*N_2); 135.2 (BC(*C*$H)_2(CCF_3)_2CH$); 134.3, 133.4 (*para*-Dipp); 130.1, 129.4 (*para*-Dipp); 129.3 (qq, $^2J_{^{13}C-^{19}F}$ = 31 Hz, $^4J_{^{13}C-^{19}F}$ = 2 Hz; $BC(CH)_2$(*C*$CF_3)_2CH$); 126.5, 125.7 (*meta*-Dipp); 125.1 (q, $^1J_{^{13}C-^{19}F}$ = 271 Hz; $BC(CH)_2$(C*C*$F_3)_2CH$); 117.9 (sept, $^3J_{^{13}C-^{19}F}$ = 4 Hz; $BC(CH)_2(CCF_3)_2$*C*H); 29.8, 29.7 ($C_6H_3\{CH(CH_3)_2\}_2$); 26.5, 24.6, 24.2, 23.2 ($C_6H_3\{CH(CH_3)_2\}_2$).

7.2.3.13 [51]Br (51: $[(aIPr)_2SbBr_2]^+$)

To a solution of IPr (555 mg, 1.430 mmol) in an ampoule in THF (5 mL) was added a solution of $SbBr_3$ (259 mg, 0.715 mmol) in THF (5 mL) rapidly while stirring at ambient temperature to afford a colourless solution. The ampoule was then closed and the solution heated to 80 °C overnight to afford large colourless crystals suitable for single crystal X-ray diffraction. The supernatant was then decanted and the crystals dried thoroughly under vacuum (785 mg, 96% crystalline yield). Anal. Calcd for $C_{54}H_{72}Br_3N_4Sb$ (1138.65): C 56.96%, H 6.37%, N 4.92%. Anal. Calcd for $C_{58}H_{80}Br_3N_4OSb$ (1210.75): C 57.54%, H 6.66%, N 4.63%. Found: C 57.70%, H 6.58%, N 4.71%. ^1H NMR (500.30 MHz, CD_2Cl_2): δ (ppm) 9.71 (s, 2H; *H*CN_2); 7.60 (s, 2H; NCC*H*N); 7.60 (t, $^3J_{H-H}$ = 8 Hz, 4H; *para*-Dipp); 7.38 (d, $^3J_{H-H}$ = 8 Hz, 4H; *meta*-Dipp); 7.36 (d, $^3J_{H-H}$ = 8 Hz, 4H; *meta*-Dipp); 2.73 (sept, $^3J_{H-H}$ = 7 Hz, 4H; $C_6H_3\{CH(CH_3)_2\}_2$); 2.46 (sept, $^3J_{H-H}$ = 7 Hz, 4H; $C_6H_3\{CH(CH_3)_2\}_2$); 1.38 (d, $^3J_{H-H}$ = 7 Hz, 12H; $C_6H_3\{CH(CH_3)_2\}_2$); 1.22 (d, $^3J_{H-H}$ = 7 Hz, 12H; $C_6H_3\{CH(CH_3)_2\}_2$); 1.14 (d, $^3J_{H-H}$ = 7 Hz, 24H; $C_6H_3\{CH(CH_3)_2\}_2$). $^{13}C\{^1H\}$ NMR (125.80 MHz, CD_2Cl_2): δ (ppm) 146.2, 145.5 (*ortho*-Dipp); 143.4 (NC*C*HN); 139.2 (H*C*N_2); 133.8 (NC*C*HN); 132.7, 132.5 (*para*-Dipp); 130.9, 130.1 (*ipso*-Dipp); 125.3, 125.2 (*meta*-Dipp); 29.6, 29.4 ($C_6H_3\{CH(CH_3)_2\}_2$); 27.0, 24.5, 24.4, 22.8 ($C_6H_3\{CH(CH_3)_2\}_2$).

7.2.3.14 [51][B(3,5-{CF_3}$_2$$C_6H_3$)$_4$] (51: [(aIPr)$_2$$SbBr_2$]$^+$)

To a mixture of [(aIPr)$_2$$SbBr_2$]Br (82 mg, 0.068 mmol) and Na[B(3,5-{CF_3}$_2$$C_6H_3$)$_4$] (60 mg, 0.068 mmol) was added DCM (5 mL) while stirring at ambient temperature to afford a colourless solution and colourless precipitate. The solution was stirred for one hour then filtered and the volatiles removed in vacuo to afford a colourless solid. The solid was then dissolved in THF, filtered, then layered with hexane to afford colourless crystals of [(aIPr)$_2$$SbBr_2$][B(3,5-{$CF_3$}$_2$$C_6H_3$)$_4$]·3THF suitable for single crystal X-ray diffraction. (93 mg, 72% crystalline yield). Anal. Calcd for $C_{86}H_{84}BBr_2F_{24}N_4Sb$ (1921.96): C 53.74%, H 4.41%, N 2.92%. Anal. Calcd for $C_{98}H_{108}BBr_2F_{24}N_4O_3Sb$ (2138.27): C 55.05%, H 5.09%, N 2.62%. Found: C 55.46%, H 5.04%, N 2.64%. ESI-MS, positive ion mode (DCM, 60 °C, 4.5 kV): *m*/*z* 1057.4980 (100%) [(aIPr)$_2$$SbBr_2$]$^+$ (Calcd 1057.3142). ^{1}H NMR (500.30 MHz, CD_2Cl_2): δ (ppm) 8.94 (s, 2H; *H*CN_2); 7.74 (s, 8H; BC(C*H*)$_2$(CCF_3)$_2$CH); 7.65 (s, 2H; NCC*H*N); 7.63 (t, $^3J_{H–H}$ = 8 Hz, 2H; *para*-Dipp); 7.60 (t, $^3J_{H–H}$ = 8 Hz, 2H; *para*-Dipp); 7.56 (s, 4H; BC(CH)$_2$(CCF_3)$_2$C*H*); 7.41 (d, $^3J_{H–H}$ = 8 Hz, 4H; *meta*-Dipp); 7.38 (d, $^3J_{H–H}$ = 8 Hz, 4H; *meta*-Dipp); 2.75 (sept, $^3J_{H–H}$ = 7 Hz, 4H; C_6H_3{C*H*(CH_3)$_2$}$_2$); 2.45 (sept, $^3J_{H–H}$ = 7 Hz, 4H; C_6H_3{C*H*(CH_3)$_2$}$_2$); 1.41 (d, $^3J_{H–H}$ = 7 Hz, 12H; C_6H_3{CH(C*H*$_3$)$_2$}$_2$); 1.20 (d, $^3J_{H–H}$ = 7 Hz, 12H; C_6H_3{CH(C*H*$_3$)$_2$}$_2$); 1.16 (d, $^3J_{H–H}$ = 7 Hz, 12H; C_6H_3{CH(C*H*$_3$)$_2$}$_2$); 1.11 (d, $^3J_{H–H}$ = 7 Hz, 12H; C_6H_3{CH(C*H*$_3$)$_2$}$_2$). ^{13}C{^{1}H} NMR (125.80 MHz, CD_2Cl_2): δ (ppm) 162.2 (m, $^1J_{^{13}C–^{11}B}$ = 50 Hz, $^1J_{^{13}C–^{10}B}$ = 17 Hz; B*C*(CH)$_2$(CCF_3)$_2$CH); 146.1, 145.5 (*ortho*-Dipp); 144.3 (N*C*CHN); 137.6 (H*C*N_2); 135.3 (BC(*C*H)$_2$(CCF_3)$_2$CH); 133.9 (NC*C*HN); 133.1, 133.0 (*para*-Dipp); 130.7, 129.7 (*ipso*-Dipp); 129.3 (qq, $^2J_{^{13}C–^{19}F}$ = 31 Hz, $^4J_{^{13}C–^{19}F}$ = 2 Hz; BC(CH)$_2$(*C*CF_3)$_2$CH); 125.6, 125.5 (*meta*-Dipp); 125.1 (q, $^1J_{^{13}C–^{19}F}$ = 271 Hz; BC(CH)$_2$(*C*CF_3)$_2$CH); 117.9 (sept, $^3J_{^{13}C–^{19}F}$ = 4 Hz; BC(CH)$_2$(CCF_3)$_2$*C*H); 29.7, 29.5 (C_6H_3{*C*H(CH_3)$_2$}$_2$); 27.0, 25.5, 25.4, 22.7 (C_6H_3{CH(*C*H_3)$_2$}$_2$). ^{11}B NMR (128.39 MHz, CD_2Cl_2): δ (ppm) –6.6 (s). ^{19}F NMR (376.54 MHz, CD_2Cl_2): δ (ppm) –62.8 (s).

7.2.3.15 [51][$AlBr_4$] (51: [(aIPr)$_2$$SbBr_2$]$^+$)

To a mixture of [(aIPr)$_2$$SbBr_2$]Br (90 mg, 0.079 mmol) and $AlBr_3$ (21 mg, 0.079 mmol) was added DCM (5 mL) while stirring at ambient temperature to afford a colourless solution. The solution was stirred for one hour then filtered and layered with hexane to afford colourless crystals suitable for single crystal X-ray diffraction. (82 mg, 74% crystalline yield). Anal. Calcd for $C_{54}H_{72}AlBr_6N_4Sb$ (1405.34): C 46.15%, H 5.16%, N 3.99%. Found: C 45.87%, H 5.19%, N 3.99%. ^{1}H NMR (500.30 MHz, CD_2Cl_2): δ (ppm) 8.31 (d, $^4J_{H–H}$ = 2 Hz, 2H; *H*CN$_2$); 7.68 (d, $^4J_{H–H}$ = 2 Hz, 2H; NCC*H*N); 7.66 (t, $^3J_{H–H}$ = 8 Hz, 2H; *para*-Dipp); 7.64 (t, $^3J_{H–H}$ = 8 Hz, 2H; *para*-Dipp); 7.42 (d, $^3J_{H–H}$ = 8 Hz, 8H; *meta*-Dipp); 2.75 (sept, $^3J_{H–H}$ = 7 Hz, 4H; $C_6H_3\{CH(CH_3)_2\}_2$); 2.44 (sept, $^3J_{H–H}$ = 7 Hz, 4H; $C_6H_3\{CH(CH_3)_2\}_2$); 1.41 (d, $^3J_{H–H}$ = 7 Hz, 12H; $C_6H_3\{CH(CH_3)_2\}_2$); 1.21 (d, $^3J_{H–H}$ = 7 Hz, 12H; $C_6H_3\{CH(CH_3)_2\}_2$); 1.18 (d, $^3J_{H–H}$ = 7 Hz, 12H; $C_6H_3\{CH(CH_3)_2\}_2$); 1.11 (d, $^3J_{H–H}$ = 7 Hz, 12H; $C_6H_3\{CH(CH_3)_2\}_2$). ^{13}C{^{1}H} NMR (125.80 MHz, CD_2Cl_2): δ (ppm) 146.0, 145.3 (*ortho*-Dipp); 144.2 (NCCHN); 137.2 (H*C*N$_2$); 133.9 (NC*C*HN); 133.1 (×2) (*para*-Dipp); 130.6, 129.6 (*ipso*-Dipp); 125.5 (×2) (*meta*-Dipp); 29.6, 29.5 ($C_6H_3\{CH(CH_3)_2\}_2$); 27.1, 24.6, 24.5, 22.7 ($C_6H_3\{CH(CH_3)_2\}_2$). ^{1}H NMR (500.30 MHz, d_8-THF): δ (ppm) 9.58 (d, $^4J_{H–H}$ = 1 Hz, 2H; *H*CN$_2$); 8.15 (d, $^4J_{H–H}$ = 1 Hz, 2H; NCC*H*N); 7.68 (t, $^3J_{H–H}$ = 8 Hz, 2H; *para*-Dipp); 7.61 (t, $^3J_{H–H}$ = 8 Hz, 2H; *para*-Dipp); 7.51 (d, $^3J_{H–H}$ = 8 Hz, 4H; *meta*-Dipp); 7.45 (d, $^3J_{H–H}$ = 8 Hz, 4H; *meta*-Dipp); 2.88 (sept, $^3J_{H–H}$ = 7 Hz, 4H; $C_6H_3\{CH(CH_3)_2\}_2$); 2.57 (sept, $^3J_{H–H}$ = 7 Hz, 4H; $C_6H_3\{CH(CH_3)_2\}_2$); 1.41 (d, $^3J_{H–H}$ = 7 Hz, 12H; $C_6H_3\{CH(CH_3)_2\}_2$); 1.24 (d, $^3J_{H–H}$ = 7 Hz, 12H; $C_6H_3\{CH(CH_3)_2\}_2$); 1.22 (d, $^3J_{H–H}$ = 7 Hz, 12H; $C_6H_3\{CH(CH_3)_2\}_2$); 1.11 (d, $^3J_{H–H}$ = 7 Hz, 12H; $C_6H_3\{CH(CH_3)_2\}_2$). ^{13}C{^{1}H} NMR (125.80 MHz, d_8-THF): δ (ppm) 147.2, 146.4 (*ortho*-Dipp); 143.9 (NCCHN); 140.6 (H*C*N$_2$); 134.2 (NC*C*HN); 133.5, 133.4 (*para*-Dipp); 131.8, 131.4 (*ipso*-Dipp); 126.0, 125.9 (*meta*-Dipp); 30.1, 30.0

($C_6H_3\{CH(CH_3)_2\}_2$); 27.1, 24.9, 24.6, 23.1 ($C_6H_3\{CH(CH_3)_2\}_2$). ^{27}Al NMR (104.27 MHz, CD_2Cl_2): δ (ppm) 80.7 (s).

7.2.3.16 [52][B(3,5-{CF_3}$_2$$C_6H_3$)$_4$]$_2$ (52: [(aIPr)$_2$SbBr]$^{2+}$)

To a mixture of [(aIPr)$_2$SbBr$_2$]Br (143 mg, 0.126 mmol) and Na[B(3,5-{CF_3}$_2$$C_6H_3$)$_4$] (223 mg, 0.252 mmol) was added DCM (5 mL) while stirring at ambient temperature to afford a colourless solution and precipitate. The solution was stirred for one hour then filtered and the solution layered with hexane to afford a colourless oil. Crystals suitable for single crystal X-ray diffraction spontaneously formed from the oil after standing for one month. (268 mg, 76% yield). ESI-MS, positive ion mode (DCM, 60 °C, 4.5 kV): *m*/*z* 489.2186 (100%) [(aIPr)$_2$SbBr]$^{2+}$ (Calcd 489.1976). ^{1}H NMR (500.30 MHz, CD_2Cl_2): δ (ppm) 8.62 (s, $^4J_{H–H}$ = 1 Hz, 2H; *H*CN_2); 7.73 (m, 20H; BC(C*H*)$_2$(CCF_3)$_2$CH and *para*-Dipp and NCC*H*N); 7.68 (t, $^3J_{H–H}$ = 8 Hz, 2H; *para*-Dipp); 7.56 (s, 8H; BC(CH)$_2$(CCF_3)$_2$C*H*); 7.50 (dd, $^3J_{H–H}$ = 8 Hz, $^4J_{H–H}$ = 1 Hz, 2H; *meta*-Dipp); 7.45 (dd, $^3J_{H–H}$ = 8 Hz, $^4J_{H–H}$ = 1 Hz, 2H; *meta*-Dipp); 7.44 (dd, $^3J_{H–H}$ = 8 Hz, $^4J_{H–H}$ = 1 Hz, 2H; *meta*-Dipp); 7.42 (dd, $^3J_{H–H}$ = 8 Hz, $^4J_{H–H}$ = 1 Hz, 2H; *meta*-Dipp); 2.27 (sept, $^3J_{H–H}$ = 7 Hz, 2H; $C_6H_3\{CH(CH_3)_2\}_2$); 2.24 (sept, $^3J_{H–H}$ = 7 Hz, 2H; $C_6H_3\{CH(CH_3)_2\}_2$); 2.18 (sept, $^3J_{H–H}$ = 7 Hz, 2H; $C_6H_3\{CH(CH_3)_2\}_2$); 2.11 (sept, $^3J_{H–H}$ = 7 Hz, 2H; $C_6H_3\{CH(CH_3)_2\}_2$); 1.35 (d, $^3J_{H–H}$ = 7 Hz, 6H; $C_6H_3\{CH(CH_3)_2\}_2$); 1.23 (d, $^3J_{H–H}$ = 7 Hz, 6H; $C_6H_3\{CH(CH_3)_2\}_2$); 1.21 (d, $^3J_{H–H}$ = 7 Hz, 6H; $C_6H_3\{CH(CH_3)_2\}_2$); 1.18 (d, $^3J_{H–H}$ = 7 Hz, 6H; $C_6H_3\{CH(CH_3)_2\}_2$), 1.16 (d, $^3J_{H–H}$ = 7 Hz, 6H; $C_6H_3\{CH(CH_3)_2\}_2$); 1.15 (d, $^3J_{H–H}$ = 7 Hz, 6H; $C_6H_3\{CH(CH_3)_2\}_2$); 1.14 (d, $^3J_{H–H}$ = 7 Hz, 6H; $C_6H_3\{CH(CH_3)_2\}_2$); 1.05 (d, $^3J_{H–H}$ = 7 Hz, 6H; $C_6H_3\{CH(CH_3)_2\}_2$). ^{13}C{^{1}H} NMR (125.80 MHz, CD_2Cl_2): δ (ppm) 162.2 (m, $^1J_{^{13}C–^{11}B}$ = 50 Hz, $^1J_{^{13}C–^{10}B}$ = 17 Hz; B*C*(CH)$_2$(CCF_3)$_2$CH); 145.7, 145.1, 144.4, 144.1 (*ortho*-Dipp); 140.9 (H*C*N_2); 135.7 (N*C*CHN); 135.4 (NC*C*HN); 135.3 (BC(*C*H)$_2$(CCF_3)$_2$CH); 134.5, 134.3 (*para*-Dipp); 129.3 (qq, $^2J_{^{13}C–^{19}F}$ = 31 Hz, $^4J_{^{13}C–^{19}F}$ = 2 Hz;

$BC(CH)_2(CCF_3)_2CH$); 128.6 (×2) (*ipso*-Dipp); 127.3, 126.6, 126.4, 126.0 (*meta*-Dipp); 125.1 (q, $^1J_{^{13}C-^{19}F}$ = 271 Hz; $BC(CH)_2(CCF_3)_2CH$); 117.9 (sept, $^3J_{^{13}C-^{19}F}$ = 4 Hz; $BC(CH)_2(CCF_3)_2CH$); 30.3, 30.2, 30.1, 30.0 ($C_6H_3\{CH(CH_3)_2\}_2$); 26.5, 25.4, 24.7, 24.4, 24.2, 23.9, 23.3, 22.7 ($C_6H_3\{CH(CH_3)_2\}_2$).

7.2.4 Chapter 5 – Redox chemistry of IPr complexes of group 15 bromides

7.2.4.1 [53]Br (53: $[(IPr)_2P_2Br_3]^+$)

To a solution of IPr (3.117 g, 8.034 mmol) in THF (50 mL) was added PBr_3 (2.175 g, 7.088 mmol) while stirring at ambient temperature to afford a yellow solution. The solution was then heated without stirring to 55 °C for three days. During this time, a colour change from yellow to red is observed followed by the formation of large, deep red crystals which were suitable for single crystal X-ray diffraction. The red solution is then filtered and the crystals washed with warm THF until the washings remain colourless. The crystals were then dried thoroughly under vacuum at 55 °C (3.468 g, 75% crystalline yield). Anal. Calcd for $C_{54}H_{72}Br_4N_4P_2$ (1158.74): C 55.97%, H 6.26%, N 4.84%. Found: C 56.79%, H 6.34%, N 4.90%. ESI-MS, positive ion mode (DCM, 60 °C, 4.5 kV): *m*/*z* 1079.2753 (100%) $[(IPr)_2P_2Br_3]^+$ (Calcd 1079.2739). ^{1}H NMR (500.30 MHz, CD_2Cl_2): δ (ppm) 7.60 (t, $^3J_{H-H}$ = 8 Hz, 2H; *para*-Dipp); 7.55 (d, $^3J_{H-H}$ = 2 Hz, 2H; N(C*H*)(CH)N); 7.51 (t, $^3J_{H-H}$ = 8 Hz, 2H; *para*-Dipp); 7.43 (d, $^3J_{H-H}$ = 2 Hz, 2H; N(CH)(C*H*)N); 7.41 (dd, $^3J_{H-H}$ = 8 Hz, $^4J_{H-H}$ = 1 Hz, 2H; *meta*-Dipp); 7.36 (dd, $^3J_{H-H}$ = 8 Hz, $^4J_{H-H}$ = 1 Hz, 2H; *meta*-Dipp); 7.27 (dd, $^3J_{H-H}$ = 8 Hz, $^4J_{H-H}$ = 1 Hz, 2H; *meta*-Dipp); 7.06 (dd, $^3J_{H-H}$ = 8 Hz, $^4J_{H-H}$ = 1 Hz, 2H; *meta*-Dipp); 2.81 (sept, $^3J_{H-H}$ = 7 Hz, 2H; $C_6H_3\{CH(CH_3)_2\}_2$); 2.72 (sept, $^3J_{H-H}$ = 7 Hz, 2H; $C_6H_3\{CH(CH_3)_2\}_2$); 2.56 (sept, $^3J_{H-H}$ = 7 Hz, 2H; $C_6H_3\{CH(CH_3)_2\}_2$); 2.55 (sept, $^3J_{H-H}$ = 7 Hz, 2H; $C_6H_3\{CH(CH_3)_2\}_2$); 1.37 (d, $^3J_{H-H}$ = 7 Hz, 6H; $C_6H_3\{CH(CH_3)_2\}_2$); 1.33 (d, $^3J_{H-H}$ = 7 Hz, 6H; $C_6H_3\{CH(CH_3)_2\}_2$); 1.28 (d, $^3J_{H-H}$ = 7 Hz, 6H; $C_6H_3\{CH(CH_3)_2\}_2$); 1.07 (d,

$^{3}J_{H–H}$ = 7 Hz, 6H; $C_6H_3\{CH(CH_3)_2\}_2$); 1.05 (d, $^{3}J_{H–H}$ = 7 Hz, 6H; $C_6H_3\{CH(CH_3)_2\}_2$); 1.00 (d, $^{3}J_{H–H}$ = 7 Hz, 6H; $C_6H_3\{CH(CH_3)_2\}_2$); 0.81 (d, $^{3}J_{H–H}$ = 7 Hz, 6H; $C_6H_3\{CH(CH_3)_2\}_2$); 0.51 (d, $^{3}J_{H–H}$ = 7 Hz, 6H; $C_6H_3\{CH(CH_3)_2\}_2$). $^{13}C\{^{1}H\}$ NMR (125.80 MHz, CD_2Cl_2): δ (ppm) 150.2 (m, CN_2); 148.1 (t, $D^{13C–31P}$ = 3 Hz; *ortho*-Dipp); 147.3, 147.2, 146.8 (*ortho*-Dipp); 133.4, 132.9 (*para*-Dipp); 131.4 (t, $D^{13C–31P}$ = 2 Hz; *ipso*-Dipp); 131.2 (*ipso*-Dipp); 128.7 (N(*C*H)(CH)N); 126.7 (N(CH)(*C*H)N); 125.9, 125.6, 125.1, 124.3 (*meta*-Dipp); 30.3, 30.0, 29.7 ($C_6H_3\{CH(CH_3)_2\}_2$); 28.9 (t, $D^{13C–31P}$ = 2 Hz; ($C_6H_3\{CH(CH_3)_2\}_2$); 27.1, 26.8, 26.6, 26.3, 23.2, 23.1, 23.0 ($C_6H_3\{CH(CH_3)_2\}_2$); 21.1 (t, $D^{13C–31P}$ = 4 Hz; $C_6H_3\{CH(CH_3)_2\}_2$). ^{31}P NMR (202.38 MHz, CD_2Cl_2): δ (ppm) –27.3 (s). UV/Vis (C_6H_5F): λ_{max} 461 nm.

7.2.4.2 [53][B(3,5-{CF₃}₂C₆H₃)₄] (53: [(IPr)₂P₂Br₃]⁺)

To a mixture of $[(IPr)_2P_2Br_3]Br$ (329 mg, 0.284 mmol) and $Na[B(3,5\text{-}\{CF_3\}_2C_6H_3)_4]$ (252 mg, 0.284 mmol) was added THF (25 mL) and the resulting suspension stirred overnight to afford an orange solution and colourless precipitate. The solution was filtered and the solvent removed in vacuo to afford an orange solid (347 mg, 63% yield). Orange crystals suitable for single crystal X-ray diffraction were grown by layering a THF solution with hexane. Anal. Calcd for $C_{86}H_{84}BBr_3F_{24}N_4P_2$ (1942.05): C 53.19%, H 4.36%, N 2.89%. Found: C 53.25%, H 4.40%, N 2.98%. ^{1}H NMR (500.30 MHz, d_8-THF): δ (ppm) 8.05 (s, 2H; N(C*H*)(CH)N); 7.97 (s, 2H; N(CH)(C*H*)N); 7.79 (s, 8H; BC(C*H*)$_2$(CCF_3)$_2$CH); 7.62 (t, $^{3}J_{H–H}$ = 8 Hz, 2H; *para*-Dipp); 7.57 (s, 4H; BC(CH)$_2$(CCF_3)$_2$C*H*); 7.53 (t, $^{3}J_{H–H}$ = 8 Hz, 2H; *para*-Dipp); 7.48 (d, $^{3}J_{H–H}$ = 8 Hz, 2H; *meta*-Dipp); 7.43 (d, $^{3}J_{H–H}$ = 8 Hz, 2H; *meta*-Dipp); 7.34 (d, $^{3}J_{H–H}$ = 8 Hz, 2H; *meta*-Dipp); 7.12 (d, $^{3}J_{H–H}$ = 8 Hz, 2H; *meta*-Dipp); 2.92 (sept, $^{3}J_{H–H}$ = 7 Hz, 2H; $C_6H_3\{CH(CH_3)_2\}_2$; 2.80 (sept, $^{3}J_{H–H}$ = 7 Hz, 2H; $C_6H_3\{CH(CH_3)_2\}_2$); 2.67 (sept, $^{3}J_{H–H}$ = 7 Hz, 2H; $C_6H_3\{CH(CH_3)_2\}_2$); 2.60 (sept, $^{3}J_{H–H}$ = 7 Hz, 2H; $C_6H_3\{CH(CH_3)_2\}_2$); 1.41 (d, $^{3}J_{H–H}$ = 7 Hz, 6H; $C_6H_3\{CH(CH_3)_2\}_2$); 1.36 (d, $^{3}J_{H–H}$ = 7 Hz, 6H; $C_6H_3\{CH(CH_3)_2\}_2$); 1.32 (d,

$^{3}J_{H–H}$ = 7 Hz, 6H; $C_6H_3\{CH(CH_3)_2\}_2$); 1.09 (d, $^{3}J_{H–H}$ = 7 Hz, 6H; $C_6H_3\{CH(CH_3)_2\}_2$); 1.06 (d, $^{3}J_{H–H}$ = 7 Hz, 6H; $C_6H_3\{CH(CH_3)_2\}_2$); 1.01 (d, $^{3}J_{H–H}$ = 7 Hz, 6H; $C_6H_3\{CH(CH_3)_2\}_2$); 0.84 (d, $^{3}J_{H–H}$ = 7 Hz, 6H; $C_6H_3\{CH(CH_3)_2\}_2$); 0.57 (d, $^{3}J_{H–H}$ = 7 Hz, 6H; $C_6H_3\{CH(CH_3)_2\}_2$). $^{13}C\{^{1}H\}$ NMR (125.80 MHz, CD_2Cl_2): δ (ppm) 163.0 (m, $^{1}J_{^{13}C–^{11}B}$ = 50 Hz, $^{1}J_{^{13}C–^{10}B}$ = 17 Hz; $BC(CH)_2(CCF_3)_2CH$); 150.3 (m, CN_2); 148.8 (t, $D_{^{13}C–^{31}P}$ = 2 Hz; *ortho*-Dipp); 148.1, 148.0, 147.5 (*ortho*-Dipp); 135.8 ($BC(CH)_2(CCF_3)_2CH$); 134.0, 133.4 (*para*-Dipp); 132.7 (t, $D_{^{13}C–^{31}P}$ = 2 Hz; *ipso*-Dipp); 132.4 (*ipso*-Dipp); 130.3 (N(*C*H)(CH)N); 130.2 (qq, $^{2}J_{^{13}C–^{19}F}$ = 31 Hz, $^{4}J_{^{13}C–^{19}F}$ = 2 Hz; $BC(CH)_2(CCF_3)_2CH$); 128.2 (N(CH)(*C*H)N); 126.7, 126.4 (*meta*-Dipp); 125.7 (q, $^{1}J_{^{13}C–^{19}F}$ = 271 Hz; $BC(CH)_2(CCF_3)_2CH$); 125.7, 124.9 (*meta*-Dipp); 118.4 (sept, $^{3}J_{^{13}C–^{19}F}$ = 4 Hz; $BC(CH)_2(CCF_3)_2CH$); 31.0, 30.7, 30.5 ($C_6H_3\{CH(CH_3)_2\}_2$); 29.7 (t, $D_{^{13}C–^{31}P}$ = 2 Hz; ($C_6H_3\{CH(CH_3)_2\}_2$); 26.8, 26.4, 26.3, 26.2, 23.7, 23.5, 23.4 ($C_6H_3\{CH(CH_3)_2\}_2$); 21.8 (t, $D_{^{13}C–^{31}P}$ = 4 Hz; $C_6H_3\{CH(CH_3)_2\}_2$). ^{31}P NMR (202.38 MHz, d_8-THF): δ (ppm) –26.8 (s).

7.2.4.3 [54]Cl (54: $[(IPr)_2P_2Cl_3]^+$)

$[(IPr)_2P_2Br_3]Br$ (283 mg, 0.244 mmol) was dissolved in DCM (15 mL) and stirred at 60 °C in an ampoule overnight to afford a yellow solution. The solution was filtered and concentrated to 5 mL and layered with hexane to afford large yellow crystals. The pale yellow solution was filtered from the crystals which were then dried thoroughly under vacuum (164 mg, 67% crystalline yield). Crystals of $[(IPr)_2P_2Cl_3]Br·4DCM$ suitable for single crystal X-ray diffraction were grown from slow diffusion of hexane into a crude reaction solution. Anal. Calcd for $C_{54}H_{72}Cl_4N_4P_2$ (980.94): C 66.12%, H 7.40%, N 5.71%. Anal. Calcd for $C_{54}H_{72}Cl_4N_4P_2(CH_2Cl_2)_{0.2}$ (997.92): C 65.23%, H 7.31%, N 5.61%. Found: C 65.18%, H 7.34%, N 5.60%. ESI-MS, positive ion mode (DCM, 60 °C, 4.5 kV): *m/z* 945.4067 (100%) $[(IPr)_2P_2Cl_3]^+$ (Calcd 945.4267). ^{1}H NMR (500.30 MHz, CD_2Cl_2): δ (ppm) 7.59 (t,

$^{3}J_{H–H}$ = 8 Hz, 2H; *para*-Dipp); 7.51 (d, $^{3}J_{H–H}$ = 2 Hz, 2H; N(C*H*)(CH)N); 7.50 (t, $^{3}J_{H–H}$ = 8 Hz, 2H; *para*-Dipp); 7.44 (d, $^{3}J_{H–H}$ = 2 Hz, 2H; N(CH)(C*H*)N); 7.40 (dd, $^{3}J_{H–H}$ = 8 Hz, $^{4}J_{H–H}$ = 1 Hz, 2H; *meta*-Dipp); 7.35 (dd, $^{3}J_{H–H}$ = 8 Hz, $^{4}J_{H–H}$ = 1 Hz, 2H; *meta*-Dipp); 7.27 (dd, $^{3}J_{H–H}$ = 8 Hz, $^{4}J_{H–H}$ = 1 Hz, 2H; *meta*-Dipp); 7.04 (dd, $^{3}J_{H–H}$ = 8 Hz, $^{4}J_{H–H}$ = 1 Hz, 2H; *meta*-Dipp); 2.60 (sept, $^{3}J_{H–H}$ = 7 Hz, 2H; $C_6H_3\{CH(CH_3)_2\}_2$); 2.49 (m, 6H; $C_6H_3\{CH(CH_3)_2\}_2$); 1.31 (d, $^{3}J_{H–H}$ = 7 Hz, 6H; $C_6H_3\{CH(CH_3)_2\}_2$); 1.27 (d, $^{3}J_{H–H}$ = 7 Hz, 6H; $C_6H_3\{CH(CH_3)_2\}_2$); 1.23 (d, $^{3}J_{H–H}$ = 7 Hz, 6H; $C_6H_3\{CH(CH_3)_2\}_2$); 1.07 (d, $^{3}J_{H–H}$ = 7 Hz, 6H; $C_6H_3\{CH(CH_3)_2\}_2$); 1.05 (d, $^{3}J_{H–H}$ = 7 Hz, 6H; $C_6H_3\{CH(CH_3)_2\}_2$); 1.02 (d, $^{3}J_{H–H}$ = 7 Hz, 6H; $C_6H_3\{CH(CH_3)_2\}_2$); 0.84 (d, $^{3}J_{H–H}$ = 7 Hz, 6H; $C_6H_3\{CH(CH_3)_2\}_2$); 0.44 (d, $^{3}J_{H–H}$ = 7 Hz, 6H; $C_6H_3\{CH(CH_3)_2\}_2$). $^{13}C\{^{1}H\}$ NMR (125.80 MHz, CD_2Cl_2): δ (ppm) 152.7 (m, *C*N_2); 148.2 (t, $D^{13C–31P}$ = 3 Hz; *ortho*-Dipp); 147.3, 147.1, 146.6 (*ortho*-Dipp); 133.3, 132.8 (*para*-Dipp); 131.1 (*ipso*-Dipp); 131.0 (t, $D^{13C–31P}$ = 2 Hz; *ipso*-Dipp); 128.3 (N(*C*H)(CH)N), 126.2 (N(CH)(*C*H)N), 125.7, 125.5, 124.9, 124.1 (*meta*-Dipp); 29.9, 29.8, 29.4 ($C_6H_3\{CH(CH_3)_2\}_2$); 28.9 (t, $D^{13C–31P}$ = 3 Hz; ($C_6H_3\{CH(CH_3)_2\}_2$); 26.9, 26.7, 26.5, 26.4, 22.9, 22.7, 22.3 ($C_6H_3\{CH(CH_3)_2\}_2$); 21.0 (t, $D^{13C–31P}$ = 4 Hz; $C_6H_3\{CH(CH_3)_2\}_2$). ^{31}P NMR (202.38 MHz, CD_2Cl_2): δ (ppm) –35.4 (s). UV/Vis (C_6H_5F): λ_{max} 435 nm.

7.2.4.4 [55][B(3,5-{CF₃}₂C₆H₃)₄]₂ (55: [(IPr)₂P₂Br₂]²⁺)

To a mixture of $[(IPr)_2P_2Br_3][B(3,5\text{-}\{CF_3\}_2C_6H_3)_4]$ (105 mg, 0.0541 mmol) and $Na[B(3,5\text{-}\{CF_3\}_2C_6H_3)_4]$ (48 mg, 0.0541 mmol) was added DFB (5 mL) while stirring at ambient temperature to afford a cloudy yellow solution. The solution was then filtered and the solvent removed in vacuo to afford a pale yellow crystalline solid which was then washed with DCM (5 mL) and the solid dried thoroughly under vacuum (145 mg, 99% yield). Crystals suitable for single crystal X-ray diffraction were grown from a saturated DCM solution at room temperature or by slow diffusion of hexane into a DFB solution. Anal. Calcd for

$C_{118}H_{96}B_2Br_2F_{48}N_4P_2$ (2725.36): C 52.00%, H 3.55%, N 2.06%. Found: C 52.28%, H 3.42%, N 1.86%. ESI-MS, positive ion mode (DFB, 60 °C, 4.5 kV): *m/z* 1861.5209 (3%) $[(IPr)_2P_2Br_2(B(3,5\text{-}\{CF_3\}_2C_6H_3)_4)]^+$ (Calcd 1861.4248), 1079.2500 (76%) $[(IPr)_2P_2Br_3]^+$ (Calcd 1079.2739), 1015.3296 (100%) $[(IPr)_2P_2Br_2(OH)]^+$ (Calcd 1015.3608), 499.1745 (15%) $[(IPr)_2P_2Br_2]^{2+}$ (Calcd 499.1787), 468.2322 (5%) $[(IPr)_2P_2Br(OH)]^{2+}$ (Calcd 468.2208). ^{1}H NMR (500.30 MHz, DFB): δ (ppm) 8.31 (s, 16H; BC(C*H*)$_2$(CCF$_3$)$_2$CH); 8.06 (s, 4H; N(C*H*)$_2$N); 7.79 (t, $^3J_{H–H}$ = 8 Hz, 4H; *para*-Dipp); 7.69 (s, 8H; BC(CH)$_2$(CCF$_3$)$_2$C*H*); 7.46 (d, $^3J_{H–H}$ = 8 Hz, 4H; *meta*-Dipp); 7.38 (d, $^3J_{H–H}$ = 8 Hz, 4H; *meta*-Dipp); 2.40 (overlapping sept, $^3J_{H–H}$ = 7 Hz, 8H; C$_6$H$_3${C*H*(CH$_3$)$_2$}$_2$); 1.34 (d, $^3J_{H–H}$ = 7 Hz, 12H; C$_6$H$_3${CH(C*H*$_3$)$_2$}$_2$); 1.27 (d, $^3J_{H–H}$ = 7 Hz, 12H; C$_6$H$_3${CH(C*H*$_3$)$_2$}$_2$); 1.19 (d, $^3J_{H–H}$ = 7 Hz, 24H; C$_6$H$_3${CH(C*H*$_3$)$_2$}$_2$). ^{13}C{^{1}H} NMR (125.80 MHz, DFB): δ (ppm) 163.0 (m, $^1J_{^{13}C–^{11}B}$ = 50 Hz, $^1J_{^{13}C–^{10}B}$ = 17 Hz; B*C*(CH)$_2$(CCF$_3$)$_2$CH); 146.3, 146.1 (*ortho*-Dipp); 138.5 (m, *C*N$_2$); 135.6 (BC(*C*H)$_2$(CCF$_3$)$_2$CH); 134.7 (N(*C*H)(CH)N); 132.2 (*para*-Dipp); 130.2 (s, *ipso*-Dipp and qq, $^2J_{^{13}C–^{19}F}$ = 31 Hz, $^4J_{^{13}C–^{19}F}$ = 2 Hz; BC(CH)$_2$(*C*CF$_3$)$_2$CH); 128.2 (N(CH)(*C*H)N); 126.1, 125.8 (*meta*-Dipp); 125.4 (q, $^1J_{^{13}C–^{19}F}$ = 271 Hz; BC(CH)$_2$(C*C*F$_3$)$_2$CH); 118.1 (sept, $^3J_{^{13}C–^{19}F}$ = 4 Hz; BC(CH)$_2$(CCF$_3$)$_2$*C*H); 30.5, 30.3 (C$_6$H$_3${*C*H(CH$_3$)$_2$}$_2$); 26.2, 25.9, 21.9 (×2) (C$_6$H$_3${CH(*C*H$_3$)$_2$}$_2$). ^{31}P NMR (202.38 MHz, DFB): δ (ppm) –1.8 (s). ^{11}B NMR (128.39 MHz, DFB): δ (ppm) –6.2 (s). ^{19}F NMR (376.54 MHz, DFB): δ (ppm) –63.1 (s). UV/Vis (DFB): λ_{max} 382 nm.

7.2.4.5 [56][B(3,5-{CF$_3$}$_2$C$_6$H$_3$)$_4$]$_2$ (56: [(IPr)$_2$P$_2$Cl$_2$]$^{2+}$)

To a mixture of [(IPr)$_2$P$_2$Cl$_3$]Cl (32 mg, 0.0326 mmol) and Na[B(3,5-{CF$_3$}$_2$C$_6$H$_3$)$_4$] (11 mg, 0.0652 mmol) in an NMR tube was added DFB (500 μL) at ambient temperature to afford a cloudy yellow solution. The solution was then filtered and the solvent removed in vacuo to afford a pale yellow solid which was then washed with DCM (5 mL) and the solid dried

thoroughly under vacuum (52 mg, 79% yield). Crystals suitable for single crystal X-ray diffraction were grown by slow diffusion of hexane into a DFB solution. ESI-MS, positive ion mode (DFB, 60 °C, 4.5 kV): *m/z* 1773.9340 (1%) $[(IPr)_2P_2Cl_2(B(3,5\text{-}\{CF_3\}_2C_6H_3)_4)]^+$ (Calcd 1773.5228), 945.6427 (57%) $[(IPr)_2P_2Cl_3]^+$ (Calcd 945.4268), 455.3389 (100%) $[(IPr)_2P_2Cl_2]^{2+}$ (Calcd 455.2290), 445.3757 (14%) $[(IPr)_2P_2Cl(OH)]^{2+}$ (Calcd 445.2474), 436.3769 (60%) $[(IPr)_2P_2(OH)_2]^{2+}$ (Calcd 436.2644). ^{1}H NMR (500.30 MHz, DFB): δ (ppm) 8.31 (s, 16H; BC(C*H*)$_2$(CCF$_3$)$_2$CH); 8.07 (s, 4H; N(C*H*)$_2$N); 7.79 (t, $^3J_{H–H}$ = 8 Hz, 4H; *para*-Dipp); 7.68 (s, 8H; BC(CH)$_2$(CCF$_3$)$_2$C*H*); 7.45 (d, $^3J_{H–H}$ = 8 Hz, 4H; *meta*-Dipp); 7.38 (d, $^3J_{H–H}$ = 8 Hz, 4H; *meta*-Dipp); 2.35 (sept, $^3J_{H–H}$ = 7 Hz, 4H; C$_6$H$_3${C*H*(CH$_3$)$_2$}$_2$); 2.32 (sept, $^3J_{H–H}$ = 7 Hz, 4H; C$_6$H$_3${C*H*(CH$_3$)$_2$}$_2$); 1.33 (d, $^3J_{H–H}$ = 7 Hz, 12H; C$_6$H$_3${CH(C*H*$_3$)$_2$}$_2$); 1.23 (d, $^3J_{H–H}$ = 7 Hz, 12H; C$_6$H$_3${CH(C*H*$_3$)$_2$}$_2$); 1.21 (d, $^3J_{H–H}$ = 7 Hz, 12H; C$_6$H$_3${CH(C*H*$_3$)$_2$}$_2$); 1.19 (d, $^3J_{H–H}$ = 7 Hz, 12H; C$_6$H$_3${CH(C*H*$_3$)$_2$}$_2$). ^{31}P NMR (202.38 MHz, DFB): δ (ppm) 20.5 (s). ^{11}B NMR (128.39 MHz, DFB): δ (ppm) –6.2 (s). ^{19}F NMR (376.54 MHz, DFB): δ (ppm) –63.1 (s). UV/Vis (DFB): λ_{max} 375 nm.

7.2.4.6 [57][SnBr$_5$(THF)] (57: [(IPr)$_2$P$_2$Br]$^+$)

To a suspension of $[(IPr)_2P_2Br_3]Br$ (234 mg, 0.201 mmol) in THF (5 mL) was added a solution of $SnBr_2$ (56 mg, 0.201 mmol) in THF (5 mL) while stirring at ambient temperature to afford a deep red solution. The mixture was stirred for five minutes before the solvent was removed in vacuo to afford a deep red solid (290 mg, 95% yield). Crystals of $[(IPr)_2P_2Br]_2[SnBr_6]$ suitable for single crystal X-ray diffraction were grown from the reaction mixture on addition of half an equivalent of IPr (which reacts with the $[SnBr_5(THF)]^-$ anion to afford $(IPr)SnBr_4$ and $[SnBr_6]^{2-}$) Anal. Calcd for $C_{58}H_{80}Br_6N_4OP_2Sn$ (1509.36): C 46.15%, H 5.34%, N 3.71%. Found: C 45.54%, H 5.26%, N 3.70%. ESI-MS, positive ion mode (DCM, 60 °C, 4.5 kV): *m/z* 919.5514 (100%) $[(IPr)_2P_2Br]^+$ (Calcd 919.4394). ^{1}H NMR (500.30 MHz, d_8-THF,

338 K): δ (ppm) 7.72 (s, 4H; N(C*H*)$_2$N); 7.50 (t, $^3J_{H–H}$ = 8 Hz, 4H; *para*-Dipp); 7.25 (d, $^3J_{H–H}$ = 8 Hz, 8H; *meta*-Dipp); 2.50 (sept, 8H; $^3J_{H–H}$ = 7 Hz, C$_6$H$_3${C*H*(CH$_3$)$_2$}$_2$); 1.07 (d, $^3J_{H–H}$ = 7 Hz, 48H; C$_6$H$_3${CH(C*H*$_3$)$_2$}$_2$). ^{1}H NMR (500.30 MHz, d_8-THF, 208 K): δ (ppm) 8.24 (s, 1H; N(C*H*)$_2$N); 8.20 (s, 1H; N(C*H*)$_2$N); 7.80 (s, 2H; N(C*H*)$_2$N); 7.64 (br t, $^3J_{H–H}$ = 8 Hz, 1H; *para*-Dipp); 7.46–7.58 (m, 5H; *meta*-Dipp and *para*-Dipp); 7.40 (br d, $^3J_{H–H}$ = 8 Hz, 1H; *meta*-Dipp); 7.34 (d, $^3J_{H–H}$ = 8 Hz, 2H; *meta*-Dipp); 7.26 (d, $^3J_{H–H}$ = 8 Hz, 2H; *meta*-Dipp); 7.00 (br d, $^3J_{H–H}$ = 8 Hz, 1H; *meta*-Dipp); 3.14 (br sept, 1H; $^3J_{H–H}$ = 7 Hz, C$_6$H$_3${C*H*(CH$_3$)$_2$}$_2$); 2.60 (br sept, 1H; $^3J_{H–H}$ = 7 Hz, C$_6$H$_3${C*H*(CH$_3$)$_2$}$_2$); 2.51 (sept, 2H; $^3J_{H–H}$ = 7 Hz, C$_6$H$_3${C*H*(CH$_3$)$_2$}$_2$); 2.30 (sept, 2H; $^3J_{H–H}$ = 7 Hz, C$_6$H$_3${C*H*(CH$_3$)$_2$}$_2$); 2.15 (br sept, 1H; $^3J_{H–H}$ = 7 Hz, C$_6$H$_3${C*H*(CH$_3$)$_2$}$_2$); 2.96 (br sept, 1H; $^3J_{H–H}$ = 7 Hz, C$_6$H$_3${C*H*(CH$_3$)$_2$}$_2$); 1.29 (d, $^3J_{H–H}$ = 7 Hz, 3H; C$_6$H$_3${CH(C*H*$_3$)$_2$}$_2$); 1.22 (d, $^3J_{H–H}$ = 7 Hz, 12H; C$_6$H$_3${CH(C*H*$_3$)$_2$}$_2$); 1.17 (d, $^3J_{H–H}$ = 7 Hz, 3H; C$_6$H$_3${CH(C*H*$_3$)$_2$}$_2$); 1.12 (d, $^3J_{H–H}$ = 7 Hz, 6H; C$_6$H$_3${CH(C*H*$_3$)$_2$}$_2$); 1.08 (d, $^3J_{H–H}$ = 7 Hz, 3H; C$_6$H$_3${CH(C*H*$_3$)$_2$}$_2$); 1.01 (d, $^3J_{H–H}$ = 7 Hz, 9H; C$_6$H$_3${CH(C*H*$_3$)$_2$}$_2$); 0.95 (d, $^3J_{H–H}$ = 7 Hz, 3H; C$_6$H$_3${CH(C*H*$_3$)$_2$}$_2$); 0.79 (d, $^3J_{H–H}$ = 7 Hz, 6H; C$_6$H$_3${CH(C*H*$_3$)$_2$}$_2$); 0.57 (d, $^3J_{H–H}$ = 7 Hz, 3H; C$_6$H$_3${CH(C*H*$_3$)$_2$}$_2$). ^{13}C{^{1}H} NMR (125.80 MHz, d_8-THF, 338 K): δ (ppm) 157.8 (v br, *C*N$_2$); 147.0 (*ortho*-Dipp); 133.4 (*ipso*-Dipp); 132.9 (*para*-Dipp); 128.3 (N(*C*H)$_2$N); 125.9 (*meta*-Dipp); 30.2 (C$_6$H$_3${*C*H(CH$_3$)$_2$}$_2$); 25.9, 23.5 (C$_6$H$_3${CH(*C*H$_3$)$_2$}$_2$). ^{13}C{^{1}H} NMR (125.80 MHz, d_8-THF, 208 K): δ (ppm) 164.2 (dd, $^1J_{^{13}C–^{31}P}$ = 118 Hz, $^2J_{^{13}C–^{31}P}$ = 32 Hz; *C*N$_2$); 150.6 (dd, $^1J_{^{13}C–^{31}P}$ = 85 Hz, $^2J_{^{13}C–^{31}P}$ = 26 Hz; *C*N$_2$); 147.2 (x2), 147.1, 146.7, 146.6, 145.9 (x2), 145.4 (*ortho*-Dipp); 133.7, 133.5 (x2), 133.0 (*ipso*-Dipp); 132.7, 132.6 (x2), 132.4 (*para*-Dipp); 130.5, 127.3, 127.2 (x2) (N(*C*H)$_2$N); 126.6, 126.3 (x2), 126.1, 126.0, 125.5, 125.2 (x2) (*meta*-Dipp); 30.3, 30.2 (x2), 29.9 (C$_6$H$_3${*C*H(CH$_3$)$_2$}$_2$); 24.2, 23.9, 23.6 (x2), 23.3, 23.1, 22.0 (x2) (C$_6$H$_3${CH(*C*H$_3$)$_2$}$_2$). No observable resonances in the ^{31}P NMR spectrum at 338 K. ^{31}P NMR (202.38 MHz, d_8-THF, 208 K): δ (ppm) 145.4 (d, $^1J_{^{31}P–^{31}P}$ = 391 Hz;

(IPr)*P*PBr(IPr)); –7.6 (d, $^{1}J_{^{31}P-^{31}P}$ = 391 Hz; (IPr)P*P*Br(IPr)). $^{119}Sn\{^{1}H\}$ NMR (186.43 MHz, d_8-THF, 298 K): δ (ppm) –1657.7 (s).

7.2.4.7 [58][B(3,5-{CF_3}$_2$$C_6H_3$)$_4$] (58: [(IPr)$_2$$P_2$]$^{\bullet+}$)

To a solution of [(IPr)$_2$$P_2$$Br_3$][B(3,5-{$CF_3$}$_2$$C_6H_3$)$_4$] (44 mg, 0.023 mmol) in THF (500 μL) was added tetrakis(dimethylamino)ethylene (7 mg, 0.034 mmol) via microsyringe to instantly afford a deep purple solution. After 30 minutes, the solvent was removed in vacuo and the product extracted with diethyl ether (5 mL). After filtration, the solvent was removed in vacuo to afford a black solid (20 mg, 52% yield). Crystals suitable for single crystal X-ray diffraction were grown by layering a THF solution with hexane. Anal. Calcd for $C_{86}H_{84}BF_{24}N_4P_2$ (1700.32): C 60.68%, H 4.97%, N 3.29%. Found: C 58.75%, H 5.11%, N 3.22%. ESI-MS, positive ion mode (DCM, 60 °C, 4.5 kV): *m/z* 838.5018 (100%) [(IPr)$_2$$P_2$]$^+$ (Calcd 838.5227). No observable resonances in the ^{31}P NMR spectrum. UV/Vis (C_6H_5F): λ_{max} 464 nm; 588 nm.

7.2.4.8 [59]Br (59: [(IPr)$_2$$As_2$$Br_3$]$^+$)

To a solution of (IPr)$AsBr_3$ (340 mg, 0.484 mmol) in DCM (2 mL) was added a solution of TDAE (48 mg, 0.242 mmol) in DCM (2 mL) rapidly while stirring at ambient temperature. The reaction mixture quickly turned a brighter orange and over two minutes developed a deep green to brown solution and colourless precipitate. After stirring for a further five minutes, the mixture had afforded a deep pink solution and colourless precipitate. The mixture was allowed to stir for a further two hours before the solution was filtered and layered with hexane to afford deep pink crystals of [(IPr)$_2$$As_2$$Br_3$]Br·3DCM suitable for single crystal X-ray diffraction (182 mg, 60% crystalline yield). Anal. Calcd for $C_{54}H_{72}As_2Br_4N_4$ (1246.64): C 52.03%, H 5.82%, N 4.49%. Found: C 52.02%, H 5.92%, N 4.50%. ESI-MS, positive ion mode (DCM, 60 °C, 4.5 kV): *m/z* 1167.3397 (100%) [(IPr)$_2$$As_2$$Br_3$]$^+$ (Calcd 1167.1696).

^{1}H NMR (500.30 MHz, CD_2Cl_2): δ (ppm) 7.63 (t, $^{3}J_{H–H}$ = 8 Hz, 2H; *para*-Dipp); 7.58 (d, $^{3}J_{H–H}$ = 2 Hz, 2H; N(C*H*)(CH)N); 7.52 (t, $^{3}J_{H–H}$ = 8 Hz, 2H; *para*-Dipp); 7.43 (dd, $^{3}J_{H–H}$ = 8 Hz, $^{4}J_{H–H}$ = 1 Hz, 2H; *meta*-Dipp); 7.42 (d, $^{3}J_{H–H}$ = 1 Hz, 2H; N(CH)(C*H*)N); 7.39 (dd, $^{3}J_{H–H}$ = 8 Hz, $^{4}J_{H–H}$ = 1 Hz, 2H; *meta*-Dipp); 7.31 (dd, $^{3}J_{H–H}$ = 8 Hz, $^{4}J_{H–H}$ = 1 Hz, 2H; *meta*-Dipp); 7.05 (dd, $^{3}J_{H–H}$ = 8 Hz, $^{4}J_{H–H}$ = 1 Hz, 2H; *meta*-Dipp); 2.78 (sept, $^{3}J_{H–H}$ = 7 Hz, 2H; $C_6H_3\{CH(CH_3)_2\}_2$); 2.76 (sept, $^{3}J_{H–H}$ = 7 Hz, 2H; $C_6H_3\{CH(CH_3)_2\}_2$); 2.57 (sept, $^{3}J_{H–H}$ = 7 Hz, 2H; $C_6H_3\{CH(CH_3)_2\}_2$); 2.50 (sept, $^{3}J_{H–H}$ = 7 Hz, 2H; $C_6H_3\{CH(CH_3)_2\}_2$); 1.39 (d, $^{3}J_{H–H}$ = 7 Hz, 6H; $C_6H_3\{CH(CH_3)_2\}_2$); 1.36 (d, $^{3}J_{H–H}$ = 7 Hz, 6H; $C_6H_3\{CH(CH_3)_2\}_2$); 1.31 (d, $^{3}J_{H–H}$ = 7 Hz, 6H; $C_6H_3\{CH(CH_3)_2\}_2$); 1.08 (d, $^{3}J_{H–H}$ = 7 Hz, 6H; $C_6H_3\{CH(CH_3)_2\}_2$); 1.05 (d, $^{3}J_{H–H}$ = 7 Hz, 6H; $C_6H_3\{CH(CH_3)_2\}_2$); 1.03 (d, $^{3}J_{H–H}$ = 7 Hz, 6H; $C_6H_3\{CH(CH_3)_2\}_2$); 0.83 (d, $^{3}J_{H–H}$ = 7 Hz, 6H; $C_6H_3\{CH(CH_3)_2\}_2$); 0.67 (d, $^{3}J_{H–H}$ = 7 Hz, 6H; $C_6H_3\{CH(CH_3)_2\}_2$). $^{13}C\{^{1}H\}$ NMR (125.80 MHz, CD_2Cl_2): δ (ppm) 150.1 (CN_2); 147.6, 147.5, 146.9, 146.8 (*ortho*-Dipp); 133.6, 133.0 (*para*-Dipp); 131.6, 131.1 (*ipso*-Dipp); 128.7 (N(*C*H)(CH)N); 126.9 (N(CH)(*C*H)N); 126.6, 125.6, 125.0, 124.2 (*meta*-Dipp); 30.0, 29.8, 29.7, 29.1 ($C_6H_3\{CH(CH_3)_2\}_2$); 27.3, 26.8, 26.7, 26.4, 23.3, 23.2, 23.1, 22.0 ($C_6H_3\{CH(CH_3)_2\}_2$). UV/Vis (DCM): λ_{max} 502 nm.

7.2.4.9 [60][B(3,5-{CF_3}$_2$$C_6H_3$)$_4$]$_2$ (60: [(IPr)$_2$$As_2Br_2$]$^+$)

To a mixture of $[(IPr)_2As_2Br_3]Br$ (350 mg, 0.281 mmol) and $Na[B(3,5\text{-}\{CF_3\}_2C_6H_3)_4]$ (498 mg, 0.562 mmol) was added DFB (5 mL) while stirring at ambient temperature to rapidly afford a bright yellow solution and colourless precipitate. The solution was stirred for one hour then filtered and layered with hexane to afford orange crystals suitable for single crystal X-ray diffraction (672 mg, 85% crystalline yield). Anal. Calcd for $C_{118}H_{96}As_2B_2Br_2F_{48}N_4$ (2813.25): C 50.38%, H 3.44%, N 1.99%. ^{1}H NMR (500.30 MHz, DFB and C_6D_6): δ (ppm) 8.42 (s, 16H; BC(C*H*)$_2$(CCF_3)$_2$CH); 7.82 (s, 4H; N(C*H*)$_2$N); 7.79 (t, $^{3}J_{H–H}$ = 8 Hz, 4H;

para-Dipp); 7.77 (s, 8H; BC(CH)$_2$(CCF$_3$)$_2$C*H*); 7.46 (d, $^3J_{H–H}$ = 8 Hz, 4H; *meta*-Dipp); 7.44 (d, $^3J_{H–H}$ = 8 Hz, 4H; *meta*-Dipp); 2.42 (overlapping sept, $^3J_{H–H}$ = 7 Hz, 8H; C$_6$H$_3${C*H*(CH$_3$)$_2$}$_2$); 1.36 (d, $^3J_{H–H}$ = 7 Hz, 12H; C$_6$H$_3${CH(C*H*$_3$)$_2$}$_2$); 1.30 (d, $^3J_{H–H}$ = 7 Hz, 12H; C$_6$H$_3${CH(C*H*$_3$)$_2$}$_2$); 1.22 (d, $^3J_{H–H}$ = 7 Hz, 12H; C$_6$H$_3${CH(C*H*$_3$)$_2$}$_2$); 1.20 (d, $^3J_{H–H}$ = 7 Hz, 12H; C$_6$H$_3${CH(C*H*$_3$)$_2$}$_2$). ^{13}C{^{1}H} NMR (125.80 MHz, DFB): δ (ppm) 163.0 (m, $^1J_{^{13}C–^{11}B}$ = 50 Hz, $^1J_{^{13}C–^{10}B}$ = 17 Hz; B*C*(CH)$_2$(CCF$_3$)$_2$CH); 146.7, 146.8 (*ortho*-Dipp); 142.6 (m, *C*N$_2$); 135.6 (BC(*C*H)$_2$(CCF$_3$)$_2$CH); 134.9 (*para*-Dipp); 130.8 (N(*C*H)(CH)N); 130.2 (qq, $^2J_{^{13}C–^{19}F}$ = 31 Hz, $^4J_{^{13}C–^{19}F}$ = 2 Hz; BC(CH)$_2$(*C*CF$_3$)$_2$CH); 130.1 (s, *ipso*-Dipp); 127.1 (N(CH)(*C*H)N); 126.2, 126.1 (*meta*-Dipp); 125.4 (q, $^1J_{^{13}C–^{19}F}$ = 271 Hz; BC(CH)$_2$(C*C*F$_3$)$_2$CH); 118.1 (sept, $^3J_{^{13}C–^{19}F}$ = 4 Hz; BC(CH)$_2$(CCF$_3$)$_2$*C*H); 30.5, 30.3 (C$_6$H$_3${*C*H(CH$_3$)$_2$}$_2$); 26.2, 26.0, 22.2, 22.1 (C$_6$H$_3${CH(*C*H$_3$)$_2$}$_2$). ^{11}B NMR (128.39 MHz, DFB): δ (ppm) –6.2 (s). ^{19}F NMR (376.54 MHz, DFB): δ (ppm) –63.1 (s). UV/Vis (DFB): λ_{max} 371 nm; 442 nm.

7.2.5 Chapter 6 – Further work and conclusions

7.2.5.1 (IPr)SnBr$_2$ (61)

To a mixture of IPr (280 mg, 0.722 mmol) and SnBr$_2$ (201 mg, 0.722 mmol) was added THF (10 mL) while stirring at ambient temperature to afford a colourless solution. The solution was filtered and layered with hexane to afford colourless crystals suitable for single crystal X-ray diffraction (452 mg, 94% crystalline yield). ^{1}H NMR (500.30 MHz, d_8-THF): δ (ppm) 7.72 (s, 2H; N(C*H*)$_2$N); 7.50 (t, $^3J_{H–H}$ = 8 Hz, 2H; *para*-Dipp); 7.35 (d, $^3J_{H–H}$ = 8 Hz, 4H; *meta*-Dipp); 2.77 (sept, $^3J_{H–H}$ = 7 Hz, 4H; C$_6$H$_3${C*H*(CH$_3$)$_2$}$_2$); 1.39 (d, $^3J_{H–H}$ = 7 Hz, 12H; C$_6$H$_3${CH(C*H*$_3$)$_2$}$_2$); 1.18 (d, $^3J_{H–H}$ = 7 Hz, 12H; C$_6$H$_3${CH(C*H*$_3$)$_2$}$_2$). ^{13}C{^{1}H} NMR (125.80 MHz, d_8-THF): δ (ppm) 177.4 (*C*N$_2$); 146.9 (*ortho*-Dipp); 134.7 (*ipso*-Dipp); 131.8

(*para*-Dipp); 127.1 (N(*C*H)$_2$N); 125.1 (*meta*-Dipp); 30.0 (C$_6$H$_3${*C*H(CH$_3$)$_2$}$_2$); 26.0, 23.7 (C$_6$H$_3${CH(*C*H$_3$)$_2$}$_2$). ^{119}Sn{^{1}H} NMR (149.24 MHz, d_8-THF): δ (ppm) –12.1 (s).

7.2.5.2 [62][AlBr$_4$] (62: [(IPr)BBr$_2$]$^+$)

To a mixture of (IPr)BBr$_3$ (260 mg, 0.407 mmol) and AlBr$_3$ (109 mg, 0.407 mmol) was added DFB (5 mL) while stirring at ambient temperature to afford a colourless solution. The mixture was stirred for 30 minutes before the solution was filtered and layered with hexane to afford colourless crystals suitable for single crystal X-ray diffraction (310 mg, 82% yield). Anal. Calcd for C$_{27}$H$_{36}$AlBBr$_6$N$_2$ (905.80): C 35.80%, H 4.01%, N 3.09%. ^{1}H NMR (500.30 MHz, DFB): δ (ppm) 8.16 (s, 2H; N(C*H*)$_2$N); 7.59 (t, $^3J_{H–H}$ = 8 Hz, 2H; *para*-Dipp); 7.36 (d, $^3J_{H–H}$ = 8 Hz, 4H; *meta*-Dipp); 2.49 (sept, $^3J_{H–H}$ = 7 Hz, 4H; C$_6$H$_3${C*H*(CH$_3$)$_2$}$_2$); 1.30 (d, $^3J_{H–H}$ = 7 Hz, 12H; C$_6$H$_3${CH(C*H*$_3$)$_2$}$_2$); 1.28 (d, $^3J_{H–H}$ = 7 Hz, 12H; C$_6$H$_3${CH(C*H*$_3$)$_2$}$_2$). ^{13}C{^{1}H} NMR (125.80 MHz, CD$_2$Cl$_2$): δ (ppm) 145.4 (*ortho*-Dipp); 133.6 (*para*-Dipp); 131.3 (N(*C*H)$_2$N); 130.7 (*ipso*-Dipp); 125.8 (*meta*-Dipp); 30.1 (C$_6$H$_3${*C*H(CH$_3$)$_2$}$_2$); 25.3, 22.7 (C$_6$H$_3${CH(*C*H$_3$)$_2$}$_2$). ^{11}B NMR (128.39 MHz, DFB): δ (ppm) 48.9 (s). ^{27}Al NMR (104.27 MHz, CD$_2$Cl$_2$): δ (ppm) 81.3 (s).

7.2.5.3 (IPr)$_2$Ga$_2$Br$_4$ (63)

To a solution of IPr (1.740 g, 4.485 mmol) in THF (30 mL) was added a solution of 'GaBr$_2$' (1.029 g, 4.485 mmol) in THF (10 mL) while stirring at ambient temperature to afford an orange solution. The mixture was stirred for 30 minutes before the solution was the solution was filtered and the volatiles were removed in vacuo to afford an amorphous solid. Diethyl ether (20 mL) was added and the resulting orange solution left to stand for one hour to afford a crystalline precipitate. The orange solution was filtered from the precipitate which was then washed with a further 10 mL of diethyl ether and subsequently dried thoroughly under vacuum

(1.646 g, 59% yield). Colourless crystals suitable for single crystal X-ray diffraction were grown by slow diffusion of hexane into a THF solution. ^{1}H NMR (500.30 MHz, CD_2Cl_2): δ (ppm) 7.41 (t, $^{3}J_{H–H}$ = 8 Hz, 2H; *para*-Dipp); 7.23 (d, $^{3}J_{H–H}$ = 8 Hz, 4H; *meta*-Dipp); 7.01 (s, 2H; N(C*H*)$_2$N); 2.74 (sept, $^{3}J_{H–H}$ = 7 Hz, 4H; $C_6H_3\{CH(CH_3)_2\}_2$); 1.29 (d,$^{3}J_{H–H}$ = 7 Hz, 12H; $C_6H_3\{CH(CH_3)_2\}_2$); 1.00 (d, $^{3}J_{H–H}$ = 7 Hz, 12H; $C_6H_3\{CH(CH_3)_2\}_2$). $^{13}C\{^{1}H\}$ NMR (125.80 MHz, CD_2Cl_2): δ (ppm) 166.4 (*C*N$_2$); 146.3 (*ortho*-Dipp); 135.1 (*ipso*-Dipp); 130.8 (*para*-Dipp); 126.3 (N(*C*H)$_2$N); 124.8 (*meta*-Dipp); 29.0 ($C_6H_3\{CH(CH_3)_2\}_2$); 26.2, 23.7 ($C_6H_3\{CH(CH_3)_2\}_2$).

7.3 Characterisation techniques

7.3.1 Single crystal X-ray diffraction

Single crystal X-ray diffraction data were collected using either an Oxford Diffraction Supernova dual-source diffractometer equipped with a 135 mm Atlas CCD area detector or an Enraf-Nonius kappa-CCD diffractometer equipped with a 95 mm CCD area detector. Crystals were selected under Paratone-N® oil, mounted on micromount loops, and quench-cooled using an Oxford Cryosystems open flow N_2 cooling device. Data were collected at 150 K using mirror monochromated Cu Kα radiation (λ = 1.54178 Å; Oxford Diffraction Supernova) or graphite-monochromated Mo Kα radiation (λ = 0.71073 Å; Enraf-Nonius kappa-CCD). Data collected on the Oxford Diffraction Supernova diffractometer were processed using the CrysAlisPro package, including unit cell parameter refinement and interframe scaling (which was carried out using SCALE3 ABSPACK within CrysAlisPro).[8] Equivalent reflections were merged, and diffraction patterns processed with the CrysAlisPro suite. For data collected on the Enraf-Nonius kappa-CCD, diffractometer equivalent reflections were merged and the diffraction patterns processed with the DENZO

and SCALEPACK programs.[9] Structures were subsequently solved using direct methods or using the charge flipping algorithm as implemented in the program SUPERFLIP[10] and refined on F^2 using the SHELXL-2013 package.[11–13]

7.3.2 NMR spectroscopy

NMR samples were prepared inside a glovebox under nitrogen in NMR tubes equipped with a gas-tight valve. ^{1}H, ^{7}Li, ^{11}B, ^{13}C{^{1}H}, ^{19}F, ^{27}Al, ^{29}Si{^{1}H}, ^{31}P, ^{119}Sn{^{1}H}, ^{199}Hg{^{1}H} and ^{207}Pb{^{1}H} NMR spectra were acquired on a Bruker AVII or AVIII 500 MHz NMR spectrometer at 298 K unless otherwise stated. ^{1}H and ^{13}C{^{1}H} spectra are reported relative to tetramethylsilane (TMS) and were referenced to the most downfield residual solvent resonance (C_6D_6: δ_H 7.16 ppm, δ_C 128.1 ppm; CD_2Cl_2: δ_H 5.32 ppm, δ_C 53.8 ppm; d_8-THF: δ_H 3.58 ppm, δ_C 67.6 ppm; d_8-toluene: δ_H 7.09 δ_C 137.5; DFB: δ_H 6.95–7.11 ppm, δ_C 151.2 ppm). ^{7}Li, ^{11}B, ^{19}F, ^{27}Al, ^{29}Si{^{1}H}, ^{31}P, ^{119}Sn{^{1}H}, ^{199}Hg{^{1}H} and ^{207}Pb{^{1}H} NMR spectra were externally referenced to LiCl in D_2O, $Et_2O{\cdot}BF_3$, $CFCl_3$, $Al(NO_3)_3$ in D_2O, $SiMe_4$, an 85% solution of H_3PO_4 in H_2O, $SnMe_4$, $HgMe_2$ and $PbMe_4$ respectively.

7.3.3 EPR spectroscopy

EPR measurements were carried out by Dr. William Myers at the Centre for Advanced Electron Spin Resonance (CAESR) of the Chemistry Department of the University of Oxford. The X-band spectrometer was a Bruker-Biospin EMXplus with a PremiumX microwave bridge, and a Bruker BioSpin SHQE-W resonator.

7.3.4 Mass spectrometry

Negative ion mode electrospray mass spectra (ESI-MS) were recorded on a Waters MassLynx LCT Time of Flight mass spectrometer with a Z-spray source. The samples (10–20 μM) were

made up inside a glovebox under nitrogen and rapidly transferred to the spectrometer via a 1 mL air-tight SGE syringe and syringe pump at a rate of 10 μL·min^{-1}.

Positive ion mode electrospray mass spectra were recorded on a Bruker MicrOTOF mass spectrometer. The samples (10–20 μM) were prepared inside a glovebox under argon and the sample injected through a standard PEEK tubing feedthrough directly to the mass analyser at 10 μL·min^{-1}.[14]

Electron ionisation mass spectrometry (EI-MS) were carried out by Colin Sparrow of the University of Oxford. Samples were submitted as solids and spectra were obtained using a Waters GCT Time of Flight mass spectrometer with a temperature-programmed solids probe inlet.

7.3.5 UV/Vis spectroscopy

UV/Vis spectra were recorded on a Lambda 750 spectrophotometer. Samples were prepared inside a glovebox under nitrogen in a 1 mm wide silica cuvette equipped with a J. Young valve.

7.3.6 Elemental analyses

Elemental analyses were performed by Elemental Microanalysis Ltd, Devon. 10–15 mg samples were sent in sealed, evacuated Pyrex ampoules. All values are an average of at least two data collections and are given as percentages.

7.4 References

(1) Hintermann, L. *Beilstein J. Org. Chem.* **2007**, *3*, 22.

(2) Wang, Y.; Xie, Y.; Abraham, M. Y.; Wei, P.; Schaefer III, H. F.; Schleyer, P. v. R.; Robinson, G. H. *J. Am. Chem. Soc.* **2010**, *132* (41), 14370–14372.

(3) Jafarpour, L.; Stevens, E. D.; Nolan, S. P. *J. Organomet. Chem.* **2000**, *606* (1), 49–54.

(4) Arduengo III, A. J.; Krafczyk, R.; Schmutzler, R.; Craig, H. A.; Goerlich, J. R.; Marshall, W. J.; Unverzagt, M. *Tetrahedron* **1999**, *55* (51), 14523–14534.

(5) Bürger, H.; Sawodny, W.; Wannagat, U. *J. Organomet. Chem.* **1965**, *3* (2), 113–120.

(6) Gynane, M. J. S.; Harris, D. H.; Lappert, M. F.; Power, P. P.; Rivière, P.; Rivière-Baudet, M. *J. Chem. Soc., Dalton Trans.* **1977**, 2004–2009.

(7) Brookhart, M.; Grant, B.; Volpe, A. F. *Organometallics* **1992**, *11* (11), 3920–3922.

(8) CrysAlisPro, Agilent Technologies, Versions 1.171.35.8 and 1.171.37.35.

(9) Otwinowski, Z.; Minor, W. *Macromol. Crystallogr. Part A* **1997**, *276*, 307–326.

(10) Palatinus, L.; Chapius, G. *J. Appl. Crystallogr.* **2007**, *40*, 786–790.

(11) Sheldrick, G. M. *Acta Crystallogr. A* **1990**, *46* (6), 467–473.

(12) Sheldrick, G. M. *Acta Crystallogr. A* **2008**, *64* (1), 112–122.

(13) Sheldrick, G. M. *SHELXL-2013, Programs for Crystal Structure Analysis* **2013**.

(14) Lubben, A. T.; McIndoe, J. S.; Weller, A. S. *Organometallics* **2008**, *27* (13), 3303–3306.

Appendix A

Supporting information

A.1 Supplementary results

A crystal of $[(IPr)_2Hg][B(3,5\text{-}\{CF_3\}_2C_6H_3)_4]_2$ suitable for single crystal X-ray diffraction was obtained from the reaction mixture of $[IPrH][B(3,5\text{-}\{CF_3\}_2C_6H_3)_4]$ with HgO in refluxing THF after filtration and addition of hexane. Due to the insolubility of HgO in THF, $[(IPr)_2Hg][B(3,5\text{-}\{CF_3\}_2C_6H_3)_4]_2$ could only be observed to form in trace amounts.

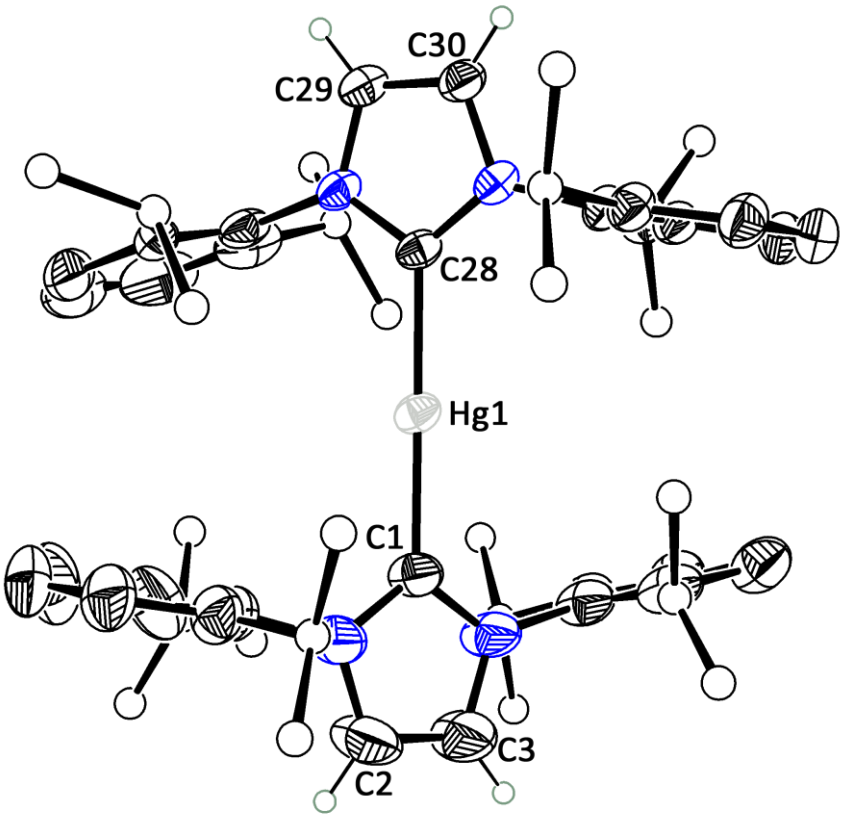

Figure A.1: Structure of dication $[(IPr)_2Hg]^{2+}$. Anisotropic displacement ellipsoids pictured are set at 50% probability. Hydrogen atoms (with the exception of the imidazole protons) have been omitted for clarity. Atoms of the ^{i}Pr groups and hydrogen atoms are pictured as spheres of arbitrary radii.

Addition of four equivalents of IPr to $SiCl_4$ in d_8-THF followed by heating at 65 °C for four days gave rise to a mixture of colourless crystals which could be identified as [IPrH]Cl·THF and $[(aIPr)_2SiCl_3]Cl$·THF as determined by single crystal X-ray diffraction. Analysis of the solution by ^1H NMR spectroscopy gave no evidence for the formation of **18**.

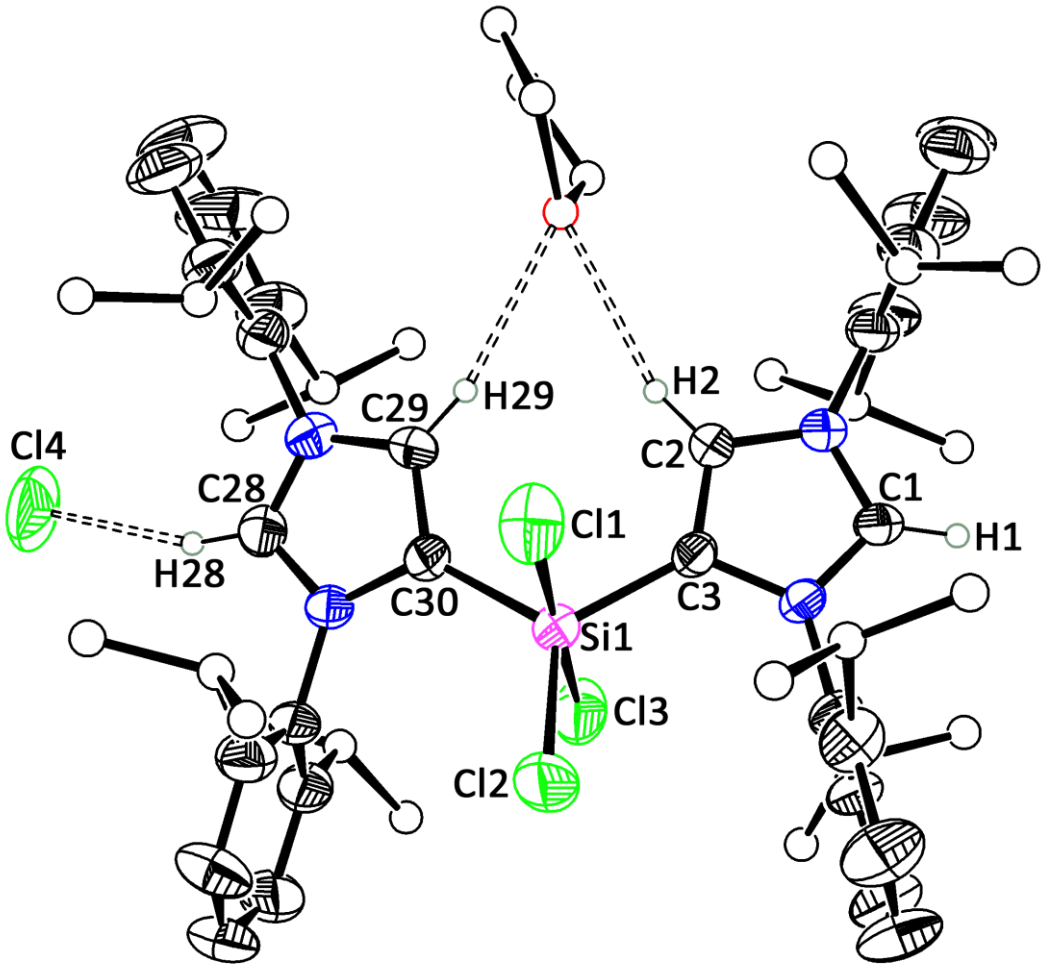

Figure A.2: Molecular structure of $[(aIPr)_2SiCl_3]Cl$·THF. Anisotropic displacement ellipsoids pictured are set at 50% probability. Hydrogen atoms (with the exception of the imidazole protons labelled H1, H2, H28 and H29) have been omitted for clarity. Atoms of the ^{i}Pr groups, the THF molecule and hydrogen atoms are pictured as spheres of arbitrary radii.

Addition of IPr to $GeBr_4$ in diethyl ether results in the immediate precipitation of a colourless, crystalline precipitate which could be identified as [IPrBr]Br·$^1/_3$THF by single crystal X-ray diffraction. [IPrBr]Br appears to form despite a 1 : 1 stoichiometry of IPr and $GeBr_4$. There was no evidence for the formation of (IPr)$GeBr_4$ and (IPr)$GeBr_2$ could be isolated as a crystalline sample from the diethyl ether reaction solution in 68% yield.

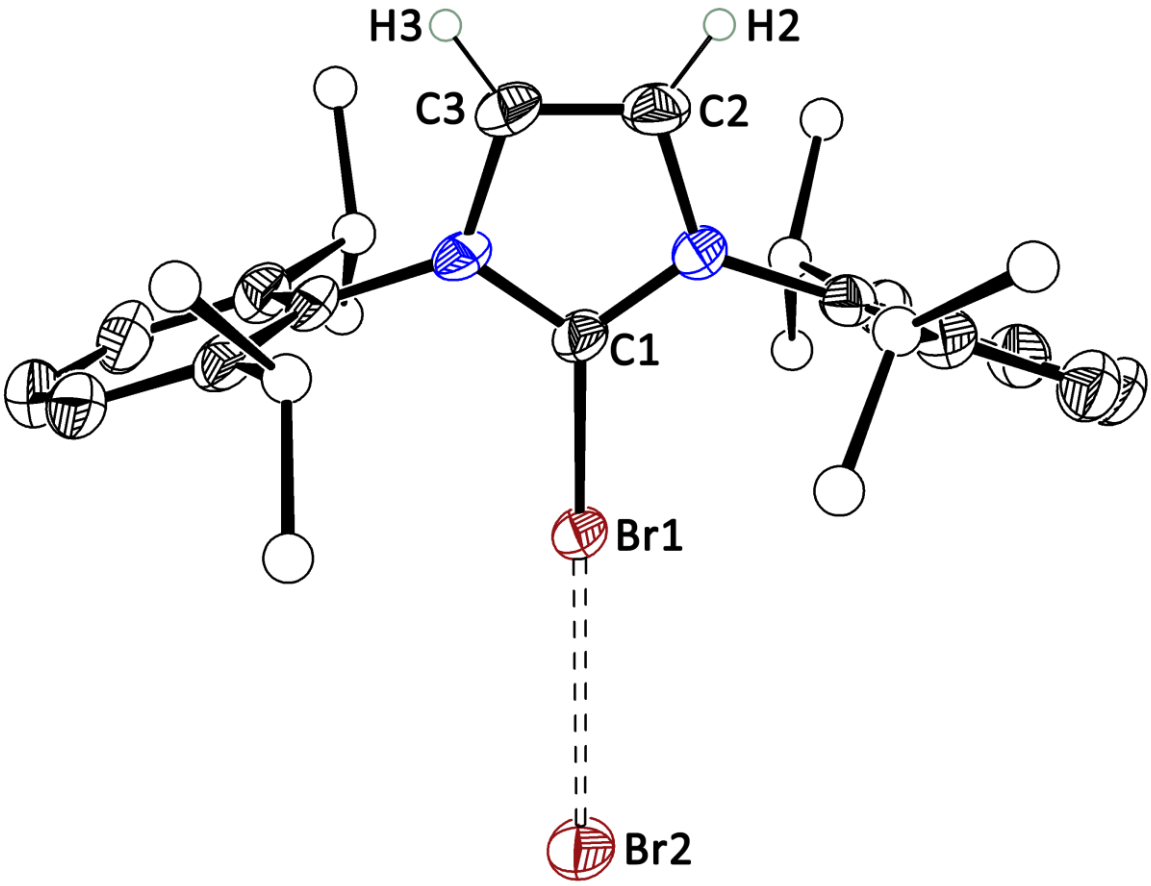

Figure A.3: Molecular structure of [IPrBr]Br. Anisotropic displacement ellipsoids pictured are set at 50% probability. Hydrogen atoms (with the exception of the imidazole protons labelled H2 and H3) have been omitted for clarity. Atoms of the ^{i}Pr groups and hydrogen atoms are pictured as spheres of arbitrary radii.

During the crystallisation of **23**, hydrolysis of the sample as a result of the presence of adventitious moisture resulted in the crystallisation of $[(aIPr)_2Si(OH)_2][OTf]_2 \cdot DFB$ as a side product which could be identified by single crystal X-ray diffraction.

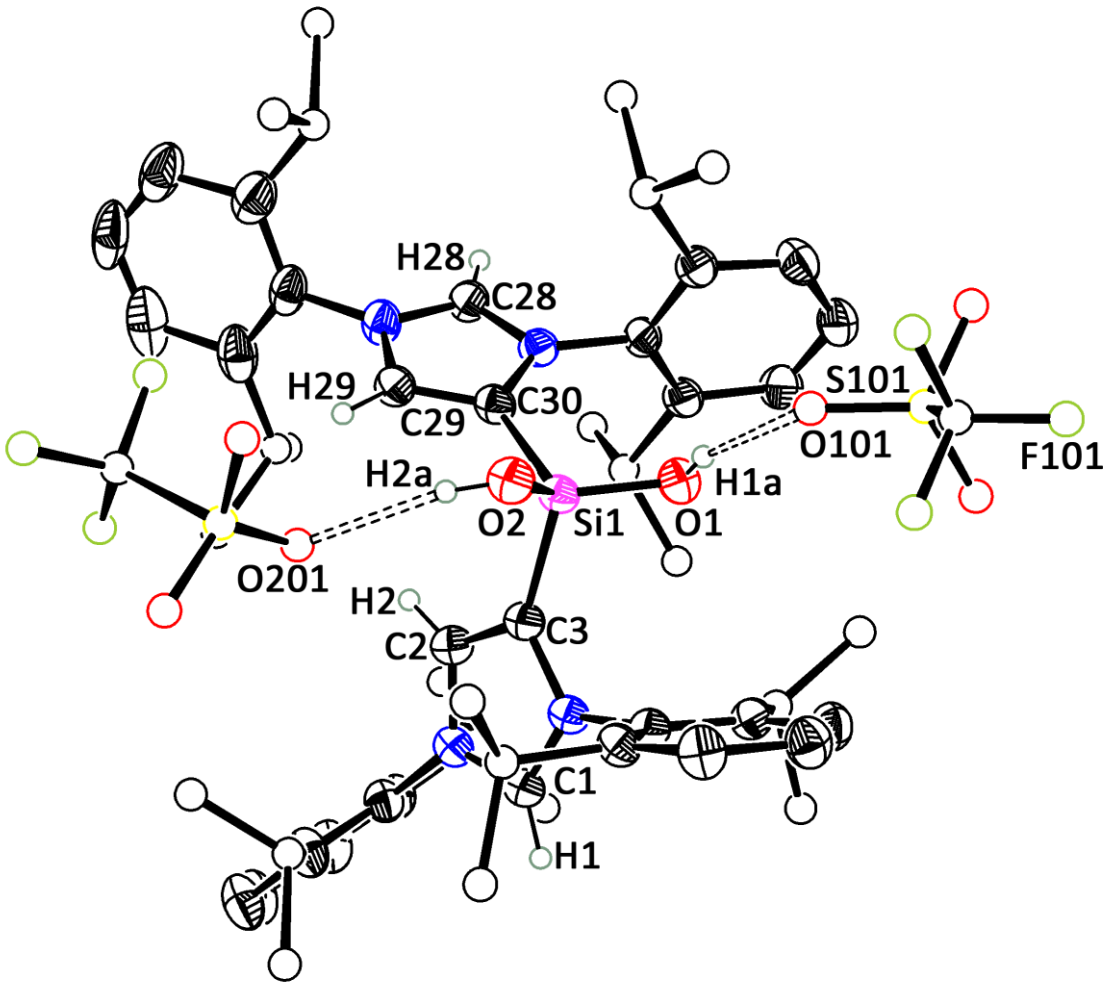

Figure A.4: Molecular structure of $[(aIPr)_2Si(OH)_2][OTf]_2$. Anisotropic displacement ellipsoids pictured are set at 50% probability. Hydrogen atoms (with the exception of the imidazole protons labelled H1, H2, H28 and H29 and the hydroxyl protons labelled H1a and H2a) have been omitted for clarity. Atoms of the ^{i}Pr groups, the triflate anions and hydrogen atoms are pictured as spheres of arbitrary radii.

Immediate diffusion of hexane into a THF solution containing one equivalent of IPr and $SnBr_4$ allowed for crystallisation of (IPr)$SnBr_4$ prior to isomerisation of the ligand in solution.

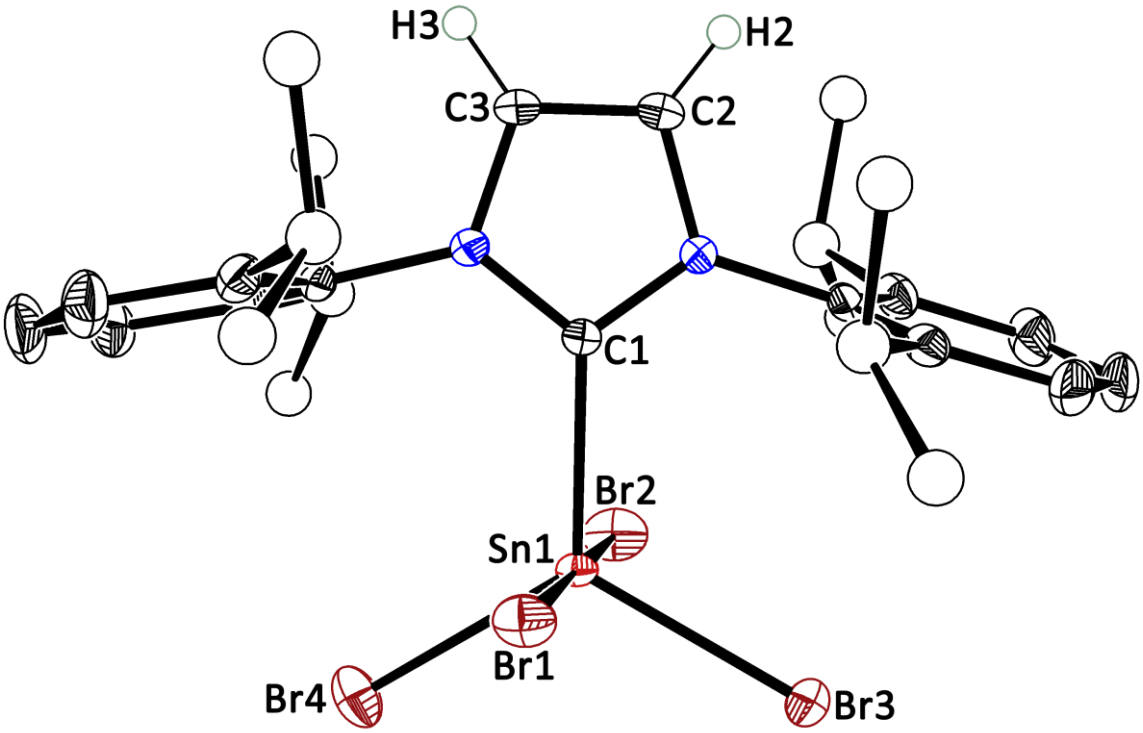

Figure A.5: Molecular structure of (IPr)$SnBr_4$. Anisotropic displacement ellipsoids pictured are set at 50% probability. Hydrogen atoms (with the exception of the imidazole protons labelled H2 and H3) have been omitted for clarity. Atoms of the ^{i}Pr groups, H2 and H3 are pictured as spheres of arbitrary radii.

On standing of a THF solution of (IPr)$AsBr_3$ or upon standing of a reaction solution containing a second equivalent of IPr to (IPr)$AsBr_3$ at room temperature results in the precipitation of a mixture of [IPrH]Br and pale pink crystals which were suitable for single crystal X-ray diffraction, analysis of which reveals a species bearing one IPr and one aIPr ligand coordinated to the arsenic centre upon elimination of one bromide, [(IPr)(aIPr)$AsBr_2$]Br. [(IPr)(aIPr)$AsBr_2$]Br could not be isolated as a pure material due to the formation of [IPrH]Br and attempts to form [(IPr)(aIPr)$AsBr_2$]Br by heating the reaction solutions in THF resulted in side reactions involving redox chemistry which is discussed in Chapter 5. Analysis of the crystalline precipitate by ESI-MS in DCM reveals a mass envelope at 1011.3232 which can be ascribed to $[(IPr)(aIPr)AsBr_2]^+$ (Calcd 1011.3319).

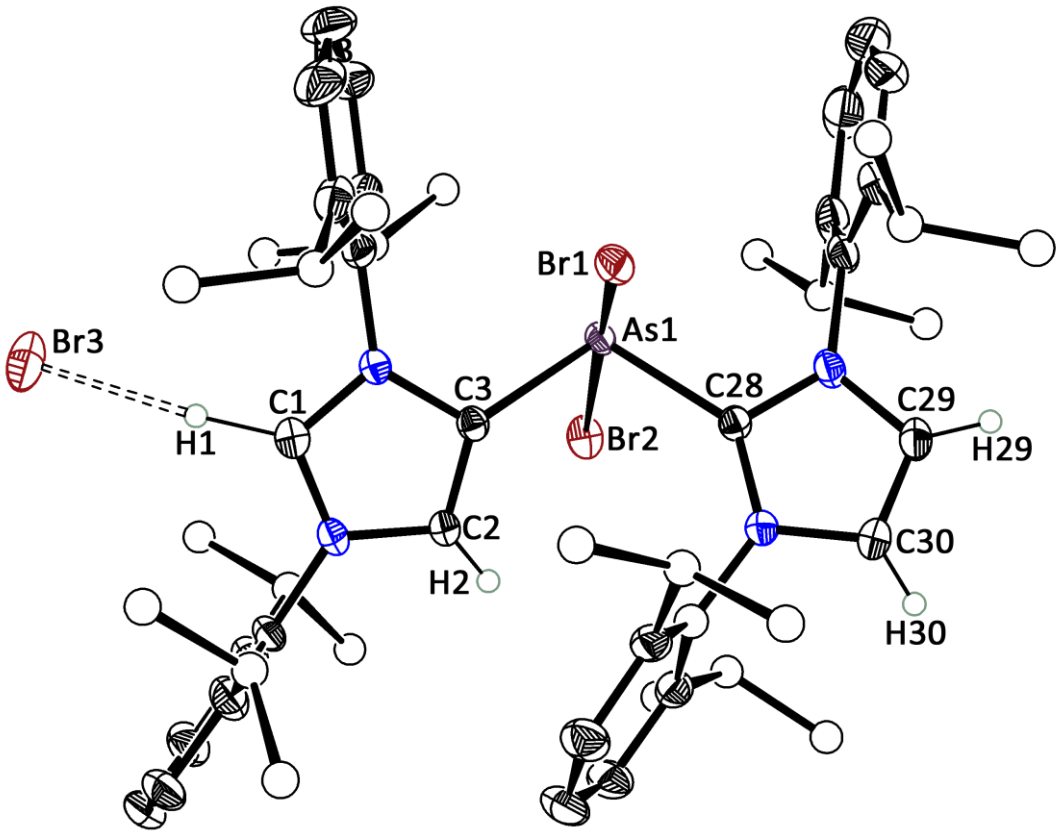

Figure A.6: Molecular structure of [(IPr)(aIPr)$AsBr_2$]Br. Anisotropic displacement ellipsoids pictured are set at 50% probability. Hydrogen atoms (with the exception of the imidazole protons labelled H1, H2, H29 and H30) have been omitted for clarity. Atoms of the ^{i}Pr groups and hydrogen atoms are pictured as spheres of arbitrary radii.

Slow diffusion of hexane into a THF solution of [**52**][B(3,5-{CF_3}$_2$$C_6H_3$)$_4$]$_2$ results in a colourless oil which spontaneously gives rise to small colourless crystals over an extended period of time (greater than two months). Analysis of the molecular structure by single crystal X-ray diffraction provides evidence for the formation of **52** which is accompanied by a second species which lies disordered on an inversion centre.

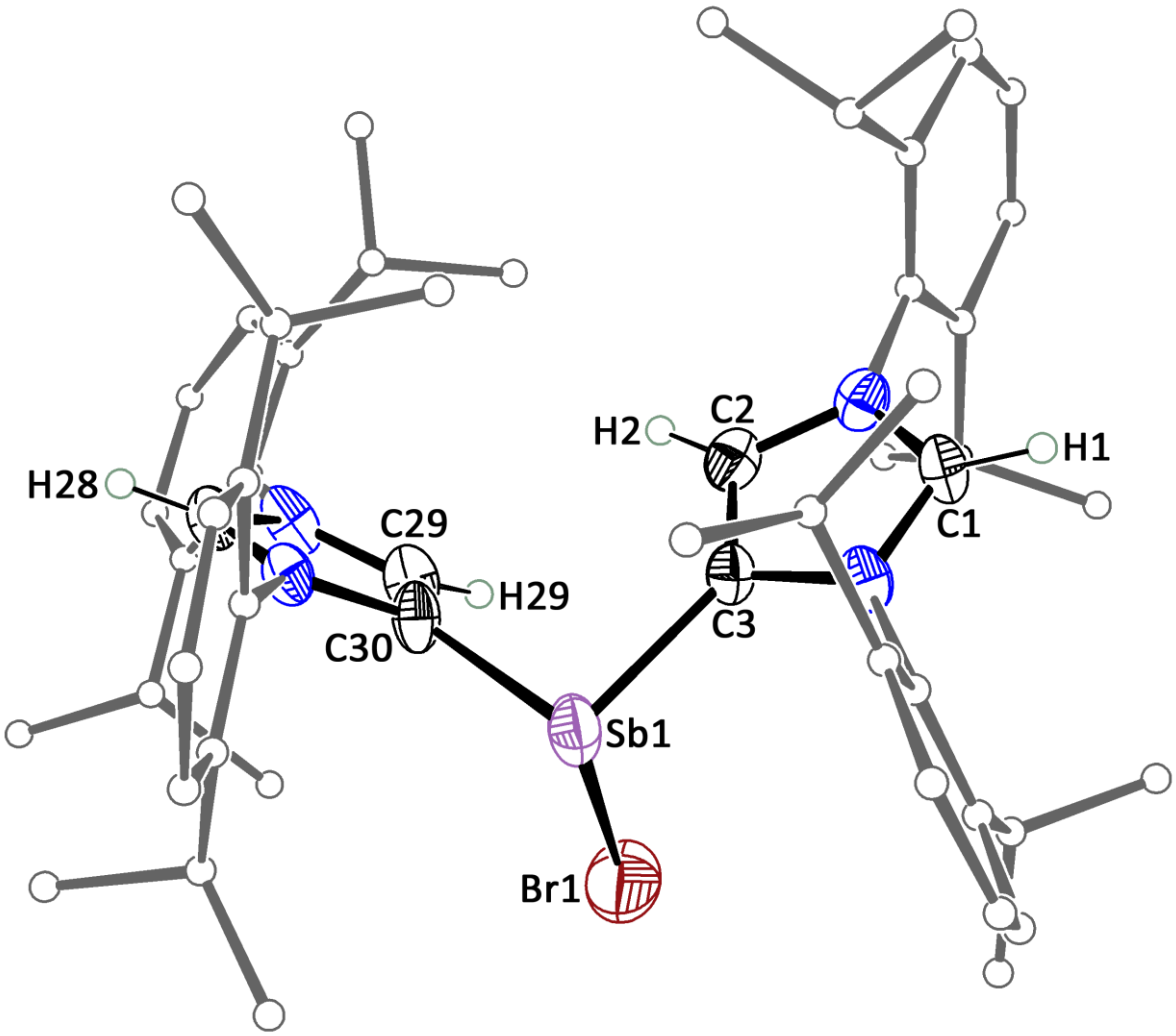

Figure A.7: Structure of dication **52** in [**52**][B(3,5-{CF_3}$_2$$C_6H_3$)$_4$]$_2$. Anisotropic displacement ellipsoids pictured are set at 50% probability. Hydrogen atoms (with the exception of the imidazole protons labelled H1, H2, H28 and H29) have been omitted for clarity. Atoms of the Dipp groups and hydrogen atoms are pictured as spheres of arbitrary radii.

Appendix B

EPR spectra

EPR measurements were performed at the Centre for Advanced Electron Spin Resonance (CAESR) of the Chemistry Department of the University of Oxford. The X-band spectrometer was a Bruker-Biospin EMXplus with a PremiumX microwave bridge, and a Bruker BioSpin SHQE-W resonator. The EPR spectra of **58** (Figure B.1) are characteristic of the proposed molecular structure. The predominant spin density is located about the ^{31}P nuclei, giving rise to a 1 : 2 : 1 hyperfine pattern (found 0.46 : 1.00 : 0.45), with unequal intensities due to slow tumbling of the molecule on the time scale of the microwave frequency. This resonance has a g_{iso} value of 2.0090 (+/– 0.0001), consistent with the data previously reported by Bertrand and co-workers. The isotropic hyperfine splitting for the ^{31}P nuclei, $A_{iso}(^{31}P)$, is 126 MHz. The hyperfine interactions of the four ^{14}N atoms of the imidazolyl groups are resolved as a nine-peak pattern on the central peak, consistent with the hyperfine splitting rule of $2nI+1$. The ^{14}N isotropic hyperfine splitting, $A_{iso}(^{14}N)$, is 4.2 (+/–0.1) MHz. Further splitting within the central feature was observed by using a smaller field modulation value, 90 milliGauss (mG), but this is incompletely-resolved.

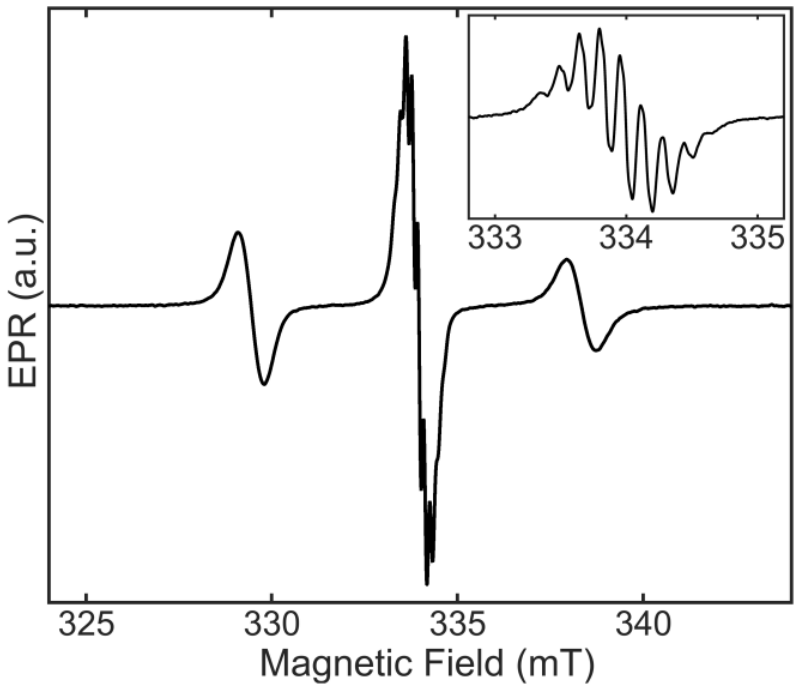

Figure B.1 CW-EPR of [**58**][B(3,5-{CF_3}$_2$$C_6H_3$)$_4$] at X-band (ν = 9.3761 GHz) and room temperature, at a concentration of 100 μM in fluorobenzene. Non-saturating conditions were found at 5 mW, with 100 kHz modulation amplitudes of 1 G and inset, 90 mG.

Appendix C

Single crystal X-ray diffraction data

	[**1**]·2THF	[K(2,2,2-crypt)][**2**]·THF	[K(18-crown-6)(THF)$_2$][**3**]·$^1/_2$THF	[K(18-crown-6)(THF)$_2$]$_2$[**4**][**6**]·THF
Formula	$C_{35}H_{51}KN_2O_2$	$C_{61}H_{115}KN_6O_7Si_4Zn$	$C_{61}H_{115}KN_4O_{8.5}Si_4Sn$	$C_{143}H_{247}Ge_2K_2N_9O_{17}Si_6$
Fw [g mol^{-1}]	570.88	1261.42	1310.72	2756.42
Crystal system	Orthorhombic	Monoclinic	Monoclinic	Triclinic
Space group	$P2_12_12_1$	$P2_1/n$	$P2_1/c$	$P\bar{1}$
a (Å)	10.8804(1)	19.8505(1)	10.5971(1)	20.3166(2)
b (Å)	14.4926(1)	19.5586(1)	34.5475(2)	20.3325(2)
c (Å)	21.7725(2)	20.5305(1)	20.9338(1)	21.3303(2)
α (°)	90	90	90	104.643(1)
β (°)	90	113.518(1)	104.365(1)	100.585(1)
γ (°)	90	90	90	102.584(1)
V (Å^3)	3433.20(5)	7308.82(8)	7424.32(9)	8049.90(14)
Z	4	4	4	2
Radiation, λ (Å)	Mo Kα, 0.71073	Mo Kα, 0.71073	Mo Kα, 0.71073	Mo Kα, 0.71073
ρ_{calc} (g cm^{-3})	1.104	1.146	1.173	1.137
μ (mm^{-1})	0.185	0.507	0.513	0.528
Reflections collected	75520	32762	32574	60361
Independent reflections	7781	16634	16832	36417
Parameters	365	779	860	1666
R(int)	0.0510	0.0174	0.0343	0.0327
R1/wR2,[a] I ≥ 2σI (%)	5.48/14.75	3.52/8.56	4.61/11.60	5.36/12.24
R1/wR2,[a] all data (%)	6.49/15.64	4.73/9.39	6.98/12.75	8.88/14.29
GOF	1.035	1.039	1.021	1.016

[a] $R1 = [\Sigma||F_o| - |F_c||]/\Sigma|F_o|$; $wR2 = \{[\Sigma w[(F_o)^2 - (F_c)^2]^2]/[\Sigma w(F_o^2)^2\}^{1/2}$; $w = [\sigma^2(F_o)^2 + (AP)^2 + BP]^{-1}$, where $P = [(F_o)^2 + 2(F_c)^2]/3$ and the A and B values are 0.0946 and 0.94 for [**1**]·2THF, 0.0424 and 3.35 for [K(2,2,2-crypt)][**2**]·THF, 0.0631 and 6.00 for [K(18-crown-6)(THF)$_2$][**3**]·$^1/_2$THF and 0.0578 and 5.55 for [K(18-crown-6)(THF)$_2$]$_2$[**4**][**6**]·THF.

	[K(18-crown-6)(THF)$_2$][**6**]·THF	[K(18-crown-6)(THF)$_2$][**7**]·THF	[**8**]·$^3/_2$THF	[**9**]·3THF
Formula	$C_{84}H_{136}GeKN_5O_9Si_2$	$C_{84}H_{136}KN_5O_9PbSi_2$	$C_{74}H_{116}GeLiN_5O_{3.5}Si_2$	$C_{74}H_{116}LiN_5O_{3.5}Si_2Sn$
Fw [g mol^{-1}]	1527.85	1662.45	1267.43	1313.52
Crystal system	Triclinic	Monoclinic	Triclinic	Triclinic
Space group	$P\bar{1}$	$P2_1/n$	$P\bar{1}$	$P\bar{1}$
a (Å)	13.2441(1)	22.8186(1)	13.0844(1)	13.1845(4)
b (Å)	17.9105(2)	26.9545(2)	14.7140(1)	14.8099(4)
c (Å)	20.1807(2)	29.4392(2)	22.8790(3)	22.7961(7)
α (°)	78.741(1)	90	94.483(1)	93.051(2)
β (°)	71.387(1)	90.504(1)	103.507(1)	104.080(3)
γ (°)	89.273(1)	90	116.150(1)	115.489(3)
V (Å^3)	4443.00(7)	18106.30(20)	3760.87(6)	3818.30(20)
Z	2	8	2	2
Radiation, λ (Å)	Mo Kα, 0.71073	Mo Kα, 0.71073	Mo Kα, 0.71073	Mo Kα, 0.71073
ρ_{calc} (g cm^{-3})	1.142	1.220	1.119	1.142
μ (mm^{-1})	0.472	1.989	0.486	0.412
Reflections collected	35110	73916	24520	40242
Independent reflections	20161	40687	13124	20206
Parameters	964	1881	847	864
R(int)	0.0241	0.0448	0.0281	0.0351
R1/wR2,[a] $I \geq 2\sigma I$ (%)	4.71/11.48	5.82/11.77	4.59/11.57	4.70/10.01
R1/wR2,[a] all data (%)	6.42/12.66	10.23/13.67	6.18/12.22	6.62/11.29
GOF	1.020	1.038	1.047	1.059

[a] $R1 = [\Sigma||F_o| - |F_c||]/\Sigma|F_o|$; $wR2 = \{[\Sigma w[(F_o)^2 - (F_c)^2]^2]/[\Sigma w(F_o^2)^2\}^{1/2}$; $w = [\sigma^2(F_o)^2 + (AP)^2 + BP]^{-1}$, where $P = [(F_o)^2 + 2(F_c)^2]/3$ and the A and B values are 0.0580 and 2.77 for [K(18-crown-6)(THF)$_2$][**6**]·THF, 0.0469 and 43.44 for [K(18-crown-6)(THF)$_2$][**7**]·THF, 0.0628 and 1.76 for [**8**]·$^3/_2$THF and 0.0716 and 3.0 for [**9**]·3THF.

	[**10**]·$^3/_2$THF	[**11**]·THF	**12**	[**13**]·C_6H_{14}
Formula	$C_{74}H_{116}LiN_5O_{3.5}PbSi_2$	$C_{64}H_{97}GeN_5OSi_2$	$C_{74}H_{121}LiN_6O_2Si_4Sn_2$	$C_{80}H_{135}LiN_6O_2Pb_2Si_4$
Fw [g mol^{-1}]	1402.02	1081.23	1483.45	1746.61
Crystal system	Triclinic	Monoclinic	Monoclinic	Monoclinic
Space group	$P\bar{1}$	$P2_1$	$P2_1/n$	$P2_1$
a (Å)	13.2827(1)	12.7705(2)	14.9991(1)	12.4297(1)
b (Å)	14.8623(1)	20.1586(2)	19.7540(1)	20.8700(2)
c (Å)	22.7948(2)	12.9807(2)	28.3678(2)	17.6567(1)
α (°)	93.588(1)	90	90	90
β (°)	104.670(1)	104.936(1)	103.266(1)	105.368(1)
γ (°)	115.201(1)	90	90	90
V (Å^3)	3863.54(6)	3228.79(8)	8180.87(9)	4416.51(6)
Z	2	2	4	2
Radiation, λ (Å)	Mo Kα, 0.71073	Cu Kα, 1.54178	Mo Kα, 0.71073	Mo Kα, 0.71073
ρ_{calc} (g cm^{-3})	1.205	1.112	1.204	1.313
μ (mm^{-1})	2.260	1.308	0.712	3.905
Reflections collected	28887	22934	26924	69232
Independent reflections	17456	10733	14226	19365
Parameters	839	708	812	883
R(int)	0.0403	0.0218	0.0244	0.0636
R1/wR2,[a] $I \geq 2\sigma I$ (%)	3.97/6.95	2.96/7.82	4.69/11.31	4.72/10.38
R1/wR2,[a] all data (%)	6.15/7.57	2.98/7.85	5.94/11.80	6.59/11.23
GOF	1.019	1.039	1.062	1.032

[a] $R1 = [\Sigma||F_o| - |F_c||]/\Sigma|F_o|$; $wR2 = \{[\Sigma w[(F_o)^2 - (F_c)^2]^2]/[\Sigma w(F_o^2)^2\}^{1/2}$; $w = [\sigma^2(F_o)^2 + (AP)^2 + BP]^{-1}$, where $P = [(F_o)^2 + 2(F_c)^2]/3$ and the A and B values are 0.0240 and 3.12 for [**10**]·$^3/_2$THF, 0.0506 and 0.66 for [**11**]·THF, 0.0486 and 16.31 for **12** and 0.0660 and 2.92 for [**13**]·C_6H_{14}.

	[13]·C_6H_{14}	[**15**]·THF·C_6H_{14}	[**16**][B(3,5-{CF_3}$_2C_6H_3$)$_4$]$_2$	[**17**][B(3,5-{CF_3}$_2C_6H_3$)$_4$]
Formula	$C_{80}H_{135}LiN_6O_2Pb_2Si_4$	$C_{106}H_{156}HgKN_8O_7$	$C_{130}H_{126}B_2F_{48}HgN_4O_3$	$C_{86}H_{84}BClF_{24}HgN_4$
Fw [g mol^{-1}]	1746.61	1894.08	2926.55	1876.42
Crystal system	Monoclinic	Monoclinic	Triclinic	Monoclinic
Space group	$P2_1$	$P2_1$	$P\bar{1}$	$P2_1/c$
a (Å)	15.199(3)	16.1359(1)	12.9967(2)	21.9411(1)
b (Å)	18.155(4)	28.5079(1)	19.5411(3)	23.7222(1)
c (Å)	17.723(4)	22.8886(1)	28.2509(4)	16.8264(1)
α (°)	90	90	73.582(1)	90
β (°)	109.11(3)	95.071(1)	86.460(1)	104.527(1)
γ (°)	90	90	81.915(1)	90
V (Å^3)	4621.0(18)	10487.56(9)	6812.09(18)	8478.00(8)
Z	2	4	2	4
Radiation, λ (Å)	Mo Kα, 0.71073	Cu Kα, 1.54178	Cu Kα, 1.54178	Cu Kα, 1.54178
ρ_{calc} (g cm^{-3})	1.255	1.200	1.427	1.470
μ (mm^{-1})	3.732	3.408	0.553	4.412
Reflections collected	87166	211014	139512	341138
Independent reflections	23567	43508	28261	17670
Parameters	864	2215	2017	1100
R(int)	0.0713	0.0211	0.0279	0.0191
R1/wR2,[a] $I \geq 2\sigma I$ (%)	4.93/12.30	3.83/10.11	3.49/9.07	3.59/9.34
R1/wR2,[a] all data (%)	5.90/12.90	3.93/10.21	3.69/9.29	4.00/9.79
GOF	1.090	1.082	1.043	1.037

[a] $R1 = [\Sigma||F_o| - |F_c||]/\Sigma|F_o|$; $wR2 = \{[\Sigma w[(F_o)^2 - (F_c)^2]^2]/[\Sigma w(F_o^2)^2\}^{1/2}$; $w = [\sigma^2(F_o)^2 + (AP)^2 + BP]^{-1}$, where $P = [(F_o)^2 + 2(F_c)^2]/3$ and the A and B values are 0.0555 and 19.17 for [**13**]·C_6H_{14}, 0.0536 and 11.93 for [**15**]·THF·C_6H_{14}, 0.0523 and 4.59 for [**16**][B(3,5-{CF_3}$_2C_6H_3$)$_4$]$_2$ and 0.0526 and 14.34 for [**17**][B(3,5-{CF_3}$_2C_6H_3$)$_4$].

	[18]·$^{3}/_{8}C_6H_{14}$	**19**	**20**	**21**
Formula	$C_{56.25}H_{75.25}Cl_2N_4Si$	$C_{54}H_{70}Br_2N_4Si$	$C_{54}H_{70}Cl_2GeN_4$	$C_{54}H_{70}Br_2GeN_4$
Fw [g mol^{-1}]	906.44	963.05	918.63	1007.55
Crystal system	Triclinic	Monoclinic	Triclinic	Orthorhombic
Space group	$P\bar{1}$	$P2_1/n$	$P1$	$Pbca$
a (Å)	13.1787(3)	14.2968(1)	9.7437(4)	16.6715(2)
b (Å)	18.6181(4)	19.3605(1)	11.9641(5)	19.8566(2)
c (Å)	25.2314(6)	19.9807(1)	13.0266(8)	31.2559(3)
α (°)	111.057(2)	90	67.438(5)	90
β (°)	103.009(2)	106.665(1)	68.377(5)	90
γ (°)	92.168(2)	90	66.987(4)	90
V (Å^3)	5581.00(20)	5298.23(8)	1247.37(13)	10346.99(19)
Z	4	4	1	8
Radiation, λ (Å)	Cu Kα, 1.54178	Cu Kα, 1.54178	Cu Kα, 1.54178	Cu Kα, 1.54178
ρ_{calc} (g cm^{-3})	1.079	1.207	1.223	1.294
μ (mm^{-1})	1.523	2.428	2.105	2.890
Reflections collected	68225	70108	11700	125612
Independent reflections	23086	11018	6154	10820
Parameters	1285	661	550	550
R(int)	0.0314	0.0312	0.0191	0.0489
R1/wR2,[a] $I \geq 2\sigma I$ (%)	6.18/17.89	4.92/13.17	3.06/8.18	5.34/14.89
R1/wR2,[a] all data (%)	7.28/19.25	5.59/13.93	3.10/8.21	6.06/15.54
GOF	1.035	1.035	1.040	1.141

[a] $R1 = \lceil\Sigma||F_o| - |F_c||\rceil/\Sigma|F_o|$; $wR2 = \{\lceil\Sigma w\lceil(F_o)^2 - (F_c)^2\rceil^2\rceil/\lceil\Sigma w(F_o^2)^2\}^{1/2}$; $w = \lceil\sigma^2(F_o)^2 + (AP)^2 + BP\rceil^{-1}$, where $P = \lceil(F_o)^2 + 2(F_c)^2\rceil/3$ and the A and B values are 0.1151 and 3.03 for [**18**]·$^{3}/_{8}C_6H_{14}$, 0.0703 and 4.71 for **19**, 0.0582 and 0.32 for **20** and 0.0535 and 37.17 for **21**.

	22	**[24]**[OTf]$_2$	[**25**][B(3,5-{CF$_3$}$_2$C$_6$H$_3$)$_4$]$_2$·2Et$_2$O	[**26**][B(3,5-{CF$_3$}$_2$C$_6$H$_3$)$_4$]$_2$·3THF
Formula	$C_{27}H_{36}Br_2GeN_2$	$C_{64}H_{88}Br_2F_6N_4O_8S_2Si$	$C_{126}H_{116}B_2Cl_2F_{48}GeN_4O_2$	$C_{130}H_{120}B_2Br_2F_{48}GeN_4O_3$
Fw [g mol^{-1}]	620.99	1407.41	2795.33	2952.32
Crystal system	Orthorhombic	Triclinic	Triclinic	Monoclinic
Space group	$P2_12_12_1$	$P\bar{1}$	$P\bar{1}$	$P2_1/n$
a (Å)	9.1741(1)	12.7960(2)	13.1647(1)	12.6604(1)
b (Å)	15.4830(1)	25.2837(6)	17.9055(2)	30.2886(2)
c (Å)	19.7624(1)	26.8061(5)	29.0625(3)	35.2249(3)
α (°)	90	116.638(2)	79.903(1)	90
β (°)	90	92.781(2)	86.763(1)	95.952(1)
γ (°)	90	97.287(2)	87.641(1)	90
V (Å^3)	2807.10(4)	7634.90(30)	6724.05(12)	13434.73(18)
Z	4	4	2	4
Radiation, λ (Å)	Cu Kα, 1.54178	Cu Kα, 1.54178	Mo Kα, 0.71073	Cu Kα, 1.54178
ρ_{calc} (g cm^{-3})	1.469	1.531	1.381	1.460
μ (mm^{-1})	4.928	3.172	0.383	2.059
Reflections collected	32780	93637	38658	160765
Independent reflections	5853	31699	24968	27978
Parameters	297	1627	1823	1783
R(int)	0.0183	0.0444	0.0309	0.1151
R1/wR2,[a] $I \geq 2\sigma I$ (%)	1.73/4.40	13.36/36.03	7.85/18.45	10.87/32.78
R1/wR2,[a] all data (%)	1.73/4.40	14.94/39.20	13.23/21.77	12.02/35.68
GOF	1.091	1.673	1.024	1.427

[a] $R1 = [\Sigma||F_o| - |F_c||]/\Sigma|F_o|$; $wR2 = \{[\Sigma w[(F_o)^2 - (F_c)^2]^2]/[\Sigma w(F_o^2)^2\}^{1/2}$; $w = [\sigma^2(F_o)^2 + (AP)^2 + BP]^{-1}$, where $P = [(F_o)^2 + 2(F_c)^2]/3$ and the A and B values are 0.0216 and 1.20 for **22**, 0.2000 and 0 for **[24]**[OTf]$_2$, 0.0944 and 9.23 for [**25**][B(3,5-{CF$_3$}$_2$C$_6$H$_3$)$_4$]$_2$·2Et$_2$O and 0.2000 and 0 for [**26**][B(3,5-{CF$_3$}$_2$C$_6$H$_3$)$_4$]$_2$·3THF.

	[**26**][OTf]$_2$·2THF	**[27]**·3C_7H_8	**[28]**·3C_6H_6	[K(2,2,2-crypt)][**31**]·THF·C_6H_{14}
Formula	$C_{60}H_{80}Br_2F_6GeN_4O_7S_2$	$C_{77}H_{94}Br_2N_4O_4Si$	$C_{74}H_{88}Cl_2GeN_4O_4$	$C_{82}H_{128}ClGeKN_6O_7$
Fw [g mol^{-1}]	1379.81	1327.47	1240.97	1457.04
Crystal system	Monoclinic	Monoclinic	Monoclinic	Orthorhombic
Space group	$P2_1/n$	Pn	$C2/c$	$Pna2_1$
a (Å)	15.8447(2)	13.3400(4)	49.5045(16)	29.9379(10)
b (Å)	19.3501(2)	12.2933(3)	12.5632(5)	13.7188(5)
c (Å)	22.4808(2)	22.2984(5)	25.6274(9)	20.7963(6)
α (°)	90	90	90	90
β (°)	104.039(1)	91.511(2)	115.879(4)	90
γ (°)	90	90	90	90
V (Å^3)	6686.66(13)	3655.50(16)	14340.2(10)	8541.3(5)
Z	4	2	8	4
Radiation, λ (Å)	Cu Kα, 1.54178	Cu Kα, 1.54178	Cu Kα, 1.54178	Cu Kα, 1.54178
ρ_{calc} (g cm^{-3})	1.371	1.206	1.150	1.133
μ (mm^{-1})	3.170	1.940	1.634	1.613
Reflections collected	90469	44358	50444	40996
Independent reflections	13949	12695	14787	11812
Parameters	740	883	933	1082
R(int)	0.0573	0.0506	0.0567	0.0438
R1/wR2,[a] $I \geq 2\sigma I$ (%)	5.01/13.19	4.35/10.80	8.71/24.60	7.12/19.06
R1/wR2,[a] all data (%)	6.29/14.52	5.80/12.09	12.40/28.71	7.96/20.00
GOF	1.030	1.036	1.035	1.086

[a] $R1 = [\Sigma||F_o| - |F_c||]/\Sigma|F_o|$; $wR2 = \{[\Sigma w[(F_o)^2 - (F_c)^2]^2]/[\Sigma w(F_o^2)^2\}^{1/2}$; $w = [\sigma^2(F_o)^2 + (AP)^2 + BP]^{-1}$, where $P = [(F_o)^2 + 2(F_c)^2]/3$ and the A and B values are 0.0738 and 6.98 for [**26**][OTf]$_2$·2THF, 0.0594 and 1.24 for [**27**]·3C_7H_8, 0.1750 and 16.48 for **[28]**·3C_6H_6 and 0.1228 and 2.51 for [K(2,2,2-crypt)][**31**]·THF·C_6H_{14}.

	32	[K(2,2,2-crypt)][**33**]·2THF	[K(2,2,2-crypt)][**34**]	[**35**]·C_6H_{14}
Formula	$C_{54}H_{70}Cl_2N_4Sn$	$C_{107}H_{157}Cl_2KN_8O_8Sn$	$C_{99}H_{141}KN_8O_6Sn$	$C_{60}H_{86}Cl_4N_4Sn$
Fw [g mol^{-1}]	964.73	1912.09	6787.92	749.21
Crystal system	Triclinic	Triclinic	Monoclinic	Triclinic
Space group	*P*1	$P\bar{1}$	$P2_1/c$	$P\bar{1}$
a (Å)	9.7341(2)	16.3382(1)	14.7129(3)	13.4869(4)
b (Å)	12.0062(2)	17.2536(1)	38.9745(8)	15.0599(5)
c (Å)	13.2468(3)	21.0534(1)	19.6668(3)	15.1690(5)
α (°)	66.563(2)	69.054(1)	90	89.467(3)
β (°)	68.948(2)	80.919(1)	103.963(2)	84.582(2)
γ (°)	67.246(2)	73.804(1)	90	84.353(3)
V (Å^3)	1270.70(5)	5311.46(7)	10944.3(4)	3052.35(17)
Z	1	2	1	2
Radiation, λ (Å)	Cu Kα, 1.54178	Mo Kα, 0.71073	Cu Kα, 1.54178	Cu Kα, 1.54178
ρ_{calc} (g cm^{-3})	1.261	1.196	1.030	1.223
μ (mm^{-1})	5.247	0.386	2.566	5.222
Reflections collected	38736	47614	91377	32944
Independent reflections	9950	29605	22665	12606
Parameters	566	1163	1026	640
R(int)	0.0259	0.0247	0.0439	0.0365
R1/wR2,[a] $I \geq 2\sigma I$ (%)	1.90/5.08	4.25/10.28	9.52/28.00	7.03/18.78
R1/wR2,[a] all data (%)	1.91/5.09	6.31/11.23	10.72/29.37	7.45/19.16
GOF	1.052	1.006	1.093	1.095

[a] $R1 = [\Sigma||F_o| - |F_c||]/\Sigma|F_o|$; $wR2 = \{[\Sigma w[(F_o)^2 - (F_c)^2]^2]/[\Sigma w(F_o^2)^2\}^{1/2}$; $w = [\sigma^2(F_o)^2 + (AP)^2 + BP]^{-1}$, where $P = [(F_o)^2 + 2(F_c)^2]/3$ and the A and B values are 0.0347 and 0.24 for **32**, 0.0535 and 2.84 for [K(2,2,2-crypt)][**33**]·2THF, 0.1745 and 31.99 for [K(2,2,2-crypt)][**34**] and 0.0897 and 9.73 for [**35**]·C_6H_{14}.

	[**36**]·3C_6H_6	[**37**][$AlCl_4$]$_2$·DFB	**39**	**40**
Formula	$C_{72}H_{90}Br_4N_4Sn$	$C_{60}H_{76}Al_2Cl_{10}F_2N_4Sn$	$C_{27}H_{36}Br_3N_2P$	$C_{27}H_{36}AsBr_3N_2$
Fw [g mol^{-1}]	1449.80	1418.39	659.28	703.23
Crystal system	Triclinic	Monoclinic	Monoclinic	Monoclinic
Space group	$P\bar{1}$	$P2_1/c$	$P2_1/c$	$P2_1/c$
a (Å)	12.2759(2)	18.2362(2)	10.2830(1)	11.1710(1)
b (Å)	12.9815(2)	19.3150(3)	18.3022(1)	16.0492(2)
c (Å)	13.1079(3)	39.4696(5)	15.6495(1)	16.2497(2)
α (°)	91.893(2)	90	90	90
β (°)	115.880(2)	92.848(1)	108.079(1)	99.391(1)
γ (°)	110.672(2)	90	90	90
V (Å^3)	1714.38(6)	13885.3(3)	2799.85(4)	2874.29(6)
Z	1	8	4	4
Radiation, λ (Å)	Cu Kα, 1.54178	Cu Kα, 1.54178	Cu Kα, 1.54178	Cu Kα, 1.54178
ρ_{calc} (g cm^{-3})	1.404	1.357	1.564	1.625
μ (mm^{-1})	6.009	7.062	6.011	6.608
Reflections collected	34434	92431	31191	18839
Independent reflections	7092	28791	5822	5946
Parameters	396	1553	326	307
R(int)	0.0248	0.0372	0.0198	0.0244
R1/wR2,[a] $I \geq 2\sigma I$ (%)	2.05/5.46	5.07/12.85	2.36/5.77	2.58/6.89
R1/wR2,[a] all data (%)	2.06/5.48	5.95/13.70	2.42/5.80	2.71/6.98
GOF	1.030	1.285	1.138	1.054

[a] $R1 = [\Sigma||F_o| - |F_c||]/\Sigma|F_o|$; $wR2 = \{[\Sigma w[(F_o)^2 - (F_c)^2]^2]/[\Sigma w(F_o^2)^2\}^{1/2}$; $w = [\sigma^2(F_o)^2 + (AP)^2 + BP]^{-1}$, where $P = [(F_o)^2 + 2(F_c)^2]/3$ and the A and B values are 0.0339 and 0.75 for [**36**]·3C_6H_6, 0.0583 and 32.66 for [**37**][$AlCl_4$]$_2$·DFB, 0.0242 and 2.67 for **39** and 0.0422 and 1.97 for **40**.

	[**41**]·2THF	[**42**]·$^1/_2$THF	[**43**][$AlBr_4$]·$^1/_2$DCM	[**44**][$AlBr_4$]
Formula	$C_{35}H_{52}Br_3N_2O_2Sb$	$C_{29}H_{36}BiBr_3N_2O_{0.5}$	$C_{27.5}H_{37}AlBr_6ClN_2P$	$C_{27}H_{36}AlAsBr_6N_2$
Fw [g mol^{-1}]	894.26	869.31	968.45	969.94
Crystal system	Monoclinic	Monoclinic	Triclinic	Monoclinic
Space group	$P2_1/n$	$P2_1/c$	$P\bar{1}$	$P2_1/c$
a (Å)	12.9636(3)	35.3941(3)	15.6279(4)	11.7311(1)
b (Å)	20.2935(4)	17.9516(1)	18.8579(5)	14.6592(1)
c (Å)	14.3419(3)	20.0953(2)	28.3542(10)	2.9300(1)
α (°)	90	90	98.285(3)	90
β (°)	96.532(2)	95.253(1)	104.752(3)	103.216(1)
γ (°)	90	90	111.205(3)	90
V (Å^3)	3748.53(14)	12714.54(18)	7270.5(4)	3503.97(4)
Z	4	16	8	4
Radiation, λ (Å)	Cu Kα, 1.54178	Cu Kα, 1.54178	Mo Kα, 0.71703	Cu Kα, 1.54178
ρ_{calc} (g cm^{-3})	1.585	1.817	1.770	1.839
μ (mm^{-1})	9.821	15.457	6.789	9.715
Reflections collected	75905	202772	112558	37115
Independent reflections	7831	26537	38491	7297
Parameters	462	1403	1420	382
R(int)	0.0673	0.0714	0.0625	0.0317
R1/wR2,[a] $I \geq 2\sigma I$ (%)	4.66/12.07	4.76/12.31	8.80/23.19	4.02/10.61
R1/wR2,[a] all data (%)	5.07/12.62	4.97/12.49	15.80/28.14	4.15/10.73
GOF	1.046	1.105	1.033	1.049

[a] $R1 = [\Sigma||F_o| - |F_c||]/\Sigma|F_o|$; $wR2 = \{[\Sigma w[(F_o)^2 - (F_c)^2]^2]/[\Sigma w(F_o^2)^2\}^{1/2}$; $w = [\sigma^2(F_o)^2 + (AP)^2 + BP]^{-1}$, where $P = [(F_o)^2 + 2(F_c)^2]/3$ and the A and B values are 0.0678 and 9.31 for [**41**]·2THF, 0.0579 and 160.94 for [**42**]·$^1/_2$THF, 0.1468 and 21.21 for [**43**][$AlBr_4$]·$^1/_2$DCM and 0.0590 and 9.61 for [**44**][$AlBr_4$].

	[**45**][$AlBr_4$]·$^1/_2$DCM	[**46**][$AlBr_4$]·$^1/_2$DCM	[**47**]·2THF	[**48**]·2THF
Formula	$C_{27.5}H_{37}AlBr_6ClN_2Sb$	$C_{27.5}H_{37}AlBiBr_6ClN_2$	$C_{35}H_{52}Br_3N_2O_2Sb$	$C_{35}H_{52}BiBr_3N_2O_2$
Fw [g mol^{-1}]	1059.23	1146.46	894.26	981.49
Crystal system	Triclinic	Triclinic	Triclinic	Triclinic
Space group	$P\bar{1}$	$P\bar{1}$	$P\bar{1}$	$P\bar{1}$
a (Å)	12.2078(3)	12.2474(3)	11.8063(3)	11.105(2)
b (Å)	17.4963(3)	17.4318(6)	11.8231(2)	11.908(2)
c (Å)	18.3277(4)	18.3406(6)	15.2363(3)	15.263(3)
α (°)	76.528(2)	77.136(2)	98.938(2)	98.77(3)
β (°)	79.988(2)	79.952(2)	101.958(2)	102.17(3)
γ (°)	81.945(2)	82.507(2)	95.680(2)	96.09(3)
V (Å^3)	3728.61(14)	3741.60(20)	1912.17(7)	1929.7(7)
Z	4	4	2	2
Radiation, λ (Å)	Cu Kα, 1.54178	Cu Kα, 1.54178	Cu Kα, 1.54178	Mo Kα, 0.71703
ρ_{calc} (g cm^{-3})	1.887	2.035	1.553	1.689
μ (mm^{-1})	14.440	17.789	9.626	7.705
Reflections collected	50023	41661	38814	14807
Independent reflections	15405	15503	7943	8734
Parameters	710	710	426	426
R(int)	0.0410	0.0325	0.0402	0.0389
R1/wR2,[a] $I \geq 2\sigma I$ (%)	4.03/10.52	3.58/9.39	4.30/11.05	5.24/12.54
R1/wR2,[a] all data (%)	4.31/10.98	3.68/9.48	4.60/11.44	6.99/13.69
GOF	1.057	1.076	1.051	1.052

[a] $R1 = [\Sigma||F_o| - |F_c||]/\Sigma|F_o|$; $wR2 = \{[\Sigma w[(F_o)^2 - (F_c)^2]^2]/[\Sigma w(F_o^2)^2\}^{1/2}$; $w = [\sigma^2(F_o)^2 + (AP)^2 + BP]^{-1}$, where $P = [(F_o)^2 + 2(F_c)^2]/3$ and the A and B values are 0.0643 and 15.88 for [**45**][$AlBr_4$]·$^1/_2$DCM, 0.0580 and 8.96 for [**46**][$AlBr_4$]·$^1/_2$DCM, 0.0581 and 3.72 for [**47**]·2THF and 0.0646 and 6.32 for [**48**]·2THF.

	[**48**]$_2$·DCM	[**49**][B(3,5-{CF_3}$_2$$C_6H_3$)$_4$]·4THF	[**50**][B(3,5-{CF_3}$_2$$C_6H_3$)$_4$]·$^5/_2$THF	[**51**]Br·$^1/_2$THF
Formula	$C_{55}H_{74}Bi_2Br_6Cl_2N_4$	$C_{75}H_{80}BBr_2F_{24}N_2O_4Sb$	$C_{77}H_{84}BBiBr_2F_{24}N_2O_{4.5}$	$C_{56}H_{76}Br_3N_4O_{0.5}Sb$
Fw [g mol^{-1}]	1759.50	1821.79	1945.07	1174.68
Crystal system	Monoclinic	Triclinic	Triclinic	Monoclinic
Space group	$P2_1/c$	$P\bar{1}$	$P\bar{1}$	$P2_1/n$
a (Å)	12.1030(2)	13.2348(2)	12.7012(3)	14.8865(2)
b (Å)	35.0769(5)	16.9730(4)	18.9400(4)	18.9920(2)
c (Å)	14.9733(3)	18.9206(4)	19.7427(4)	20.8333(2)
α (°)	90	72.072(2)	113.243(2)	90
β (°)	98.804(2)	83.509(2)	93.206(2)	98.610(1)
γ (°)	90	87.014(2)	106.828(2)	90
V (Å^3)	6281.80(19)	4017.25(15)	4098.06(17)	5823.70(12)
Z	4	2	2	4
Radiation, λ (Å)	Cu Kα, 1.54178	Cu Kα, 1.54178	Cu Kα, 1.54178	Cu Kα, 1.54178
ρ_{calc} (g cm^{-3})	1.860	1.506	1.576	1.340
μ (mm^{-1})	16.401	4.802	6.275	6.445
Reflections collected	76854	81697	83484	79376
Independent reflections	13131	16691	16981	12155
Parameters	667	1092	1091	620
R(int)	0.0430	0.0541	0.0473	0.0359
R1/wR2,[a] $I \geq 2\sigma I$ (%)	3.37/8.68	5.84/15.71	5.67/14.07	3.91/10.28
R1/wR2,[a] all data (%)	3.41/8.72	6.23/16.16	6.33/14.79	4.08/10.49
GOF	1.159	1.047	1.034	1.053

[a] $R1 = [\Sigma||F_o| - |F_c||]/\Sigma|F_o|$; $wR2 = \{[\Sigma w[(F_o)^2 - (F_c)^2]^2]/[\Sigma w(F_o^2)^2\}^{1/2}$; $w = [\sigma^2(F_o)^2 + (AP)^2 + BP]^{-1}$, where $P = [(F_o)^2 + 2(F_c)^2]/3$ and the A and B values are 0.0471 and 19.77 for [**48**]$_2$·DCM, 0.0818 and 6.86 for [**49**][B(3,5-{CF_3}$_2$$C_6H_3$)$_4$]·4THF, 0.0643 and 14.41 for [**50**][B(3,5-{CF_3}$_2$$C_6H_3$)$_4$]·$^5/_2$THF and 0.0569 and 8.14 [**51**]Br·$^1/_2$THF.

	[**51**][$AlBr_4$]	[**51**][$B(3,5\text{-}\{CF_3\}_2C_6H_3)_4$]·3THF	[**53**]Br·3THF	[**53**][$B(3,5\text{-}\{CF_3\}_2C_6H_3)_4$]
Formula	$C_{54}H_{72}AlBr_6N_4Sb$	$C_{98}H_{108}BBr_2F_{24}N_4O_3Sb$	$C_{66}H_{96}Br_4N_4O_3P_2$	$C_{86}H_{84}BBr_3F_{24}N_4P_2$
Fw [g mol^{-1}]	1405.34	2138.27	1375.04	1942.05
Crystal system	Orthorhombic	Orthorhombic	Triclinic	Triclinic
Space group	$P2_12_12_1$	$P2_12_12_1$	$P\bar{1}$	$P\bar{1}$
a (Å)	10.5273(1)	18.6015(3)	12.7442(6)	12.8207(1)
b (Å)	18.6503(1)	23.3299(4)	15.5789(7)	23.5342(3)
c (Å)	30.8129(2)	70.1897(11)	18.8569(6)	30.8558(4)
α (°)	90	90	76.130(3)	90.475(1)
β (°)	90	90	81.932(3)	99.027(1)
γ (°)	90	90	68.427(3)	105.727(1)
V ($Å^3$)	6049.72(8)	30460.3(9)	3374.4(3)	8837.79(18)
Z	4	12	2	4
Radiation, λ (Å)	Cu Kα, 1.54178	Cu Kα, 1.54178	Cu Kα, 1.54178	Cu Kα, 1.54178
ρ_{calc} (g cm^{-3})	1.543	1.399	1.353	1.460
μ (mm^{-1})	8.669	3.884	3.708	2.880
Reflections collected	63776	90656	35659	127655
Independent reflections	12555	49603	13975	36533
Parameters	611	3628	728	2283
R(int)	0.0317	0.0877	0.0288	0.0257
R1/wR2,[a] $I \geq 2\sigma I$ (%)	2.43/5.88	11.81/30.47	4.47/13.35	4.27/11.63
R1/wR2,[a] all data (%)	2.50/5.95	13.83/32.67	4.69/13.58	4.73/12.09
GOF	1.023	1.074	1.023	1.026

[a] $R1 = [\Sigma||F_o| - |F_c||]/\Sigma|F_o|$; $wR2 = \{[\Sigma w[(F_o)^2 - (F_c)^2]^2]/[\Sigma w(F_o^2)^2\}^{1/2}$; $w = [\sigma^2(F_o)^2 + (AP)^2 + BP]^{-1}$, where $P = [(F_o)^2 + 2(F_c)^2]/3$ and the A and B values are 0.0254 and 6.37 for [**51**][$AlBr_4$], 0.1730 and 149.23 for [**51**][$B(3,5\text{-}\{CF_3\}_2C_6H_3)_4$]·3THF, 0.0758 and 8.12 for [**53**]Br·3THF and 0.0643 and 10.80 for [**53**][$B(3,5\text{-}\{CF_3\}_2C_6H_3)_4$].

	[**54**]Br·4DCM	[**55**][B(3,5-{CF_3}$_2$$C_6H_3$)$_4$]$_2$·$^3/_2$DCM	[**55**][B(3,5-{CF_3}$_2$$C_6H_3$)$_4$]$_2$·2DFB	[**56**][B(3,5-{CF_3}$_2$$C_6H_3$)$_4$]$_2$·DFB
Formula	$C_{58}H_{80}BrCl_{11}N_4P_2$	$C_{119.5}H_{99}B_2Br_2Cl_3F_{48}N_4P_2$	$C_{130}H_{104}B_2Br_2F_{52}N_4P_2$	$C_{124}H_{100}B_2Cl_2F_{50}N_4P_2$
Fw [g mol^{-1}]	1365.06	2852.75	2953.55	2750.53
Crystal system	Monoclinic	Triclinic	Triclinic	Triclinic
Space group	$P2_1/n$	$P\bar{1}$	$P\bar{1}$	$P\bar{1}$
a (Å)	12.0636(2)	12.9265(1)	12.8045(4)	12.8289(5)
b (Å)	28.5186(3)	19.5862(2)	16.4182(5)	16.4297(7)
c (Å)	20.4019(3)	25.8965(3)	17.5699(4)	17.5090(7)
α (°)	90	91.462(1)	73.042(2)	73.077(4)
β (°)	104.232(1)	100.922(1)	84.650(2)	84.604(3)
γ (°)	90	103.341(1)	67.727(3)	67.356(4)
V (Å^3)	6803.58(17)	6247.54(11)	3268.83(18)	3257.8(3)
Z	4	2	1	1
Radiation, λ (Å)	Cu Kα, 1.54178	Cu Kα, 1.54178	Cu Kα, 1.54178	Cu Kα, 1.54178
ρ_{calc} (g cm^{-3})	1.333	1.516	1.500	1.402
μ (mm^{-1})	5.536	2.739	2.135	1.754
Reflections collected	96280	107268	32251	34428
Independent reflections	14191	25881	11539	13471
Parameters	741	1676	921	846
R(int)	0.0417	0.0286	0.0300	0.0333
R1/wR2,[a] I ≥ 2σI (%)	5.72/17.87	5.95/15.58	5.70/15.97	10.80/30.87
R1/wR2,[a] all data (%)	6.13/18.44	6.32/15.94	6.05/16.36	11.41/32.13
GOF	1.021	1.054	1.065	2.644

[a] $R1 = [\Sigma||F_o| - |F_c||]/\Sigma|F_o|$; $wR2 = \{[\Sigma w[(F_o)^2 - (F_c)^2]^2]/[\Sigma w(F_o^2)^2\}^{1/2}$; $w = [\sigma^2(F_o)^2 + (AP)^2 + BP]^{-1}$, where $P = [(F_o)^2 + 2(F_c)^2]/3$ and the A and B values are 0.1133 and 12.13 for [**54**]Br·4DCM, 0.0777 and 12.79 for [**55**][B(3,5-{CF_3}$_2$$C_6H_3$)$_4$]$_2$·$^3/_2$DCM, 0.1031 and 2.78 for [**55**][B(3,5-{CF_3}$_2$$C_6H_3$)$_4$]$_2$·2DFB and 0.2000 and 0 for [**56**][B(3,5-{CF_3}$_2$$C_6H_3$)$_4$]$_2$·DFB.

	[**57**]$_2$[$SnBr_6$]·THF	[**58**][B(3,5-{CF_3}$_2$$C_6H_3$)$_4$]	[**59**]Br·3DCM	[**60**][B(3,5-{CF_3}$_2$$C_6H_3$)$_4$]$_2$·2DFB
Formula	$C_{112}H_{152}Br_8N_8OP_4Sn$	$C_{86}H_{84}BF_{24}N_4P_2$	$C_{57}H_{78}As_2Br_4Cl_6N_4$	$C_{130}H_{104}As_2B_2Br_2F_{52}N_4$
Fw [g mol^{-1}]	2508.26	1702.32	1501.41	3041.45
Crystal system	Monoclinic	Triclinic	Triclinic	Monoclinic
Space group	*Ia*	$P\bar{1}$	$P\bar{1}$	$P2_1/c$
a (Å)	21.5603(2)	12.6812(2)	12.8050(4)	14.5097(2)
b (Å)	26.1169(2)	17.0730(3)	15.7709(4)	23.4608(4)
c (Å)	22.7679(2)	20.7995(4)	18.6208(4)	20.2944(4)
α (°)	90	81.712(2)	74.190(3)	90
β (°)	111.375(1)	74.258(2)	79.812(3)	109.658(2)
γ (°)	90	86.832(2)	66.879(3)	90
V (Å^3)	11938.48(19)	4288.73(14)	3317.14(19)	6505.8(2)
Z	4	2	2	2
Radiation, λ (Å)	Cu Kα, 1.54178	Cu Kα, 1.54178	Cu Kα, 1.54178	Cu Kα, 1.54178
ρ_{calc} (g cm^{-3})	1.396	1.318	1.503	1.553
μ (mm^{-1})	5.708	1.317	6.577	2.478
Reflections collected	72532	84078	36675	39801
Independent reflections	18569	17780	13717	13482
Parameters	1240	1080	693	1021
R(int)	0.0228	0.0268	0.0226	0.0239
R1/wR2,[a] I ≥ 2σI (%)	2.98/8.38	5.07/13.18	4.68/12.84	5.64/16.48
R1/wR2,[a] all data (%)	3.03/8.44	5.71/13.78	5.22/13.41	6.37/17.42
GOF	1.045	1.049	1.045	1.035

[a] $R1 = [\Sigma||F_o| - |F_c||]/\Sigma|F_o|$; $wR2 = \{[\Sigma w[(F_o)^2 - (F_c)^2]^2]/[\Sigma w(F_o^2)^2\}^{1/2}$; $w = [\sigma^2(F_o)^2 + (AP)^2 + BP]^{-1}$, where $P = [(F_o)^2 + 2(F_c)^2]/3$ and the A and B values are 0.0528 and 17.82 for [**57**]$_2$[$SnBr_6$]·THF, 0.0620 and 3.01 for [**58**][B(3,5-{CF_3}$_2$$C_6H_3$)$_4$], 0.0701 and 9.06 for [**59**]Br·3DCM and 0.1055 and 7.29 for [**60**][B(3,5-{CF_3}$_2$$C_6H_3$)$_4$]$_2$·2DFB.

	61	**[**(IPr)$_2$Sn$_2$Br$_3$][AlBr$_4$]	[**62**][AlBr$_4$]	**63**
Formula	$C_{27}H_{36}Br_2N_2Sn$	$C_{54}H_{72}AlBr_7N_4Sn_2$	$C_{27}H_{36}AlBBr_6N_2$	$C_{54}H_{72}Br_4Ga_2N_4$
Fw [g mol^{-1}]	667.09	1600.88	905.83	1236.23
Crystal system	Monoclinic	Monoclinic	Monoclinic	Monoclinic
Space group	$P2_1/c$	$P2_1/c$	$C2$	$P2_1/n$
a (Å)	16.7886(2)	10.5493(1)	26.3717(3)	12.7294(2)
b (Å)	19.5529(2)	16.2618(1)	9.7638(1)	13.7839(2)
c (Å)	19.0022(2)	37.8845(3)	29.4827(5)	15.9632(2)
α (°)	90	90	90	90
β (°)	111.561(1)	92.164(1)	114.299(2)	94.060(1)
γ (°)	90	90	90	90
V (Å^3)	5801.29(12)	6494.47(9)	6918.92(19)	2793.89(7)
Z	8	4	8	2
Radiation, λ (Å)	Cu Kα, 1.54178	Cu Kα, 1.54178	Cu Kα, 1.54178	Cu Kα, 1.54178
ρ_{calc} (g cm^{-3})	1.528	1.637	1.739	1.470
μ (mm^{-1})	10.342	11.555	8.771	4.809
Reflections collected	118365	80998	46980	31430
Independent reflections	12080	13522	11703	5824
Parameters	577	629	705	290
R(int)	0.0390	0.0535	0.0299	0.0443
R1/wR2,[a] $I \geq 2\sigma I$ (%)	3.22/7.93	4.81/12.41	4.16/10.07	3.55/9.32
R1/wR2,[a] all data (%)	3.93/8.50	5.20/12.80	4.21/10.12	3.62/9.42
GOF	1.120	1.040	0.658	1.072

[a] $R1 = [\Sigma||F_o| - |F_c||]/\Sigma|F_o|$; $wR2 = \{[\Sigma w[(F_o)^2 - (F_c)^2]^2]/[\Sigma w(F_o^2)^2\}^{1/2}$; $w = [\sigma^2(F_o)^2 + (AP)^2 + BP]^{-1}$, where $P = [(F_o)^2 + 2(F_c)^2]/3$ and the A and B values are 0.0280 and 14.81 for **61**, 0.0595 and 25.32 for [(IPr)$_2$Sn$_2$Br$_3$][AlBr$_4$], 0.0681 and 143.65 for [**62**][AlBr$_4$] and 0.0631 and 1.48 for **63**.